

Novel regulators of chromatin response to DNA damage

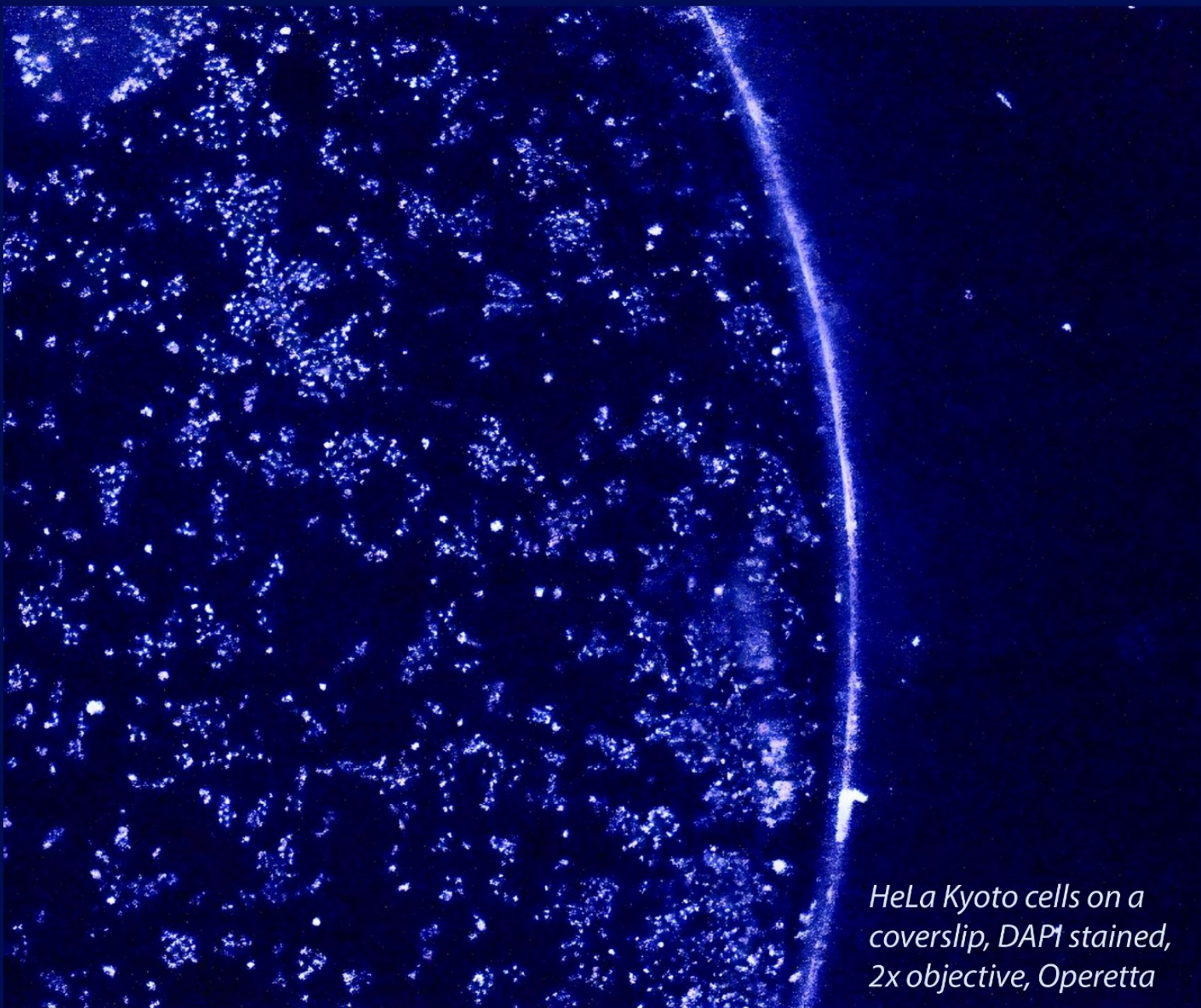
Neuartige Regulatoren der Chromatin Reaktion auf DNA-Schäden

by **Ksenia G. Kolobynina**



TECHNISCHE
UNIVERSITÄT
DARMSTADT

Cell Biology and Epigenetics



*HeLa Kyoto cells on a
coverslip, DAPI stained,
2x objective, Operetta*

2024, Darmstadt

Novel regulators of chromatin response to DNA damage
Neuartige Regulatoren der Chromatin Reaktion auf DNA-Schäden

Vom Fachbereich Biologie der Technischen Universität Darmstadt
zur Erlangung des akademischen Grades
Doctor rerum naturalium
genehmigte Dissertation von

Ksenia G. Kolobynina

M. Sc. in Molecular Biology and Genetics
aus Kasan, Russland

1. Referentin: Prof. Dr. M. Cristina Cardoso
2. Referent: Prof. Dr. Markus Löbrich

Darmstadt, Technische Universität Darmstadt
2024

Novel regulators of chromatin response to DNA damage

Neuartige Regulatoren der Chromatin Reaktion auf DNA-Schäden © 2024

Genehmigte Dissertation von Ksenia G. Kolobynina, M.Sc. aus Kasan, Russland

1. Referent/Referentin: Prof. Dr. M. Cristina Cardoso

2. Referent/Referentin: Prof. Dr. Markus Löbrich

Darmstadt, Technische Universität Darmstadt

Jahr der Veröffentlichung der Dissertation auf TUpriints: 2024

Tag der Einreichung: 22.05.2024

Tag der mündlichen Prüfung: 1.07.2024

Veröffentlicht unter CC BY-SA 4.0. International

<https://creativecommons.org/licenses/by-sa/4.0/>

Science is a horizon to search for, not a prize to hold in your hand.

Alex Hirsch

Deep roots are safe from frost.

The current work is devoted to my family who patiently endured years of separation between us and never doubted that I could do it and deserve it. Since the first day when my PhD route started, the world has changed beyond our imagination, and despite the distance between us my family and I went through life storms together. I know that no matter where my way will bring me and how many good and bad days will come, I always have a home to come back to.

The ornament that marks the start and end of the thesis' main body is a national tatar ornament usually used for the decoration of fabrics, various objects of art and everyday life, in architecture.



Preface

Before you lies the doctoral thesis entitled “Novel regulators of chromatin response to DNA damage”. The work combines the results of two high-throughput screens and characterization of one of the hit proteins, PHF19, for its function in the DNA damage signaling and repair. The introduction is partially based on Kolobynina *et al.*, 2022. To facilitate the interpretation of the data obtained from the screens, the discussion to each part was merged together with the corresponding results. The results and discussion section is followed by the general conclusions and perspectives. The Annex part contains supplementary figures and tables that are referred in the text as (Annex: Table XX) and (Annex: Figure XX).

Summary

The DNA damage response (DDR) signaling maintains genome stability, thus protecting cells from aging or malignant transformation. DNA damage and following DDR occur in the context of chromatin, and chromatin governs the damage response at multiple levels including post-translational modifications of histone and non-histone proteins. Among these modifications reported at the sites of DNA double-strand breaks (DSBs) are phosphorylation, acetylation, methylation, and ubiquitination.

DSB signaling and repair take place in a defined chromatin domain characterized by the enrichment of specific post-translational modifications and accumulated proteins. These structures are microscopically visible and are termed "DNA repair foci". Phosphorylation of serine 139 of histone H2AX (termed γ H2AX) is the key event and forms the platform for subsequent repair. The formation and persistence of γ H2AX domains reflect chromatin architecture and the efficiency of DSB repair.

Another important post-translational modification involved in DSB repair is ubiquitination. Ubiquitination is a covalent protein modification, which requires a three-enzyme cascade. The high abundance of ubiquitin ligases, internal ubiquitin modification sites, and a variety of possible ubiquitin signal structures make ubiquitination one of the most complex modification types in DDR. Due to the complexity large part of the ubiquitin-dependent network remains to be discovered, although several ubiquitin ligases were shown to be involved in the DDR.

To identify novel ubiquitin ligases involved in the DDR a human ubiquitinome-wide (663 E3 ubiquitin ligases) high-throughput screening was performed using the formation and persistence of γ H2AX foci as a proxy for DSB repair following X-ray exposure. More than 100 novel ubiquitin modifiers that affect DNA damage signaling (30 min post-irradiation) and/or repair (24 h post-irradiation) were identified in the screening. Of the identified hits 62.2% are associated with the damage signaling only (early time point, 107 ubiquitin modifiers), while 15.1 % of the hits are exclusively associated with the late repair point (24 h, 26 ubiquitin modifiers). The remaining 22.7% of the identified target genes affect both repair stages (39 ubiquitin modifiers). Gene ontology analysis and in silico protein-protein interaction analysis identified clusters of physically interacting hits for each time point. This data provided a list of novel chromatin modifiers involved in the DNA damage response and repair and their potential molecular function.

In a second screen 33 of the identified hits, which affected both early and late repair time points, were studied in more detail. This screen used more time points and additionally made use of the immunohistochemical detection of RAD51 (homologous recombination) and 53BP1 (non-homologous end joining) foci to gain information about the affected DSB repair pathways. In addition, we performed the cluster analysis and identified four time-independent DNA repair phenotypes represented by CXXC1, XIAP, RNF8 and RNF168 proteins.

In the third part of this work, the molecular function of one hit, the PHF19, was studied in the context of the chromatin response to DSBs. PHF19 was shown to be crucial for the γ H2AX signaling and formation of the repair focus. PHF19-depleted cells experienced global chromatin decondensation and a significant decrease in γ H2AX foci intensity post-X-ray irradiation. Moreover, PHF19 knockdown caused DSB repair delay compared to wild type cells. In accordance with the γ H2AX signaling impairment, the lack of the PHF19 protein hindered RAD51, RAD52, 53BP1, pATM and RNF8 recruitment to sites of DSBs. Both general ubiquitination and H2AK119ub specifically were decreased at the sites of breaks. With the use of ubiquitin binder probes, we showed that ubiquitination is reduced at the sites of the damage in living PHF19 knockdown cells. Additionally, we showed that PHF19 association with the DSB site reaches its maximum one hour post-irradiation.

In conclusion, these findings provide previously unknown ubiquitin-dependent signaling cascades in the DDR and underline the role of chromatin ubiquitination in DSB repair suggesting possible targets for anti-cancer therapy.

Zusammenfassung

Die DNA-Schadensreaktion (engl. DNA damage response, DDR) sorgt für die Aufrechterhaltung der Genomstabilität und schützt so die Zellen vor Alterung oder maligner Transformation. DNA-Schäden und die anschließende DNA-Schadensreaktion finden im Kontext des Chromatins statt. Das Chromatin steuert dabei die Schadensreaktion auf mehreren Ebenen, einschließlich posttranslationaler Veränderungen von Histon- und Nicht-Histon-Proteinen. Zu diesen Modifikationen, die an den Stellen von DNA-Doppelstrangbrüchen (DSB) festgestellt wurden, gehören Phosphorylierung, Acetylierung, Methylierung und Ubiquitinierung.

DSB-Signaling und -Reparatur finden in einer definierten Chromatin-Domäne statt, die durch die Anreicherung spezifischer posttranslationaler Modifikationen und akkumulierter Proteine gekennzeichnet ist. Diese Strukturen sind mikroskopisch sichtbar und werden als "DNA-Reparatur Foci" bezeichnet. Die Phosphorylierung von Serin 139 des Histons H2AX (als γ H2AX bezeichnet) ist das Schlüsselereignis und bildet die Plattform für die anschließende Reparatur. Die Bildung und das Fortbestehen von γ H2AX-Domänen spiegeln die Chromatinarchitektur und die Effizienz der DSB-Reparatur wider.

Eine weitere wichtige posttranslationale Modifikation, die an der DSB-Reparatur beteiligt ist, ist die Ubiquitinierung. Ubiquitinierung ist eine kovalente Proteinmodifikation, die eine Drei-Enzym-Kaskade erfordert. Die große Anzahl an Ubiquitin-Ligasen, internen Ubiquitin-Modifikationsstellen und eine Vielzahl möglicher Ubiquitin-Signalstrukturen machen die Ubiquitinierung zu einer der komplexesten Modifikationsarten in der DNA-Schadensreaktion. Um neue Ubiquitin-Ligasen zu identifizieren, die an der DDR beteiligt sind, haben wir ein humanes Ubiquitinom-weites (663 E3-Ubiquitin-Ligasen) Hochdurchsatz-Screening durchgeführt, bei dem die Bildung und Persistenz von γ H2AX-Foci als Indikator für die DSB-Reparatur nach Röntgenexposition verwendet wurde. Mehr als 100 neue Ubiquitin-Modifikatoren, die das Signaling der DNA-Reparatur (30 Minuten nach der Bestrahlung) und/oder die Reparatur selbst (24 Stunden nach der Bestrahlung) beeinflussen, wurden bei diesem Screening identifiziert. Von den identifizierten Treffern sind 62,2 % nur mit der Schadenssignalisierung assoziiert (früher Zeitpunkt, 107 Ubiquitin-Modifikatoren), während 15,1 % der Treffer ausschließlich mit dem späten Reparaturzeitpunkt (24 h, 26 Ubiquitin-Modifikatoren) in Verbindung stehen. Die restlichen 22,7 % der identifizierten Zielgene betreffen beide Reparaturphasen (39 Ubiquitin-Modifikatoren). Eine Gen-Ontologie-Analyse und eine in silico Analyse der Protein-Protein-Interaktion ergaben für jeden Zeitpunkt Cluster von physisch interagierenden Treffern. Diese Daten lieferten eine Liste neuartiger Chromatin-Modifikatoren, die an der DNA-Schadensreaktion und -Reparatur beteiligt sind, sowie deren potenzielle molekulare Funktion. 33 der identifizierten Treffer, die sowohl frühe als auch späte Reparaturzeitpunkte betrafen, wurden in einem zweiten Screening genauer untersucht. Bei diesem Screening wurden zusätzliche Zeitpunkte verwendet und darüber hinaus der immunhistochemische Nachweis von Rad51- (homologe Rekombination) und 53BP1- (nicht-homologe Endverbindung) Foci genutzt, um Informationen über die durch den Knockdown der Ubiquitin-Ligasen betroffenen DSB-Reparaturwege zu gewinnen. Darüber hinaus haben wir eine Clusteranalyse durchgeführt und vier zeitunabhängige DNA-Reparatur-Phänotypen identifiziert, die durch die Proteine CXXC1, XIAP, RNF8 und RNF168 repräsentiert werden.

Im dritten Teil dieser Arbeit wurde die molekulare Funktion eines der Treffer, PHF19, im Zusammenhang mit der Chromatinreaktion auf DSBs untersucht. Es wurde gezeigt, dass PHF19

für das γ H2AX-Signaling und die Bildung des Reparaturfokus entscheidend ist. Bei PHF19-depletierten Zellen kam es zu einer globalen Chromatinkondensations- und einer signifikanten Abnahme der Intensität der γ H2AX-Foci nach Röntgenbestrahlung. Darüber hinaus führte der PHF19-Knockdown zu einer Verzögerung der DSB-Reparatur im Vergleich zu Wildtyp-Zellen. In Übereinstimmung mit der Beeinträchtigung der γ H2AX-Signalisierung behinderte das Fehlen des PHF19-Proteins die Rekrutierung von RAD51, 53BP1 und RNF8 an DSB-Stellen. Sowohl die allgemeine Ubiquitinierung als auch die spezifische H2AK119ub waren an den Bruchstellen verringert. Mit Hilfe von Ubiquitin-Binder-Sonden konnte ich zeigen, dass die Ubiquitinierung an den Stellen der Schädigung in lebenden PHF19-Knockdown-Zellen reduziert ist.

Außerdem konnte ich zeigen, dass die Assoziation von PHF19 mit der DSB-Stelle eine Stunde nach der Bestrahlung ihr Maximum erreicht. Zusammenfassend lässt sich sagen, dass diese Ergebnisse bisher unbekannte, von Ubiquitin abhängige Signalkaskaden in der DDR aufzeigen und die Rolle der Ubiquitinierung von Chromatin bei der DSB-Reparatur unterstreichen, was mögliche neuartige Ansatzpunkte für eine Krebstherapie bietet.

Contents

Preface	7
Summary	9
List of Main Figures	15
List of Main Tables	16
Main abbreviations	18
1. Introduction	20
1.1. DNA damage response-associated chromatin remodeling	20
1.2 Local and global chromatin changes mediated by ubiquitination	24
Ubiquitin-dependent chromatin network	25
Local chromatin changes: damage signaling	31
Local chromatin changes: repair pathway choice	33
Global chromatin changes	37
1.3 Crosstalk between ubiquitination and other modifications in DDR.....	40
Phosphorylation and ubiquitination	40
Poly(ADP-ribos)ylation and ubiquitination	44
Acetylation and ubiquitination	47
SUMOylation and ubiquitination	49
Neddylatation and ubiquitination	51
1.4 Polycomb-associated ubiquitination in DNA damage signaling and repair	51
1.5 Ubiquitination, DNA damage and disease	56
2. Aims of the study	59
3. Materials and Methods	61
3.1 Cell culture.....	61
3.2 Expression constructs for live-cell DNA damage assay	61
Ubiquitinome-wide high-throughput screening: methods	61
3.3 siRNA library preparation, array mapping and layout	61
3.4 Ubiquitinome-wide high-content high-throughput screening	62
3.5 High-throughput microscopy.....	62
3.6 Image analysis.....	62
3.7 Image and image analysis quality control.....	63
3.8 Data analysis	64
3.9 Enrichment analysis and bioinformatics	64
Small-scale 4D screen: methods	64
3.10 siRNA library preparation, plate mapping and layout.....	64
3.11 Small-scale 4D screening for the repair pathway preference.....	64
3.12 High-throughput microscopy.....	65
3.13 Image analysis	65
3.14 Data analysis	66
3.15 Hierarchical clustering	66
PHF19 as a novel player in ubiquitin-dependent chromatin response to double-strand	

breaks: methods	67
3.16 Irradiation	67
3.17 Cell cycle distribution	67
3.18 Neon transfection	67
3.19 PHF19 knockdown	68
3.20 Immunofluorescence	68
3.21 Comet assay.....	68
3.22 Live-cell DNA damage assay.....	68
3.23 Microscopy	69
3.24 Image analysis	69
3.25 Data analysis	70
3.26 Immunoblotting	70
3.27 Apoptosis analysis	71
4. Results and discussion	72
4.1 Ubiquitinome-wide high-throughput screening to identify novel ubiquitin modifiers in chromatin response to double-strand break.....	72
Ubiquitinome-wide screening for novel players of DNA damage signaling and repair: design and rationale	72
Construction of the image analysis pipeline for the ubiquitome-wide screen	74
Establishment of the data analysis strategy	77
4.2 Hits recognition and evaluation	84
Chromatin proteins involved in DNA damage signaling and repair revealed by ubiquitinome-wide screening.....	84
In silico analysis of protein interactions revealed the connection between DDR proteins and chromatin remodelers among novel ubiquitin modifiers	89
Ubiquitination controls DNA repair early after the damage and cell fate decision at the late time point	94
4.3 Small-scale 4D screen for mapping repair pathway preference	99
Small-scale 4D screen design and rationale	99
Validation of small-scale 4D screen	106
Downregulation of hits identified in the screening alters kinetics of repair proteins	111
Depletion of hits led to the formation of four DNA repair phenotypes.....	116
4.4 PHF19 as a novel player in ubiquitin-dependent chromatin response to double-strand breaks	122
PHF19 knockdown lowers DNA damage signaling.....	122
Lack of PHF19 changes the recruitment of selected repair factors to the sites of DNA damage.....	125
PHF19 is a facultative heterochromatin-associated protein that functions in early-mid stages of double-strand break repair.....	134
PHF19 depletion causes chromatin decompaction in undamaged human cells.....	136
PHF19 is required to keep the general ubiquitination signaling as well as H2AK119ub specifically at the sites of double-strand breaks	138
5. General conclusions and perspectives	145
6. Bibliography	149

7. Annex	187
Acknowledgements	299
CV.....	301

List of Main Figures

Figure 1.1. Chromatin is an essential context for DNA damage signaling and repair	22
Figure 1.2. Histone modifications in the double-strand break repair pathway choice	24
Figure 1.3. The ubiquitin-dependent system is complex and versatile	26
Figure 1.4. Ubiquitination in the DNA repair pathway choice	35
Figure 1.5. Crosstalk between ubiquitination and other posttranslational modifications in the double-strand break repair. Phosphorylation and ubiquitination	42
Figure 1.6. (a) PARylation and ubiquitination. (b) Acetylation and ubiquitination	46
Figure 1.7. (a) SUMOylation and ubiquitination. (b) NEDDylation and ubiquitination	50
Figure 1.8. Polycomb-associated ubiquitination in the DNA damage signaling and repair	54
Figure 2. Aims of the study: graphical abstract	59
Figure 4.1. Ubiquitinome-wide high-content screen for the players of chromatin response to DNA damage	73
Figure 4.2. Image analysis workflow for the high-throughput data collected in the ubiquitinome-wide screening	76
Figure 4.3. Image data quality control	78
Figure 4.4. Data normalization and dose response	80
Figure 4.5. Data analysis of the ubiquitinome-wide high-throughput screening data	82
Figure 4.6. Analysis of the hits from the ubiquitinome-wide screening revealed seven scenarios	88
Figure 4.7. Custom network of the GO terms and protein-protein interactions for hits list for both post-irradiation time points	90
Figure 4.8. Protein-protein interaction networks for the hits of 0.5 h and 24 h post-irradiation highlighted connection between DNA repair proteins and chromatin remodelers	92
Figure 4.9. Comparative functional and protein-protein interaction profiling of the hits at 0.5 h and 24 h post-irradiation time points	96
Figure 4.10. Protein-protein interaction components and hits overlap identified between the hit lists at 0.5 h and 24 h post-irradiation	98
Figure 4.11. Gene ontology analysis of the 4D small-scale screen genes	102
Figure 4.12. Small-scale 4D screen design	103
Figure 4.13. Image analysis of the data obtained in the small-scale 4D screen	105

Figure 4.14. Irradiation response of mock/non-siRNA transfected cells in the small-scale 4D screen	108
Figure 4.15. Depletion of the known ubiquitin modifiers alters DDR kinetics	110
Figure 4.16. Downregulation of the hits identified in the screening alters the kinetics of repair proteins	112
Figure 4.17. Altered repair kinetics and pathway preference at the whole-nuclear intensity level	114
Figure 4.18. Altered repair kinetics and pathway preference at the single-focus level	115
Figure 4.19. Clustering analysis identified four clusters of the DDR kinetics at each time point post-irradiation	118
Figure 4.20. Cluster analysis identified four time-independent phenotypes of the DDR kinetics	120
Figure 4.21. PHF19 knockdown lowers DNA damage signaling and repair	124
Figure 4.22. Lack of PHF19 hinders the recruitment of selected factors to the sites of DNA damage	130
Figure 4.23. PHF19 knockdown affected the writer and the reader of the γ H2AX	133
Figure 4.24. PHF19 is facultative heterochromatin-associated protein and involved in the early-mid DNA repair	135
Figure 4.25. PHF19 depletion causes chromatin decompaction in undamaged and irradiated human cells	137
Figure 4.26. PHF19 depletion impairs ubiquitination signaling at the DSBs	139
Figure 4.27. PHF19-depleted cells fail to retain ubiquitination at the damage spot	142
Figure 4.28. The hypothesis	148

List of Main Tables

Table 1.1. Histone modifications in the DNA damage signaling and repair	27
Table 1.2. Summary of ubiquitin-binding domains	30
Table 1.3. Inhibitors of ubiquitin modifiers	56
Table 4.1. Screening hits known to be associated with other posttranslational modifications	93
Table 4.2. Summary of the hits chosen for the small-scale 4D screen for the DNA repair pathway preference	100

Main abbreviations

ATM - ataxia-telangiectasia mutated

ATR - ATM and RAD3-related

BER - base-excision repair

CDK - cell cycle-dependent kinase

CFS - common fragile sites

cNHEJ - canonical NHEJ

DDR – DNA damage response

DEVD - amino acid sequence Asp-Glu-Val-Asp

DNA-PKcs - DNA-dependent protein kinase catalytic subunit

DSB – double-strand break

DTC - Deltex C-terminal domain

DUB - deubiquitinase

ERK - extracellular signal-regulated kinase

FA - Fanconi anemia

FC - fold change

FRRUC - FBXL10-RNF68-RNF2 ubiquitin ligase complex

HDAC - histone deacetylase

HR – homologous recombination

IR - ionizing radiation

IRIF – irradiation-induced focus

LET - linear energy transfer

LLPS - liquid-liquid phase separation

MIU - motif interacting with ubiquitin

NEDD8 - neural precursor cell expressed developmentally downregulated 8

NER - nucleotide excision repair

NHEJ – non-homologous end joining

NZF - Npl4 Zinc Finger domain

PAR - poly(ADP-ribose)

PARP - poly (ADP-ribose) polymerase

PI3 - phosphoinositide 3

PI3KK - phosphoinositide 3 kinase-related protein kinase

polyUb - polyubiquitin

PPI - protein-protein interaction

PRC - polycomb repressive complex

PTM – post-translational modification

pUb - phosphoubiquitin

RIDDLE - Radiosensitivity, ImmunoDeficiency Dysmorphic features and LEarning difficulties syndrome

RNAi - RNA interference

ssDNA - single-strand DNA

STUbL - SUMO-targeted ubiquitin ligase

SUMO – small ubiquitin-like modifier

TAD - topologically associated domain

TSA - Trichostatin A

Ub – ubiquitin

UBA - ubiquitin-associated domain

UBD - ubiquitin-binding domain

UBZ - ubiquitin-binding zinc-finger

UIM - ubiquitin-interacting motif

1. Introduction¹

DNA damage is a major threat to genome stability, especially in the form of a double-strand break (DSB). Unrepaired breaks are one of the most harmful damage types, causing cell cycle arrest, apoptosis, or malignant transformation (Bartkova et al., 2005; Gorgoulis et al., 2005; Negrini et al., 2010). To cope with the threat, DNA damage response (DDR) systems have evolved. Naturally, DNA damage and the DDR both happen in the context of chromatin. Chromatin, comprising DNA together with associated histone and non-histone proteins, determines the structure and function of the genome. At the primary level, chromatin is constituted by approximately 147 base pairs of DNA wrapped twice around eight core histones (H2A, H2B, H3, H4) forming nucleosomes (Luger et al., 1997). Nucleosome arrays compact and fold further into high-order structures creating a complex multilevel 3D chromatin architecture. With each new level of folding, more and more factors are involved in the decision process that regulates the chromatin structure. In addition, DNA and histones can be chemically modified. Histone post-translational modifications (PTM), such as phosphorylation, methylation, acetylation, and ubiquitination as well as histone variants modulate histone dynamics and DNA association. Together with the linker histone H1 and many non-histone proteins these factors directly define the physical properties of the chromatin fiber including secondary structure, accessibility, phase separation properties, and mobility, hence ultimately affecting damage induction, recognition, and processing.

1.1. DNA damage response-associated chromatin remodeling

In an undamaged state, chromatin exists in a variety of functionally and topologically different domains, which can change dynamically. Based on the degree of compaction, originally based upon contrast staining with basic dyes (Heitz, 1928) chromatin is classified into more compacted, usually defined as transcriptionally inert heterochromatin and open, transcriptionally active, gene-rich euchromatin. Each of them is characterized by unique epigenetic and structural properties. Chromatin conformation reflects the role of the underlying sequences in the genome: centromeric and pericentromeric regions of chromosomes are organized into constitutive heterochromatin, which is believed to stay repressed among all cell types (Saksouk et al., 2015). On the other hand, facultative heterochromatin contains genes, which are silent in the corresponding cell type dependent on the developmental state. In response to various stimuli, facultative heterochromatin is remodeled into euchromatin and vice versa, which ensures that the correct genes are expressed.

The pre-existing conformation of chromatin is a factor that affects DNA damage induction. Additional factors include the cell cycle stage (Ward and Chen, 2001), transcriptional activity (Falk et al., 2008; Herrera-Moyano et al., 2014; Prendergast et al., 2020; Bayona-Feliu and Aguilera, 2021), DNA secondary structure such as G-quadruplexes (Kumari et al., 2019), as well as the type of DNA damage and its source (e.g. LET (linear energy transfer) of ionizing radiation (Löbrich et al., 1996; Sutherland et al., 2001; Radulescu et al., 2004). When exposed to ionizing irradiation, the more compacted heterochromatin environment has been reported to physically shield DNA from damage and thus decrease the frequency and severity of the lesions formed

¹ The introduction is taken in part from the review by Kolobynina *et al.*, 2022

(Yoshikawa et al., 2008; Takata et al., 2013; Brambilla et al., 2020; Elia and Bradley, 1992; Cannan et al., 2014). The number of water molecules available for radiolysis and subsequent DNA damage generation in condensed regions is considered to be lower than in decondensed ones. Along with this line, tightly packed nucleosomes in heterochromatin should show decreased accessibility for damage sensors and repair proteins, and consequently, decreased repair efficiency. Yet, this hypothesis of the impervious heterochromatin was questioned (Caridi et al., 2017). Chromatin compaction affects lesion induction, but compacted regions are not as irresponsive as was suggested before (Jakob et al., 2011; Chagin et al., 2019). The complex relationship between the initial chromatin structure and the DDR was summarized in two models. The “access-repair-restore” model came first and depicted chromatin as an obstacle for the repair machinery (Smerdon, 1991). Later this model was revised according to the evidence that chromatin actively participates in the DDR and provides the necessary context for repair. The updated model was named “prime-repair-restore”, where the prime step comprises both the contribution of the initial chromatin landscape and its remodeling to facilitate damage signaling (Soria et al., 2012). At the prime step, the PTMs on histone and non-histone proteins, corresponding to the pre-existing eu- or heterochromatin epigenetic landscape, change to the ones of the repair-associated epigenetic landscape, thus, promoting the formation of a 3D repair domain (Figure 1.1). Interaction of proteins and successful crosstalk between damage signaling and repair mechanism at the sites of DSBs is achieved by a highly controlled network of PTMs. The latter changes protein stability, charge, activity, structure, or interaction with other players of the pathway. Among the various PTMs of proteins at the sites of DNA lesions are phosphorylation, acetylation, methylation, poly(ADP-ribosyl)ation, ubiquitination, and sumoylation (Kouzarides, 2007). The *de novo* establishment of the PTMs is catalyzed by writer enzymes, with the removal of the PTMs being done by eraser enzymes and the transduction of the signal downstream in the cascade being carried out by reader proteins. The chromatin modifications and their role are, therefore, highly dynamic and tightly regulated at multiple levels.

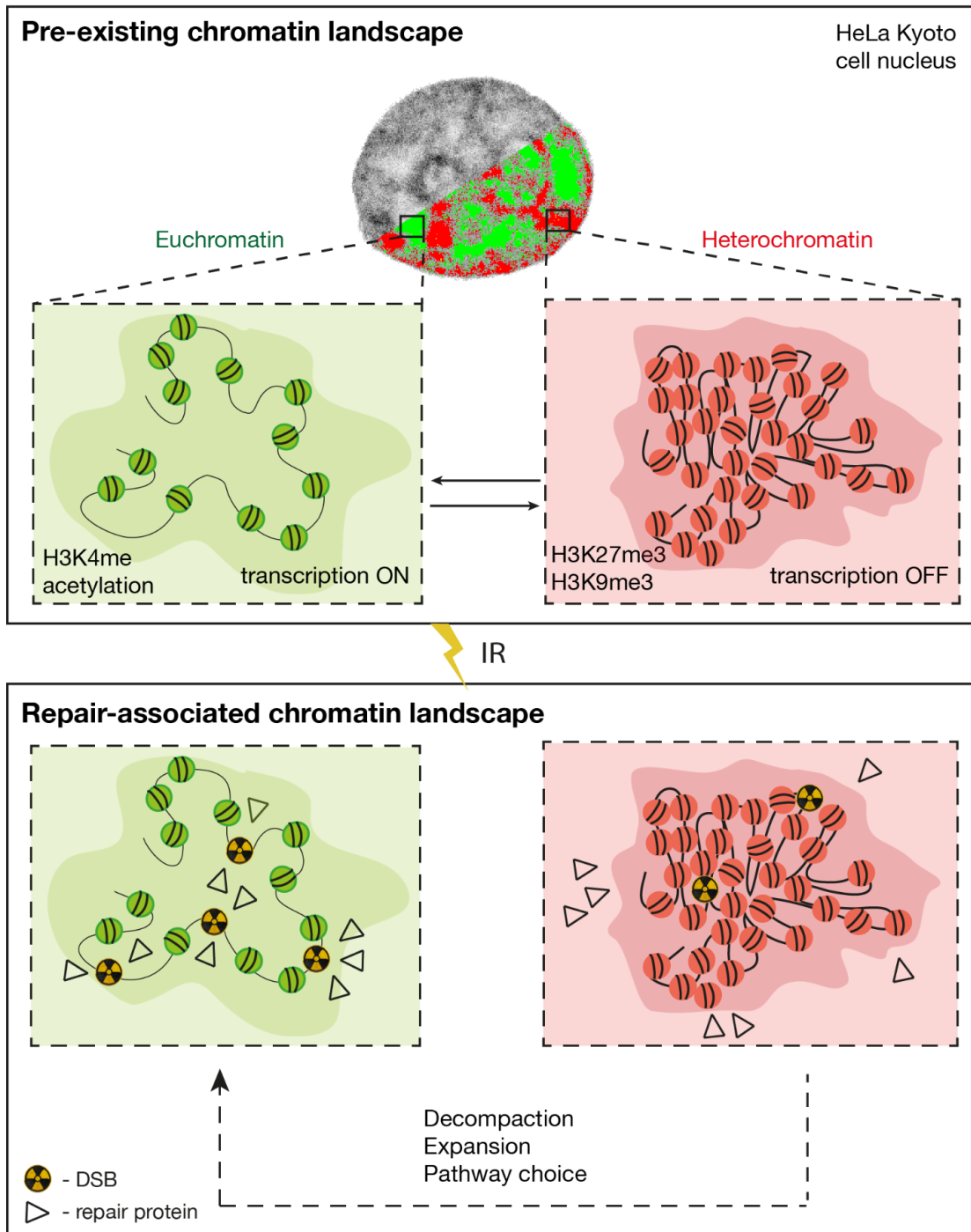


Figure 1.1. Chromatin is an essential context for DNA damage signaling and repair. DNA damage occurs in the context of chromatin, which is organized in a variety of functionally and topologically different domains such as euchromatin and heterochromatin. Decompacted euchromatin allows easy access of repair proteins to the lesions, however, the number of lesions can be higher than in heterochromatin. The compacted heterochromatic regions physically shield DNA from damaging agents, but the compaction partially restricts access of the repair proteins. Both euchromatin and heterochromatin get remodeled in the course of DDR. IR - ionizing irradiation.

To maintain genome stability, two major DSB repair pathways (non-homologous end joining (NHEJ) and homologous recombination (HR)) evolved. Both pathways are characterized by a different chromatin landscape (Figure 1.2).

The upstream DDR event is the phosphorylation of serine 139 (termed γ H2AX) on the histone variant H2AX by the PI3 kinase-related protein kinases ATM, ATR and DNA-PKcs (Rogakou et al., 1998; Sedelnikova et al., 2002). This signaling step is common for all DSBs independent of the repair pathway choice. The γ H2AX-mediated downstream cascade involves such reader and writer enzymes as MDC1, RNF8, and RNF168 (Kolas et al., 2007; Doil et al., 2009). The RNF8-RNF168 ubiquitination cascade recruits the main regulators of the repair pathway choice, 53BP1 for NHEJ and BRCA1 for HR. The RNF8-RNF168 axis promotes two chromatin modification marks, which 53BP1 binds in a bivalent mode: the H2AK15ub mark and the H4K20me2 (Fradet-Turcotte et al., 2013; Acs et al., 2011; Mallette et al., 2012). Interestingly, the H2AK15 site is a target for both ubiquitination and acetylation and is crucial for repair pathway decisions (Figure 1.2). When HR is preferred, the TIP60/NuA4 acetyltransferase complex acetylates H2AK15 and directly blocks ubiquitination which impairs the binding of 53BP1 (Jacquet et al., 2016). The histone acetyltransferase (HAT) TIP60 is also responsible for acetylation of the H4K16 site which physically inhibits 53BP1 binding to H4K20me2 and, thus, promotes HR (Figure 1.2) (Tang et al., 2013). On the other hand, the removal of H4K16ac from chromatin by the deacetylases HDAC1 and HDAC2 promotes NHEJ (Miller et al., 2010). The removal or absence of methylation at H4K20 (H4K20me0) was reported to guide the pathway choice toward HR by opening the binding site for BRCA1-BARD1, the main HR player (Nakamura et al., 2019). As H4K20me0 is abundant in post-replicative cells, these data provide evidence for how HR can be promoted once the sister chromatid is available as a template. The BRCA1-BARD1 ubiquitinates H2AK127/129 which is read by the ubiquitin reader SMARCAD1 to start a cascade of chromatin remodeling and blocks 53BP1 from binding on damaged chromatin (Densham et al., 2016). There are several chromatin modifications at the DSB sites that mediate the pathway choice in cooperation with the transcription activity of damaged loci, e.g. H3K36me3, H2BK120ac, H2AK118/119ub (Shanbhag et al., 2010; Clouaire et al., 2018). Usually, these modifications are associated with the NHEJ repair pathway but some were shown to be involved in both and additionally regulated by other epigenetic marks or factors (Figure 1.2).

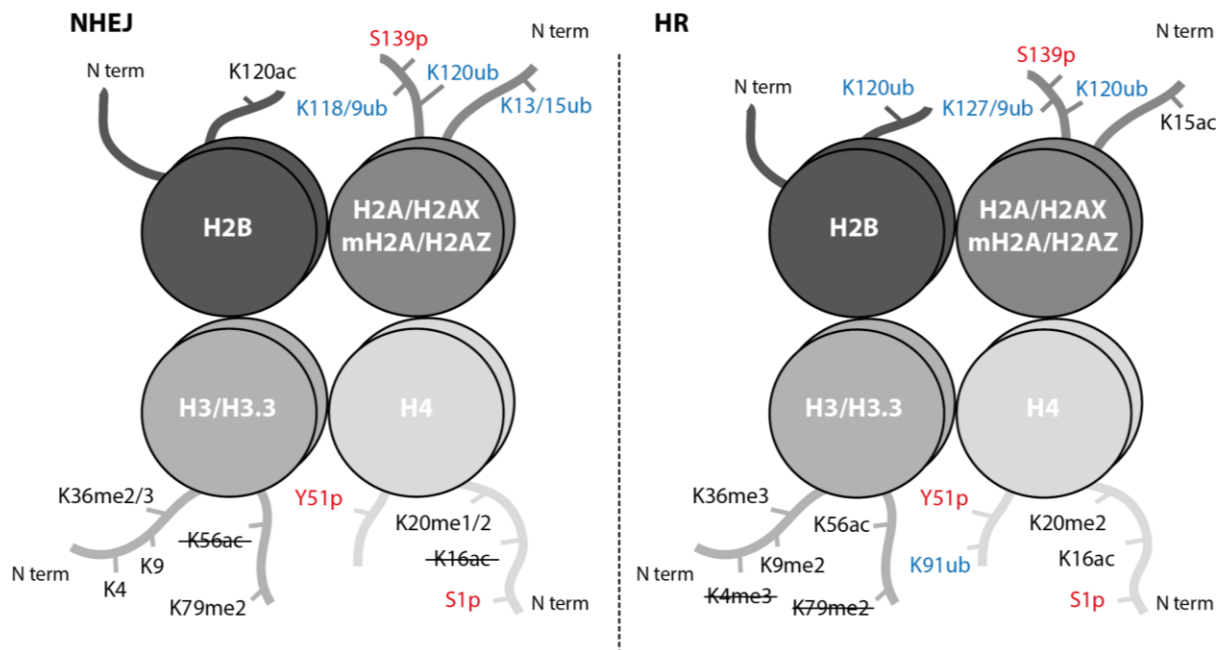


Figure 1.2. Histone post-translational modifications associated with NHEJ and HR repair pathways. Interaction of proteins and successful crosstalk between damage signaling and repair mechanism at the sites of DSBs is achieved by a highly controlled network of PTMs. Histone PTMs play a role in DSB repair pathway choice and serve as binding sites for repair proteins. Ubiquitination marks are in blue and phosphorylation marks are in red; ub - ubiquitination, p - phosphorylation, ac - acetylation, me - methylation, N term - N terminus. The crossed-out mark means it is removed in the repair pathway.

Many more chromatin modifications cooperate at the site of DNA damage to fine-tune the damage signaling, control chromatin remodeling and ensure a successful repair (Figure 1.2; Table 1.1). Combined, these data reveal the importance and complexity of chromatin remodeling in DDR.

1.2 Local and global chromatin changes mediated by ubiquitination

Ubiquitination is one of the major chromatin modifications happening globally in a cell and at the sites of DSB in particular. It was discovered as a process of covalent protein modification (Goldknopf et al., 1977) when small chemical modifications like phosphorylation and acetylation were already reported to affect protein properties and function. In the 1980s ubiquitination was shown to be part of the protein degradation pathway via the 26S proteasome and for a long time, the proteasomal role of ubiquitin was the only known (Hershko and Ciechanover, 1998). In the last decades, however, an ever-growing number of studies described a non-proteolytical or non-classical role of ubiquitination in intracellular signaling, membrane trafficking, DNA repair, and cell cycle (Dwane et al., 2017; Liao et al., 2022). Through multiple large-scale quantitative proteomic screens, it was confirmed that there are more than 1000 players in the ubiquitin system and more than 10,000 known individual ubiquitination sites in human proteins, which could mean that every cellular protein is ubiquitinated at some point in its existence (Kim et al., 2011; Wagner et al., 2011; Clague et al., 2015). Despite the intense research on ubiquitination, which led to the Nobel Prize in Chemistry for Aaron Ciechanover, Avram Hershko, and Irwin Rose in 2004, there is still a lot unknown about its players and their regulation.

Ubiquitin-dependent chromatin network

Ubiquitin (Ub) is a highly conserved 76 amino acids protein, its name due to its massive abundance in all eukaryotic cell types (Goldstein et al., 1975). Ubiquitin is the main building block in ubiquitination which is a process of covalent attachment of ubiquitin to a target protein. There are four genes encoding ubiquitin in the human genome: UBB, UBC, UBA52, and RPS27A (Kimura and Tanaka, 2010). Translation of these genes does not directly produce free active ubiquitin but requires cleavage of precursors by deubiquitinases (DUB). In addition, DUBs can reverse ubiquitination by cleaving the isopeptide bond between ubiquitin and its substrate protein. In humans, there are nearly 90 DUB genes, which can be classified into seven classes (Clague et al., 2019).

The enzymatic cascade of ubiquitination includes three steps and three types of enzymes (Pickart, 2004) (Figure 1.3A). At first, the free ubiquitin moiety is activated by the E1 enzyme in an ATP-dependent manner by building a thioester bond between the C-terminal Gly carboxyl group of Ub and the Cys in the active site of E1. Then, the activated Ub is delivered to the Cys residue of the E2 conjugating enzyme via E1-E2 thioester transfer. The third step is the substrate-specific transfer of the ubiquitin chain to the target molecule. This is achieved by the substrate-specific E3 ligase, which recognizes the E2-Ub complex and catalyzes the formation of an isopeptide bond between the C-terminal carboxyl group of a Ub moiety and an ϵ -NH₂ group on a lysine on the target protein. There is recent evidence that ubiquitination could also take place on other residues like cysteine, serine, and threonine (McClellan et al., 2019; Mabbitt et al., 2020). There are two ubiquitin E1 genes, around 40 E2, around 90 DUBs, and around 663 E3 ubiquitin ligases genes in the human genome representing around 5% of the total number of genes (Li et al., 2008; George et al., 2018). Interestingly, the number of E3 ubiquitin ligases in the human genome is larger than the number of kinases (518 genes) (Li et al., 2008). The difference in number between the three classes of ubiquitination enzymes evolutionary originates from the ability of one E2 enzyme to cooperate with several different E3 ligases depending on the context, the so-called combinatorial effect. Although there are some E2 proteins able to mediate the direct transfer of Ub to the target, in most cases the E3 ligase is the enzyme that promotes selectivity and specificity of the ubiquitination.

The complexity of the ubiquitin system is also expanded by the fact that ubiquitin itself contains seven lysine residues available for modification: K6, K11, K27, K29, K33, K48, and K63. Multiple ubiquitination events result in the formation of elongated polyubiquitin chains with various structures depending on which lysine was modified (Figure 1.3B). Apart from the seven internal lysines, there is the eighth site for ubiquitination, which is the methionine at position 1. This results in the formation of non-canonical “linear” chains (Ikeda et al., 2011; Iwai et al., 2014). The topology of the chains defines their function. The K48-linked chains are predominant in cells and usually target their substrate for degradation (Finley, 2009), while K63- and K6-linked chains were shown to regulate DDR (Elia et al., 2015; Takahashi et al., 2018). The wide variety of all the ubiquitination types, like monoubiquitination, multi-monoubiquitination, homotypic polyubiquitination (through the same lysine residue), and heterotypic polyubiquitination (mixed, branched) was named the “ubiquitination code” (Komander and Rape, 2012). The ubiquitin code is steadily expanding with recent findings that ubiquitin itself can be further modified post-translationally by, e.g., phosphorylation at eleven potential sites (Thr7, Thr12, Thr14, Ser20,

step is conjugation, where ubiquitin is transferred to the E2 enzyme. At the last step, ubiquitination occurs, e.g. modification of a target protein by ubiquitin-mediated by E3 ligase. The ubiquitination process is opposed by deubiquitination, which is the removal of the ubiquitin mark from the target protein by deubiquitinases (DUB). (b) Variety of ubiquitin chains, with or without modifications. P- phosphorylation, Ac - acetylation, SUMO - SUMOylation, NEDD8 - NEDDylation, Ub - ubiquitin, UBD - ubiquitin-binding domain, target - target protein harboring ubiquitin modification.

The ubiquitination network not only includes writers but also erasers and readers for its function. Some of the proteins might have more than one function and each function is activated by a different signal. While the E3 ligases (RING, HECT, and RBR families) write the ubiquitination and DUBs erase it, the ubiquitination readers are the proteins containing ubiquitin-binding domains (UBD). There are at least 20 types of UBDs present on a wide range of signaling proteins (Dikic et al., 2009). Interestingly, certain types of UBDs are present in proteins enriched at the sites of DSB, namely UIM (ubiquitin-interacting motif), MIU (motif interacting with ubiquitin), and UBZ (ubiquitin-binding zinc-finger) domains (Table 1.2). The affinity of a single UBD towards ubiquitin marks is low, and, therefore, various mechanisms were developed to increase the sensitivity and specificity of recognition. Some Ub readers contain multiple UBDs, e.g., the BRCA1-interacting protein RAP80 contains two UIM domains recognizing K63-linked polyubiquitin chains (Sato et al., 2009). Another way for UBD-containing proteins to ensure correct context-specific reading of ubiquitination is to cooperate. Such cooperation was reported for RNF168, RNF169, and RAD18 (Panier et al., 2012). Novel mechanisms of Ub reading and novel UBDs are yet to be identified. Taken together, all the variations of the ubiquitin code, alternative Ub modifications, complex networks of regulating proteins, and a large number of putative ubiquitin ligases with still unknown functions constitute a complex, highly dynamic, and largely unexplored ubiquitin-dependent epigenetic system. Due to its remarkable versatility and exceptional ability to fine-tune a signal transfer, ubiquitination is ideally suited for the regulation of dynamic and complex cellular processes like DSB signaling and repair.

Table 1.1. Histone modifications in the DDR.

PTM	Histone site	Writer	Eraser	Pathway	Reference
Phosphorylation	H2AXS139	ATM, ATR, DNA-PKcs	PP2A, PP4, PP6, Wip1	NHEJ, HR	(Rogakou et al., 1998; Ward and Chen, 2001; Stucki et al., 2005; Chowdhury et al., 2005, 2008; Douglas et al., 2010; Macurek et al., 2010)
	H2AXY142	WSTF	EYA1	NHEJ, HR	(Xiao et al., 2009; Cook et al., 2009)
	H4Y51	TIE2	-	NHEJ	(Hossain et al., 2016)

	H4S1	Casein kinase 2	-	NHEJ, HR	(Cheung et al., 2005; Clouaire et al., 2018)
	H3S10	Aurora-B	-	-	(Tjeertes et al., 2009)
	H4T80	Cla4	-	-	(Millan-Zambrano et al., 2018)
	H3T45	Akt	-	-	(Lee et al., 2015)
	H2BS14	MST1	-		(Fernandez-Capetillo et al., 2004)
Ubiquitination	H1	RNF8	-	-	(Thorslund et al., 2015)
	H2AK13/15	RNF168	OTUB1, USP3, USP11, USP44, USP51, USP26, USP37, A20, Dub3	NHEJ	(Fradet-Turcotte et al., 2013; Mailand et al., 2007; Kolas et al., 2007; Mattioli et al., 2012; Nakada et al., 2010; Sharma et al., 2014; Mosbech et al., 2013; Wang et al., 2016; Typas et al., 2015; Delgado-Díaz et al., 2014; Yu et al., 2016; Horn et al., 2019)
	H2AK118/119	RING1B, FBXL10-RNF68-RNF2	USP16, BAP1	NHEJ	(Shanbhag et al., 2010; Rona et al., 2018; Daou et al., 2015)
	H2AXK118/ K119	RING1B/BMI1	-	NHEJ	(Pan et al., 2011; Wu et al., 2011a)
	H2AK127/129	BRCA1/BARD1	BAP1/ASXL, USP48	HR	(Kalb et al., 2014; Densham et al., 2016; Uckelmann et al., 2018)
	H2AZ	RNF168	-	-	(O'Connor et al., 2015)
	H2BK120	RNF20/40, UBR7	SAGA	HR	(Henry et al., 2003; Nakamura et al., 2011; Moyal

					et al., 2011; Ramachandran et al., 2016; Dasgupta et al., 2022)
	H4K91	BBAP	-		(Yan et al., 2009, 2013)
	H2AZK126/K133	-	-		(Kalocsay et al., 2009)
Acetylation	H2AK15	TIP60	-	HR	(Jacquet et al., 2016)
	H2AXK36	CBP/p300	-	-	(Jiang et al., 2010)
	H2BK120	SAGA, PCAF	-	HR	(Clouaire et al., 2018; Kim et al., 2019)
	H3K9	GCN5, PCAF	SIRT6, HDAC3	-	(Tjeertes et al., 2009)
	H3K14	GCN5, PCAF	HDAC3	-	(Duan and Smerdon, 2014)
	H3K18	GCN5, p300, CBP	SIRT7	NHEJ	(Vazquez et al., 2016)
	H3K56	GCN5, CBP/p300	HDAC1, HDAC2, SIRT1, SIRT2, SIRT6	HR	(Masumoto et al., 2005; Tjeertes et al., 2009; Das et al., 2009; Miller et al., 2010; Toiber et al., 2013)
	H4K16	TIP60, MOF, GCN5, p300	HDAC1, HDAC2, SIRT1	HR	(Tang et al., 2013; Gong et al., 2015)
Methylation	H2AR3	PRMT7	-	-	(Karkhanis et al., 2012)
	H2AXK134	SUV39H2	-	-	(Sone et al., 2014)
	H3K4	Set1p	LSD1, KDM5A, KDM5B	NHEJ	(Faucher and Wellinger, 2010; Mosammamparas t et al., 2013; Li et al., 2014; Gong et al., 2017)
	H3K9	KMT1A, DMT1B, SETDB1, PRDM2, SUV39h1	KDM4B, KDM4D	HR	(Sun et al., 2009; Young et al., 2013; Khoury-Haddad et al., 2014;

					Ayrapetov et al., 2014; Khurana et al., 2014; Alagoz et al., 2015)
	H3K27	EZH2	-	-	(O'Hagan et al., 2008; Campbell et al., 2013)
	H3K36	SETD2, SETMAR	KDM2A, KDM4A	NHEJ, HR	(Aymard et al., 2014; Pfister et al., 2014; Carvalho et al., 2014; Fnu et al., 2011; Pai et al., 2014; Amendola et al., 2017)
	H3K79	DOT1L	-	NHEJ, HR	(Huyen et al., 2004; Wakeman et al., 2012)
	H4R3	PRMT7	-	-	(Karkhanis et al., 2012)
	H4K20	KMT5A, KMT5B, KMT5C, SET8	-	NHEJ, HR	(Botuyan et al., 2006; Pei et al., 2011; Acs et al., 2011)

Table 1.2. Ubiquitin-binding domains.

UBD family	UBD	Representative protein	Ub epitope	Reference
α helix	UIM	RAP80	I44	(Yan et al., 2007)
	MIU	RNF168	I44	(Pinato et al., 2009; Doil et al., 2009)
	UMI	RNF168	I44	(Pinato et al., 2011)
	UBA	hHR23a	I44	(Wang et al., 2003)
	CUE	FANCD2	I44	(Rego et al., 2012)
	GAT	GGA3, TOM1	I44	(Prag et al., 2007)
	VHS	STAM, GGA3	-	(Wang et al., 2010)

	NUB	NEMO, ABIN1-3	I44	(Ea et al., 2006)
Zinc finger	NZF	NPL4, VPS36	I44	(Meyer et al., 2002; Sato et al., 2011; Ohkuni et al., 2022)
	ZnF_UBP (PAZ)	USP20, HDAC6	71LRLRGG7, L8, I36	(Reyes-Turcu et al., 2006; Yang et al., 2019; Balmik et al., 2021)
	ZnF_A20	ZNF216	D58	(Huang et al., 2004)
	UBZ	RAD18, FAAP20	I44	(Rizzo et al., 2014; Yang et al., 2010; Toma et al., 2015)
Ubc-like	UEV	BRE, FANCL2, MMS2	I44, Q62	(Andersen et al., 2005; Hodson et al., 2011; Rabl et al., 2019)
	UBC	UBE2O, BRUCE	I44	(Ge et al., 2015; Huang et al., 2022)
PH domain	GLUE	VPS36	I44	(Slagsvold et al., 2005)
	PRU	RPN13	I44 and others	(Husnjak et al., 2008)
Others	UBM	Pol ι , REV1	-	(Bomar et al., 2010; Niu et al., 2019)
	SH3	BCR/ABL	I44	(Slupianek et al., 2009)
	PFU	UFD3	-	(Fu et al., 2009)

Local chromatin changes: damage signaling

The first ubiquitin modifier identified in the DNA damage response was the DNA repair gene RAD6, an E2 enzyme in *S. cerevisiae* (Jentsch et al., 1987). It was also in the DDR where the first evidence of a non-proteolytic function of K63-linked ubiquitination was observed (Spence et al., 1995). Since then evidence has accumulated confirming the essential role of the ubiquitination system in the cellular response to DNA damage.

The first DDR-associated ubiquitination event takes place within minutes after DNA break induction, and it is the monoubiquitination of histone H2AX at lysine 119/120 by the canonical Polycomb Repressive Complex 1 (PRC1) complex including BMI1-RING1 proteins (Pan et al., 2011; Wu et al., 2011a). Additionally, H2A gets ubiquitinated at the same residues and it is believed that this modification induces transcriptional repression, in turn facilitating repair

(Ismail et al., 2010; Chou et al., 2010). H2AXK119/120ub modification happens in a DSB-dependent manner and possibly even earlier than the γ H2AX formation. It was reported that the H2AXK119/120ub maintains the γ H2AX foci stability by directly recruiting ATM to breaks, thus playing a significant role in initiating DNA damage signaling. Alternatively, ATM can also be activated in the absence of H2AX ubiquitination by the MRN complex recognizing the breaks (Uziel et al., 2003). Since γ H2AX is the apical modification event in the reaction cascade of damage response, H2AXK119/120 monoubiquitination subsequently indirectly affects the downstream repair factors. The phosphorylated H2AX is recognized by MDC1 which, when phosphorylated by ATM, tethers both L3MBTL2 and RNF8 to the vicinity of the DNA lesion (Stucki et al., 2005; Nowsheen et al., 2018). At the sites of DSB, the E3 ligase RNF8 performs various types of ubiquitination on different targets: firstly, it polyubiquitinates L3MBTL2 via K63-linkage formation, and secondly, histone H2A (Mailand et al., 2007; Stewart et al., 2009; Panier et al., 2012). RNF8-mediated ubiquitination attracts another E3 ligase RNF168 whose activity, in turn, is essential for chromatin rearrangements and recruitment of 53BP1 and BRCA1 via K63- and K27-linked ubiquitination (Gatti et al., 2015). Attracted by RNF8-mediated ubiquitination, RNF168 primes monoubiquitination of H2A at lysine 13 and 15 and with the help of RNF8 builds K63-linked chains (Doil et al., 2009; Mattioli et al., 2012). RNF168 binds modified H2A itself and further accumulates at the DSBs, thereby spreading the ubiquitination. Interestingly, RNF168 activity is mediated not only by recognizing upstream ubiquitination but also by binding an acidic patch on the nucleosome (Mattioli et al., 2014; Leung et al., 2014). This fact once again confirms how precisely and multitiered the ubiquitination is regulated to ensure the specificity of the signal.

A recent finding revealed another functional layer in the RNF8/RNF168 cascade. It was reported that RNF8 E3 ligase and UBC13 E2 conjugating enzyme mediate the K63-linked ubiquitination of H1 linker histones and, thus, provide a binding platform for RNF168 (Thorslund et al., 2015). This step is required for the further accumulation of ubiquitination at sites of DSBs. The RNF8/RNF168-mediated ubiquitination initiates the recruitment of other ubiquitin modifiers to the vicinity of DNA damage, e.g., HERC2, RAD18, BRCA1, and RNF169 (Huang et al., 2009; Bekker-Jensen et al., 2010; Kraiss et al., 2021).

Ubiquitination takes the form of a highly regulated dynamic network with multiple interconnected levels of regulation. One layer is the removal of Ub modifications by DUBs. The ubiquitination of H2A at lysine 13/15 is erased by USP51 and USP3 enzymes (Sharma et al., 2014; Wang et al., 2016; Nicassio et al., 2007; Lancini et al., 2014). Other Ub marks catalyzed by the RNF8/RNF168 tandem are removed by USP11 and USP44 DUBs (Mosbech et al., 2013; Yu et al., 2016). Another way to regulate the ubiquitination at DSBs is by controlling the protein levels of E3 ligases. So TRIP12 and UBR5 ubiquitin modifiers negatively control the RNF168 levels by ubiquitin-mediated degradation and, therefore, restrain ubiquitination spreading around damaged chromatin (Gudjonsson et al., 2012), while the RNF8 turnover was reported to be maintained by the p97/VCP/Ataxin complex in a proteasome-dependent manner (Singh et al., 2019). Remarkably, the negative regulation of ubiquitination at DSBs can be achieved not only by active removal of the mark or its writers but by changing the message of the signal as well. Accumulation of the K48- and K6-linked chains at the lesion targets proteins to proteasomal degradation, thus controlling the subsequent recruitment of repair factors (Meerang et al., 2011; Acs et al., 2011; Ali et al., 2018). Finally, there is evidence that there might be a non-catalytic competition present at the damage sites. The paralog of RNF168, RNF169 competes for RNF168-

generated ubiquitination products with other proteins and, by that, it affects RNF8/RNF168 kinetics and removes 53BP1 from damaged chromatin (Chen et al., 2012; Poulsen et al., 2012; Kitevski-LeBlanc et al., 2017; An et al., 2018).

The RNF8/RNF168 is one of the multiple ubiquitination axes, which take place in DDR. The monoubiquitination of histone H2B at lysine 120 mediated by the RNF20/RNF40 E3 ligases happens in response to DNA damage. The modified H2BK120 attracts the chromatin remodeler SMARCA5 thereby promoting chromatin relaxation and facilitating the recruitment of repair factors (Moyal et al., 2011; Nakamura et al., 2011; So et al., 2019). The removal of the H2BK120ub mark from the chromatin by USP22 and the SAGA complex was reported to regulate the early stage of damage response, however, a lot about this axis is still to be identified.

There is another ubiquitination axis identified that promotes RAP80/BRCA1-A, RAD18, and 53BP1 recruitment to DSBs. Remarkably, it is based on the crosstalk between K63- and K11-polyubiquitin signaling mediated by one reader and eraser protein, Cezanne (Wu et al., 2019). Downstream of RNF8/RNF168, the DUB Cezanne in complex with Cezanne2 binds to K63-linked ubiquitin chains at the sites of damage and removes K11-linked ubiquitination from mixed polyUb chains as well. As the RAP80/BRCA1-A are not able to bind mixed K63-/K11-polyubiquitin chains, the erasure of K11 facilitates its binding.

There are other ubiquitination cascades at the sites of the DSBs but many of them are largely understudied. Not much is known about histones H3 and H4 ubiquitination in the DDR. The CUL4-DDB1-ROC1 complex was shown to ubiquitinate mammalian H3 and H4 histones *in vivo* and *in vitro* in response to UV irradiation (Wang et al., 2006). The homolog of this complex in yeast, however, appeared as a hit in a genetic screen for players of homologous recombination (Moss et al., 2010). Interestingly, the ubiquitination targets of this E3 ligase complex in two different DDR pathways are different as well: while in the nucleotide excision repair (NER) pathway the histones get ubiquitinated, in response to DSBs the CUL4-DDB1-ROC1 complex ubiquitinates the Spd1 protein. This shows that one ubiquitin writer can modify histone and non-histone targets and, therefore, serve various functions in different repair pathways depending on the stimulus.

Another E3 ligase was reported to ubiquitinate histone H4 in response to the DNA damage. The BBAP monoubiquitinates H4K91 and protects cells exposed to hydroxyurea and doxorubicin (Yan et al., 2009). Although the levels of γ H2AX and MDC1 were not affected in the BBAP knockdown cells, the lack of the H4K91ub mark significantly delayed 53BP1 recruitment to the DSBs. Subsequent investigation of the chromatin marks H4K20me2 and H2AK15 necessary for 53BP1 to bind damaged chromatin showed that their levels were decreased upon the BBAP knockdown. Based on these data, the authors suggested that the H4K91ub is somehow required before the H4K20me1/2 and other PTMs taking place at the damage sites, however, the exact mechanism is unknown.

Local chromatin changes: repair pathway choice

Ubiquitination is a fundamental part of DNA damage signaling. DSB repair pathway choice is also modulated by various ubiquitin modifiers. As mentioned above, there are two main DSB repair pathways, NHEJ and HR. The principal difference is reflected in the fidelity of repair, whether or not DSB ends are resected, that is 5' to 3' degradation of one strand at each side of the break. The NHEJ, or mammalian canonical NHEJ (cNHEJ), is a very fast repair pathway that employs end

ligation with minimum resection and sequence homology. In contrast, the multi-step HR is driven by homology search and broken ends resection, where single-strand DNA uses an intact copy of the damaged locus as a template for repair and, therefore, requires significant homology between sequences. As a result, this difference leads to the concept of HR being the pathway that provides the most accurate repair of DSB, while NHEJ might serve as a source of point mutations and small deletions.

The correct choice of repair pathway at every DSB is of utmost importance for cell survival. Both pathways co-exist in a cell at the same time and partially compete for the DSBs (Beucher et al., 2009). Multiple factors affect the repair pathway decision in a spatio-temporal manner. One of the approaches suggested structuring our knowledge about all these factors and their coordination with each other in a way we could predict the pathway choice in a so-called “decision tree” (Scully et al., 2019). The first factor that affects the pathway choice is open DNA ends. Depending on the source of damage and initial chromatin state, the composition of the break may significantly vary, which in turn affects the binding affinity of damage sensor proteins, e.g. Ku70/80 shows weak binding affinity to long ssDNA (Mimori and Hardin, 1986). The Ku70/80 binding to the break initiates NHEJ, while the displacement of the Ku70/80 heterodimer from the broken DNA ends is a necessary step to initiate resection and turn the repair in the direction of HR (Langerak et al., 2011). The Ku70/80 removal from the ends can be achieved by ubiquitin-mediated degradation via K48-linked chains added to Ku70 (Postow et al., 2008; Ismail et al., 2015). Another important factor in the pathway choice is the cell cycle stage (Hustedt and Durocher, 2016). The NHEJ is functional throughout the cell cycle while the HR is a preferable choice in the S-G2 stages when a sister chromatid is available for template-guided repair, therefore the cell cycle stage is directly related to the resection (Mao et al., 2008). The cell cycle status can be directly transmitted from the cell cycle-dependent kinases (CDK) to the repair machinery, e.g. through phosphorylation of resection players CtIP and EXO1 (Tomimatsu et al., 2014; Anand et al., 2016). In G1 cells instead, CtIP gets ubiquitinated and targeted for degradation by the anaphase-promoting complex APC/C thus blocking resection (Lafranchi et al., 2014). Recently another way for the APC/C complex to regulate pathway choice in a ubiquitin-dependent manner was identified. The authors showed that in G1 cells the BRCA1 recruitment to DSB is obstructed due to the USP1-mediated removal of K63-linked polyubiquitin chains from histones. In contrast, in the S-G2 phases, USP1 is ubiquitinated by the APC/C complex and degraded. This process requires Chk1 activation as well (Ha et al., 2017). Aside from USP1, there were more DUB enzymes identified lately that modulate pathway choice by facilitating retention of resection proteins CtIP and EXO1 at the sites of damage, namely USP4 and UCHL5 (Liu et al., 2015; Wijnhoven et al., 2015).

Another ubiquitin modifier that affects repair pathway choice is the E3 ligase RNF138 (Figure 1.4). Interestingly, RNF138 promotes HR by ubiquitination of two substrates. First, RNF138 ubiquitinates CtIP and causes its retention at DSBs, second, RNF138 ubiquitinates the Ku80 subunit of the Ku70/80 heterodimer which results in Ku70/80 displacement (Ismail et al., 2015; Schmidt et al., 2015). The ubiquitination of Ku80 happens in the S phase only and, thus, there must be an additional cell cycle-dependent regulation mechanism.

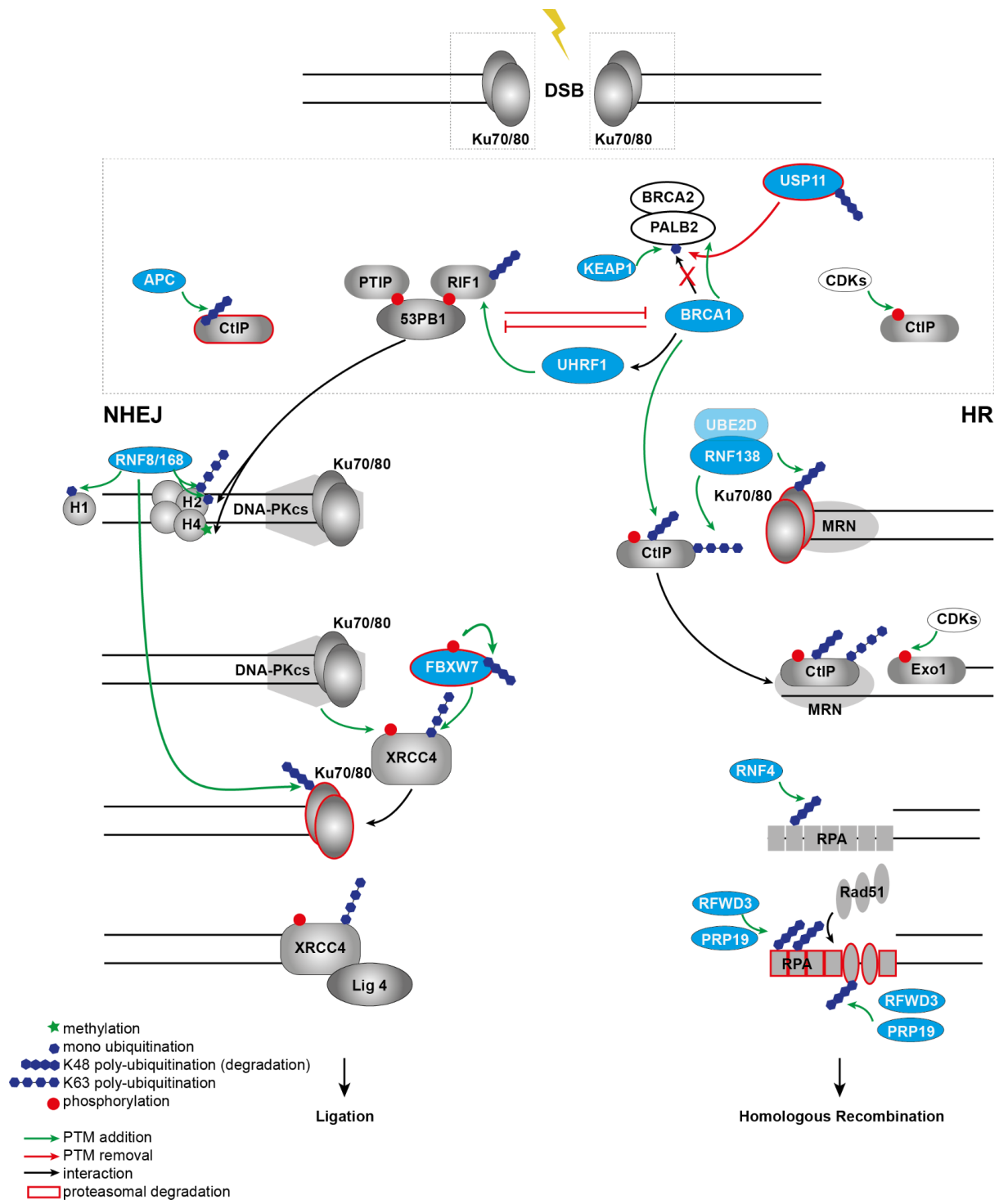


Figure 1.4. Ubiquitination in DSB repair pathway choice. The DSB is rapidly recognized by the Ku70/80 heterodimer. The choice between NHEJ and HR at the DSB is controlled by the competition between 53BP1 and BRCA1. In an NHEJ-permissive environment, 53BP1 builds a complex via ATM phosphorylation-dependent interactions with its binding partners RIF1 and PTIP. The 53BP1-PTIP-RIF1 complex prevents recruitment of BRCA1 to the break and, therefore, antagonizes HR. The E3 ubiquitin ligase KEAP1 ubiquitinates PALB2 at the BRCA1 binding site and prevents the assembling of the BRCA1-BRCA2-PALB2 complex, thus, promoting NHEJ. This process is balanced by the DUB USP11 and controlled by the cell cycle. BRCA1 antagonizes NHEJ by impairing the retention of RIF1 at DSB sites in a CtIP- or UHRF1-dependent manner. Ubiquitin-dependent degradation of CtIP by the APC/C in NHEJ prevents the resection

process, in contrast to HR, where CtIP is not degraded but phosphorylated by the CDKs. The RNF8-RNF168-mediated ubiquitination on chromatin provides a binding platform for both 53BP1 and BRCA1. Later RNF8 also ubiquitinates Ku70/80 to facilitate its proteasomal degradation and removal from the broken ends. In the HR-permissive environment, the E3 ubiquitin ligase RNF138 ubiquitinates Ku to remove it from DSB, allowing end-resection factors to gain access to the deprotected ends. RNF138 also ubiquitinates CtIP, enhancing its retention on damaged chromatin. At the later steps of NHEJ, the ligation of broken ends is promoted by FBXW7 which recognizes phosphorylated XRRC4 and subsequently ubiquitinates it. At the later steps of HR, RPA SUMOylation-guided ubiquitination by RNF4 promotes RPA turnover and RAD51 recruitment. Multi-site ubiquitination of RPA by the ubiquitin ligases RFW3 and PRP19 also facilitates HR.

The RNF138-mediated dual ubiquitination of two different targets in one process is an important example of the versatility of the ubiquitin-dependent network in DDR. Another example is when one target can be ubiquitinated by multiple different writers, e.g. the Ku70/80 can be removed from DSB ends by various ubiquitin E3 ligases. The RNF8 and SCF-FBXL12 ligases promote ubiquitination and subsequent removal of Ku70/80 as well (Feng and Chen, 2012; Postow and Funabiki, 2013).

At the sites of DSBs, 53BP1 and BRCA1 proteins antagonize each other in repair pathway choice. It was shown that both of them are recruited to the break via the RNF8/RNF168 ubiquitination cascade. We discussed earlier that 53BP1 uses bivalent recognition of both RNF8/RNF168-mediated H2AK15ub ubiquitination and H4K20me2 methylation to bind to damaged chromatin. In undamaged cells, the methylation mark is hidden from 53BP1 interaction by KDM4A (JMJD2A) and L3MBTL1, but at DSB sites both of them are targeted to proteasomal degradation (Mallette et al., 2012; Acs et al., 2011; Fradet-Turcotte et al., 2013). Once bound to chromatin in G1, 53BP1 promotes NHEJ through the recruitment of its interaction factors telomere-associated protein RIF1, PTIP, and REV7 and suppression of BRCA1 (Chapman et al., 2013; Di Virgilio et al., 2013; Wang et al., 2014a; Xu et al., 2015a; Noordermeer et al., 2018; Mirman et al., 2018).

Moreover, a new ubiquitin-dependent mechanism for suppression of HR in G1 cells was identified (Orthwein et al., 2015). The ubiquitination of PALB2, one of the interacting partners for BRCA1, by KEAP1 E3 ligase complex blocks its interaction with BRCA1 and thus HR in G1 cells (Figure 1.4). This process is opposed by the DUB USP11 that removes ubiquitin from PALB2, promoting BRCA1-PALB2-BRCA2 complex formation in S/G2 cells (Schoenfeld et al., 2004; Orthwein et al., 2015). In contrast, the HR-favoring conditions are characterized by the ubiquitination of histone H2A at K125/127/129 by BRCA1-BARD1 (Kalb et al., 2014). The H2AK125/127/129ub in response to DSBs supports SMARCAD1 recruitment which in turn facilitates the repositioning of 53BP1 to the periphery of the repair focus and promotes resection (Densham et al., 2016). Later the same group also identified the DUB for negative regulation of BRCA1-mediated resection (Uckelmann et al., 2018). The very recent studies further expanded our knowledge about the BRCA1-BARD1 repair mechanism in post-replicative chromatin (Hu et al., 2021; Becker et al., 2021). With the help of cryo-electron microscopy, the authors revealed that BRCA1-BARD1 specifically binds to nucleosomal histones, DNA, and H2AK13/K15 monoubiquitination at the DSB sites and subsequently promotes ubiquitination at the C terminus of H2A (Hu et al., 2021). Via multivalent interactions, BARD1 mediates recruitment of BRCA1 to ubiquitinated chromatin, but other ubiquitin modifiers control the BARD1 itself. Newly identified E3 ligase RNF19A ubiquitinates BARD1 to prevent its retention and homologous recombination in the NHEJ-favored chromatin context (Zhu et al., 2021). Even more

mechanisms of how BRCA1 antagonizes 53BP1 were identified. Several studies reported that BRCA1 impairs the retention of 53BP1 interacting partner RIF1 at the damaged chromatin in the S phase in either a CtIP-dependent manner (Escribano-Díaz et al., 2013) or via UHRF1 E3 ligase recruitment (Zhang et al., 2016a). Interestingly, CtIP ubiquitination by BRCA1 does not result in its degradation but instead strengthens its role in the G2/M checkpoint. BRCA1 recruitment to DSBs was shown to be mediated by deubiquitination events as well (Li et al., 2017). The DUB enzyme USP13 deubiquitinates RAP80 which facilitates its interaction with BRCA1 and subsequent recognition of the K63-ubiquitinated chromatin (histones) in the vicinity of DSBs. Ubiquitination affects DNA repair pathway choice at all steps of DDR. At the later steps like RPA-coated ssDNA formation and homology search the E3 ligases PRP19 and RFWD3 control the stability of RPA and RAD51 nucleofilaments thus promoting HR (Figure 1.4). At the sites of DNA damage, RFWD3 polyubiquitinates both RPA and RAD51 in a phosphorylation-dependent manner which requires the help of ATM and ATR (Dubois et al., 2017; Inano et al., 2017). The RFWD3 polyubiquitination stimulates VCP/p97-mediated protein degradation and subsequent removal of RPA and RAD51 from the DSB sites. In contrast to RFWD3, the E3 ligase PRP19 binds RPA not permanently but only in a DSB-dependent manner (Maréchal et al., 2014). Together these ubiquitin modifiers support late-HR progression in time and space. Despite the seeming abundance of our knowledge about ubiquitination-guided repair pathway choice, a lot of questions remain unanswered and a lot of new ubiquitin modifiers and regulation mechanisms are to be discovered in the future.

The ubiquitination events are omnipresent throughout all steps of DDR from damage recognition to successful repair of the lesion. Ubiquitination signaling orchestrates DDR not only locally at the site of broken ends but also participates in the formation of a repair domain at a larger scale.

Global chromatin changes

Chromatin domains affect DSB formation and get affected by it at multiple hierarchically organized structural levels. On higher folding levels newly built breaks initiate the formation of repair domains, microscopically visible as foci, in the case of radiation known as radiation-induced foci (IRIF). The foci can be visualized by immunofluorescent labeling of various damage signaling and repair proteins but the most important for chromatin structure study is the labeling of γ H2AX. The phosphorylation of H2AX spreads far beyond the actual break location over megabase-pair distance (Rogakou et al., 1999). It is generally believed that every single focus at the conventional microscopy level represents one break and the large spreading of phosphorylation was an intriguing fact back then. There is a lot of evidence that chromatin architecture controls the formation of the γ H2AX-decorated repair domain. The super-resolution light microscopy showed that CTCF protein, which restrains cohesin-mediated loop extrusion and therefore essentially shapes the 3D organization of large chromatin domains, is juxtaposed to γ H2AX foci. Moreover, the depletion of CTCF heavily impaired DDR signaling and repair efficiency in cells subjected to radiation (Natale et al., 2017). Other studies utilizing endonuclease AsiSI for targeted DSB generation in mammalian cells showed NIPBL-, MRN-, and ATM-mediated accumulation of cohesin at the DSB site (Arnould et al., 2021). With the help of chromosome conformation capture mapping and chromatin immunoprecipitation (ChIP) assays, the authors revealed a surprising discrepancy between γ H2AX spreading and accumulation of its kinase ATM around the break that suggests that H2AX phosphorylation is not

just a linear, ATM-dependent process. Their study highlights the one-sided loop extrusion on either side of the break as a prime mechanism of γ H2AX domain formation. Also, chromatin structural domains (TAD, topologically associated domain) are a template for the repair domain (Arnould et al., 2021). Thus, DDR utilizes a large-scale chromatin structure remodeling for genome maintenance.

Interestingly, a similar γ H2AX cohesin-dependent arrangement on chromatin was reported for other repair proteins like 53BP1, ubiquitination events, and H1 histone eviction (Clouaire et al., 2018; Ochs et al., 2019). Remarkably, ubiquitination of damaged chromatin follows γ H2AX spreading almost precisely (Clouaire et al., 2018), not being restricted to the vicinity of the break. It is evident now that various histone/non-histone ubiquitin modifications and ubiquitin modifiers contribute as well to the formation of the 3D repair-permissive domain to facilitate the repair and, in the end, to maintain chromatin topology at sites of DNA breakage.

The chromatin domains vary in their properties. Pre-existing heterochromatin allows the entrance of some macromolecules and chromatin remodelers, e.g. due to the formation of a phase-separated domain with selective permeability (Gibson et al., 2019; Wang et al., 2019). Liquid-liquid phase separation (LLPS) as a force driving and maintaining chromatin compartmentalization is promoted by the chromatin scaffold, histone modifications, and their multiple reader proteins (Snead and Gladfelter, 2019). A newly formed lesion starts a cascade of changes in the chromatin context, which leads to its reorganization at a large scale to form a 3D domain outlining a repair-prone environment. In recent years, a growing number of publications highlighted the role of phase separation in DNA damage response. All levels, initiation, spatial organization/clustering of damage, maintenance of damage domain 3D architecture, and repair are affected (Kilic et al., 2019; Singatulina et al., 2019; Pessina et al., 2019; Oshidari et al., 2020; Levone et al., 2021; Ghodke et al., 2021; Miné-Hattab et al., 2021; Frattini et al., 2021). Remarkably, PTMs, namely ubiquitination and its crosstalk play a significant role in it. For example, it was proposed that 53BP1-seeded phase separation requires interaction between 53BP1 and H4K20me₂, and 53BP1 and RNF168-mediated, DNA damage-induced H2AK15 ubiquitin marks (Kilic et al., 2019). Therefore modifiers like RNF169, TRIP12, and UBR5 that antagonize the RNF168-mediated ubiquitination spreading, indirectly control phase separation at the sites of the DSBs. Not only monoubiquitination but also K63-ubiquitin chains promote LLPS at the DSBs. A recent publication described the RAP80 protein undergoing a phase separation at the sites of the breaks, which is required for the recruitment of the BRCA1 and efficient repair (Qin et al., 2023). The phase separation required interaction between the UIM ubiquitin-binding domains of RAP80 and K63-polyubiquitin chains at the γ H2AX, and was dependent on the length of the ubiquitin chains. Interestingly, the K48-polyubiquitin chains showed no impact on the RAP80 phase separation, which confirms the multivalent and interaction-specific nature of the LLPS.

Another seeding factor for the phase separation in DDR is poly(ADP-ribosylation) (PARylation), which is mediated by PARP1 activation. It was shown before that PAR chains can synergize with various intrinsically disordered proteins, e.g. FUS, to initiate LLPS, however, a recent study described a DUB enzyme to bind PAR chains in a damage-dependent manner (Kim et al., 2021). The USP39 deubiquitinase is recruited to the DSBs by the poly(ADP-ribosylation) with the help of its tripartite RG domain, thus inducing liquid demixing and promoting NHEJ. The authors also suggested that the USP39 function is required for HR, however, it is not related to PAR or phase

separation. Additionally, the USP39 activity is an important example of PAR-ubiquitination crosstalk in the DDR.

The ubiquitination and other PTMs on histones and non-histone proteins not only change the chemical properties of the target proteins but also control the abundance of other molecules like RNA in the phase-separated domain. However, our understanding of how ubiquitination contributes to the phase separation in damaged chromatin is only starting to form, and more studies are needed to uncover this network.

It is exciting to think about how phase separation integrates with active molecular processes at the DNA damage sites. Although some repair proteins like 53BP1 are observed to initiate the phase separation, upstream γ H2AX and MDC1 accumulation do not seem to be involved in it (Kilic et al., 2019). This fact hints that the formation of the repair domain is a product of multiple different processes, and their interplay is yet to be investigated.

Chromatin responds dynamically to the damage. Upon DNA damage, mammalian and yeast chromatin domains go through decompaction and expansion, which in turn changes the mobility and accessibility of the damaged locus. It is well documented now that the mobility of damaged locus increases, reflecting exploration of the nuclear space by DSB end during “homology search” (Hauer and Gasser, 2017; Herbert et al., 2017; Miné-Hattab et al., 2017). However, undamaged loci in damaged cells were observed to elevate their mobility as well but to a lesser extent, which points out that changes in chromatin mobility are a general feature of the whole-genome response to DSBs (Chiolo et al., 2011; Miné-Hattab et al., 2017; Caridi et al., 2018; Smith et al., 2019). Moreover, the DSBs in *Drosophila* and mouse cells were observed to relocalize to subnuclear domains facilitating repair: from pericentromeric heterochromatin regions to the nuclear periphery in flies and from the core to the outer layer of chromocenters in mice (Chiolo et al., 2011; Tsouroula et al., 2016; Jakob et al., 2011). Tsouroula et al and Natale et al additionally showed that damage-induced global expansion in centromeric and pericentromeric domains was not accompanied by the removal of silent chromatin marks and was not connected to the relocalization happening in mammals (Tsouroula et al., 2016; Natale et al., 2017). This finding supported the previously stated integral function of localized recompaction in checkpoint signaling but not in repair (Burgess et al., 2014). This suggests that chromatin compaction may regulate the timing of different steps of the DDR. A recent study described HR in centromeric regions in G1 in the absence of the sister chromatid and taking advantage of centromeric transcripts forming DNA-RNA hybrids. In addition, the DUB USP11 was shown to promote the recruitment of the RAD51-BRCA1-BRCA2 complex to centromeres by interaction with the centromeric histone CENP-A and HJURP (Yilmaz et al., 2021).

The transient chromatin decompaction occurs at the sites of DSBs independently of the repair pathway. Such decompaction and accompanying increased mobility correlated to significant depletion of nucleosomes on DNA with proteolytic degradation of 30-40% of core histones in yeast (Hauer et al., 2017). A similar effect was shown when core histone reduction was achieved by deletion of genes coding for histones H3 and H4 (Liang et al., 2012). Recent work of the Gasser group further explored the chromatin remodeling effect mediated by histone depletion and revealed the paramount role of ubiquitin ligases and chromatin ubiquitination in the mobility of the damaged site in yeast (Cheblal et al., 2020; Challa et al., 2021). They showed that five ubiquitin-conjugating factors are recruited to the damage sites in a checkpoint- and INO80C-dependent manner which results in depletion of core and H1 histones up to 20%-40%, chromatin decompaction, and enhanced DNA locus mobility (Challa et al., 2021). Remarkably, a homolog

of one of them was proposed to cause chromatin decompaction in mammalian cells as well. The RNF20/40 ligases (Bre1 in yeast) promote the formation of the H2BK120ub mark in damaged cells, which facilitates chromatin relaxation and repair proteins recruitment by promoting nucleosome disassembly (Moyal et al., 2011; Nakamura et al., 2011; Zheng et al., 2018; Chernikova et al., 2010; So et al., 2019; Liu et al., 2021). Interestingly, the monoubiquitination of histone H2B itself directly impairs the compaction of higher-order chromatin structures and results in open conformation (Fierz et al., 2011). The mechanism is different from the acetylation-mediated decompaction and in contrast to it, monoubiquitination spreads over larger distances. Lastly, the H2BK120ub was shown to crosstalk with other chromatin modifications at the damage sites, namely H4K20 and H4K9 methylation, which could lead to a pleiotropic chromatin reorganization.

Speaking of chromatin mobility in DDR, we cannot ignore the clustering of DNA damage. The clustering is thought to be happening to DSBs which require the resection of broken ends or concentration of several damaged sites into the large domain to facilitate repair (Aymard et al., 2017; Schrank et al., 2018; Schrank and Gautier, 2019). It was recently identified that actin filament nucleators are the driving force for DSB clustering and are a factor in the repair (Schrank et al., 2018). Lastly, the clustering can also protect DSBs from improper repair, where one of the examples is coordination between end resection degree and amount of damage inflicted on cells.

1.3 Crosstalk between ubiquitination and other modifications in DDR

Crosstalk between various PTMs on histone and non-histone proteins lies at the basis of DNA damage signaling and repair. A single PTM affects the properties and function of its target, but only coordination of phosphorylation, acetylation, methylation, poly(ADP-ribosyl)ation, ubiquitination, and their readers ensure the spatiotemporal recruitment of repair proteins and chromatin remodeling at the sites of damage. There are several classifications of crosstalk proposed, e.g. based on how modifications are hierarchically organized in a cascade (Dantuma and van Attikum, 2016). According to it, the PTMs can be serial, when one modification sequentially promotes other modifications; parallel, when one reader containing multiple binding domains recognizes multiple independent modifications; and combinatorial, when two or more modifications are equally required for one reader to induce a signal. Above, we described some of the examples of ubiquitin-dependent regulatory cascades, but the ubiquitination crosstalk with other PTMs constitutes an integrated signaling network in DDR.

Phosphorylation and ubiquitination

Phosphorylation is among the most abundant and most studied modifications at the sites of DNA damage. Crosstalk between phosphorylation and ubiquitination is essential for the correct execution of DDR. One of the examples of this crosstalk is phosphorylation-guided proteasomal degradation with the help of phosphodegrons. Phosphodegrons are one or several residues on a target protein that can be phosphorylated by a kinase and subsequently bound by an E3 ubiquitin ligase to initiate proteasomal degradation via K48-linked ubiquitin chains (Ang and Wade Harper, 2005). At the sites of DSB, the NHEJ E3 ligase FBXW7 stability is controlled by phosphorylation and the creation of the phosphodegron signal (Figure 1.5). The extracellular

signal-regulated kinase (ERK) directly interacts with and phosphorylates FBXW7 at Thr205, which results in the degradation of FBXW7 in a PIN-1-dependent manner by an unknown E3 ligase (Ji et al., 2015). When FBXW7 is phosphorylated at Ser58 and Thr284 by kinase PLK1, it autoubiquitinates itself which also leads to its degradation (Xiao et al., 2016). Remarkably, FBXW7 can not only be a substrate for simultaneous phosphorylation and ubiquitination but also acts as the degradation-inducing E3 ligase for other substrates, e.g. p53 (Cui et al., 2020) (Figure 1.5). In response to etoposide-induced DNA damage, ATM phosphorylates p53 on Ser33 and Ser37, which facilitates the FBXW7 binding and subsequent p53 degradation. The knockdown/knockout or chemical inhibition of FBXW7 increased p53 protein half-life upon DNA damage in an MDM2-independent manner, therefore sensitizing cells to radiation and etoposide treatment. Thus, the phosphorylation and ubiquitination crosstalk is finely tuned to ensure the protection of genome stability. Importantly, the “phosphodegron” signal does not necessarily result in degradation (Figure 1.5). Phosphorylated by ATM at Ser26, FBXW7 is recruited to the sites of DSB, where it recognizes another phosphorylated protein XRCC4. Upon phosphorylation at Ser325/326 by DNA-PKcs, XRCC4 is bound and ubiquitinated by FBXW7 via K63-chains at lysine 296 (Figure 1.5). The K63-linked polyubiquitination of XRCC4 enhances its association with the Ku70/80 complex to facilitate NHEJ repair (Zhang et al., 2016b). Recently, a systematic analysis of MARKs-phosphorylated degron motifs recognized by FBXW7 identified new targets among chromatin proteins (Singh et al., 2022). The exact mechanism remains elusive, however, it provides a look at the large regulation network managed by phosphorylation and ubiquitination.

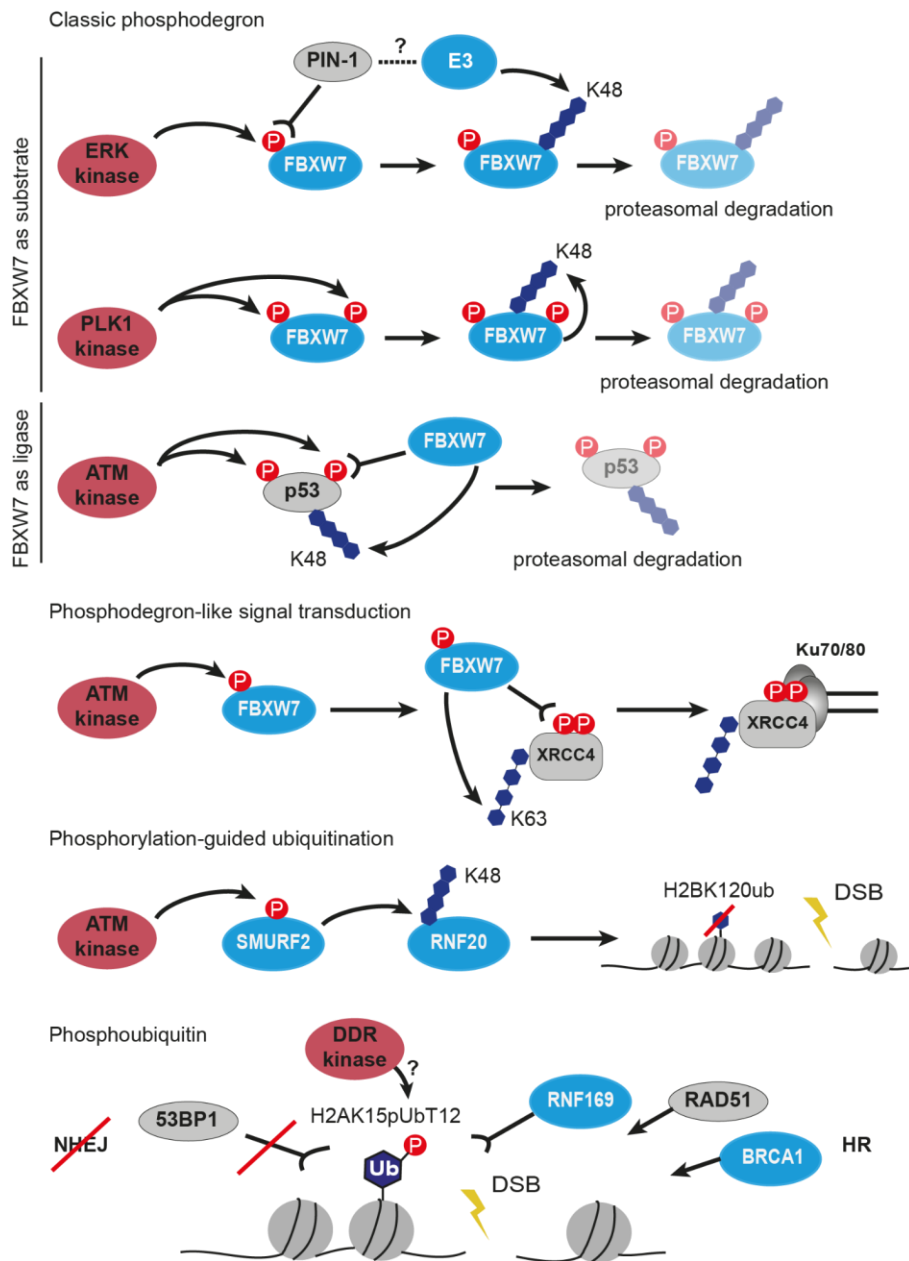


Figure 1.5. Crosstalk between phosphorylation and ubiquitination in DSB signaling and repair. The first three panels describe the classic phosphodegron situations highlighting FBXW7 as substrate to phosphorylation and as phosphorylation reading ubiquitin ligase. Next, phosphodegron-like signal transduction by FBXW7 is shown, which results in ubiquitination and stabilization of XRCC4 at Ku70/80 covered DSB. The next panel depicts phosphorylation-guided ubiquitination involving sequential signal transfer by two ubiquitin ligases SMURF2 and RNF20. The last example of the crosstalk between phosphorylation and ubiquitination is the phosphorylation of the ubiquitin moiety. The H2AK15pUbT12 is recognized by the HR factors such as RNF169, RAD51 and BRCA1, but prevents the binding of 53BP1 at DSB. P, phosphorylation, Ub, ubiquitin.

Phosphodegron cascades are possible due to the proteins containing both phosphorylation and ubiquitination sites. A comprehensive statistical analysis of the sequence and spatial distributions of PTMs revealed that among all the PTM pairs studied, phosphorylation and ubiquitination sites have a smaller distance between each other on the same proteins compared

to random distance distribution (Korkuć and Walther, 2017). Such conserved distances are ensured by protein sequences and related to the ability of ubiquitination to sterically hinder subsequent phosphorylation of the sites in its vicinity. For example, ubiquitination sites enrichment near the domain activation loop and in the glycine-rich region of kinases were reported to serve for reversible inhibition (Swaney et al., 2013). The same proteome-wide study identified 466 yeast proteins with 2100 phosphorylation sites co-occurring with 2189 ubiquitination sites using mass spectrometry-based methods. Interestingly, greater conservation of phosphorylation on ubiquitinated proteins was observed than the other way around, which highlights the existence of crosstalk directionality where phosphorylation tends to precede ubiquitination (Swaney et al., 2013).

One of the central phosphorylation events in DDR is γ H2AX formation mediated by ATM, ATR, and DNA-PKcs. Above we have already discussed in detail the γ H2AX-dependent chromatin-associated RNF8/RNF168 ubiquitination axis (Kolas et al., 2007; Doil et al., 2009). Yet ATM phosphorylates various substrates in various damage response contexts and subsequently promotes various multifaceted ubiquitination events. Together with the CHK2 kinase, ATM phosphorylates CABIN1 which acts as a negative regulator of p53 activity. The phosphorylated CABIN1 is recognized and targeted to the ubiquitin-dependent proteasomal degradation mediated by the CRL4DDB2 ubiquitin ligase complex, thus activating p35 in response to the genotoxic stress (Choi et al., 2013). There are more negative regulators of p53 at the damage sites, HDMX (human ortholog of Mdmx) is one of them as well. It was shown that in response to the lesion ATM phosphorylates HDMX at Ser395 and promotes its degradation by the E3 ligase HDM2 (human ortholog of Mdm2) (Pereg et al., 2005). The precise regulation of the ATM-mediated p53 activation and stabilization remains elusive due to the abundance of the phosphorylation-ubiquitination circuits. It was recently reported that the E3 ligase Mdm2 can be phosphorylated by ATM as well which leads to its autoubiquitination and subsequent degradation (Magnussen et al., 2020). More evidence is required to fill the gap in our knowledge about the organization of separate cascades and their crosstalk within the DDR network.

Apart from the p53 regulation, ATM was observed to phosphorylate Ser384 on the E3 ligase SMURF2, an interaction partner of RNF20 (Tang et al., 2020) (Figure 1.5). In turn, phosphoSMURF2 binds and ubiquitinates RNF20 promoting its proteasomal degradation. The SMURF2-mediated RNF20 ubiquitination results in a decrease of H2BK120 ubiquitination, thereby promoting chromatin compaction and protecting cells from DNA damage. However, in the absence of phosphorylation or SMURF2 knockout, the repair was shown to proceed faster than in wild type cells as measured by γ H2AX disappearance, probably, due to excessive relaxation of chromatin and facilitated recruitment of repair proteins. Despite faster DSB repair, the mouse embryonic fibroblasts with the mutant SMURF2 showed higher sensitivity to etoposide treatment which means that timely chromatin remodeling is of utmost importance for DDR (Tang et al., 2020).

Phosphoubiquitin (pUb) was shown for the first time to play a role in DNA damage signaling and repair only recently (Figure 1.5). Walser and colleagues described that the ubiquitin moiety phosphorylated at Thr12 (pUbT12) is used for the formation of a new chromatin mark H2AK15pUbT12 (Walser et al., 2020). Authors reported that the H2AK15pUbT12 levels increase in response to the radiation- and etoposide-induced DSBs and return back to the basal state after DNA repair. The H2AK15pUbT12 is differently recognized by ubiquitin readers in DDR: the phosphorylation of H2AK15 abolishes 53BP1 binding while being still bound by RNF169. Thus,

chromatin modified by pUbT12 is inaccessible to 53BP1 but permissive to the HR proteins like RNF169, RAD51, and the BRCA1/BARD1 complex, which makes the H2AK15pUbT12 an HR-specific chromatin modification. Interestingly, the pUbT12 prevents the removal of the H2AK15pUbT12 mark by DUB USP51 from chromatin which results in the retention of ubiquitination and formation of the HR-prone environment. The DDR kinase responsible for this phosphorylation on ubiquitin is unknown as well as its mechanism, although the authors revealed that it depends on preceding ubiquitination events mediated by RNF168 (Walser et al., 2020). Taken together, the phosphoubiquitin modifications represent a new type of DDR signaling.

Poly(ADP-ribos)ylation and ubiquitination

Poly(ADP-ribose) (PAR) is a PTM that consists of at least two or more ADP-ribose molecules covalently linked by glycosidic ribose–ribose bonds. Formation of the poly(ADP-ribose) chains or PARylation can occur at different amino acid residues, including aspartate, glutamate, and lysine residues, mediated by the family of the poly(ADP-ribose) polymerases (PARPs) (Leung, 2014). At the sites of DNA damage, the most abundant PARP is poly(ADP-ribose) polymerase 1 (PARP1) whose recruitment results in rapid and reversible PARylation at histone, non-histone proteins, and PARP1 itself (Tallis et al., 2014).

Poly(ADP-ribose)ylation has extensive crosstalk with other PTM types in DDR, including ubiquitination. CHFR is one of the E3 ubiquitin ligases recruited to DSBs by direct interaction between its zinc finger domain and PAR chains (Oberoi et al., 2010) (Figure 1.6A). Interestingly, CHFR shares structural similarities with RNF8, with the exception that RNF8 is recruited to lesions in a phosphorylation-dependent manner. At the sites of DSBs, CHFR ubiquitinates auto-PARylated PARP1 with the K48- and K63-linked ubiquitin chains and promotes PARP1 degradation (Liu et al., 2013). It is thought that CHFR can bind and ubiquitinate PARylated histones as well, however, direct evidence is missing. Ubiquitination of PARP1 by CHFR leads to extraction of PARP1 from chromatin and spatiotemporal restriction of PAR spreading, thus controlling the early stage of damage response in a negative feedback loop. CHFR, therefore, belongs to the early-response ubiquitin modifiers in DDR. The E3 ligase TRIP12 can recognize the PAR chains on PARP1 and promote its removal from chromatin as well (Gatti et al., 2020). Another E3 ubiquitin ligase promoting proteasomal degradation of repair proteins and PARP1 in a PAR-dependent manner is RNF146 (Kang et al., 2011) (Figure 1.6A). Interestingly, RNF146 requires PARylation not only for interaction with its targets but also for ubiquitin ligase activity (DaRosa et al., 2015). The RNF146 RING domain responsible for ubiquitination requires non-covalent binding to PAR to undergo conformational change and switch from an inactive to an active state. Therefore, PARylation serves both as an upstream signal to ubiquitination and as a physical activator of ubiquitin modifiers.

The master regulator of DNA repair BRCA1 was reported to recruit to the sites of DSBs in a PAR-dependent manner as well (Li and Yu, 2013; Li et al., 2013; Hu et al., 2014a). It requires the BRCT domain of the BRCA1 interaction partner BARD1 to bind PAR and initiate the homologous recombination pathway. This example of the poly(ADP-ribose)ylation and ubiquitination crosstalk and its importance for cell survival provided a strategy for cancer therapies.

The F-box containing ubiquitin modifiers was observed to have crosstalk with poly(ADP-ribos)ylation as well. The mammalian FBXL10-RNF68-RNF2 ubiquitin ligase complex (FRRUC) is

known as part of the non-canonical Polycomb Repressive Complex 1.1 (variant PRC1.1) which monoubiquitinates H2A histones on K119 to initiate transcriptional repression in undamaged cells (Wang et al., 2004a; Wu et al., 2013). The FRRUC complex is rapidly recruited to the sites of DNA damage in a PARP1- and TIMELESS-dependent manner, however, the exact mechanism is still unknown (Rona et al., 2018). When at the DSBs, the FRRUC complex facilitates recruitment of the canonical PRC1 complexes containing the E3 ligases RNF51 and RNF110 and mediates H2AK119 ubiquitination. The FBXL10-RNF68-RNF2 complex was shown to be required for the transcriptional repression, the H2A/H2A.Z histone exchange, and HR damage signaling. Interestingly, the depletion of FRRUC impaired the K63-linked ubiquitination by the RNF8/RNF168 axis, but not γ H2AX or MDC1 foci formation (Rona et al., 2018). Another F-box E3 ligase that binds PAR chains at double-strand breaks was already mentioned in the previous chapter. FBXW7 is a factor in the NHEJ pathway and is recruited to the sites of DSBs in the ATM-mediated manner. How exactly was not clear until it was discovered that the WD40 domain of FBXW7 binds to PARP1-produced PAR chains (Zhang et al., 2019). Thus, the rapid recruitment of FBXW7 to PAR on damaged chromatin promotes ATM-dependent phosphorylation and retention at damage sites, XRCC4 ubiquitination, and activation of NHEJ. Which PARylated targets are exactly recognized by the FBXW7 reader domain is yet to be discovered, since PAR chains occur not only on histones but on PARP1, PARP2, and repair proteins as well. It is important to mention, that due to almost immediate poly(ADP-ribos)ylation at the DSB sites, its readers are recruited rapidly too.

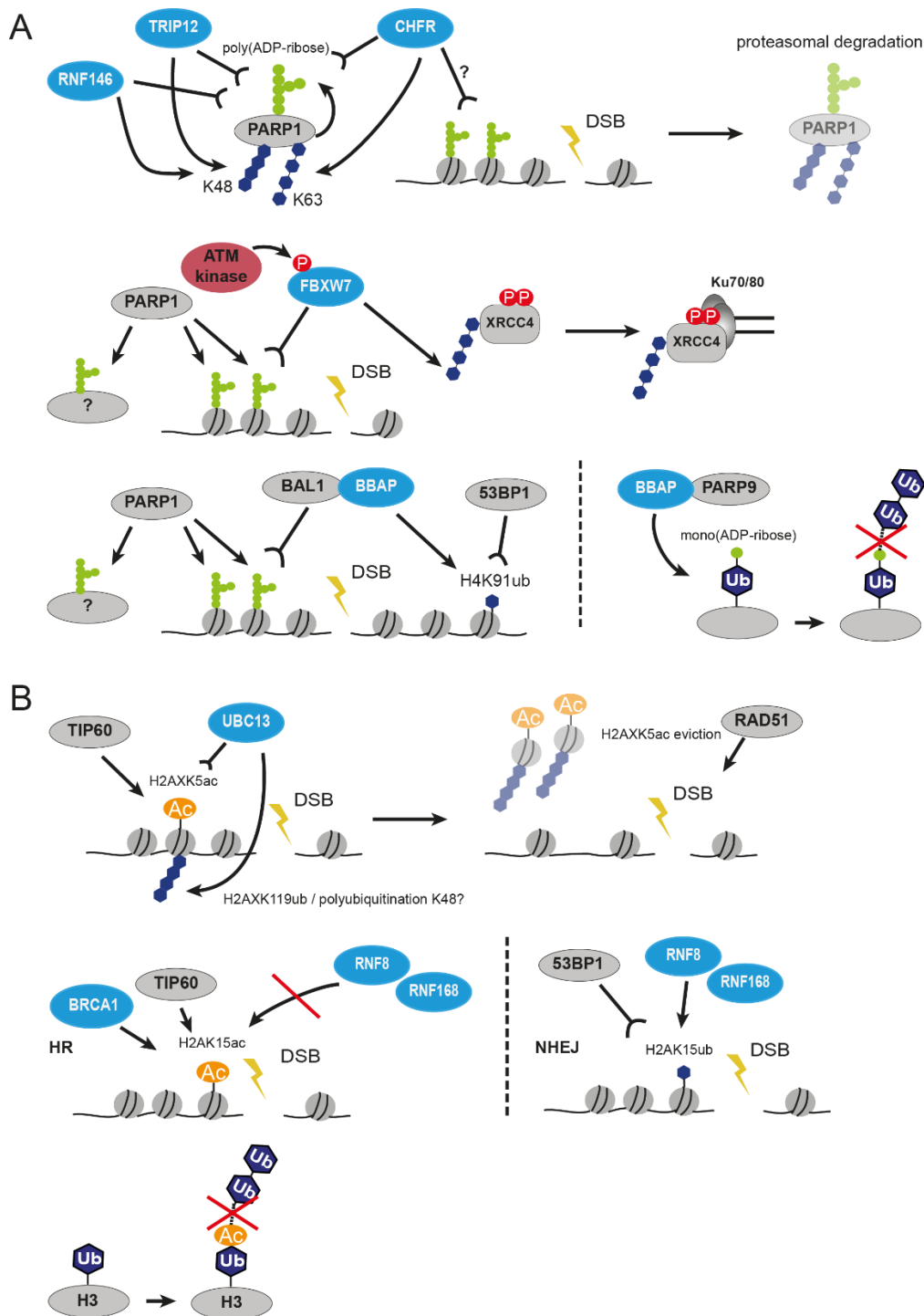


Figure 1.6. Crosstalk between PARylation and ubiquitination, as well as acetylation and ubiquitination in DSB signaling and repair. (A) Crosstalk between PARylation and ubiquitination. PARP1 auto-PARylates itself followed by recognition of PAR chains by several ubiquitin ligases such as CHFR, RNF146, TRIP12 and subsequent polyubiquitination. This results in proteasomal degradation of PARP1. PARP1-mediated modification of histones at DSBs can be recognized by FBXW7, which polyubiquitinates XRCC4 and leads to its interaction with Ku70/80. On the other hand, PARP1-mediated modification of histones can also be recognized by BAL1-BBAP which leads to ubiquitination of H4K91 creating a binding site for 53BP1. Interaction of BBAP with PARP9 leads to mono(ADP-ribosylation) of ubiquitin moiety preventing elongation of the ubiquitin chain. (B) Crosstalk between acetylation and ubiquitination. TIP60 acetylates H2AXK5 creating a recognition site for UBC13, which then polyubiquitinates H2AXK119 resulting in the eviction of

H2AX. H2AK15 can be acetylated or ubiquitinated. When acetylated by TIP60, it is recognized by BRCA1 but prevents the action of RNF8/RNF168, thus promoting HR. When ubiquitinated by RNF8/RNF168, it is recognized by 53BP1 promoting NHEJ. Acetylation of the ubiquitin moiety similarly to mono(ADP-ribosyl)ation prevents elongation of the ubiquitin chain. P, phosphorylation, Ac, acetylation, Ub, ubiquitin.

The BBAP E3 ligase (also known as DTX3L) was shown to selectively ubiquitinate histone H4 and indirectly promote 53BP1 recruitment to DSBs (Yan et al., 2009). Together with its partner, the macrodomain-containing protein BAL1, BBAP forms a complex that specifically binds PARP1-mediated PAR chains (Figure 1.6A). Interestingly, it is the BAL1 protein that recognizes PAR and BBAP is tethered to the sites of DNA damage via its interaction with BAL1 (Yan et al., 2013). Only together with BAL1 BBAP ligase is able to recruit to DSB and initiate the early ubiquitination wave, which ensures correct damage signaling and repair. The study also revealed that the PARP-BAL1-BBAP ubiquitination axis is functionally independent and nonredundant from the ATM-MDC1-RNF8 one, and they both significantly impair repair both at early and late time points (Yan et al., 2013). Strikingly, 53BP1, RAP80, and BRCA1 recruitment via PARP1-mediated BAL1-BBAP ubiquitination and via γ H2AX-dependent RNF8-induced ubiquitination were shown to be separate mechanisms as well, which hints that the recruitment of the major repair proteins is a multi-regulated process. The BBAP ligase can form a complex with other partners apart from BAL1. Another study showed that BBAP can interact with PARP9, a mono-ADP-ribosyltransferase, which was reported as being enzymatically inactive (Yang et al., 2017) (Figure 1.6A). When heterodimerized with BBAP, the BBAP-PARP9 heterodimer complex mediates reversible NAD^+ -dependent mono-ADP-ribosylation of the ubiquitin moiety on Gly76 which is used for conjugation to substrates. As a result, the ADP-ribosylated Ub can no longer be used for ubiquitination and that restricts the E3 ligase activity of BBAP. It was observed that the BBAP-PARP9 complex is recruited to sites of DNA damage. The function of BBAP in NHEJ is regulated by the NAD^+ concentration and PAR chains. This, in turn, modulates ubiquitin mono-ADP-ribosylation by PARP9. The authors suggested that under normal conditions the effect of ubiquitin mono-ADP-ribosylation is not necessary to inhibit ubiquitin-conjugation, but rather to suppress the formation of polyubiquitin chains by restricting the reaction to a single round of ubiquitin transfers (Yang et al., 2017).

BBAP E3 ligase belongs to the family of the DELTEX ubiquitin ligases (DTX1 to DTX4 and DTX3L), which contain the RING domain and the conserved Deltex C-terminal (DTC) domain. A recent comprehensive study on the interactome and ubiquitination targets of the DTX2 E3 ligase found a large share of the DDR proteins among them (Ahmed et al., 2020). The DTC domain was reported as a new PAR-binding domain involved in PAR-guided ubiquitination by DTX2. This process is organized similarly to the phosphodegrons but in this case, DTX2 ubiquitinates proteins modified by PARP1/PARP2.

As PAR chains and intrinsically disordered proteins are involved in the formation of phase-separated domains, there might be more ubiquitin modifiers to modulate this process at the sites of DNA damage.

Acetylation and ubiquitination

The acetyltransferase TIP60 has several effects on ubiquitination in DDR. The TRRAP-TIP60 complex together with the ATPase p400 acetylates histones H4, H2AX, and ATM and promotes

chromatin relaxation at DSBs (Sun et al., 2005; Murr et al., 2006; Ikura et al., 2007; Xu et al., 2010b). This facilitates the binding of RNF8/RNF168 and subsequent ubiquitination in the vicinity of breaks. Activating transcription factor 2 ATF2 and E3 ligase complex Cul3/Roc1 in turn control the stability of TIP60 and, therefore, activity of ATM (Bhoumik et al., 2008). The depletion of either component of the TRRAP-TIP60 complex impaired both acetylation and ubiquitination at chromatin and in turn, hindered the recruitment of 53BP1 and BRCA1. In response to DNA damage, TIP60 acetylates H2AX histone on K5 independently of its phosphorylation (Figure 1.6B). In turn, acetylated H2AX is required for the UBC13-mediated polyubiquitination of H2AX on K119 (Ikura et al., 2007). This acetylation-guided ubiquitination cascade promotes H2AX release from chromatin, which further relaxes the structure and facilitates RAD51 recruitment. Interestingly, the acetylation of the H2A N-terminal region in pre-existing chromatin was found to directly impair subsequent RNF20-RNF40-dependent ubiquitination of H2BK120 (Wojcik et al., 2018). This can bring novel insight into how acetylation regulates downstream ubiquitination in DDR. The competition between acetylation and ubiquitination for the same residues was shown to regulate pathway choice and chromatin structure at the damage sites. Acetylated in a TIP60-mediated manner H2AK15 blocks the ubiquitination and therefore inhibits 53BP1 recruitment promoting HR (Jacquet et al., 2016) (Figure 1.6B). Another site that can be both exclusively acetylated and ubiquitinated is H2BK120. The levels of acetylation were reported to increase in response to DSBs and the levels of ubiquitinated H2BK120 decreased (Clouaire et al., 2018). As both modifications were shown to alter the higher-order compaction state of the chromatin fiber (Fierz et al., 2011), it is clear that the acetylation-ubiquitination switch is an important part of chromatin remodeling at the sites of the breaks.

The ubiquitin modifiers can be tethered to DSBs by binding acetylated histone marks. The bromodomain-containing E3 ligase TRIM66 was observed to bind unmethylated H3R2-H3K4 and H3K56ac in a combinatorial manner at the damage sites (Chen et al., 2019). In wild type cells, H3K56ac is rapidly deacetylated by SIRT6, HDAC1, and HDAC2 at the very early stage of DDR, but the knockdown of TRIM66 causes retention of this mark and impairs repair (Tjeertes et al., 2009; Miller et al., 2010; Battu et al., 2011; Toiber et al., 2013). TRIM66 was found to localize to DSBs in an H3K56ac-dependent manner and subsequently recruit SIRT6 to induce deacetylation, however, it is unknown if this regulatory circuit involves the ubiquitination activity of TRIM66.

The acetylation factors have been shown to compete with the E3 ligases for the targets. In undamaged cells, the deacetylase HDAC6 interacts with H2A/H2AX preventing its ubiquitination by RNF168 (Qiu et al., 2023). Upon the induction of the double-strand break, RNF168 ubiquitinates HDAC6 and targets it to degradation, opening the access to the H2A/H2AX ubiquitination.

Moreover, the ubiquitin moiety can be acetylated on either K6 or K48 which does not affect the monoubiquitination but inhibits the formation of K11-, K48-, and K63-linked polyubiquitin chains (Ohtake et al., 2015). Interestingly, one of the targets getting modified with acetylated ubiquitin is histone H3 (Figure 1.6B). Another study analyzed the effect of acetylated ubiquitin on the catalytic activity of the E1 enzyme UBA1. It was observed that acetylation on all seven internal lysines can impair the conformational change required for the E1-E2 transfer and Ub-conjugation to the E2 enzyme, thus resulting in impaired target ubiquitination (Lacoursiere and Shaw, 2021). The role of acetylated ubiquitin in DDR signaling is yet to be investigated.

SUMOylation and ubiquitination

The addition of SUMO (small ubiquitin-related modifier) is also involved in DDR. There are three functionally redundant SUMO proteins encoded in mammalian cells, SUMO1, SUMO2, and SUMO3. However very similar to ubiquitination, SUMOylation uses its own enzymatic system consisting of an E1 activating enzyme (SAE1/SAE2), an E2 ligase (UBC9 also known as UBE2I), and various E3 ligases (Celen and Sahin, 2020). Ubiquitination has tight crosstalk with SUMOylation, the cascades vary in their directionality and organization. While homogeneously distributed in undamaged cells, SUMO proteins recruit to IRIF 4 hours after damage (Galanty et al., 2009). The recruitment occurs in a PIAS1- and PIAS4-dependent manner, two E3 ligases of the SUMO system. It was found that the RNF8/RNF168-mediated ubiquitination on chromatin is required for the SUMO signaling at DSBs and the SUMOylation is functionally divided into 53BP1-SUMO1 and BRCA1-SUMO2/3 pathways (Figure 1.7A). So far SUMOylation has been reported for multiple repair proteins, including MDC1, 53BP1, BRCA1, RPA, CtIP, RNF8, and HERC2 (Morris et al., 2009; Galanty et al., 2009, 2012; Luo et al., 2012; Yin et al., 2012; Danielsen et al., 2012; Locke et al., 2021). Many DDR ubiquitin modifiers require being SUMOylated for their E3 ligase activity, e.g. BRCA1/BARD1 heterodimer. Interestingly, SUMO signaling not only relies on RNF8 and K63-linked ubiquitination on chromatin but also participates in ubiquitination stability and spreading (Danielsen et al., 2012).

One of the essential SUMO cascades at the sites of DNA damage is mediated by the SUMO-targeted ubiquitin ligase (STUbL) RNF4. RNF4 is recruited to DSBs in a PIAS1-, PIAS4-dependent manner and requires its SUMO interaction motifs (Galanty et al., 2012). When bound to SUMOylated proteins like MDC1, RNF4 ubiquitinates them and targets them for proteasomal degradation thus ensuring the correct timing of DDR steps (Figure 1.7A). The lack of RNF4 results in severe DNA repair defects and constant phosphorylation of H2AX histone as a signal of persistent damage (Yin et al., 2012; Luo et al., 2012). Additionally, deSUMOylation by the deSUMOylase SENP2 provides a further pathway-specific switch. It was shown that the extraction of MDC1 after RNF4-mediated ubiquitination and simultaneous SUMOylation is blocked by the SENP2-mediated deSUMOylation and thus promotes NHEJ (Garvin et al., 2019). Aside from repair proteins removal, RNF4 was proposed to facilitate ubiquitination signaling at the DSBs. The RAP80 protein is an important mediator of BRCA1 recruitment to damaged chromatin and requires both SUMO and ubiquitin modifications (Hu et al., 2012; Guzzo et al., 2012). RNF4 is thought to produce the hybrid SUMO-ubiquitin chains that tether RAP80 and subsequently BRCA1 promoting HR (Figure 1.7A). The crucial role of SUMOylation and ubiquitination crosstalk in DNA repair pathway choice is getting more evidence with time. A recent study identified Sp1 as a target for SUMO-dependent RNF4 ubiquitination (Swift and Azizkhan-Clifford, 2022). The cascade involves DNA damage-induced phosphorylation of Sp1 by ATM and Cyclin A/CDK2 upon entry in the S phase, which is necessary for subsequent SUMOylation of Sp1 on K16 (Figure 1.7A). The serial events of phosphorylation and SUMOylation on Sp1 are recognized by RNF4 which ubiquitinates Sp1 and initiates its degradation. As Sp1 affects the localization of 53BP1, its degradation results in the removal of both Sp1 and 53BP1 from DSBs. The search for targets of RNF4 is ongoing and the number of players identified in SUMOylation-ubiquitination crosstalk is growing (Kumar et al., 2017).

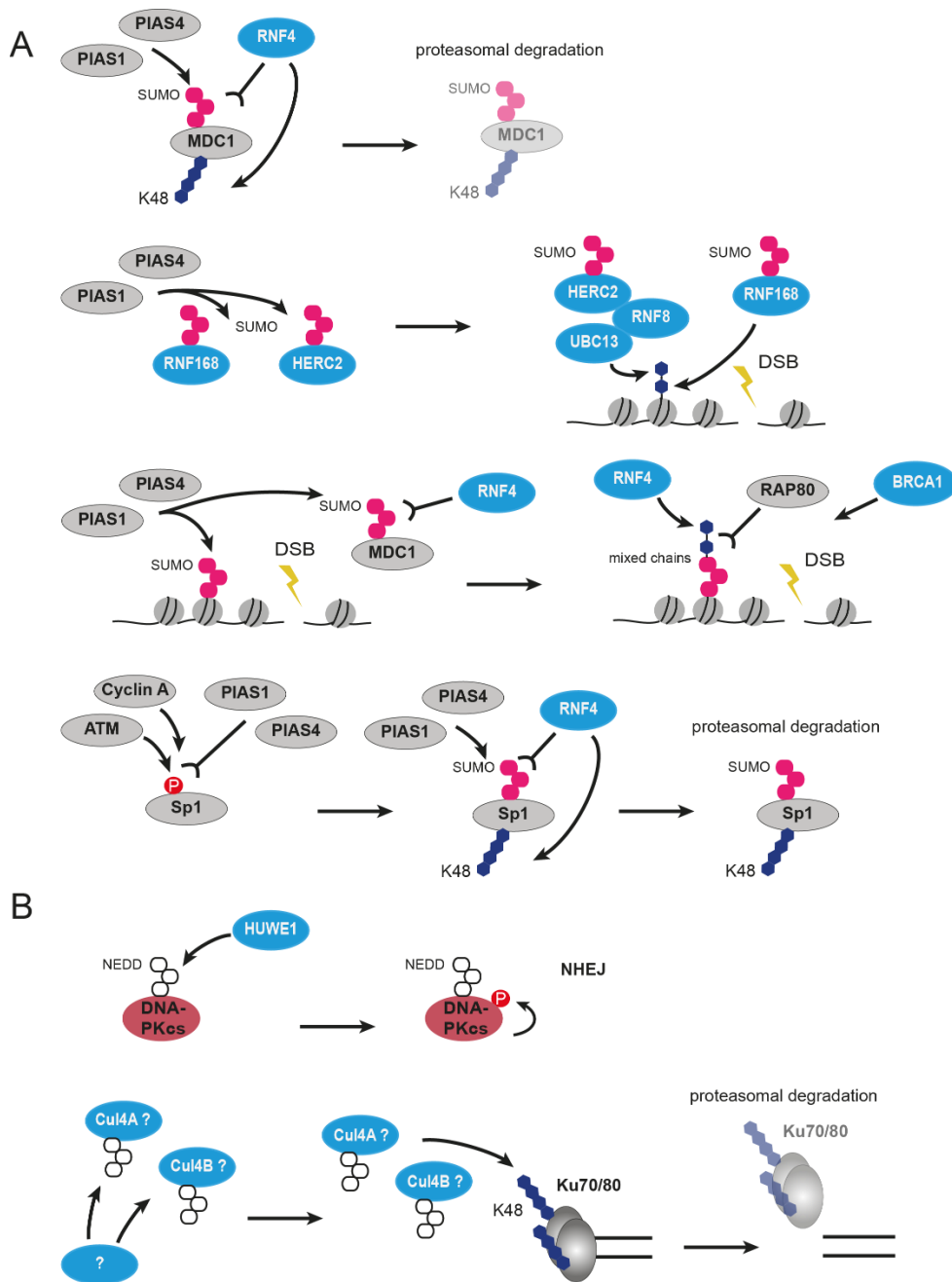


Figure 1.7. Crosstalk between SUMOylation and ubiquitination, as well as NEDDylation and ubiquitination in DSB signaling and repair. (A) Crosstalk between SUMOylation and ubiquitination. MDC1 can be SUMOylated by PIAS1 and PIAS4 and then recognized by RNF4 leading to its polyubiquitination and degradation. PIAS1 and PIAS4 can also SUMOylate RNF168 and HERC2 leading to their activation. Activated HERC2 interacts with RNF8 and UBC13 and ubiquitinates histones together with activated RNF168. PIAS1 and PIAS4-mediated SUMOylation of MDC1 and histones recruits RNF4, which builds mixed SUMO-ubiquitin chains recognized by RAP80. Phosphorylated Sp1 is recognized by PIAS1 and PIAS4 leading to its SUMOylation. SUMOylated Sp1 is recognized by RNF4 and gets polyubiquitinated and degraded. (B) Crosstalk between NEDDylation and ubiquitination. HUWE1 ubiquitin ligase can NEDDylate DNA-PKcs leading to its autophosphorylation and promoting NHEJ. NEDDylation of potentially cullins leads to polyubiquitination of Ku70/80 and their degradation. The enzyme performing NEDDylation is unknown. P, phosphorylation; SUMO, SUMOylation; NEDD8, NEDDylation; U, ubiquitin.

Neddylation and ubiquitination

NEDD8 (neural precursor cell expressed developmentally downregulated 8) is another ubiquitin-like protein that shares the highest similarity to ubiquitin, it is ~60% identical and ~80% homologous to ubiquitin (Jentsch and Pyrowolakis, 2000). However, as SUMOylation, the neddylation has its own enzymatic system in tight coordination with ubiquitination, and some ubiquitin ligases were shown to be able to perform neddylation due to the high similarity between NEDD8 and ubiquitin. The modification with NEDD8 was identified as the second most abundant ubiquitin-like modification following SUMO that accumulates at DSBs (Ma et al., 2013). At the DSBs, this NEDD8 accumulation was observed to be mediated by the E3 ubiquitin ligase RNF111 on the histone H4 N-terminus. Interestingly, H4 polyneddylation can be recognized by the MIU domain of RNF168, thus providing another regulating node for the RNF8/RNF168 ubiquitination axis (Ma et al., 2013).

Neddylation-guided ubiquitination at the sites of DNA damage regulates repair machinery and repair pathway choice as well. Ku70/80 was reported to be ubiquitinated on K195, K265, and K481 in Ku80 and K114 in Ku70 in a neddylation-dependent manner by a yet unknown factor (Brown et al., 2015) (Figure 1.7B). The ubiquitination of Ku70/80 causes its disassembly from the broken ends and therefore can promote resection-dependent repair. Consistently with the fact that cullins are the predominant targets of neddylation, the authors observed CUL4A and CUL4B as neddylation-dependent interacting partners of Ku70/80.

The dynamic regulation of neddylation and deneddylation at the DSBs was confirmed to guide repair pathway choice by controlling the length of CtIP-resected DNA (Jimeno et al., 2015). The authors reported that the RNF111/UBE2M-dependent neddylation inhibits resection and promotes NHEJ, while the deneddylation is required to initiate HR. At the sites of DNA damage, CtIP and its partner BRCA1 constitutively interact with neddylated proteins, therefore the balance between neddylation and its removal is crucial for the correct repair choice. Interestingly, the neddylation level on damaged chromatin regulates not only NHEJ/HR choice but also the fine balance between various variants of HR (Jimeno et al., 2015).

As a further example, DNA-PKcs was shown to be polyneddylated at its kinase domain by the E3 ubiquitin ligase HUWE1 (Guo et al., 2020) (Figure 1.7B). This modification is necessary for the autophosphorylation of DNA-PKcs on Ser2056 and efficient NHEJ.

1.4 Polycomb-associated ubiquitination in DNA damage signaling and repair

Polycomb group proteins (PcG) are a large group of diverse and highly conserved proteins that maintain transcriptional repression during embryonic development, stem cell differentiation and tissue homeostasis from flies to vertebrates. They were first identified in *Drosophila* as transcriptional repressors of homeotic (HOX) genes and important regulators of tissue morphogenesis (Lewis, 1978). Human orthologues were discovered in the 1990s with their direct role in oncogenesis and as of today it is well established that misregulation of polycomb protein activity causes various types of cancer (Piunti and Shilatifard, 2016). Based on the functional diversity the PcG proteins are viewed as two enzymatic complexes named Polycomb repressive complex 1 (PRC1) and Polycomb repressive complex 2 (PRC2), with sometimes adding the third complex, Polycomb Repressive DeUbiquitinase (PR-DUB) (Scheuermann et al., 2010).

All PRC1 complexes contain a ubiquitin ligase that monoubiquitinates histone H2A at the lysine 119 (H2AK119ub). It was also reported that the PRC1 complexes can perform ubiquitin-independent non-enzymatic compaction of chromatin and possibly directly interact with the transcription machinery (Francis et al., 2004; Stock et al., 2007; Eskeland et al., 2010). There are multiple proteins that serve as subunits for different variations of the PRC1 complexes; currently, six different PRC1 complexes with different compositions are classified. The core component of all known PRC1 complexes is RING1A/B ubiquitin ligases and the subcomplex classification is based on their exclusive association with one of the six PCGF proteins (PCGF1/2/3/4/5/6) (Figure 1.8A). Traditionally, the complexes with the highest similarity to the initial PRC1 complex in *Drosophila* are referred to as canonical PRC1 complexes (cPRC1). Canonical mammalian PRC1 complexes contain PCGF2 and PCGF4 (PRC1.2/4), various chromodomain proteins (CBX2/4/6/8), three Polyhomeotic Homologs (PHC1/2/3), and substoichiometric amounts of Scm homologs (SCMH1, SCML1, and SCML2). In addition to the RING1A/B ubiquitin ligases, PCGF2 (MEL18) and PCGF4 (BMI1) proteins harbor RING ubiquitin-writing domains in the canonical PRC1 complexes (Figure 1.8A). PCGF4 (BMI1) stimulates the function of RING1A/B and together they form the ubiquitin ligase that ubiquitinates histone H2A (Ben-Saadon et al., 2006; Buchwald et al., 2006). The RING1B ligase was shown to recruit to the sites of UV-induced (Bergink et al., 2006) and laser-induced DNA damage (Ginjala et al., 2011). The RING1B-mediated monoubiquitination was shown to recruit ATM to the sites of DNA damage, thus affecting the formation and stability of the γ H2AX (Wu et al., 2011a; Pan et al., 2011). For BMI1, some studies showed that it recruits to the damage sites in the biphasic mode, where the initial transient recruitment is pATM-independent but the persistent accumulation requires pATM and the γ H2AX (Ginjala et al., 2011; Ismail et al., 2010). The RING1 protein and its cofactor BMI1 are among the most studied for their function in the DDR PRC components. It was shown that the accumulation of the BMI1/RING1 at the sites of the UV laser damage depends on the activity of the poly(ADP-ribose) polymerases (PARPs) (Figure 1.8B) (Chou et al., 2010). The PAR-mediated recruitment to the damage sites was described for MEL18, a homolog of BMI1 and cofactor of RING1, for CBX4, PRC1 component (Ismail et al., 2010, 2012), and CBX8 (Oza et al., 2016). Interestingly, CBX4 sumoylates BMI1 at lysine 88 which is required for BMI1 recruitment to DNA damage (Figure 1.8B). The CBX4 and CBX8 activity appeared to be independent of the H2AX, RNF8, BMI1 or PI-3-related kinases. It is clear that there are multiple pathways controlling the BMI1 recruitment to the sites of DNA damage but it is still not completely clear how they are connected.

Importantly, a defect in monoubiquitination of H2AX caused by BMI1/RNG1 depletion profoundly enhances ionizing radiation sensitivity. In fact, the depletion of BMI1 in mouse embryonic fibroblasts led to two-fold decrease of DSB repair at 5 h after the calicheamicin treatment (Ismail et al., 2010). The homologous recombination repair defect was also observed by an I-SceI endonuclease-based *in vivo* HR assay in human embryonic kidney HEK293T cells (Ginjala et al., 2011). The nuclear localization of BMI1 was shown to be critical for the efficient processing of the stalled replication forks where it recruits RAD51 and promotes HR (Azzoni et al., 2022). Accordingly, BMI1 appeared to control end resection as well. The BMI1-mediated H2AK119ub chromatin mark is bound by the resection factor CtIP, thus allowing RPA and RAD51 accumulation at DNA damage sites (Figure 1.8B) (Fitieh et al., 2022).

A lot more evidence exists suggesting the molecular function of PRC1 components in the homologous recombination than in the non-homologous end joining. It was shown that BMI1 can

interact with 53BP1 (Abdouh et al., 2009; Ismail et al., 2010). However, the early data was obtained in the context of dysfunctional telomere-initiated NHEJ and the BMI1/RING1 depletion did not affect the repair of the DSBs caused by gamma irradiation (Bartocci et al., 2014). Importantly, the BMI1/RING1-mediated H2A monoubiquitination seem to be in part functionally redundant with the RNF8/RNF168-mediated ubiquitination axis. Both RNF8 and BMI1/RING1 monoubiquitinate the H2A and H2AX and the monoubiquitination can serve as a docking site for the polyubiquitin chains produced by RNF168. The depletion of RNF8 and depletion of BMI1 similarly abolished the recruitment of 53BP1, RAP80 and BRCA1. It was demonstrated that both RNF8/RNF168 and BMI1/RING1 bind the nucleosome acid patch to mediate H2A/H2AX ubiquitination (Leung et al., 2014). Thus, both the RNF8/RNF168 and BMI1/RING1 ubiquitination signaling contribute to the radiation resistance.

The human PRC2 complex consists of the core subunits Enhancer of Zeste Homolog 1 or 2 (EZH1/2), Suppressor of Zeste 12 protein homolog (SUZ12), Embryonic Ectoderm Development protein (EED), and Retinoblastoma protein Associated protein 46/48 (RbAp46/48) (Figure 1.8A). The main molecular function of the PRC2 complex is to mediate the formation of H3K27me3 transcriptionally repressive mark (Figure 1.8B). The active methyltransferase is formed by EZH1/2, SUZ12 and EED (Pasini et al., 2004; Cao and Zhang, 2004; Montgomery et al., 2005). The EZH1 and EZH2 proteins both possess methyltransferase activity but act in different cellular contexts. While EZH1 is present in dividing and differentiated cells, EZH2 is only active in dividing cells. The methyltransferase activity of the EZH1 was shown to be lower and EZH1-containing PRC2 complexes were described to have different chromatin compacting properties than EZH2 (Margueron et al., 2008). PRC2 exists in the form of two major subcomplexes, PRC2.1 and PRC2.2, and the accessory proteins define the subcomplex. In addition to the core components, the PRC2.1 complex consists of the three polycomb-like proteins PHF1 (polycomb-like protein 1, PCL1), MTF2 (polycomb-like protein 2) and PHF19 (polycomb-like protein 3) (Figure 1.8A). The PRC2.2 complex contains JARID2 and AEBOP accessory proteins. Remarkably, the accessory proteins were shown to guide the recruitment of distinct PRC2 subcomplexes. The polycomb-like proteins of the PRC2.1 drive its recruitment to the Polycomb target genes to catalyze the majority of H3K27me3 mark and to promote subsequent recruitment of CBX2/4-containing PRC1. Conversely, the PRC2.2 complex with JARID2 subunit appear to be essential for recruitment of CBX7-containing PRC1 and the consequent 3D chromatin interactions at Polycomb target gene sites but not H3K27me3 deposition (Glancy et al., 2023).

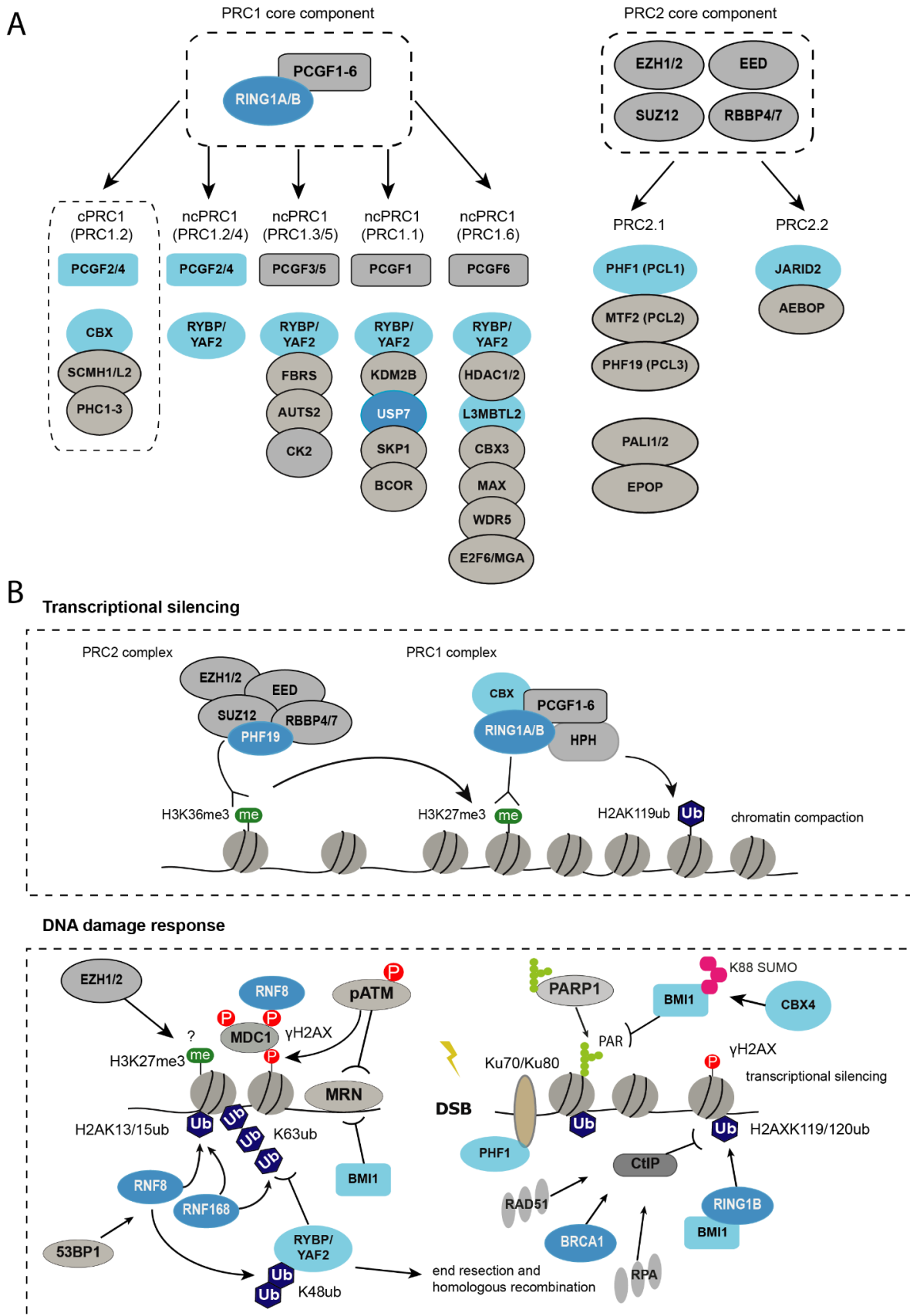


Figure 1.8. Polycomb-associated ubiquitination in the DNA damage signaling and repair. (A) Composition of PRC1 and PRC2 complexes. The proteins in the dark blue circles are the E3 ubiquitin ligases, the proteins in the light blue circles or rectangles are the ubiquitin modulators, the proteins in gray circles or rectangles

are the rest of the proteins. (B) Polycomb-associated transcriptional gene silencing and polycomb-associated DDR signaling. The proteins in the dark blue circles are the E3 ubiquitin ligases, the proteins in the light blue circles or rectangles are the ubiquitin modulators, the proteins in gray circles or rectangles are the rest of the proteins. *me* - methylation, *p* - phosphorylation, *ub* - ubiquitination, *PAR* - PARylation, *SUMO* - sumoylation.

Multiple PRC2 components were shown to recruit to UV laser damage in living cells: EZH1/2, EED, SUZ12, PHF1 (Chou et al., 2010; Hong et al., 2008; O'Hagan et al., 2008). Some studies reported the early and rapid accumulation of the H3K27me₃ at the damage sites, for example at the *I-SceI* endonuclease-generated DSBs (Figure 1.8B) (O'Hagan et al., 2008). This fact, however, appeared to be controversial as it was not supported by other studies (Campbell et al., 2013). The PRC2 components were described to recruit to the damage sites, but the mechanism of the recruitment seems to be different for different components. Thus, EZH2 recruitment was independent of H2AX and the PI-3-related kinases ATM and DNA-PKcs but required PARylation to retain. PHF1 recruitment was explained by direct interaction with the Ku70/Ku80 proteins (Figure 1.8B). If the PRC2 components are recruited to DSBs as a complex or via separate mechanisms is yet to be elucidated. Importantly, depletion of various PRC2 components led to increased X-ray and gamma radiation sensitivity.

The PRC1 and PRC2 complexes are tightly interconnected. The traditional scheme of the PRC-mediated transcriptional silencing depicts PRC1 and PRC2 as a signaling cascade, where PRC2 is targeted to active genes marked by the H3K36me₃ mark and facilitates its replacement with the H3K27me₃ (Figure 1.8B). In turn, the PRC1 complex recognizes the H3K27me₃ mark and mediates the deposition of the H2AK119ub to propagate the silencing. This scheme, however, is complicated by several facts. First of all, the recruitment of the PRC complexes to chromatin does not seem to be one directional. Both PRC2 and PRC1 recognize the H3K27me₃ mark (Hansen et al., 2008; Xu et al., 2010a). The JARID2 subunit of the PRC2.2 complex was shown to bind the H2AK119ub (Cooper et al., 2016), and the existing H2AK119ub was shown to facilitate subsequent PRC2 methyltransferase activity (Ohtomo et al., 2023). Interestingly, the H2AK119ub deposition can be stimulated and maintained independently of H3K27me₃ mark (Sijm et al., 2022). Secondly, the PRC-mediated gene silencing is complicated and varies from the loose silencing observed at bivalent chromatin domains to complete silencing of not expressed genes. Additionally, numerous different PRC-mediated silencing mechanisms involving various PRC subcomplexes were described for the silencing at different genetic loci.

The crosstalk between transcription regulation and DNA repair at the sites of DNA damage is one of the central questions in regard to the PRC complexes. In the light of growing evidence that various PRC components contribute to DNA repair and even to DNA repair pathway choice, it is important to investigate if the PRC-mediated transcriptional silencing and PRC-mediated DNA repair share the same mechanism. Once a double-strand break occurs in an actively transcribed region, the transcription is to be silenced. It was shown that pATM is one of the central regulators of the transcriptional silencing program *in cis* to DSBs (Shanbhag et al., 2010). With the help of additional proteins, pATM was described to recruit the PRC1 components BMI1/RING1 which, in turn, facilitate formation of the UBR5 damage-inducible nuclear foci (Ui et al., 2015; Sanchez et al., 2016). The PRC-mediated H2AK119ub mark was shown to initiate local chromatin compaction and at the same time establish a transcriptionally repressive zone in the vicinity of DSBs (Fitieh et al., 2022). The condensed chromatin structure at DNA damage sites appear to be

actually required for proper DNA repair when the lesions occurred near a gene. Taken together, the PRC complexes represent an example of chromatin structure connecting molecular DNA processes.

1.5 Ubiquitination, DNA damage and disease

Due to the abundance and versatility of the ubiquitin network, the dysregulation of any of its components can potentially lead to pathogenesis. Ubiquitination defects were reported to cause cancer, neurodegenerative diseases, immune pathologies, and muscle atrophy-related diseases (Popovic et al., 2014; Zheng et al., 2016). Since the first successful clinical application of proteasomal inhibitors (Hideshima et al., 2001), the search for a druggable ubiquitinome never stopped (Table 1.3).

Table 1.3. Inhibitors of ubiquitin modifiers.

Target	Name	Reference
VCP	NMS-873	(Magnaghi et al., 2013)
p97	CB-5083	(Kilgas et al., 2021)
MDM2	Nutlin	(Vassilev et al., 2004)
MDM2	APG-115	(Rasco et al., 2019a)
MDM2	CGM097	(Holzer et al., 2015)
E3 ligases	PROTACs	(Bondeson et al., 2015)
TRIM24	dTRIM24	(Gechijian et al., 2018)
Cullin-RING ligases	MLN4924	(Zhao et al., 2014; Tong et al., 2017)
KEAP1	Omaveloxolone	(Lynch et al., 2019)
Proteasome components	PS-341	(Teicher et al., 1999)
Proteasome components	Marizomib	(Potts et al., 2011)
Proteasome components	MLN9708	(Kupperman et al., 2010)
Proteasome components	NPI-0052	(Chauhan et al., 2005)
Proteasome components	CEP-18770	(Piva et al., 2008)
E3 ligases	CC-122	(Rasco et al., 2019b)
E3 ligases	CC-220	(Bjorklund et al., 2020)
SMURF1	HS-152	(Tian et al., 2019)
DUBs	VLX1570	(Wang et al., 2015)

The ubiquitination defects in DNA damage and repair are mostly related to genome instability. A well-known example is germline mutations in the BRCA1 gene, often in the RING domain region,

that predispose to breast and ovarian cancer (Maxwell and Domchek, 2012). BRCA1 recruitment is mediated by the RNF8/RNF168 ubiquitination signaling and its dysregulation leads to severe consequences. Mutations inactivating the RNF168 gene were shown to cause the RIDDLE syndrome, a rare disease characterized by radiosensitivity, immunodeficiency, dysmorphic features, pulmonary failure, and learning disabilities (Stewart et al., 2009, 2007). The RNF168 can harbor various mutations and therefore result in different symptoms. A nonsense mutation leading to the loss of both ubiquitin-binding domains MIU1 and MIU2 was described to cause ataxia, growth retardation, microcephaly, immunodeficiency, and radiosensitivity (Devgan et al., 2011). Interestingly, the disease phenotype was accompanied by persistent chronic inflammation from unrepaired DNA damage that caused the idiopathic pulmonary fibrosis. RNF168 mutated in MIU1 and 2 was not able to retain 53BP1 and BRCA1 at the sites of the damage, thus impairing the RNF8-RNF168-HERC2-BRCA1 chromatin ubiquitin ligase cascade in DDR (Devgan et al., 2011). The paramount role of the ubiquitin ligases in maintaining genome stability is highlighted in the Fanconi anemia disease. Fanconi anemia is a rare disorder that results in bone marrow failure, cancer predisposition, and genomic instability. Fanconi anemia patients suffer chromosome fragility and hypersensitivity to drugs that induce DNA interstrand crosslinks. Often patients develop solid tumors such as squamous cell carcinomas in their 20s (Pollard and Gatti, 2009). There are more than 20 genes identified in the Fanconi anemia (FA) pathway that assemble in multiple complexes in the FA-BRCA DNA-damage response network (Wang, 2007; Fang et al., 2020). Eight of them (FANCA, B, C, E, F, G, L, and M) form the so-called FA core complex together with FANCA-associated polypeptides FAAP100 and FAAP24, a nuclear E3 ubiquitin ligase complex that monoubiquitinates the FANCD2/FANCI heterodimer (FA-ID complex) in response to damage. This results in the stabilization of the FA-ID complex on DNA and subsequent interaction with BRCA2, PALB2, RAD51, and BRIP1 to promote homologous recombination (Garcia-Higuera et al., 2001; Alcón et al., 2020). Most FA cases harbor mutations that lead to the ubiquitination defect (Tan and Deans, 2017). The FA-ID ubiquitination is required for prevention of the bone marrow failure, and FA patients with FANCD2 mutations were reported to have an early bone marrow failure onset (Boisvert and Howlett, 2014; Tan et al., 2020). The depletion of FA proteins responsible for the ubiquitination sensitizes cisplatin-resistant human lung adenocarcinoma cells to cisplatin treatment (Chen et al., 2016). Mutations in the FA genes deregulate the DDR and the predisposition to the BRCA1- and BRCA2-dependent cancers (Kais et al., 2016).

Various combinations of mutations in genes coding for different ubiquitin modifiers result in various pathological phenotypes. The genetic deletion of RNF8 and CHFR sensitizes mice to ionizing radiation and results in the development of T-cell lymphoma, emphasizing the importance of the combined action of these phospho- and PAR-targeted ubiquitin ligases in the DDR (Wu et al., 2011b). The RNF8 knockout in mice causes growth retardation, sensitivity to ionizing radiation, impaired spermatogenesis, and defective immunoglobulin class-switch-recombination, similar to RNF168 and 53BP1 knockouts (Manis et al., 2004; Santos et al., 2010; Li et al., 2010). Interestingly, similar effects as for RNF8 and RNF168 knock-out were observed for RNF4 deficiency, which links SUMOylation to ubiquitination cascades in DDR (Vyas et al., 2013).

The susceptibility of the ubiquitination cascades involved in DDR is not only the source of genetic instability in normal cells but can be also used to sensitize cancer cells to ionizing radiation or chemotherapy. A well-known example is PARP inhibition, which leads to impaired homologous

recombination in cells with BRCA1 and BRCA2 mutations (Bryant et al., 2005). The p97/VCP complex mediates K48-linked ubiquitination of multiple targets at the DSBs thus promoting the repair proteins turnover and facilitating timely repair. The VCP inhibitor NMS-873 was shown to induce unfolded protein response, autophagy, and cell death (Magnaghi et al., 2013). Additionally, p97 inhibition by the specific small-molecule inhibitor CB-5083 leads to cell death after IR due to excessive MRN-mediated resection (Kilgas et al., 2021). Many tumors overexpress MDM2 (human analog HDM2), the E3 ubiquitin ligase that ubiquitinates p53 and negatively controls its levels thus promoting cell survival (Ladanyi et al., 1993). Therefore, the inhibitors of MDM2 are promising anti-cancer drugs. One of the most potent MDM2 small-molecule inhibitors identified in high-throughput screening is the Nutlin family, analogs of cis-imidazoline (Vassilev et al., 2004). Currently, two MDM2 inhibitors are in clinical trials: APG-115 is in Phase I, and CGM097 is in Phase II (Holzer et al., 2015; Rasco et al., 2019a). Inhibiting MDM2 activity, the inhibitors restore the anti-cancer activity of p53 and lead to apoptosis. The MLN4924 inhibitor blocks Cullins NEDDylation and inactivates Cullin-RING ligases which, in turn, triggers cell cycle arrest, apoptosis, senescence, and autophagy in many cancer cells (Zhao et al., 2014; Tong et al., 2017). In addition, it was reported that the accumulation of substrates of the Cullin-RING ligases (p21, p27, Wee1), triggers DNA damage, and induces cell cycle arrest at the G2/M stage (Tong et al., 2017).

The development of new small-molecule inhibitors targeting ubiquitin modifiers in the DDR pathways for the treatment of cancer and other diseases is underway and requires the expansion of our knowledge about the ubiquitination network.

2. Aims of the study

Chromatin has proven to play a major role in the regulation of DNA damage signaling and repair, with ubiquitin modifications entering the repair stage recently. Due to the immense complexity of the ubiquitin-dependent epigenetic system (over 660 genes in humans), it is likely that many more yet unknown ubiquitin modifiers play a role in DNA damage repair.

Hence, the aims of this study are:

- identify novel ubiquitin modifiers involved in chromatin response to DNA damage at early and late post-irradiation time points
- classify and select the hits based on the time point and the effect on damage signaling
- evaluate repair pathway preference for selected hits
- characterize the role of a selected hit (PHF19) in the DDR

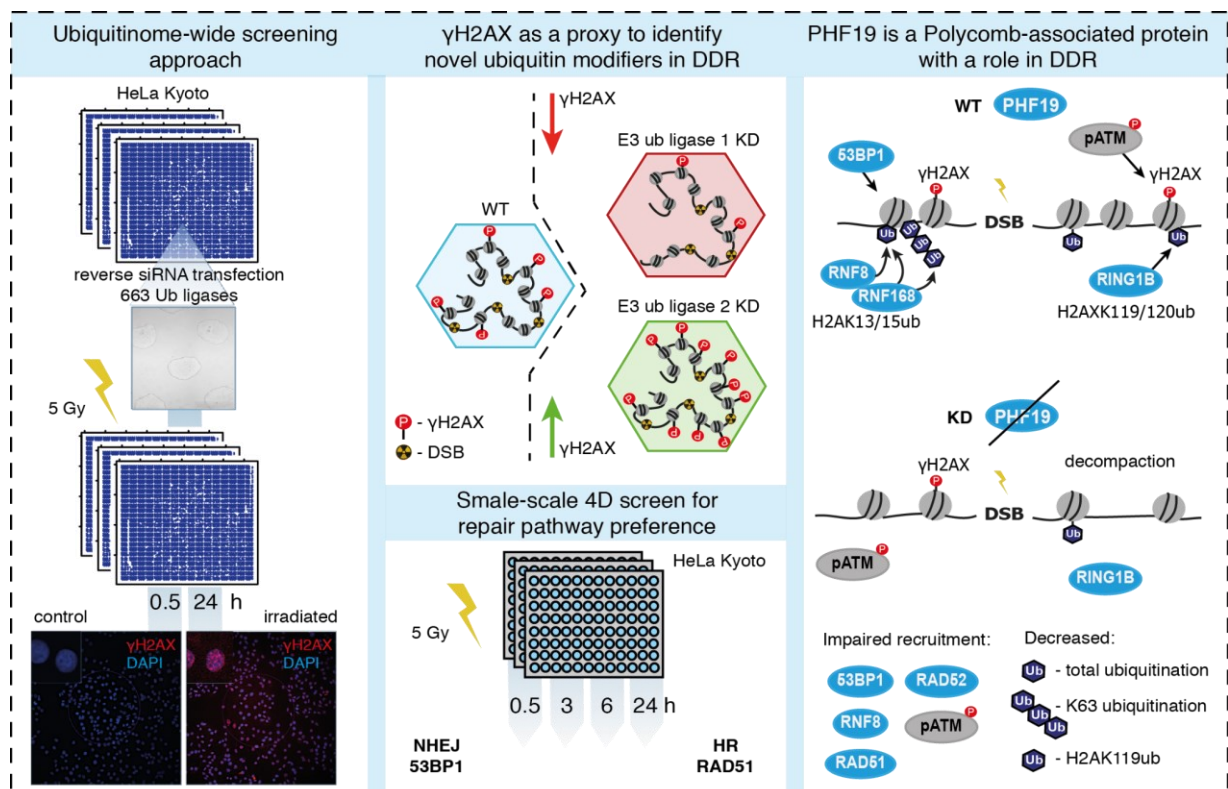


Figure 2. Aim of the study: graphical abstract. The current study consists of four parts. First part is the ubiquitinome-wide high-throughput screening for the novel ubiquitin modifiers in chromatin response to DNA damage. Second part is the selection of the hits and classification of them based on the effect the knockdown has on the γ H2AX signaling at the early and late DNA repair time points. The third part is the small-scale 4D screen for the hits that are common for the both early and late DNA repair time points; the screen was set to study the DSB repair pathway preference. The fourth and the last part aimed to characterize one of the selected hits in the chromatin response to DSB. The knockdown of the PHF19 protein leads to chromatin decompaction, γ H2AX signaling and ubiquitination downregulation, impaired recruitment of 53BP1, RNF8, pATM, RAD51 and RAD52.

Procrastination is not a virtue

3. Materials and Methods

3.1 Cell culture

HeLa Kyoto cells (Erflé et al., 2007) (a kind gift from Jan Ellenberg) were grown in Dulbecco's modified Eagle's medium (DMEM) (4.5 g L⁻¹ D-glucose, Gibco), supplemented with 10% fetal calf serum (FCS, Sigma), 2 mM L-glutamine (Sigma) and 100 U per ml penicillin and 100 µg ml⁻¹ streptomycin (Sigma) at 37° C in a humidified atmosphere of 5% CO₂.

HeLa Kyoto PHF19-GFP cells were generated using the Flp-In recombination system based on the Flp site-specific recombinase in a course of a DAAD-supported master thesis by Maruthi Kumar Pabba. The HeLa Kyoto FRTLacZ cells containing a genomically integrated FRT site as described earlier (Chagin et al., 2016), were cotransfected with pFRT-B-PHF19GFP (encoding mouse protein PHF19 tagged with GFP) and pOG44 Flp-recombinase using Neon transfection (MPK5000, Invitrogen). Four hours after transfection the cell culture medium was exchanged and cells were grown for 48 h and transfected cells were selected with 2.5 mg ml⁻¹ blasticidin (R210-01, Invitrogen). A stable monoclonal line was isolated using blasticidin selection. HeLa Kyoto GFP-PCNA cells were generated previously as described above by cotransfecting the HeLa Kyoto FRTLacZ cells with pFRT-B-GFPPCNA (encoding human protein PCNA tagged with GFP) and pOG44 Flp-recombinase (Chagin et al., 2016).

HeLa Kyoto Cherry-NZF and Cherry-2UBA cells were obtained by the Neon transfection with the plasmids bearing mCherry gene and NZF and 2UBA genes, respectively. Positively transfected cells were selected visually. Cells were seeded on the µ-Dish35 mm (81158, ibidi) in a concentration of 200000 cells per dish. Cells were incubated for 24 h after transfection as described above.

3.2 Expression constructs for live-cell DNA damage assay

The generation of expression constructs for Cherry-2UBA and Cherry-NZF was described previously (Qin et al., 2022). Briefly, the coding sequence of the UBA domain of RAD23 (amino acids 158 to 212) and the NZF domain of TAB2 (amino acids 663–693) was amplified using cDNA from mouse embryonic stem cells (mESCs) E14. To generate the constructs, a duplicate UBA and NZF coding sequences was subcloned into the pCAG-Cherry-IB vector.

Ubiquitinome-wide high-throughput screening: methods

3.3 siRNA library preparation, array mapping and layout

The library of siRNAs (Ambion, Annex: Table 7.1, attached separately due to the size) was spotted on glass bottom arrays as described previously (Starkuviene et al., 2019). Every gene was targeted by at least three different siRNAs and every siRNA variant was spotted at least three times (layout is shown in Annex: Table 7.1, Figure 7.1). Negative control siRNAs were present in 105 spots that were distributed through the arrays according to the layout, as well as a total of 2211 spots that did not receive any siRNA.

3.4 Ubiquitinome-wide high-content high-throughput screening

A high-throughput microscopy-based screening for the novel ubiquitin modifiers in chromatin response to the DNA double-strand breaks was developed to allow the quantification of the total γ H2AX and DAPI intensity per single cell.

Cervical carcinoma HeLa Kyoto cells (ATCC No. CCL-2) cells were used throughout the experiment. For the arrays, 2.5×10^6 HeLa Kyoto cells per array were plated on the replicate glass bottom arrays with already preprinted siRNA variants for the 663 genes of the annotated and potential E3 ubiquitin ligases and substrate-recognition subunits of E3 complexes. After 48 hours, all the replicate arrays except the 3 replicate arrays of the unirradiated control were irradiated with 5 Gy of gamma irradiation (90 kV, 33.7 mA, 1.643 min^{-1} , GE Isovolt Titan) to induce DNA breaks. After the exposure to IR, cells were incubated in a humidified environment, with 5% CO_2 at 37 °C as indicated. All irradiated arrays were fixed for 30 min with 3.7% formaldehyde (Sigma) in PBS at different time points after damage at 0.5 h and 24 h, as well as the unirradiated control array. The cells were washed once with PBS and permeabilized in 0.7% Triton X-100 (Neolab Migge) for 30 min in PBS at room temperature. After the permeabilization, the arrays were washed once with PBS and subjected to blocking in 1% (w/v) bovine serum albumin (BSA, Carl Roth) in PBS for 45 min at room temperature. The cells were incubated with the primary antibody against γ H2AX (mouse monoclonal antibody, clone JBW301, Millipore) diluted 1:1000 in the blocking solution for 2 h at room temperature on a shaker. Post antibody incubation, the cells were washed twice with PBS and once with 0.001% Tween 20 (Carl Roth) in PBS for 5 min each step. The signal was detected with the secondary goat anti-mouse-IgG-AlexaFluor 488 antibody (A11029, 2120125, Invitrogen, 1:1000), and the DNA was counterstained with 1 $\mu\text{g}/\text{mL}$ DAPI (Carl Roth). The secondary antibody and DAPI both were diluted in the blocking solution 1:1000 and the cells were incubated in the mix for 1.5 h at room temperature on a shaker. Following the incubation, the cells were washed with PBS and Tween 20 in PBS as described above. The stained arrays were kept in the mounting medium (30% Glycerol (Sigma) and 100 mM DABCO (Sigma) in PBS) at 4°C protected from light until imaging.

3.5 High-throughput microscopy

High-content imaging was performed using a home-made high-content screening microscope using a 20x 0.75 NA UPlanSApo (Olympus) objective lens. The arrays were aligned using prestained reference points printed together with the siRNAs and then the cells at the known location of the printed siRNA spots were recorded after contrast-based software autofocus in the DAPI channel. One image per siRNA spot was recorded using a Hamamatsu ORCA-FLASH 4.0LT camera (Hamamatsu, Hamamatsu, Shizuoka, Japan) containing approximately 200-300 cells as described in (Starkuviene et al., 2019).

3.6 Image analysis

The images acquired were analyzed with the custom-made image analysis pipeline for high-throughput data in the KNIME Analytics Platform (software version 3.4.0, KNIME AG, Switzerland). The KNIME software can be freely downloaded at the official webpage: <https://www.knime.com/downloads>. After downloading the user is required to manually update the Install/Upload preferences and add the “KNIME Community Contributions” as an available update site. The next step is to install an image processing extension, which can be found under

the name “KNIME Community Contributions - Image Processing and Analysis”. The image analysis pipeline was constructed as follows. The dataset for each of the 9 replicates was loaded and run separately. The images in the γ H2AX and DAPI channels corresponding to one siRNA spot were loaded simultaneously and analyzed in parallel. Both channels were preprocessed. Briefly, the DAPI channel was subjected to the background subtraction (rolling ring, $\sigma=400$), then to the Gaussian blur smoothing ($\sigma=2$). The DAPI channel was used for the nuclei segmentation. Nuclei were segmented based on applying the Watershed Transform (one iteration, two dimensions transform). The segmented nuclei were converted into a mask with each nucleus's DAPI intensity features and texture features recorded. The nuclei population was further thresholded by nucleus area and circularity to eliminate segmentation artifacts. The nuclei population was also thresholded by the X and Y position coordinates of the nuclei on an image, excluding the edge areas from the analysis. For each image in the DAPI channel, a variance/mean² value of the pixel intensities was calculated and recorded. The γ H2AX channel was subjected to the background subtraction as well (rolling ring, $\sigma=50$). The nuclear mask and the corresponding image in the γ H2AX channel were overlaid and the total whole-nuclear γ H2AX intensity was recorded inside the nuclear areas per cell. The γ H2AX intensity parameters (total intensity, mean intensity, minimum intensity, maximum intensity, standard deviation), DAPI intensity parameters (total intensity, mean intensity, minimal intensity, maximum intensity, standard deviation), nuclear area, circularity per nucleus and variance/mean² were exported as XLSX files for further analysis.

3.7 Image and image analysis quality control

The image quality control and image analysis quality control were performed in R Studio (<https://posit.co/download/rstudio-desktop/>). Briefly, each replicate dataset was analyzed separately. The image quality control was performed per image by controlling two parameters: variance/mean² of the DAPI pixel intensities per siRNA spot and mean of the total whole-nuclear γ H2AX intensity per siRNA spot. First, the variance/mean² values of all the spots on an array were plotted as a histogram and the spot images with the highest and the lowest values were manually controlled for imaging artifacts or autofocus failure (Bray et al., 2012; Caicedo et al., 2017). Based on the observation the lower and higher threshold for the sufficient quality imaging data was applied. The images with insufficient quality were removed from the analysis, and the images with artifacts such as debris were manually corrected by substituting the affected region with the background values in the ImageJ software (software version 2.9.0/1.53t, ImageJ, USA) (Schindelin et al., 2012) and returned to the image analysis pipeline. Next, the data was controlled for the mean of the total whole-nuclear γ H2AX intensity per siRNA spot. The mean value was plotted for each spot with its X and Y positions to control for artifacts like spatial effects and debris. The images with the highest and the lowest mean values were manually examined to confirm the sufficient quality for further analysis. The images of insufficient quality were removed from the analysis, and the images with artifacts such as debris (usually contributing to the brightest pixel intensities and wrongly segmented) were manually corrected by substituting the affected region with the background values in the ImageJ software.

The next step of the quality control was performed on a single nucleus level. The single-cell total DAPI intensity and nuclear area were visualized as a scatterplot to control for the nuclear segmentation artifacts. The data for each replicate was examined manually and the lower and higher threshold values for the nuclear area and total DAPI intensity were chosen. The wrongly

segmented nuclei manifesting as the outliers outside the thresholds were removed from the further analysis.

3.8 Data analysis

Data analysis was performed in R Studio (<https://posit.co/download/rstudio-desktop/>). Each replicate dataset was analyzed separately. Briefly, after the quality control procedures the total whole-nuclear γ H2AX intensity was normalized by total whole-nuclear DAPI intensity per nucleus to correct for the cell cycle in the cell population. The resulting value, the relative γ H2AX intensity, was used for the next analysis steps and hit identification. The relative γ H2AX intensity of all the nuclei at the siRNA spot was summarized as mean γ H2AX intensity and median γ H2AX intensity per spot. The mean γ H2AX intensity per spot was subsequently converted to the fold change (FC) and Z score values, both relating the value of each siRNA spot to the level of control siRNA spots at the same array (non-siRNA treated/mock-transfected cells). Lastly, the p-value per siRNA spot was calculated by using the Wilcoxon rank-sum significance test. Based on the p-value and fold change each siRNA on a replicate array was visualized as a Volcano plot. The standard significance thresholds were applied for the hit selection: -1.5 and 1.5 for the log fold change, and 0.05 for the p-value.

3.9 Enrichment analysis and bioinformatics

Protein network analysis and functional enrichment analysis were determined using Metascape (Zhou et al., 2019), gProfiler (ELIXIR Infrastructure) (Raudvere et al., 2019), STRING (ELIXIR Infrastructure) (Snel et al., 2000; Szklarczyk et al., 2023) on those genes whose γ H2AX signal scored with the highest significance. The analysis was performed separately on the full gene list and on each gene list (0.5 h, 24 h, unirradiated) in categories of Biological process, Molecular function, and Subcellular localization. Statistically enriched categories were then submitted to the protein-protein interaction (PPI) network identification. The PPI networks were analyzed and processed in the Cytoscape software (version 3.10.1) (Shannon et al., 2003).

Small-scale 4D screen: methods

3.10 siRNA library preparation, plate mapping and layout

3 siRNAs for each target gene were purchased from Ambion (Annex: Table 7.8). 384-well plates were coated with these siRNAs and transfection reagent as described in Erfle *et al.*, 2007. Every siRNA was present at least 3 times/plate (for a layout, see Annex: Table 7.8). All replicates of the 384-well plates were coated simultaneously to ensure reliability of the validation experiments.

3.11 Small-scale 4D screening for the repair pathway preference

For a small-scale high-content screen with the preprinted siRNAs against the 33 ubiquitin hits, the HeLa Kyoto cells were seeded in a concentration of 1500 cells per well in replicate 384-well plates (Greiner Bio-One # 781090). After 48 hours, all plates except the unirradiated control were irradiated with 5 Gy of gamma irradiation (90 kV, 33.7 mA, 1.643 min⁻¹, GE Isovolt Titan) to induce DNA breaks. Irradiated cells were allowed to recover at 37°C, 5% CO₂ for the indicated time points after damage (0.5 h, 3 h, 6 h and 24 h). All plates were fixed with 3.7% formaldehyde in PBS as previously described, washed with PBS and permeabilized. Permeabilization and blocking were performed as described before in Chapter 1. The primary antibody against γ H2AX (mouse monoclonal antibody, clone JBW301, Millipore), 53BP1 (rabbit polyclonal antibody, A300-272A,

Bethyl Laboratories Inc.) and RAD51 (rabbit polyclonal antibody, PC130, 3474043, Calbiochem) were diluted 1:1000, 1:3000 and 1:2000 in the blocking solution, respectively. The cells were incubated with the primary antibodies overnight at 4°C. The next day, the cells were washed once with 0.02% Tween 20 (Carl Roth) in PBS for 10 min and two times with PBS for 10 min. The cells then were incubated with the secondary antibodies diluted 1:800 in the blocking solution for 1 h at room temperature. The signal was detected with the donkey anti-mouse-IgG-AlexaFluor 594 (144883, Jackson ImmunoResearch Europe Ltd.) and with the donkey anti-rabbit-IgG-AlexaFluor 488 (A11034, 2380031, Invitrogen). The washing was performed as described above. Nuclei were counterstained with DAPI for 10 min and cells were kept in the mounting medium (30% Glycerol (Sigma) and 100 mM DABCO (Sigma) in PBS) at 4°C until imaging.

3.12 High-throughput microscopy

The 384-well plates were scanned using the automated confocal spinning disk microscope CREST V2 mounted on a Nikon TiE2 (Nikon, Japan) equipped with a 40x air (NA 0.95, WD 250 µm) objective. Nine positions per well were selected and at each position, one image stack was acquired in DAPI, γH2AX and 53BP1 or RAD51 channels. The DAPI channel was used for the contrast based autofocus at each imaging position. The images were recorded as z-stacks of 7 planes with a z-spacing of 1 µm using the following filters: DAPI: excitation wavelength (ex): 378/52 nm, emission wavelength (em): 432/25, dichroic (dc) 409 nm; Alexa488: ex: 474/24 nm, em: 515/25 nm, dc: 493 nm; Alexa594: ex: 578/21 nm, em: 702/100 nm, dc: 595 nm.

3.13 Image analysis

Images were analyzed with the custom-made image analysis pipeline for high-throughput data in the KNIME Analytics Platform (software version 3.4.0, KNIME AG, Switzerland). The KNIME software can be freely downloaded at the official webpage: <https://www.knime.com/downloads>. After downloading the user is required to manually update the Install/Upload preferences and add the “KNIME Community Contributions” as an available update site. The next step is to install an image processing extension, which can be found under the name “KNIME Community Contributions - Image Processing and Analysis”. The image analysis pipeline was constructed as follows. The dataset for each 10 replicate plates was loaded and run separately. Images in the DAPI, γH2AX and 53BP1 or RAD51 channels corresponding to one well on the plate were loaded simultaneously and analyzed in parallel. The image analysis had two parts: whole-nuclear intensity analysis and 3D foci analysis. For the whole-nuclear intensity analysis, three channels of the images were maximum intensity projected. The DAPI channel was used for the nuclei segmentation. Nuclei were segmented based on the global intensity threshold (method Otsu). The segmented nuclei were converted into a mask with each nucleus's DAPI intensity and texture features recorded. The nuclei population was further thresholded by nucleus area (the lower and higher thresholds were chosen manually, 4000-20000 pix) and circularity (>0.7 where 1 is the maximum and corresponds to the 100% circular object) to eliminate segmentation artifacts. The γH2AX, 53BP1 and RAD51 channels were maximum intensity projected as well. The nuclear mask and γH2AX, 53BP1 and RAD51 channels were overlaid, and the intensity parameters were recorded inside the nuclear areas. The γH2AX, 53BP1, RAD51 and DAPI intensity parameters (total whole-nuclear intensity, mean intensity, minimum intensity, maximum intensity, standard deviation), nuclear area and texture parameters per nucleus were exported as XLSX files for further analysis.

For the 3D foci analysis, only the DAPI channel was maximum intensity projected for creating a nuclear mask. The nuclear mask was created as described above. The γ H2AX, 53BP1 and RAD51 channels were subjected to foci segmentation based on a wavelet transform algorithm in 3D (Olivo-Marin, 2002). The algorithm parameters were selected individually for each type of the repair protein and maintained the same between all the replicates. The segmented foci were converted into a mask for each channel. The nuclear mask and γ H2AX, 53BP1 and RAD51 foci masks were overlaid to filter only the foci inside the nuclear areas. The γ H2AX, 53BP1 and RAD51 foci intensity parameters (total intensity, mean intensity, minimum intensity, maximum intensity, standard deviation), γ H2AX, 53BP1 and RAD51 foci diameter, size and number per nucleus, DAPI intensity parameters (total intensity, mean intensity, minimal intensity, maximum intensity, standard deviation) per nucleus were exported as XLSX files for further analysis.

3.14 Data analysis

The data analysis was performed in R Studio (<https://posit.co/download/rstudio-desktop/>). Each replicate dataset was analyzed separately. Briefly, the correct nuclei segmentation was confirmed by evaluating total whole-nuclear DAPI intensity and nuclear size per cell. The lower and higher thresholds for both parameters were set manually. The wrongly segmented cells were removed from the analysis.

For the whole-nuclear intensity analysis, the total whole-nuclear γ H2AX, 53BP1, and RAD51 intensity was normalized by total whole-nuclear DAPI intensity per nucleus to correct for the cell cycle in the cell population. The resulting value, the relative γ H2AX, 53BP1, RAD51 intensity was used for the next analysis steps and hit identification. The relative γ H2AX, 53BP1 and RAD51 intensity of all the nuclei in the well was summarized as mean and median γ H2AX, 53BP1 and RAD51 intensity per well. The mean intensity per well was subsequently converted to the fold change (FC), referring to the difference between the siRNA wells and control siRNA wells at the same array (non-siRNA treated/mock-transfected cells). The fold change for the 53BP1 and RAD51 per gene was summarized for all the time points including unirradiated control. Based on fold change value and direction (upregulation or downregulation or no effect) over the post-irradiation time scale a kinetics line plot was created for each gene. The genes were separated into groups according to the effect the knockdown had on the γ H2AX, 53BP1, and RAD51 signaling.

For the 3D foci analysis, mean and median 53BP1 and RAD51 foci parameters (sum intensity, volume, number per nucleus) were calculated per well. The fold change was calculated as described above.

3.15 Hierarchical clustering

The agglomerative hierarchical clustering was performed in R Studio to identify the phenotypes of the DDR kinetics. A matrix was built in which each gene was associated with a vector of the combined γ H2AX, 53BP1, and RAD51 foci parameters. The matrix was then used to group the genes by hierarchical clustering. For this, Euclidian distances of the variables were computed, and their linkage was determined by the average method. The result was presented as a dendrogram where the height of the fusion, provided on the vertical axis, indicates the dissimilarity between the two clusters.

PHF19 as a novel player in ubiquitin-dependent chromatin response to double-strand breaks: methods

3.16 Irradiation

A single exposure to 5 Gy X-ray was applied (90 kV, 33.7 mA, 1.643 min⁻¹, GE Isovolt Titan) to induce DNA damage and trigger DDR. After exposure to IR, cells were incubated in a humidified environment, with 5% CO₂ at 37 °C for the indicated times. Unirradiated control cells were included.

3.17 Cell cycle distribution

HeLa Kyoto cells were transfected by the Neon electroporation with 25 nM siRNA targeting human PHF19 (siPHF19) (s25161, GCCUCGUGACUUUCGAAGATT, Thermo Fisher Scientific). After 72 h, the transfected cells and the wild type control cells were irradiated with 5 Gy of gamma irradiation (90 kV, 33.7 mA, 1.643 min⁻¹, GE Isovolt Titan). The cells were harvested at 0.5 h, 1 h, 1.5 h, 2 h, 4 h and 24 h post irradiation, including unirradiated control, and fixed in 70% ice-cold ethanol in ddH₂O. Cell cycle distribution was evaluated by flow cytometry after staining with propidium iodide (PI, Biomol GbmH) staining buffer (PI 20 µg/ml, RNase A 0.2 mg/ml, Triton X-100 0.1% in 1xPBS) for 30 min at room temperature and data were analyzed using the FlowJo software (Tree Star, Inc.).

3.18 Neon transfection

All the transfections were done with the Neon electroporation system (Invitrogen). Briefly, an asynchronous population of cells was washed with PBS/EDTA, trypsinized, and collected in a 15 ml tube. The cells were pelleted at 300 x g for 5 minutes. The media was removed, cells were washed once with sterile prewarmed PBS and pelleted again. Next, the cells were resuspended in 100 µl resuspension buffer R (Invitrogen) to achieve the concentration of 10⁶ cells per mL and transferred to a 1.5 mL microcentrifuge tube. Either 5 µg of plasmid DNA or 25 nM siRNA was added to the cell mixture. The Neon TM tip was immersed into the cell mixture and the mixture was sucked into the tip, taking care to avoid bubbles. The tip was immersed in the electrolytic buffer E2, and cells were electroporated: voltage - 1005 V, width - 35, pulses - 2 for HeLa Kyoto cells. The electroporated mixture was transferred to 60 mm plates (3022021, Sarstedt) with DMEM medium without antibiotics. After transfection cells were allowed to attach overnight and the next day the medium was changed to regular DMEM with antibiotics. As a control for the transfection, the siRNA targeting GFP (#EHUEGFP, MISSION® esiRNA, GTGAGCAAGGGCGAGGAGCTGTTACCGGGTGGTGCCCATCCTGGTCGAGCTGGACGGCGAC GTAAACGGCCACAAGTTCAGCGTGTCCGGCGAGGGCGAGGGCGATGCCACCTACGGCAAGCTG ACCCTGAAGTTCATCTGCACCACCGGCAAGCTGCCCGTGCCCTGGCCCACCCTCGTGACCACC CTGACCTACGGCGTGCAGTGCTTACGCCGCTACCCCGACCACATGAAGCAGCAGCACTTCTTCA AGTCCGCCATGCCCGAAGGCTACGTCCAGGAGCGCACCATCTTCTTCAAGGACGACGGCAACTA CAAGACCCGCGCCGAGGTGAAGTTCGAGGGCGACACCCTGGTGAACCGCATCGAGCTGAAGGG CATCGACTTCAAGGAGGACGGCAACATCCTGGGGCACAAGCTGGAGTACAACACTACAACAGCCAC AACGTCTATATCATGGCCGACAAGCAGAAGAACGGCATCAAGGTGAACTTCAAGATCCGCCACAA CATCGAGGACGGCAGCGTGCAGCTCGCCGACCACTACCAGCAGAACACCCCATCGGCGACG GCCCGTGCTGCTGCCCGACAACCACTACCTGAGCACCCAGTCCGCCCTGAGCAAAGACCCCA ACGAGAAGCGCGATCACATGGTCTGCTGGAGTTCGTGACCGCCGCGGGATCACTCTCGGCAT GGACGAGCTGTA, Sigma) was used, further in the text referred to as mock transfection.

3.19 PHF19 knockdown

A number of 200 000 cells were transfected with 25 nM of a siRNA targeting human PHF19 (siPHF19) (s25161, GCCUCGUGACUUUCGAAGATT, targeting third exon, Thermo Fisher Scientific) using Neon electroporation system (Invitrogen). The PHF19 siRNA binds to the region between 692 and 1195 of the human PHF19 transcript (NM_006565.3). Cells were incubated 24–72 h post transfection and knockdown efficiency was monitored every 24 h.

3.20 Immunofluorescence

Cells were fixed in 3.7% formaldehyde and permeabilized in 0.7% Triton X-100 in PBS at room temperature for 10 min and 20 min, respectively. The following primary antibodies were used: mouse anti- γ H2AX (clone JBW301, Millipore, 1:1000), rabbit anti-RAD51 (PC130, 3474043, Calbiochem, 1:2000), rabbit anti-53BP1 (A300-272A, Bethyl Laboratories Inc., 1:3000), mouse anti-phospho-ATM (pS1981) (#MAB3806, Millipore, 1:100); rabbit anti-PHF19 (#7727S, Cell Signaling, 1:800); rabbit anti-PHF19 (GTX32787, GeneTex, 1:500); mouse anti-ubiquitin (FK2, 3720630, ST1200, Calbiochem, 1:500); rabbit anti-H2AK119ub (D27C4, #8240, Cell Signaling, 1:1600). The cells were fixed in 3.7% formaldehyde for 10 min at room temperature. Antibody incubation was performed at 4 °C overnight in 1% BSA in PBS in dilution specified. The signals were detected with donkey anti-mouse-IgG-AlexaFluor 594 (144883, Jackson ImmunoResearch Europe Ltd., 1:800), donkey anti-rabbit-IgG-AlexaFluor 488 (A11034, 2380031, Invitrogen, 1:800), donkey anti-mouse-IgG-Cy5 (155896, Jackson ImmunoResearch Europe Ltd., 1:800), donkey anti-rabbit-IgG-Cy3 (159772, Jackson ImmunoResearch Europe Ltd., 1:800). DNA was counterstained with 1 μ g/mL DAPI (Carl Roth) before cells were mounted with Vectashield antifade medium (H-1000-10, Vectorlabs).

3.21 Comet assay

DNA repair kinetics in PHF knockdown cells were measured using the neutral comet assay. In brief, PHF19 was depleted as described above and 48 h post siRNA transfection, the cells were exposed to 5 Gy X-ray as described above. At the indicated time points, cells were trypsinized and 2×10^5 cells ml^{-1} were embedded in 0.8% low-melting point agarose (Sigma type VII). Lysis was performed for 4 h at 4 °C in lysis buffer (10 mM Tris, 150 mM NaCl, 1% N-lauryl-sarcosinate, 1% Triton X-100, 0.5% DMSO, pH 8.0) and electrophoresis was done in 1 \times TBE at 4 °C (1 V cm^{-1}) for 30 min. Slides were then dehydrated in 100% ethanol and rehydrated in ddH₂O. DNA was stained in a SYBRGold (S11494, Invitrogen) staining buffer (1 \times TBE supplemented with SYBRGold, 1:10,000). Two biological replicates (with three technical replicates) were performed and 50 comets per slide were scored using Komet 7.1 (Andor, Oxford Instruments).

3.22 Live-cell DNA damage assay

Live-cell DNA damage assay was performed as previously described (Chagin et al., 2019). Imaging and microirradiation experiments were done using a Leica TCS SP5II confocal laser scanning microscope (Leica Microsystems, Wetzlar, Germany) equipped with an oil immersion Plan-Apochromat \times 100/1.44 NA objective lens (pixel size in XY set to 76 nm) and laser lines at 405, 488, 561 and 633 nm. All imaging was conducted in a closed live-cell microscopy chamber (ACU, Olympus) at 37°C with 5% CO₂ and 60% humidity, mounted on the Leica TCS SP5II microscope. The emission of GFP and mCherry was captured using the detection range 495–549

and 610–680, respectively. For standard microirradiation, a preselected spot in non-S phase cells (1 μm diameter) within the nucleus was microirradiated for 0.6 s with the laser line 405 nm laser set to 100%. Before and after microirradiation, confocal image series of one mid-nucleus z-section were recorded in 15 s intervals.

All analysis steps for the confocal microscopy images from microirradiation experiments were performed using ImageJ. Images were first corrected for cell movement and subsequently mean intensity of the irradiated region was divided by the mean intensity of the whole nucleus (both corrected for background) using ImageJ software. For each experimental condition, at least 25 cells were used. Half-times for ubiquitin probes accumulation were calculated from the time of microirradiation till maximal accumulation with one phase association (single exponential function: $Y = Y_0 + (\text{Plateau} - Y_0) \times (1 - e^{-K \times X})$).

FRAP data were normalized by pre-bleach fluorescence intensity. All fits were performed on averaged normalized FRAP curves and the resulting fit parameters are reported as the mean \pm SEM for two or three independent experiments. Curve fitting was done to double the exponential equation.

3.23 Microscopy

Confocal microscopy images were acquired using a Leica TCS SP5 (Leica Microsystems, Wetzlar, Germany) confocal microscope with an oil immersion Plan-Apochromat $\times 100/1.44$ NA objective lens. Cells were recorded as z-stacks with a z-spacing of 0.29 μm . The images were recorded using the following filters: DAPI: excitation wavelength (ex): 360/40 nm, emission wavelength (em): 425 LP, dichroic (dc) 400 nm; Alexa488/GFP: ex: 470/40 nm, em: 515 LP nm, dc: 510 nm; Alexa594/Cy3: ex: 570/20 nm, em: 640/40 nm, dc: 600 nm.

High-content imaging was performed using the automated confocal spinning disk microscope CREST V2 mounted on a Nikon TiE2 (Nikon, Japan) equipped with a 40x air (NA 0.95, WD 250 μm) objective. Each replicate was divided into 32 positions and at each position, one image was acquired in the channels specified. The images were recorded using the following filters: DAPI: excitation wavelength (ex): 378/52 nm, emission wavelength (em): 432/25, dichroic (dc) 409 nm; Alexa488/GFP: ex: 474/24 nm, em: 515/25 nm, dc: 493 nm; Alexa594/Cy3: ex: 578/21 nm, em: 702/100 nm, dc: 595 nm. For the comet imaging a Plan Fluor DIC 10x (NA 0.3) air objective was used.

High-content imaging was performed using the Operetta system (Perkin Elmer). Samples were imaged using 20x (NA 0.45) air objective, using the following filters: DAPI: excitation wavelength (ex): 360–400 nm, emission wavelength (em): 420–480 nm; Alexa488/GFP: ex: 460–490 nm, em: 500–550 nm; Alexa594/Cy3: ex: 560–580 nm, em: 590–640 nm.

3.24 Image analysis

The images acquired were analyzed with the custom-made image analysis pipeline for high-throughput data in the KNIME Analytics Platform (software version 3.4.0, KNIME AG, Switzerland). The KNIME software can be freely downloaded at the official webpage: <https://www.knime.com/downloads>. After downloading the user is required to manually update the Install/Upload preferences and add the “KNIME Community Contributions” as an available update site. The next step is to install an image processing extension, which can be found under the name “KNIME Community Contributions - Image Processing and Analysis”. The image analysis pipeline was constructed as follows. The dataset for each condition was loaded and run

separately. The images in the corresponding channels were loaded simultaneously and analyzed in parallel. The image analysis had two parts: whole-nuclear intensity analysis and 3D foci analysis. The DAPI channel was used for the nuclei segmentation. Nuclei were segmented based on the global intensity threshold (method Otsu). The segmented nuclei were converted into a mask with each nucleus's DAPI intensity and texture features recorded. The nuclei population was further thresholded by nucleus area and circularity to eliminate segmentation artifacts. The nuclear mask and channels of interest were overlaid, and the intensity parameters were recorded inside the nuclear areas. The intensity parameters for all the channels (total whole-nuclear intensity, mean intensity, minimum intensity, maximum intensity, standard deviation), nuclear area and texture parameters per nucleus were exported as XLSX files for further analysis.

3.25 Data analysis

Sample size was chosen so that groups (for example, time points) had comparable numbers (for example, number of imaged cells), whenever possible. High-content microscopy provided large data sets ensuring statistical significance. All statistical analysis has been performed using R. Briefly, in case data were normally distributed (Shapiro–Wilk test), ANOVA or Student's t-test were performed for groups or pairs, respectively. Else, Wilcoxon/Mann–Whitney rank sum tests were used for groups or pairs, respectively. For visualization of the box plots, the box plot lower and upper hinges correspond to the first and third quartiles (the 25th and 75th percentiles), and the upper whisker extends from the hinge to the largest value no further than $1.5 \times$ IQR from the hinge (where IQR is the interquartile range or distance between the first and third quartiles). The lower whisker extends from the hinge to the smallest value at most $1.5 \times$ IQR of the hinge. The horizontal line represents the median value. The outliers are presented as single dots in the plot outside of the box area, unless other specified.

3.26 Immunoblotting

Cells for western blot were washed with 5 ml ice-cold $1 \times$ PBS once and 2 ml of ice-cold $1 \times$ PBS was added, and cells were scraped using a cell scraper. Cells were then centrifuged in a 15 ml tube at $500 \times g$ for 5 min. Cells were lysed for total cell lysates for 1 hr at 4°C using the IP lysis buffer with 150 mM NaCl (0601.2, Carl Roth), 200 mM TrisCl pH 8 (A1086.500, Diagonal), 5 mM EDTA (8040.2, Carl Roth), 0.5% NP-40 (74385, Sigma) and protease and phosphatase inhibitors PMSF (6367.1, Carl Roth), PepA (2936.2, Carl Roth), NaF (67414-1-ML-F, Sigma), Na_3VO_4 (S6508-10G, Sigma). Whole-cell extracts were prepared by lysis with the IP buffer (150 mM NaCl, 25 mM Tris-HCl pH 7.4, 1% NP-40, 1 mM EDTA, 5% glycerol). All lysates were then centrifuged at 13,000 rpm for 20 min at 4°C . The supernatant was collected into a new 1.5 mL tube. The protein concentration was quantified by using Pierce 660 nm Protein Assay (22660, Thermo Fisher Scientific) with the Pre-Diluted Protein Assay Standards Bovine Serum Albumin (BSA) Set (23208, Thermo Fisher Scientific) according to the manufacturer's protocol. After loading 30, 40 and 50 μg of protein extract, the electrophoresis was performed for 1.5 h in ice-cold $1 \times$ Laemmli electrophoresis running buffer. Then, the protein was transferred to the $0.2 \mu\text{m}$ nitrocellulose membrane using a semi-dry transfer system (#1703940, Trans-Blot SD Semi-Dry Transfer Cell, Bio-Rad) for 55 min at 25 V using $1 \times$ transfer buffer (Pierce Western Blot Transfer Buffer $10 \times$, Thermo Fisher Scientific). After the transfer, the blotting membrane was incubated in a blocking buffer (5% low-fat milk in $1 \times$ PBS) for 30 min. The primary antibodies rabbit anti-PHF19 (#7727S, Cell Signaling, 1:1000) and rat anti-GFP (3H9, Chromotek, 1:1000) were diluted in blocking buffer

to 5% milk and incubated at 4°C overnight. The next day the membrane was washed three times with 1×PBS-T (0.075 %) 10 min each. The membrane was then incubated with secondary antibodies goat anti-rat IgG HRP (112-035-068, The Jackson Laboratory, 1:5000) and goat anti-rabbit IgG HRP (026M4782V, A-0545, Sigma, 1:10000) for 1 h at room temperature. The membrane was washed again with 1×PBS-T (0.075 %) three times 10 min each and incubated with 1:1 ECL chemiluminescence solution (Clarity Western ECL, #170-5061, Bio-Rad Laboratories). Signal was detected with the enhanced chemiluminescence detection system Amersham AI600 imager (Amersham Biosciences). Quantification was performed using ImageJ.

3.27 Apoptosis analysis

We analyzed the level of apoptosis by measuring the activity of caspase-3 and other DEVD-specific proteases. We used the EnzChek® Caspase-3 Assay Kit #2 (E-13184, Molecular Probes) according to the manufacturer's protocol. Briefly, the wild type, mock-transfected and PHF19-depleted cells were submitted to X-ray radiation. At the corresponding time points, cells were harvested and washed once with ice-cold 1xPBS. Cell pellets were lysed in the 1x cell lysis buffer (Component C, provided in the kit) on ice for 30 min. Then the lysates were centrifuged at 5000 rpm for 5 min to pellet the cellular debris. The supernatant was transferred to the microplate and mixed with 2x substrate working solution. The mix was incubated for 30 min at the room temperature protected from light. The fluorescence (excitation/emission 496/520 nm) was measured using multimode plate reader Tecan (Tecan). The fluorescent readout per sample was recorded in triplicates and presented as a bar plot. The fluorescent readout of the cell lysis buffer alone was measured as well and subtracted from the other samples.

4. Results and discussion

4.1 Ubiquitinome-wide high-throughput screening to identify novel ubiquitin modifiers in chromatin response to double-strand break

Ubiquitinome-wide screening for novel players of DNA damage signaling and repair: design and rationale

In the search for novel chromatin factors regulating DNA damage signaling and repair, we focused on ubiquitin-dependent chromatin modifiers. This modification has been gaining significant attention in the context of DDR regulation in the last years. To identify ubiquitin modifiers and the cellular pathways in DDR, we chose an RNAi high-throughput screening as a technique that is suitable for analyzing a wide variety of cellular phenotypes (Mohr et al., 2014). Using a previously published strategy for siRNA screening (Erflle et al., 2007), we designed and performed a ubiquitinome-wide cell-based siRNA screen targeting 663 genes reported to code annotated and putative E3 ubiquitin ligases and substrate-recognition subunits of E3 complexes in the human genome (Li et al., 2008) (Figure 4.1, and Annex: Table 7.1). Together with 663 putative ubiquitin ligase genes, the library included non-targeted siRNAs (NCscr1) as a negative control for transfection effects. Each gene was covered by three or more siRNA, each in triplicate, variants targeting different gene exons to maximize the efficiency of knockdown and provide additional statistical control (Annex: Table 7.1). In contrast to the usual multi-plate approach, this screen was performed on custom glass-bottom arrays using printed siRNAs. The advantages of these arrays are the large area and the absence of walls inside this area avoiding spatial effects and pipetting biases. To achieve the knockdown of the 663 genes, the reverse transfection strategy was chosen. HeLa Kyoto cells were seeded on the glass bottom arrays with pre-printed siRNAs (at least three different per gene) in triplicates. The knockdown effect for all the siRNAs was evaluated at 48 h post-seeding and the cells were subjected to 5 Gy of X-ray irradiation to induce DNA double-strand breaks (Figure 4.1). Cells were fixed, then stained for γ H2AX as a readout of DNA damage signaling/repair and the DNA dye DAPI as nuclear and cell cycle progression proxy. The γ H2AX intensity at each siRNA spot size (ca. 250 μ m diameter) was recorded by fluorescence microscopy on an automated imaging platform. We selected an unirradiated control and two post-irradiation time points for analysis: 0.5 h post-irradiation to catch the peak of damage signaling (early) and 24 h post-irradiation indicating repair efficiency (late). Each timepoint was represented by three replicate arrays, with each array accommodating 8 064 spots (663 genes x 3 siRNAs x triplicates = 8 064 spots) which totaled as 8 064 x 9 arrays = 72 576 siRNA spots. With each siRNA spot accommodating around 300 cells, we imaged and analyzed more than 20 million cells (Figure 4.1).

We chose γ H2AX as a proxy for the screen due to its central role in the DNA damage response (Stiff et al., 2004). The γ H2AX signaling kinetics at the DNA double-strand breaks is well-studied (Ciccica and Elledge, 2010) and it was established that the γ H2AX is one of the most proximal events in the DDR. In the control cells (including cells transfected with scrambled siRNA and cells not transfected), the γ H2AX signal increase was already detectable some minutes after exposure to irradiation and reached the maximum phosphorylation signal at around 0.5 h timepoint in agreement with other reports (Sedelnikova et al., 2002) (Figures 4.1, 4.2). The γ H2AX signal stayed stable for at least an hour, after which it started to decrease as the damage was

repaired. At 24 h post-irradiation, only unresolved double-strand breaks were left and were visible as residual γ H2AX foci (Figure 4.1).

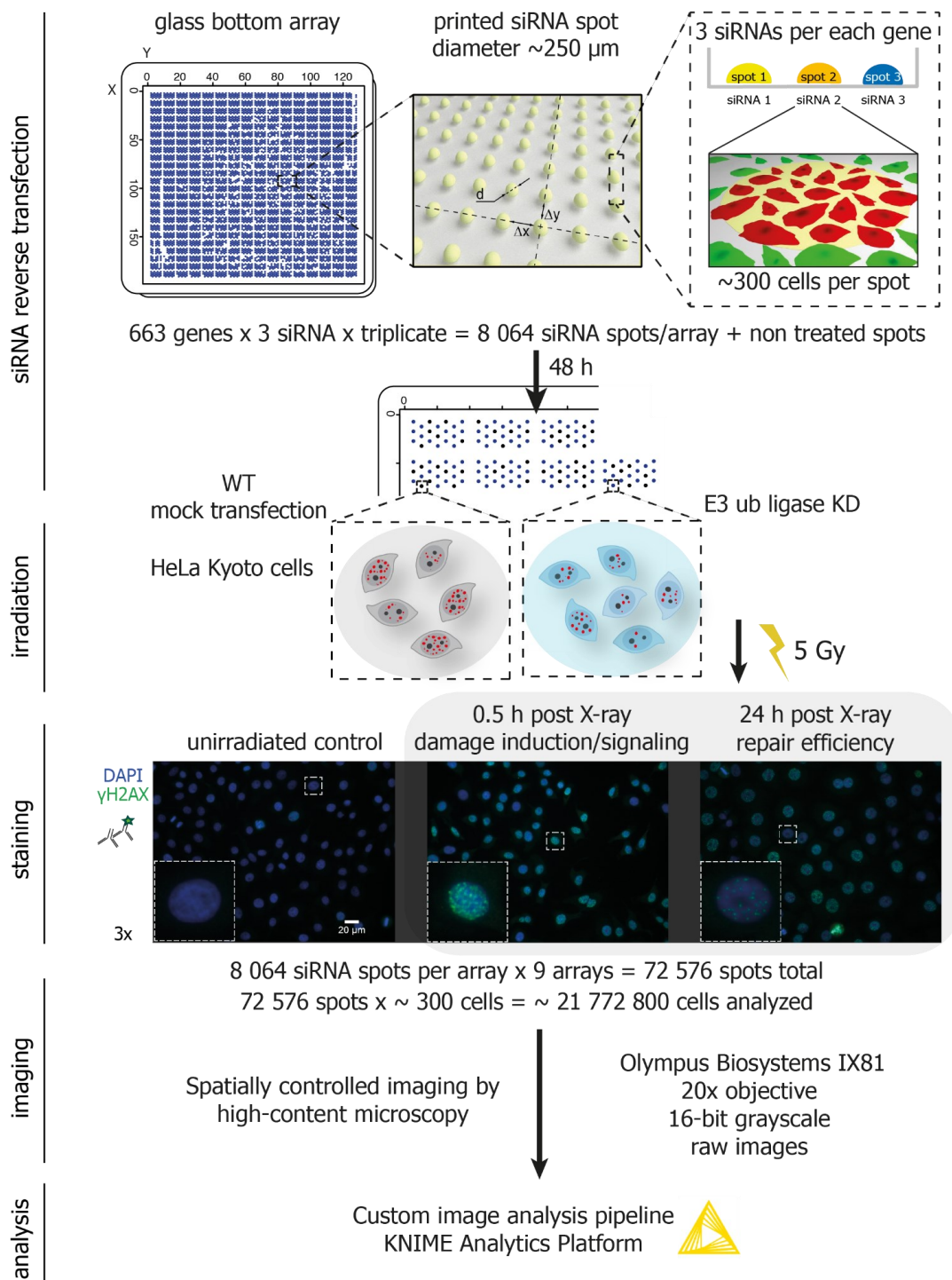


Figure 4.1. Ubiquitinome-wide high-content screen for the players of chromatin response to DNA damage. The scheme is presented in the form of a modified flowchart consisting of five major parts: reverse transfection, irradiation, staining, imaging, and analysis. The magnified area of an array describes the reverse transfection principle where only cells positioned on the spot get transfected with an siRNA. After 48 h the cells reach the knockdown phenotype and are subjected to 5 Gy of gamma irradiation. The arrays

are fixed at the chosen time points post-irradiation, including unirradiated arrays. The image panel represents the γ H2AX signal in control non-siRNA transfected cells. The arrays were imaged with an automated imaging platform and the data was analyzed in the KNIME Analytics Platform. The detailed version of the image analysis with a description of the filters and data thresholding is described in the part “Construction of the image analysis pipeline for the ubiquitinome-wide screen”.

Another argument for choosing γ H2AX signaling as a proxy was that it is a known part of chromatin response to DNA damage. It was shown before that the γ H2AX spreading and clustering directly reflects a high-order chromatin structure and 3D organization in response to the DNA damage (Natale et al., 2017; Aymard et al., 2017; Arnould et al., 2021). Additionally, the γ H2AX is recognized by multiple reader proteins and, therefore, indicates the recruitment of downstream repair factors and accumulation of phosphorylation-dependent ubiquitination and acetylation chromatin marks.

Construction of the image analysis pipeline for the ubiquitinome-wide screen

The ubiquitinome-wide screening is a high-throughput/high-content approach and it was designed to screen and profile a large collection of RNAi reagents (siRNA library). At the center of the ubiquitinome-wide screening is a robust phenotyping assay. As a microscopy-based screening, it produced a large number of images each containing information about hundreds of cells. The cells in a heterogeneous population are in different cell cycle stages which might influenced the resulting knockdown phenotype at the single siRNA spot. To have a cell cycle marker on the screen we introduced the second channel, DAPI, that stains DNA. The individual cells in a cell population were reported to behave differently towards the same siRNA due to their microenvironment, for example, due to the cell density on a plate/array (Snijder et al., 2012). Additionally, due to the individual differences cells can have varying siRNA uptake efficiency and knockdown level. Therefore, the aim was to design an image analysis protocol that can perform a single-cell analysis.

Our high-throughput imaging approach allowed us to record hundreds of parameters defining the knockdown-caused phenotypes at nuclear and subnuclear scales, as well as the classification of subphenotypes. The standard image analysis pipelines are not suitable for handling this type of data and extracting the relevant information. Hence, we designed a single-cell image analysis pipeline for the high-throughput image data that allowed robust extraction of the fluorescence intensity, texture, and geometric features. We chose the KNIME Analytics Platform (KNIME, Switzerland) software to construct the image analysis pipeline due to the advantages it offers. The KNIME software has a modular environment that enables visual assembly and interactive execution of pipelines. KNIME as a single platform comprises all the functionalities that a bioimage analysis requires (Dietz and Berthold, 2016). Another advantage is that the KNIME combines functionalities of other different analysis tools and domains, including ImageJ. Moreover, when the analysis workflow was created, it could be applied to large data sets of images by using a loop function.

Each siRNA spot was imaged in two fluorescent channels, DAPI and γ H2AX, and subjected to image analysis using the KNIME Analytics Platform (see Materials and Methods). The image analysis workflow for the high-throughput imaging data (“The Last Jedi” version) was constructed as follows (Figure 4.2A). All the data sets and their metadata were loaded in the first node “List files”. The workflow contained two loops, one inside another, to first loop iterates over datasets,

then over images. The images loop loaded only a couple of images at each iteration, DAPI and γ H2AX images corresponding to one spot. The channels were split in the node “Splitter” to be analyzed in parallel. The DAPI channel was used to create the mask of the nuclei, record nuclei intensity, geometry, and texture features and filter the segmented nuclei population by the area and circularity threshold. The DAPI channel was preprocessed in the ImageJ Macro node (“Subtract background”, “Gaussian Blur”, “Watershed”) which resulted in the binary segmentation image (Figure 4.2B, 4.2C). The binary image was corrected for holes in the “Fill holes” node. In the next step, the subsets of connected segmented objects are uniquely labeled using a connected component analysis algorithm to create a mask of the nuclei (“Connected component analysis” node). The resulting mask of the objects was overlaid with the original DAPI channel image to record the DAPI intensity features, geometry and texture features for a single nucleus (“Image segment features” node). In the next node, “Row filter”, the nuclei population was filtered to remove the segmentation artifacts by applying nuclear size, circularity and XY thresholds (Figure 4.2C). In the parallel line of the workflow, the γ H2AX image was subjected to two types of preprocessing: first preprocessing used only the “Subtract background” functionality of the ImageJ Macro node, and second had additional “Gaussian Blur”. Both preprocessed γ H2AX images were subjected to further analysis and later were compared for the resulting γ H2AX intensity value (Figure 4.2C, 4.2D). The comparison showed the one-to-one correlation between the resulting γ H2AX intensity values, indicating no advantage delivered by the additional Gaussian smoothing (Figure 4.2D). Therefore, only the minimally preprocessed γ H2AX image (“Subtract background”) was used for the data analysis and hits identification. The preprocessed γ H2AX image was overlaid with the final nuclei mask and intensity, geometry (X/Y position, area, circularity, convexity, and diameter), and texture features (Haralick texture features, different aspects of the gray-level distribution in the object area, helps object segmentation) were recorded per single nucleus. At the end of the loop, the γ H2AX parameters were recorded in the nuclear area delineated by the DAPI mask at two levels, as data per siRNA spot and as data per cell nucleus (Figure 4.2). From over 30 different parameters collected from more than seven million cells (at each time point), we selected (1) the number of nuclei, and (2) the total intensity of γ H2AX per nucleus for subsequent data analysis. In parallel to the image processing part, intensity features were calculated for each DAPI image (“Image math (QC)” workflow line) (Figure 4.2A). The image features were used in the following “Math Formula” node to calculate the variance/mean² DAPI intensity value per image. The variance/mean² values were recorded and exported together with other DAPI and γ H2AX parameters in the results table and were later used for the quality control of the imaging data.

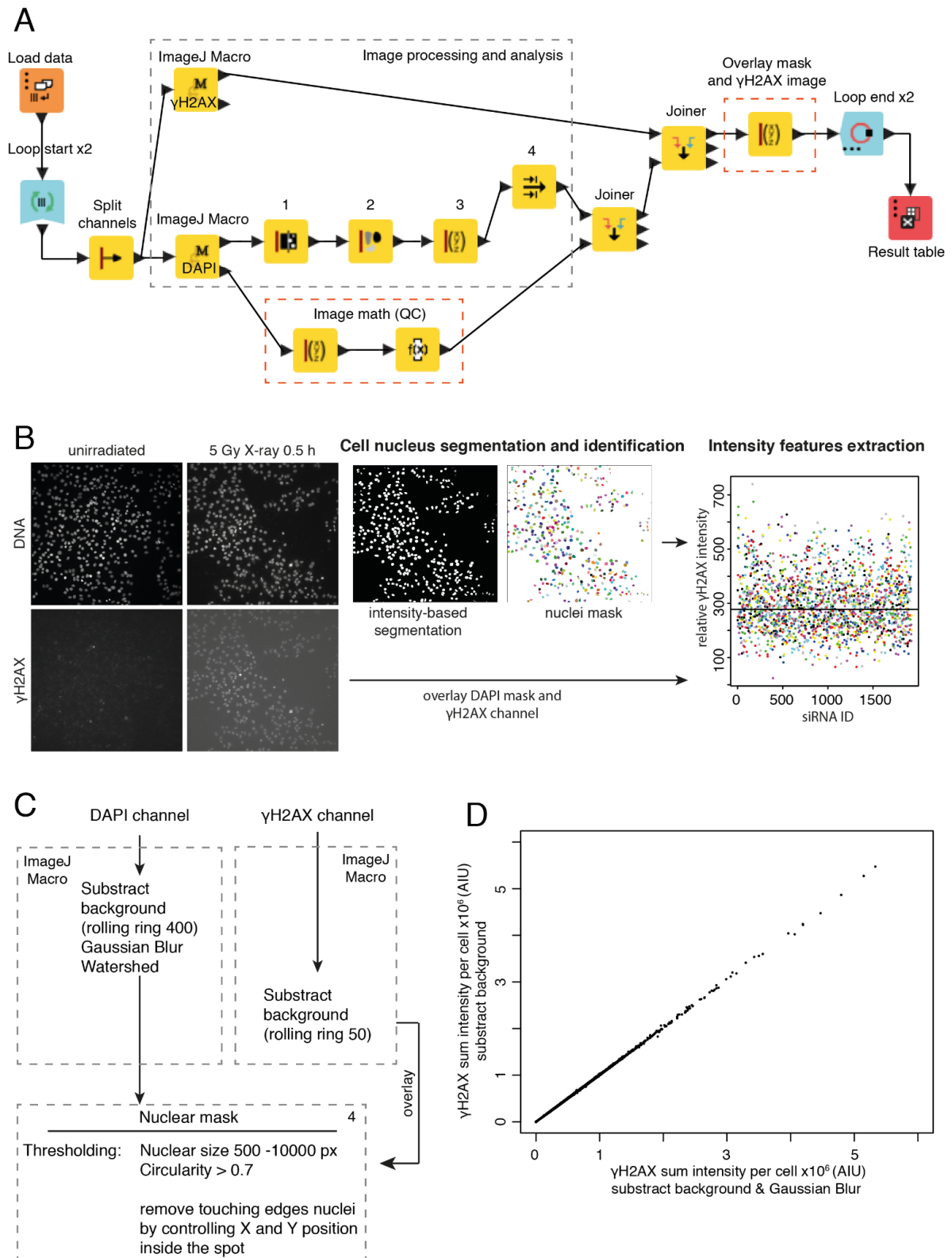


Figure 4.2. Image analysis workflow for the high-throughput data collected in the ubiquitinome-wide screening. (A) Simplified version of the modular image analysis workflow used for the analysis of the high-throughput data in KNIME software. The KNIME original node icons are presented. 1- “Fill Holes” node, 2- “Connected component analysis” node, 3 - “Image segment features” node, 4 - “Row filter” node. Full workflow is in the Annex Figure 7.2. (B) The outcome of the image processing nodes. Original DAPI and γ H2AX images for unirradiated and irradiated arrays are presented. The outcome of the sequential

execution of “ImageJ Macro” (“Subtract background”, “Gaussian Blur”, “Watershed”) and “Fill Holes” nodes is presented under the number 1. The outcome of the “Connected component analysis” node is presented under the number 2 (nuclear mask). Upon overlay of the nuclear mask and preprocessed γ H2AX image (ImageJ Macro node, “Subtract background”, “Gaussian blur”) the single-cell γ H2AX intensity features are recorded. (C) Schematic representation of the DAPI and γ H2AX channel preprocessing parameters in the ImageJ Macro nodes and nuclear population thresholding parameters. 4 - nuclear population thresholding parameters in the Row Filter node. After nuclei segmentation and connected component analysis the nuclear size, circularity and XY positioning thresholds were applied to remove the segmentation artifacts. (D) Correlation between total whole-nuclear single-cell γ H2AX values obtained by two types of preprocessing in ImageJ Macro nodes.

Establishment of the data analysis strategy

This section describes the data analysis steps applied to the single-cell raw γ H2AX and DAPI intensity measurements to identify the siRNAs that significantly change γ H2AX intensity compared to non-treated/mock-transfected cells.

The following steps describe the overall data analysis:

1. Image quality control
 - 1.1. Identification of the imaging artifacts by variance/mean² ratio of the image pixel intensities and manual filtering
 - 1.2. Identification of the imaging artifacts by abnormal total γ H2AX intensity values and manual filtering
2. Cell-level quality control
3. Transform into raw single cell γ H2AX intensities to log scale
4. Correct γ H2AX signal for DNA content
5. Calculation of γ H2AX intensity fold change and Z score values
6. Calculation of p-values per siRNA spot
7. Rank the significant genes by the reproducibility between the replicates

The image quality control measures were applied to correct for the imaging problems (e.g. automatic focus failure at a siRNA spot, blurring, bright debris at a siRNA spot with saturated pixels) and for the segmentation artifacts (under-segmentation of the crowded nuclei, over-segmentation of a single nucleus). One of the two statistical approaches used to reflect the image quality was variance and the square mean ratio of the image pixel intensities (Caicedo et al., 2017; Groen et al., 1985). The variance/mean² (further in the text referred to as normalized variance) value was calculated for the DAPI image of every siRNA spot during the high-throughput image analysis. The normalized variance value represents the variability between the pixel intensity in the image and is affected by the number of cells (represented by the bright pixels). Generally, the lowest normalized variance value that can be obtained is 0, which signals that the image has no variation in pixel intensity, is heavily blurred and is out of focus. The higher the value is, the more pixel intensity varies due to the signal of interest (cell nuclei stained by DAPI) or the contribution of saturated pixels (bright artifacts). For each array, the distribution of the normalized variance values among the siRNA spots was inspected and the lower and upper thresholds were chosen by manual examination. Based on the thresholds chosen, the spot IDs with too low or too high normalized variance values were compiled and the corresponding images were manually examined. The images with insufficient quality were removed from the analysis. The images that appear well-focused but contain artifacts such as debris or inappropriately bright aggregations were manually edited in Fiji to remove the artifacts and subjected to repeated

image analysis (Figure 4.3A). In total, most of the images from the arrays appeared to have sufficient image quality, and less than 1% of the siRNA spots were removed from the analysis.

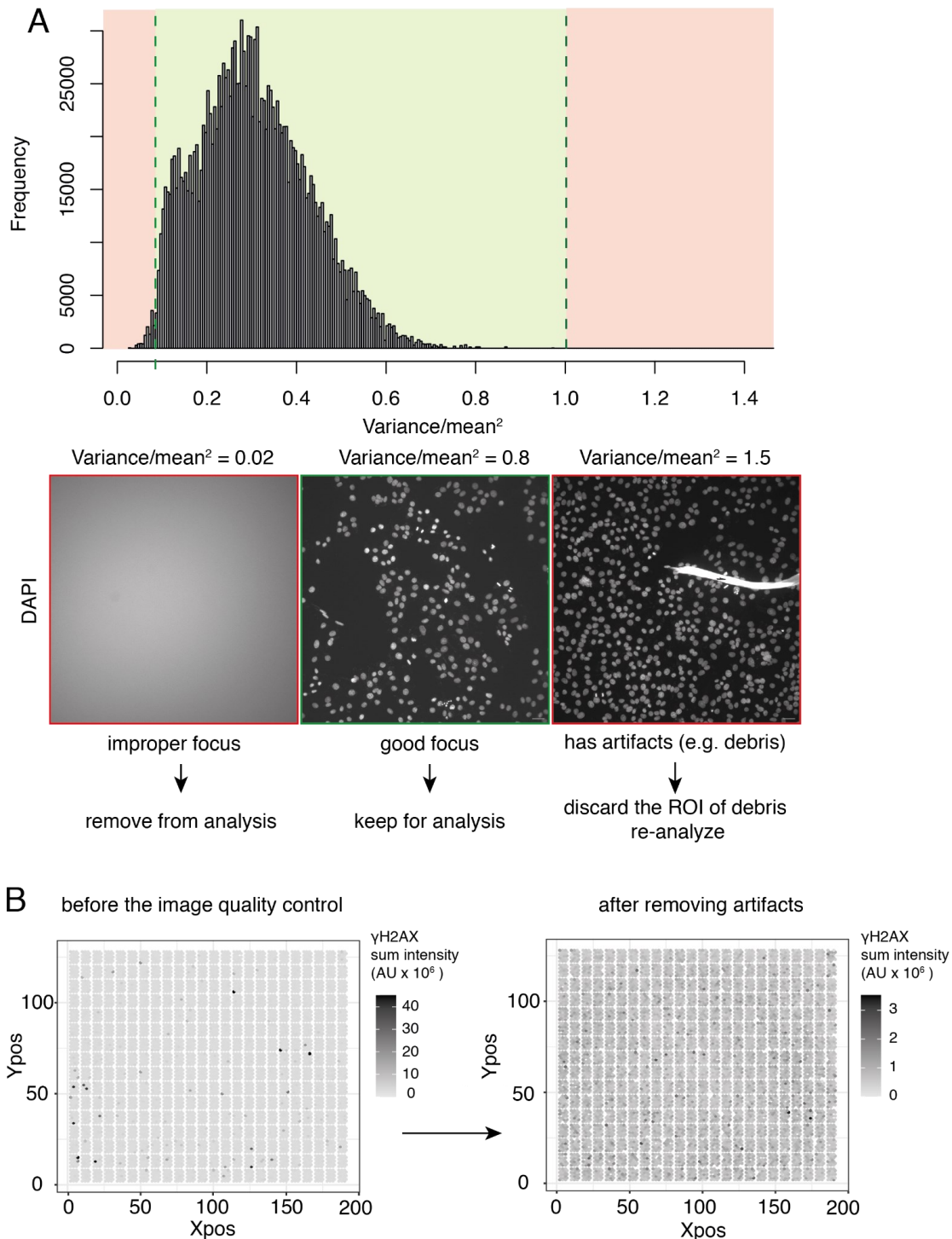


Figure 4.3. Image data quality control. (A) The histogram of the normalized variance values per image (siRNA spot), array 0.5 h post-irradiation. The red areas highlight the range of the values beyond the selected threshold, lower corresponding to the improper focus (lower panel), and higher corresponding to the images with artifacts (lower panel). The green area highlights the range of values corresponding to the well-focused images. (B) The array layout is colored by the mean of the total γ H2AX intensities per cell, each dot represents a siRNA spot on the array. The left array layout shows the distribution of the values

before the image quality control. The right one shows the distribution of the values after the image control (note the different color scale).

A similar image quality examination was performed using total γ H2AX intensity per siRNA spot for each array separately. The distribution and the range of the total γ H2AX intensity values were inspected and the images with the highest γ H2AX intensity were manually controlled for the saturated pixels. As before, the images with insufficient quality have been removed from the analysis, while the images that were only partially affected by artifacts such as debris present or saturated pixels were manually corrected and re-analyzed. The spatial distribution of the affected siRNA spots appeared not related to the position on an array. After removing the images with the artifacts, the data showed more variability in total γ H2AX intensity among the siRNA spots highlighting potential hits (Figure 4.3B).

The cell-level quality control was performed based on individual nuclei size and total DAPI intensity per cell for each array. This step was designed to correct possible nuclei segmentation issues. As expected, the total DAPI intensity of the segmented regions directly correlated with their size. Most of the segmented nuclei appeared to form one distinct population based on their size and total DAPI intensity with approximately 5% (variable between the arrays) spreading in the direction of the size and the intensity increase. Manual image comparison showed that this population was represented by the under-segmented nuclei aggregates. The threshold values were defined for each array individually and were consistent among the different replicates and time points.

The raw data was represented by the total whole-nuclear γ H2AX intensity and total whole-nuclear DAPI intensity per nucleus (Figure 4.5A). As we noticed before (Natale et al., 2017), the whole-nuclear γ H2AX intensity was highly correlated with the whole-nuclear DAPI intensity, that is the γ H2AX signal strength/amount is DNA content dependent. Therefore, to identify the siRNA treatment effects we corrected the whole-nuclear γ H2AX intensity of each cell by its whole-nuclear DAPI intensity. The value obtained was called relative γ H2AX intensity (Figure 4.5A). The raw values were transformed to a log scale to correct the signal skewness of the data distribution and normalize it for further statistical analysis. The log transformation significantly improved the shape of the data distribution, which was used for the later analysis steps to calculate a p value (Figure 4.4A). For simplicity, we will still use the term γ H2AX intensity, but from here on we are referring to the relative log transformed γ H2AX intensity.

The data analysis was performed per array, the raw γ H2AX intensity values were normalized by the DNA content. As expected, most of the spots on the arrays showed the raw and normalized γ H2AX intensity values similar to the cells on the control spots with a small subset showing a significant change that was selected as potential hits (Figure 4.3B). That was also shown by pooling all array spots together during the time course, which showed the expected γ H2AX intensity kinetics. Remarkably, some spots had a significantly strong γ H2AX intensity effect noticeable as the raw values, further confirmed by the statistical analysis (Figure 4.4C). The robustness of the screening (Z' factor ranging between a maximum of 1 and a minimum of minus infinity, calculated as difference between the value of the siRNA control spots and siRNA spots) was assessed as high by the data distribution and the Z' factor value reaching 0.7 (Birmingham et al., 2009). In total, these results prove the sensitivity, robustness, and reproducibility of our method and, thus, its potential application in the discovery of different DNA repair modifiers.

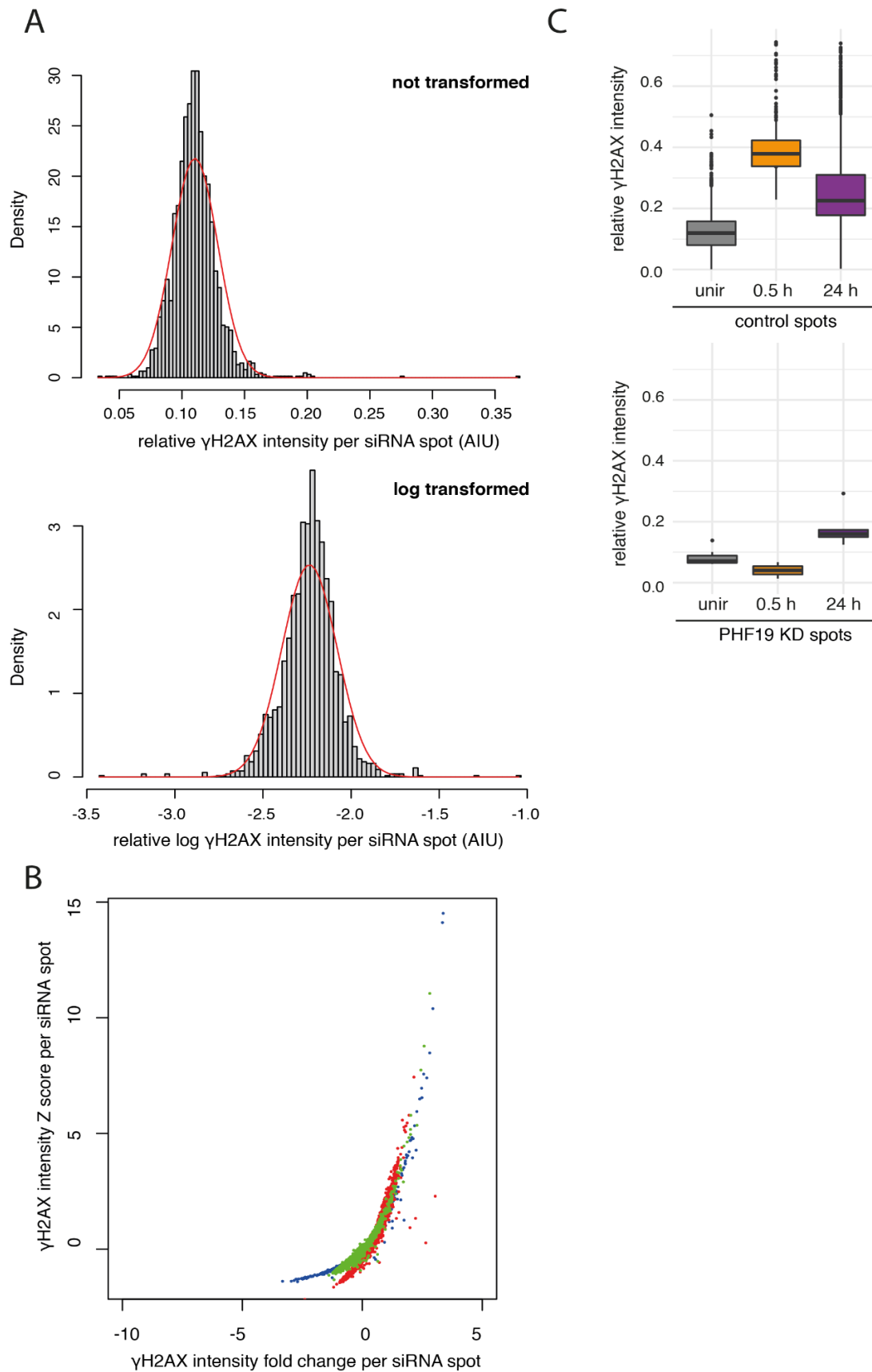


Figure 4.4. Data normalization and dose response. (A) Histograms depicting transformed and log transformed relative γ H2AX intensity per spot values from one array, 0.5 h post-irradiation. The red line is a

trendline. After the log transformation, the data assumed normal distribution. (B) Data distribution of three replicate arrays according to the γ H2AX intensity fold change values and the γ H2AX intensity Z score values per siRNA spot. Each point is a siRNA spot, three colors correspond to the three replicate arrays of the same time point (24 h post-irradiation). (C) The dose response of control no siRNA/control siRNA spots and the siRNA spots for the PHF19 gene. The box plots of relative γ H2AX intensity per spot kinetics on control spots (no siRNA/ control siRNA) and on one of the hit spots, PHF19 (one array replicate per time point is shown). The relative γ H2AX intensity per spot was calculated as the mean of total nuclear γ H2AX intensity per cell normalized by total DAPI intensity. The bar of the box plot represents the median. The box plot lower and upper hinges correspond to the first and third quartiles (the 25th and 75th percentiles), and the upper whisker extends from the hinge to the largest value no further than $1.5 \times$ IQR from the hinge (where IQR is the interquartile range or distance between the first and third quartiles). The lower whisker extends from the hinge to the smallest value at most $1.5 \times$ IQR of the hinge. The outliers are presented as single dots outside of the box area.

The summary statistics per siRNA spot were carefully examined. The siRNA spots containing less than 5 cells have been removed from the further analysis and compiled as a separate list to be investigated for the potential cell lethality effect. The mean, median, and standard deviation were calculated for the total γ H2AX single-cell intensity and nuclear size. Both the γ H2AX intensity and nuclear size were further analyzed and hits lists were combined separately. The γ H2AX intensity values summarized per spot were subsequently converted to fold change (FC) and Z score values, both referring to the difference between the observed effect and control cell population (irradiated but not siRNA-treated cells) (Figure 4.5A). The fold change per siRNA spot on each array was calculated as follows:

$$\text{fold change} = \log_2 \frac{\text{mean}(\text{relative } \gamma\text{H2AX intensity}) \text{ of } a}{\text{mean}(\text{mean}(\text{relative } \gamma\text{H2AX intensity}) \text{ of } C)},$$

where a - a siRNA spot, and C - pooled control spots (no siRNA/ control siRNA).

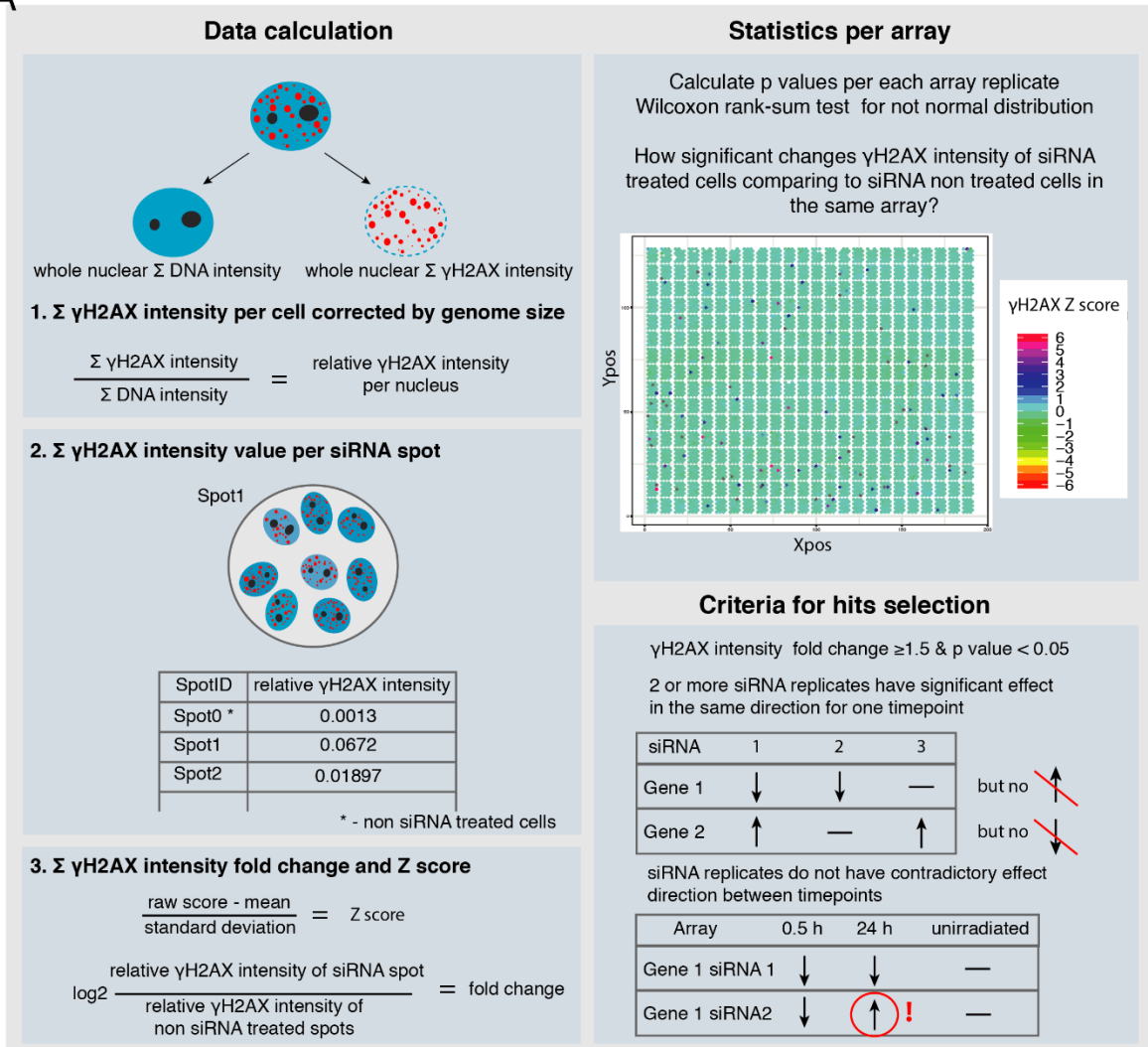
The siRNA spots were compared to the control spots on the same array. Since most of the siRNA spots intensity values were not different from the control spots, the Z score per spot was calculated as follows:

$$Z \text{ score} = \frac{\text{mean}(\text{relative } \gamma\text{H2AX intensity}) \text{ of } a - \text{mean}(\text{mean}(\text{relative } \gamma\text{H2AX intensity}) \text{ of all spots})}{\text{standard deviation}(\text{mean}(\text{relative } \gamma\text{H2AX intensity}) \text{ of all spots})},$$

where a - single siRNA spot, all spots - all spots on an array including the controls.

The Z score calculation is a way to normalize the values to the normally distributed population based on the standard deviation and the mean of the values of all the spots (Birmingham et al., 2009; Williams et al., 2017). In contrast to the fold change value, the Z score value does not show a direct difference between a siRNA spot and the control spots, rather gives an impression of how different the test value of a siRNA spot is from the mean of all spots on an array. The Z score calculation implies that most spots on an array are indistinguishable from the controls, therefore we could use it in our analysis. We compared the fold change values with the Z score values for the spots between the same time point replicates and found them to have only small differences. The data from the time point replicates showed a similar value range (Figure 4.4B).

A



B

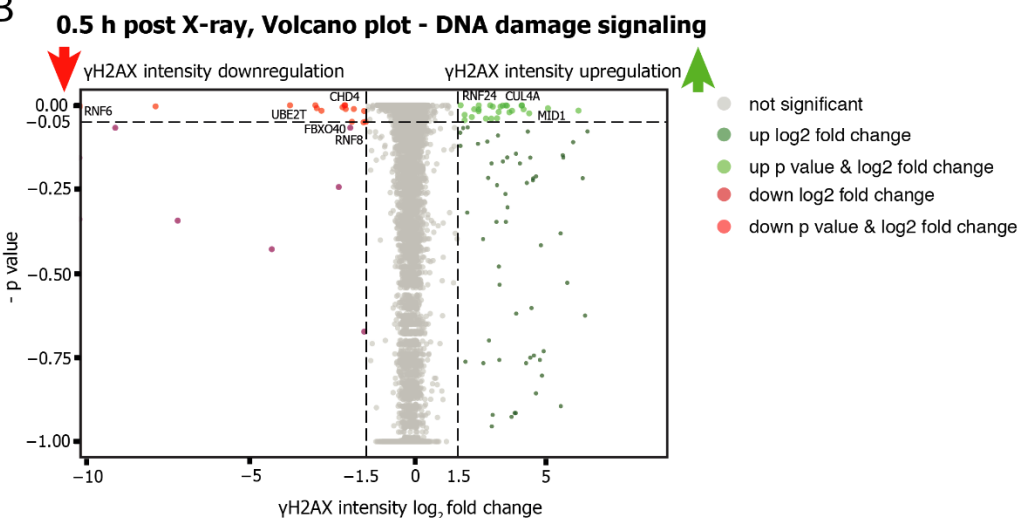


Figure 4.5. Data analysis of the ubiquitinome-wide high-throughput screening data. (A) The step-by-step scheme of the data analysis. Only the main steps are depicted. The analysis consisted of three parts. The first part is data calculation, which includes 1 - total γ H2AX intensity per cell corrected by genome size (total DAPI intensity per cell). 2 - calculation of the total γ H2AX per spot (per siRNA spot summary statistics

such as mean, median, standard deviation of the total single-cell γ H2AX intensity), the exemplary table shows the difference between the siRNA spots. 3 - calculation of the total γ H2AX intensity fold change and Z score values per siRNA spot. The second part is the calculation of statistics per array and p value calculation. The heatmap showing the nuclear γ H2AX intensity difference compared to untreated cells in cells transfected with different siRNAs at 0.5 h time point. Each spot contains cells transfected with a particular siRNA. γ H2AX nuclear intensity is represented as a Z score parameter and it is displayed with a color code. The zero value depicts no difference in γ H2AX nuclear intensity compared to control spots at the same array (same timepoint, no siRNA/control siRNA). The positive Z score represents an increase of γ H2AX nuclear intensity compared to corresponding control spots, negative Z score represents a decrease of γ H2AX nuclear intensity compared to corresponding control spots. The value of the Z score shows the magnitude of the difference in γ H2AX nuclear intensity between individual siRNA spots and control spots. The third part comprises the rules for hits selection and ranking of the hits. The part describes the handling of the siRNA variant replicates on the same array and the time point replicates. (B) Volcano plot depicting the genes according to their p value and \log_2 fold change value for a 0.5 h array, DNA damage signaling. Each point represents a single gene. The γ H2AX intensity \log_2 fold change is represented by positive and negative values, where the positive value represents an increase of γ H2AX nuclear intensity compared to corresponding control spots (green), negative value represents a decrease of γ H2AX nuclear intensity compared to corresponding control spots (red). The p value ranges from 0 to 1, the scale is $-p$ value. The thresholds are set up as -1.5 and 1.5 for the γ H2AX intensity \log_2 fold change and 0.05 for the p value. Based on the thresholds the plot is divided into areas and points are colored accordingly: grey points are genes whose γ H2AX total intensity is not significantly different from the cells on the no siRNA/control siRNA spots, green points are the genes whose KD increased γ H2AX total intensity, red points are the genes whose KD decreased γ H2AX total intensity. Some of the highly significant genes have their names written.

To find out the siRNA spots showing the γ H2AX intensity significantly different from the control spots, we performed multiple nonparametric Wilcoxon rank-sum tests. Single-cell relative γ H2AX intensity values corresponding to one siRNA spot on an array were compared in the Wilcoxon rank-sum test to the single-cell relative γ H2AX intensity from the control spots on the same array. The significance threshold was set at a lower than 0.05 p value.

For the visual analysis and preliminary selection of the hits on each array, a Volcano plot was chosen. A Volcano plot is a type of scatter plot that shows statistical significance (p value) versus magnitude of change (fold change), it is widely used for the visualization of the hits in differential gene expression studies (McDermaid et al., 2019). We used the R script "Enhanced Volcano" (Blighe et al. 2018) and modified it to fit our data analysis. The spots were plotted according to their \log_2 fold change and -p values. The thresholds were applied as -1.5 and 1.5 for the \log_2 fold change and 0.5 for the p value, dividing the plot with the spots into five areas: nonsignificant values, significantly upregulating the γ H2AX intensity according to the \log_2 FC, significantly downregulating the γ H2AX intensity according to the \log_2 FC, significantly upregulating according to both the \log_2 FC and p value and significantly downregulating according to both the \log_2 FC and p value (Figure 4.5B). The genes with both statistical significance and the magnitude of effect in either up- or downregulation direction were chosen as hits and subjected to the further selection procedure (Annex: Table 7.2). The genes with significantly higher or lower \log_2 FC were separated into a list of interesting candidates but were not analyzed further.

The hits lists were further subjected to the selection procedure. Since all the previous analysis steps were performed per array, the selection rules were chosen based on the reproducibility of the replicates, which gave us a data range of at least 27 observations per gene at one time point (3 siRNA replicates per plate x 3 siRNAs per gene x 3 replicated plates per time point). (Figure

4.5A). The first rule dealt with the siRNA variants and their replicates per gene on the same array. The gene was selected as a hit if the siRNA variants/replicates γ H2AX intensity log₂ FC values did not show contradicting effects (upregulation effect or downregulation effect). It was allowed for some of the siRNA variants of a gene candidate not to show a significant effect due to the siRNA variants targeting different exons and variability in the transfection efficiency. The hit candidates that passed the in-array siRNA variability rule were tested for their reproducibility at the second selection step. The second selection step cross-referenced the hits from the replicate arrays for the same time point. The general rule was to keep only the genes that have a consistent effect for each time point among three replicates. The genes with contradicting effects were removed from the list. The genes with the different effects (up- or downregulation) for the two different time points were kept in the list and considered particularly interesting.

The last step of the selection procedure was the ranking of the hits according to their reproducibility. The reproducibility rank was calculated as an arbitrary value represented by the sum of the observations, where the significant effect was counted as one and non-significant as zero. The gene set was further ranked to identify the strongest and most reproducible hits. Taken together, the hits list was assembled according to the reproducibility rank, significance, and direction of the effect on the γ H2AX intensity (Annex: Table 7.2).

4.2 Hits recognition and evaluation

Chromatin proteins involved in DNA damage signaling and repair revealed by ubiquitinome-wide screening

The whole nuclear γ H2AX intensity of cells at the siRNA spots was analyzed with the help of the following statistical parameters: log fold change (FC), Z score, and p value. The final hit identification was based on the cut-offs of the log fold change set as >1.5 and <-1.5 and <0.05 for the p value. The hits were scored in two directions: significantly downregulating and upregulating the γ H2AX intensity (corresponding to negative and positive log FC, respectively) compared to the scramble siRNA-transfected/non-transfected spots per time point (Figure 4.5B, Annex: Figure 7.3). The hits were scored separately for each array and cross-referenced for reproducibility by time point.

Based on the log FC, p-value, and reproducibility factor, we identified 143 hits for the 0.5 h post-irradiation time point and 65 hits for the 24 h time point, with 39 of them being common for both time points (Figure 4.6A). Cell death-inducing gene knockdowns formed a separate category of hits due to the potential importance of their function for cell survival. As we cannot exclude technical reasons leading to cell mortality and, as these genes may play general functions in cell cycle and apoptosis, we excluded them from the present analysis.

The knockdown of the hits common for both time points could induce γ H2AX intensity change in the same direction at both time points (uniform effect through time) as well as in different directions (multifactorial effect through time). Based on the direction of the effect on γ H2AX intensity, we have identified several hit “scenarios” depicting a possible mode of action (Figure 4.6B). The most abundant scenario (scenario 3) was characterized by a significant increase of DNA damage signaling at 0.5 h after damage (33.4% of all phenotypes). The second most abundant scenario (scenario 4) was characterized by the delay of DNA damage signaling at 0.5 h after damage (28.8% of all phenotypes). Interestingly, the most frequent phenotypes appeared to be caused by the knockdown of the regulators of the 0.5 h (DNA damage signaling) time point

only. Next in rank scenario (scenario 1) showed a decrease of γ H2AX signaling at 0.5 h as well as its extinction at 24 h, and it represents a prolonged disturbance of the DNA damage signaling (15.4%). A similar but smaller frequency (12.1%) was observed for scenario 5 characterized by the significantly lower γ H2AX signaling at 24 h time point. The lack of the residual γ H2AX late in the signaling is often recognized in this type of high-throughput assays as a sign of the fast and efficient repair (Martinez-Pastor et al., 2021), but we, however, considered a bigger picture. Not denying the connection between the amount of the γ H2AX signal and the DNA damage persisting, we considered such factors as the 3D chromatin architecture, stability of the phosphorylated domains over time and crosstalk between the phosphorylation and ubiquitination. Scenario 2 showed an increased signal of DNA repair at the 0.5 h time point and its disappearance 24 h after damage (Figure 4.6B). Much less abundant among all was scenario 7, in which the signaling was lower at 0.5 h after damage but significantly elevated at 24 h. We considered this phenotype a delay in the γ H2AX signal activation, and the hits that fell into this category are mostly known cell cycle regulators, e.g. cyclin D1. One hit showed a permanent overactivation of DNA damage signaling across both time points (TRIM60), however, the phenotype was associated with high cell lethality that led to insufficient statistics. Thus, TRIM60 was removed from further analysis. Importantly, the hit list included the proteins known for their function in the DNA damage signaling and repair, which validates the specificity, validity, and completeness of the screen. These factors include key ubiquitin modifiers such as: RNF8 (downregulation of γ H2AX intensity at 0.5 h and 24 h) and RNF168 (upregulation of γ H2AX intensity at 0.5 h) (Malette et al., 2012; Nowsheen et al., 2018; Lu et al., 2021), HUWE1 (downregulation at 0.5 h) (Yi et al., 2015; Kunz et al., 2020; Mandemaker et al., 2017), RAD18 (upregulation at 0.5 h) (Huang et al., 2009; Kobayashi et al., 2015), TRIP12 (upregulation at 0.5 h and downregulation at 24 h) (Liu et al., 2016), UHRF1 (downregulation at 0.5 h and 24 h) (Hahm et al., 2019; Zhang et al., 2016a), APC (downregulation at 24 h) (Lafranchi et al., 2014), XIAP (downregulation at 24 h) (Bruno et al., 2008), CUL4A (upregulation at 0.5 h) (Wang et al., 2006), HLTF (downregulation at 24 h) and SHPRH (downregulation in undamaged cells) (Lin et al., 2011; Seelinger and Otterlei, 2020). Additionally, we identified as hits some of the known ubiquitin-dependent DDR factors such as CHD4 (downregulation at 0.5 h) (Polo et al., 2010), BAZ1B (downregulation at 0.5 h and 24 h) (Xiao et al., 2009) and CDK2 (upregulation at 0.5 h and downregulation at 24 h) (Liu et al., 2020). Confirming the screen's specificity, we discovered among the hits general ubiquitination cascade regulators, for example, UBA1 (E1 enzyme, common for the ubiquitination cascades) (Lacoursiere and Shaw, 2021), UBB (one of the four ubiquitin-producing genes) (Baker and Board, 1987), and players of the ubiquitin-like modifications like ufmylation (UFM1) (Lee et al., 2021) and SUMOylation (PIAS2, PIAS4) (Galanty et al., 2009; Han et al., 2021) (Figure 4.6C, Annex: Table 7.2). The presence of these proteins among the identified hits further confirms the sensitivity and specificity of the ubiquitinome-wide screening for the novel modifiers of chromatin response in the DDR.

To further characterize the identified hits, we ran a functional profiling of the full hits list (post-irradiation time points, 0.5 h and 24 h, further in the text - full hits list, unless otherwise specified) irrespective of the time point affected and the up- or downregulation effect. The functional profiling was done by cross-referencing the hits list with the Gene Ontology: Biological Process (GO:BP) database in the gProfiler software (Raudvere et al., 2019). The database contains annotations of all the genes in the human genome, each gene is assigned a term, or category, based on the evidence provided. The types of evidence include experiments, high-throughput

experiments, expression patterns, sequencing results, structural similarity, and reviewed computational analysis. Most of the terms have a hierarchical structure with the more general terms having a wider description (“parental”) and more specialized terms clustered into groups under the parental ones. Since our screen specifically targeted human ubiquitinome, the functional profiling showed “Protein ubiquitination” as the most represented term with the highest adjusted p value (GO:0016567, adjusted p value 1.752×10^{-123}). To reveal the categories with lower but highly significant p values we capped the parental terms (28 terms total, all describing the general ubiquitination process) and analyzed the hits content of the more specialized terms (Figure 4.6D). In total, we could identify 148 highly significant overrepresented categories and proceeded to analyze 120 specialized ones. The 120 terms identified roughly fell into categories of DNA damage signaling/repair, cell cycle control, chromatin organization and apoptosis. Interestingly, the hits were highly enriched in terms of K48-ubiquitination (GO:0070936, adjusted p value 2.88×10^{-24}) and K63-ubiquitination (GO:0070534, adjusted p value 6.881×10^{-17}), which is 10^4 times more enriched than the same terms in the hits list from the unirradiated cells (Figure 4.6D, Annex: Table 7.3, 7.4). The terms “DNA damage response” (GO:0006974) and “DNA repair” (GO:0006281) had very high p values, 5.199×10^{-10} and 8.839×10^{-7} , respectively, and they comprised the hits known for a role in the DDR (Figure 4.6D, category 1). Another interesting group of the overrepresented terms among the hits characterized the various aspects of chromatin posttranslational modifications and remodeling (Figure 4.6D, category 2). We identified a significant group of the hits represented by the terms “Histone ubiquitination” (GO:0016574, adjusted p value 3.84×10^{-6}), “Chromatin organization” (GO:0006325, adjusted p value 5.14×10^{-4}) and “Histone H2A ubiquitination” (GO:0033522, adjusted p value 1.04×10^{-3}). The next larger category of the hits fell into the terms describing various aspects of the cell cycle control: “Cell cycle process” (GO:0022402, adjusted p value 2.432×10^{-4}), “Negative regulation of cell cycle process” (GO:001094, adjusted p value 9.531×10^{-6}), “Cell cycle G1/S phase transition” (GO:0044843, adjusted p value 7.4×10^{-4}) and “Cell cycle G2/M phase transition” (GO:0044839, adjusted p value 3.13×10^{-2}) (Figure 4.6D, category 3). The terms related to the processes of cell death were assigned to the category of apoptosis (Figure 4.6D, category 4). The category included functional terms like “Cell death” (GO:0008219, adjusted p value 2.114×10^{-2}), “Regulation of apoptotic process” (GO:0042981, adjusted p value 3.316×10^{-3}) and “Autophagy” (GO:0006914, adjusted p value 1.507×10^{-3}).

We also compared the enrichment of the terms between the hits list from the irradiated cells (0.5 h and 24 h) with those from the unirradiated cells and identified the terms that are present only in response to IR and terms that disappear in response to IR (Annex: Table 7.3, 7.4). In this regard, the post-irradiation time points included hits in 75 unique IR-associated categories such as “Protein K11-linked ubiquitination”, “DNA metabolic process”, “Negative regulation of cell cycle phase transition”, “Cell cycle G1/S phase transition”, “Apoptotic process”, “Innate immune response”, “DNA damage checkpoint signaling”, “DNA integrity checkpoint signaling”, “Signal transduction in response to DNA damage”, “Autophagy”, and “Negative regulation of DNA-templated transcription”. Another large group of IR-associated terms was related to cellular responses to various stimuli, such as cytokines, tumor necrosis factor, and stress. Moreover, the ubiquitin modifiers that are annotated to fill the categories of transcription control were found to be IR-specific (“Epigenetic regulation of gene expression”, “DNA metabolic process”). In contrast to the hit list from the post-irradiation time points, the novel ubiquitin modifiers in undamaged cells were enriched in the terms describing RNA-related processes, such as

“Regulation of RNA metabolic process” and “RNA biosynthetic process” (Annex: Figure 7.4, Table 7.4). In general, when compared to the hits from the irradiated cells, the hits from the unirradiated samples had lower p values of the terms’ enrichment. It is directly related to the smaller number of the hits in unchallenged cells scored, but also to the various γ H2AX-mediated processes not directly tied to the DNA damage response.

We further proceeded with the hits scored in 0.5 h and 24 h post-irradiation time points to discover novel ubiquitin modifiers in the DDR, leaving the hits from the unirradiated cells for future analysis. Taken together, the results provided us with an accurate prediction of the processes involved in the DNA damage signaling and repair that require ubiquitination events.

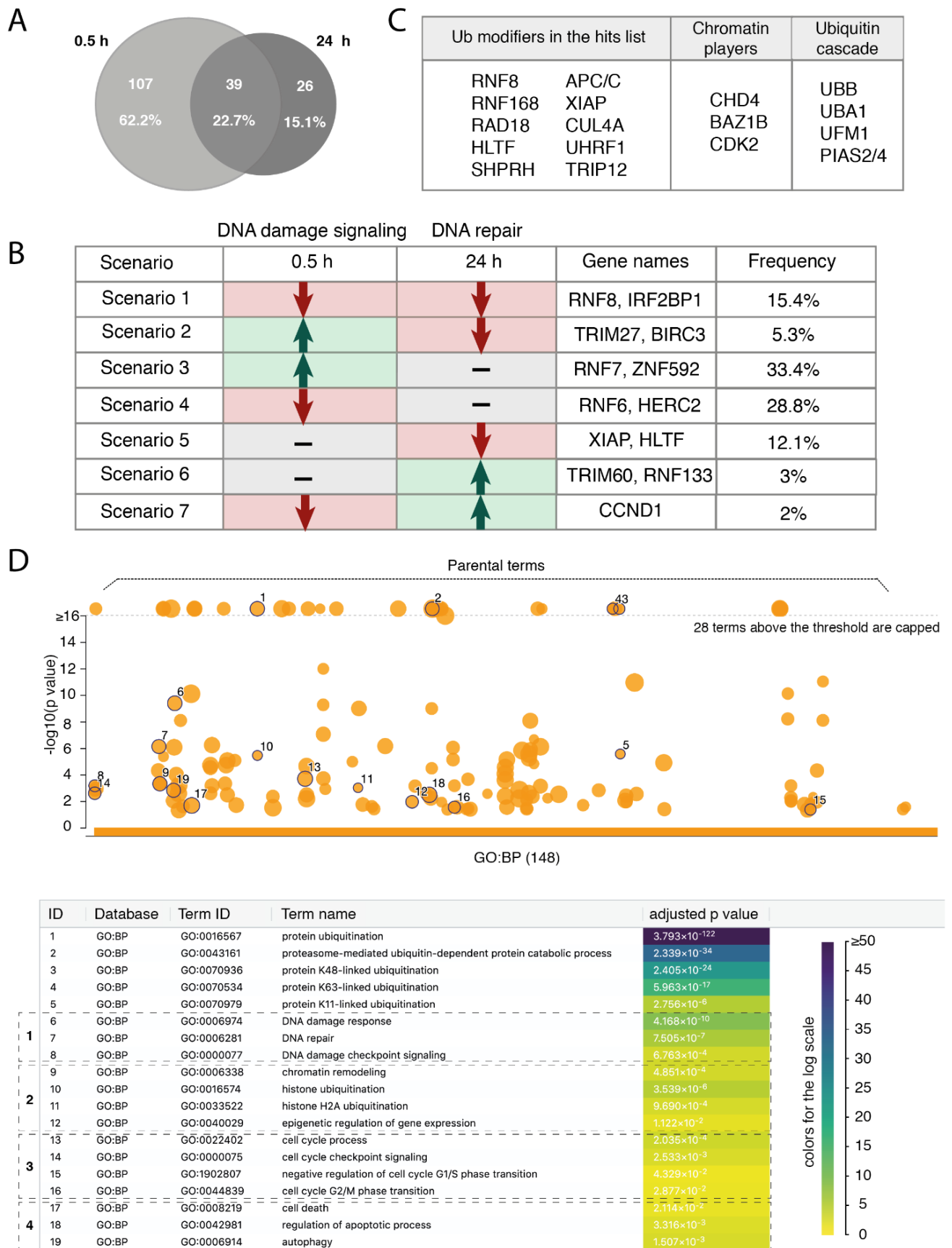


Figure 4.6. Analysis of the hits from the ubiquitinome-wide screening revealed seven scenarios. (A) Venn diagram showing how many hits are significant for the 0.5 h, 24 h, or both time points irrespective of the up-

or downregulation effect. (B) The summary of the proteins known for the function in the DDR pathway. The table has three columns, known ubiquitin modifiers, known chromatin proteins, and general players of the ubiquitin cascade. (C) The schematic table of the possible scenarios of action among the hits. The scenarios are the phenotypes that we identified among the hits depending on the time point affected and the up- (green arrow) or down-regulating (red arrow) effect on γ H2AX signal intensity. Exemplary hits are given. (D) Results summary of the functional profiling for the hits irrespective of the time point and up- or downregulation effect, GO:BP - biological process category. The hits list was cross-referenced with the biological process database comprising such evidence types as experiment, expression patterns, sequence or structural similarity, genomic context, and computational analysis. The resulting *p* values were corrected for the multiple testing with the in-house algorithm, significance threshold was set at 0.05. Only significant categories are plotted. In total 148 terms are represented as circles, where its size is proportional to the number of hit genes that fall into that term. 28 overrepresented terms (parental terms) with the highest *p* values were capped on the top of the plot to allow the visualization of the less represented but significant categories. 19 terms were manually selected, numbered and clustered in the categories (1, 2, 3, 4). The terms are listed in the table below. Each term has a corresponding ID number and the name presented. Category 1 - DNA damage signaling/repair terms, 2 - chromatin organization terms, 3 - cell cycle terms, 4 - apoptosis terms.

In silico analysis of protein interactions revealed the connection between DDR proteins and chromatin remodelers among novel ubiquitin modifiers

As ubiquitination generally involves several steps and multiple protein complexes, the similarity of knockdown effects between hits potentially resulted from protein-protein interactions. We combined functional profiling and protein-protein interaction analysis to elucidate the functional interactions between our hits. First, we built a network of the gene ontology terms identified before (Figure 4.6D) by modeling it as an undirected multigraph within the Metascape software (Zhou et al., 2019). The network connected the GO terms by the edges representing the GO similarity score. Next, we manually remodeled the network by keeping the input of the nodes and substituting the edges of the GO similarity score with the arbitrarily calculated protein-protein interaction score. The resulting network consisted of several tightly inter- and intraconnected clusters (Figure 4.7). As expected, the clusters represented the groups of similar GO terms with similar functional profiles and protein content and, therefore, enriched for the protein-protein interactions. Among the clusters, we clearly distinguished previously identified GO categories such as DNA damage signaling and repair, cell cycle transition and chromatin remodeling (Figure 4.7). The high level of interactions between the clusters showed that the ubiquitin modifiers identified in our screen form a functional chromatin network in response to DNA damage. Two GO clusters with the highest level of protein-protein interactions between the hits inside them were identified as “Polyubiquitination” and “K63-ubiquitination and oncogenic transformation” (Figure 4.7, highlighted red). The K63-ubiquitination was previously shown in multiple studies to be associated with DNA damage signaling and repair (Liu et al., 2018). Interestingly, although strongly connected to the DNA damage signaling/repair cluster, the “K63-ubiquitination and oncogenic transformation” cluster was still spatially separated. The analysis of the single GO terms and hits inside them revealed that the total hits list for both 0.5 h and 24 h time points was enriched for the players of cancer pathways. The interactions identified could be a part of the same ubiquitin-dependent cascades controlling response to DNA damage and long-term genome stability.

To identify the single protein-protein interactions (PPI) enriched in our hits list, we separated the hits significant for the early (0.5 h) and late (24 h) DNA damage signaling time points and analyzed them for functional and physical interactions using experimental/biochemical databases (DIP, BioGRID, HPRD, InAct, MINT, PDB) and curated databases (Biocarta, BioCyc, GO, KEGG, Reactome) (Figure 4.8, Annex: Tables 7.5, 7.6). Expectedly, we identified more protein-protein interactions among the 0.5 h hits than 24 h, which is in agreement with the total number of hits per time point. Interestingly, the share of the hits with known functional or physical interactions from the total number of hits was around 60% for both time points. In this analysis, we only considered functional and physical interactions between single proteins that are known from experimental physical and functional interaction data. The functional interaction meant proteins jointly contribute to a shared function (part of the signaling cascade), either by physical binding or not.

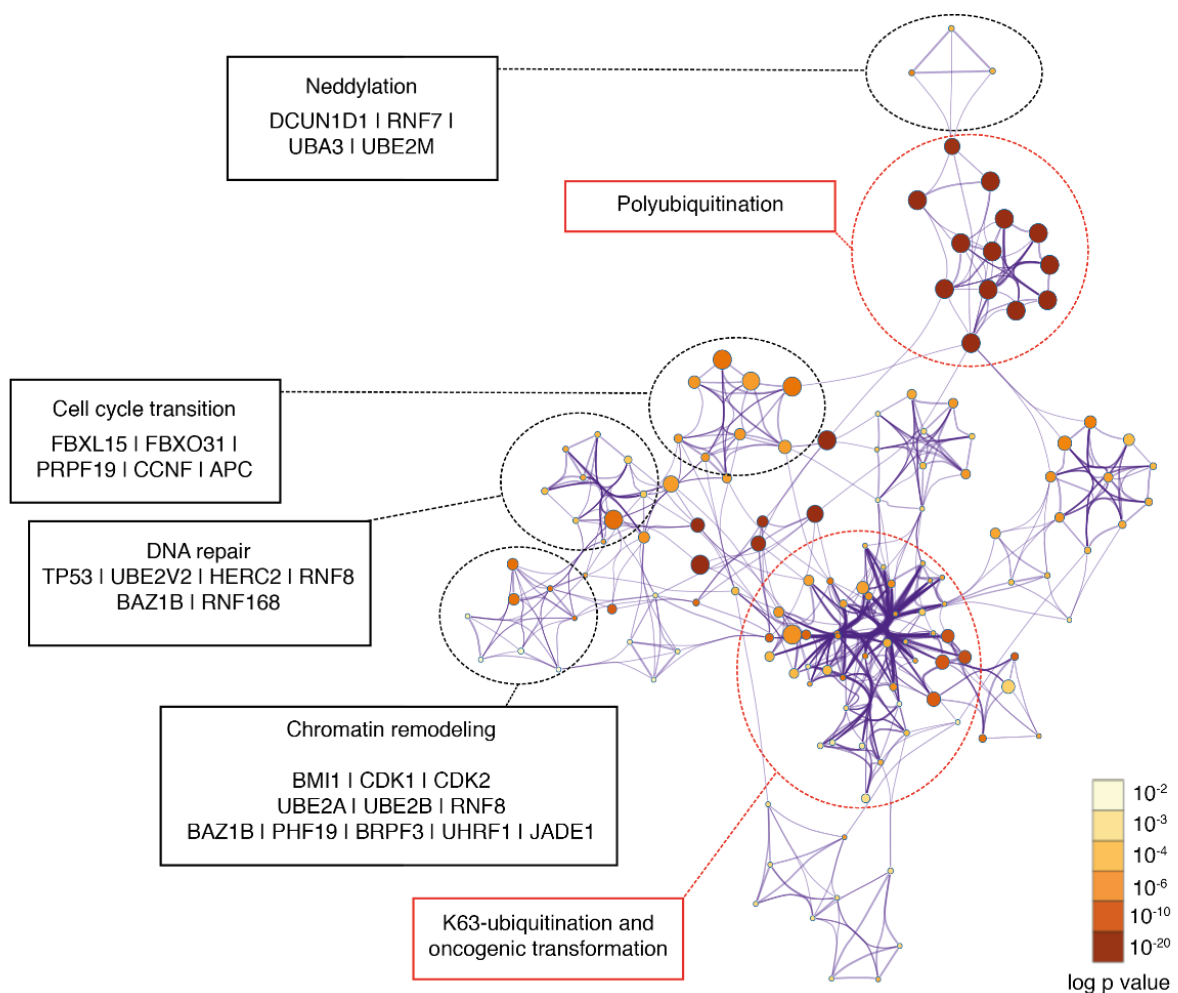


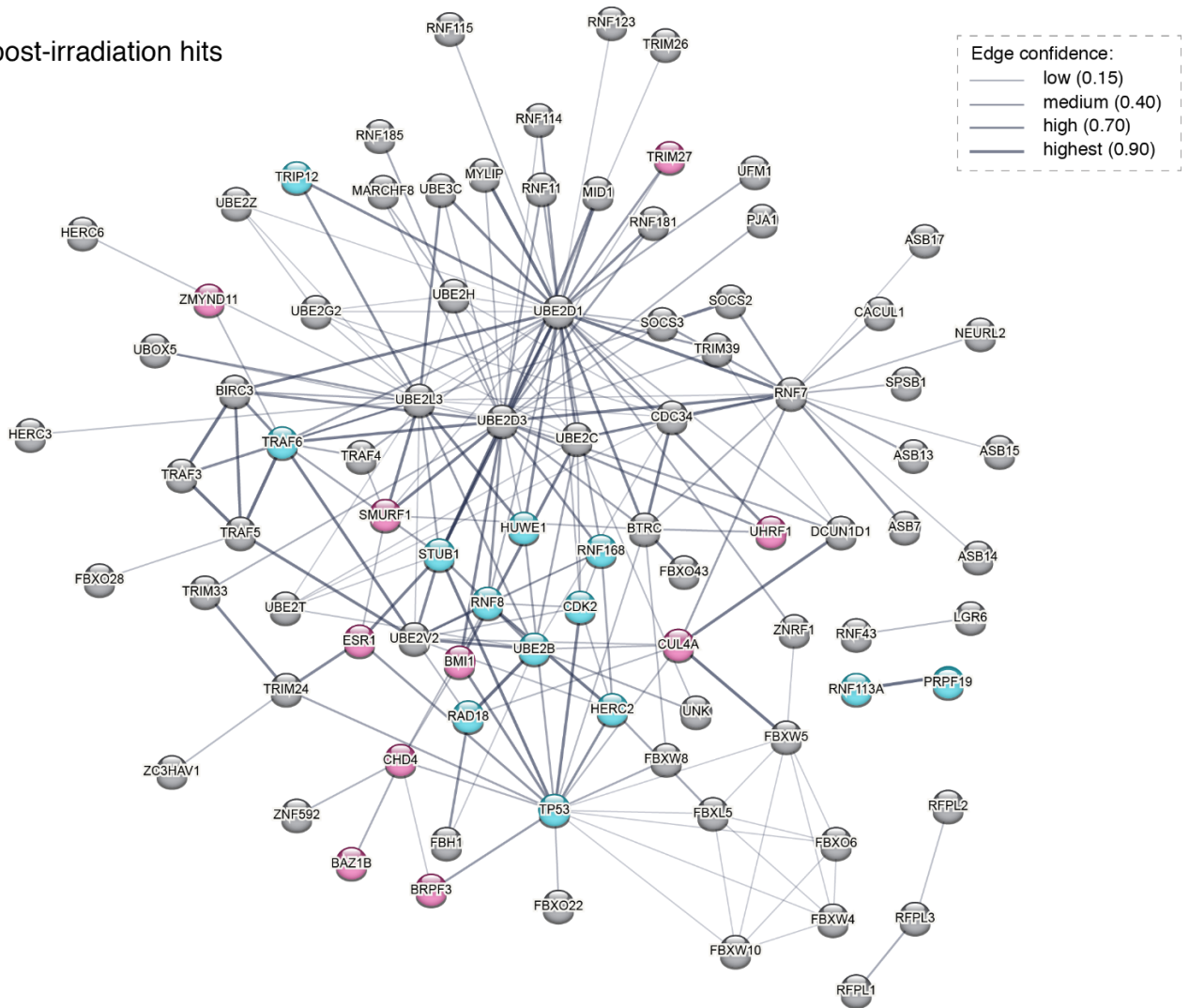
Figure 4.7. Custom network of the GO terms and protein-protein interactions for hits list for both post-irradiation time points. Each term is represented by a circle node, where its size is proportional to the number of hit genes that fall into that term, and its color represents its p value. The edges represent the functional and physical protein-protein interaction score. Terms with the score > 0.4 are linked by an edge with the thickness of the edge representing the strength of the data supporting it. The network was visualized with Metascape and Cytoscape with “force-directed” layout and with edge bundled for clarity. Selected clusters of terms are highlighted in the network, their names and examples of hits are given. Two

of the clusters are highlighted with a red dashed circle representing two clusters each with a high level of interactions.

A part of the protein-protein interactions enriched at both 0.5 h and 24 h time points were aggregated near several E2 type enzyme of the hits (UBE2B, UBE2D1, UBE2D3 for 0.5 h, UBE2D2 for 24 h), likely due to the ability of a single E2 enzyme to accommodate multiple E3 ligases (Figure 4.8). Most of the interactions, however, appeared to be centered around the known players of the DNA damage signaling and repair (Figure 4.8, blue)). Remarkably, the first level of interaction of the DDR proteins for both time points were proteins annotated as chromatin remodelers (Figure 4.8, pink). The functionally and/or physically interacting DDR proteins and chromatin remodelers made up 30-40% of all the interactions identified for both time points and were supported by the highly confident data evidence (edge confidence ≥ 0.7). To identify novel functional signaling cascades, we analyzed the proteins with the highest number of interactions together with their first and second-level interacting partners. Almost all of the network elements identified included a hit previously not reported for a function in the DDR. Next, we scanned the PPI networks for the hits common for both time points. We found that the same proteins identified as hits for the early and late DNA damage signaling have different interaction partners at the 0.5 h and 24 h networks (Figure 4.8). For example, at 0.5 h post-irradiation FBXW8 protein showed first-level interactions with TP53 and BTRC, while at 24 h - with BTRC, CCND1 and DCUN1D3. Different combinations of partners of the same ubiquitin modifier at 0.5 h and 24 h with high probability reflected the combinatorial nature of the molecular processes involved in early and late DNA damage signaling. Another proof of the interaction enrichment not being a random effect was derived from the comparison of our networks with a network built from a random gene set of the same size. After multiple comparisons, the PPI enrichment p value for the network of 0.5 h hits was $<10^{-15}$, and for the network of 24 h 3.46×10^{-14} . The result signified that our hits had more interactions among themselves than what would be expected for a random set of proteins drawn from the genome and that the proteins are biologically connected.

To investigate ubiquitination crosstalk with other posttranslational modifications among our hits, we expanded the PPI networks to other protein-protein interactions not identified in our screen. The enzymes known for the ubiquitin-like modifications like neddylation, SUMOylation and ufmylation were identified in our list as a part of the GO terms. We further analyzed the interacting partners of our hits and identified several of them associated with phosphorylation, acetylation, and methylation (Table 4.1). As expected, we found the DDR players and chromatin remodelers highly enriched for the ubiquitination crosstalk with other posttranslational modifications: RNF8 and RNF168 for methylation, UHRF1 for methylation and acetylation. A significant group of hits was recognized for the crosstalk between ubiquitination and phosphorylation. The majority of the hits in this group was represented by the phosphodegron-regulated ubiquitination (FBXW8, FBXO6, BTRC, CBL) and some hits required phosphorylation to get activated (e.g. SMURF1). The hit list for both time points was enriched for the components of the PRC complexes, which is one of the prominent examples of crosstalk between ubiquitination and chromatin methylation (BMI1, PHF19). Several ubiquitin modifiers among the hits were annotated for recruiting acetyltransferase complexes (PHF20) and deacetylase complexes (UHRF1). The crosstalk with PARylation was represented by the TRIP12 protein that recognizes the PAR chains. This type of crosstalk was the most underrepresented.

0.5 h post-irradiation hits



24 h post-irradiation hits

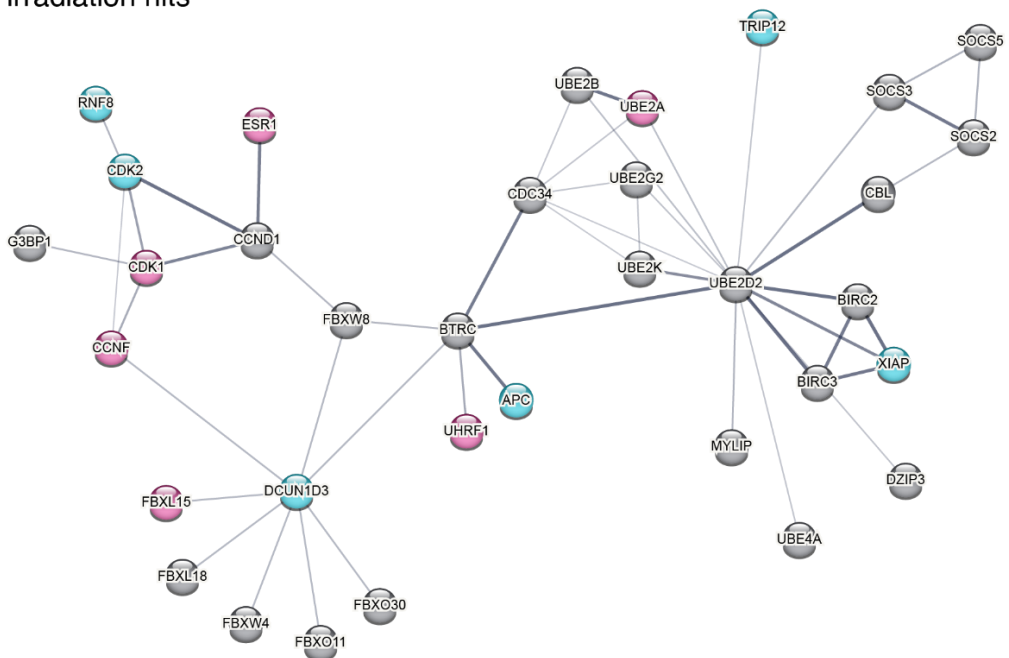


Figure 4.8. Protein-protein interaction networks for the hits of 0.5 h and 24 h post-irradiation highlighted connection between DNA repair proteins and chromatin remodelers. Functional and physical interactions

are represented by edges. Each node is a hit protein, the label is written on the nodes. Blue nodes are hits known for DNA damage signaling/repair, pink nodes are hits known for chromatin remodeling, and grey nodes are the hits not fitting in either of the two prior categories. The thickness of the edges represents the confidence of the supporting data, with the thickest edges being the most confident. Only the interactions with a minimum required interaction score > 0.4 (medium confidence) are shown. The hits with a score < 0.4 are not shown.

Table 4.1. Screening hits known to be associated with other posttranslational modifications.

Hit protein	Time point	PTM type	Interactions
BMI1	0.5 h	Methylation	PRC components
FBXW8	0.5 h 24 h	Phosphorylation	MAP4K1/HPK1, IRS1, GORASP1
CUL4A	0.5 h	Neddylation	TIP120A/CAND1
CDK2	0.5 h 24 h	Phosphorylation	CTNNB1, USP37, p53/TP53, NPM1, CDK7, RB1, BRCA2, MYC, NPAT, EZH2, ERCC6
RNF8	0.5 h 24 h	Methylation	JMJD2A/KDM4A
RNF168	0.5 h	Methylation	JMJD2A/KDM4A
UHRF1	0.5 h 24 h	Methylation Acetylation	DNMT1, DNMT3A, DNMT3B HDAC1
DCUN1D3	24 h	Neddylation	CUL3, RBX1
TRIM26	0.5 h	Acetylation Methylation	PHF20, KDM6B
BTRC	0.5 h 24 h	Phosphorylation	NFKB1, ATF4, CDC25A, DLG1, FBXO5, PER1, SMAD3, SMAD4, SNAI1
FBXO6	0.5 h	Phosphorylation	CHEK1
CBL	24 h	Phosphorylation	KIT, FLT1, FGFR1, FGFR2, PDGFRA, PDGFRB, CSF1R, EPHA8, KDR
TRIM60	0.5 h 24 h	SUMOylation	TRAF6/TAB2/TAK1
PHF17	24 h	Acetylation	KAT7, NPHP4
TRIP12	0.5 h 24 h	PARylation	MYC, UBP7
SMURF1	0.5 h	Phosphorylation	AKT1/2

Thus, we functionally characterized the novel ubiquitin modifiers identified in the ubiquitinome-wide screening for the novel players of DNA damage signaling and repair. With the help of the

pathway and protein-protein interaction analysis, we found signaling cascades involving previously known as well as new DDR factors. The hits list appeared to be enriched for the chromatin remodelers and their interactions with the DDR proteins. Additionally, among our hits, we uncovered the ubiquitination crosstalk with other posttranslational modifications in response to DNA damage.

Ubiquitination controls DNA repair early after the damage and cell fate decision at the late time point

To further investigate the ubiquitin-dependent signaling at the early (0.5 h post-irradiation) and late (24 h post-irradiation) time points we compared the functional profiling and protein-protein interactions between the two hit lists. First, we modified the GO/PPI network we built for all the hits from the post-irradiation time points (Figure 4.7). Each GO term enriched was analyzed for its hits content and association with 0.5 h and/or 24 h time points. The resulting network kept the structure and only the nodes were annotated differently. We found the clusters associated mostly with the early DNA damage signaling, the clusters associated mostly with the late DNA damage signaling, and the clusters enriched for both time points more or less equally. As expected, the big polyubiquitination cluster containing the general parental GO categories was associated with both time points (Figure 4.9A). A similar distribution was observed for all the terms of the cell cycle transition cluster with, however, the more significant contribution of 24 h hits. Interestingly, the DNA repair cluster was almost completely represented by the 0.5 h hits as well as neddylation (Figure 4.9A). The chromatin remodeling terms were tightly interconnected by protein-protein interactions but had a preference for either early or late DNA damage signaling time point. That signified that the ubiquitin-dependent signaling on the chromatin caused by the hits takes place throughout the DNA damage response likely in the form of interacting multiprotein complexes. The cluster of the “K63-linked ubiquitination and oncogenic transformation” was associated with both time points, with some terms enriched only at 0.5 h and some only at 24 h post-irradiation. Additionally, we identified the functional clusters enriched only at 24 h post-irradiation. The novel ubiquitin modifiers that fell into these categories supported the cell fate decision pathways post-damage, such as PI3K, MAPK, JAK-STAT-regulated pathways, and the Wnt pathway (Figure 4.9A). Despite the lack of protein-protein interactions between each other, the clusters represent phosphorylation-guided ubiquitination. Next, we compared the enrichment of the functional terms and identified the ones with the biggest difference between the two time points (Figure 4.9B). We identified all statistically enriched terms (KEGG Pathway, GO Biological Processes, Reactome Gene Sets, Canonical Pathways, CORUM, WikiPathways, and PANTHER Pathway), accumulative hypergeometric p values (Zar, 1999) and enrichment factors were calculated and used for filtering. Terms with a p value <0.01, a minimum count of 3 hits, and an enrichment factor >1.5 (the enrichment factor is the ratio between the observed counts and the counts expected by chance) are collected and grouped into a tree of the hierarchical clusters based on their functional similarities (sub-trees with a similarity Kappa score >0.3 were considered a cluster) (Cohen, 1960). The term with the best p value within each cluster was selected as its representative term and displayed in a dendrogram (Figure 4.9B). The terms “Protein autoubiquitination”, “Neddylation”, “DNA damage response”, “DNA repair”, “Positive regulation of histone modification”, “Regulation of canonical NF-kappaB signal transduction” and “RING-type E3 ligases ubiquitinate target proteins” were significantly more enriched for the early DNA damage signaling time point compared with late

one. The functional groups “Protein monoubiquitination”, “Protein K27-linked ubiquitination” and “p53 regulation pathway” were unique for the early time point (Figure 4.9B). In contrast, the late time point showed higher enrichment in terms of “PI3K-, MAPK-, JAK-STAT pathways”, “Negative regulation of cell cycle process” and “Small cell lung cancer”. The unique functional categories for the 24 h post-irradiation included “Regulation of canonical Wnt signaling pathway” and “Regulation of plasma membrane bounded cell projection organization”, the latter referred to the processes of plasma membrane organization. Thus, we observed that in response to the DNA damage, the ubiquitination events predominantly promote DNA repair and chromatin remodeling at the early DDR stages, while controlling cell cycle transition and cell fate at the late ones.

To compare the transcriptional regulatory interactions and disease associations between the early and late DDR time points, we performed the analysis described above using the TRRUST (Han et al., 2015) and the DisGeNET (Piñero et al., 2017) databases, respectively (Annex: Figure 7.5). We found that the 24-hour time point was in general more enriched for the transcription factor regulatory interactions. We identified a total of seven significantly overrepresented regulatory networks, four of which were significantly overrepresented for 0.5 h time point. Interestingly, the terms with the highest significance for 24 h were the TP53-regulated network and MYC-regulated network, and MYC-regulated network for 0.5 h (Annex: Figure 7.5A). Both TP53 and MYC were shown to regulate a wide range of genes coding proteins and RNAs that coordinate key processes in cancer (Sullivan et al., 2018; Gabay et al., 2014). The TP53 was found to be inactivated in many cancers, while MYC was found to be activated. The enrichment of the two different regulatory networks at early and late DDR signaling could signify the different ubiquitin-dependent processes but has to be considered carefully due to the obvious cell type bias (May et al., 1991).

The analysis of the disease associations showed an overrepresentation of various cancer types among the terms (Annex: Figure 7.5B), which agrees with the result of the transcriptionally regulated networks. In total 20 disease terms were overrepresented among the hits of the 24 h time point, 10 of which were overrepresented among the 0.5 h hits. The 24 h post-irradiation time point was more enriched with the functional terms than the 0.5 h with the higher p values. Among the disease terms, only two were not directly related to cancer but were annotated as congenital skin disorders linked to genome instability and overrepresented among the hits of 24 h post-irradiation: poikiloderma of Kindler (Kindler photodermatitis syndrome) and aplasia cutis congenita. Taken together, the findings indicate that the novel ubiquitin modifiers identified in the screen could be potential targets for anti-cancer therapy.

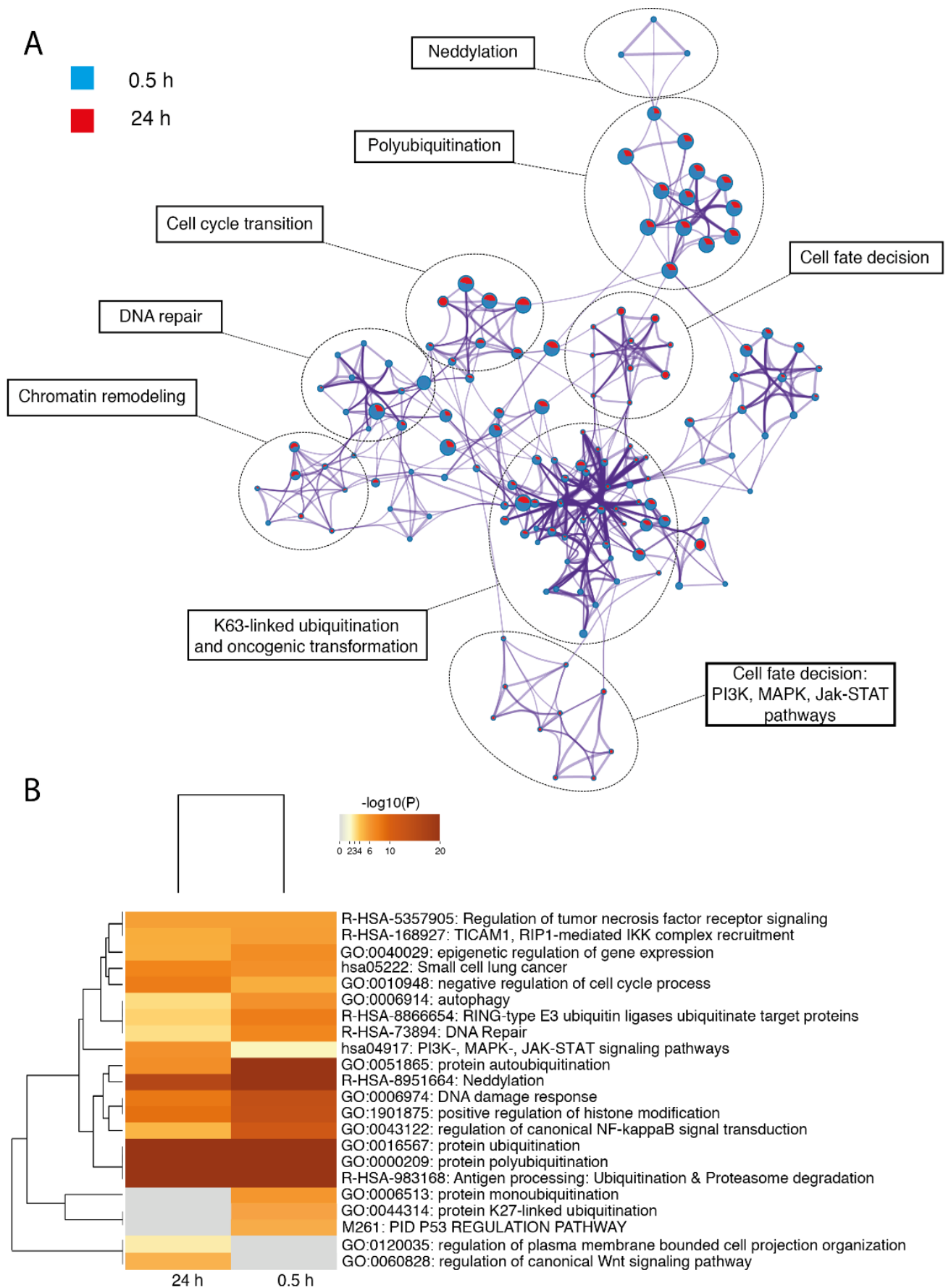


Figure 4.9. Comparative functional and protein-protein interaction profiling of the hits at 0.5 h and 24 h post-irradiation time points. (A) Custom network of the GO terms and protein-protein interactions. Each

term is represented by a circle node. The nodes are shown as pie charts, where the size of a pie is proportional to the total number of hits that fall into that specific term. The pie charts are color-coded based on the hit list identities, where the size of a slice represents the percentage of hits under the term that originated from a time point. The edges represent the functional and physical protein-protein interaction score. Terms with a score > 0.4 are linked by an edge with the thickness of the edge representing the strength of the data supporting it. The network was visualized with Metascape and Cytoscape with “force-directed” layout and with edge bundled for clarity. Selected clusters of terms are highlighted in the network, and their names and examples of hits are given. (B) Comparative heatmap of enriched GO terms across 0.5 h and 24 h hits lists, colored by p values. Terms with a p-value < 0.01, a minimum count of 3, and an enrichment factor > 1.5 are collected and grouped into clusters based on their membership similarities. Significant terms were then hierarchically clustered into a tree based on Kappa-statistical similarities among their gene memberships. Then 0.3 kappa score was applied as the threshold to cast the tree into term clusters. The term with the best p value within each cluster was chosen as its representative term and displayed in a dendrogram. The heatmap cells are colored by their p values, grey cells indicate the lack of enrichment for that term in the corresponding hit list.

We hypothesized that these differences at least partially come from the protein-protein interactions and sharing of the ubiquitin modifiers between the enzymatic complexes. To test this assumption, we performed protein-protein enrichment analysis for physical interactions between single hits. The resulting network was further narrowed down by applying the MCODE algorithm (Bader and Hogue, 2003). As a result, we obtained the densely connected network components that corresponded to the hits with the highest physical interaction confidence (Figure 4.10A). We identified six network components, all of them except one including the hits of both time points. The biggest network component was represented by a big cluster of hits united by interactions between themselves and CDC34, the hit common for both 0.5 h and 24 h time points. Inside this network component, CDC34 was found to physically interact with 14 hits at 0.5 h post-irradiation and with five hits at 24 h, two of which are common for both time points as well. Most of the network components identified included one or more hits shared between 0.5 h and 24 h, which confirmed our hypothesis.

To investigate ubiquitin-dependent events significant for both DNA damage signaling and repair, we selected the hits that showed an effect on the γ H2AX intensity at 0.5 h and 24 h post-irradiation. As was mentioned before, the hit lists for the early and late DNA damage signaling shared 39 proteins changing the γ H2AX signal intensity either in the same direction (uniform effect through time) or in different directions (multifactorial effect through time) (Figure 4.10B, Table 4.2). To find out how many of the shared hits were functionally annotated in our analysis, we visualized the hits for 0.5 h and 24 h according to both GO terms and gene identity. As we showed before, the time points were highly connected by the hits falling in the same functional categories. However, only 18 of the shared hits showed enrichment in the GO functional terms compared to the single-time point genes (Figure 4.10B). The rest of the shared hits were represented by the underrepresented functional terms or lack of annotation. Thus, most of the shared hits significant for the early and late DDR are novel ubiquitin modifiers with unknown molecular functions in DNA repair.

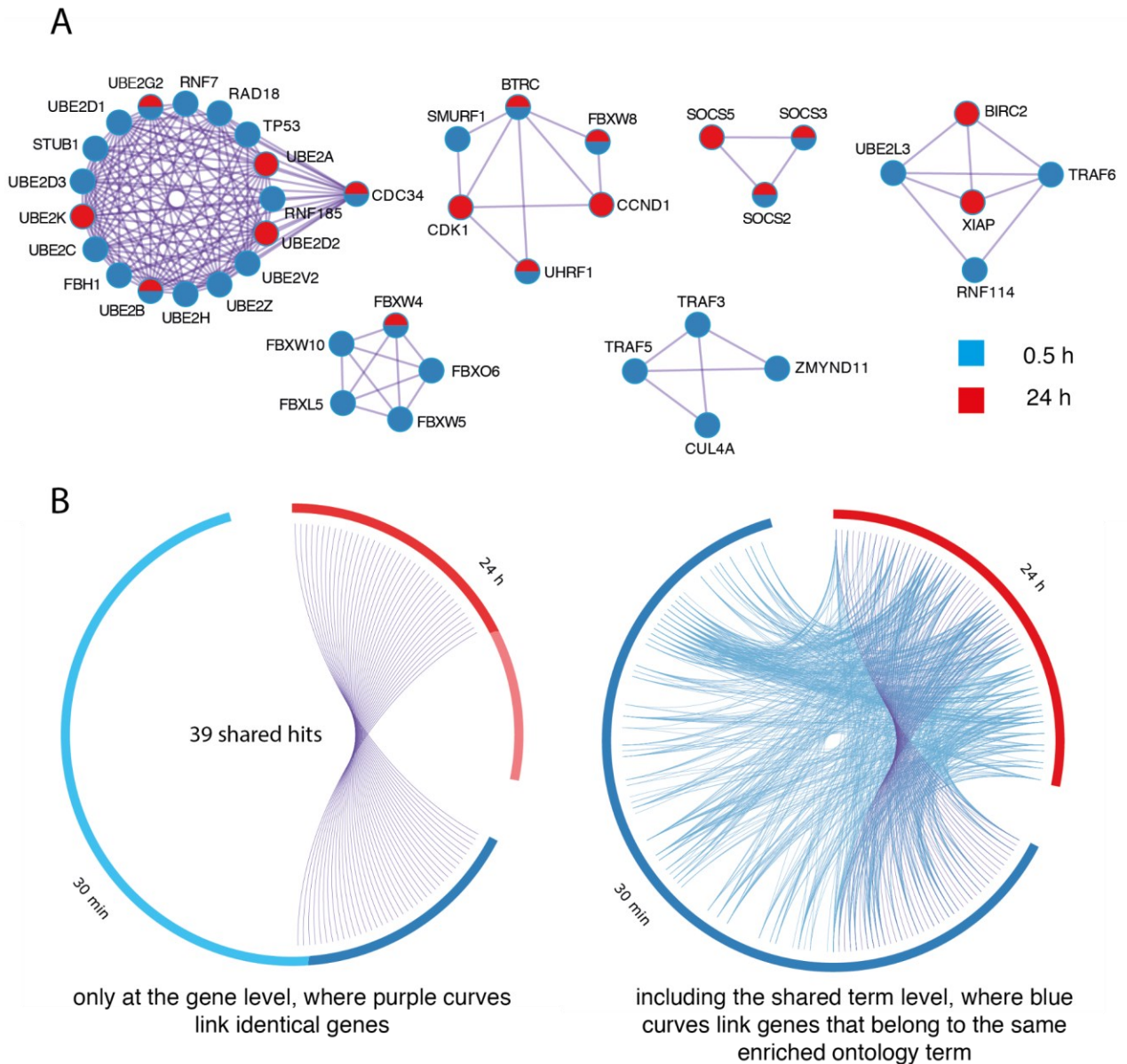


Figure 4.10. Protein-protein interaction components and hits overlap identified between the hit lists at 0.5 h and 24 h post-irradiation. (A) Protein-protein interaction network components of both 0.5 h and 24 h hit lists identified by the Molecular Complex Detection (MCODE) algorithm. Each hit is shown as a node, label is positioned next to the node. Nodes are colored according to the time point: blue - 0.5 h post-irradiation, red - 24 h post-irradiation, both blue and red - scored at both time points. The edges represent physical interaction only. (B) Overlap between hit lists at the gene level and at both the gene and the shared term level, shown as a Circos plot. The blue arc represents the 0.5 h hit list, where hits are arranged along the arc. The red arc represents the 24 h hit list, where hits are arranged along the arc. Hits common for both time points are connected by purple lines, and hits with the functional terms common for both time points are connected by blue lines.

Interestingly, most of the hits shared between the 0.5 h and 24 h post-irradiation had uniform downregulation effect through time corresponding to our scenario 1 of prolonged γ H2AX signaling disturbance (Figure 4.6B, Annex: Table 7.7). The second enriched scenario 2 with upregulation at 0.5 h and downregulation at 24 h suggested the overactivation of γ H2AX signaling

with more efficient repair. Among the shared hits only CCND1 protein showed the upregulation of the γ H2AX signal intensity at 24 h post-irradiation, corresponding to the scenario 7. Among the shared hits we identified proteins of the same families having the same effect on the γ H2AX intensity: FBXL15 and FBXL18 both downregulated γ H2AX intensity through time, FBXW4 and FBXW8 both upregulated γ H2AX intensity at 0.5 h and downregulated it at 24 h, the latter was observed for the E2 enzymes UBE2B and UBE2G2. Moreover, the proteins known to be involved in the same biological process, e.g. transcriptional silencing by the PRCs, showed the same effect on γ H2AX intensity as well (BMI1 and PHF19 - downregulation through time) (Annex: Table 7.7). The correlation observed between the protein families and the effect on the γ H2AX signaling suggested novel physical and functional interactions potentially within an E3 ligase complex. In summary, we identified 39 novel ubiquitin modifiers involved in the chromatin response to double-strand break from early till late DDR stage. The structural and functional clustering of the hits revealed novel interactions within the ubiquitin-dependent DDR signaling.

4.3 Small-scale 4D screen for mapping repair pathway preference

Small-scale 4D screen design and rationale

We aimed to validate the role of the hits obtained in the DNA damage signaling and elucidate the DNA repair pathway preference of the E3 ligases identified. We analyzed the 39 genes identified as common for the both time points for their cellular localization, molecular function in the DDR and antibody availability. For the small-scale 4D screen we chose the genes that are localized in the nucleus, preferentially with functional interactions with known DDR factors and high-quality antibody available with high sensitivity for immunofluorescence. As a result, we compiled a list of 33 genes for a small-scale 4D screen for the DNA repair pathway preference based on the following criteria: (1) proteins affect both 0.5 h and 24 h time points and are annotated or predicted to be localized in the nucleus, (2) they are hit proteins with highly statistically significant effect for either 0.5 h or 24 h time points, (3) they are hit proteins holding structural domains reported in DDR (Table 4.2). Additionally, we included four genes encoding known DDR factors that we identified as hits in the ubiquitinome-wide screening. We named the four genes “positive controls” for their well-studied molecular function in DNA repair (RAD18, RNF168, HUWE1, BRCA1). We ran a gene ontology (GO) analysis on the subset of the genes chosen for the 4D small-scale screen (Figure 4.11). We identified several GO functional clusters connected, some being more expected than others, for example, DNA repair and ubiquitination clusters. Among others, the hits fell into DNA replication and transcription, chromatin remodeling, cell cycle progression, and immune response clusters. Remarkably, the genes selected for the 4D small-scale screen showed a strong clustering into such categories as phosphorylation-directed signaling, neddylation, and neurogenesis. The cell death and cancer cluster was tightly connected to the clusters of DNA repair, cell cycle, and ubiquitination, suggesting a potential of the hits for anti-cancer therapy (Figure 4.11).

We assembled a small siRNA library by selecting the siRNA variants per gene that showed the most significant effect in the ubiquitinome-wide screening (Annex: Table 7.7). We chose three siRNA variants for each gene that showed a statistically significant effect (p value) on the γ H2AX intensity with the highest effect magnitude (fold change). For the small-scale screen design, we chose a layout of 384-well plates. The 33 selected genes represented by 3 siRNA variants in triplicates made up 297 wells per plate, the rest of the wells were covered by positive controls (in 3 siRNA variants in triplicates) and negative controls (non-targeted siRNAs and wells without

siRNAs). As for the ubiquitinome-wide screening, we used reverse transfection to obtain the knockdown phenotypes: the siRNAs were pre-printed as described in Materials and Methods (3.12), and HeLa Kyoto cells were seeded on top. The cells were subjected to 5 Gy of X-ray irradiation to induce DNA double-strand breaks and fixed at 0.5 h (early), 3 h (mid), 6 h (mid-late), and 24 h (late) post-irradiation (Figure 4.12). We have chosen two repair proteins as markers of two main double-strand break repair pathways: 53BP1 as a marker of non-homologous end joining (NHEJ) and RAD51 as a marker of homologous recombination (HR). In total, each time point post-irradiation and unirradiated control was represented by two 384-well plates, one plate was stained for the γ H2AX and 53BP1 and the other for γ H2AX and RAD51 (Figure 4.12). To characterize the effect of the hits on the DNA repair pathways, we acquired high-content imaging data in the form of Z stacks. We used the γ H2AX signal as a proxy for the DNA damage signaling as well as the quantification of 53BP1 and RAD51 to identify the DSB repair pathway affected. 4D foci quantification as well as colocalization analysis were performed. As expected from the literature (Doil et al., 2009; Feng and Zhang, 2012; Zhao et al., 2017), we detected the impairment in 53BP1 recruitment in irradiated cells defective for RNF168 and impairment in RAD51 recruitment in irradiated cells lacking BRCA1 (Figure 4.12), validating that the assay design is suitable. The data were further subjected to a custom image analysis workflow (Figure 4.13).

Table 4.2. Summary of the hits chosen for the small-scale 4D screen for the DNA repair pathway preference. The gene names, Ensembl ID, Gene ID, and effect on the γ H2AX intensity at 0.5 h and 24 h time points are given. D&R - the column identifies whether the hit has a significant effect for both time points (Y - yes) or only one (N - no).

	Gene name	Highest siRNA identifier	Ensembl ID	Gene ID	Damage 0.5 h	Repair 24 h
1	RNF8	s17201	ENSG00000112130	9025	↓	↓
2	TRIM27	s11960	ENSG00000204713	5987	↑	↓
3	PHF19	s25161	ENSG00000119403	26147	↓	↓
4	TRIM46	s36935	ENSG00000163462	80128	↑	-
5	IRF2BP1	s25155	ENSG00000170604	26145	↓	↓
6	TRIM60	s46624	ENSG00000176979	166655	↑	↑
7	FBXO11	s37047	ENSG00000138081	80204	↓	↓
8	CDK2	s204	ENSG00000123374	1017	↑	↓
9	PHF17	s36724	ENSG00000077684	79960	-	↑
10	CDC34	s2764	ENSG00000099804	997	↑	↓
11	HLTF	s13136	ENSG00000071794	6596	-	↓
12	RNF7	s18475	ENSG00000114125	9616	↑	-
13	CCNB1	s2516	ENSG00000134057	891	↓	↑
14	BIRC3	s1451	ENSG00000023445	330	↑	↓
15	FBXO38	s37604	ENSG00000145868	81545	↓	↓
16	CBLC	s24225	ENSG00000142273	23624	↑	-
17	CCND1	s230	ENSG00000110092	595	↓	↑
18	TRIP12	s17810	ENSG00000153827	9320	↑	↓

19	SOCS3	s17190	ENSG00000184557	9021	↓	↓
20	XIAP	s1454	ENSG00000101966	331	-	↓
21	FBXL18	s36852	ENSG00000155034	80028	↓	↓
22	HERC2	s17062	ENSG00000128731	8924	↓	-
23	ZNF592	s18534	ENSG00000166716	9640	↑	↓
24	BRPF3	s25918	ENSG00000096070	27154	↓	↓
25	PHRF1	s33541	ENSG00000070047	57661	↓	-
26	BAZ1B	s17210	ENSG00000009954	9031	↓	↓
27	STUB1	s195025	ENSG00000103266	10273	↑	-
28	UBOX5	s22597	ENSG00000185019	22888	↑	↓
29	PRPF19	s223754	ENSG00000110107	27339	↓	↓
30	BAHD1	s22604	ENSG00000140320	22893	↓	-
31	CXXC1	s26937	ENSG00000154832	30827	↑	-
32	CHD4	s2985	ENSG00000111642	1108	↓	-
33	DCUN1D1	s28891	ENSG00000043093	54165	↓	-
Positive controls						
34	RAD18	s32296	ENSG00000070950	56852	↑	-
35	RNF168	s46599	ENSG00000163961	165918	↑	-
36	BRCA1	s458	ENSG00000012048	672	↓	-
37	HUWE1	s19596	ENSG00000086758	10075	↓	-

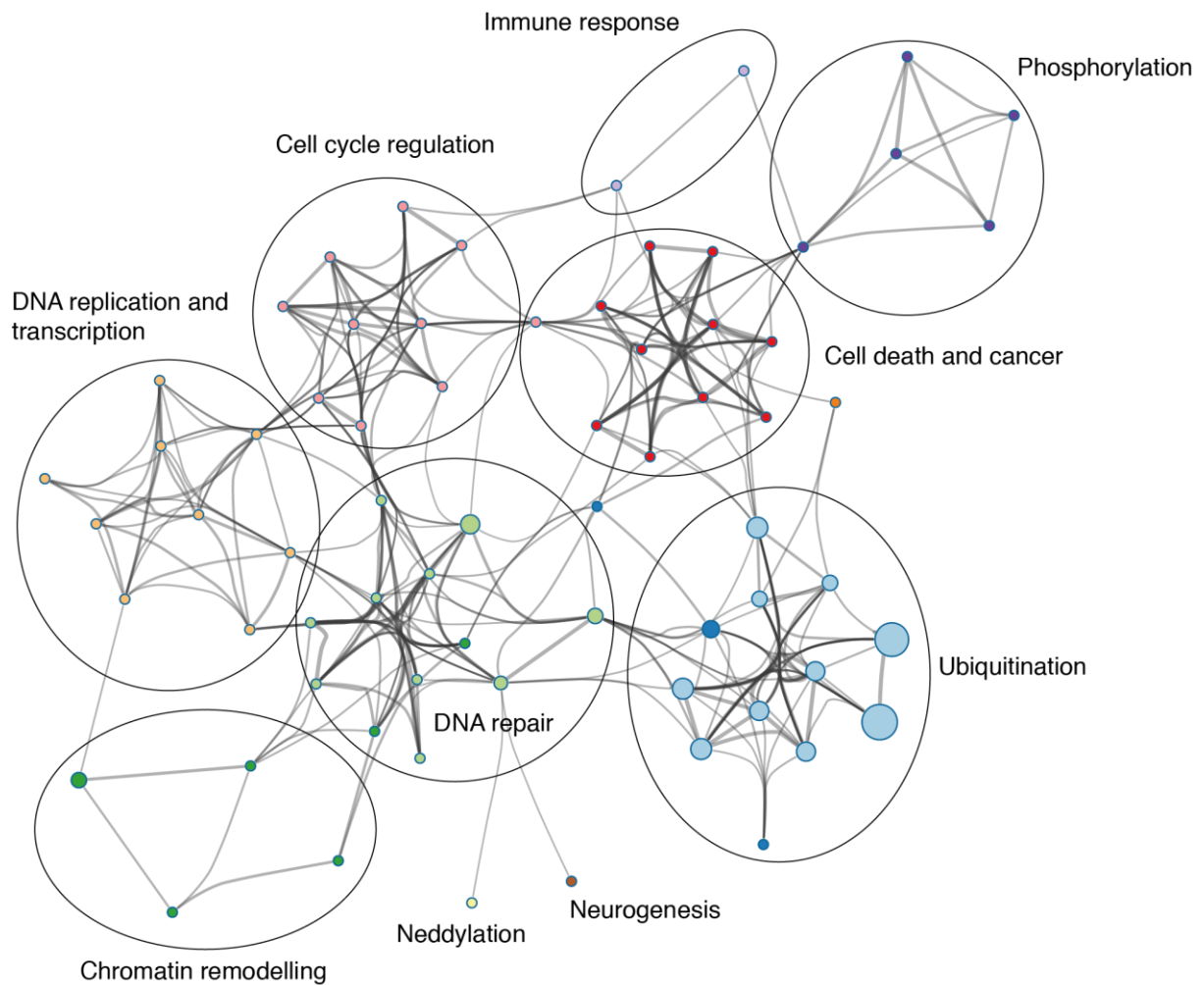


Figure 4.11. Gene ontology analysis of the 4D small-scale screen genes. Each GO term is represented by a circle node, where its size is proportional to the number of hit genes that fall into that term, the nodes that belong to the same parental GO term are colored the same. The edges represent the functional and physical protein-protein interaction score. Terms with a score > 0.4 are linked by an edge with the thickness of the edge representing the strength of the data supporting it. The network was visualized with Metascape and Cytoscape with “force-directed” layout and with edge bundled for clarity. Selected clusters of terms are highlighted in the network, their names are given.

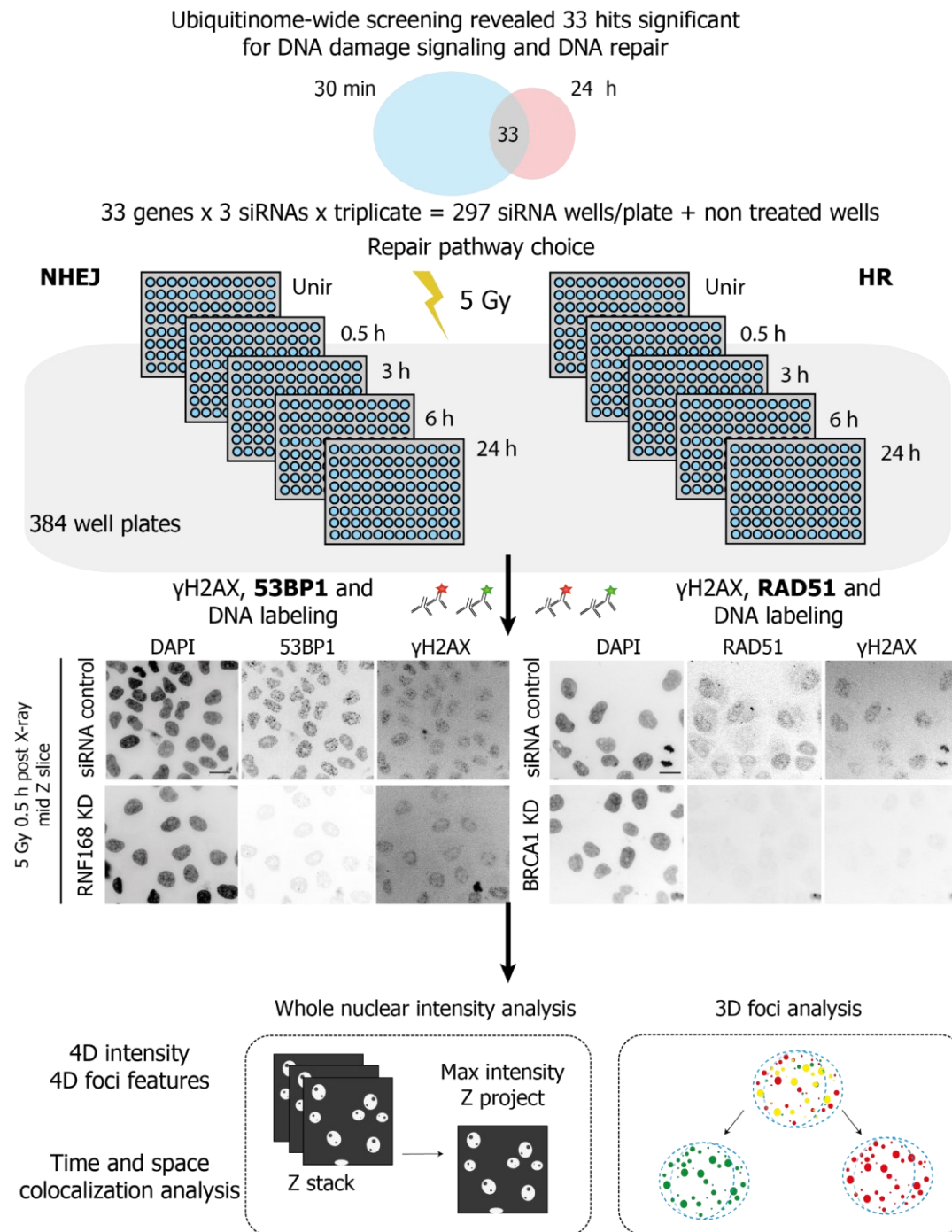


Figure 4.12. Small-scale 4D screen design. The scheme is presented in the form of a flowchart consisting of three major parts: reverse transfection in the plate layout, staining, and analysis. The reverse transfection of the HeLa Kyoto cells on the 384-well plates was performed as described for the ubiquitinome-wide screen. After 48 h the cells reach knockdown phenotype and are subjected to 5 Gy X-rays. The arrays are fixed according to the time points post-irradiation, including unirradiated arrays. The images represent the γ H2AX, 53BP1, and RAD51 signals in siRNA control cells and in the cells with knockdown of RNF168 or BRCA1, respectively. The arrays were imaged with an automated imaging platform and the data were analyzed in the KNIME Analytics Platform. The image analysis was performed as a whole-nuclear intensity analysis and 3D foci analysis. The detailed version of the image analysis with a description of the filters and data thresholding is described in Figure 4.13.

We created a custom image analysis workflow in the KNIME Analytics Platform to interpret the data obtained in the small-scale 4D screen. As mentioned before, we performed two types of image analysis on the same imaging data using two image analysis workflows. The whole-nuclear intensity analysis was performed similarly to the image analysis of the ubiquitinome-wide screening data (Figure 4.13A, whole-nuclear intensity analysis) with the difference that the 3D stack images were projected to maximum intensity. To ensure the correct quantification of the fluorescent signal, the dynamic range was adjusted before the imaging on the control wells and on the test wells expected to show the γ H2AX intensity increase. The data were acquired as 16-bit images to allow better discrimination between the pixel intensities. The images projected were used to extract total γ H2AX, 53BP1 and RAD51 intensity per nucleus. The total intensity was normalized by the total DAPI intensity as described previously and intensity fold change was calculated between the siRNA wells and control wells (no siRNA treatment/non-targeted siRNA wells) per plate. Mean and median intensities of γ H2AX, 53BP1, RAD51 per nucleus, nuclei number and the fold change value per well for each time point were used in the analysis.

To characterize the γ H2AX, 53BP1 and RAD51 signaling change at the single double-strand break level, the images were subjected to custom 3D foci analysis. As before, the DAPI channels were used for nuclei segmentation, and γ H2AX, 53BP1 and RAD51 channels were used for the foci segmentation by the custom wavelet transform algorithm (Figure 4.13A, 3D foci analysis). The parameters of the wavelet transform algorithm were adjusted for segmentation of the γ H2AX, 53BP1 and RAD51 separately on the mock/non-siRNA transfected cells (Figure 4.13B). The foci masks were overlaid with the nuclei mask for foci quantification and with each other to quantify colocalization events (Figure 4.13C). Mean, sum focus intensities and focus size of γ H2AX, 53BP1, RAD51 per nucleus, foci count per nucleus, colocalization number and the fold change value per well for each time point were used in the analysis.

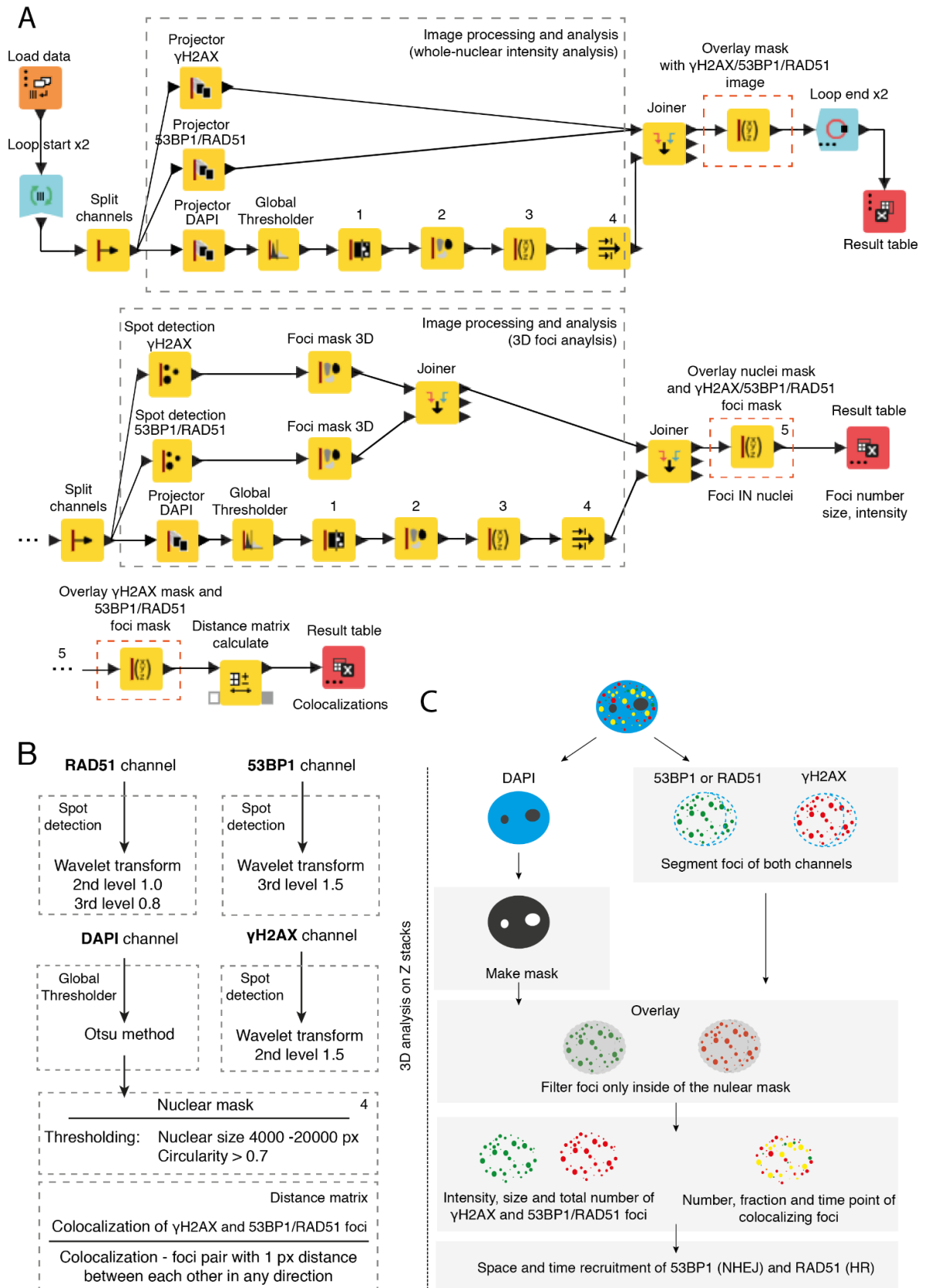


Figure 4.13. Image analysis of the data obtained in the small-scale 4D screen. (A) A simplified version of the modular image analysis workflow used for the analysis of the high-throughput data in KNIME software. The KNIME original node icons are presented. Two main workflows are depicted: whole-nuclear intensity

analysis and 3D foci analysis. The identical parts of the workflow are hidden behind a three-dot ellipsis. 1- “Fill Holes” node, 2 - “Connected component analysis” node, 3 - “Image segment features” node, 4 - “Row filter” node, 5 - “Image segment features” (Overlay nuclear mask and γ H2AX/53BP1/RAD51 foci mask). (B) Schematic representation of the DAPI, γ H2AX, 53BP1, RAD51 channels segmentation parameters in the Global Thresholding (DAPI) and Spot detection node, nuclear population thresholding parameters, and colocalization parameters. 4 - nuclear population thresholding parameters in the Row Filter node. (C) Scheme of the 3D foci analysis steps.

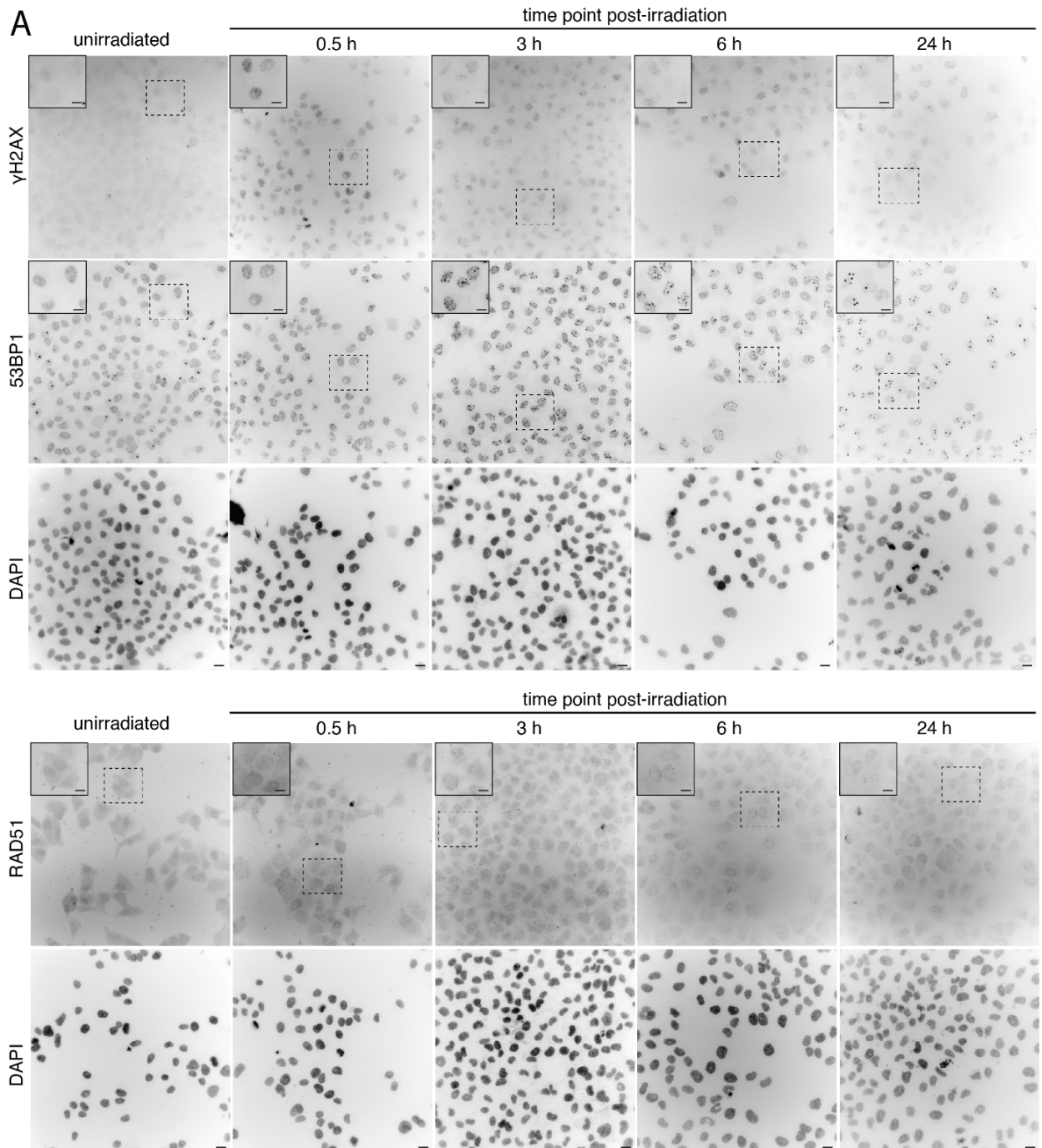
Validation of small-scale 4D screen

As expected, the total nuclear γ H2AX signal in the mock/non-siRNA transfected cells was increased at 0.5 h post-irradiation and gradually decreased over time showing lower phosphorylation levels at 3 h and 6 h post-irradiation with residual γ H2AX signal detected at 24 h (Figure 4.14A, B). That same kinetics was true for the number of γ H2AX foci per nucleus observed in the non-siRNA transfected cells. The sum intensity of γ H2AX focus per nucleus increased post-irradiation and showed the highest value at 3 h, reflecting the increase in average focus size (Figure 4.14B). After the irradiation, the accumulation of the 53BP1 repair protein started rapidly reaching its maximum at 3 h as shown by quantification of the whole nuclear 53BP1 intensity and sum focus intensity per nucleus. In comparison to the chromatin DDR signaling such as the γ H2AX, 53BP1 was expected to accumulate at the later time points to participate in the repair pathway choice. Interestingly, although the intensity parameters confirmed this idea, the highest number of 53BP1 foci per nucleus was observed as early as 0.5 h post-irradiation (Figure 4.14B). The response of the homologous recombination player RAD51 started with the increase in the protein amount in the nucleus at 0.5 h post-irradiation, however, with only a few foci formed. At the later time points, RAD51 got recruited to the DNA breaks shown by the increase in the foci number, foci size, and sum focus intensity per nucleus (Figure 4.14B). In agreement with other studies (Osipov et al., 2015), the mock/non-siRNA transfected cells in the small-scale screen showed RAD51 response increase up to 6 h post-irradiation.

Next, we verified the DDR effect in the cells with knockdown of the “positive controls” (RAD18, RNF168, BRCA1, HUWE1) (Table 4.2). The four proteins are known as ubiquitin modifiers with a role in DNA damage signaling and repair. The cells with the depletion of the RNF168 protein in the ubiquitinome-wide screening layout showed upregulation of the γ H2AX signal at 0.5 h post-irradiation. In the small-scale screen, we confirmed this effect by quantifying the whole nuclear γ H2AX intensity, γ H2AX sum focus intensity, and foci number per nucleus (Figure 4.15). The γ H2AX signal parameters increased not only at 0.5 h post-irradiation but at the later time points, showing both upregulation and persistence of the signal. The RNF168 ligase was previously characterized as a factor upstream to 53BP1 and, together with RNF8, necessary for 53BP1 recruitment to the site of a double-strand break (Mattioli et al., 2012; Nowsheen et al., 2018). In agreement with it, we observed a significant decrease in the 53BP1 total focus intensity and foci number per nucleus after the irradiation in cells with knockdown of RNF168 (Figure 4.15). Interestingly, the cells with knockdown of RNF8 showed similar defects of the 53BP1 signaling, reflecting the synergistic role of both RNF8 and RNF168 in the assembly of the repair focus (Annex: Figure 7.6).

In the ubiquitinome-wide screen, cells with depletion of BRCA1 showed significant downregulation of the γ H2AX signal at the early stage of the damage signaling (Table 4.2) and that

was observed in the format of the 4D small-scale screen as well, both at the level of foci number and mean focus intensity per nucleus (Figure 4.15). Damaged cells with knockdown of the BRCA1 demonstrated impaired RAD51 recruitment to the sites of the damage in agreement with the previously published data (Feng and Zhang, 2012; Zhao et al., 2017).



B

mock/non-siRNA transfected cells

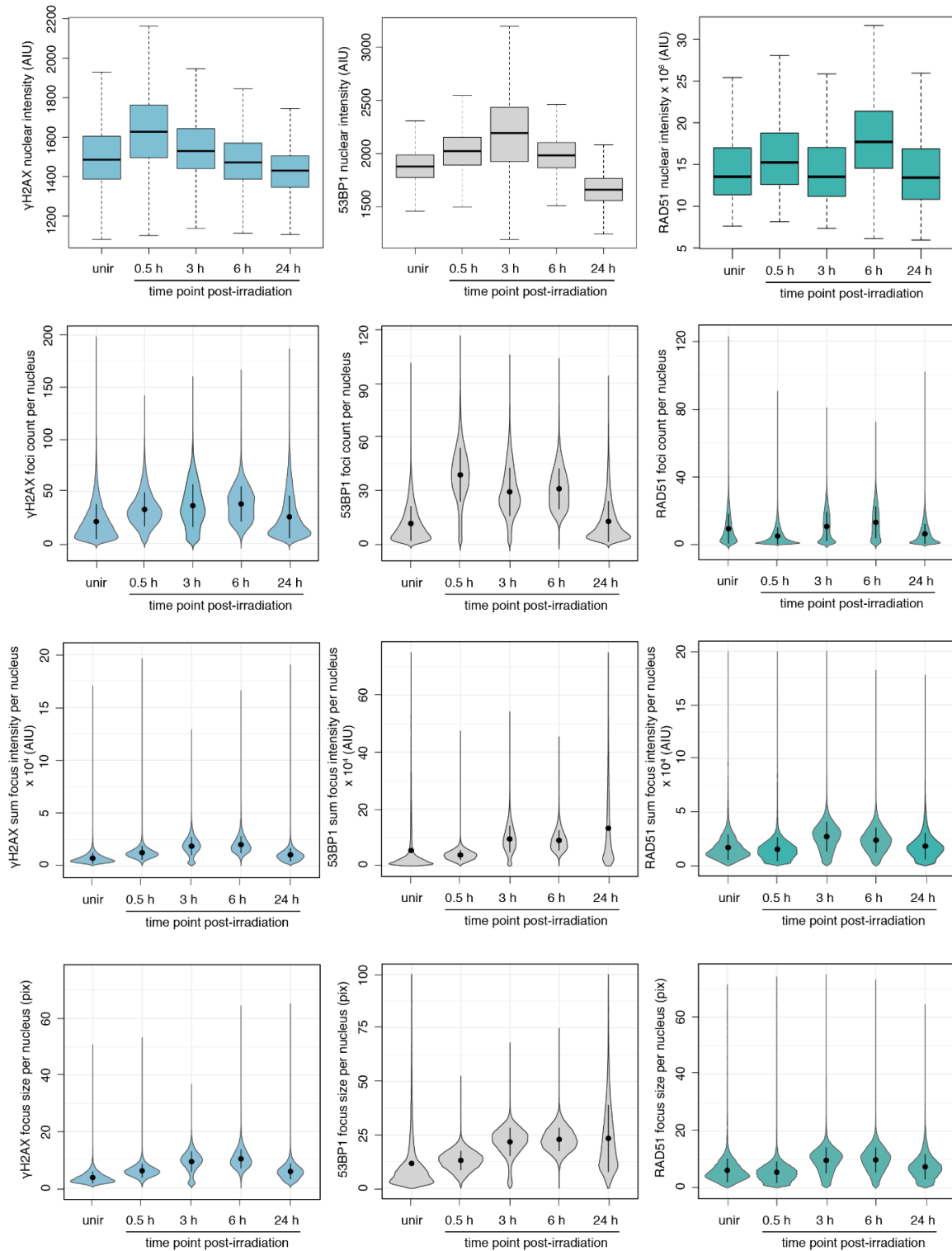
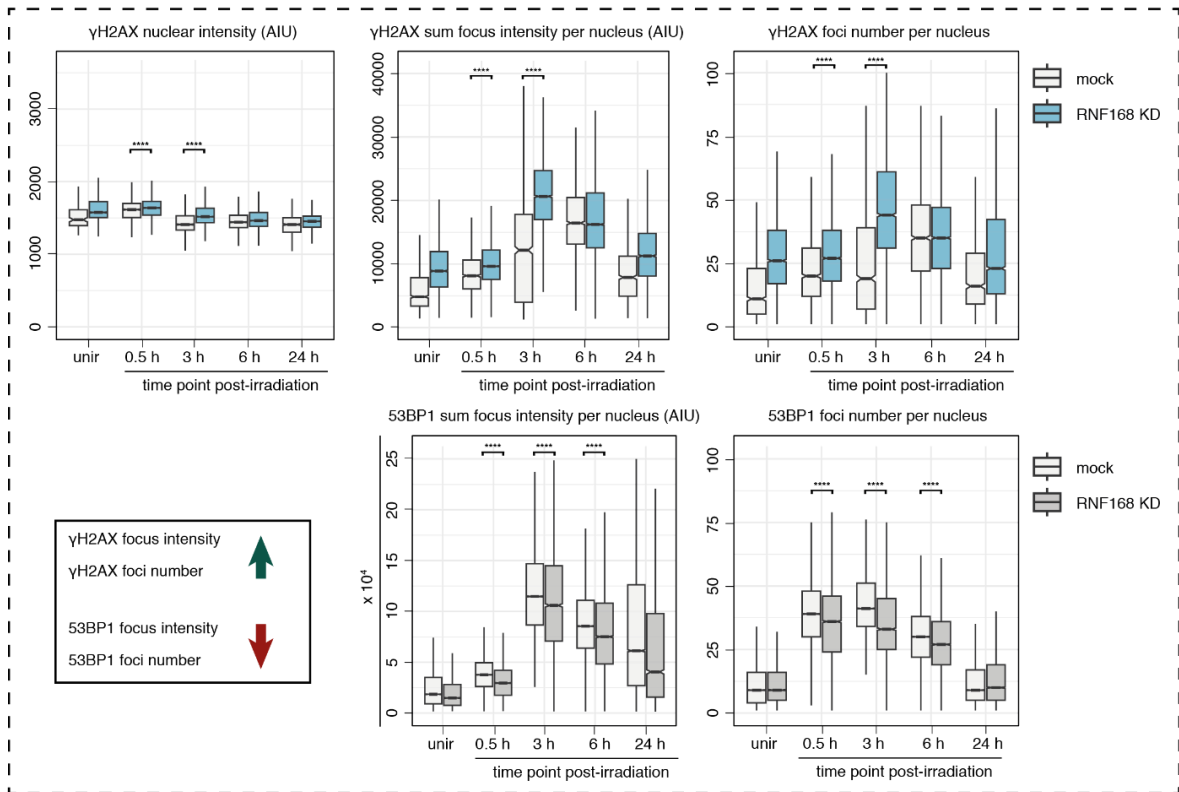


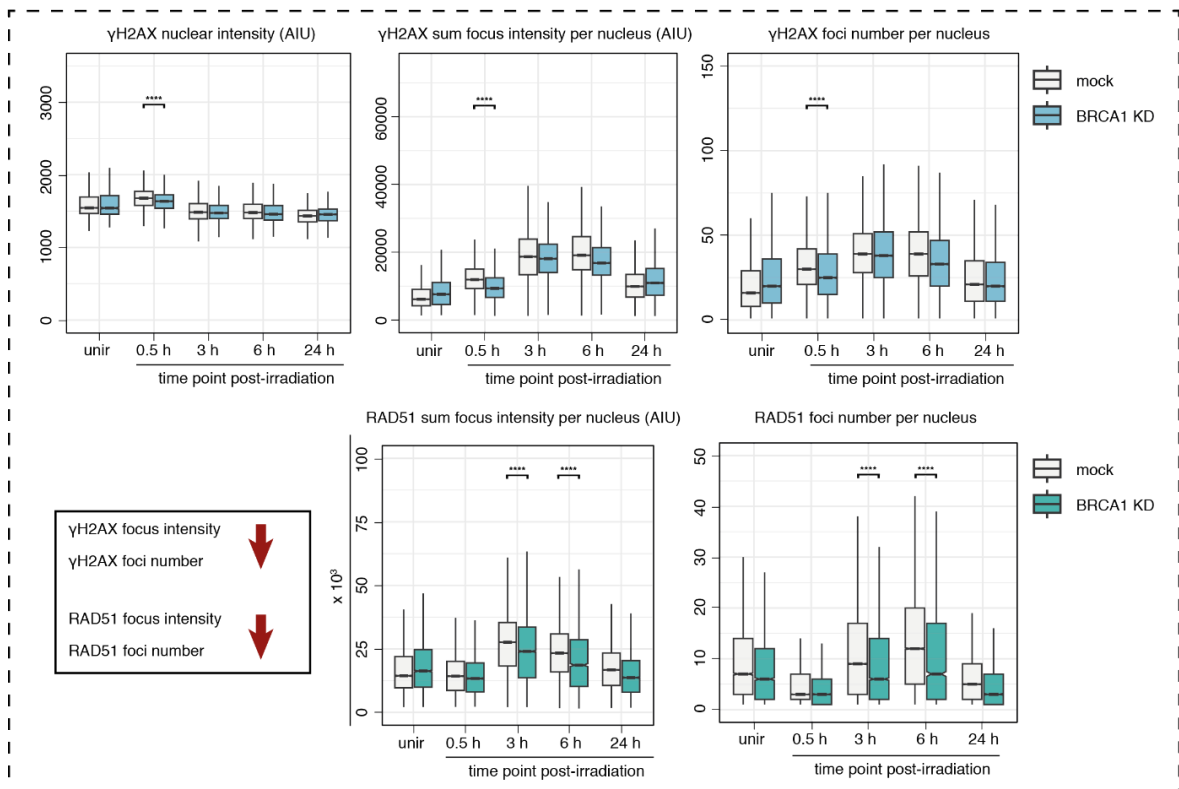
Figure 4.14. Irradiation response of mock/non-siRNA transfected cells in the small-scale 4D screen. (A) Representative images of mock/non-siRNA transfected cells showing accumulation and resolution of the γ H2AX, 53BP1, RAD51 signal in HeLa Kyoto nuclei after exposure to X-ray irradiation (5 Gy). The dashed rectangle depicts the area of the image that is zoomed up. Scale bar 10 μ m. (B) Quantification of the γ H2AX, 53BP1, RAD51 whole nuclear intensity, foci number, and sum focus intensity per nucleus in mock/non-siRNA transfected cells at the indicated times after irradiation. For box plots: the horizontal line represents

the mean. For violin plots: the black dot represents the mean, and the vertical line represents the mean \pm standard deviation.

RNF168 KD



BRCA1 KD



HUWE1 KD

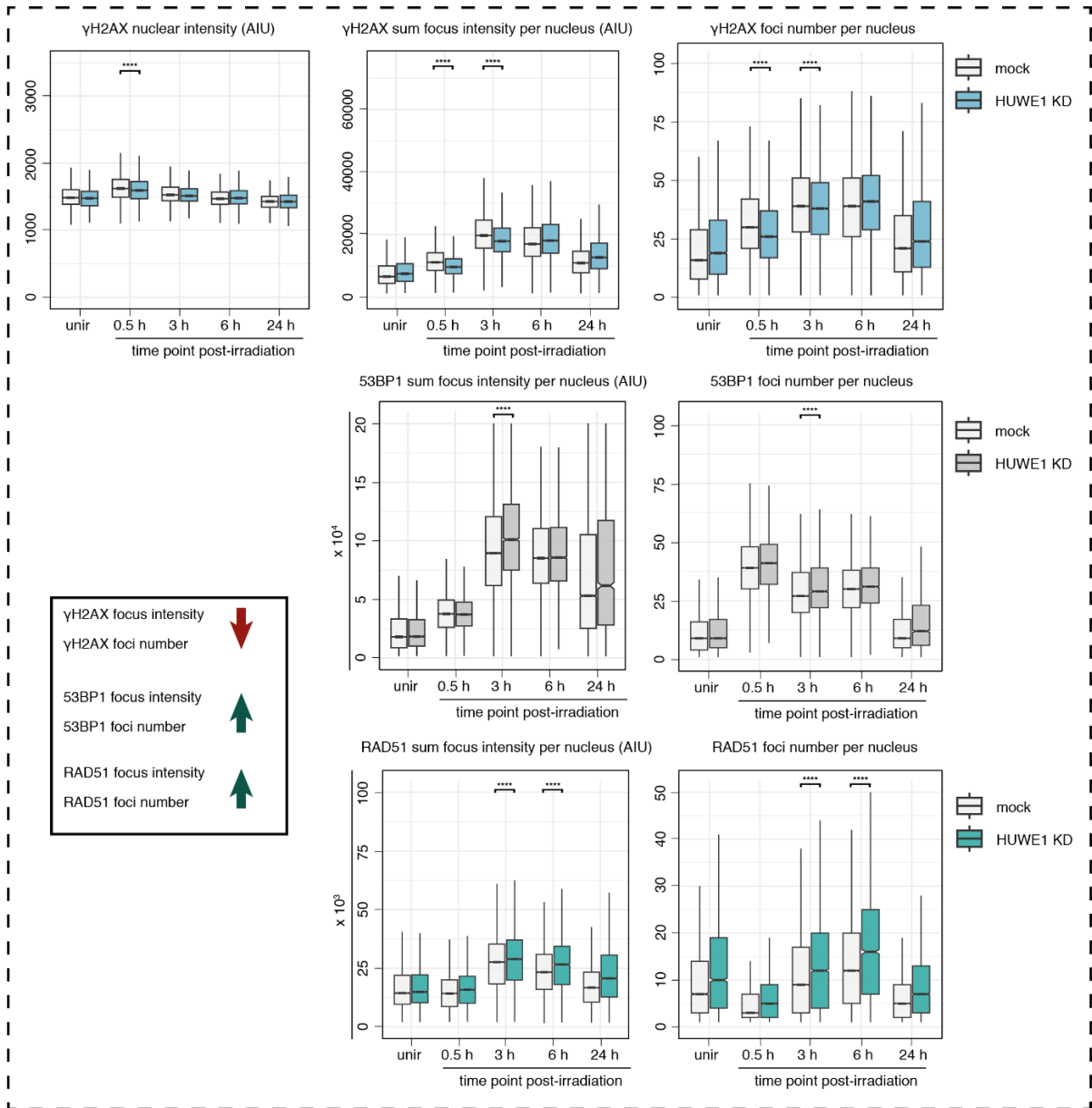


Figure 4.15. Depletion of the known ubiquitin modifiers alters DDR kinetics. The quantification of the DDR kinetics in cells with knockdown of four ubiquitin modifiers with known function in DNA damage signaling and repair: RNF168, BRCA1, HUWE1. For all plots, mock is a pooled population of mock-transfected and non-siRNA transfected cells from either one plate corresponding to the indicated time point (53BP1 and RAD51 response quantification, total 51 wells per plate, approximately 200 cells per well) or two replicate plates corresponding to the indicated time point (γ H2AX response quantification, total 102 wells, approx 200 cells per well). The knockdown population was represented by the wells with three siRNA variants per gene of interest and their replicates (total minimum 9 wells per plate per gene, approximately 200 cells per well) corresponding to the indicated time point. Whole nuclear intensity of γ H2AX per nucleus, mean focus intensity of γ H2AX, 53BP1, RAD51 foci per nucleus, and number of γ H2AX, 53BP1, RAD51 foci per nucleus were determined in HeLa Kyoto cells at the indicated times after DNA damage induction (5 Gy). The box plot description as above. The outliers were omitted and not presented in the plot. **** $p < 0.001$ by Wilcoxon rank-sum test, for knockdown sample versus mock/non-siRNA transfected sample.

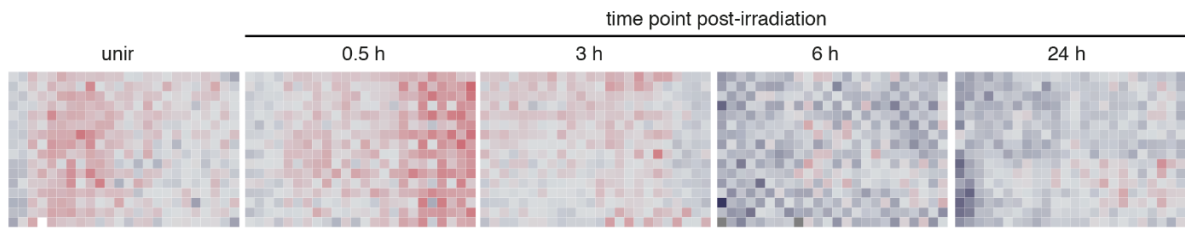
The HUWE1 ubiquitin ligase was described to ubiquitinate and neddylate multiple targets involved in the DNA damage response (Yi et al., 2015; Mandemaker et al., 2017; Cassidy et al., 2020; Guo et al., 2020). It was shown that HUWE1 mediates the ubiquitination and subsequent degradation of the histone H2AX in undamaged cells. At the same time, upon DNA damage formation, the HUWE1 activity is blocked and H2AX phosphorylation is promoted by the ATM kinase and SIRT6/SNF2H (Atsumi et al., 2015). Moreover, the γ H2AX is monoubiquitinated by HUWE1 at the stalled replication forks and this monoubiquitination was shown to be crucial for the stability of the phosphorylation similar to the monoubiquitination written by RNF168 and BMI1 (Choe et al., 2016; Wu et al., 2011a; Pan et al., 2011). Supporting the latter, both the ubiquitinome-wide screen and 4D small-scale screen demonstrated a decrease in the γ H2AX whole-nuclear and mean focus intensity as well as in the foci number per nucleus in the HUWE1 knockdown cells at 0.5 h post-irradiation and an increase in the foci number per cell later in the DDR indicating slower decay (Table 4.2, Figure 4.15). Interestingly, the HUWE1 loss induced upregulation of both 53BP1 and RAD51 signaling in damaged HeLa cells (Figure 4.15). While the molecular mechanism of the 53BP1 upregulation is unknown, the effect on the RAD51 was shown to be caused by ubiquitin-dependent MYC activation (Adhikary et al., 2005; Clements et al., 2020) or by affecting BRCA1 stability (Wang et al., 2014b).

Downregulation of hits identified in the screening alters kinetics of repair proteins

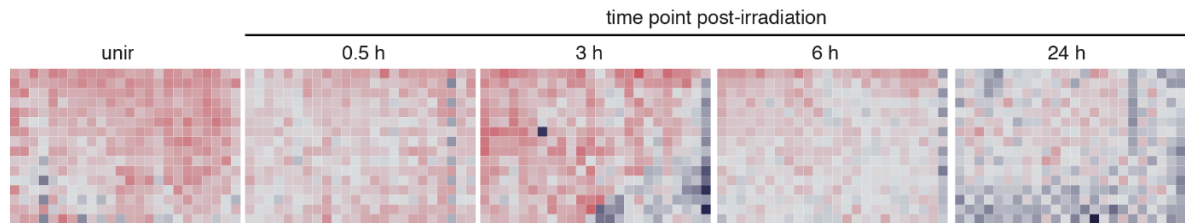
Next, we addressed the alterations in the cells with downregulation of the hits without known function in the DDR. The γ H2AX, RAD51, and 53BP1 whole-nuclear intensity and foci feature read-outs were transformed into the fold change values representing the difference from the non-siRNA-treated/mock-transfected controls. We observed different fold change values for the 53BP1 and RAD51 whole-nuclear intensity at the same time points and in the same knockdown cells (Figure 4.16A). Most of the knockdown cells showed a decline in the RAD51 whole-nuclear intensity at 6 h and 24 h post-irradiation compared to the control cells. In contrast, the 53BP1 whole-nuclear intensity was predominantly upregulated in the knockdown cells after the damage induction up until the 24 h time, when most cells failed to retain 53BP1 (Figure 4.16A). Two types of image analysis that we performed allowed us to relate the whole-nuclear protein levels directly to the single repair focus parameters (Annex: Figure 7.7). Upon DNA damage induction, we observed 53BP1 and RAD51 foci number per nucleus and sum focus intensity per nucleus changing in the knockdown and control wells (Figure 4.14B, 4.16B). Heat maps generated with data from the single focus analysis showed the hits whose depletion led to an increased number of both 53BP1 and RAD51 foci at the same time points after DNA damage compared with controls (Figure 4.16B). Likewise, we identified the hits whose depletion led to the opposite effect on the 53BP1 and RAD51 foci number at the same time points. The hits were qualified as universal players of both DSB repair pathways.

A

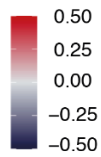
RAD51 - HR



53BP1 - NHEJ



log fold change sum protein intensity



B

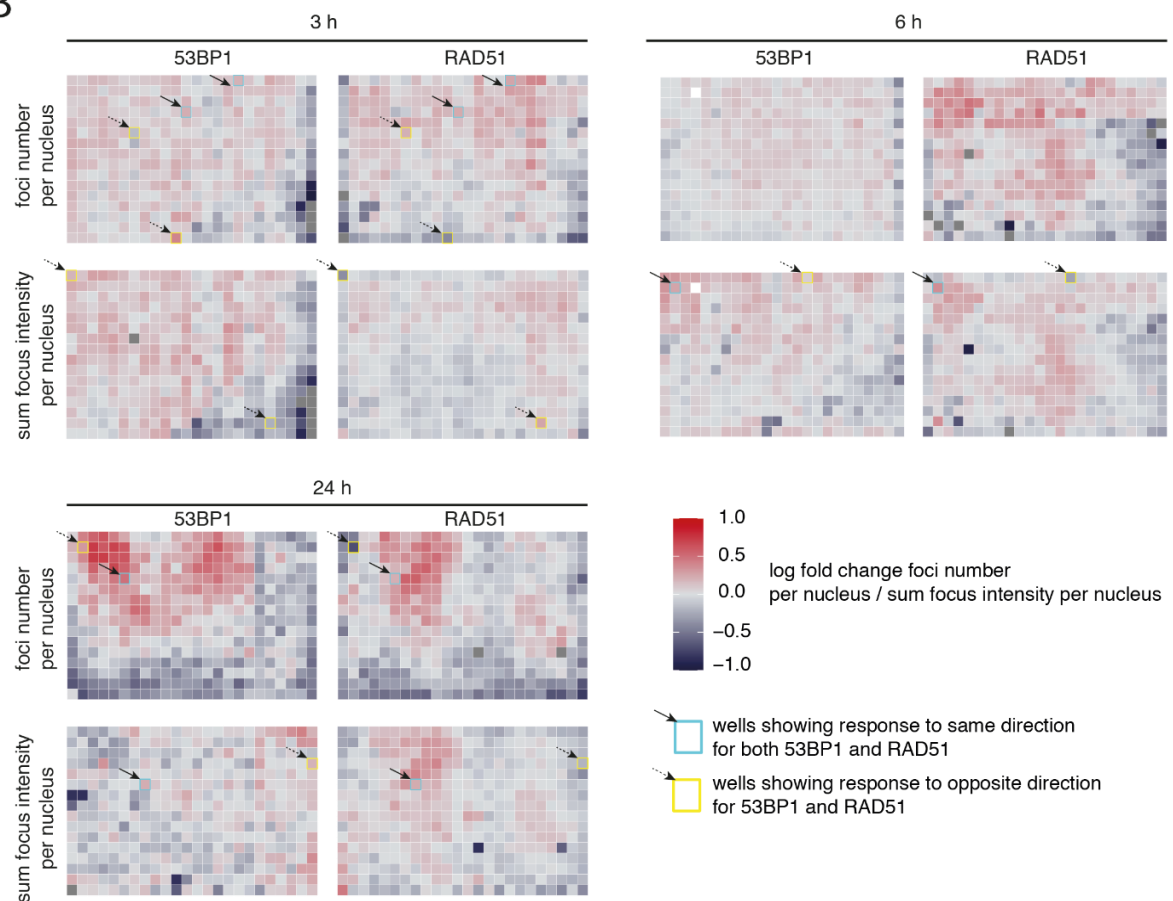


Figure 4.16. Downregulation of the hits identified in the screening alters the kinetics of repair proteins. (A) The repair proteins 53BP1 and RAD51 whole-nuclear intensity changes are represented by logarithmically

transformed fold change values and depicted as heat maps with the plate layout. According to the scale, the red color represents the upregulation of the signal compared to the non-siRNA-treated/mock-transfected controls, the blue color represents the downregulation of the signal compared to the non-siRNA-treated/mock-transfected controls, the white color represents the value equal to the mean value of the non-siRNA-treated/mock-transfected controls. The grey wells represent a value outside of the range presented. (B) The repair proteins 53BP1 and RAD51 foci number and sum focus intensity changes are represented by logarithmically transformed fold change values and depicted as heat maps with the plate layout. The scale is as in (A). The wells with the cyan frame highlight the same effect on the 53BP1 and RAD51 foci number or sum focus intensity at the same time point in the knockdown cells, and the wells with the yellow frame highlight the different effect on the 53BP1 and RAD51 foci number or sum focus intensity at the same time point in the knockdown cells. The wells show only a small share of all cases for representation.

The same was observed for the 53BP1 and RAD51 sum focus intensity (Figure 4.16B). We compared the sum focus intensity fold change between 53BP1 and RAD51 plates and identified knockdown phenotypes that led to either the same or opposite direction of kinetics change. Importantly, when compared for the same protein, the foci number and sum focus intensity per nucleus resembled each other in most cases for most time points, showing the connection between repair foci incidence and stability (Figure 4.16B, Annex: Figure 7.7).

The knockdown of the significant hits for both the NHEJ and HR pathways altered the kinetics of the repair proteins differently. For example, the lack of TRIM60 protein led to 53BP1 whole-nuclear levels upregulation at all time points post-irradiation except for 24 h when the 53BP1 levels decreased compared to the control cells (Figure 4.17). At the same time, the RAD51 whole-nuclear levels successively decreased in the knockdown cells after the damage induction. Another example of the hits whose knockdown led to the altered repair kinetics of both NHEJ and HR was the ZNF592 protein. The knockdown cells demonstrated a decrease of the 53BP1 and RAD51 levels in the mid-late time points post-irradiation (Figure 4.17).

In addition to the hits affecting both the NHEJ and HR and considered by us as universal components of the pathways irrespective of their direction of effect, we observed the hits whose depletion affected only one of the pathways for any given time point post-irradiation. The hits were considered to show a preference for the NHEJ or the HR (Figure 4.17). For example, among all the hits we identified TRIP12 and PRPF19 as the ubiquitin modifiers with a preference for the non-homologous end joining that was manifested through an altered 53BP1 response (Figure 4.17). Depletion of both of the hits led to upregulated whole-nuclear levels of 53BP1 protein in the knockdown cells and to minor or no difference in RAD51. Interestingly, the TRIP12 knockdown and PRPF19 knockdown provoked the upregulation in unchallenged and irradiated cells. The PRPF19 depletion affected only 3 h time point post-irradiation, while the lack of TRIP12 led to 53BP1 upregulation till 24 h after damage (Figure 4.17). For the HR, we found STUB1 and FBXO38 proteins to be a part of the pathway. Depletion of each of them led to a similar RAD51 kinetics phenotype where RAD51 was significantly upregulated early post-irradiation but was exhausted later compared to the non-siRNA-treated cells. The knockdown phenotypes of the STUB1 and FBXO38 proteins did not show a significant effect on the 53BP1 whole-nuclear intensity levels, thus we concluded that they showed a preference for the HR pathway.

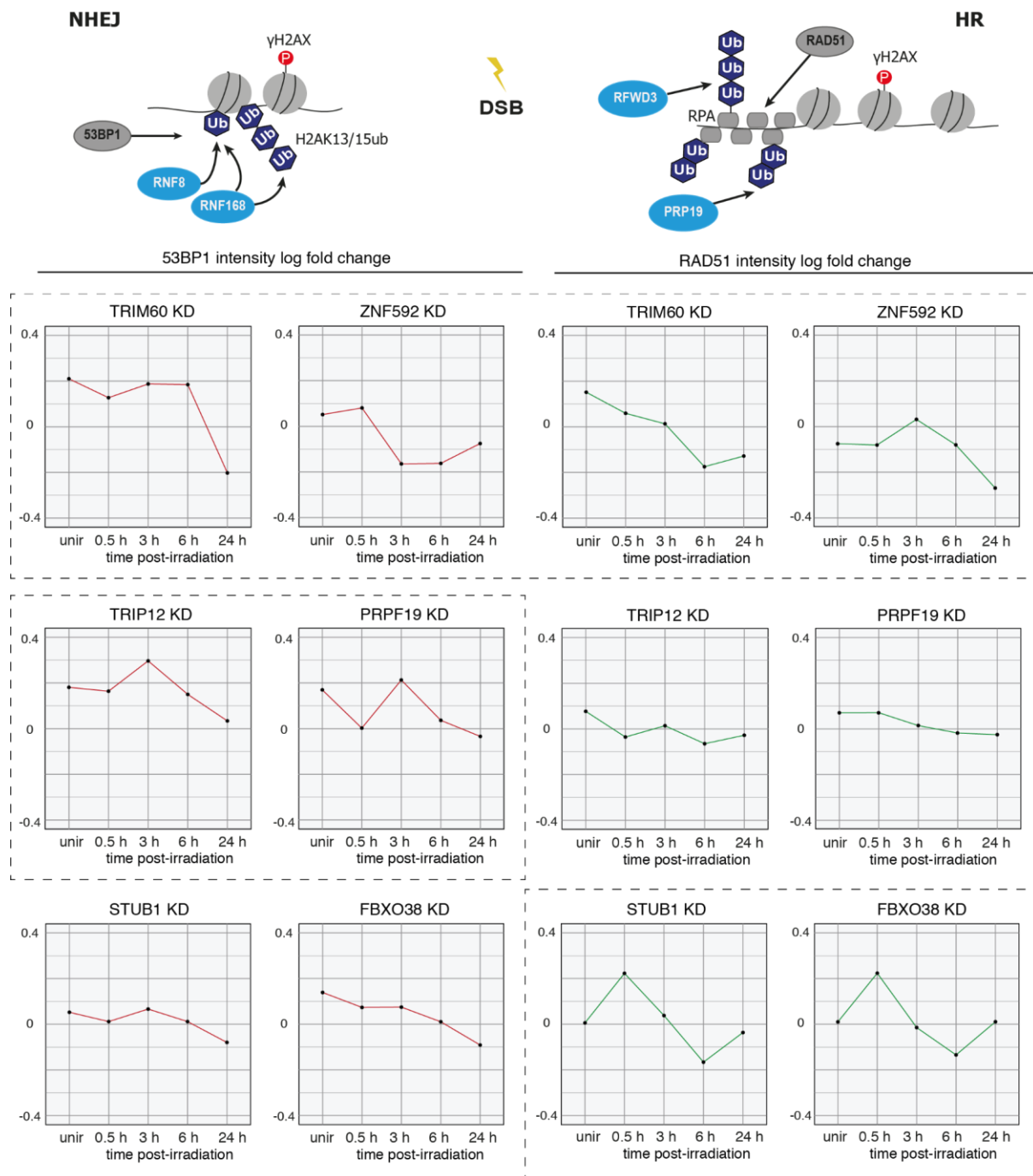


Figure 4.17. Altered repair kinetics and pathway preference at the whole-nuclear intensity level. The repair proteins 53BP1 and RAD51 whole-nuclear intensity changes are represented by logarithmically transformed fold change values and depicted as line plots to highlight the intensity difference from the non-siRNA-treated/mock-transfected controls per time point. The knockdown population was represented by the wells with three siRNA variants per gene of interest and their replicates (total minimum 9 wells per plate per gene, approximately 200 cells per well) corresponding to the indicated time point. The dashed boxes highlight the plots with repair pathway preference, where the first row of the plots shows hits significant for both the NHEJ and HR, the second row shows hits with a preference for the NHEJ, and the third row shows hits with a preference for the HR.

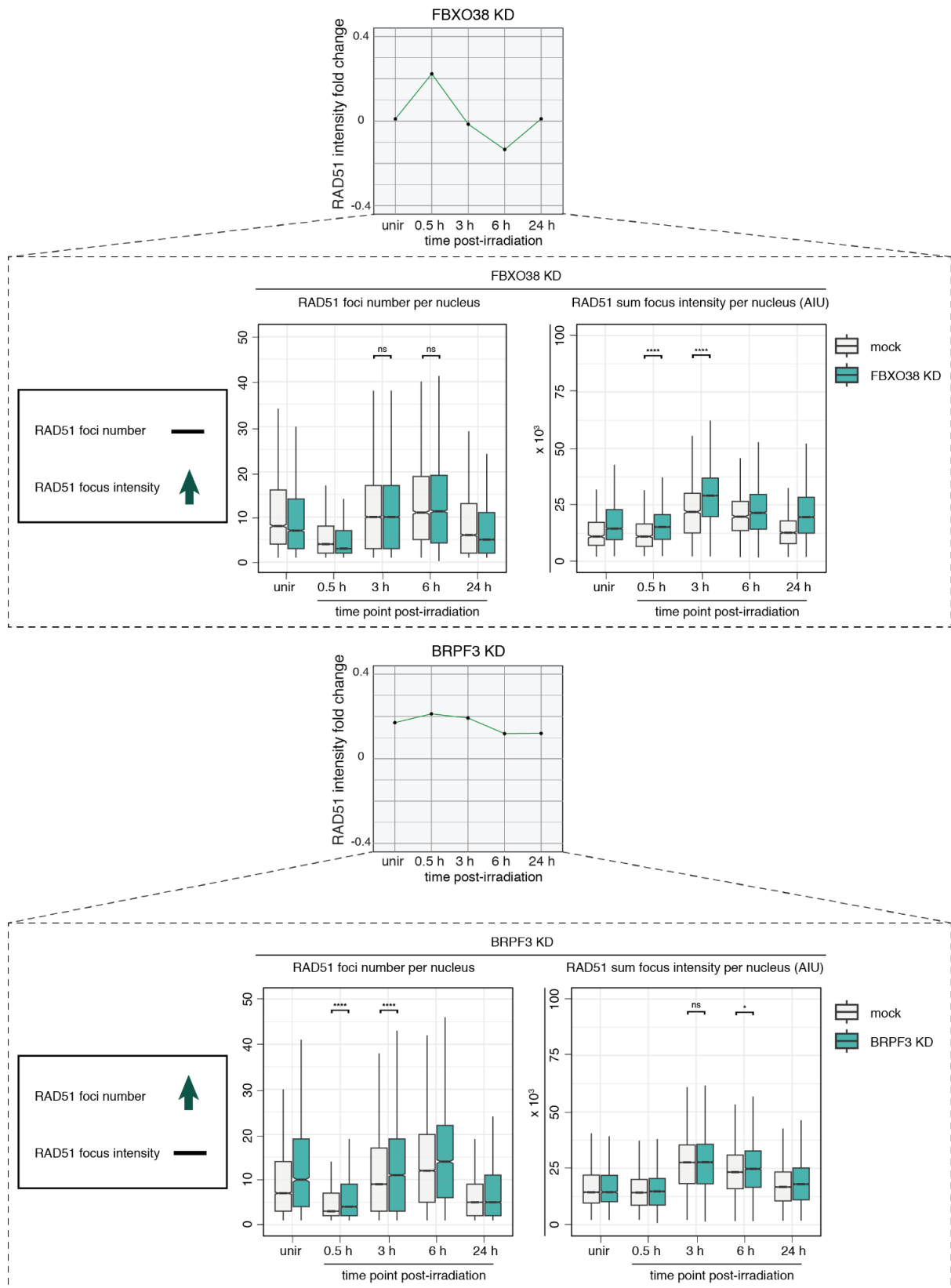


Figure 4.18. Altered repair kinetics and pathway preference at the single-focus level. The repair protein RAD51 whole-nuclear intensity changes are represented by logarithmically transformed fold change values and depicted as line plots to highlight the intensity difference from the non-siRNA-treated/mock-transfected controls per time point. The knockdown population was represented by the wells with three

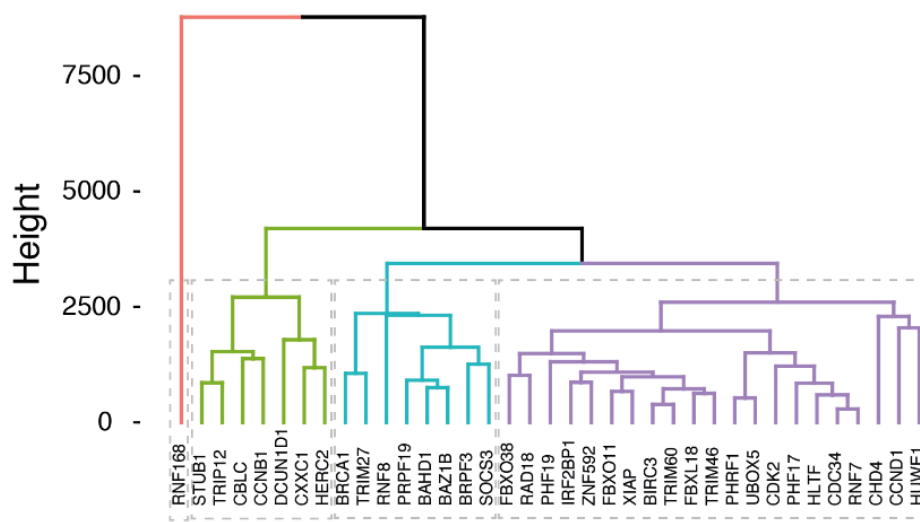
*siRNA variants per gene of interest and their replicates (total minimum 9 wells per plate per gene, approximately 200 cells per well) corresponding to the indicated time point. The sum focus intensity of RAD51 foci per nucleus and the number of RAD51 foci per nucleus were determined in HeLa Kyoto cells at the indicated times after DNA damage induction (5 Gy). The box plot lower and upper hinges correspond to the first and third quartiles (the 25th and 75th percentiles), and the upper whisker extends from the hinge to the largest value no further than 1.5 x IQR from the hinge (where IQR is the interquartile range or distance between the first and third quartiles). The lower whisker extends from the hinge to the smallest value at most 1.5 x IQR of the hinge. The horizontal line represents the median value. The outliers were omitted and not presented in the plot. *** $p < 0.001$, * $p < 0.05$ by Wilcoxon rank-sum test, for knockdown sample versus mock/non-siRNA transfected sample; ns $p > 0.05$ by Wilcoxon rank-sum test, for knockdown sample versus mock/non-siRNA transfected sample.*

To find out what part of the chromatin response to DNA damage was altered in the absence of the novel ubiquitin modifiers, we analyzed the 53BP1 and RAD51 response at the single-focus level. We discovered that the foci parameters such as foci number and sum focus intensity per nucleus were changed differently in the knockdown cells. The depletion of the FBXO38 protein led to the upregulation of the RAD51 whole-nuclear intensity at 0.5 h post-irradiation and subsequent downregulation until 6 h time point. This alteration of the kinetics was predominantly caused by significant changes in RAD51 sum focus intensity per nucleus but not foci number (Figure 4.18). In contrast, the cells with knockdown of the BRPF3 protein showed an increase of RAD51 whole-nuclear intensity at 0.5 h and 3 h time points induced by an increase in sum focus intensity per nucleus with a constant foci number (Figure 4.18). The increase in the RAD51 foci number could signify the increase in DNA damage sites after the X-ray irradiation or stimulation of the homologous recombination pathway at a single damage site. In contrast, the focus intensity increase could be caused by excess resection of the DNA ends.

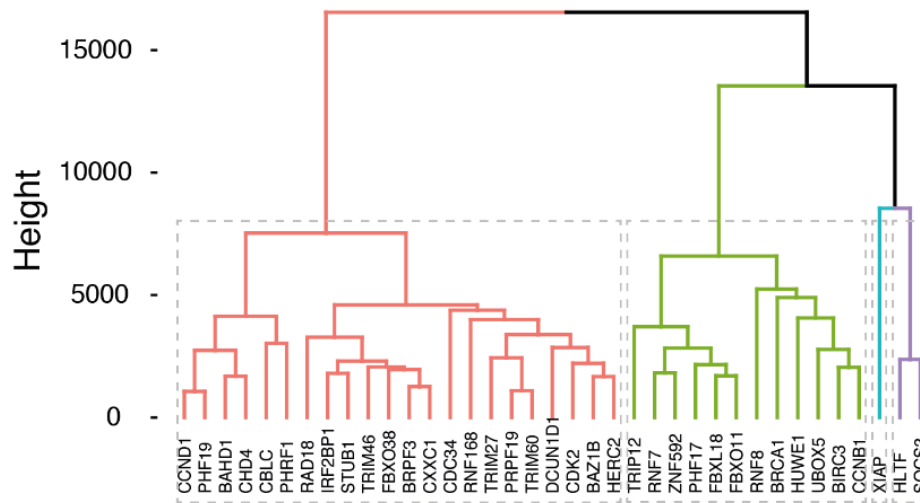
Depletion of hits led to the formation of four DNA repair phenotypes

The 4D single-focus analysis summed up the information about the γ H2AX, 53BP1, and RAD51 foci parameters for each gene knockdown: mean focus size, mean focus intensity, sum focus intensity, and foci number per nucleus. We applied an agglomerative hierarchical clustering algorithm for each time point to interpret the data and identify similarities in the altered DNA repair kinetics. We focused on the 0.5 h, 3 h, 6 h, and 24 h post-irradiation and used the mean foci parameters of 53BP1 and RAD51 per nucleus per gene. The clustering analysis identified four main phenotypes of the DDR kinetics caused by the depletion of the hits at each time point post-irradiation with variable gene content (Figure 4.19). Interestingly, RNF8 and RNF168 depletion altered the repair phenotype specifically enough to form a separate cluster either single or together at 0.5 h, 6 h, and 24 h time points post-irradiation. This result supports the distinctive role of the RNF8/RNF168 proteins acting together as a cascade in the chromatin response to DNA damage throughout the repair.

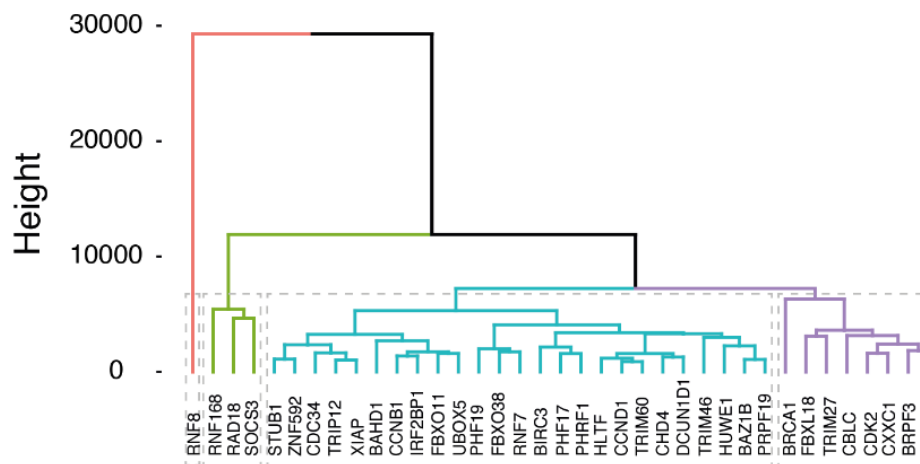
Cluster Dendrogram 0.5 h post-irradiation



Cluster Dendrogram 3 h post-irradiation



Cluster Dendrogram 6 h post-irradiation



Cluster Dendrogram 24 h post-irradiation

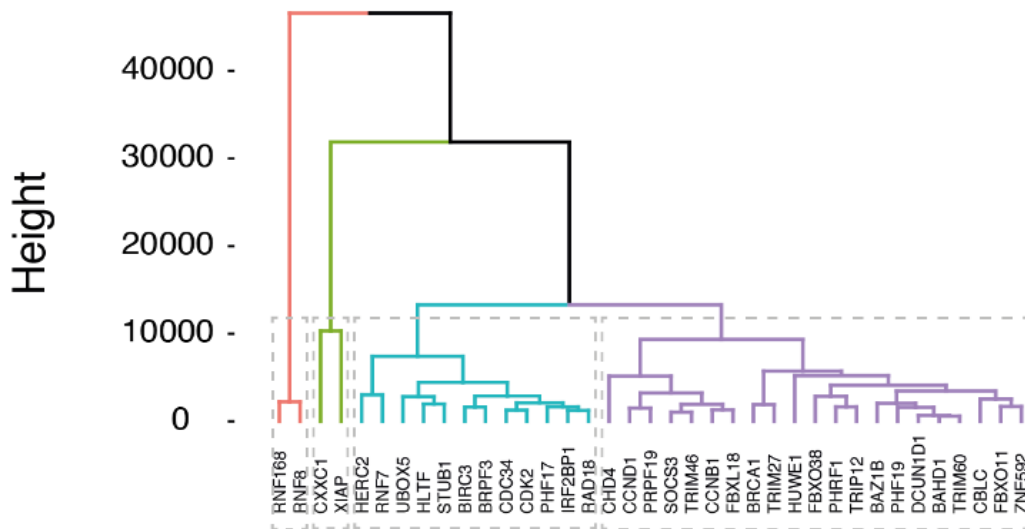
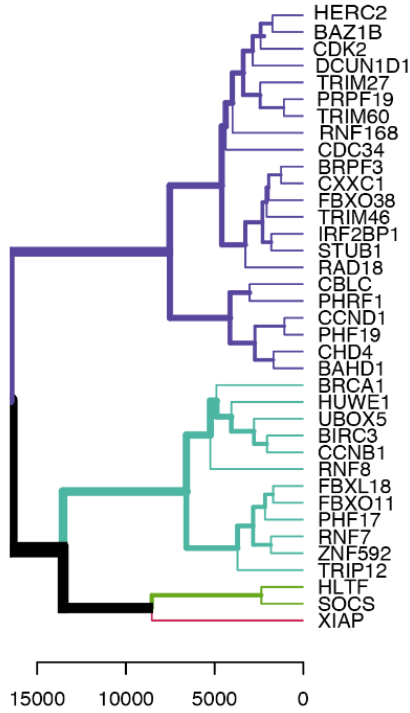


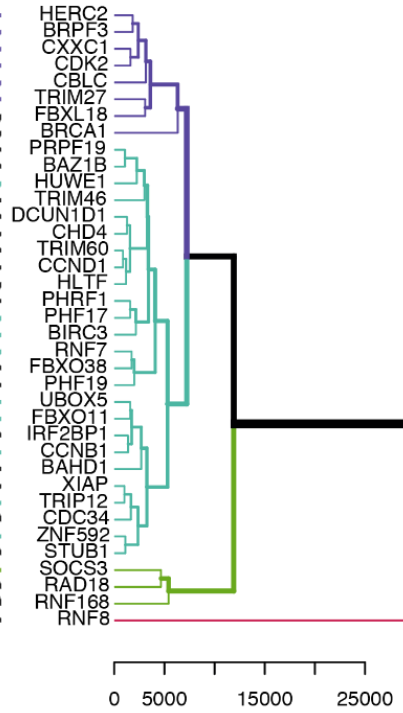
Figure 4.19. Clustering analysis identified four clusters of the DDR kinetics at each time point post-irradiation. The γ H2AX, 53BP1, and RAD51 foci parameters were averaged per gene and per time point post-irradiation and used as variables for cluster analysis. The clusters are colored, the height represents the Euclidean distance measuring the dissimilarity between each pair of gene knockdowns.

A

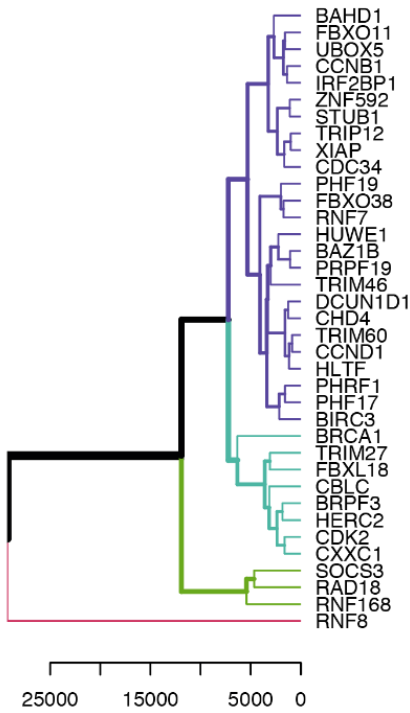
3 h post-irradiation



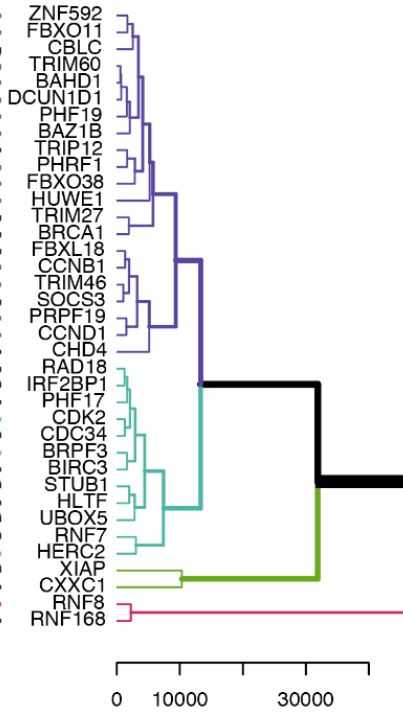
6 h post-irradiation



6 h post-irradiation



24 h post-irradiation



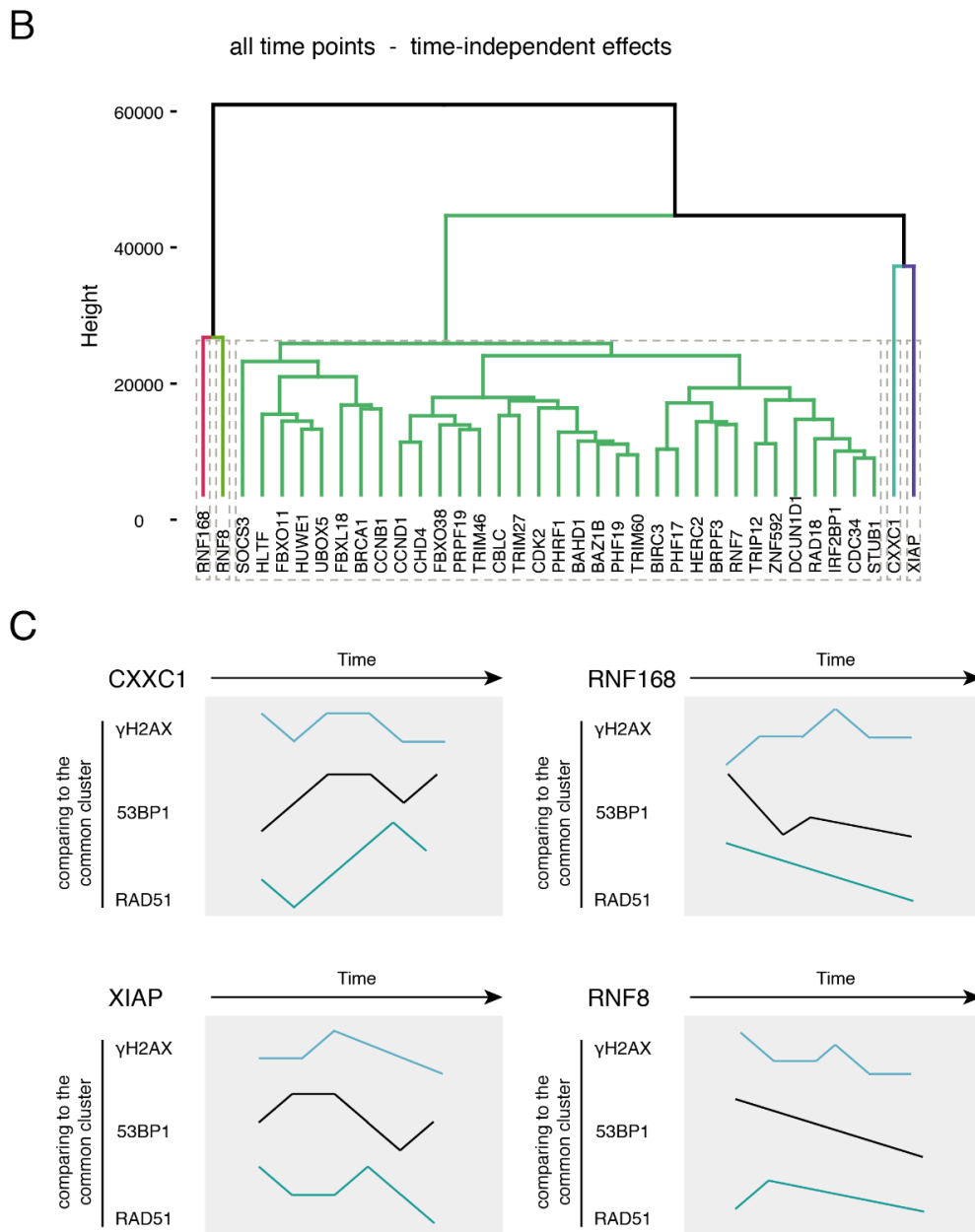


Figure 4.20. Cluster analysis identified four time-independent phenotypes of the DDR kinetics. (A) The cluster dendrograms were compared between the 3 h and 6 h time points, and 6 h and 24 h time points. The γ H2AX, 53BP1, and RAD51 average foci parameters per gene were used as variables to perform the clustering, the clustering was performed per time point. The branches corresponding to the clusters are colored. The lines connect the identical genes between the two dendrograms, black lines represent genes that changed the cluster between the time points, colored lines represent genes that kept the cluster, and the color of the connecting line matches the cluster's color. The x-axis shows the height. The height was calculated as the Euclidean distance measuring the dissimilarity between each pair of gene knockdowns. (B) Cluster dendrogram of all time points. Five clusters are identified, and each cluster is colored accordingly. The y-axis shows the height. The height was calculated as the Euclidean distance measuring the dissimilarity between each pair of gene knockdowns. (C) A simplified summary of the time-independent DDR kinetics phenotypes compared to the common cluster.

To determine if the clusters identified per time point consist of the same genes, we compared the 3 h versus 6 h time points clusters, and 6 h versus 24 h time points clusters (Figure 4.20A). Some of the genes tended to cluster together over time after the damage induction, and more genes were shared between the clusters of 6 h and 24 h than between 3 h and 6 h time points. We found that BRPF3, HERC2, and CDK2 proteins clustered together and did not change the cluster at 3 h, 6 h, and 24 h, suggesting that their depletion led to a similar and consistent DDR phenotype over time (Figure 4.20A). Most of the hits, however, were characterized by higher variability at different time points post-irradiation. Matching the identified clusters with the foci parameter changes at the corresponding time points suggested the existence of unknown protein-protein interactions among the hits.

To find the time-independent effects of the hits on the DDR kinetics, we combined the γ H2AX, 53BP1, and RAD51 foci parameters of all the knockdowns at all time points and ran the hierarchical cluster analysis. We hypothesized that combining the time points would highlight the hits with time-independent uniform effects of the knockdown. With all the time points combined, four proteins were identified that uniquely impacted the 53BP1 and RAD51 kinetics: RNF8, RNF168, CXXC1, and XIAP (Figure 4.20B). The rest of the genes fell into one cluster due to the variability of their effects on the DDR foci in time. The separation of the RNF8-RNF168 from other hits in the time-independent clustering may signal the existence of other functions of these ligases in the DDR signaling and repair in addition to the previously reported, while CXXC1 and XIAP are novel regulators of the chromatin response to DNA damage.

We sought to characterize the knockdown phenotypes of RNF8, RNF168, XIAP, and CXXC1 and find out what caused them to separate in the time-independent cluster analysis (Figure 4.20C, Annex: Figure 7.8). The four phenotypes showed at least a two-fold difference in foci intensity and/or foci count at most of the time points compared to the knockdown phenotypes in the big cluster. We observed that the remarkable strength of the response over a long period was one of the deciding factors for the genes to found a cluster. The RNF168 and RNF8 knockdowns were both characterized by the strong downregulation of 53BP1 and RAD51 foci intensity and count before the irradiation and up to 24 h after due to their central function in the DDR response. However, they were not assigned to the same cluster because of the distinct effect on the γ H2AX (Figure 4.20C, Annex: Figure 7.8). The depletion of RNF168 led to upregulating the γ H2AX foci parameters in undamaged cells in contrast to the RNF8 depletion. RNF168 depletion showed a more prominent effect on the γ H2AX foci count than RNF8 after irradiation, suggesting higher DSB incidence and chromosome fragility. Despite acting together in the DDR cascade, RNF8 and RNF168 possess unique noninterchangeable functions as was suggested previously (Zhang et al., 2013; Kelliher et al., 2020) and formed separate phenotypes in the cluster analysis.

The strength of the effect was the deciding factor for the XIAP knockdown as well. Notably, the depletion of the XIAP protein caused the γ H2AX, 53BP1, and RAD51 foci parameters to change at the later DDR time points (3 h, 6 h, 24 h post-irradiation), and the foci count was affected as well as the foci intensity (Figure 4.20C, Annex: Figure 7.8). The γ H2AX damage signaling, 53BP1, and RAD51 signaling were upregulated at the early time points and extinguished at the late time points. It might suggest more efficient repair, however, additional tests have to be done to test this hypothesis.

CXXC1 formed a cluster due to upregulation of the RAD51 foci count and intensity at all post-irradiation time points except for 24 h (Figure 4.20C, Annex: Figure 7.8). The unirradiated cells and 24 h post-irradiation time point were characterized by the decrease of RAD51 foci count. The

increased recruitment of RAD51 as early as 0.5 h could signify the increase in single-stranded DNA due to excessive resection or replication stress that has to be tended by RAD51. Remarkably, the knockdown of CXXC1 affected 53BP1 intensity but not the foci count in damaged cells.

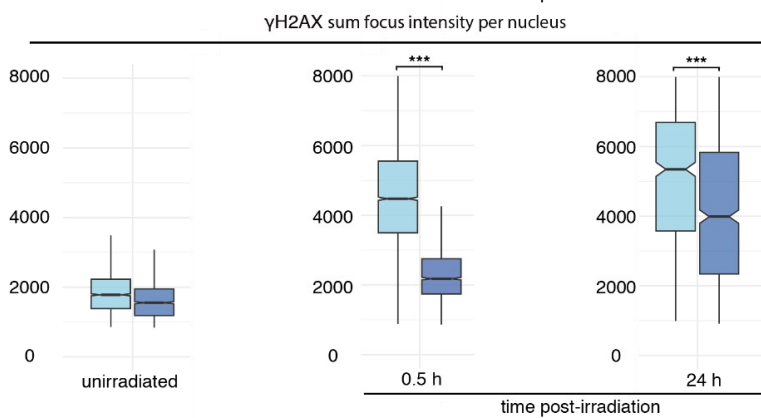
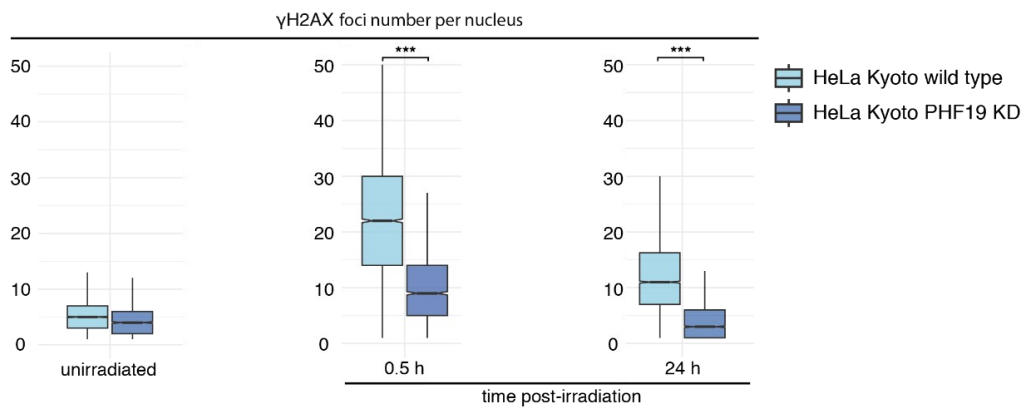
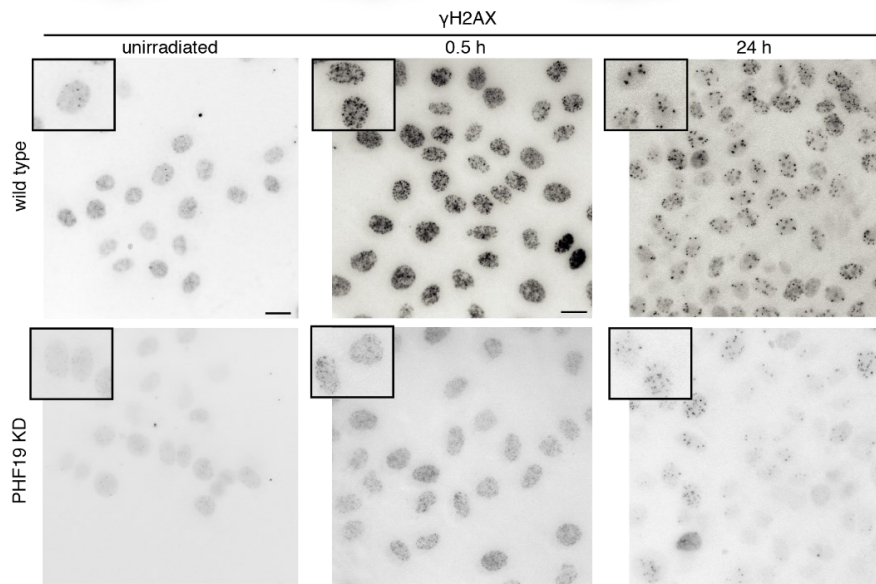
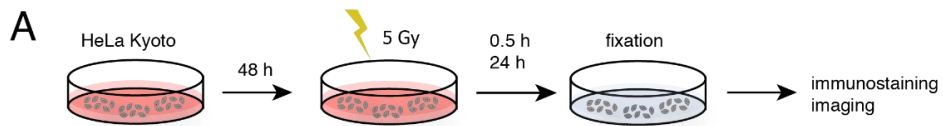
The cluster analysis revealed the similarities between the knockdown phenotypes based on how the depletion of the chromatin modifiers affected DNA damage signaling, NHEJ and HR. Combined with *in silico* analysis of protein interactions among our hits, the clusters could be interpreted as novel signaling cascades in damaged chromatin.

4.4 PHF19 as a novel player in ubiquitin-dependent chromatin response to double-strand breaks

PHF19 knockdown lowers DNA damage signaling

We identified PHF19 as a protein whose knockdown downregulates γ H2AX intensity at 0.5 h post-irradiation in the ubiquitinome-wide and the 4D small-scale screens (Annex: Figure 7.9A). PHF19 is a PRC2.1 polycomb repressive complex component with roles in transcriptional silencing, associated with embryonic development, cell differentiation, and maintenance of cell identity. PHF19 long and short splicing variants were found overexpressed in various tumor types (Wang et al., 2004b; Ghislin et al., 2012; Xu et al., 2015b; Cai et al., 2018; Deng et al., 2018; Gollavilli et al., 2018; Jain et al., 2020; Ruan et al., 2020; Wang et al., 2020; Mason et al., 2020; García-Montolio et al., 2021; Li et al., 2021), but no active role of PHF19 in the regulation of DNA repair has been reported. Indeed, *Phf19*-KO mice appear viable with a normal life span but display anterior-to-posterior homeotic transformations such as an increased number of ribs and various defects of the hematopoietic system, presumably as a result of PHF19 functions in transcriptional regulation and differentiation (Vizán et al., 2020). Interestingly, the murine *Phf19*-KO hematopoietic stem cells resembled aged ones and were less functional under stress conditions.

To validate the loss of the whole-nuclear γ H2AX intensity, we induced the knockdown of PHF19 in the HeLa Kyoto cells using the same siRNA variant that led to the strongest downregulation effect in our screens. The cells with PHF19 depletion (up to 60% endogenous protein loss, Annex: Figure 7.9B) failed to reach the same intensity levels of the H2AX phosphorylation as the wild type at 0.5 h and 24 h post-irradiation (Figure 4.21A). Remarkably, the PHF19 depletion affected the damage signaling without changing the cell cycle distribution (Annex: Figure 7.9C). Together with the severe intensity defect, the γ H2AX foci number per nucleus decreased as well. To find out if the γ H2AX foci number per nucleus decreased in the knockdown cells or the foci were undersegmented due to intensity loss, we compared the intensity-based (local maxima segmentation) and geometric (wavelet transformation, both intensity- and texture-based) foci segmentation algorithms to characterize the γ H2AX signaling defect (Annex: Figure 7.9D). The local maxima segmentation algorithm was in total less powerful to identify the foci compared to the wavelet transform, both in the wild type and PHF19-depleted cells. Both segmentation algorithms confirmed the significant decrease in the γ H2AX foci intensity and number per nucleus post-irradiation in the knockdown cells (Figure 4.21A, Annex: Figure 7.9D). Remarkably, the γ H2AX signaling was impaired in the unchallenged cells as well, meaning that PHF19 loss affected the processing of exogenously and endogenously caused DNA damage.



B

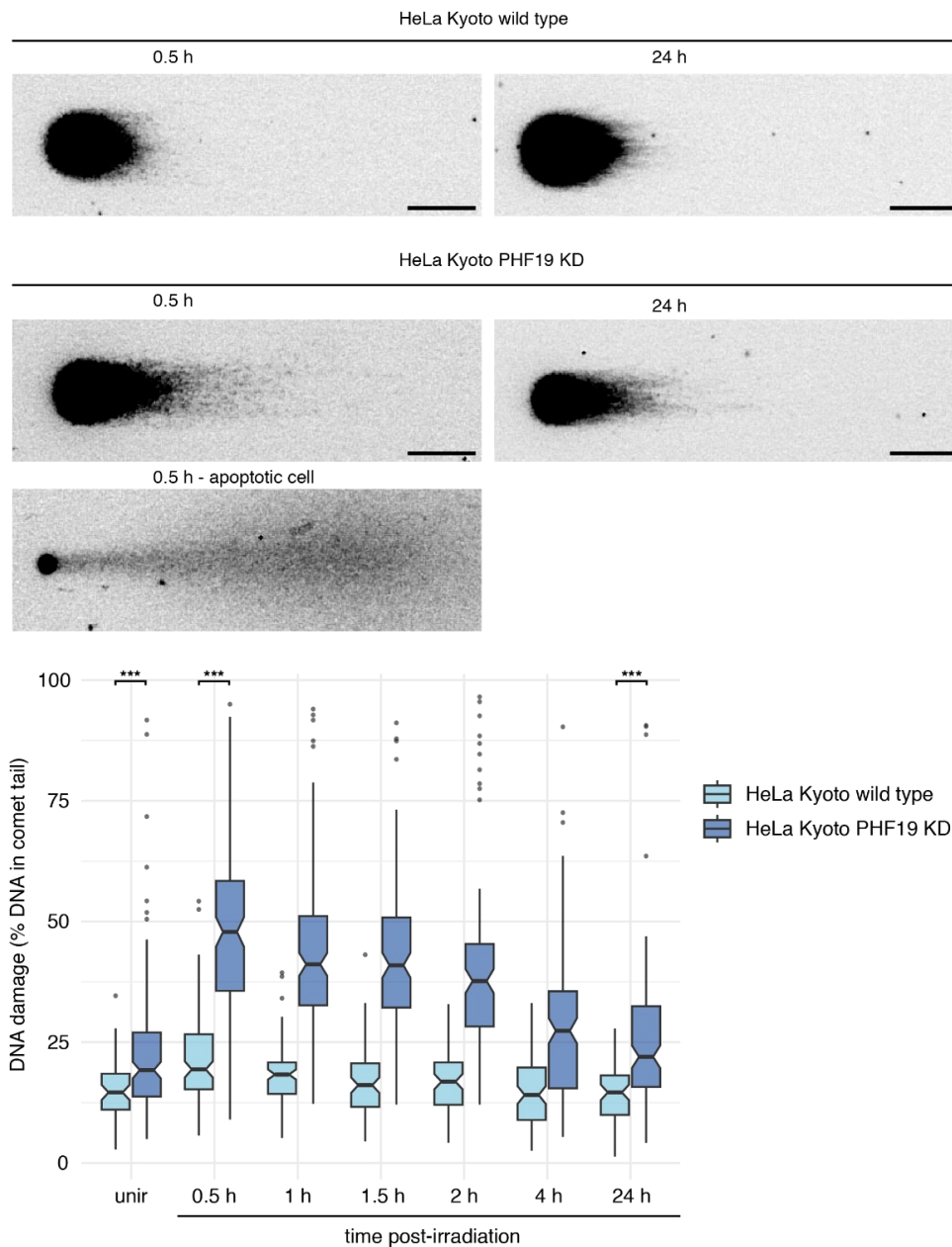


Figure 4.21. PHF19 knockdown lowers DNA damage signaling and repair. (A) Scheme of the experiment, representative images, and foci quantification of the γ H2AX signal in the HeLa Kyoto wild type cells and HeLa Kyoto PHF19 knockdown cells. The wavelet transformation was used to segment the γ H2AX foci. At least 2000 cells were analyzed per condition. The box plot lower and upper hinges correspond to the first and third quartiles (the 25th and 75th percentiles), and the upper whisker extends from the hinge to the largest value no further than $1.5 \times$ IQR from the hinge (where IQR is the interquartile range or distance between the first and third quartiles). The lower whisker extends from the hinge to the smallest value at most $1.5 \times$ IQR of the hinge. The horizontal line represents the median value. The outliers are presented as single dots in the plot outside of the box area. *** $p < 0.001$ by t-test, for knockdown sample versus wild type sample. Scale bar $20 \mu\text{m}$. (B) DNA fragmentation was measured by the neutral comet assay. The percent of DNA in the tail was plotted per comet from six replicates (two biological replicates in triplicate),

each consisting of at least 50 comet measurements. The box plot description as above. *** $p < 0.001$ by t -test, for knockdown sample versus wild type sample. Scale bar 50 μm .

The depletion of PHF19 impaired not only DNA damage signaling in the chromatin but the DNA repair outcome as well. We quantified the DNA fragmentation before and after irradiation by neutral comet assay (Figure 4.21B). The PHF19 knockdown cells failed to repair the double-strand breaks as efficiently as the wild type at all the time points post-irradiation. The undamaged cells showed a higher level of DNA damage than the control as well. Interestingly, the knockdown phenotype was characterized by the presence of the apoptotic cells independent of the radiation (Figure 4.21B, the representative image of the apoptotic cell, outliers in the box plot). Additionally, we measured the apoptosis in the wild type and PHF19-depleted cell populations by detecting the activity of the caspase 3 and other DEVD-specific proteases. The caspase proteases were shown to be the main drivers of apoptosis and increase in their activity was linked to the loss of cell viability (Wolf et al., 1999; Walsh et al., 2008). We compared the caspase activity in the undamaged and radiated wild type and PHF19 knockdown cells. In fact, in the absence of PHF19, the cells showed higher levels of apoptosis without the damage (Annex: Figure 7.9E). Post-irradiation, the level of apoptosis in the wild type, mock-transfected and knockdown gradually increased with the time point. At 5 h and 19 h after the damage induction, the caspases activity in the PHF19 knockdown cells was higher than in the wild type and mock cells. That changed at the later time points such as 24 h and 48 h when the apoptosis in the PHF19 knockdown cells increased by up to 30% compared to the wild type and mock transfection (Annex: Figure 7.9E). This observation suggests that the inability to efficiently repair DSBs caused by lack of PHF19 leads to long-term viability decrease, potentially due to accumulation of unrepaired lesions.

Lack of PHF19 changes the recruitment of selected repair factors to the sites of DNA damage

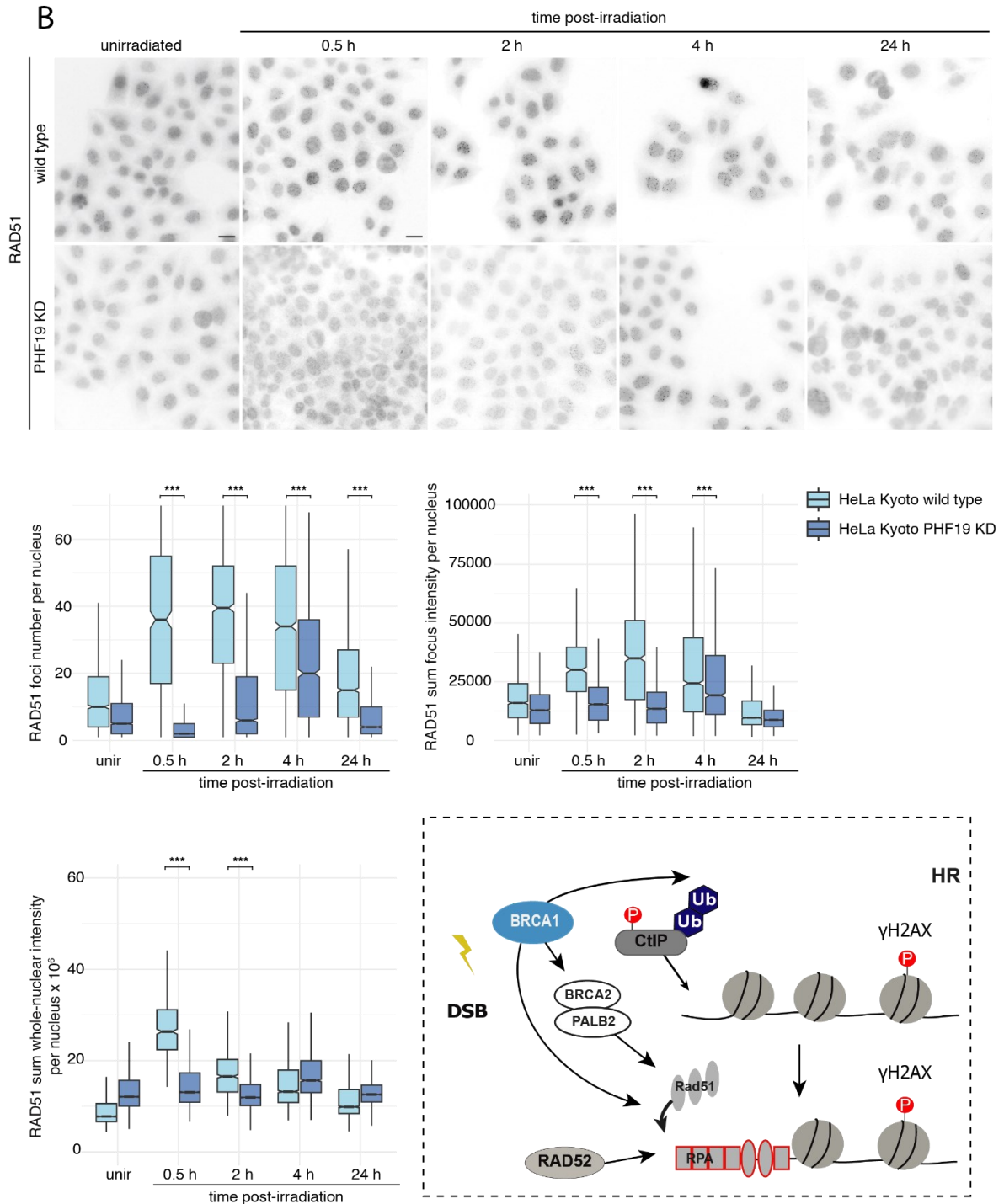
Since the γH2AX is one of the central chromatin modifications for recruitment of DNA repair factors, we next examined if PHF19-depleted cells have different repair proteins kinetics than the wild type. In the absence of PHF19, 53BP1 NHEJ repair protein showed impaired recruitment to the DNA damage sites (Figure 4.22A). The 53BP1 foci number and intensity per nucleus were significantly lower in unchallenged as well as irradiated knockdown cells compared to the wild type. The same was observed for the whole-nuclear levels, indicating that PHF19 depletion perturbed the 53BP1 production or stability in the nuclei. Interestingly, in contrast to the γH2AX signaling, at 24 h post-irradiation the 53BP1 signaling had almost returned to the wild type level. This can be explained by either the delay of the 53BP1 recruitment in the knockdown cells or by the partial reverse of the knockdown phenotype 24 hours post-siRNA treatment.

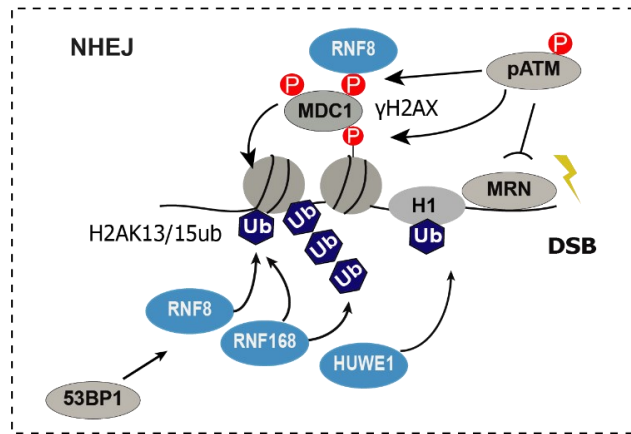
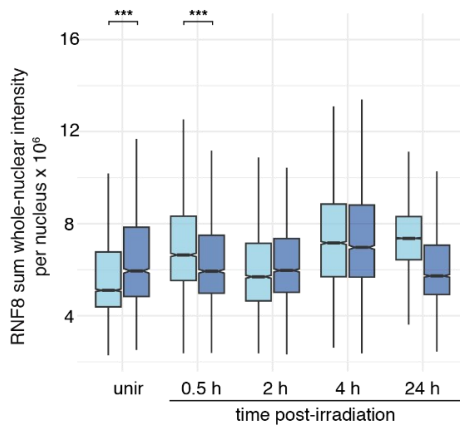
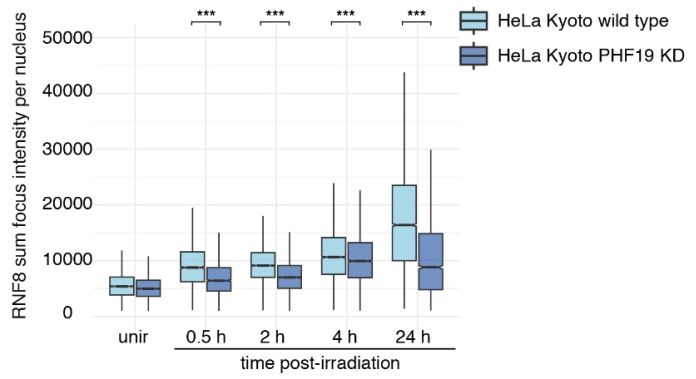
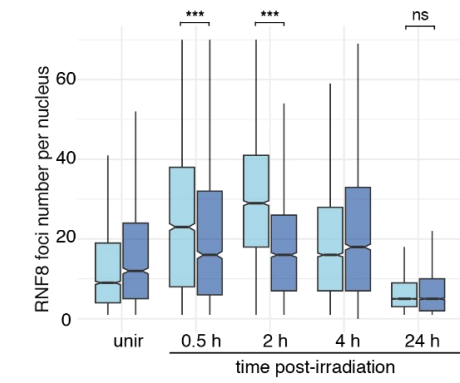
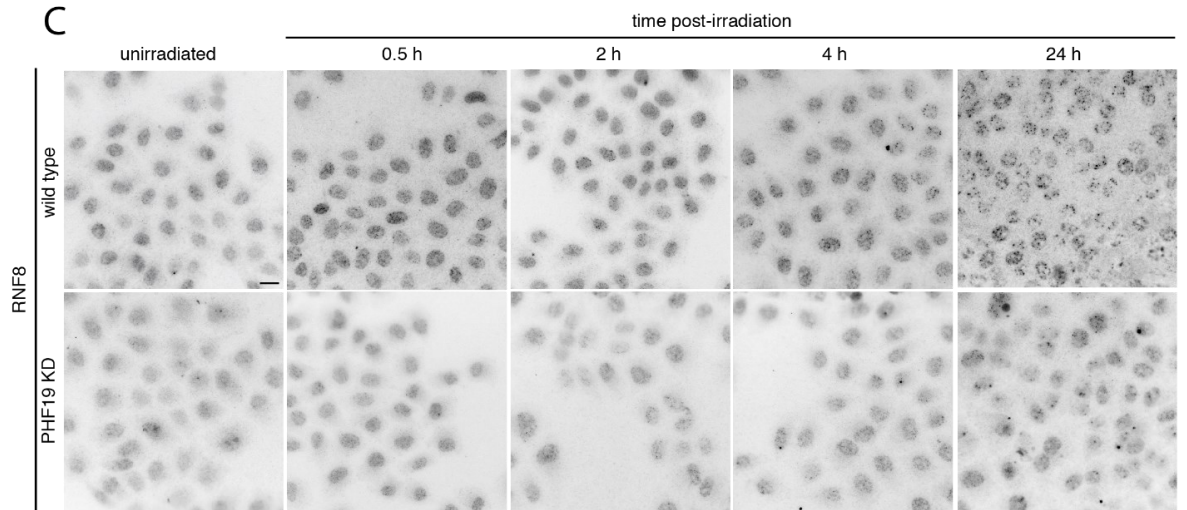
Together with the perturbed NHEJ, we observed a defect in the homologous recombination protein recruitment. The RAD51 foci number and intensity were downregulated in the unchallenged and damaged cells with the lack of PHF19 and the 24 h time point was affected as well (Figure 4.22B). Compared to the 53BP1 defect, the RAD51 foci signaling was disturbed without recovery, however, the whole-nuclear RAD51 levels were upregulated compared to the control at 4 h and 24 h post-irradiation. The abolished recruitment together with increased whole-nuclear levels could be explained by the transcriptional changes caused by PHF19 depletion or by the attempt to compensate defective recruitment. The 53BP1 and RAD51 are different in the

ways they are recruited to the double-strand breaks and that PHF19 knockdown cells fail to recruit both of them under the stress highlights the universal chromatin rearrangement.

The recruitment of 53BP1 (Malette et al., 2012; Hu et al., 2014b) and to a lesser extent RAD51 (Nakada et al., 2012; Kobayashi et al., 2015) to the damage sites requires upstream RNF8 accumulation. In turn, RNF8 was shown to bind ATM-phosphorylated MDC1 on the damaged chromatin (Mailand et al., 2007). In the absence of PHF19, RNF8 recruitment and retention at the double-strand breaks were impaired (Figure 4.22C). The RNF8 foci intensity was downregulated at all time points post-irradiation, while the RNF8 foci number per nucleus was affected predominantly at 0.5 h and 2 h post-irradiation. Interestingly, the number of the RNF8 foci was equal to the wild type at 24 h similar to the 53BP1 signaling. Since RNF8-mediated chromatin ubiquitination is a prerequisite to the 53BP1 recruitment in the wild type cells, the 53BP1 recruitment delay could be at least partially caused by an RNF8 defect.

Another repair protein kinetics that was affected by the PHF19 depletion was RAD52. RAD52 participates in several DNA repair pathways such as homologous recombination, alternative end-joining, and single-strand annealing (Kan et al., 2017). Although *RAD52-null* mammals do not exhibit observable viability phenotype (Rijkers et al., 1998), RAD52 protein supports the correct performance of multiple damage signaling cascades and shares the function with BRCA2. In the PHF19-depleted cells, both foci number and sum focus intensity per nucleus were downregulated (Figure 4.22D). No signaling recovery to the pre-damage and 0.5 h time points was observed at the foci level. Since the RAD52 also showed a pan-nuclear signal, we analyzed the whole-nuclear RAD52 intensity levels of the wild type and knockdown cells. The knockdown cells showed decreased levels of RAD52 before the damage and at all time points after except for 24 h. The 24 h time point in the PHF19-depleted cells was characterized by the increase of the pan-nuclear RAD52 levels but decreased formation of RAD52 foci (Figure 4.22D). The observed response could be caused by defects in recruitment and attempted compensation by RAD52 production.





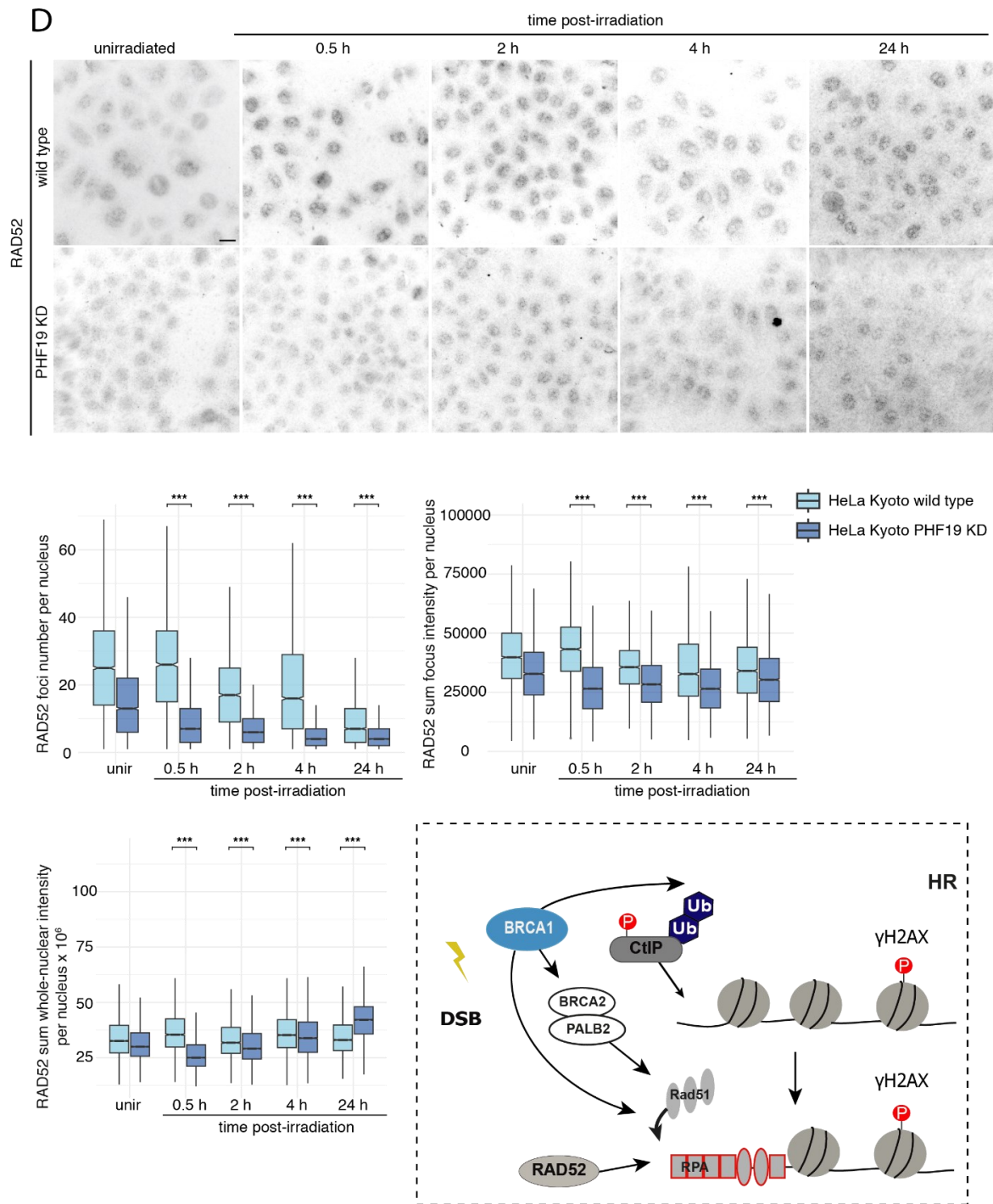
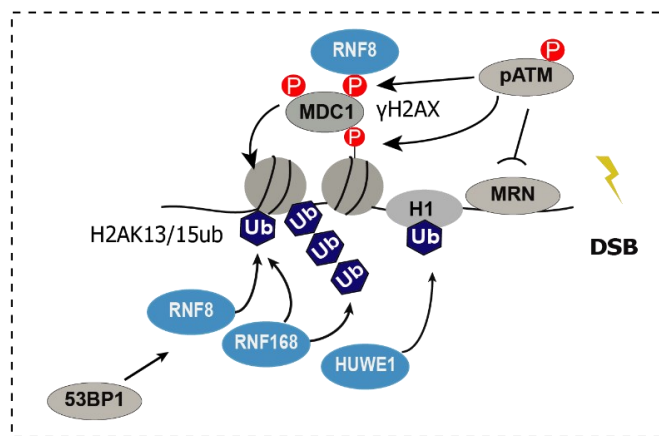
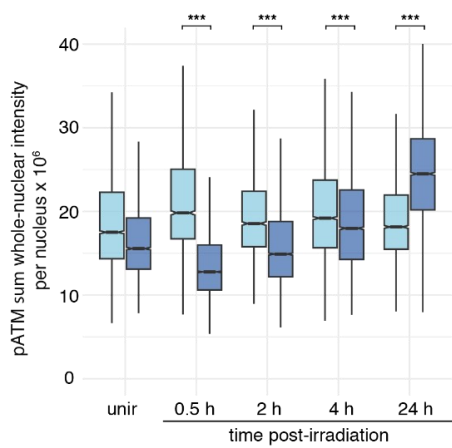
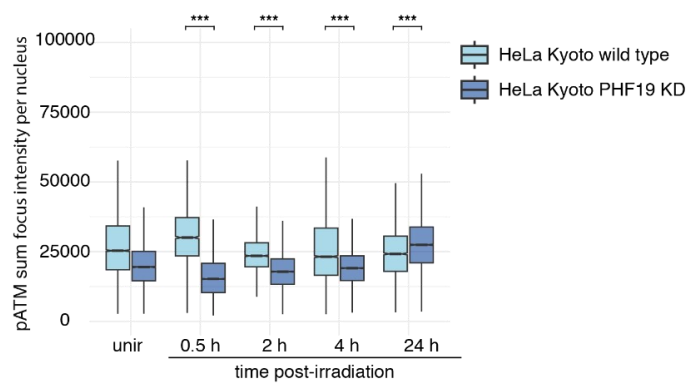
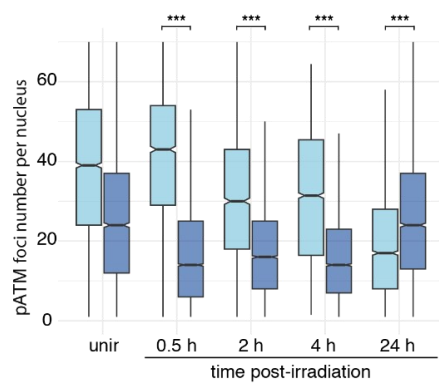
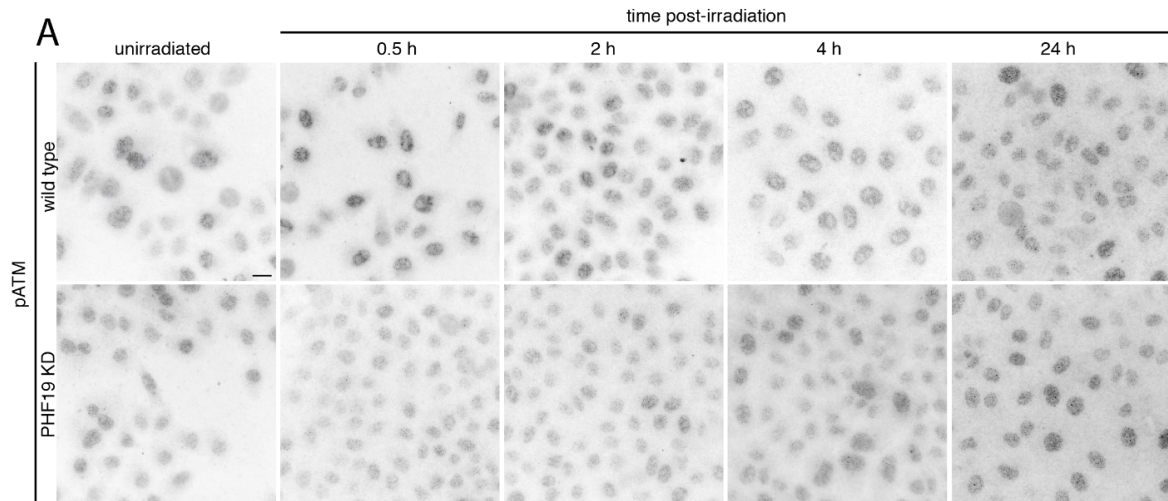


Figure 4.22. Lack of PHF19 hinders the recruitment of selected factors to the sites of DNA damage. Quantification of the repair factors signaling in the wild type and PHF19-depleted HeLa Kyoto cells. The schemes at each part of the figure depict the place of the 53BP1, RAD51, RNF8 and RAD52 in the DDR pathway. The box plot description as above. The outliers are not presented in the plot. ns: not significant ($p > 0.05$), * $p < 0.05$, *** $p < 0.001$ by t-test, for knockdown sample versus wild type sample. Scale bar 20 μm . (A) 53BP1 (B) RAD51 (C) RNF8 (D) RAD52.

The γH2AX is one of the first chromatin modifications happening at the sites of the double-strand breaks and the one that was shown to outline the repair focus in 3D. We examined if the kinetics of the selected repair proteins were affected only by the insufficient H2AX phosphorylation and,

subsequently, insufficient signal transduction by the readers upwards in the cascade. First, we tested the pATM foci formation in the wild type and knockdown cells under stress. As well as γ H2AX, pATM accumulates at the DSBs within minutes post-irradiation and together with ATR and DNA-PKcs phosphorylates H2AX and multiple other targets. In the absence of PHF19, the pATM foci number and sum focus intensity per nucleus were decreased at all time points post-irradiation except for 24 h when the foci parameters were upregulated compared to the wild type levels (Figure 4.23A). The whole-nuclear levels of the pATM showed the same kinetics as the pATM foci parameters indicating that not only pATM recruitment but also the levels of phosphorylated ATM were affected by PHF19 depletion. By similarity with the 53BP1 and RNF8, the pATM kinetics appeared delayed in time. Interestingly, the γ H2AX signaling was not restored in the PHF19 knockdown cells at 24 h post-irradiation despite the accumulation of the pATM, suggesting that the pATM recruitment was insufficient to restart the repair focus formation. Surprisingly, the reader of the γ H2AX MDC1 showed the opposite kinetics. The MDC1 foci number was significantly higher in the PHF19-depleted cells than in the wild type after the damage induction (Figure 4.23B). The MDC1 foci intensity was upregulated in a damage-dependent manner as well except for the 24 h time point when the foci intensity was not different from the wild type cells. The MDC1 foci kinetics profile of the PHF19-depleted cells was similar to the one of the wild type: the maximum of the MDC1 recruitment was observed at 0.5h post-irradiation with the gradual decrease till 24 h. Interestingly, the whole-nuclear intensity of the MDC1 was upregulated in the damaged PHF19-depleted cells but not at the 24 h time point (Figure 4.23B). At the 24 h, the MDC1 total levels appeared to be decreased compared to the wild type control. The reduction of both the MDC1 foci intensity and total nuclear intensity at the 24 h post-irradiation indicated the MDC1 degradation. Compared to the delayed kinetics of pATM, 53BP1, RNF8, and abolished recruitment of RAD52 and RAD51, the MDC1 excessive accumulation seems unexpected. Previous studies have shown that although γ H2AX is important for DNA repair, it is not strictly necessary (Celeste et al., 2002, 2003). According to the recent findings (Salguero et al., 2019), the DNA repair in the absence of γ H2AX is promoted by MDC1. The MDC1 PST-repeat region directly interacts with chromatin via the nucleosome acidic patch and mediates DNA damage- and γ H2AX-independent association of MDC1 with chromatin. This association was described as necessary for 53BP1 recruitment in the *H2AX*^{-/-} cells. However, in the PHF19-depleted cells, the MDC1 recruitment was not enough to recruit 53BP1 and repair the damage as efficiently as in the wild type. Additionally, MDC1 was shown to associate with the genomic loci upon their transcriptional activation (Salifou et al., 2021). Independently of DNA damage, MDC1 and the MRN complex (MRE11-RAD50-NBS1) interact with factors involved in gene expression and RNA processing. Moreover, the MRN subunits colocalize at the transcription start sites and actively transcribed gene bodies in the RNAPII transcriptional complex-dependent manner. The transcriptional changes and activation due to chromatin compaction loss could explain the MDC1 overrecruitment in the PHF19-depleted cells, however, not the pATM recruitment defect.



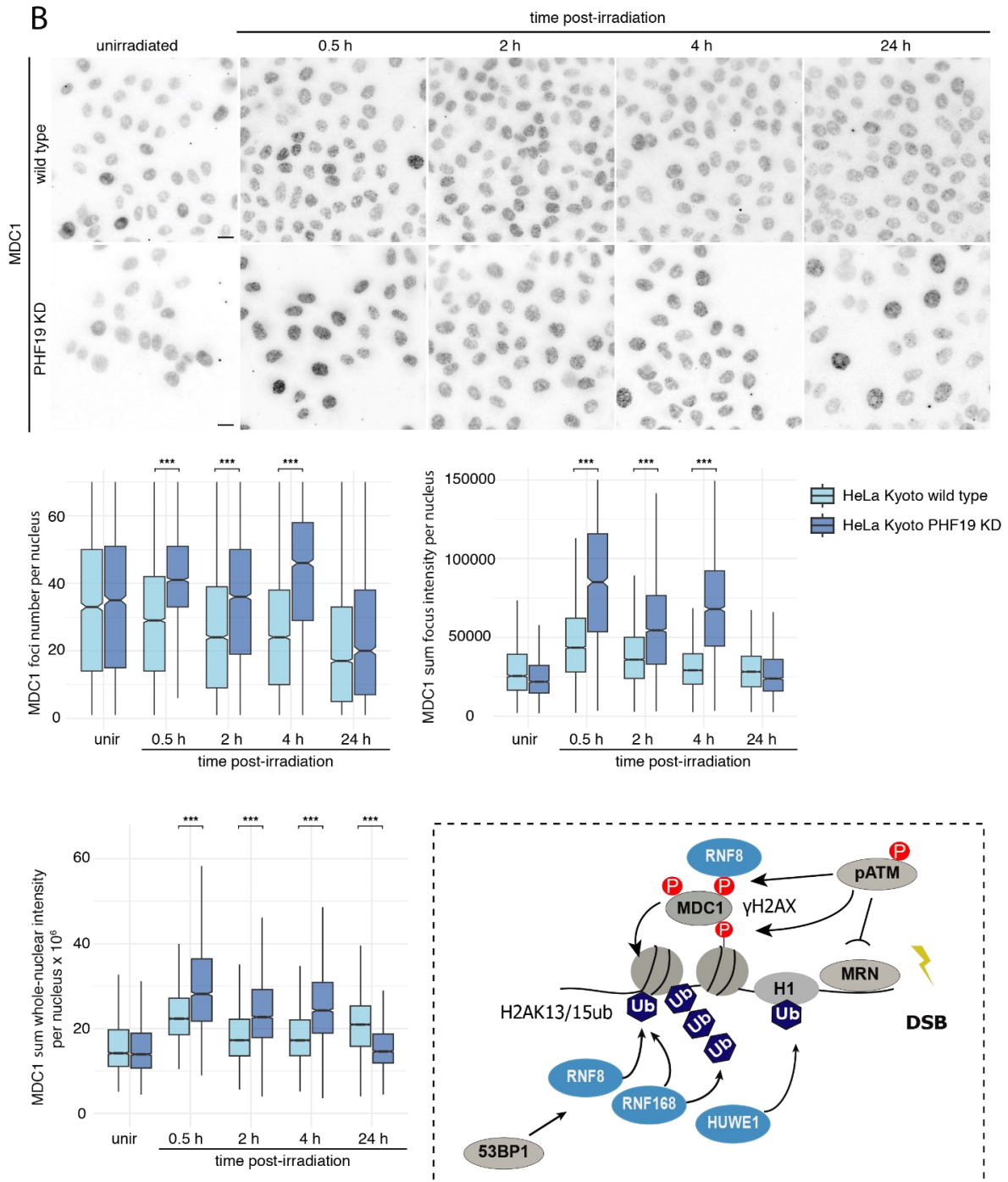


Figure 4.23. PHF19 knockdown affected the writer and the reader of the γ H2AX. (A) Quantification of the pATM signaling in the wild type and PHF19-depleted HeLa Kyoto cells. The wavelet transformation was used to segment the pATM foci, at least 2000 cells were analyzed per condition in triplicates. The scheme depicts the place of the pATM in the DDR pathway. The box plot description as above. The outliers are not presented in the plot. ns: not significant *** $p < 0.001$ by t-test, for knockdown sample versus wild type sample. Scale bar 20 μ m. (B) Quantification of the MDC1 signaling in the wild type and PHF19-depleted HeLa Kyoto cells. The scheme depicts the place of the MDC1 in the DDR pathway. The wavelet transformation was used to segment the MDC1 foci, at least 2000 cells were analyzed per condition in

triplicates. The box plot description as above. The outliers are not presented in the plot. ns: not significant, *** $p < 0.001$ by t-test, for knockdown sample versus wild type sample. Scale bar 20 μm .

PHF19 is a facultative heterochromatin-associated protein that functions in early-mid stages of double-strand break repair

To inspect PHF19 intracellular localization, we generated a HeLa Kyoto cell line stably overexpressing mouse PHF19 tagged with EGFP fluorescent protein (mPHF19-GFP). Remarkably, in undamaged cells, mPHF19-GFP showed a recognizable association with compacted facultative heterochromatin regions (Figure 4.24A, Annex: Figure 7.10A). The association of the recombinant PHF19 protein with the facultative heterochromatin regions is in line with it being an adaptor protein for the PRC2-mediated transcriptional silencing.

Next, we evaluated the dynamics of PHF19 association with the repair foci. The endogenous whole-nuclear protein levels showed an increase in response to the damage as early as 0.5 h post-irradiation (Figure 4.24B, C). Interestingly, the maximum colocalization with the γH2AX foci per nucleus was reached at 1 h gradually decreasing after, suggesting that PHF19 is required for the DNA repair events in the early-mid timing.

To further specify the timing of the PHF19 involvement in the repair, we measured the PHF19 intensity in the γH2AX -decorated chromatin domains before and after irradiation. Strikingly, although the maximum of colocalizations per nucleus was reached at 1 h post-irradiation, the maximum level of PHF19 at the repair foci was observed at 1.5 h post-irradiation (Figure 4.24C). The time point difference for the number of colocalizations per nucleus and for the protein amount per γH2AX focus could indicate that the PHF19 levels are enough for many DSBs at 1 h post-irradiation to be processed and PHF19 accumulates more for the ones that require more processing. The PHF19 amount at the γH2AX foci in the undamaged cells was much lower compared to all time points post-irradiation suggesting that PHF19 colocalization with γH2AX foci is damage-dependent.

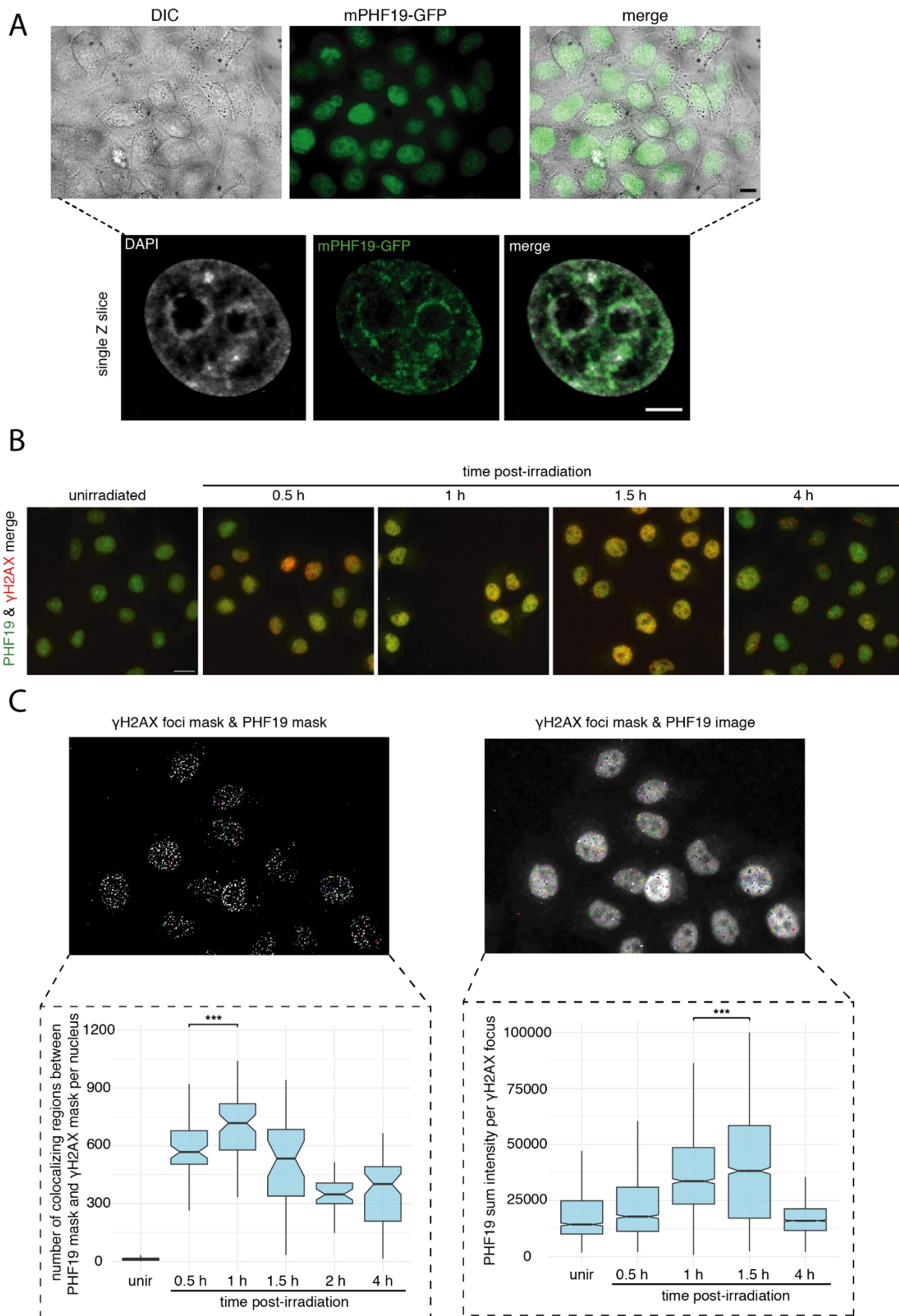


Figure 4.24. PHF19 is facultative heterochromatin-associated protein and involved in the early-mid DNA repair. (A) Representative images of the HeLa Kyoto mPHF19-GFP cell line. The upper row contains wide-

field images, scale bar 10 μm . The lower row shows a mid Z slice of a single cell at higher resolution, scale bar 5 μm . (B) Representative images of the HeLa Kyoto cells stained for endogenous PHF19 protein and γH2AX . Merge of the two channels shown for unirradiated cells and time points post-irradiation. PHF19 is shown in green false color, γH2AX is shown in red false color. Scale bar 20 μm . (C) Two ways of measuring the time point of the highest association between PHF19 and γH2AX foci. The overlay between the segmentation masks from the PHF19 and γH2AX signals was used to calculate the number of the colocalizing regions per nucleus. The overlay between the γH2AX signal mask and PHF19 original image was used to measure the PHF19 sum intensity per γH2AX focus. The results of both quantifications are shown as box plots. At least 2000 cells were analyzed per condition in triplicates. The box plot description as above. The outliers are not presented in the plot. *** $p < 0.001$ by t-test, for knockdown sample versus wild type sample.

PHF19 depletion causes chromatin decompaction in undamaged human cells

Next, we sought to investigate if the PHF19 depletion affects chromatin. The knockdown of PHF19 caused a general whole-nuclear decompaction of the heterochromatin domains in unchallenged cells (Figure 4.25A). To quantify the decompaction effect, we compared the standard deviation pixel value per nucleus in the wild type and knockdown cells stained with the DAPI DNA fluorescent label (Figure 4.25B). The high standard deviation value per nucleus corresponds to the presence of the pixels with various intensity values translating into the presence of compacted and decompacted nuclear areas. In contrast, the low standard deviation value suggests that most pixels in the nuclear area have similar intensity values, therefore most of the chromatin in the nucleus has a similar compaction level. The nuclei of the wild type HeLa Kyoto cells showed an expected distribution of decompacted euchromatin and compacted heterochromatin regions in undamaged as well as irradiated cells (Figure 4.25A). In the absence of PHF19, chromatin regions appeared to be more homogeneously compacted. The DAPI standard deviation value per nucleus confirmed the observation. The DAPI standard deviation value per nucleus in the wild type cells was higher than in the knockdown without damage induction (Figure 4.25C). The trend persisted at 0.5 h and 2 h post-irradiation. In addition, we compared the DAPI mean intensity value per nucleus. The mean intensity value of the PHF19-depleted cells was lower than the one of the wild type population, both in undamaged and irradiated cells (Figure 4.25C).

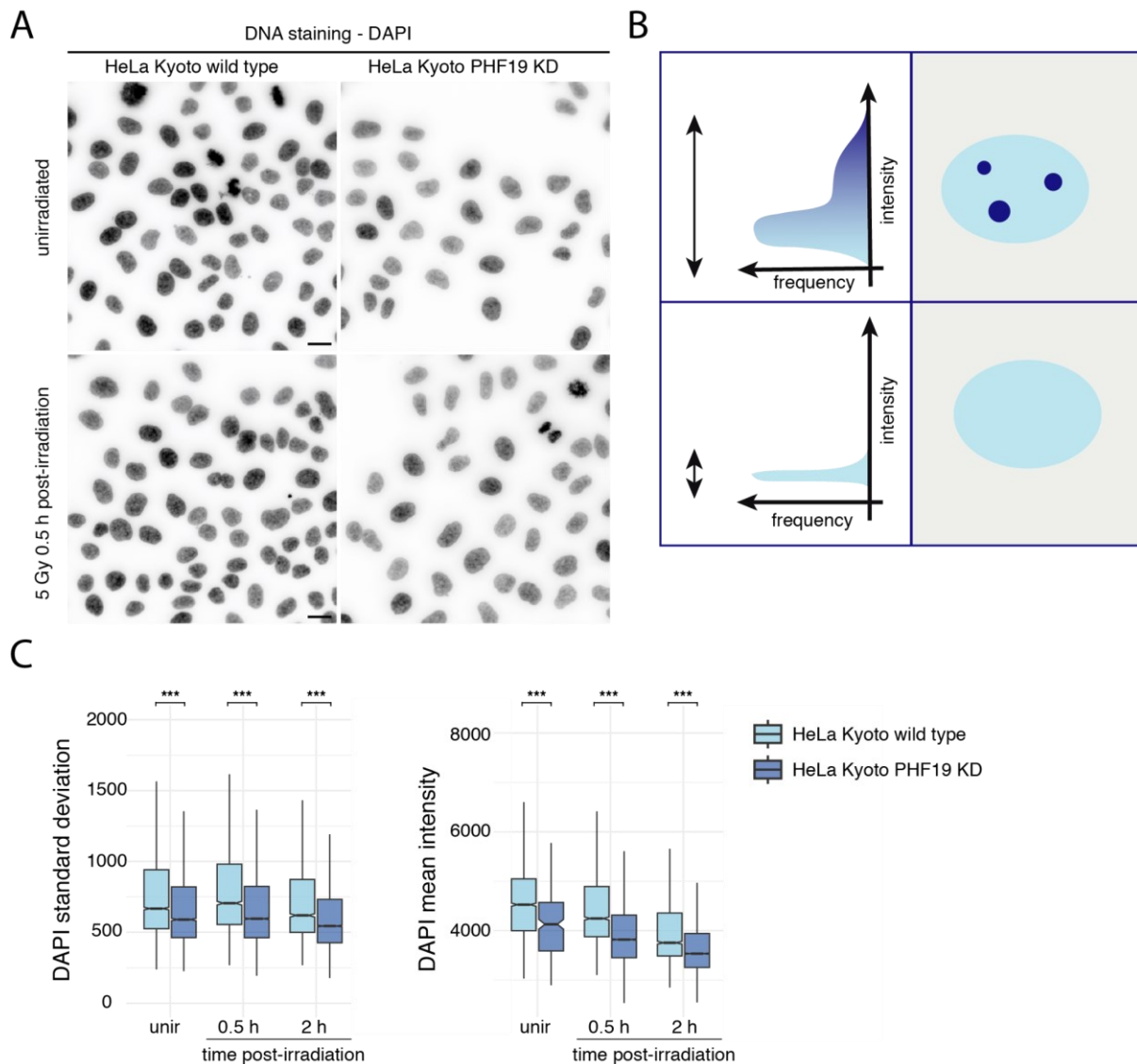


Figure 4.25. PHF19 depletion causes chromatin decompaction in undamaged and irradiated human cells. (A) Representative images of the HeLa Kyoto wild type and PHF19 knockdown nuclei stained by DAPI to label the DNA. Scale bar 20 μ m. (B) The scheme describes the principle of DNA compaction quantification using DAPI standard deviation. (C) Quantification of the DAPI standard deviation and mean intensity values per nucleus in the wild type and PHF19-depleted cells. At least 2000 cells were analyzed per condition. The box plot description as above. The outliers are not presented in the plot. *** $p < 0.001$ by t-test, for knockdown sample versus wild type sample.

The PHF19 protein was described to be involved in the PRC-mediated transcriptional silencing and associated with the facultative heterochromatin domains, therefore it could contribute to the stability of chromatin compaction. The results obtained through compaction analysis support this hypothesis and explain the impaired γ H2AX signaling in the irradiated cells due to the destruction of the 3D structure. As shown before (Natale et al., 2017), the H2AX phosphorylation is not linear and requires the accommodation of the chromatin loops in 3D to form the repair focus. Hence, the PHF19 depletion causes the chromatin defect that is primary to the DNA damage signaling and repair defect.

PHF19 is required to keep the general ubiquitination signaling as well as H2AK119ub specifically at the sites of double-strand breaks

Next, we sought to compare the damage-associated ubiquitination in the wild type and PHF19 knockdown cells. PHF19 is not known as an annotated but putative E3 ubiquitin ligase due to the presence of the two Zn-finger domains. Despite the lack of ubiquitination activity, we showed that the knockdown cells fail to retain at the damage spot the accumulation of the ubiquitin ligase RNF8 (Figure 4.22C). To investigate if the PHF19 knockdown changed the ubiquitination levels at the sites of the double-strand breaks, we used the well-characterized antibody against mono- and polyubiquitinated proteins (FK2 clone) (Fujimuro et al., 1994). The PHF19-depleted cells showed less accumulation of ubiquitination compared to the wild type (Figure 4.26A). In the absence of PHF19, the spreading of ubiquitination on the chromatin was impaired similarly to the spreading of the γ H2AX and both, repair foci number and sum focus intensity per nucleus, were downregulated (Figure 4.26A). The general ubiquitination decrease at the sites of the double-strand breaks could be a direct consequence of the failed recruitment of the multiple repair factors in the knockdown phenotype.

Not only depletion of the ubiquitination sites in the vicinity of the break but the change of the chromatin ubiquitination before or after the damage could cause the observed knockdown phenotype. PHF19 is known for its role in PRC-mediated transcriptional silencing, which acts as an adaptor and facilitator of the H3K27me3 mark propagation. The *de novo* H3K27me3 deposition, in turn, promotes H2AK119 ubiquitination by the PRC1 complex. The H2AK119ub chromatin mark was shown to be locally induced in the vicinity of the double-strand breaks and promote the HR (Fitieh et al., 2022). Thus, we hypothesized that the PHF19 depletion would affect the global and local levels of the H2AK119ub. We compared the global whole-nuclear H2AK119ub levels in the wild type and PHF19 knockdown cells before and after the damage induction. The PHF19 depletion caused global loss of the H2AK119 ubiquitination in the unchallenged cells (Figure 4.26B). After the damage induction, global H2AK119ub levels remained to be lower in the PHF19 absence. Next, we tested if the PHF19 knockdown changed the H2AK119 ubiquitination at the sites of the damage. We used the γ H2AX signaling as a mask demarcating the repair foci to measure the H2AK119ub locally. Interestingly, the local post-irradiation H2AK119ub levels were upregulated both in the wild type and knockdown cells (Figure 4.26B). However, the PHF19 knockdown hindered the local H2AK119ub induction near the breaks, suggesting that the hierarchical PRC recruitment to the damaged chromatin was impaired.

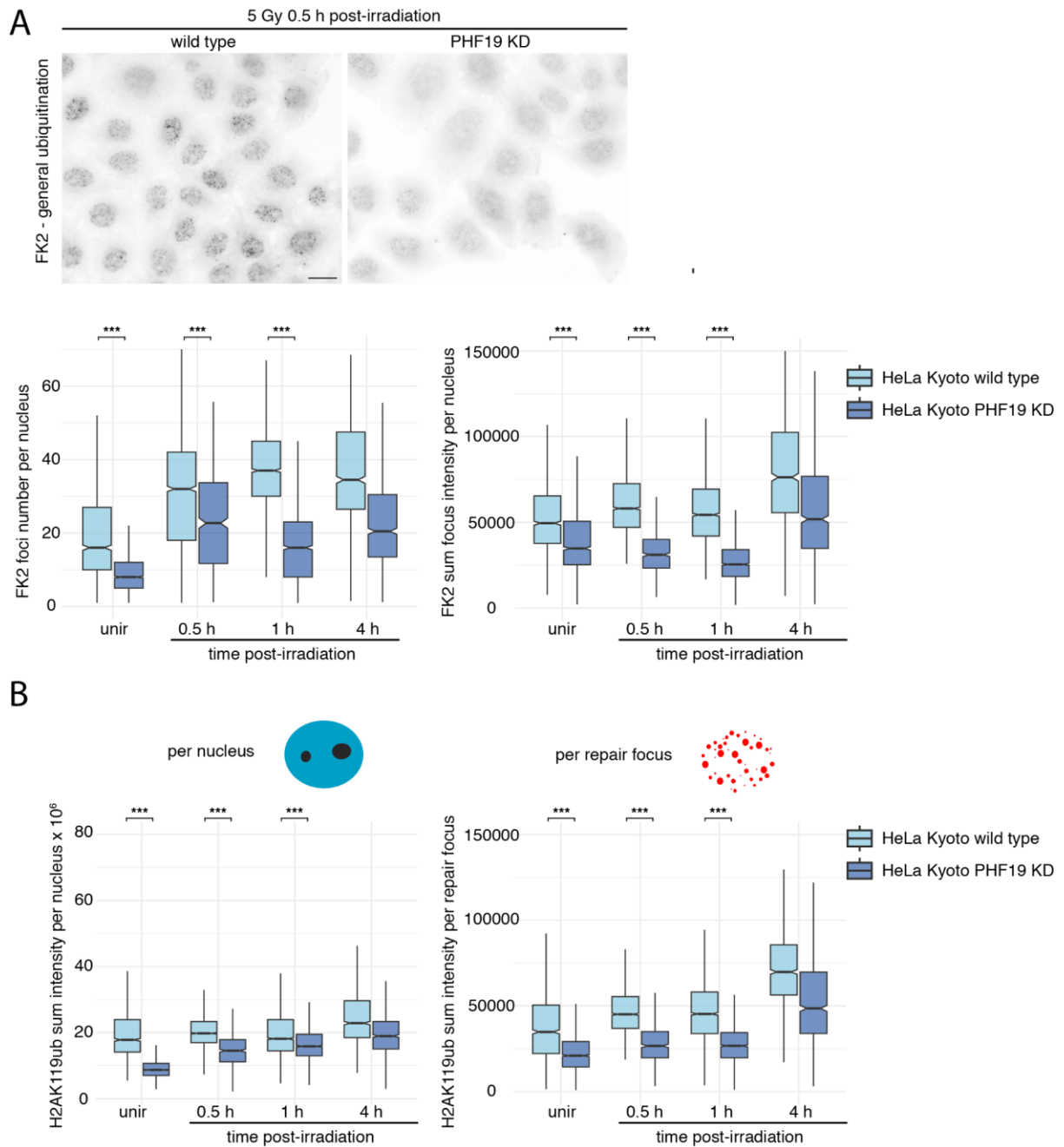
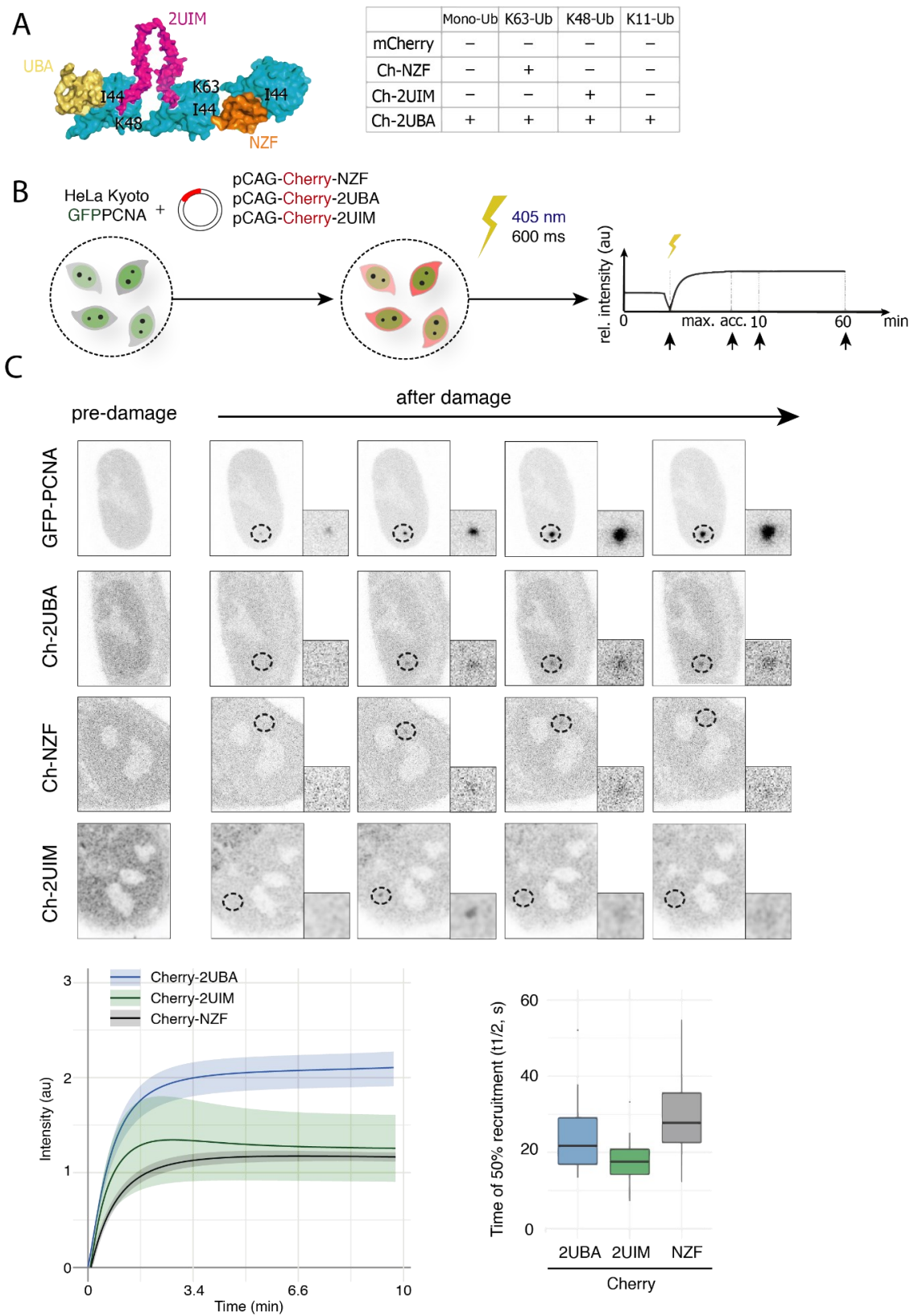


Figure 4.26. PHF19 depletion impairs ubiquitination signaling at the DSBs. (A) Representative images and quantification of the general ubiquitination (FK2) at the damage spots, at least 1000 cells analyzed per condition. The box plot description as above. The outliers are not presented in the plot. *** $p < 0.001$ by t -test, for knockdown sample versus wild type sample. Scale bar 20 μm . (B) Quantification of the whole-nuclear H2AK119ub intensity and H2AK119ub intensity at the repair foci in the wild type and PHF19-depleted cells, at least 1000 cells analyzed per condition. The box plot description as above. The outliers are not presented in the plot. *** $p < 0.001$ by t -test, for knockdown sample versus wild type sample.

To discriminate ubiquitination constructed by different linkages, we used the ubiquitin probes combining the ubiquitin interacting motifs 2UBA from RAD23, 2UIM from USP25 and the NZF from TAK1 binding protein 2 (TAB2) fused with mCherry fluorescent protein published before (Qin et al., 2022). The 2UIM specifically recognizes K48 ubiquitin linkage via binding the proximal

ubiquitin with UIM2 and to the distal one with UIM1 domain (Kawaguchi et al., 2017), the NZF binds the Ile44 patch of both proximal and distal ubiquitin to specifically recognize the K63 ubiquitin linkage (Kulathu et al., 2009; van Wijk et al., 2012), and the 2UBA showed linkage-independent binding (Bertolaet et al., 2001; Qin et al., 2022) (Figure 4.27A). First, we characterized the accumulation kinetics of the ubiquitin probes at the DNA damage site in the live cells stably expressing GFP-tagged PCNA protein (GFP-PCNA) and ectopically expressing mCherry tagged ubiquitin probes (Figure 4.27B). To locally induce DNA damage, we irradiated a spot in the nucleus with a focused 405 nm laser. Using live-cell imaging, we monitored GFP-PCNA accumulation as a readout of DNA damage and the ubiquitin probes as a readout of the ubiquitination (Figure 4.27B, C). By comparing the probes, we calculated the ubiquitination dynamics during DNA repair. We found that Cherry-2UIM (K48) showed the fastest association with DNA damage sites (time of 50% recruitment ($t_{1/2}$): ~17 sec) versus Cherry-2UBA (K48 and K63, $t_{1/2}$: ~24 s) and Ch-NZF (K63, $t_{1/2}$: ~30 s) (Figure 4.27C). In line with previous studies (Acs et al., 2011; Ali et al., 2018; Feng and Chen, 2012; Mallette et al., 2012; Meerang et al., 2011), we found that K48-linked polyubiquitination mediates protein degradation and nucleosome eviction at DNA damage sites and facilitates following K63-linked ubiquitination mediated signaling repair pathways. Interestingly, Cherry-2UBA and Cherry-NZF exhibited stable association with damage sites over one hour, whereas Cherry-2UIM dissociated from DNA damage sites after 10 min and its retention time was more variable between cells than of the other two probes (Annex: Figure 7.11). Our observation that the stability of Cherry-2UIM binding to the damaged spot was lower indicating its rapid turnover (Figure 4.27C), suggests that the K48 chain formation is short-lived, and less uniform compared to K63 during DNA damage response. In contrast to the wild type cells, the ubiquitination probes showed different recruitment kinetics in the PHF19-depleted cells. The Cherry-2UBA accumulation was slower than in the wild type cells and the accumulation intensity was much lower (Figure 4.27D). Interestingly, the damage spot marked by the Cherry-2UBA accumulation took up a bigger area in the nucleus and together with the low intensity appeared as decompacted (Figure 4.27D). The effect observed might be another line of evidence for the chromatin remodeling happening in the PHF19-depleted cells prior to the DNA damage. However, the mechanism of the ubiquitination signaling defect remains to be elucidated.



D

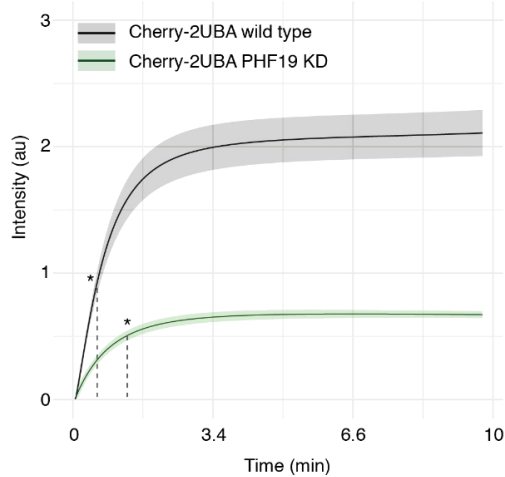
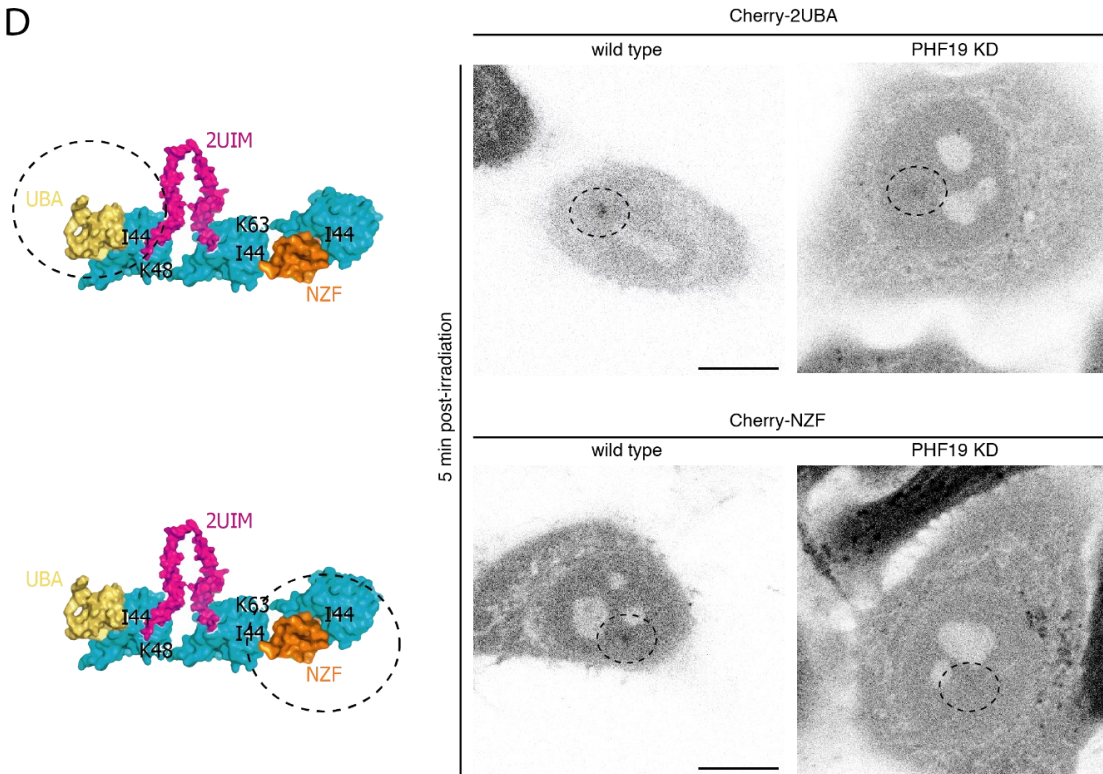


Figure 4.27. PHF19-depleted cells fail to retain ubiquitination at the damage spot. (A) Scheme of the ubiquitin-binding preferences of the ubiquitin probes used. (B) Scheme of the laser microirradiation experiment. (C) Representative images corresponding to the time points indicated in (B) with black arrowheads. DNA damage was locally induced by microirradiation (black dotted circle) and zoomed images are shown. The Ch-2UIM image was processed for better representation of the signal: raw image was multiplied by itself, then processed with ROF denoise filter (theta 100) and Gaussian filter (sigma 1.5). Ubiquitin probes recruitment curves displayed as mean \pm SEM for two or three independent experiments after DNA damage. For each experimental condition at least 25 cells were used. Times of 50% recruitment of ubiquitin probes at DNA damage sites represented as box plots. Middle line depicts the median value among the cell population. (D) Representative images of the Cherry-2UBA and Cherry-NZF ubiquitin probes recruitment to the laser-induced damage spot in the wild type and PHF19-depleted cells. Scale bar 20 μ m.

Ubiquitin probes recruitment curves displayed as mean ± SEM for two or three independent experiments after DNA damage. For each experimental condition at least 25 cells were used.

Interestingly, the accumulation of the Cherry-NZF probe that specifically binds K63-ubiquitination was severely impaired in the absence of PHF19 (Figure 4.27D). The accumulation intensity was as weak as the background nuclear intensity rendering the calculation of the recruitment curve not possible. Thus, the PHF19 depletion specifically impaired the DNA damage and repair ubiquitination signaling in the cells under stress.

Taken together, the PHF19 is a novel modulator of chromatin response to DNA damage. Predominantly localizing to the facultative heterochromatin regions, PHF19 is involved in the formation and stability of the compacted domains as a part of the PRC2-mediated transcriptional silencing. Accordingly, the depletion of PHF19 in unchallenged cells leads to the global loss of chromatin compaction and downregulation of both total ubiquitin signaling and PRC1-specific chromatin ubiquitination (H2AK119ub). After the exposure to X-ray radiation, the global chromatin compaction loss remains up until 2 h post-irradiation. The PHF19-depleted cells fail to initiate and maintain the DNA damage-specific chromatin H2AX phosphorylation (γ H2AX). The γ H2AX formation is known as one of the earliest events in the DNA damage response and serves for DNA damage signaling cascade amplification. In line with the observed disruption of the γ H2AX domains, PHF19 depletion causes delay in the recruitment of repair factors downstream to the γ H2AX, RNF8 and 53BP1. Remarkably, the γ H2AX writer (pATM) and γ H2AX reader (MDC1) behave differently in the PHF19 knockdown cells. The pATM shows significant delay in its recruitment to the double-strand breaks, which, however, cannot completely explain the γ H2AX defect. In contrast, MDC1 is extensively recruited to the damaged chromatin independently of the impaired γ H2AX in the PHF19 knockdown cells but does not rescue RNF8 and 53BP1 recruitment. The PHF19 depletion abolishes the recruitment of the homologous recombination factors such as RAD51 and RAD52 despite the upregulation of their protein levels at the late time points post-damage. Interestingly, the phenotype we describe here for the PHF19 possesses similarity to the depletion phenotype of BMI1, the PRC1 component with the ubiquitin stimulating activity (Ismail et al., 2010; Fiteh et al., 2022). The depletion of BMI1 was reported to hinder 53BP1, BRCA1, RAD51 and RAP80 recruitment to the double-strand breaks and impaired the homologous recombination. Similar to PHF19, BMI1 appears to be upstream or independent of the γ H2AX and RNF8 cascade, several studies describe BMI1 to be recruited to the damage sites by recognizing PARylation and the MRN complex (Chou et al., 2010; Ismail et al., 2010; Rona et al., 2018). Interestingly, the γ H2AX loss in the BMI1/RING1-depleted cells was observed only in the presence of the DNA-PKcs inhibitor (Pan et al., 2011). In contrast to PHF19 depletion characterized by overrecruitment of MDC1, the BMI1 depletion in the presence of the DNA-PKcs inhibitor led to decrease of MDC1 accumulation. The homologous recombination defect of BMI1 depletion is particularly important, since the PHF19 depletion abolishes both RAD51 and RAD52 recruitment and elevates DNA damage levels. The homologous recombination defect caused by the absence of BMI1 is partially caused by the cell cycle changes (Ginjala et al., 2011), which is not the case for PHF19 depletion. Remarkably, the common feature of both BMI1 and PHF19 depletion phenotypes is downregulation of the H2AK119ub chromatin mark. The recent findings demonstrate that the H2AK119ub is required for the γ H2AX stability, the end resection and the homologous recombination (Fiteh et al., 2022). While lowering of the H2AK119ub levels could

explain the repair defect and impaired recruitment of the HR repair factors by similarity with the BMI1 depletion phenotype, the changed chromatin compaction, prolonged disruption of the γ H2AX in the presence of other phosphoinositide 3-related kinases (ATR, DNA-PKcs), prolonged disruption of the general ubiquitination domains and impaired recruitment of the NHEJ proteins remain unexplained. Interestingly, another PRC2 component of the PHF protein family that is recruited to the sites of DNA damage is PHF1. In contrast to the BMI1/RING1 recruitment, it physically interacts with Ku70/Ku80 break sensors and impairs DNA repair leading to the X-ray sensitivity (Hong et al., 2008). Unlike BMI1 and PHF19, PHF1 appear to recruit within 10 min after the damage and to dissociate fast. It is yet to be elucidated if the observed effect in the PHF19-depleted cells is caused by the change in the transcriptional silencing *in cis* to the breaks, since the extent of the crosstalk between the PRC-mediated transcriptional silencing at the damage sites and PRC-mediated chromatin response to damage remains to be uncovered.

In summary, we describe here a novel PRC-associated ubiquitin modulator of chromatin response to DNA damage discovered in our screens. We show that the loss of PHF19 changes chromatin structure, impairs ubiquitination signaling and recruitment of the NHEJ and HR factors to double-strand breaks that leads to DNA damage accumulation. Our work provides novel lines of evidence for the involvement of PRC complexes in genome maintenance.

5. General conclusions and perspectives

We have developed and performed two high-throughput siRNA-based screenings for the discovery of ubiquitin modulators involved in the repair of DNA double-strand breaks. We used a large glass array layout to accommodate more than 24000 siRNA spots for 663 genes and 2×10^6 cells per glass array. We quantified DNA damage signaling and repair through γ H2AX whole-nuclear intensity, the marker of double-strand breaks. We used an automatic imaging platform with a motorized stage to image the precise locations of the siRNA and mock-transfected spots. We constructed the image analysis pipeline for the high-throughput single-cell analysis of imaging data across siRNA spots, arrays, and timepoints.

The outcome of the screen allowed the identification of more than 100 ubiquitin modulators either up- or downregulating the γ H2AX intensity compared to the control cells at 0.5 h and 24 h post-irradiation. Thirty nine of them were shared between the time points indicating their significance for all stages of DSB repair. We analyzed the hits and distinguished seven scenarios of action among them based on the γ H2AX response and the time parameter. The functional profiling and PPI/pathway analysis uncovered previously unknown aspects of ubiquitin-dependent signaling in DNA repair.

The second 4D small-scale screen determined the DNA repair pathway preference and kinetics of the 39 shared hits through γ H2AX, RAD51 and 53BP1 nuclear foci quantification in single cells. The automatic imaging allowed us to monitor the formation of the knockdown phenotypes at the single repair focus level. We created the image analysis pipeline tailored for high-throughput analysis of the γ H2AX, RAD51 and 53BP1 foci parameters in 2D and 3D. Based on the foci parameters readouts, we performed cluster analysis and identified four time-independent knockdown repair phenotypes caused by the depletion of CXXC1, XIAP, RNF8 and RNF168.

Both screens demonstrated high sensitivity: (1) by identifying the expected or so called “positive control” factors as hits and (2) by identifying distinct phenotypes of delayed or accelerated DNA damage signaling and repair.

The methodology described in this thesis has potential for the large varieties of the assays to study the chromatin response to DNA damage. The large format of the glass bottom array with pre-printed siRNAs can be used with various libraries to target various chromatin modulators in various damage contexts, such as UV damage, alkylating agents and others. The automatic imaging combined with the developed high-throughput image analysis protocols allows monitoring of the dynamics of the multiple DNA repair factors at the single focus level. The repair foci parameters and the individual foci colocalization analysis can be successfully applied to the identification of novel DNA repair phenotypes caused by the depletion of both unidentified and known chromatin proteins.

More than 100 ubiquitin modulators identified in the primary and second screens are yet to be annotated for their molecular function in the DDR. Uncovering of the signaling cascades among the hits at the different stages of DNA repair is of paramount importance. On the one hand, it would put non-proteolytic ubiquitination on chromatin in the limelight. On the other hand, finding the protein-protein interactions among hits would provide a link between the chromatin structure and molecular DNA processes and essential for our understanding of chromatin being an active regulator.

Among the hits identified we focused on PHF19, whose depletion led to downregulation of γ H2AX signaling at 0.5 h and 24 h post-irradiation. PHF19 has been described as part of the PRC2 complex involved in the transcriptional silencing where it recognizes the H3K36me3 chromatin mark and facilitates its replacement by the H3K27me3 (Brien et al., 2012; Ballaré et al., 2012; Cai et al., 2013). No role of PHF19 in DNA damage signaling and repair has been reported so far, however, there is extensive evidence of PHF19 overexpression as a marker for poor prognosis in various cancer types (Wang et al., 2004b; Ghislin et al., 2012; Xiaoyun et al., 2021; Jain et al., 2020). We found that PHF19 is required to retain the ubiquitination signaling globally and at the sites of the double-strand breaks. We showed that PHF19 depletion permanently impairs the spreading of the H2AX phosphorylation on chromatin, thus hindering the formation of DNA repair foci in 3D. The accumulation of downstream repair factors at double-strand breaks was delayed up to 24 h post damage (53BP1, RNF8, pATM) or completely abolished (RAD51, RAD52). We showed that both NHEJ and HR repair pathways are inhibited in the PHF19-depleted cells leading to elevated levels of DNA damage in both unchallenged and X-ray radiated cells. The absence of PHF19 sensitized cells to DNA damage and increased the frequency of apoptosis, without affecting cell cycle distribution. Importantly, we observed that PHF19 depletion alters the chromatin compaction levels in a DNA damage-independent manner. The decreased compaction of usually tightly packed chromatin domains appears to facilitate over-recruitment of repair factors that are able to bind nucleosomes independently of other repair pathways (MDC1). Additionally, we showed that the lack of PHF19 hinders ubiquitination in multiple ways. First, the recruitment of DNA damage E3 ubiquitin ligases (RNF8) was impaired causing the reduction of the K63-linked ubiquitin marks near the breaks. We confirmed this observation in live cells by demonstrating the slowed down accumulation of 2UBA and NZF ubiquitin binding probes. Next, we found that PRC1-mediated H2AK119ub mark that was recently connected to DNA repair (Fitieh et al., 2022) is depleted globally and locally at the DSBs in the absence of PHF19. Several other components of the PRC1 and PRC2 complexes such as BMI1, RING2, EZH2, EED, PHF1 and SUZ12 (Campbell et al., 2013; Fitieh et al., 2021; Chou et al., 2010) show recruitment to damaged chromatin in microirradiation experiments suggesting that PRC complexes have an active role in DNA damage signaling and repair independent of their canonical function in transcription. Interestingly, it was reported that some PRC complex subunits were recruited to the damage sites even prior to γ H2AX and independently of it. This fact suggests that PRC components and PHF19 represent an alternative chromatin signaling cascade in response to DNA damage, however, the extent of its crosstalk with the γ H2AX-RNF8/RNF168-53BP1 cascade is yet to be uncovered.

We demonstrate that PHF19 depletion changes chromatin independent of DNA damage, characterizing PHF19 not only as a novel repair factor but as a novel ubiquitin dependent chromatin remodeler. In line with this hypothesis, other PRC components were shown to interact with chromatin remodeler KAP1/TRIM27 (Cheng et al., 2014; Maat et al., 2021). KAP1 is enriched in endogenous heterochromatic loci. Upon damage, KAP1 is phosphorylated by ATM and involved in DNA repair (White et al., 2012). PHF19 could have a similar role providing both formation of chromatin domains without DNA damage and formation of repair foci under stress (Figure 4.28). Additionally, it was shown that PRC1 shapes 3D genome organization by mediating long-range interactions that are independent of CTCF and can bridge sites at a megabase scale (Boyle et al., 2020). These long-range interactions were shown to be independent of transcription. As PRC1 is recruited by PRC2 (including PHF19), this suggests that PHF19 is

involved in establishing long-range chromatin interactions. The global chromatin decompaction in the PHF19-depleted cells observed supports this hypothesis. Hence, PHF19 role in chromatin organization and DDR are additional functions to its role as a transcriptional silencing factor. Finally, the H2AK119ub chromatin mark facilitated by the PHF19 activity itself promotes chromatin compaction and its loss impairs the DDR (Arends et al., 2024). The H2AK119ub-dependent chromatin compaction was shown to be directly antagonized by the PRC-associated deubiquitinases (Bonnet et al., 2022). This fact supports chromatin compaction being dependent from chromatin ubiquitination. In summary, our work highlights the pivotal role of chromatin and its structure in DNA damage signaling and repair.

Although the current work does not describe the precise molecular mechanism of the novel ubiquitin modulator PHF19 in the DDR, it summarizes main effects of its depletion on both chromatin and repair proteins. Several additional experiments would help to complete the PHF19 characterization. The protein-protein interaction analysis together with the mass spectrometry could be used to identify the interaction partners of PHF19 on the damaged chromatin. There is a high probability that at least some of them would be other PRC components, for example, such as SUZ12, direct interaction partner of PHF19 in the PRC2, which would bring us closer to deciphering the crosstalk between transcription and genome maintenance processes in nucleus. The global and local transcriptional changes caused by PHF19 depletion are to be elucidated. Since the global chromatin compaction changes in the absence of PHF19, it is probable that alone or together with other PRC components PHF19 mediates long-range chromatin contacts and DNA looping. Another open question is how exactly PHF19 depletion changes the ubiquitination at the DNA damage sites. We hypothesize that PHF19 is not only governs the chromatin structure but also serves as a part of ubiquitin-dependent signaling cascades in response to DNA damage. The phenotype we describe here is characterized by the prominent loss of general ubiquitination levels, which is unusual of for other PRC components depletion phenotypes. Looking at other DDR-specific chromatin ubiquitination marks and finding changed ubiquitination cascades would expand our knowledge on how chromatin ubiquitination controls the molecular DNA processes.

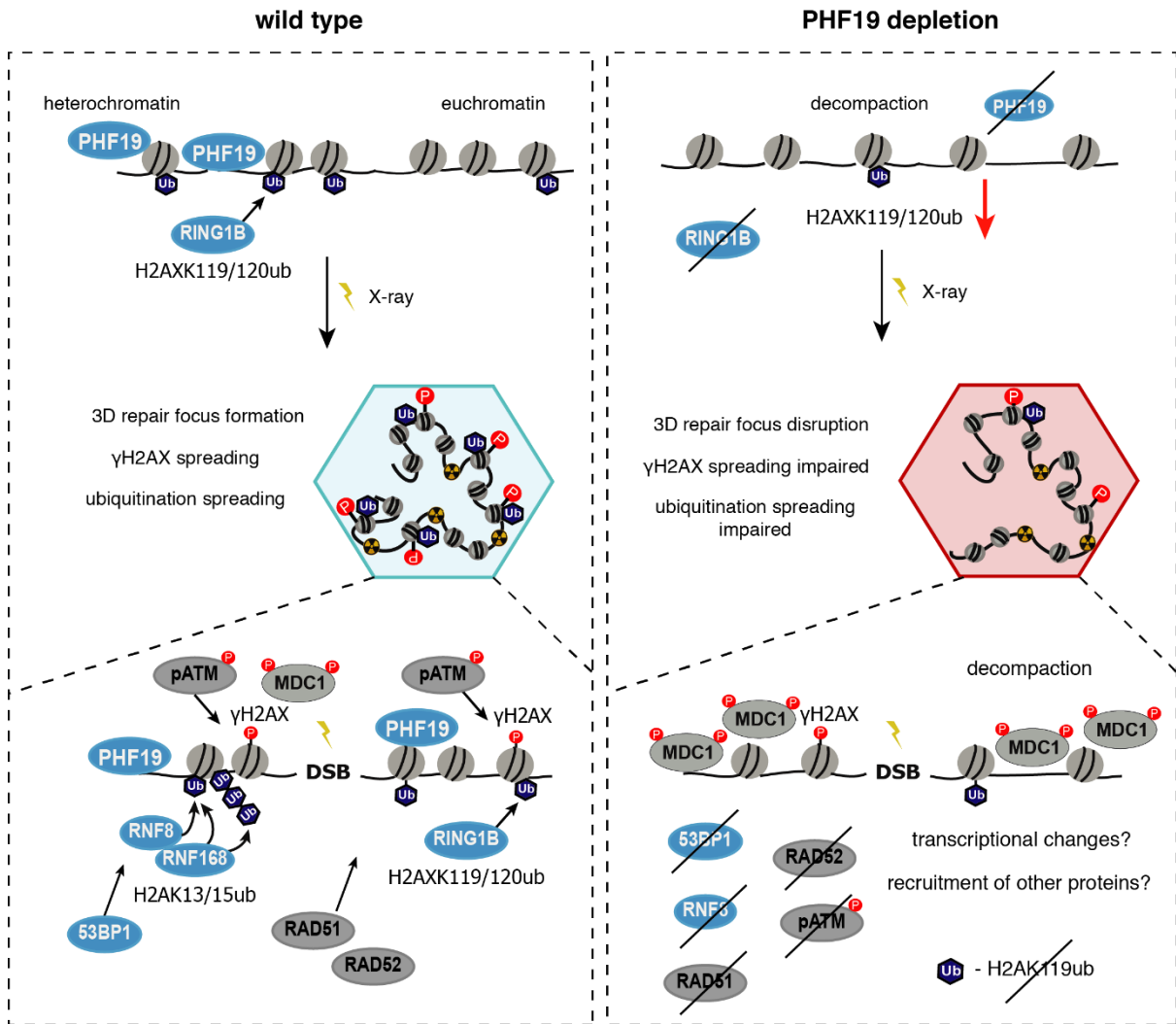


Figure 4.28. The hypothesis.

6. Bibliography

- Abdouh, M., Facchino, S., Chatoo, W., Balasingam, V., Ferreira, J., and Bernier, G. (2009). BMI1 sustains human glioblastoma multiforme stem cell renewal. *J. Neurosci.* 29, 8884–8896. doi:10.1523/JNEUROSCI.0968-09.2009.
- Acs, K., Luijsterburg, M. S., Ackermann, L., Salomons, F. A., Hoppe, T., and Dantuma, N. P. (2011). The AAA-ATPase VCP/p97 promotes 53BP1 recruitment by removing L3MBTL1 from DNA double-strand breaks. *Nat. Struct. Mol. Biol.* 18, 1345–1350. doi:10.1038/nsmb.2188.
- Adhikary, S., Marinoni, F., Hock, A., Hulleman, E., Popov, N., Beier, R., Bernard, S., Quarto, M., Capra, M., Goettig, S., et al. (2005). The ubiquitin ligase HectH9 regulates transcriptional activation by Myc and is essential for tumor cell proliferation. *Cell* 123, 409–421. doi:10.1016/j.cell.2005.08.016.
- Ahmed, S. F., Buetow, L., Gabrielsen, M., Lilla, S., Chatrin, C., Sibbet, G. J., Zanivan, S., and Huang, D. T. (2020). DELTEX2 C-terminal domain recognizes and recruits ADP-ribosylated proteins for ubiquitination. *Sci. Adv.* 6. doi:10.1126/sciadv.abc0629.
- Alagoz, M., Katsuki, Y., Ogiwara, H., Ogi, T., Shibata, A., Kakarougkas, A., and Jeggo, P. (2015). SETDB1, HP1 and SUV39 promote repositioning of 53BP1 to extend resection during homologous recombination in G2 cells. *Nucleic Acids Res.* 43, 7931–7944. doi:10.1093/nar/gkv722.
- Alcón, P., Shakeel, S., Chen, Z. A., Rappsilber, J., Patel, K. J., and Passmore, L. A. (2020). FANCD2-FANCI is a clamp stabilized on DNA by monoubiquitination of FANCD2 during DNA repair. *Nat. Struct. Mol. Biol.* 27, 240–248. doi:10.1038/s41594-020-0380-1.
- Ali, M. A. M., Strickfaden, H., Lee, B. L., Spyrapoulos, L., and Hendzel, M. J. (2018). RYBP Is a K63-Ubiquitin-Chain-Binding Protein that Inhibits Homologous Recombination Repair. *Cell Rep.* 22, 383–395. doi:10.1016/j.celrep.2017.12.047.
- Amendola, P. G., Zaghet, N., Ramalho, J. J., Vilstrup Johansen, J., Boxem, M., and Salcini, A. E. (2017). JMJD-5/KDM8 regulates H3K36me2 and is required for late steps of homologous recombination and genome integrity. *PLoS Genet.* 13, e1006632. doi:10.1371/journal.pgen.1006632.
- Anand, R., Ranjha, L., Cannavo, E., and Cejka, P. (2016). Phosphorylated CtIP Functions as a Co-factor of the MRE11-RAD50-NBS1 Endonuclease in DNA End Resection. *Mol. Cell* 64, 940–950. doi:10.1016/j.molcel.2016.10.017.
- Andersen, P. L., Zhou, H., Pastushok, L., Moraes, T., McKenna, S., Ziola, B., Ellison, M. J., Dixit, V. M., and Xiao, W. (2005). Distinct regulation of Ubc13 functions by the two ubiquitin-conjugating enzyme variants Mms2 and Uev1A. *J. Cell Biol.* 170, 745–755. doi:10.1083/jcb.200502113.
- Ang, X. L., and Wade Harper, J. (2005). SCF-mediated protein degradation and cell cycle control. *Oncogene* 24, 2860–2870. doi:10.1038/sj.onc.1208614.
- An, L., Dong, C., Li, J., Chen, J., Yuan, J., Huang, J., Chan, K. M., Yu, C.-H., and Huen, M. S. Y. (2018). RNF169 limits 53BP1 deposition at DSBs to stimulate single-strand annealing repair. *Proc Natl Acad Sci USA* 115, E8286–E8295. doi:10.1073/pnas.1804823115.

- Arends, T., Tsuchida, H., Adeyemi, R. O., and Tapscott, S. J. (2024). DUX4-induced HSATII transcription causes KDM2A/B-PRC1 nuclear foci and impairs DNA damage response. *J. Cell Biol.* 223. doi:10.1083/jcb.202303141.
- Arnould, C., Rocher, V., Finoux, A.-L., Clouaire, T., Li, K., Zhou, F., Caron, P., Mangeot, P. E., Ricci, E. P., Mourad, R., et al. (2021). Loop extrusion as a mechanism for formation of DNA damage repair foci. *Nature* 590, 660–665. doi:10.1038/s41586-021-03193-z.
- Atsumi, Y., Minakawa, Y., Ono, M., Dobashi, S., Shinohe, K., Shinohara, A., Takeda, S., Takagi, M., Takamatsu, N., Nakagama, H., et al. (2015). ATM and SIRT6/SNF2H Mediate Transient H2AX Stabilization When DSBs Form by Blocking HUWE1 to Allow Efficient γ H2AX Foci Formation. *Cell Rep.* 13, 2728–2740. doi:10.1016/j.celrep.2015.11.054.
- Aymard, F., Aguirrebengoa, M., Guillou, E., Javierre, B. M., Bugler, B., Arnould, C., Rocher, V., Iacovoni, J. S., Biernacka, A., Skrzypczak, M., et al. (2017). Genome-wide mapping of long-range contacts unveils clustering of DNA double-strand breaks at damaged active genes. *Nat. Struct. Mol. Biol.* 24, 353–361. doi:10.1038/nsmb.3387.
- Aymard, F., Bugler, B., Schmidt, C. K., Guillou, E., Caron, P., Briois, S., Iacovoni, J. S., Daburon, V., Miller, K. M., Jackson, S. P., et al. (2014). Transcriptionally active chromatin recruits homologous recombination at DNA double-strand breaks. *Nat. Struct. Mol. Biol.* 21, 366–374. doi:10.1038/nsmb.2796.
- Ayrappetov, M. K., Gursoy-Yuzugullu, O., Xu, C., Xu, Y., and Price, B. D. (2014). DNA double-strand breaks promote methylation of histone H3 on lysine 9 and transient formation of repressive chromatin. *Proc Natl Acad Sci USA* 111, 9169–9174. doi:10.1073/pnas.1403565111.
- Azzoni, V., Wicinski, J., Macario, M., Castagné, M., Finetti, P., Ambrosova, K., Rouault, C. D., Sergé, A., Farina, A., Agavnián, E., et al. (2022). BMI1 nuclear location is critical for RAD51-dependent response to replication stress and drives chemoresistance in breast cancer stem cells. *Cell Death Dis.* 13, 96. doi:10.1038/s41419-022-04538-w.
- Bader, G. D., and Hogue, C. W. V. (2003). An automated method for finding molecular complexes in large protein interaction networks. *BMC Bioinformatics* 4, 2. doi:10.1186/1471-2105-4-2.
- Baker, R. T., and Board, P. G. (1987). The human ubiquitin gene family: structure of a gene and pseudogenes from the Ub B subfamily. *Nucleic Acids Res.* 15, 443–463. doi:10.1093/nar/15.2.443.
- Ballaré, C., Lange, M., Lapinaite, A., Martin, G. M., Morey, L., Pascual, G., Liefke, R., Simon, B., Shi, Y., Gozani, O., et al. (2012). Phf19 links methylated Lys36 of histone H3 to regulation of Polycomb activity. *Nat. Struct. Mol. Biol.* 19, 1257–1265. doi:10.1038/nsmb.2434.
- Balmik, A. A., Sonawane, S. K., and Chinnathambi, S. (2021). The extracellular HDAC6 ZnF UBP domain modulates the actin network and post-translational modifications of Tau. *Cell Commun. Signal.* 19, 49. doi:10.1186/s12964-021-00736-9.
- Bartkova, J., Horejsí, Z., Koed, K., Krämer, A., Tort, F., Zieger, K., Guldberg, P., Sehested, M., Nesland, J. M., Lukas, C., et al. (2005). DNA damage response as a candidate anti-cancer barrier in early human tumorigenesis. *Nature* 434, 864–870. doi:10.1038/nature03482.
- Bartocci, C., Diedrich, J. K., Ouzounov, I., Li, J., Piunti, A., Pasini, D., Yates, J. R., and Lazzarini Denchi, E. (2014). Isolation of chromatin from dysfunctional telomeres reveals an important role for Ring1b in NHEJ-mediated chromosome fusions. *Cell Rep.* 7, 1320–1332. doi:10.1016/j.celrep.2014.04.002.

- Battu, A., Ray, A., and Wani, A. A. (2011). ASF1A and ATM regulate H3K56-mediated cell-cycle checkpoint recovery in response to UV irradiation. *Nucleic Acids Res.* 39, 7931–7945. doi:10.1093/nar/gkr523.
- Bayona-Feliu, A., and Aguilera, A. (2021). The role of chromatin at transcription-replication conflicts as a genome safeguard. *Biochem. Soc. Trans.* doi:10.1042/BST20210691.
- Becker, J. R., Clifford, G., Bonnet, C., Groth, A., Wilson, M. D., and Chapman, J. R. (2021). BARD1 reads H2A lysine 15 ubiquitination to direct homologous recombination. *Nature* 596, 433–437. doi:10.1038/s41586-021-03776-w.
- Bekker-Jensen, S., Rendtlew Danielsen, J., Fugger, K., Gromova, I., Nerstedt, A., Lukas, C., Bartek, J., Lukas, J., and Mailand, N. (2010). HERC2 coordinates ubiquitin-dependent assembly of DNA repair factors on damaged chromosomes. *Nat. Cell Biol.* 12, 80–6; sup pp 1. doi:10.1038/ncb2008.
- Ben-Saadon, R., Zaaroor, D., Ziv, T., and Ciechanover, A. (2006). The polycomb protein Ring1B generates self atypical mixed ubiquitin chains required for its in vitro histone H2A ligase activity. *Mol. Cell* 24, 701–711. doi:10.1016/j.molcel.2006.10.022.
- Bergink, S., Salomons, F. A., Hoogstraten, D., Groothuis, T. A. M., de Waard, H., Wu, J., Yuan, L., Citterio, E., Houtsmuller, A. B., Neefjes, J., et al. (2006). DNA damage triggers nucleotide excision repair-dependent monoubiquitylation of histone H2A. *Genes Dev.* 20, 1343–1352. doi:10.1101/gad.373706.
- Bertolaet, B. L., Clarke, D. J., Wolff, M., Watson, M. H., Henze, M., Divita, G., and Reed, S. I. (2001). UBA domains of DNA damage-inducible proteins interact with ubiquitin. *Nat. Struct. Biol.* 8, 417–422. doi:10.1038/87575.
- Beucher, A., Birraux, J., Tchouandong, L., Barton, O., Shibata, A., Conrad, S., Goodarzi, A. A., Krempler, A., Jeggo, P. A., and Löbrich, M. (2009). ATM and Artemis promote homologous recombination of radiation-induced DNA double-strand breaks in G2. *EMBO J.* 28, 3413–3427. doi:10.1038/emboj.2009.276.
- Bhoomik, A., Singha, N., O’Connell, M. J., and Ronai, Z. A. (2008). Regulation of TIP60 by ATF2 modulates ATM activation. *J. Biol. Chem.* 283, 17605–17614. doi:10.1074/jbc.M802030200.
- Birmingham, A., Selfors, L. M., Forster, T., Wrobel, D., Kennedy, C. J., Shanks, E., Santoyo-Lopez, J., Dunican, D. J., Long, A., Kelleher, D., et al. (2009). Statistical methods for analysis of high-throughput RNA interference screens. *Nat. Methods* 6, 569–575. doi:10.1038/nmeth.1351.
- Bjorklund, C. C., Kang, J., Amatangelo, M., Polonskaia, A., Katz, M., Chiu, H., Couto, S., Wang, M., Ren, Y., Ortiz, M., et al. (2020). Iberdomide (CC-220) is a potent cereblon E3 ligase modulator with antitumor and immunostimulatory activities in lenalidomide- and pomalidomide-resistant multiple myeloma cells with dysregulated CRBN. *Leukemia* 34, 1197–1201. doi:10.1038/s41375-019-0620-8.
- Boisvert, R. A., and Howlett, N. G. (2014). The Fanconi anemia ID2 complex: dueling axes at the crossroads. *Cell Cycle* 13, 2999–3015. doi:10.4161/15384101.2014.956475.
- Bomar, M. G., D’Souza, S., Bienko, M., Dikic, I., Walker, G. C., and Zhou, P. (2010). Unconventional ubiquitin recognition by the ubiquitin-binding motif within the Y family DNA polymerases iota and Rev1. *Mol. Cell* 37, 408–417. doi:10.1016/j.molcel.2009.12.038.

- Bondeson, D. P., Mares, A., Smith, I. E. D., Ko, E., Campos, S., Miah, A. H., Mulholland, K. E., Routly, N., Buckley, D. L., Gustafson, J. L., et al. (2015). Catalytic in vivo protein knockdown by small-molecule PROTACs. *Nat. Chem. Biol.* 11, 611–617. doi:10.1038/nchembio.1858.
- Bonnet, J., Boichenko, I., Kalb, R., Le Jeune, M., Maltseva, S., Pieropan, M., Finkl, K., Fierz, B., and Müller, J. (2022). PR-DUB preserves Polycomb repression by preventing excessive accumulation of H2Aub1, an antagonist of chromatin compaction. *Genes Dev.* 36, 1046–1061. doi:10.1101/gad.350014.122.
- Botuyan, M. V., Lee, J., Ward, I. M., Kim, J.-E., Thompson, J. R., Chen, J., and Mer, G. (2006). Structural basis for the methylation state-specific recognition of histone H4-K20 by 53BP1 and Crb2 in DNA repair. *Cell* 127, 1361–1373. doi:10.1016/j.cell.2006.10.043.
- Boyle, S., Flyamer, I. M., Williamson, I., Sengupta, D., Bickmore, W. A., and Illingworth, R. S. (2020). A central role for canonical PRC1 in shaping the 3D nuclear landscape. *Genes Dev.* 34, 931–949. doi:10.1101/gad.336487.120.
- Brambilla, F., Garcia-Manteiga, J. M., Monteleone, E., Hoelzen, L., Zocchi, A., Agresti, A., and Bianchi, M. E. (2020). Nucleosomes effectively shield DNA from radiation damage in living cells. *Nucleic Acids Res.* 48, 8993–9006. doi:10.1093/nar/gkaa613.
- Bray, M.-A., Fraser, A. N., Hasaka, T. P., and Carpenter, A. E. (2012). Workflow and metrics for image quality control in large-scale high-content screens. *J. Biomol. Screen.* 17, 266–274. doi:10.1177/1087057111420292.
- Brien, G. L., Gambero, G., O’Connell, D. J., Jerman, E., Turner, S. A., Egan, C. M., Dunne, E. J., Jurgens, M. C., Wynne, K., Piao, L., et al. (2012). Polycomb PHF19 binds H3K36me3 and recruits PRC2 and demethylase NO66 to embryonic stem cell genes during differentiation. *Nat. Struct. Mol. Biol.* 19, 1273–1281. doi:10.1038/nsmb.2449.
- Brown, J. S., Lukashchuk, N., Sczaniecka-Clift, M., Britton, S., le Sage, C., Calsou, P., Beli, P., Galanty, Y., and Jackson, S. P. (2015). Neddylation promotes ubiquitylation and release of Ku from DNA-damage sites. *Cell Rep.* 11, 704–714. doi:10.1016/j.celrep.2015.03.058.
- Bruno, T., Iezzi, S., De Nicola, F., Di Padova, M., Desantis, A., Scarsella, M., Di Certo, M. G., Leonetti, C., Floridi, A., Passananti, C., et al. (2008). Che-1 activates XIAP expression in response to DNA damage. *Cell Death Differ.* 15, 515–520. doi:10.1038/sj.cdd.4402284.
- Bryant, H. E., Schultz, N., Thomas, H. D., Parker, K. M., Flower, D., Lopez, E., Kyle, S., Meuth, M., Curtin, N. J., and Helleday, T. (2005). Specific killing of BRCA2-deficient tumours with inhibitors of poly(ADP-ribose) polymerase. *Nature* 434, 913–917. doi:10.1038/nature03443.
- Buchwald, G., van der Stoop, P., Weichenrieder, O., Perrakis, A., van Lohuizen, M., and Sixma, T. K. (2006). Structure and E3-ligase activity of the Ring-Ring complex of polycomb proteins Bmi1 and Ring1b. *EMBO J.* 25, 2465–2474. doi:10.1038/sj.emboj.7601144.
- Burgess, R. C., Burman, B., Kruhlak, M. J., and Misteli, T. (2014). Activation of DNA damage response signaling by condensed chromatin. *Cell Rep.* 9, 1703–1717. doi:10.1016/j.celrep.2014.10.060.
- Caicedo, J. C., Cooper, S., Heigwer, F., Warchal, S., Qiu, P., Molnar, C., Vasilevich, A. S., Barry, J. D., Bansal, H. S., Kraus, O., et al. (2017). Data-analysis strategies for image-based cell profiling. *Nat. Methods* 14, 849–863. doi:10.1038/nmeth.4397.

- Cai, L., Rothbart, S. B., Lu, R., Xu, B., Chen, W.-Y., Tripathy, A., Rockowitz, S., Zheng, D., Patel, D. J., Allis, C. D., et al. (2013). An H3K36 methylation-engaging Tudor motif of polycomb-like proteins mediates PRC2 complex targeting. *Mol. Cell* 49, 571–582. doi:10.1016/j.molcel.2012.11.026.
- Cai, Z., Qian, Z.-Y., Jiang, H., Ma, N., Li, Z., Liu, L.-Y., Ren, X.-X., Shang, Y.-R., Wang, J.-J., Li, J.-J., et al. (2018). hPCL3s Promotes Hepatocellular Carcinoma Metastasis by Activating β -Catenin Signaling. *Cancer Res.* 78, 2536–2549. doi:10.1158/0008-5472.CAN-17-0028.
- Campbell, S., Ismail, I. H., Young, L. C., Poirier, G. G., and Hendzel, M. J. (2013). Polycomb repressive complex 2 contributes to DNA double-strand break repair. *Cell Cycle* 12, 2675–2683. doi:10.4161/cc.25795.
- Cannan, W. J., Tsang, B. P., Wallace, S. S., and Pederson, D. S. (2014). Nucleosomes suppress the formation of double-strand DNA breaks during attempted base excision repair of clustered oxidative damages. *J. Biol. Chem.* 289, 19881–19893. doi:10.1074/jbc.M114.571588.
- Cao, R., and Zhang, Y. (2004). SUZ12 is required for both the histone methyltransferase activity and the silencing function of the EED-EZH2 complex. *Mol. Cell* 15, 57–67. doi:10.1016/j.molcel.2004.06.020.
- Caridi, C. P., D’Agostino, C., Ryu, T., Zapotoczny, G., Delabaere, L., Li, X., Khodaverdian, V. Y., Amaral, N., Lin, E., Rau, A. R., et al. (2018). Nuclear F-actin and myosins drive relocalization of heterochromatic breaks. *Nature* 559, 54–60. doi:10.1038/s41586-018-0242-8.
- Caridi, P. C., Delabaere, L., Zapotoczny, G., and Chiolo, I. (2017). And yet, it moves: nuclear and chromatin dynamics of a heterochromatic double-strand break. *Philos. Trans. R. Soc. Lond. B Biol. Sci.* 372. doi:10.1098/rstb.2016.0291.
- Carvalho, S., Vitor, A. C., Sridhara, S. C., Martins, F. B., Raposo, A. C., Desterro, J. M. P., Ferreira, J., and de Almeida, S. F. (2014). SETD2 is required for DNA double-strand break repair and activation of the p53-mediated checkpoint. *eLife* 3, e02482. doi:10.7554/eLife.02482.
- Cassidy, K. B., Bang, S., Kurokawa, M., and Gerber, S. A. (2020). Direct regulation of Chk1 protein stability by E3 ubiquitin ligase HUWE1. *FEBS J.* 287, 1985–1999. doi:10.1111/febs.15132.
- Celen, A. B., and Sahin, U. (2020). Sumoylation on its 25th anniversary: mechanisms, pathology, and emerging concepts. *FEBS J.* 287, 3110–3140. doi:10.1111/febs.15319.
- Celeste, A., Difilippantonio, S., Difilippantonio, M. J., Fernandez-Capetillo, O., Pilch, D. R., Sedelnikova, O. A., Eckhaus, M., Ried, T., Bonner, W. M., and Nussenzweig, A. (2003). H2AX haploinsufficiency modifies genomic stability and tumor susceptibility. *Cell* 114, 371–383. doi:10.1016/s0092-8674(03)00567-1.
- Celeste, A., Petersen, S., Romanienko, P. J., Fernandez-Capetillo, O., Chen, H. T., Sedelnikova, O. A., Reina-San-Martin, B., Coppola, V., Meffre, E., Difilippantonio, M. J., et al. (2002). Genomic instability in mice lacking histone H2AX. *Science* 296, 922–927. doi:10.1126/science.1069398.
- Chagin, V. O., Casas-Delucchi, C. S., Reinhart, M., Schermelleh, L., Markaki, Y., Maiser, A., Bolius, J. J., Bensimon, A., Fillies, M., Domaing, P., et al. (2016). 4D Visualization of replication foci in mammalian cells corresponding to individual replicons. *Nat. Commun.* 7, 11231. doi:10.1038/ncomms11231.

- Chagin, V. O., Reinhart, B., Becker, A., Mortusewicz, O., Jost, K. L., Rapp, A., Leonhardt, H., and Cardoso, M. C. (2019). Processive DNA synthesis is associated with localized decompaction of constitutive heterochromatin at the sites of DNA replication and repair. *Nucleus* 10, 231–253. doi:10.1080/19491034.2019.1688932.
- Challa, K., Schmid, C. D., Kitagawa, S., Cheblal, A., Iesmantavicius, V., Seeber, A., Amitai, A., Seebacher, J., Hauer, M. H., Shimada, K., et al. (2021). Damage-induced chromatome dynamics link Ubiquitin ligase and proteasome recruitment to histone loss and efficient DNA repair. *Mol. Cell* 81, 811–829.e6. doi:10.1016/j.molcel.2020.12.021.
- Chapman, J. R., Barral, P., Vannier, J.-B., Borel, V., Steger, M., Tomas-Loba, A., Sartori, A. A., Adams, I. R., Batista, F. D., and Boulton, S. J. (2013). RIF1 is essential for 53BP1-dependent nonhomologous end joining and suppression of DNA double-strand break resection. *Mol. Cell* 49, 858–871. doi:10.1016/j.molcel.2013.01.002.
- Chauhan, D., Catley, L., Li, G., Podar, K., Hideshima, T., Velankar, M., Mitsiades, C., Mitsiades, N., Yasui, H., Letai, A., et al. (2005). A novel orally active proteasome inhibitor induces apoptosis in multiple myeloma cells with mechanisms distinct from Bortezomib. *Cancer Cell* 8, 407–419. doi:10.1016/j.ccr.2005.10.013.
- Cheblal, A., Challa, K., Seeber, A., Shimada, K., Yoshida, H., Ferreira, H. C., Amitai, A., and Gasser, S. M. (2020). DNA Damage-Induced Nucleosome Depletion Enhances Homology Search Independently of Local Break Movement. *Mol. Cell* 80, 311–326.e4. doi:10.1016/j.molcel.2020.09.002.
- Cheng, B., Ren, X., and Kerppola, T. K. (2014). KAP1 represses differentiation-inducible genes in embryonic stem cells through cooperative binding with PRC1 and derepresses pluripotency-associated genes. *Mol. Cell. Biol.* 34, 2075–2091. doi:10.1128/MCB.01729-13.
- Chen, J., Feng, W., Jiang, J., Deng, Y., and Huen, M. S. Y. (2012). Ring finger protein RNF169 antagonizes the ubiquitin-dependent signaling cascade at sites of DNA damage. *J. Biol. Chem.* 287, 27715–27722. doi:10.1074/jbc.M112.373530.
- Chen, J., Wang, Z., Guo, X., Li, F., Wei, Q., Chen, X., Gong, D., Xu, Y., Chen, W., Liu, Y., et al. (2019). TRIM66 reads unmodified H3R2K4 and H3K56ac to respond to DNA damage in embryonic stem cells. *Nat. Commun.* 10, 4273. doi:10.1038/s41467-019-12126-4.
- Chen, P., Li, J., Chen, Y.-C., Qian, H., Chen, Y.-J., Su, J.-Y., Wu, M., and Lan, T. (2016). The functional status of DNA repair pathways determines the sensitization effect to cisplatin in non-small cell lung cancer cells. *Cell Oncol (Dordr)* 39, 511–522. doi:10.1007/s13402-016-0291-7.
- Chernikova, S. B., Dorth, J. A., Razorenova, O. V., Game, J. C., and Brown, J. M. (2010). Deficiency in Bre1 impairs homologous recombination repair and cell cycle checkpoint response to radiation damage in mammalian cells. *Radiat. Res.* 174, 558–565. doi:10.1667/RR2184.1.
- Cheung, W. L., Turner, F. B., Krishnamoorthy, T., Wolner, B., Ahn, S.-H., Foley, M., Dorsey, J. A., Peterson, C. L., Berger, S. L., and Allis, C. D. (2005). Phosphorylation of histone H4 serine 1 during DNA damage requires casein kinase II in *S. cerevisiae*. *Curr. Biol.* 15, 656–660. doi:10.1016/j.cub.2005.02.049.
- Chiolo, I., Minoda, A., Colmenares, S. U., Polyzos, A., Costes, S. V., and Karpen, G. H. (2011). Double-strand breaks in heterochromatin move outside of a dynamic HP1a domain to complete recombinational repair. *Cell* 144, 732–744. doi:10.1016/j.cell.2011.02.012.

- Choe, K. N., Nicolae, C. M., Constantin, D., Imamura Kawasawa, Y., Delgado-Diaz, M. R., De, S., Freire, R., Smits, V. A., and Moldovan, G.-L. (2016). HUWE1 interacts with PCNA to alleviate replication stress. *EMBO Rep.* 17, 874–886. doi:10.15252/embr.201541685.
- Choi, S.-Y., Jang, H., Roe, J.-S., Kim, S.-T., Cho, E.-J., and Youn, H.-D. (2013). Phosphorylation and ubiquitination-dependent degradation of CABIN1 releases p53 for transactivation upon genotoxic stress. *Nucleic Acids Res.* 41, 2180–2190. doi:10.1093/nar/gks1319.
- Chou, D. M., Adamson, B., Dephoure, N. E., Tan, X., Nottke, A. C., Hurov, K. E., Gygi, S. P., Colaiácovo, M. P., and Elledge, S. J. (2010). A chromatin localization screen reveals poly (ADP ribose)-regulated recruitment of the repressive polycomb and NuRD complexes to sites of DNA damage. *Proc Natl Acad Sci USA* 107, 18475–18480. doi:10.1073/pnas.1012946107.
- Chowdhury, D., Keogh, M.-C., Ishii, H., Peterson, C. L., Buratowski, S., and Lieberman, J. (2005). gamma-H2AX dephosphorylation by protein phosphatase 2A facilitates DNA double-strand break repair. *Mol. Cell* 20, 801–809. doi:10.1016/j.molcel.2005.10.003.
- Chowdhury, D., Xu, X., Zhong, X., Ahmed, F., Zhong, J., Liao, J., Dykxhoorn, D. M., Weinstock, D. M., Pfeifer, G. P., and Lieberman, J. (2008). A PP4-phosphatase complex dephosphorylates gamma-H2AX generated during DNA replication. *Mol. Cell* 31, 33–46. doi:10.1016/j.molcel.2008.05.016.
- Ciccia, A., and Elledge, S. J. (2010). The DNA damage response: making it safe to play with knives. *Mol. Cell* 40, 179–204. doi:10.1016/j.molcel.2010.09.019.
- Clague, M. J., Heride, C., and Urbé, S. (2015). The demographics of the ubiquitin system. *Trends Cell Biol.* 25, 417–426. doi:10.1016/j.tcb.2015.03.002.
- Clague, M. J., Urbé, S., and Komander, D. (2019). Breaking the chains: deubiquitylating enzyme specificity begets function. *Nat. Rev. Mol. Cell Biol.* 20, 338–352. doi:10.1038/s41580-019-0099-1.
- Clements, K. E., Schleicher, E. M., Thakar, T., Hale, A., Dhoonmoon, A., Tolman, N. J., Sharma, A., Liang, X., Imamura Kawasawa, Y., Nicolae, C. M., et al. (2020). Identification of regulators of poly-ADP-ribose polymerase inhibitor response through complementary CRISPR knockout and activation screens. *Nat. Commun.* 11, 6118. doi:10.1038/s41467-020-19961-w.
- Clouaire, T., Rocher, V., Lashgari, A., Arnould, C., Aguirrebengoa, M., Biernacka, A., Skrzypczak, M., Aymard, F., Fongang, B., Dojer, N., et al. (2018). Comprehensive Mapping of Histone Modifications at DNA Double-Strand Breaks Deciphers Repair Pathway Chromatin Signatures. *Mol. Cell* 72, 250-262.e6. doi:10.1016/j.molcel.2018.08.020.
- Cohen, J. (1960). A Coefficient of Agreement for Nominal Scales. *Educ. Psychol. Meas.* 20, 37–46. doi:10.1177/001316446002000104.
- Cook, P. J., Ju, B. G., Telese, F., Wang, X., Glass, C. K., and Rosenfeld, M. G. (2009). Tyrosine dephosphorylation of H2AX modulates apoptosis and survival decisions. *Nature* 458, 591–596. doi:10.1038/nature07849.
- Cooper, S., Grijzenhout, A., Underwood, E., Ancelin, K., Zhang, T., Nesterova, T. B., Anil-Kirmizitas, B., Bassett, A., Kooistra, S. M., Agger, K., et al. (2016). Jarid2 binds mono-ubiquitylated H2A lysine 119 to mediate crosstalk between Polycomb complexes PRC1 and PRC2. *Nat. Commun.* 7, 13661. doi:10.1038/ncomms13661.

- Cui, D., Xiong, X., Shu, J., Dai, X., Sun, Y., and Zhao, Y. (2020). FBXW7 confers radiation survival by targeting p53 for degradation. *Cell Rep.* 30, 497-509.e4. doi:10.1016/j.celrep.2019.12.032.
- Danielsen, J. R., Povlsen, L. K., Villumsen, B. H., Streicher, W., Nilsson, J., Wikström, M., Bekker-Jensen, S., and Mailand, N. (2012). DNA damage-inducible SUMOylation of HERC2 promotes RNF8 binding via a novel SUMO-binding Zinc finger. *J. Cell Biol.* 197, 179-187. doi:10.1083/jcb.201106152.
- Dantuma, N. P., and van Attikum, H. (2016). Spatiotemporal regulation of posttranslational modifications in the DNA damage response. *EMBO J.* 35, 6-23. doi:10.15252/embj.201592595.
- Daou, S., Hammond-Martel, I., Mashtalir, N., Barbour, H., Gagnon, J., Iannantuono, N. V. G., Nkwe, N. S., Motorina, A., Pak, H., Yu, H., et al. (2015). The BAP1/ASXL2 histone H2A deubiquitinase complex regulates cell proliferation and is disrupted in cancer. *J. Biol. Chem.* 290, 28643-28663. doi:10.1074/jbc.M115.661553.
- DaRosa, P. A., Wang, Z., Jiang, X., Pruneda, J. N., Cong, F., Klevit, R. E., and Xu, W. (2015). Allosteric activation of the RNF146 ubiquitin ligase by a poly(ADP-ribosylation) signal. *Nature* 517, 223-226. doi:10.1038/nature13826.
- Dasgupta, A., Mondal, P., Dalui, S., Das, C., and Roy, S. (2022). Molecular characterization of substrate-induced ubiquitin transfer by UBR7-PHD finger, a newly identified histone H2BK120 ubiquitin ligase. *FEBS J.* 289, 1842-1857. doi:10.1111/febs.16262.
- Das, C., Lucia, M. S., Hansen, K. C., and Tyler, J. K. (2009). CBP/p300-mediated acetylation of histone H3 on lysine 56. *Nature* 459, 113-117. doi:10.1038/nature07861.
- Delgado-Díaz, M. R., Martín, Y., Berg, A., Freire, R., and Smits, V. A. J. (2014). Dub3 controls DNA damage signalling by direct deubiquitination of H2AX. *Mol. Oncol.* 8, 884-893. doi:10.1016/j.molonc.2014.03.003.
- Deng, Q., Hou, J., Feng, L., Lv, A., Ke, X., Liang, H., Wang, F., Zhang, K., Chen, K., and Cui, H. (2018). PHF19 promotes the proliferation, migration, and chemosensitivity of glioblastoma to doxorubicin through modulation of the SIAH1/ β -catenin axis. *Cell Death Dis.* 9, 1049. doi:10.1038/s41419-018-1082-z.
- Densham, R. M., Garvin, A. J., Stone, H. R., Strachan, J., Baldock, R. A., Daza-Martin, M., Fletcher, A., Blair-Reid, S., Beesley, J., Johal, B., et al. (2016). Human BRCA1-BARD1 ubiquitin ligase activity counteracts chromatin barriers to DNA resection. *Nat. Struct. Mol. Biol.* 23, 647-655. doi:10.1038/nsmb.3236.
- Devgan, S. S., Sanal, O., Doil, C., Nakamura, K., Nahas, S. A., Pettijohn, K., Bartek, J., Lukas, C., Lukas, J., and Gatti, R. A. (2011). Homozygous deficiency of ubiquitin-ligase ring-finger protein RNF168 mimics the radiosensitivity syndrome of ataxia-telangiectasia. *Cell Death Differ.* 18, 1500-1506. doi:10.1038/cdd.2011.18.
- Dietz, C., and Berthold, M. R. (2016). KNIME for Open-Source Bioimage Analysis: A Tutorial. *Adv. Anat. Embryol. Cell Biol.* 219, 179-197. doi:10.1007/978-3-319-28549-8_7.
- Dikic, I., Wakatsuki, S., and Walters, K. J. (2009). Ubiquitin-binding domains - from structures to functions. *Nat. Rev. Mol. Cell Biol.* 10, 659-671. doi:10.1038/nrm2767.
- Di Virgilio, M., Callen, E., Yamane, A., Zhang, W., Jankovic, M., Gitlin, A. D., Feldhahn, N., Resch, W., Oliveira, T. Y., Chait, B. T., et al. (2013). Rif1 prevents resection of DNA breaks and

promotes immunoglobulin class switching. *Science* 339, 711–715.
doi:10.1126/science.1230624.

Doil, C., Mailand, N., Bekker-Jensen, S., Menard, P., Larsen, D. H., Pepperkok, R., Ellenberg, J., Panier, S., Durocher, D., Bartek, J., et al. (2009). RNF168 binds and amplifies ubiquitin conjugates on damaged chromosomes to allow accumulation of repair proteins. *Cell* 136, 435–446. doi:10.1016/j.cell.2008.12.041.

Douglas, P., Zhong, J., Ye, R., Moorhead, G. B. G., Xu, X., and Lees-Miller, S. P. (2010). Protein phosphatase 6 interacts with the DNA-dependent protein kinase catalytic subunit and dephosphorylates gamma-H2AX. *Mol. Cell. Biol.* 30, 1368–1381. doi:10.1128/MCB.00741-09.

Duan, M.-R., and Smerdon, M. J. (2014). Histone H3 lysine 14 (H3K14) acetylation facilitates DNA repair in a positioned nucleosome by stabilizing the binding of the chromatin Remodeler RSC (Remodels Structure of Chromatin). *J. Biol. Chem.* 289, 8353–8363. doi:10.1074/jbc.M113.540732.

Dubois, J.-C., Yates, M., Gaudreau-Lapierre, A., Clément, G., Cappadocia, L., Gaudreau, L., Zou, L., and Maréchal, A. (2017). A phosphorylation-and-ubiquitylation circuitry driving ATR activation and homologous recombination. *Nucleic Acids Res.* 45, 8859–8872. doi:10.1093/nar/gkx571.

Dwane, L., Gallagher, W. M., Ní Chonghaile, T., and O'Connor, D. P. (2017). The Emerging Role of Non-traditional Ubiquitination in Oncogenic Pathways. *J. Biol. Chem.* 292, 3543–3551. doi:10.1074/jbc.R116.755694.

Ea, C.-K., Deng, L., Xia, Z.-P., Pineda, G., and Chen, Z. J. (2006). Activation of IKK by TNFalpha requires site-specific ubiquitination of RIP1 and polyubiquitin binding by NEMO. *Mol. Cell* 22, 245–257. doi:10.1016/j.molcel.2006.03.026.

Elia, A. E. H., Boardman, A. P., Wang, D. C., Huttlin, E. L., Everley, R. A., Dephoure, N., Zhou, C., Koren, I., Gygi, S. P., and Elledge, S. J. (2015). Quantitative proteomic atlas of ubiquitination and acetylation in the DNA damage response. *Mol. Cell* 59, 867–881. doi:10.1016/j.molcel.2015.05.006.

Elia, M. C., and Bradley, M. O. (1992). Influence of chromatin structure on the induction of DNA double strand breaks by ionizing radiation. *Cancer Res.* 52, 1580–1586.

Erfle, H., Neumann, B., Liebel, U., Rogers, P., Held, M., Walter, T., Ellenberg, J., and Pepperkok, R. (2007). Reverse transfection on cell arrays for high content screening microscopy. *Nat. Protoc.* 2, 392–399. doi:10.1038/nprot.2006.483.

Escibano-Díaz, C., Orthwein, A., Fradet-Turcotte, A., Xing, M., Young, J. T. F., Tkáč, J., Cook, M. A., Rosebrock, A. P., Munro, M., Canny, M. D., et al. (2013). A cell cycle-dependent regulatory circuit composed of 53BP1-RIF1 and BRCA1-CtIP controls DNA repair pathway choice. *Mol. Cell* 49, 872–883. doi:10.1016/j.molcel.2013.01.001.

Eskeland, R., Leeb, M., Grimes, G. R., Kress, C., Boyle, S., Sproul, D., Gilbert, N., Fan, Y., Skoultchi, A. I., Wutz, A., et al. (2010). Ring1B compacts chromatin structure and represses gene expression independent of histone ubiquitination. *Mol. Cell* 38, 452–464. doi:10.1016/j.molcel.2010.02.032.

Falk, M., Lukášová, E., and Kozubek, S. (2008). Chromatin structure influences the sensitivity of DNA to gamma-radiation. *Biochim. Biophys. Acta* 1783, 2398–2414. doi:10.1016/j.bbamcr.2008.07.010.

- Fang, C.-B., Wu, H.-T., Zhang, M.-L., Liu, J., and Zhang, G.-J. (2020). Fanconi anemia pathway: mechanisms of breast cancer predisposition development and potential therapeutic targets. *Front. Cell Dev. Biol.* 8, 160. doi:10.3389/fcell.2020.00160.
- Faucher, D., and Wellinger, R. J. (2010). Methylated H3K4, a transcription-associated histone modification, is involved in the DNA damage response pathway. *PLoS Genet.* 6. doi:10.1371/journal.pgen.1001082.
- Feng, L., and Chen, J. (2012). The E3 ligase RNF8 regulates KU80 removal and NHEJ repair. *Nat. Struct. Mol. Biol.* 19, 201–206. doi:10.1038/nsmb.2211.
- Feng, Z., and Zhang, J. (2012). A dual role of BRCA1 in two distinct homologous recombination mediated repair in response to replication arrest. *Nucleic Acids Res.* 40, 726–738. doi:10.1093/nar/gkr748.
- Fernandez-Capetillo, O., Allis, C. D., and Nussenzweig, A. (2004). Phosphorylation of histone H2B at DNA double-strand breaks. *J. Exp. Med.* 199, 1671–1677. doi:10.1084/jem.20032247.
- Fierz, B., Chatterjee, C., McGinty, R. K., Bar-Dagan, M., Raleigh, D. P., and Muir, T. W. (2011). Histone H2B ubiquitylation disrupts local and higher-order chromatin compaction. *Nat. Chem. Biol.* 7, 113–119. doi:10.1038/nchembio.501.
- Finley, D. (2009). Recognition and processing of ubiquitin-protein conjugates by the proteasome. *Annu. Rev. Biochem.* 78, 477–513. doi:10.1146/annurev.biochem.78.081507.101607.
- Fitieh, A., Locke, A. J., Mashayekhi, F., Khaliqdina, F., Sharma, A. K., and Ismail, I. H. (2022). BMI-1 regulates DNA end resection and homologous recombination repair. *Cell Rep.* 38, 110536. doi:10.1016/j.celrep.2022.110536.
- Fitieh, A., Locke, A. J., Motamedi, M., and Ismail, I. H. (2021). The role of polycomb group protein BMI1 in DNA repair and genomic stability. *Int. J. Mol. Sci.* 22. doi:10.3390/ijms22062976.
- Fnu, S., Williamson, E. A., De Haro, L. P., Brennehan, M., Wray, J., Shaheen, M., Radhakrishnan, K., Lee, S.-H., Nickoloff, J. A., and Hromas, R. (2011). Methylation of histone H3 lysine 36 enhances DNA repair by nonhomologous end-joining. *Proc Natl Acad Sci USA* 108, 540–545. doi:10.1073/pnas.1013571108.
- Fradet-Turcotte, A., Canny, M. D., Escribano-Díaz, C., Orthwein, A., Leung, C. C. Y., Huang, H., Landry, M.-C., Kitevski-LeBlanc, J., Noordermeer, S. M., Sicheri, F., et al. (2013). 53BP1 is a reader of the DNA-damage-induced H2A Lys 15 ubiquitin mark. *Nature* 499, 50–54. doi:10.1038/nature12318.
- Francis, N. J., Kingston, R. E., and Woodcock, C. L. (2004). Chromatin compaction by a polycomb group protein complex. *Science* 306, 1574–1577. doi:10.1126/science.1100576.
- Frattini, C., Promonet, A., Alghoul, E., Vidal-Eychenie, S., Lamarque, M., Blanchard, M.-P., Urbach, S., Basbous, J., and Constantinou, A. (2021). TopBP1 assembles nuclear condensates to switch on ATR signaling. *Mol. Cell* 81, 1231–1245.e8. doi:10.1016/j.molcel.2020.12.049.
- Fujimuro, M., Sawada, H., and Yokosawa, H. (1994). Production and characterization of monoclonal antibodies specific to multi-ubiquitin chains of polyubiquitinated proteins. *FEBS Lett.* 349, 173–180. doi:10.1016/0014-5793(94)00647-4.

- Fu, Q.-S., Zhou, C.-J., Gao, H.-C., Jiang, Y.-J., Zhou, Z.-R., Hong, J., Yao, W.-M., Song, A.-X., Lin, D.-H., and Hu, H.-Y. (2009). Structural basis for ubiquitin recognition by a novel domain from human phospholipase A2-activating protein. *J. Biol. Chem.* 284, 19043–19052. doi:10.1074/jbc.M109.009126.
- Gabay, M., Li, Y., and Felsher, D. W. (2014). MYC activation is a hallmark of cancer initiation and maintenance. *Cold Spring Harb. Perspect. Med.* 4. doi:10.1101/cshperspect.a014241.
- Galanty, Y., Belotserkovskaya, R., Coates, J., and Jackson, S. P. (2012). RNF4, a SUMO-targeted ubiquitin E3 ligase, promotes DNA double-strand break repair. *Genes Dev.* 26, 1179–1195. doi:10.1101/gad.188284.112.
- Galanty, Y., Belotserkovskaya, R., Coates, J., Polo, S., Miller, K. M., and Jackson, S. P. (2009). Mammalian SUMO E3-ligases PIAS1 and PIAS4 promote responses to DNA double-strand breaks. *Nature* 462, 935–939. doi:10.1038/nature08657.
- García-Higuera, I., Taniguchi, T., Ganesan, S., Meyn, M. S., Timmers, C., Hejna, J., Grompe, M., and D'Andrea, A. D. (2001). Interaction of the Fanconi anemia proteins and BRCA1 in a common pathway. *Mol. Cell* 7, 249–262. doi:10.1016/s1097-2765(01)00173-3.
- García-Montolio, M., Ballaré, C., Blanco, E., Gutiérrez, A., Aranda, S., Gómez, A., Kok, C. H., Yeung, D. T., Hughes, T. P., Vizán, P., et al. (2021). Polycomb factor PHF19 controls cell growth and differentiation toward erythroid pathway in chronic myeloid leukemia cells. *Front. Cell Dev. Biol.* 9, 655201. doi:10.3389/fcell.2021.655201.
- Garvin, A. J., Walker, A. K., Densham, R. M., Chauhan, A. S., Stone, H. R., Mackay, H. L., Jamshad, M., Starowicz, K., Daza-Martin, M., Ronson, G. E., et al. (2019). The deSUMOylase SENP2 coordinates homologous recombination and nonhomologous end joining by independent mechanisms. *Genes Dev.* 33, 333–347. doi:10.1101/gad.321125.118.
- Gatti, M., Imhof, R., Huang, Q., Baudis, M., and Altmeyer, M. (2020). The ubiquitin ligase TRIP12 limits PARP1 trapping and constrains PARP inhibitor efficiency. *Cell Rep.* 32, 107985. doi:10.1016/j.celrep.2020.107985.
- Gatti, M., Pinato, S., Maiolica, A., Rocchio, F., Prato, M. G., Aebbersold, R., and Penengo, L. (2015). RNF168 promotes noncanonical K27 ubiquitination to signal DNA damage. *Cell Rep.* 10, 226–238. doi:10.1016/j.celrep.2014.12.021.
- Gechijian, L. N., Buckley, D. L., Lawlor, M. A., Reyes, J. M., Paulk, J., Ott, C. J., Winter, G. E., Erb, M. A., Scott, T. G., Xu, M., et al. (2018). Functional TRIM24 degrader via conjugation of ineffectual bromodomain and VHL ligands. *Nat. Chem. Biol.* 14, 405–412. doi:10.1038/s41589-018-0010-y.
- George, A. J., Hoffiz, Y. C., Charles, A. J., Zhu, Y., and Mabb, A. M. (2018). A comprehensive atlas of E3 ubiquitin ligase mutations in neurological disorders. *Front. Genet.* 9, 29. doi:10.3389/fgene.2018.00029.
- Ge, C., Che, L., and Du, C. (2015). The UBC Domain Is Required for BRUCE to Promote BRIT1/MCPH1 Function in DSB Signaling and Repair Post Formation of BRUCE-USP8-BRIT1 Complex. *PLoS ONE* 10, e0144957. doi:10.1371/journal.pone.0144957.
- Ghislin, S., Deshayes, F., Middendorp, S., Boggetto, N., and Alcaide-Loridan, C. (2012). PHF19 and Akt control the switch between proliferative and invasive states in melanoma. *Cell Cycle* 11, 1634–1645. doi:10.4161/cc.20095.

- Ghodke, I., Remisova, M., Furst, A., Kilic, S., Reina-San-Martin, B., Poetsch, A. R., Altmeyer, M., and Soutoglou, E. (2021). AHNAK controls 53BP1-mediated p53 response by restraining 53BP1 oligomerization and phase separation. *Mol. Cell* 81, 2596-2610.e7. doi:10.1016/j.molcel.2021.04.010.
- Gibson, B. A., Doolittle, L. K., Schneider, M. W. G., Jensen, L. E., Gamarra, N., Henry, L., Gerlich, D. W., Redding, S., and Rosen, M. K. (2019). Organization of chromatin by intrinsic and regulated phase separation. *Cell* 179, 470-484.e21. doi:10.1016/j.cell.2019.08.037.
- Ginjala, V., Nacerddine, K., Kulkarni, A., Oza, J., Hill, S. J., Yao, M., Citterio, E., van Lohuizen, M., and Ganesan, S. (2011). BMI1 is recruited to DNA breaks and contributes to DNA damage-induced H2A ubiquitination and repair. *Mol. Cell. Biol.* 31, 1972–1982. doi:10.1128/MCB.00981-10.
- Glancy, E., Wang, C., Tuck, E., Healy, E., Amato, S., Neikes, H. K., Mariani, A., Mucha, M., Vermeulen, M., Pasini, D., et al. (2023). PRC2.1- and PRC2.2-specific accessory proteins drive recruitment of different forms of canonical PRC1. *Mol. Cell* 83, 1393-1411.e7. doi:10.1016/j.molcel.2023.03.018.
- Goldknopf, I. L., French, M. F., Musso, R., and Busch, H. (1977). Presence of protein A24 in rat liver nucleosomes. *Proc Natl Acad Sci USA* 74, 5492–5495. doi:10.1073/pnas.74.12.5492.
- Goldstein, G., Scheid, M., Hammerling, U., Schlesinger, D. H., Niall, H. D., and Boyse, E. A. (1975). Isolation of a polypeptide that has lymphocyte-differentiating properties and is probably represented universally in living cells. *Proc Natl Acad Sci USA* 72, 11–15. doi:10.1073/pnas.72.1.11.
- Gollavilli, P. N., Pawar, A., Wilder-Romans, K., Natesan, R., Engelke, C. G., Dommeti, V. L., Krishnamurthy, P. M., Nallasivam, A., Apel, I. J., Xu, T., et al. (2018). EWS/ETS-Driven Ewing Sarcoma Requires BET Bromodomain Proteins. *Cancer Res.* 78, 4760–4773. doi:10.1158/0008-5472.CAN-18-0484.
- Gong, F., Chiu, L.-Y., Cox, B., Aymard, F., Clouaire, T., Leung, J. W., Cammarata, M., Perez, M., Agarwal, P., Brodbelt, J. S., et al. (2015). Screen identifies bromodomain protein ZMYND8 in chromatin recognition of transcription-associated DNA damage that promotes homologous recombination. *Genes Dev.* 29, 197–211. doi:10.1101/gad.252189.114.
- Gong, F., Clouaire, T., Aguirrebengoa, M., Legube, G., and Miller, K. M. (2017). Histone demethylase KDM5A regulates the ZMYND8-NuRD chromatin remodeler to promote DNA repair. *J. Cell Biol.* 216, 1959–1974. doi:10.1083/jcb.201611135.
- Gorgoulis, V. G., Vassiliou, L.-V. F., Karakaidos, P., Zacharatos, P., Kotsinas, A., Liloglou, T., Venere, M., Ditullio, R. A., Kastriakis, N. G., Levy, B., et al. (2005). Activation of the DNA damage checkpoint and genomic instability in human precancerous lesions. *Nature* 434, 907–913. doi:10.1038/nature03485.
- Groen, F. C., Young, I. T., and Ligthart, G. (1985). A comparison of different focus functions for use in autofocus algorithms. *Cytometry* 6, 81–91. doi:10.1002/cyto.990060202.
- Gudjonsson, T., Altmeyer, M., Savic, V., Toledo, L., Dinant, C., Grøfte, M., Bartkova, J., Poulsen, M., Oka, Y., Bekker-Jensen, S., et al. (2012). TRIP12 and UBR5 suppress spreading of chromatin ubiquitylation at damaged chromosomes. *Cell* 150, 697–709. doi:10.1016/j.cell.2012.06.039.

- Guo, Z., Wang, S., Xie, Y., Han, Y., Hu, S., Guan, H., Xie, D., Bai, C., Liu, X., Gu, Y., et al. (2020). HUWE1-dependent DNA-PKcs neddylation modulates its autophosphorylation in DNA damage response. *Cell Death Dis.* 11, 400. doi:10.1038/s41419-020-2611-0.
- Guzzo, C. M., Berndsen, C. E., Zhu, J., Gupta, V., Datta, A., Greenberg, R. A., Wolberger, C., and Matunis, M. J. (2012). RNF4-dependent hybrid SUMO-ubiquitin chains are signals for RAP80 and thereby mediate the recruitment of BRCA1 to sites of DNA damage. *Sci. Signal.* 5, ra88. doi:10.1126/scisignal.2003485.
- Hahm, J. Y., Kim, J.-Y., Park, J. W., Kang, J.-Y., Kim, K.-B., Kim, S.-R., Cho, H., and Seo, S.-B. (2019). Methylation of UHRF1 by SET7 is essential for DNA double-strand break repair. *Nucleic Acids Res.* 47, 184–196. doi:10.1093/nar/gky975.
- Hansen, K. H., Bracken, A. P., Pasini, D., Dietrich, N., Gehani, S. S., Monrad, A., Rappsilber, J., Lerdrup, M., and Helin, K. (2008). A model for transmission of the H3K27me3 epigenetic mark. *Nat. Cell Biol.* 10, 1291–1300. doi:10.1038/ncb1787.
- Han, H., Shim, H., Shin, D., Shim, J. E., Ko, Y., Shin, J., Kim, H., Cho, A., Kim, E., Lee, T., et al. (2015). TRRUST: a reference database of human transcriptional regulatory interactions. *Sci. Rep.* 5, 11432. doi:10.1038/srep11432.
- Han, M. M., Hirakawa, M., Yamauchi, M., and Matsuda, N. (2021). Roles of the SUMO-related enzymes, PIAS1, PIAS4, and RNF4, in DNA double-strand break repair by homologous recombination. *Biochem. Biophys. Res. Commun.* 591, 95–101. doi:10.1016/j.bbrc.2021.12.099.
- Hauer, M. H., and Gasser, S. M. (2017). Chromatin and nucleosome dynamics in DNA damage and repair. *Genes Dev.* 31, 2204–2221. doi:10.1101/gad.307702.117.
- Hauer, M. H., Seeber, A., Singh, V., Thierry, R., Sack, R., Amitai, A., Kryzhanovska, M., Eglinger, J., Holcman, D., Owen-Hughes, T., et al. (2017). Histone degradation in response to DNA damage enhances chromatin dynamics and recombination rates. *Nat. Struct. Mol. Biol.* 24, 99–107. doi:10.1038/nsmb.3347.
- Ha, K., Ma, C., Lin, H., Tang, L., Lian, Z., Zhao, F., Li, J.-M., Zhen, B., Pei, H., Han, S., et al. (2017). The anaphase promoting complex impacts repair choice by protecting ubiquitin signalling at DNA damage sites. *Nat. Commun.* 8, 15751. doi:10.1038/ncomms15751.
- Heitz, E. (1928). Das heterochromatin der moose. *Jahrbücher für wissenschaftliche Botanik* 69, 762–818.
- Hendriks, I. A., D'Souza, R. C. J., Yang, B., Verlaan-de Vries, M., Mann, M., and Vertegaal, A. C. O. (2014). Uncovering global SUMOylation signaling networks in a site-specific manner. *Nat. Struct. Mol. Biol.* 21, 927–936. doi:10.1038/nsmb.2890.
- Henry, K. W., Wyce, A., Lo, W.-S., Duggan, L. J., Emre, N. C. T., Kao, C.-F., Pillus, L., Shilatifard, A., Osley, M. A., and Berger, S. L. (2003). Transcriptional activation via sequential histone H2B ubiquitylation and deubiquitylation, mediated by SAGA-associated Ubp8. *Genes Dev.* 17, 2648–2663. doi:10.1101/gad.1144003.
- Herbert, S., Brion, A., Arbona, J.-M., Lelek, M., Veillet, A., Lelandais, B., Parmar, J., Fernández, F. G., Almayrac, E., Khalil, Y., et al. (2017). Chromatin stiffening underlies enhanced locus mobility after DNA damage in budding yeast. *EMBO J.* 36, 2595–2608. doi:10.15252/embj.201695842.

- Herrera-Moyano, E., Mergui, X., García-Rubio, M. L., Barroso, S., and Aguilera, A. (2014). The yeast and human FACT chromatin-reorganizing complexes solve R-loop-mediated transcription-replication conflicts. *Genes Dev.* 28, 735–748. doi:10.1101/gad.234070.113.
- Hershko, A., and Ciechanover, A. (1998). The ubiquitin system. *Annu. Rev. Biochem.* 67, 425–479. doi:10.1146/annurev.biochem.67.1.425.
- Hideshima, T., Richardson, P., Chauhan, D., Palombella, V. J., Elliott, P. J., Adams, J., and Anderson, K. C. (2001). The proteasome inhibitor PS-341 inhibits growth, induces apoptosis, and overcomes drug resistance in human multiple myeloma cells. *Cancer Res.* 61, 3071–3076.
- Hodson, C., Cole, A. R., Lewis, L. P. C., Miles, J. A., Purkiss, A., and Walden, H. (2011). Structural analysis of human FANCL, the E3 ligase in the Fanconi anemia pathway. *J. Biol. Chem.* 286, 32628–32637. doi:10.1074/jbc.M111.244632.
- Holzer, P., Masuya, K., Furet, P., Kallen, J., Valat-Stachyra, T., Ferretti, S., Berghausen, J., Bouisset-Leonard, M., Buschmann, N., Pissot-Soldermann, C., et al. (2015). Discovery of a Dihydroisoquinolinone Derivative (NVP-CGM097): A Highly Potent and Selective MDM2 Inhibitor Undergoing Phase 1 Clinical Trials in p53wt Tumors. *J. Med. Chem.* 58, 6348–6358. doi:10.1021/acs.jmedchem.5b00810.
- Hong, Z., Jiang, J., Lan, L., Nakajima, S., Kanno, S., Koseki, H., and Yasui, A. (2008). A polycomb group protein, PHF1, is involved in the response to DNA double-strand breaks in human cell. *Nucleic Acids Res.* 36, 2939–2947. doi:10.1093/nar/gkn146.
- Horn, V., Uckelmann, M., Zhang, H., Eerland, J., Aarsman, I., le Paige, U. B., Davidovich, C., Sixma, T. K., and van Ingen, H. (2019). Structural basis of specific H2A K13/K15 ubiquitination by RNF168. *Nat. Commun.* 10, 1751. doi:10.1038/s41467-019-09756-z.
- Hossain, M. B., Shifat, R., Johnson, D. G., Bedford, M. T., Gabrusiewicz, K. R., Cortes-Santiago, N., Luo, X., Lu, Z., Ezhilarasan, R., Sulman, E. P., et al. (2016). TIE2-mediated tyrosine phosphorylation of H4 regulates DNA damage response by recruiting ABL1. *Sci. Adv.* 2, e1501290. doi:10.1126/sciadv.1501290.
- Huang, J., Huen, M. S. Y., Kim, H., Leung, C. C. Y., Glover, J. N. M., Yu, X., and Chen, J. (2009). RAD18 transmits DNA damage signalling to elicit homologous recombination repair. *Nat. Cell Biol.* 11, 592–603. doi:10.1038/ncb1865.
- Huang, J., Teng, L., Li, L., Liu, T., Li, L., Chen, D., Xu, L.-G., Zhai, Z., and Shu, H.-B. (2004). ZNF216 Is an A20-like and I κ B kinase γ -interacting inhibitor of NF κ B activation. *J. Biol. Chem.* 279, 16847–16853. doi:10.1074/jbc.M309491200.
- Huang, Q., Qin, D., Pei, D., Vermeulen, M., and Zhang, X. (2022). UBE2O and USP7 co-regulate RECQL4 ubiquitylation and homologous recombination-mediated DNA repair. *FASEB J.* 36, e22112. doi:10.1096/fj.202100974RRR.
- Husnjak, K., Elsasser, S., Zhang, N., Chen, X., Randles, L., Shi, Y., Hofmann, K., Walters, K. J., Finley, D., and Dikic, I. (2008). Proteasome subunit Rpn13 is a novel ubiquitin receptor. *Nature* 453, 481–488. doi:10.1038/nature06926.
- Hustedt, N., and Durocher, D. (2016). The control of DNA repair by the cell cycle. *Nat. Cell Biol.* 19, 1–9. doi:10.1038/ncb3452.

- Huyen, Y., Zgheib, O., Ditullio, R. A., Gorgoulis, V. G., Zacharatos, P., Petty, T. J., Sheston, E. A., Mellert, H. S., Stavridi, E. S., and Halazonetis, T. D. (2004). Methylated lysine 79 of histone H3 targets 53BP1 to DNA double-strand breaks. *Nature* 432, 406–411. doi:10.1038/nature03114.
- Hu, Q., Botuyan, M. V., Zhao, D., Cui, G., Mer, E., and Mer, G. (2021). Mechanisms of BRCA1-BARD1 nucleosome recognition and ubiquitylation. *Nature* 596, 438–443. doi:10.1038/s41586-021-03716-8.
- Hu, X., Paul, A., and Wang, B. (2012). Rap80 protein recruitment to DNA double-strand breaks requires binding to both small ubiquitin-like modifier (SUMO) and ubiquitin conjugates. *J. Biol. Chem.* 287, 25510–25519. doi:10.1074/jbc.M112.374116.
- Hu, Y., Petit, S. A., Ficarro, S. B., Toomire, K. J., Xie, A., Lim, E., Cao, S. A., Park, E., Eck, M. J., Scully, R., et al. (2014a). PARP1-driven poly-ADP-ribosylation regulates BRCA1 function in homologous recombination-mediated DNA repair. *Cancer Discov.* 4, 1430–1447. doi:10.1158/2159-8290.CD-13-0891.
- Hu, Y., Wang, C., Huang, K., Xia, F., Parvin, J. D., and Mondal, N. (2014b). Regulation of 53BP1 protein stability by RNF8 and RNF168 is important for efficient DNA double-strand break repair. *PLoS ONE* 9, e110522. doi:10.1371/journal.pone.0110522.
- Ikeda, F., Deribe, Y. L., Skånland, S. S., Stieglitz, B., Grabbe, C., Franz-Wachtel, M., van Wijk, S. J. L., Goswami, P., Nagy, V., Terzic, J., et al. (2011). SHARPIN forms a linear ubiquitin ligase complex regulating NF- κ B activity and apoptosis. *Nature* 471, 637–641. doi:10.1038/nature09814.
- Ikura, T., Tashiro, S., Kakino, A., Shima, H., Jacob, N., Amunugama, R., Yoder, K., Izumi, S., Kuraoka, I., Tanaka, K., et al. (2007). DNA damage-dependent acetylation and ubiquitination of H2AX enhances chromatin dynamics. *Mol. Cell. Biol.* 27, 7028–7040. doi:10.1128/MCB.00579-07.
- Inano, S., Sato, K., Katsuki, Y., Kobayashi, W., Tanaka, H., Nakajima, K., Nakada, S., Miyoshi, H., Knies, K., Takaori-Kondo, A., et al. (2017). RFWD3-Mediated Ubiquitination Promotes Timely Removal of Both RPA and RAD51 from DNA Damage Sites to Facilitate Homologous Recombination. *Mol. Cell* 66, 622-634.e8. doi:10.1016/j.molcel.2017.04.022.
- Ismail, I. H., Andrin, C., McDonald, D., and Hendzel, M. J. (2010). BMI1-mediated histone ubiquitylation promotes DNA double-strand break repair. *J. Cell Biol.* 191, 45–60. doi:10.1083/jcb.201003034.
- Ismail, I. H., Gagné, J.-P., Caron, M.-C., McDonald, D., Xu, Z., Masson, J.-Y., Poirier, G. G., and Hendzel, M. J. (2012). CBX4-mediated SUMO modification regulates BMI1 recruitment at sites of DNA damage. *Nucleic Acids Res.* 40, 5497–5510. doi:10.1093/nar/gks222.
- Ismail, I. H., Gagné, J.-P., Genois, M.-M., Strickfaden, H., McDonald, D., Xu, Z., Poirier, G. G., Masson, J.-Y., and Hendzel, M. J. (2015). The RNF138 E3 ligase displaces Ku to promote DNA end resection and regulate DNA repair pathway choice. *Nat. Cell Biol.* 17, 1446–1457. doi:10.1038/ncb3259.
- Iwai, K., Fujita, H., and Sasaki, Y. (2014). Linear ubiquitin chains: NF- κ B signalling, cell death and beyond. *Nat. Rev. Mol. Cell Biol.* 15, 503–508. doi:10.1038/nrm3836.
- Jacquet, K., Fradet-Turcotte, A., Avvakumov, N., Lambert, J.-P., Roques, C., Pandita, R. K., Paquet, E., Herst, P., Gingras, A.-C., Pandita, T. K., et al. (2016). The TIP60 Complex Regulates

- Bivalent Chromatin Recognition by 53BP1 through Direct H4K20me Binding and H2AK15 Acetylation. *Mol. Cell* 62, 409–421. doi:10.1016/j.molcel.2016.03.031.
- Jain, P., Ballare, C., Blanco, E., Vizan, P., and Di Croce, L. (2020). PHF19 mediated regulation of proliferation and invasiveness in prostate cancer cells. *eLife* 9. doi:10.7554/eLife.51373.
- Jakob, B., Splinter, J., Conrad, S., Voss, K.-O., Zink, D., Durante, M., Löbrich, M., and Taucher-Scholz, G. (2011). DNA double-strand breaks in heterochromatin elicit fast repair protein recruitment, histone H2AX phosphorylation and relocation to euchromatin. *Nucleic Acids Res.* 39, 6489–6499. doi:10.1093/nar/gkr230.
- Jentsch, S., McGrath, J. P., and Varshavsky, A. (1987). The yeast DNA repair gene RAD6 encodes a ubiquitin-conjugating enzyme. *Nature* 329, 131–134. doi:10.1038/329131a0.
- Jentsch, S., and Pyrowolakis, G. (2000). Ubiquitin and its kin: how close are the family ties? *Trends Cell Biol.* 10, 335–342. doi:10.1016/s0962-8924(00)01785-2.
- Jiang, X., Xu, Y., and Price, B. D. (2010). Acetylation of H2AX on lysine 36 plays a key role in the DNA double-strand break repair pathway. *FEBS Lett.* 584, 2926–2930. doi:10.1016/j.febslet.2010.05.017.
- Ji, S., Qin, Y., Shi, S., Liu, X., Hu, H., Zhou, H., Gao, J., Zhang, B., Xu, W., Liu, J., et al. (2015). ERK kinase phosphorylates and destabilizes the tumor suppressor FBW7 in pancreatic cancer. *Cell Res.* 25, 561–573. doi:10.1038/cr.2015.30.
- Jimeno, S., Fernández-Ávila, M. J., Cruz-García, A., Cepeda-García, C., Gómez-Cabello, D., and Huertas, P. (2015). Neddylation inhibits CtIP-mediated resection and regulates DNA double strand break repair pathway choice. *Nucleic Acids Res.* 43, 987–999. doi:10.1093/nar/gku1384.
- Kais, Z., Rondinelli, B., Holmes, A., O’Leary, C., Kozono, D., D’Andrea, A. D., and Ceccaldi, R. (2016). FANCD2 Maintains Fork Stability in BRCA1/2-Deficient Tumors and Promotes Alternative End-Joining DNA Repair. *Cell Rep.* 15, 2488–2499. doi:10.1016/j.celrep.2016.05.031.
- Kalb, R., Mallery, D. L., Larkin, C., Huang, J. T. J., and Hiom, K. (2014). BRCA1 is a histone-H2A-specific ubiquitin ligase. *Cell Rep.* 8, 999–1005. doi:10.1016/j.celrep.2014.07.025.
- Kalocsay, M., Hiller, N. J., and Jentsch, S. (2009). Chromosome-wide Rad51 spreading and SUMO-H2A.Z-dependent chromosome fixation in response to a persistent DNA double-strand break. *Mol. Cell* 33, 335–343. doi:10.1016/j.molcel.2009.01.016.
- Kan, Y., Batada, N. N., and Hendrickson, E. A. (2017). Human somatic cells deficient for RAD52 are impaired for viral integration and compromised for most aspects of homology-directed repair. *DNA Repair (Amst)* 55, 64–75. doi:10.1016/j.dnarep.2017.04.006.
- Kang, H. C., Lee, Y.-I., Shin, J.-H., Andrabi, S. A., Chi, Z., Gagné, J.-P., Lee, Y., Ko, H. S., Lee, B. D., Poirier, G. G., et al. (2011). Iduna is a poly(ADP-ribose) (PAR)-dependent E3 ubiquitin ligase that regulates DNA damage. *Proc Natl Acad Sci USA* 108, 14103–14108. doi:10.1073/pnas.1108799108.
- Karkhanis, V., Wang, L., Tae, S., Hu, Y.-J., Imbalzano, A. N., and Sif, S. (2012). Protein arginine methyltransferase 7 regulates cellular response to DNA damage by methylating promoter

- histones H2A and H4 of the polymerase δ catalytic subunit gene, POLD1. *J. Biol. Chem.* 287, 29801–29814. doi:10.1074/jbc.M112.378281.
- Kawaguchi, K., Uo, K., Tanaka, T., and Komada, M. (2017). Tandem UIMs confer Lys48 ubiquitin chain substrate preference to deubiquitinase USP25. *Sci. Rep.* 7, 45037. doi:10.1038/srep45037.
- Kelliher, J. L., West, K. L., Gong, Q., and Leung, J. W. C. (2020). Histone H2A variants alpha1-extension helix directs RNF168-mediated ubiquitination. *Nat. Commun.* 11, 2462. doi:10.1038/s41467-020-16307-4.
- Khoury-Haddad, H., Guttmann-Raviv, N., Ipenberg, I., Huggins, D., Jeyasekharan, A. D., and Ayoub, N. (2014). PARP1-dependent recruitment of KDM4D histone demethylase to DNA damage sites promotes double-strand break repair. *Proc Natl Acad Sci USA* 111, E728-37. doi:10.1073/pnas.1317585111.
- Khurana, S., Kruhlak, M. J., Kim, J., Tran, A. D., Liu, J., Nyswaner, K., Shi, L., Jailwala, P., Sung, M.-H., Hakim, O., et al. (2014). A macrohistone variant links dynamic chromatin compaction to BRCA1-dependent genome maintenance. *Cell Rep.* 8, 1049–1062. doi:10.1016/j.celrep.2014.07.024.
- Kilgas, S., Singh, A. N., Paillas, S., Then, C.-K., Torrecilla, I., Nicholson, J., Browning, L., Vendrell, I., Konietzny, R., Kessler, B. M., et al. (2021). p97/VCP inhibition causes excessive MRE11-dependent DNA end resection promoting cell killing after ionizing radiation. *Cell Rep.* 35, 109153. doi:10.1016/j.celrep.2021.109153.
- Kilic, S., Lezaja, A., Gatti, M., Bianco, E., Michelena, J., Imhof, R., and Altmeyer, M. (2019). Phase separation of 53BP1 determines liquid-like behavior of DNA repair compartments. *EMBO J.* 38, e101379. doi:10.15252/embj.2018101379.
- Kimura, Y., and Tanaka, K. (2010). Regulatory mechanisms involved in the control of ubiquitin homeostasis. *J. Biochem.* 147, 793–798. doi:10.1093/jb/mvq044.
- Kim, J. J., Lee, S. Y., Gong, F., Battenhouse, A. M., Boutz, D. R., Bashyal, A., Refvik, S. T., Chiang, C.-M., Xhemalce, B., Paull, T. T., et al. (2019). Systematic bromodomain protein screens identify homologous recombination and R-loop suppression pathways involved in genome integrity. *Genes Dev.* 33, 1751–1774. doi:10.1101/gad.331231.119.
- Kim, J. J., Lee, S. Y., Hwang, Y., Kim, S., Chung, J. M., Park, S., Yoon, J., Yun, H., Ji, J.-H., Chae, S., et al. (2021). USP39 promotes non-homologous end-joining repair by poly(ADP-ribose)-induced liquid demixing. *Nucleic Acids Res.* doi:10.1093/nar/gkab892.
- Kim, W., Bennett, E. J., Huttlin, E. L., Guo, A., Li, J., Possemato, A., Sowa, M. E., Rad, R., Rush, J., Comb, M. J., et al. (2011). Systematic and quantitative assessment of the ubiquitin-modified proteome. *Mol. Cell* 44, 325–340. doi:10.1016/j.molcel.2011.08.025.
- Kitevski-LeBlanc, J., Fradet-Turcotte, A., Kukic, P., Wilson, M. D., Portella, G., Yuwen, T., Panier, S., Duan, S., Canny, M. D., van Ingen, H., et al. (2017). The RNF168 paralog RNF169 defines a new class of ubiquitylated histone reader involved in the response to DNA damage. *eLife* 6. doi:10.7554/eLife.23872.
- Kobayashi, S., Kasaishi, Y., Nakada, S., Takagi, T., Era, S., Motegi, A., Chiu, R. K., Takeda, S., and Hirota, K. (2015). Rad18 and Rnf8 facilitate homologous recombination by two distinct mechanisms, promoting Rad51 focus formation and suppressing the toxic effect of nonhomologous end joining. *Oncogene* 34, 4403–4411. doi:10.1038/onc.2014.371.

- Kolas, N. K., Chapman, J. R., Nakada, S., Ylanko, J., Chahwan, R., Sweeney, F. D., Panier, S., Mendez, M., Wildenhain, J., Thomson, T. M., et al. (2007). Orchestration of the DNA-damage response by the RNF8 ubiquitin ligase. *Science* 318, 1637–1640. doi:10.1126/science.1150034.
- Komander, D., and Rape, M. (2012). The ubiquitin code. *Annu. Rev. Biochem.* 81, 203–229. doi:10.1146/annurev-biochem-060310-170328.
- Korkuć, P., and Walther, D. (2017). Towards understanding the crosstalk between protein post-translational modifications: Homo- and heterotypic PTM pair distances on protein surfaces are not random. *Proteins* 85, 78–92. doi:10.1002/prot.25200.
- Kouzarides, T. (2007). Chromatin modifications and their function. *Cell* 128, 693–705. doi:10.1016/j.cell.2007.02.005.
- Krais, J. J., Wang, Y., Patel, P., Basu, J., Bernhardt, A. J., and Johnson, N. (2021). RNF168-mediated localization of BARD1 recruits the BRCA1-PALB2 complex to DNA damage. *Nat. Commun.* 12, 5016. doi:10.1038/s41467-021-25346-4.
- Kulathu, Y., Akutsu, M., Bremm, A., Hofmann, K., and Komander, D. (2009). Two-sided ubiquitin binding explains specificity of the TAB2 NZF domain. *Nat. Struct. Mol. Biol.* 16, 1328–1330. doi:10.1038/nsmb.1731.
- Kumar, R., González-Prieto, R., Xiao, Z., Verlaan-de Vries, M., and Vertegaal, A. C. O. (2017). The STUbL RNF4 regulates protein group SUMOylation by targeting the SUMO conjugation machinery. *Nat. Commun.* 8, 1809. doi:10.1038/s41467-017-01900-x.
- Kumari, N., Vartak, S. V., Dahal, S., Kumari, S., Desai, S. S., Gopalakrishnan, V., Choudhary, B., and Raghavan, S. C. (2019). G-quadruplex Structures Contribute to Differential Radiosensitivity of the Human Genome. *iScience* 21, 288–307. doi:10.1016/j.isci.2019.10.033.
- Kunz, V., Bommert, K. S., Kruk, J., Schwinning, D., Chatterjee, M., Stühmer, T., Bargou, R., and Bommert, K. (2020). Targeting of the E3 ubiquitin-protein ligase HUWE1 impairs DNA repair capacity and tumor growth in preclinical multiple myeloma models. *Sci. Rep.* 10, 18419. doi:10.1038/s41598-020-75499-3.
- Kupperman, E., Lee, E. C., Cao, Y., Bannerman, B., Fitzgerald, M., Berger, A., Yu, J., Yang, Y., Hales, P., Bruzzese, F., et al. (2010). Evaluation of the proteasome inhibitor MLN9708 in preclinical models of human cancer. *Cancer Res.* 70, 1970–1980. doi:10.1158/0008-5472.CAN-09-2766.
- Lacoursiere, R. E., and Shaw, G. S. (2021). Acetylated ubiquitin modulates the catalytic activity of the E1 enzyme uba1. *Biochemistry* 60, 1276–1285. doi:10.1021/acs.biochem.1c00145.
- Ladanyi, M., Cha, C., Lewis, R., Jhanwar, S. C., Huvos, A. G., and Healey, J. H. (1993). MDM2 gene amplification in metastatic osteosarcoma. *Cancer Res.* 53, 16–18.
- Lafranchi, L., de Boer, H. R., de Vries, E. G. E., Ong, S.-E., Sartori, A. A., and van Vugt, M. A. T. M. (2014). APC/C(Cdh1) controls CtlP stability during the cell cycle and in response to DNA damage. *EMBO J.* 33, 2860–2879. doi:10.15252/embj.201489017.
- Lancini, C., van den Berk, P. C. M., Vissers, J. H. A., Gargiulo, G., Song, J.-Y., Hulsman, D., Serresi, M., Tanger, E., Blom, M., Vens, C., et al. (2014). Tight regulation of ubiquitin-mediated DNA

- damage response by USP3 preserves the functional integrity of hematopoietic stem cells. *J. Exp. Med.* 211, 1759–1777. doi:10.1084/jem.20131436.
- Langerak, P., Mejia-Ramirez, E., Limbo, O., and Russell, P. (2011). Release of Ku and MRN from DNA ends by Mre11 nuclease activity and Ctp1 is required for homologous recombination repair of double-strand breaks. *PLoS Genet.* 7, e1002271. doi:10.1371/journal.pgen.1002271.
- Lee, J.-H., Kang, B.-H., Jang, H., Kim, T. W., Choi, J., Kwak, S., Han, J., Cho, E.-J., and Youn, H.-D. (2015). AKT phosphorylates H3-threonine 45 to facilitate termination of gene transcription in response to DNA damage. *Nucleic Acids Res.* 43, 4505–4516. doi:10.1093/nar/gkv176.
- Lee, L., Perez Oliva, A. B., Martinez-Balsalobre, E., Churikov, D., Peter, J., Rahmouni, D., Audoly, G., Azzoni, V., Audebert, S., Camoin, L., et al. (2021). UFMylation of MRE11 is essential for telomere length maintenance and hematopoietic stem cell survival. *Sci. Adv.* 7, eabc7371. doi:10.1126/sciadv.abc7371.
- Leung, A. K. L. (2014). Poly(ADP-ribose): an organizer of cellular architecture. *J. Cell Biol.* 205, 613–619. doi:10.1083/jcb.201402114.
- Leung, J. W., Agarwal, P., Canny, M. D., Gong, F., Robison, A. D., Finkelstein, I. J., Durocher, D., and Miller, K. M. (2014). Nucleosome acidic patch promotes RNF168- and RING1B/BMI1-dependent H2AX and H2A ubiquitination and DNA damage signaling. *PLoS Genet.* 10, e1004178. doi:10.1371/journal.pgen.1004178.
- Levone, B. R., Lenzken, S. C., Antonaci, M., Maiser, A., Rapp, A., Conte, F., Reber, S., Mechttersheimer, J., Ronchi, A. E., Mühlemann, O., et al. (2021). FUS-dependent liquid-liquid phase separation is important for DNA repair initiation. *J. Cell Biol.* 220. doi:10.1083/jcb.202008030.
- Lewis, E. B. (1978). A gene complex controlling segmentation in *Drosophila*. *Nature* 276, 565–570. doi:10.1038/276565a0.
- Liang, D., Burkhart, S. L., Singh, R. K., Kabbaj, M.-H. M., and Gunjan, A. (2012). Histone dosage regulates DNA damage sensitivity in a checkpoint-independent manner by the homologous recombination pathway. *Nucleic Acids Res.* 40, 9604–9620. doi:10.1093/nar/gks722.
- Liao, Y., Sumara, I., and Pangou, E. (2022). Non-proteolytic ubiquitylation in cellular signaling and human disease. *Commun. Biol.* 5, 114. doi:10.1038/s42003-022-03060-1.
- Lin, J.-R., Zeman, M. K., Chen, J.-Y., Yee, M.-C., and Cimprich, K. A. (2011). SHPRH and HLTF act in a damage-specific manner to coordinate different forms of postreplication repair and prevent mutagenesis. *Mol. Cell* 42, 237–249. doi:10.1016/j.molcel.2011.02.026.
- Liu, C., Wu, J., Paudyal, S. C., You, Z., and Yu, X. (2013). CHFR is important for the first wave of ubiquitination at DNA damage sites. *Nucleic Acids Res.* 41, 1698–1710. doi:10.1093/nar/gks1278.
- Liu, G., Yan, J., Wang, X., Chen, J., Wang, X., Dong, Y., Zhang, S., Gan, X., Huang, J., and Chen, X. (2021). RPA-mediated recruitment of Bre1 couples histone H2B ubiquitination to DNA replication and repair. *Proc Natl Acad Sci USA* 118. doi:10.1073/pnas.2017497118.
- Liu, H., Zhang, H., Wang, X., Tian, Q., Hu, Z., Peng, C., Jiang, P., Wang, T., Guo, W., Chen, Y., et al. (2015). The Deubiquitylating Enzyme USP4 Cooperates with CtIP in DNA Double-Strand Break End Resection. *Cell Rep.* 13, 93–107. doi:10.1016/j.celrep.2015.08.056.

- Liu, P., Gan, W., Su, S., Hauenstein, A. V., Fu, T.-M., Brasher, B., Schwerdtfeger, C., Liang, A. C., Xu, M., and Wei, W. (2018). K63-linked polyubiquitin chains bind to DNA to facilitate DNA damage repair. *Sci. Signal.* 11. doi:10.1126/scisignal.aar8133.
- Liu, Q., Gao, J., Zhao, C., Guo, Y., Wang, S., Shen, F., Xing, X., and Luo, Y. (2020). To control or to be controlled? Dual roles of CDK2 in DNA damage and DNA damage response. *DNA Repair (Amst)* 85, 102702. doi:10.1016/j.dnarep.2019.102702.
- Liu, X., Yang, X., Li, Y., Zhao, S., Li, C., Ma, P., and Mao, B. (2016). Trip12 is an E3 ubiquitin ligase for USP7/HAUSP involved in the DNA damage response. *FEBS Lett.* 590, 4213–4222. doi:10.1002/1873-3468.12471.
- Li, L., Halaby, M.-J., Hakem, A., Cardoso, R., El Ghamrasni, S., Harding, S., Chan, N., Bristow, R., Sanchez, O., Durocher, D., et al. (2010). Rnf8 deficiency impairs class switch recombination, spermatogenesis, and genomic integrity and predisposes for cancer. *J. Exp. Med.* 207, 983–997. doi:10.1084/jem.20092437.
- Li, M., Lu, L.-Y., Yang, C.-Y., Wang, S., and Yu, X. (2013). The FHA and BRCT domains recognize ADP-ribosylation during DNA damage response. *Genes Dev.* 27, 1752–1768. doi:10.1101/gad.226357.113.
- Li, M., and Yu, X. (2013). Function of BRCA1 in the DNA damage response is mediated by ADP-ribosylation. *Cancer Cell* 23, 693–704. doi:10.1016/j.ccr.2013.03.025.
- Li, P., Sun, J., Ruan, Y., and Song, L. (2021). High PHD Finger Protein 19 (PHF19) expression predicts poor prognosis in colorectal cancer: a retrospective study. *PeerJ* 9, e11551. doi:10.7717/peerj.11551.
- Li, W., Bengtson, M. H., Ulbrich, A., Matsuda, A., Reddy, V. A., Orth, A., Chanda, S. K., Batalov, S., and Joazeiro, C. A. P. (2008). Genome-wide and functional annotation of human E3 ubiquitin ligases identifies MULAN, a mitochondrial E3 that regulates the organelle's dynamics and signaling. *PLoS ONE* 3, e1487. doi:10.1371/journal.pone.0001487.
- Li, X., Liu, L., Yang, S., Song, N., Zhou, X., Gao, J., Yu, N., Shan, L., Wang, Q., Liang, J., et al. (2014). Histone demethylase KDM5B is a key regulator of genome stability. *Proc Natl Acad Sci USA* 111, 7096–7101. doi:10.1073/pnas.1324036111.
- Li, Y., Luo, K., Yin, Y., Wu, C., Deng, M., Li, L., Chen, Y., Nowsheen, S., Lou, Z., and Yuan, J. (2017). USP13 regulates the RAP80-BRCA1 complex dependent DNA damage response. *Nat. Commun.* 8, 15752. doi:10.1038/ncomms15752.
- Löbrich, M., Cooper, P. K., and Rydberg, B. (1996). Non-random distribution of DNA double-strand breaks induced by particle irradiation. *Int. J. Radiat. Biol.* 70, 493–503. doi:10.1080/095530096144680.
- Locke, A. J., Hossain, L., McCrostie, G., Ronato, D. A., Fitieh, A., Rafique, T. A., Mashayekhi, F., Motamedi, M., Masson, J.-Y., and Ismail, I. H. (2021). SUMOylation mediates CtIP's functions in DNA end resection and replication fork protection. *Nucleic Acids Res.* 49, 928–953. doi:10.1093/nar/gkaa1232.
- Luger, K., Mäder, A. W., Richmond, R. K., Sargent, D. F., and Richmond, T. J. (1997). Crystal structure of the nucleosome core particle at 2.8 Å resolution. *Nature* 389, 251–260. doi:10.1038/38444.

- Lundby, A., Secher, A., Lage, K., Nordsborg, N. B., Dmytriiev, A., Lundby, C., and Olsen, J. V. (2012). Quantitative maps of protein phosphorylation sites across 14 different rat organs and tissues. *Nat. Commun.* 3, 876. doi:10.1038/ncomms1871.
- Luo, K., Zhang, H., Wang, L., Yuan, J., and Lou, Z. (2012). Sumoylation of MDC1 is important for proper DNA damage response. *EMBO J.* 31, 3008–3019. doi:10.1038/emboj.2012.158.
- Lu, X., Xu, M., Zhu, Q., Zhang, J., Liu, G., Bao, Y., Gu, L., Tian, Y., Wen, H., and Zhu, W.-G. (2021). RNF8-ubiquitinated KMT5A is required for RNF168-induced H2A ubiquitination in response to DNA damage. *FASEB J.* 35, e21326. doi:10.1096/fj.202002234R.
- Lynch, D. R., Farmer, J., Hauser, L., Blair, I. A., Wang, Q. Q., Mesaros, C., Snyder, N., Boesch, S., Chin, M., Delatycki, M. B., et al. (2019). Safety, pharmacodynamics, and potential benefit of omaveloxolone in Friedreich ataxia. *Ann. Clin. Transl. Neurol.* 6, 15–26. doi:10.1002/acn3.660.
- Ma, T., Chen, Y., Zhang, F., Yang, C.-Y., Wang, S., and Yu, X. (2013). RNF111-dependent neddylation activates DNA damage-induced ubiquitination. *Mol. Cell* 49, 897–907. doi:10.1016/j.molcel.2013.01.006.
- Maat, H., Atsma, T. J., Hogeling, S. M., Rodríguez López, A., Jaques, J., Olthuis, M., de Vries, M. P., Gravesteijn, C., Brouwers-Vos, A. Z., van der Meer, N., et al. (2021). The USP7-TRIM27 axis mediates non-canonical PRC1.1 function and is a druggable target in leukemia. *iScience* 24, 102435. doi:10.1016/j.isci.2021.102435.
- Mabbitt, P. D., Loreto, A., Déry, M.-A., Fletcher, A. J., Stanley, M., Pao, K.-C., Wood, N. T., Coleman, M. P., and Virdee, S. (2020). Structural basis for RING-Cys-Relay E3 ligase activity and its role in axon integrity. *Nat. Chem. Biol.* 16, 1227–1236. doi:10.1038/s41589-020-0598-6.
- Macûrek, L., Lindqvist, A., Voets, O., Kool, J., Vos, H. R., and Medema, R. H. (2010). Wip1 phosphatase is associated with chromatin and dephosphorylates gammaH2AX to promote checkpoint inhibition. *Oncogene* 29, 2281–2291. doi:10.1038/onc.2009.501.
- Magnaghi, P., D'Alessio, R., Valsasina, B., Avanzi, N., Rizzi, S., Asa, D., Gasparri, F., Cozzi, L., Cucchi, U., Orrenius, C., et al. (2013). Covalent and allosteric inhibitors of the ATPase VCP/p97 induce cancer cell death. *Nat. Chem. Biol.* 9, 548–556. doi:10.1038/nchembio.1313.
- Magnussen, H. M., Ahmed, S. F., Sibbet, G. J., Hristova, V. A., Nomura, K., Hock, A. K., Archibald, L. J., Jamieson, A. G., Fushman, D., Vousden, K. H., et al. (2020). Structural basis for DNA damage-induced phosphoregulation of MDM2 RING domain. *Nat. Commun.* 11, 2094. doi:10.1038/s41467-020-15783-y.
- Mailand, N., Bekker-Jensen, S., Fastrup, H., Melander, F., Bartek, J., Lukas, C., and Lukas, J. (2007). RNF8 ubiquitylates histones at DNA double-strand breaks and promotes assembly of repair proteins. *Cell* 131, 887–900. doi:10.1016/j.cell.2007.09.040.
- Mallette, F. A., Mattioli, F., Cui, G., Young, L. C., Hendzel, M. J., Mer, G., Sixma, T. K., and Richard, S. (2012). RNF8- and RNF168-dependent degradation of KDM4A/JMJD2A triggers 53BP1 recruitment to DNA damage sites. *EMBO J.* 31, 1865–1878. doi:10.1038/emboj.2012.47.
- Mandemaker, I. K., van Cuijk, L., Janssens, R. C., Lans, H., Bezstarosti, K., Hoeijmakers, J. H., Demmers, J. A., Vermeulen, W., and Marteijn, J. A. (2017). DNA damage-induced histone H1 ubiquitylation is mediated by HUWE1 and stimulates the RNF8-RNF168 pathway. *Sci. Rep.* 7, 15353. doi:10.1038/s41598-017-15194-y.

- Manis, J. P., Morales, J. C., Xia, Z., Kutok, J. L., Alt, F. W., and Carpenter, P. B. (2004). 53BP1 links DNA damage-response pathways to immunoglobulin heavy chain class-switch recombination. *Nat. Immunol.* 5, 481–487. doi:10.1038/ni1067.
- Mao, Z., Bozzella, M., Seluanov, A., and Gorbunova, V. (2008). DNA repair by nonhomologous end joining and homologous recombination during cell cycle in human cells. *Cell Cycle* 7, 2902–2906. doi:10.4161/cc.7.18.6679.
- Maréchal, A., Li, J.-M., Ji, X. Y., Wu, C.-S., Yazinski, S. A., Nguyen, H. D., Liu, S., Jiménez, A. E., Jin, J., and Zou, L. (2014). PRP19 transforms into a sensor of RPA-ssDNA after DNA damage and drives ATR activation via a ubiquitin-mediated circuitry. *Mol. Cell* 53, 235–246. doi:10.1016/j.molcel.2013.11.002.
- Margueron, R., Li, G., Sarma, K., Blais, A., Zavadil, J., Woodcock, C. L., Dynlacht, B. D., and Reinberg, D. (2008). Ezh1 and Ezh2 maintain repressive chromatin through different mechanisms. *Mol. Cell* 32, 503–518. doi:10.1016/j.molcel.2008.11.004.
- Martinez-Pastor, B., Silveira, G. G., Clarke, T. L., Chung, D., Gu, Y., Cosentino, C., Davidow, L. S., Mata, G., Hassanieh, S., Salsman, J., et al. (2021). Assessing kinetics and recruitment of DNA repair factors using high content screens. *Cell Rep.* 37, 110176. doi:10.1016/j.celrep.2021.110176.
- Mason, M. J., Schinke, C., Eng, C. L. P., Towfic, F., Gruber, F., Dervan, A., White, B. S., Pratapa, A., Guan, Y., Chen, H., et al. (2020). Multiple Myeloma DREAM Challenge reveals epigenetic regulator PHF19 as marker of aggressive disease. *Leukemia* 34, 1866–1874. doi:10.1038/s41375-020-0742-z.
- Masumoto, H., Hawke, D., Kobayashi, R., and Verreault, A. (2005). A role for cell-cycle-regulated histone H3 lysine 56 acetylation in the DNA damage response. *Nature* 436, 294–298. doi:10.1038/nature03714.
- Mattioli, F., Uckelmann, M., Sahtoe, D. D., van Dijk, W. J., and Sixma, T. K. (2014). The nucleosome acidic patch plays a critical role in RNF168-dependent ubiquitination of histone H2A. *Nat. Commun.* 5, 3291. doi:10.1038/ncomms4291.
- Mattioli, F., Vissers, J. H. A., van Dijk, W. J., Ikpa, P., Citterio, E., Vermeulen, W., Marteiijn, J. A., and Sixma, T. K. (2012). RNF168 ubiquitinates K13-15 on H2A/H2AX to drive DNA damage signaling. *Cell* 150, 1182–1195. doi:10.1016/j.cell.2012.08.005.
- Maxwell, K. N., and Domchek, S. M. (2012). Cancer treatment according to BRCA1 and BRCA2 mutations. *Nat. Rev. Clin. Oncol.* 9, 520–528. doi:10.1038/nrclinonc.2012.123.
- May, E., Jenkins, J. R., and May, P. (1991). Endogenous HeLa p53 proteins are easily detected in HeLa cells transfected with mouse deletion mutant p53 gene. *Oncogene* 6, 1363–1365.
- McClellan, A. J., Laugesen, S. H., and Ellgaard, L. (2019). Cellular functions and molecular mechanisms of non-lysine ubiquitination. *Open Biol.* 9, 190147. doi:10.1098/rsob.190147.
- McDermaid, A., Monier, B., Zhao, J., Liu, B., and Ma, Q. (2019). Interpretation of differential gene expression results of RNA-seq data: review and integration. *Brief. Bioinformatics* 20, 2044–2054. doi:10.1093/bib/bby067.
- Meerang, M., Ritz, D., Paliwal, S., Garajova, Z., Bosshard, M., Mailand, N., Janscak, P., Hübscher, U., Meyer, H., and Ramadan, K. (2011). The ubiquitin-selective segregase VCP/p97

- orchestrates the response to DNA double-strand breaks. *Nat. Cell Biol.* 13, 1376–1382. doi:10.1038/ncb2367.
- Meyer, H. H., Wang, Y., and Warren, G. (2002). Direct binding of ubiquitin conjugates by the mammalian p97 adaptor complexes, p47 and Ufd1-Npl4. *EMBO J.* 21, 5645–5652. doi:10.1093/emboj/cdf579.
- Millan-Zambrano, G., Santos-Rosa, H., Puddu, F., Robson, S. C., Jackson, S. P., and Kouzarides, T. (2018). Phosphorylation of histone H4T80 triggers DNA damage checkpoint recovery. *Mol. Cell* 72, 625–635.e4. doi:10.1016/j.molcel.2018.09.023.
- Miller, K. M., Tjeertes, J. V., Coates, J., Legube, G., Polo, S. E., Britton, S., and Jackson, S. P. (2010). Human HDAC1 and HDAC2 function in the DNA-damage response to promote DNA nonhomologous end-joining. *Nat. Struct. Mol. Biol.* 17, 1144–1151. doi:10.1038/nsmb.1899.
- Mimori, T., and Hardin, J. A. (1986). Mechanism of interaction between Ku protein and DNA. *J. Biol. Chem.* 261, 10375–10379. doi:10.1016/S0021-9258(18)67534-9.
- Miné-Hattab, J., Heltberg, M., Villemeur, M., Guedj, C., Mora, T., Walczak, A. M., Dahan, M., and Taddei, A. (2021). Single molecule microscopy reveals key physical features of repair foci in living cells. *eLife* 10. doi:10.7554/eLife.60577.
- Miné-Hattab, J., Recamier, V., Izeddin, I., Rothstein, R., and Darzacq, X. (2017). Multi-scale tracking reveals scale-dependent chromatin dynamics after DNA damage. *Mol. Biol. Cell.* doi:10.1091/mbc.E17-05-0317.
- Mirman, Z., Lottersberger, F., Takai, H., Kibe, T., Gong, Y., Takai, K., Bianchi, A., Zimmermann, M., Durocher, D., and de Lange, T. (2018). 53BP1-RIF1-shieldin counteracts DSB resection through CST- and Polα-dependent fill-in. *Nature* 560, 112–116. doi:10.1038/s41586-018-0324-7.
- Mohr, S. E., Smith, J. A., Shamu, C. E., Neumüller, R. A., and Perrimon, N. (2014). RNAi screening comes of age: improved techniques and complementary approaches. *Nat. Rev. Mol. Cell Biol.* 15, 591–600. doi:10.1038/nrm3860.
- Montgomery, N. D., Yee, D., Chen, A., Kalantry, S., Chamberlain, S. J., Otte, A. P., and Magnuson, T. (2005). The murine polycomb group protein Eed is required for global histone H3 lysine-27 methylation. *Curr. Biol.* 15, 942–947. doi:10.1016/j.cub.2005.04.051.
- Morris, J. R., Boutell, C., Keppler, M., Densham, R., Weekes, D., Alamshah, A., Butler, L., Galanty, Y., Pangon, L., Kiuchi, T., et al. (2009). The SUMO modification pathway is involved in the BRCA1 response to genotoxic stress. *Nature* 462, 886–890. doi:10.1038/nature08593.
- Mosammamarast, N., Kim, H., Laurent, B., Zhao, Y., Lim, H. J., Majid, M. C., Dango, S., Luo, Y., Hempel, K., Sowa, M. E., et al. (2013). The histone demethylase LSD1/KDM1A promotes the DNA damage response. *J. Cell Biol.* 203, 457–470. doi:10.1083/jcb.201302092.
- Mosbech, A., Lukas, C., Bekker-Jensen, S., and Mailand, N. (2013). The deubiquitylating enzyme USP44 counteracts the DNA double-strand break response mediated by the RNF8 and RNF168 ubiquitin ligases. *J. Biol. Chem.* 288, 16579–16587. doi:10.1074/jbc.M113.459917.
- Moss, J., Tinline-Purvis, H., Walker, C. A., Folkes, L. K., Stratford, M. R., Hayles, J., Hoe, K.-L., Kim, D.-U., Park, H.-O., Kearsey, S. E., et al. (2010). Break-induced ATR and Ddb1-Cul4(Cdt)² ubiquitin ligase-dependent nucleotide synthesis promotes homologous recombination repair in fission yeast. *Genes Dev.* 24, 2705–2716. doi:10.1101/gad.1970810.

- Moyal, L., Lerenthal, Y., Gana-Weisz, M., Mass, G., So, S., Wang, S.-Y., Eppink, B., Chung, Y. M., Shalev, G., Shema, E., et al. (2011). Requirement of ATM-dependent monoubiquitylation of histone H2B for timely repair of DNA double-strand breaks. *Mol. Cell* 41, 529–542. doi:10.1016/j.molcel.2011.02.015.
- Murr, R., Loizou, J. I., Yang, Y.-G., Cuenin, C., Li, H., Wang, Z.-Q., and Herceg, Z. (2006). Histone acetylation by Trapp-Tip60 modulates loading of repair proteins and repair of DNA double-strand breaks. *Nat. Cell Biol.* 8, 91–99. doi:10.1038/ncb1343.
- Nakada, S., Tai, I., Panier, S., Al-Hakim, A., Iemura, S.-I., Juang, Y.-C., O'Donnell, L., Kumakubo, A., Munro, M., Sicheri, F., et al. (2010). Non-canonical inhibition of DNA damage-dependent ubiquitination by OTUB1. *Nature* 466, 941–946. doi:10.1038/nature09297.
- Nakada, S., Yonamine, R. M., and Matsuo, K. (2012). RNF8 regulates assembly of RAD51 at DNA double-strand breaks in the absence of BRCA1 and 53BP1. *Cancer Res.* 72, 4974–4983. doi:10.1158/0008-5472.CAN-12-1057.
- Nakamura, K., Kato, A., Kobayashi, J., Yanagihara, H., Sakamoto, S., Oliveira, D. V. N. P., Shimada, M., Tauchi, H., Suzuki, H., Tashiro, S., et al. (2011). Regulation of homologous recombination by RNF20-dependent H2B ubiquitination. *Mol. Cell* 41, 515–528. doi:10.1016/j.molcel.2011.02.002.
- Nakamura, K., Saredi, G., Becker, J. R., Foster, B. M., Nguyen, N. V., Beyer, T. E., Cesa, L. C., Faull, P. A., Lukauskas, S., Frimurer, T., et al. (2019). H4K20me0 recognition by BRCA1-BARD1 directs homologous recombination to sister chromatids. *Nat. Cell Biol.* 21, 311–318. doi:10.1038/s41556-019-0282-9.
- Natale, F., Rapp, A., Yu, W., Maiser, A., Harz, H., Scholl, A., Grulich, S., Anton, T., Hörl, D., Chen, W., et al. (2017). Identification of the elementary structural units of the DNA damage response. *Nat. Commun.* 8, 15760. doi:10.1038/ncomms15760.
- Negrini, S., Gorgoulis, V. G., and Halazonetis, T. D. (2010). Genomic instability--an evolving hallmark of cancer. *Nat. Rev. Mol. Cell Biol.* 11, 220–228. doi:10.1038/nrm2858.
- Nicassio, F., Corrado, N., Vissers, J. H. A., Areces, L. B., Bergink, S., Marteijn, J. A., Geverts, B., Houtsmuller, A. B., Vermeulen, W., Di Fiore, P. P., et al. (2007). Human USP3 is a chromatin modifier required for S phase progression and genome stability. *Curr. Biol.* 17, 1972–1977. doi:10.1016/j.cub.2007.10.034.
- Niu, X., Chen, W., Bi, T., Lu, M., Qin, Z., and Xiao, W. (2019). Rev1 plays central roles in mammalian DNA-damage tolerance in response to UV irradiation. *FEBS J.* 286, 2711–2725. doi:10.1111/febs.14840.
- Noordermeer, S. M., Adam, S., Setiawati, D., Barazas, M., Pettitt, S. J., Ling, A. K., Olivieri, M., Álvarez-Quilón, A., Moatti, N., Zimmermann, M., et al. (2018). The shieldin complex mediates 53BP1-dependent DNA repair. *Nature* 560, 117–121. doi:10.1038/s41586-018-0340-7.
- Nowsheen, S., Aziz, K., Aziz, A., Deng, M., Qin, B., Luo, K., Jeganathan, K. B., Zhang, H., Liu, T., Yu, J., et al. (2018). L3MBTL2 orchestrates ubiquitin signalling by dictating the sequential recruitment of RNF8 and RNF168 after DNA damage. *Nat. Cell Biol.* 20, 455–464. doi:10.1038/s41556-018-0071-x.
- O'Connor, H. F., Lyon, N., Leung, J. W., Agarwal, P., Swaim, C. D., Miller, K. M., and Huibregtse, J. M. (2015). Ubiquitin-Activated Interaction Traps (UBAITs) identify E3 ligase binding partners. *EMBO Rep.* 16, 1699–1712. doi:10.15252/embr.201540620.

- O'Hagan, H. M., Mohammad, H. P., and Baylin, S. B. (2008). Double strand breaks can initiate gene silencing and SIRT1-dependent onset of DNA methylation in an exogenous promoter CpG island. *PLoS Genet.* 4, e1000155. doi:10.1371/journal.pgen.1000155.
- Oberoi, J., Richards, M. W., Crumpler, S., Brown, N., Blagg, J., and Bayliss, R. (2010). Structural basis of poly(ADP-ribose) recognition by the multizinc binding domain of checkpoint with forkhead-associated and RING Domains (CHFR). *J. Biol. Chem.* 285, 39348–39358. doi:10.1074/jbc.M110.159855.
- Ochs, F., Karemore, G., Miron, E., Brown, J., Sedlackova, H., Rask, M.-B., Lampe, M., Buckle, V., Schermelleh, L., Lukas, J., et al. (2019). Stabilization of chromatin topology safeguards genome integrity. *Nature* 574, 571–574. doi:10.1038/s41586-019-1659-4.
- Ohkuni, K., Gliford, L., Au, W.-C., Suva, E., Kaiser, P., and Basrai, M. A. (2022). Cdc48Ufd1/Npl4 segregase removes mislocalized centromeric histone H3 variant CENP-A from non-centromeric chromatin. *Nucleic Acids Res.* 50, 3276–3291. doi:10.1093/nar/gkac135.
- Ohtake, F., Saeki, Y., Sakamoto, K., Ohtake, K., Nishikawa, H., Tsuchiya, H., Ohta, T., Tanaka, K., and Kanno, J. (2015). Ubiquitin acetylation inhibits polyubiquitin chain elongation. *EMBO Rep.* 16, 192–201. doi:10.15252/embr.201439152.
- Ohtomo, H., Ito, S., McKenzie, N. J., Uckelmann, M., Wakamori, M., Ehara, H., Furukawa, A., Tsunaka, Y., Shibata, M., Sekine, S.-I., et al. (2023). H2A Ubiquitination Alters H3-tail Dynamics on Linker-DNA to Enhance H3K27 Methylation. *J. Mol. Biol.* 435, 167936. doi:10.1016/j.jmb.2022.167936.
- Olivo-Marin, J.-C. (2002). Extraction of spots in biological images using multiscale products. *Pattern Recognit.* 35, 1989–1996. doi:10.1016/S0031-3203(01)00127-3.
- Orthwein, A., Noordermeer, S. M., Wilson, M. D., Landry, S., Enchev, R. I., Sherker, A., Munro, M., Pinder, J., Salsman, J., Dellaire, G., et al. (2015). A mechanism for the suppression of homologous recombination in G1 cells. *Nature* 528, 422–426. doi:10.1038/nature16142.
- Oshidari, R., Huang, R., Medghalchi, M., Tse, E. Y. W., Ashgriz, N., Lee, H. O., Wyatt, H., and Mekhail, K. (2020). DNA repair by Rad52 liquid droplets. *Nat. Commun.* 11, 695. doi:10.1038/s41467-020-14546-z.
- Osipov, A. N., Grekhova, A., Pustovalova, M., Ozerov, I. V., Eremin, P., Vorobyeva, N., Lazareva, N., Pulin, A., Zhavoronkov, A., Roumiantsev, S., et al. (2015). Activation of homologous recombination DNA repair in human skin fibroblasts continuously exposed to X-ray radiation. *Oncotarget* 6, 26876–26885. doi:10.18632/oncotarget.4946.
- Oza, J., Ganguly, B., Kulkarni, A., Ginjaala, V., Yao, M., and Ganesan, S. (2016). A novel role of chromodomain protein CBX8 in DNA damage response. *J. Biol. Chem.* 291, 22881–22893. doi:10.1074/jbc.M116.725879.
- Pai, C.-C., Deegan, R. S., Subramanian, L., Gal, C., Sarkar, S., Blaikley, E. J., Walker, C., Hulme, L., Bernhard, E., Codlin, S., et al. (2014). A histone H3K36 chromatin switch coordinates DNA double-strand break repair pathway choice. *Nat. Commun.* 5, 4091. doi:10.1038/ncomms5091.
- Panier, S., Ichijima, Y., Fradet-Turcotte, A., Leung, C. C. Y., Kaustov, L., Arrowsmith, C. H., and Durocher, D. (2012). Tandem protein interaction modules organize the ubiquitin-dependent response to DNA double-strand breaks. *Mol. Cell* 47, 383–395. doi:10.1016/j.molcel.2012.05.045.

- Pan, M.-R., Peng, G., Hung, W.-C., and Lin, S.-Y. (2011). Monoubiquitination of H2AX protein regulates DNA damage response signaling. *J. Biol. Chem.* 286, 28599–28607. doi:10.1074/jbc.M111.256297.
- Pasini, D., Bracken, A. P., Jensen, M. R., Lazzerini Denchi, E., and Helin, K. (2004). Suz12 is essential for mouse development and for EZH2 histone methyltransferase activity. *EMBO J.* 23, 4061–4071. doi:10.1038/sj.emboj.7600402.
- Pei, H., Zhang, L., Luo, K., Qin, Y., Chesi, M., Fei, F., Bergsagel, P. L., Wang, L., You, Z., and Lou, Z. (2011). MMSET regulates histone H4K20 methylation and 53BP1 accumulation at DNA damage sites. *Nature* 470, 124–128. doi:10.1038/nature09658.
- Peng, J., Schwartz, D., Elias, J. E., Thoreen, C. C., Cheng, D., Marsischky, G., Roelofs, J., Finley, D., and Gygi, S. P. (2003). A proteomics approach to understanding protein ubiquitination. *Nat. Biotechnol.* 21, 921–926. doi:10.1038/nbt849.
- Pereg, Y., Shkedy, D., de Graaf, P., Meulmeester, E., Edelson-Averbukh, M., Salek, M., Biton, S., Teunisse, A. F. A. S., Lehmann, W. D., Jochemsen, A. G., et al. (2005). Phosphorylation of Hdmx mediates its Hdm2- and ATM-dependent degradation in response to DNA damage. *Proc Natl Acad Sci USA* 102, 5056–5061. doi:10.1073/pnas.0408595102.
- Pessina, F., Giavazzi, F., Yin, Y., Gioia, U., Vitelli, V., Galbiati, A., Barozzi, S., Garre, M., Oldani, A., Flaus, A., et al. (2019). Functional transcription promoters at DNA double-strand breaks mediate RNA-driven phase separation of damage-response factors. *Nat. Cell Biol.* 21, 1286–1299. doi:10.1038/s41556-019-0392-4.
- Pfister, S. X., Ahrabi, S., Zalmas, L.-P., Sarkar, S., Aymard, F., Bachrati, C. Z., Helleday, T., Legube, G., La Thangue, N. B., Porter, A. C. G., et al. (2014). SETD2-dependent histone H3K36 trimethylation is required for homologous recombination repair and genome stability. *Cell Rep.* 7, 2006–2018. doi:10.1016/j.celrep.2014.05.026.
- Pickart, C. M. (2004). Back to the future with ubiquitin. *Cell* 116, 181–190. doi:10.1016/s0092-8674(03)01074-2.
- Pinato, S., Gatti, M., Scandiuizzi, C., Confalonieri, S., and Penengo, L. (2011). UMI, a novel RNF168 ubiquitin binding domain involved in the DNA damage signaling pathway. *Mol. Cell. Biol.* 31, 118–126. doi:10.1128/MCB.00818-10.
- Pinato, S., Scandiuizzi, C., Arnaudo, N., Citterio, E., Gaudino, G., and Penengo, L. (2009). RNF168, a new RING finger, MIU-containing protein that modifies chromatin by ubiquitination of histones H2A and H2AX. *BMC Mol. Biol.* 10, 55. doi:10.1186/1471-2199-10-55.
- Piñero, J., Bravo, À., Queralt-Rosinach, N., Gutiérrez-Sacristán, A., Deu-Pons, J., Centeno, E., García-García, J., Sanz, F., and Furlong, L. I. (2017). DisGeNET: a comprehensive platform integrating information on human disease-associated genes and variants. *Nucleic Acids Res.* 45, D833–D839. doi:10.1093/nar/gkw943.
- Piunti, A., and Shilatifard, A. (2016). Epigenetic balance of gene expression by Polycomb and COMPASS families. *Science* 352, aad9780. doi:10.1126/science.aad9780.
- Piva, R., Ruggeri, B., Williams, M., Costa, G., Tamagno, I., Ferrero, D., Giai, V., Coscia, M., Peola, S., Massaia, M., et al. (2008). CEP-18770: A novel, orally active proteasome inhibitor with a tumor-selective pharmacologic profile competitive with bortezomib. *Blood* 111, 2765–2775. doi:10.1182/blood-2007-07-100651.

- Pollard, J. M., and Gatti, R. A. (2009). Clinical radiation sensitivity with DNA repair disorders: an overview. *Int. J. Radiat. Oncol. Biol. Phys.* 74, 1323–1331. doi:10.1016/j.ijrobp.2009.02.057.
- Polo, S. E., Kaidi, A., Baskcomb, L., Galanty, Y., and Jackson, S. P. (2010). Regulation of DNA-damage responses and cell-cycle progression by the chromatin remodelling factor CHD4. *EMBO J.* 29, 3130–3139. doi:10.1038/emboj.2010.188.
- Popovic, D., Vucic, D., and Dikic, I. (2014). Ubiquitination in disease pathogenesis and treatment. *Nat. Med.* 20, 1242–1253. doi:10.1038/nm.3739.
- Postow, L., and Funabiki, H. (2013). An SCF complex containing Fbxl12 mediates DNA damage-induced Ku80 ubiquitylation. *Cell Cycle* 12, 587–595. doi:10.4161/cc.23408.
- Postow, L., Ghenoiu, C., Woo, E. M., Krutchinsky, A. N., Chait, B. T., and Funabiki, H. (2008). Ku80 removal from DNA through double strand break-induced ubiquitylation. *J. Cell Biol.* 182, 467–479. doi:10.1083/jcb.200802146.
- Potts, B. C., Albitar, M. X., Anderson, K. C., Baritaki, S., Berkers, C., Bonavida, B., Chandra, J., Chauhan, D., Cusack, J. C., Fenical, W., et al. (2011). Marizomib, a proteasome inhibitor for all seasons: preclinical profile and a framework for clinical trials. *Curr. Cancer Drug Targets* 11, 254–284. doi:10.2174/156800911794519716.
- Poulsen, M., Lukas, C., Lukas, J., Bekker-Jensen, S., and Mailand, N. (2012). Human RNF169 is a negative regulator of the ubiquitin-dependent response to DNA double-strand breaks. *J. Cell Biol.* 197, 189–199. doi:10.1083/jcb.201109100.
- Prag, G., Watson, H., Kim, Y. C., Beach, B. M., Ghirlando, R., Hummer, G., Bonifacino, J. S., and Hurley, J. H. (2007). The Vps27/Hse1 complex is a GAT domain-based scaffold for ubiquitin-dependent sorting. *Dev. Cell* 12, 973–986. doi:10.1016/j.devcel.2007.04.013.
- Prendergast, L., McClurg, U. L., Hristova, R., Berlinguer-Palmini, R., Greener, S., Veitch, K., Hernandez, I., Pasero, P., Rico, D., Higgins, J. M. G., et al. (2020). Resolution of R-loops by INO80 promotes DNA replication and maintains cancer cell proliferation and viability. *Nat. Commun.* 11, 4534. doi:10.1038/s41467-020-18306-x.
- Qin, C., Wang, Y.-L., Zhou, J.-Y., Shi, J., Zhao, W.-W., Zhu, Y.-X., Bai, S.-M., Feng, L.-L., Bie, S.-Y., Zeng, B., et al. (2023). RAP80 phase separation at DNA double-strand break promotes BRCA1 recruitment. *Nucleic Acids Res.* 51, 9733–9747. doi:10.1093/nar/gkad686.
- Qin, W., Steinek, C., Kolobynina, K., Forné, I., Imhof, A., Cardoso, M. C., and Leonhardt, H. (2022). Probing protein ubiquitination in live cells. *Nucleic Acids Res.* doi:10.1093/nar/gkac805.
- Qiu, L., Xu, W., Lu, X., Chen, F., Chen, Y., Tian, Y., Zhu, Q., Liu, X., Wang, Y., Pei, X.-H., et al. (2023). The HDAC6-RNF168 axis regulates H2A/H2A.X ubiquitination to enable double-strand break repair. *Nucleic Acids Res.* doi:10.1093/nar/gkad631.
- Rabl, J., Bunker, R. D., Schenk, A. D., Cavadini, S., Gill, M. E., Abdulrahman, W., Andrés-Pons, A., Luijsterburg, M. S., Ibrahim, A. F. M., Branigan, E., et al. (2019). Structural basis of BRCC36 function in DNA repair and immune regulation. *Mol. Cell* 75, 483–497. doi:10.1016/j.molcel.2019.06.002.
- Radulescu, I., Elmroth, K., and Stenerlöw, B. (2004). Chromatin organization contributes to non-randomly distributed double-strand breaks after exposure to high-LET radiation. *Radiat. Res.* 161, 1–8. doi:10.1667/rr3094.

- Ramachandran, S., Haddad, D., Li, C., Le, M. X., Ling, A. K., So, C. C., Nepal, R. M., Gommerman, J. L., Yu, K., Ketela, T., et al. (2016). The SAGA Deubiquitination Module Promotes DNA Repair and Class Switch Recombination through ATM and DNAPK-Mediated γ H2AX Formation. *Cell Rep.* 15, 1554–1565. doi:10.1016/j.celrep.2016.04.041.
- Rasco, D. W., Lakhani, N. J., Li, Y., Men, L., Wang, H., Ji, J., Tang, Y., Liang, Z., Amaya, A., Estkowski, K., et al. (2019a). A phase I study of a novel MDM2 antagonist APG-115 in patients with advanced solid tumors. *JCO* 37, 3126–3126. doi:10.1200/JCO.2019.37.15_suppl.3126.
- Rasco, D. W., Papadopoulos, K. P., Pourdehnad, M., Gandhi, A. K., Hagner, P. R., Li, Y., Wei, X., Chopra, R., Hege, K., DiMartino, J., et al. (2019b). A First-in-Human Study of Novel Cereblon Modulator Avadomide (CC-122) in Advanced Malignancies. *Clin. Cancer Res.* 25, 90–98. doi:10.1158/1078-0432.CCR-18-1203.
- Raudvere, U., Kolberg, L., Kuzmin, I., Arak, T., Adler, P., Peterson, H., and Vilo, J. (2019). g:Profiler: a web server for functional enrichment analysis and conversions of gene lists (2019 update). *Nucleic Acids Res.* 47, W191–W198. doi:10.1093/nar/gkz369.
- Rego, M. A., Kolling, F. W., Vuono, E. A., Mauro, M., and Howlett, N. G. (2012). Regulation of the Fanconi anemia pathway by a CUE ubiquitin-binding domain in the FANCD2 protein. *Blood* 120, 2109–2117. doi:10.1182/blood-2012-02-410472.
- Reyes-Turcu, F. E., Horton, J. R., Mullally, J. E., Heroux, A., Cheng, X., and Wilkinson, K. D. (2006). The ubiquitin binding domain ZnF UBP recognizes the C-terminal diglycine motif of unanchored ubiquitin. *Cell* 124, 1197–1208. doi:10.1016/j.cell.2006.02.038.
- Rijkers, T., Van Den Ouweland, J., Morolli, B., Rolink, A. G., Baarends, W. M., Van Sloun, P. P., Lohman, P. H., and Pastink, A. (1998). Targeted inactivation of mouse RAD52 reduces homologous recombination but not resistance to ionizing radiation. *Mol. Cell. Biol.* 18, 6423–6429. doi:10.1128/MCB.18.11.6423.
- Rizzo, A. A., Salerno, P. E., Bezsonova, I., and Korzhnev, D. M. (2014). NMR structure of the human Rad18 zinc finger in complex with ubiquitin defines a class of UBZ domains in proteins linked to the DNA damage response. *Biochemistry* 53, 5895–5906. doi:10.1021/bi500823h.
- Rogakou, E. P., Boon, C., Redon, C., and Bonner, W. M. (1999). Megabase chromatin domains involved in DNA double-strand breaks in vivo. *J. Cell Biol.* 146, 905–916. doi:10.1083/jcb.146.5.905.
- Rogakou, E. P., Pilch, D. R., Orr, A. H., Ivanova, V. S., and Bonner, W. M. (1998). DNA double-stranded breaks induce histone H2AX phosphorylation on serine 139. *J. Biol. Chem.* 273, 5858–5868. doi:10.1074/jbc.273.10.5858.
- Rona, G., Roberti, D., Yin, Y., Pagan, J. K., Homer, H., Sassani, E., Zeke, A., Busino, L., Rothenberg, E., and Pagano, M. (2018). PARP1-dependent recruitment of the FBXL10-RNF68-RNF2 ubiquitin ligase to sites of DNA damage controls H2A.Z loading. *eLife* 7. doi:10.7554/eLife.38771.
- Ruan, S., Zhang, H., Tian, X., Zhang, Z., Huang, H., Shi, C., Liu, W., Jiang, X., Huang, D., and Tao, F. (2020). PHD finger protein 19 enhances the resistance of ovarian cancer cells to compound fufing granule by protecting cell growth, invasion, migration, and stemness. *Front. Pharmacol.* 11, 150. doi:10.3389/fphar.2020.00150.
- Saksouk, N., Simboeck, E., and Déjardin, J. (2015). Constitutive heterochromatin formation and transcription in mammals. *Epigenetics Chromatin* 8, 3. doi:10.1186/1756-8935-8-3.

- Salguero, I., Belotserkovskaya, R., Coates, J., Sczaniecka-Clift, M., Demir, M., Jhujh, S., Wilson, M. D., and Jackson, S. P. (2019). MDC1 PST-repeat region promotes histone H2AX-independent chromatin association and DNA damage tolerance. *Nat. Commun.* 10, 5191. doi:10.1038/s41467-019-12929-5.
- Salifou, K., Burnard, C., Basavarajaiah, P., Grasso, G., Helmsmoortel, M., Mac, V., Depierre, D., Franckhauser, C., Beyne, E., Contreras, X., et al. (2021). Chromatin-associated MRN complex protects highly transcribing genes from genomic instability. *Sci. Adv.* 7. doi:10.1126/sciadv.abb2947.
- Sanchez, A., De Vivo, A., Uprety, N., Kim, J., Stevens, S. M., and Kee, Y. (2016). BMI1-UBR5 axis regulates transcriptional repression at damaged chromatin. *Proc Natl Acad Sci USA* 113, 11243–11248. doi:10.1073/pnas.1610735113.
- Santos, M. A., Huen, M. S. Y., Jankovic, M., Chen, H.-T., López-Contreras, A. J., Klein, I. A., Wong, N., Barbancho, J. L. R., Fernandez-Capetillo, O., Nussenzweig, M. C., et al. (2010). Class switching and meiotic defects in mice lacking the E3 ubiquitin ligase RNF8. *J. Exp. Med.* 207, 973–981. doi:10.1084/jem.20092308.
- Sato, Y., Fujita, H., Yoshikawa, A., Yamashita, M., Yamagata, A., Kaiser, S. E., Iwai, K., and Fukai, S. (2011). Specific recognition of linear ubiquitin chains by the Npl4 zinc finger (NZF) domain of the HOIL-1L subunit of the linear ubiquitin chain assembly complex. *Proc Natl Acad Sci USA* 108, 20520–20525. doi:10.1073/pnas.1109088108.
- Sato, Y., Yoshikawa, A., Mimura, H., Yamashita, M., Yamagata, A., and Fukai, S. (2009). Structural basis for specific recognition of Lys 63-linked polyubiquitin chains by tandem UIMs of RAP80. *EMBO J.* 28, 2461–2468. doi:10.1038/emboj.2009.160.
- Scheuermann, J. C., de Ayala Alonso, A. G., Oktaba, K., Ly-Hartig, N., McGinty, R. K., Fraterman, S., Wilm, M., Muir, T. W., and Müller, J. (2010). Histone H2A deubiquitinase activity of the Polycomb repressive complex PR-DUB. *Nature* 465, 243–247. doi:10.1038/nature08966.
- Schindelin, J., Arganda-Carreras, I., Frise, E., Kaynig, V., Longair, M., Pietzsch, T., Preibisch, S., Rueden, C., Saalfeld, S., Schmid, B., et al. (2012). Fiji: an open-source platform for biological-image analysis. *Nat. Methods* 9, 676–682. doi:10.1038/nmeth.2019.
- Schmidt, C. K., Galanty, Y., Sczaniecka-Clift, M., Coates, J., Jhujh, S., Demir, M., Cornwell, M., Beli, P., and Jackson, S. P. (2015). Systematic E2 screening reveals a UBE2D-RNF138-CtIP axis promoting DNA repair. *Nat. Cell Biol.* 17, 1458–1470. doi:10.1038/ncb3260.
- Schoenfeld, A. R., Apgar, S., Dolios, G., Wang, R., and Aaronson, S. A. (2004). BRCA2 is ubiquitinated in vivo and interacts with USP11, a deubiquitinating enzyme that exhibits prosurvival function in the cellular response to DNA damage. *Mol. Cell. Biol.* 24, 7444–7455. doi:10.1128/MCB.24.17.7444-7455.2004.
- Schrank, B., and Gautier, J. (2019). Assembling nuclear domains: Lessons from DNA repair. *J. Cell Biol.* 218, 2444–2455. doi:10.1083/jcb.201904202.
- Schrank, B. R., Aparicio, T., Li, Y., Chang, W., Chait, B. T., Gundersen, G. G., Gottesman, M. E., and Gautier, J. (2018). Nuclear ARP2/3 drives DNA break clustering for homology-directed repair. *Nature* 559, 61–66. doi:10.1038/s41586-018-0237-5.
- Scully, R., Panday, A., Elango, R., and Willis, N. A. (2019). DNA double-strand break repair-pathway choice in somatic mammalian cells. *Nat. Rev. Mol. Cell Biol.* 20, 698–714. doi:10.1038/s41580-019-0152-0.

- Sedelnikova, O. A., Rogakou, E. P., Panyutin, I. G., and Bonner, W. M. (2002). Quantitative detection of (125)IdU-induced DNA double-strand breaks with gamma-H2AX antibody. *Radiat. Res.* 158, 486–492.
- Seelinger, M., and Otterlei, M. (2020). Helicase-Like Transcription Factor HLTF and E3 Ubiquitin Ligase SHPRH Confer DNA Damage Tolerance through Direct Interactions with Proliferating Cell Nuclear Antigen (PCNA). *Int. J. Mol. Sci.* 21. doi:10.3390/ijms21030693.
- Shanbhag, N. M., Rafalska-Metcalf, I. U., Balane-Bolivar, C., Janicki, S. M., and Greenberg, R. A. (2010). ATM-dependent chromatin changes silence transcription in cis to DNA double-strand breaks. *Cell* 141, 970–981. doi:10.1016/j.cell.2010.04.038.
- Shannon, P., Markiel, A., Ozier, O., Baliga, N. S., Wang, J. T., Ramage, D., Amin, N., Schwikowski, B., and Ideker, T. (2003). Cytoscape: a software environment for integrated models of biomolecular interaction networks. *Genome Res.* 13, 2498–2504. doi:10.1101/gr.1239303.
- Sharma, N., Zhu, Q., Wani, G., He, J., Wang, Q., and Wani, A. A. (2014). USP3 counteracts RNF168 via deubiquitinating H2A and γ H2AX at lysine 13 and 15. *Cell Cycle* 13, 106–114. doi:10.4161/cc.26814.
- Sijm, A., Atlasi, Y., van der Knaap, J. A., Wolf van der Meer, J., Chalkley, G. E., Bezstarosti, K., Dekkers, D. H. W., Doff, W. A. S., Ozgur, Z., van IJcken, W. F. J., et al. (2022). USP7 regulates the ncPRC1 Polycomb axis to stimulate genomic H2AK119ub1 deposition uncoupled from H3K27me3. *Sci. Adv.* 8, eabq7598. doi:10.1126/sciadv.abq7598.
- Singatulina, A. S., Hamon, L., Sukhanova, M. V., Desforges, B., Joshi, V., Bouhss, A., Lavrik, O. I., and Pastré, D. (2019). PARP-1 Activation Directs FUS to DNA Damage Sites to Form PARG-Reversible Compartments Enriched in Damaged DNA. *Cell Rep.* 27, 1809-1821.e5. doi:10.1016/j.celrep.2019.04.031.
- Singh, A. N., Oehler, J., Torrecilla, I., Kilgas, S., Li, S., Vaz, B., Guérillon, C., Fielden, J., Hernandez-Carralero, E., Cabrera, E., et al. (2019). The p97-Ataxin 3 complex regulates homeostasis of the DNA damage response E3 ubiquitin ligase RNF8. *EMBO J.* 38, e102361. doi:10.15252/embj.2019102361.
- Singh, N., Zeke, A., and Reményi, A. (2022). Systematic Discovery of FBXW7-Binding Phosphodegrons Highlights Mitogen-Activated Protein Kinases as Important Regulators of Intracellular Protein Levels. *Int. J. Mol. Sci.* 23. doi:10.3390/ijms23063320.
- Slagsvold, T., Aasland, R., Hirano, S., Bache, K. G., Raiborg, C., Trambaiolo, D., Wakatsuki, S., and Stenmark, H. (2005). Eap45 in mammalian ESCRT-II binds ubiquitin via a phosphoinositide-interacting GLUE domain. *J. Biol. Chem.* 280, 19600–19606. doi:10.1074/jbc.M501510200.
- Slupianek, A., Jozwiakowski, S. K., Gurdek, E., and Skorski, T. (2009). BCR/ABL kinase interacts with and phosphorylates the RAD51 paralog, RAD51B. *Leukemia* 23, 2308–2310. doi:10.1038/leu.2009.164.
- Smerdon, M. J. (1991). DNA repair and the role of chromatin structure. *Curr. Opin. Cell Biol.* 3, 422–428. doi:10.1016/0955-0674(91)90069-b.
- Smith, M. J., Bryant, E. E., Joseph, F. J., and Rothstein, R. (2019). DNA damage triggers increased mobility of chromosomes in G1-phase cells. *Mol. Biol. Cell* 30, 2620–2625. doi:10.1091/mbc.E19-08-0469.

- Snead, W. T., and Gladfelter, A. S. (2019). The control centers of biomolecular phase separation: how membrane surfaces, ptms, and active processes regulate condensation. *Mol. Cell* 76, 295–305. doi:10.1016/j.molcel.2019.09.016.
- Snel, B., Lehmann, G., Bork, P., and Huynen, M. A. (2000). STRING: a web-server to retrieve and display the repeatedly occurring neighbourhood of a gene. *Nucleic Acids Res.* 28, 3442–3444. doi:10.1093/nar/28.18.3442.
- Snijder, B., Sacher, R., Rämö, P., Liberali, P., Mench, K., Wolfrum, N., Burleigh, L., Scott, C. C., Verheije, M. H., Mercer, J., et al. (2012). Single-cell analysis of population context advances RNAi screening at multiple levels. *Mol. Syst. Biol.* 8, 579. doi:10.1038/msb.2012.9.
- Sone, K., Piao, L., Nakakido, M., Ueda, K., Jenuwein, T., Nakamura, Y., and Hamamoto, R. (2014). Critical role of lysine 134 methylation on histone H2AX for γ -H2AX production and DNA repair. *Nat. Commun.* 5, 5691. doi:10.1038/ncomms6691.
- Soria, G., Polo, S. E., and Almouzni, G. (2012). Prime, repair, restore: the active role of chromatin in the DNA damage response. *Mol. Cell* 46, 722–734. doi:10.1016/j.molcel.2012.06.002.
- So, C. C., Ramachandran, S., and Martin, A. (2019). E3 Ubiquitin Ligases RNF20 and RNF40 Are Required for Double-Stranded Break (DSB) Repair: Evidence for Monoubiquitination of Histone H2B Lysine 120 as a Novel Axis of DSB Signaling and Repair. *Mol. Cell. Biol.* 39. doi:10.1128/MCB.00488-18.
- Spence, J., Sadis, S., Haas, A. L., and Finley, D. (1995). A ubiquitin mutant with specific defects in DNA repair and multiubiquitination. *Mol. Cell. Biol.* 15, 1265–1273. doi:10.1128/MCB.15.3.1265.
- Starkuviene, V., Kallenberger, S. M., Beil, N., Lisauskas, T., Schumacher, B. S.-S., Bulkescher, R., Wajda, P., Gunkel, M., Beneke, J., and Erfle, H. (2019). High-Density Cell Arrays for Genome-Scale Phenotypic Screening. *SLAS Discov.* 24, 274–283. doi:10.1177/2472555218818757.
- Stewart, G. S., Panier, S., Townsend, K., Al-Hakim, A. K., Kolas, N. K., Miller, E. S., Nakada, S., Ylanko, J., Olivarius, S., Mendez, M., et al. (2009). The RIDDLE syndrome protein mediates a ubiquitin-dependent signaling cascade at sites of DNA damage. *Cell* 136, 420–434. doi:10.1016/j.cell.2008.12.042.
- Stewart, G. S., Stankovic, T., Byrd, P. J., Wechsler, T., Miller, E. S., Huissoon, A., Drayson, M. T., West, S. C., Elledge, S. J., and Taylor, A. M. R. (2007). RIDDLE immunodeficiency syndrome is linked to defects in 53BP1-mediated DNA damage signaling. *Proc Natl Acad Sci USA* 104, 16910–16915. doi:10.1073/pnas.0708408104.
- Stiff, T., O'Driscoll, M., Rief, N., Iwabuchi, K., Löbrich, M., and Jeggo, P. A. (2004). ATM and DNA-PK function redundantly to phosphorylate H2AX after exposure to ionizing radiation. *Cancer Res.* 64, 2390–2396. doi:10.1158/0008-5472.can-03-3207.
- Stock, J. K., Giadrossi, S., Casanova, M., Brookes, E., Vidal, M., Koseki, H., Brockdorff, N., Fisher, A. G., and Pombo, A. (2007). Ring1-mediated ubiquitination of H2A restrains poised RNA polymerase II at bivalent genes in mouse ES cells. *Nat. Cell Biol.* 9, 1428–1435. doi:10.1038/ncb1663.
- Stucki, M., Clapperton, J. A., Mohammad, D., Yaffe, M. B., Smerdon, S. J., and Jackson, S. P. (2005). MDC1 directly binds phosphorylated histone H2AX to regulate cellular responses to DNA double-strand breaks. *Cell* 123, 1213–1226. doi:10.1016/j.cell.2005.09.038.

- Sullivan, K. D., Galbraith, M. D., Andrysiak, Z., and Espinosa, J. M. (2018). Mechanisms of transcriptional regulation by p53. *Cell Death Differ.* 25, 133–143. doi:10.1038/cdd.2017.174.
- Sun, Y., Jiang, X., Chen, S., Fernandes, N., and Price, B. D. (2005). A role for the Tip60 histone acetyltransferase in the acetylation and activation of ATM. *Proc Natl Acad Sci USA* 102, 13182–13187. doi:10.1073/pnas.0504211102.
- Sun, Y., Jiang, X., Xu, Y., Ayrapetov, M. K., Moreau, L. A., Whetstine, J. R., and Price, B. D. (2009). Histone H3 methylation links DNA damage detection to activation of the tumour suppressor Tip60. *Nat. Cell Biol.* 11, 1376–1382. doi:10.1038/ncb1982.
- Sutherland, B. M., Bennett, P. V., Schenk, H., Sidorkina, O., Laval, J., Trunk, J., Monteleone, D., and Sutherland, J. (2001). Clustered DNA damages induced by high and low LET radiation, including heavy ions. *Phys. Med.* 17 Suppl 1, 202–204.
- Swaney, D. L., Beltrao, P., Starita, L., Guo, A., Rush, J., Fields, S., Krogan, N. J., and Villén, J. (2013). Global analysis of phosphorylation and ubiquitylation cross-talk in protein degradation. *Nat. Methods* 10, 676–682. doi:10.1038/nmeth.2519.
- Swift, M. L., and Azizkhan-Clifford, J. (2022). DNA damage-induced sumoylation of Sp1 induces its interaction with RNF4 and degradation in S phase to remove 53BP1 from DSBs and permit HR. *DNA Repair (Amst)* 111, 103289. doi:10.1016/j.dnarep.2022.103289.
- Szklarczyk, D., Kirsch, R., Koutrouli, M., Nastou, K., Mehryary, F., Hachilif, R., Gable, A. L., Fang, T., Doncheva, N. T., Pyysalo, S., et al. (2023). The STRING database in 2023: protein-protein association networks and functional enrichment analyses for any sequenced genome of interest. *Nucleic Acids Res.* 51, D638–D646. doi:10.1093/nar/gkac1000.
- Takahashi, T. S., Hirade, Y., Toma, A., Sato, Y., Yamagata, A., Goto-Ito, S., Tomita, A., Nakada, S., and Fukai, S. (2018). Structural insights into two distinct binding modules for Lys63-linked polyubiquitin chains in RNF168. *Nat. Commun.* 9, 170. doi:10.1038/s41467-017-02345-y.
- Takata, H., Hanafusa, T., Mori, T., Shimura, M., Iida, Y., Ishikawa, K., Yoshikawa, K., Yoshikawa, Y., and Maeshima, K. (2013). Chromatin compaction protects genomic DNA from radiation damage. *PLoS ONE* 8, e75622. doi:10.1371/journal.pone.0075622.
- Tallis, M., Morra, R., Barkauskaite, E., and Ahel, I. (2014). Poly(ADP-ribosyl)ation in regulation of chromatin structure and the DNA damage response. *Chromosoma* 123, 79–90. doi:10.1007/s00412-013-0442-9.
- Tang, J., Cho, N. W., Cui, G., Manion, E. M., Shanbhag, N. M., Botuyan, M. V., Mer, G., and Greenberg, R. A. (2013). Acetylation limits 53BP1 association with damaged chromatin to promote homologous recombination. *Nat. Struct. Mol. Biol.* 20, 317–325. doi:10.1038/nsmb.2499.
- Tang, L.-Y., Thomas, A., Zhou, M., and Zhang, Y. E. (2020). Phosphorylation of SMURF2 by ATM exerts a negative feedback control of DNA damage response. *J. Biol. Chem.* 295, 18485–18493. doi:10.1074/jbc.RA120.014179.
- Tan, W., and Deans, A. J. (2017). A defined role for multiple Fanconi anemia gene products in DNA-damage-associated ubiquitination. *Exp. Hematol.* 50, 27–32. doi:10.1016/j.exphem.2017.03.001.

- Tan, W., van Twest, S., Leis, A., Bythell-Douglas, R., Murphy, V. J., Sharp, M., Parker, M. W., Crismani, W., and Deans, A. J. (2020). Monoubiquitination by the human Fanconi anemia core complex clamps FANCI:FANCD2 on DNA in filamentous arrays. *eLife* 9. doi:10.7554/eLife.54128.
- Teicher, B. A., Ara, G., Herbst, R., Palombella, V. J., and Adams, J. (1999). The proteasome inhibitor PS-341 in cancer therapy. *Clin. Cancer Res.* 5, 2638–2645.
- Thorslund, T., Ripplinger, A., Hoffmann, S., Wild, T., Uckelmann, M., Villumsen, B., Narita, T., Sixma, T. K., Choudhary, C., Bekker-Jensen, S., et al. (2015). Histone H1 couples initiation and amplification of ubiquitin signalling after DNA damage. *Nature* 527, 389–393. doi:10.1038/nature15401.
- Tian, M., Zeng, T., Liu, M., Han, S., Lin, H., Lin, Q., Li, L., Jiang, T., Li, G., Lin, H., et al. (2019). A cell-based high-throughput screening method based on a ubiquitin-reference technique for identifying modulators of E3 ligases. *J. Biol. Chem.* 294, 2880–2891. doi:10.1074/jbc.RA118.003822.
- Tjeertes, J. V., Miller, K. M., and Jackson, S. P. (2009). Screen for DNA-damage-responsive histone modifications identifies H3K9Ac and H3K56Ac in human cells. *EMBO J.* 28, 1878–1889. doi:10.1038/emboj.2009.119.
- Toiber, D., Erdel, F., Bouazoune, K., Silberman, D. M., Zhong, L., Mulligan, P., Sebastian, C., Cosentino, C., Martinez-Pastor, B., Giacosa, S., et al. (2013). SIRT6 recruits SNF2H to DNA break sites, preventing genomic instability through chromatin remodeling. *Mol. Cell* 51, 454–468. doi:10.1016/j.molcel.2013.06.018.
- Toma, A., Takahashi, T. S., Sato, Y., Yamagata, A., Goto-Ito, S., Nakada, S., Fukuto, A., Horikoshi, Y., Tashiro, S., and Fukai, S. (2015). Structural basis for ubiquitin recognition by ubiquitin-binding zinc finger of FAAP20. *PLoS ONE* 10, e0120887. doi:10.1371/journal.pone.0120887.
- Tomimatsu, N., Mukherjee, B., Catherine Hardebeck, M., Ilcheva, M., Vanessa Camacho, C., Louise Harris, J., Porteus, M., Llorente, B., Khanna, K. K., and Burma, S. (2014). Phosphorylation of EXO1 by CDKs 1 and 2 regulates DNA end resection and repair pathway choice. *Nat. Commun.* 5, 3561. doi:10.1038/ncomms4561.
- Tong, S., Si, Y., Yu, H., Zhang, L., Xie, P., and Jiang, W. (2017). MLN4924 (Pevonedistat), a protein neddylation inhibitor, suppresses proliferation and migration of human clear cell renal cell carcinoma. *Sci. Rep.* 7, 5599. doi:10.1038/s41598-017-06098-y.
- Tsouroula, K., Furst, A., Rogier, M., Heyer, V., Maglott-Roth, A., Ferrand, A., Reina-San-Martin, B., and Soutoglou, E. (2016). Temporal and Spatial Uncoupling of DNA Double Strand Break Repair Pathways within Mammalian Heterochromatin. *Mol. Cell* 63, 293–305. doi:10.1016/j.molcel.2016.06.002.
- Typas, D., Luijsterburg, M. S., Wiegant, W. W., Diakatou, M., Helfricht, A., Thijssen, P. E., van den Broek, B., Mullenders, L. H., and van Attikum, H. (2015). The de-ubiquitylating enzymes USP26 and USP37 regulate homologous recombination by counteracting RAP80. *Nucleic Acids Res.* 43, 6919–6933. doi:10.1093/nar/gkv613.
- Uckelmann, M., Densham, R. M., Baas, R., Winterwerp, H. H. K., Fish, A., Sixma, T. K., and Morris, J. R. (2018). USP48 restrains resection by site-specific cleavage of the BRCA1 ubiquitin mark from H2A. *Nat. Commun.* 9, 229. doi:10.1038/s41467-017-02653-3.

- Ui, A., Nagaura, Y., and Yasui, A. (2015). Transcriptional elongation factor ENL phosphorylated by ATM recruits polycomb and switches off transcription for DSB repair. *Mol. Cell* 58, 468–482. doi:10.1016/j.molcel.2015.03.023.
- Uziel, T., Lerenthal, Y., Moyal, L., Andegeko, Y., Mittelman, L., and Shiloh, Y. (2003). Requirement of the MRN complex for ATM activation by DNA damage. *EMBO J.* 22, 5612–5621. doi:10.1093/emboj/cdg541.
- Vassilev, L. T., Vu, B. T., Graves, B., Carvajal, D., Podlaski, F., Filipovic, Z., Kong, N., Kammlott, U., Lukacs, C., Klein, C., et al. (2004). In vivo activation of the p53 pathway by small-molecule antagonists of MDM2. *Science* 303, 844–848. doi:10.1126/science.1092472.
- Vazquez, B. N., Thackray, J. K., Simonet, N. G., Kane-Goldsmith, N., Martinez-Redondo, P., Nguyen, T., Bunting, S., Vaquero, A., Tischfield, J. A., and Serrano, L. (2016). SIRT7 promotes genome integrity and modulates non-homologous end joining DNA repair. *EMBO J.* 35, 1488–1503. doi:10.15252/embj.201593499.
- Vizán, P., Gutiérrez, A., Espejo, I., García-Montolio, M., Lange, M., Carretero, A., Lafzi, A., de Andrés-Aguayo, L., Blanco, E., Thambyrajah, R., et al. (2020). The Polycomb-associated factor PHF19 controls hematopoietic stem cell state and differentiation. *Sci. Adv.* 6, eabb2745. doi:10.1126/sciadv.abb2745.
- Vyas, R., Kumar, R., Clermont, F., Helfricht, A., Kalev, P., Sotiropoulou, P., Hendriks, I. A., Radaelli, E., Hochepped, T., Blanpain, C., et al. (2013). RNF4 is required for DNA double-strand break repair in vivo. *Cell Death Differ.* 20, 490–502. doi:10.1038/cdd.2012.145.
- Wagner, S. A., Beli, P., Weinert, B. T., Nielsen, M. L., Cox, J., Mann, M., and Choudhary, C. (2011). A proteome-wide, quantitative survey of in vivo ubiquitylation sites reveals widespread regulatory roles. *Mol. Cell. Proteomics* 10, M111.013284. doi:10.1074/mcp.M111.013284.
- Wakeman, T. P., Wang, Q., Feng, J., and Wang, X.-F. (2012). Bat3 facilitates H3K79 dimethylation by DOT1L and promotes DNA damage-induced 53BP1 foci at G1/G2 cell-cycle phases. *EMBO J.* 31, 2169–2181. doi:10.1038/emboj.2012.50.
- Walser, F., Mulder, M. P. C., Bragantini, B., Burger, S., Gubser, T., Gatti, M., Botuyan, M. V., Villa, A., Altmeyer, M., Neri, D., et al. (2020). Ubiquitin phosphorylation at thr12 modulates the DNA damage response. *Mol. Cell* 80, 423-436.e9. doi:10.1016/j.molcel.2020.09.017.
- Walsh, J. G., Cullen, S. P., Sheridan, C., Lüthi, A. U., Gerner, C., and Martin, S. J. (2008). Executioner caspase-3 and caspase-7 are functionally distinct proteases. *Proc Natl Acad Sci USA* 105, 12815–12819. doi:10.1073/pnas.0707715105.
- Wang, H., Wang, L., Erdjument-Bromage, H., Vidal, M., Tempst, P., Jones, R. S., and Zhang, Y. (2004a). Role of histone H2A ubiquitination in Polycomb silencing. *Nature* 431, 873–878. doi:10.1038/nature02985.
- Wang, H., Xu, P., Sun, G., Lv, J., Cao, J., and Xu, Z. (2020). Downregulation of PHF19 inhibits cell growth and migration in gastric cancer. *Scand. J. Gastroenterol.* 55, 687–693. doi:10.1080/00365521.2020.1766555.
- Wang, H., Zhai, L., Xu, J., Joo, H.-Y., Jackson, S., Erdjument-Bromage, H., Tempst, P., Xiong, Y., and Zhang, Y. (2006). Histone H3 and H4 ubiquitylation by the CUL4-DDB-ROC1 ubiquitin ligase facilitates cellular response to DNA damage. *Mol. Cell* 22, 383–394. doi:10.1016/j.molcel.2006.03.035.

- Wang, J., Aroumougame, A., Loblrich, M., Li, Y., Chen, D., Chen, J., and Gong, Z. (2014a). PTIP associates with Artemis to dictate DNA repair pathway choice. *Genes Dev.* 28, 2693–2698. doi:10.1101/gad.252478.114.
- Wang, L., Gao, Y., Zheng, X., Liu, C., Dong, S., Li, R., Zhang, G., Wei, Y., Qu, H., Li, Y., et al. (2019). Histone modifications regulate chromatin compartmentalization by contributing to a phase separation mechanism. *Mol. Cell* 76, 646–659.e6. doi:10.1016/j.molcel.2019.08.019.
- Wang, Q., Goh, A. M., Howley, P. M., and Walters, K. J. (2003). Ubiquitin recognition by the DNA repair protein hHR23a. *Biochemistry* 42, 13529–13535. doi:10.1021/bi035391j.
- Wang, S., Robertson, G. P., and Zhu, J. (2004b). A novel human homologue of Drosophila polycomblike gene is up-regulated in multiple cancers. *Gene* 343, 69–78. doi:10.1016/j.gene.2004.09.006.
- Wang, T., Liu, N. S., Seet, L.-F., and Hong, W. (2010). The emerging role of VHS domain-containing Tom1, Tom1L1 and Tom1L2 in membrane trafficking. *Traffic* 11, 1119–1128. doi:10.1111/j.1600-0854.2010.01098.x.
- Wang, W. (2007). Emergence of a DNA-damage response network consisting of Fanconi anaemia and BRCA proteins. *Nat. Rev. Genet.* 8, 735–748. doi:10.1038/nrg2159.
- Wang, X., D’Arcy, P., Caulfield, T. R., Paulus, A., Chitta, K., Mohanty, C., Gullbo, J., Chanan-Khan, A., and Linder, S. (2015). Synthesis and evaluation of derivatives of the proteasome deubiquitinase inhibitor b-AP15. *Chem. Biol. Drug Des.* 86, 1036–1048. doi:10.1111/cbdd.12571.
- Wang, X., Lu, G., Li, L., Yi, J., Yan, K., Wang, Y., Zhu, B., Kuang, J., Lin, M., Zhang, S., et al. (2014b). HUWE1 interacts with BRCA1 and promotes its degradation in the ubiquitin-proteasome pathway. *Biochem. Biophys. Res. Commun.* 444, 549–554. doi:10.1016/j.bbrc.2014.01.075.
- Wang, Z., Zhang, H., Liu, J., Cheruiyot, A., Lee, J.-H., Ordog, T., Lou, Z., You, Z., and Zhang, Z. (2016). USP51 deubiquitylates H2AK13,15ub and regulates DNA damage response. *Genes Dev.* 30, 946–959. doi:10.1101/gad.271841.115.
- Ward, I. M., and Chen, J. (2001). Histone H2AX is phosphorylated in an ATR-dependent manner in response to replicational stress. *J. Biol. Chem.* 276, 47759–47762. doi:10.1074/jbc.C100569200.
- White, D., Rafalska-Metcalf, I. U., Ivanov, A. V., Corsinotti, A., Peng, H., Lee, S.-C., Trono, D., Janicki, S. M., and Rauscher, F. J. (2012). The ATM substrate KAP1 controls DNA repair in heterochromatin: regulation by HP1 proteins and serine 473/824 phosphorylation. *Mol. Cancer Res.* 10, 401–414. doi:10.1158/1541-7786.MCR-11-0134.
- van Wijk, S. J. L., Fiskin, E., Putyrski, M., Pampaloni, F., Hou, J., Wild, P., Kensche, T., Grecco, H. E., Bastiaens, P., and Dikic, I. (2012). Fluorescence-based sensors to monitor localization and functions of linear and K63-linked ubiquitin chains in cells. *Mol. Cell* 47, 797–809. doi:10.1016/j.molcel.2012.06.017.
- Wijnhoven, P., Konietzny, R., Blackford, A. N., Travers, J., Kessler, B. M., Nishi, R., and Jackson, S. P. (2015). USP4 Auto-Deubiquitylation Promotes Homologous Recombination. *Mol. Cell* 60, 362–373. doi:10.1016/j.molcel.2015.09.019.

- Williams, S. P., Barthorpe, A. S., Lightfoot, H., Garnett, M. J., and McDermott, U. (2017). High-throughput RNAi screen for essential genes and drug synergistic combinations in colorectal cancer. *Sci. Data* 4, 170139. doi:10.1038/sdata.2017.139.
- Wojcik, F., Dann, G. P., Beh, L. Y., Debelouchina, G. T., Hofmann, R., and Muir, T. W. (2018). Functional crosstalk between histone H2B ubiquitylation and H2A modifications and variants. *Nat. Commun.* 9, 1394. doi:10.1038/s41467-018-03895-5.
- Wolf, B. B., Schuler, M., Echeverri, F., and Green, D. R. (1999). Caspase-3 is the primary activator of apoptotic DNA fragmentation via DNA fragmentation factor-45/inhibitor of caspase-activated DNase inactivation. *J. Biol. Chem.* 274, 30651–30656. doi:10.1074/jbc.274.43.30651.
- Wu, C.-Y., Kang, H.-Y., Yang, W.-L., Wu, J., Jeong, Y. S., Wang, J., Chan, C.-H., Lee, S.-W., Zhang, X., Lamothe, B., et al. (2011a). Critical role of monoubiquitination of histone H2AX protein in histone H2AX phosphorylation and DNA damage response. *J. Biol. Chem.* 286, 30806–30815. doi:10.1074/jbc.M111.257469.
- Wu, J., Chen, Y., Lu, L.-Y., Wu, Y., Paulsen, M. T., Ljungman, M., Ferguson, D. O., and Yu, X. (2011b). Chfr and RNF8 synergistically regulate ATM activation. *Nat. Struct. Mol. Biol.* 18, 761–768. doi:10.1038/nsmb.2078.
- Wu, X., Johansen, J. V., and Helin, K. (2013). Fbxl10/Kdm2b recruits polycomb repressive complex 1 to CpG islands and regulates H2A ubiquitylation. *Mol. Cell* 49, 1134–1146. doi:10.1016/j.molcel.2013.01.016.
- Wu, X., Liu, S., Sagum, C., Chen, J., Singh, R., Chaturvedi, A., Horton, J. R., Kashyap, T. R., Fushman, D., Cheng, X., et al. (2019). Crosstalk between Lys63- and Lys11-polyubiquitin signaling at DNA damage sites is driven by Cezanne. *Genes Dev.* 33, 1702–1717. doi:10.1101/gad.332395.119.
- Xiaoyun, S., Yuyuan, Z., Jie, X., Yingjie, N., Qing, X., Yuezhen, D., and Haiguang, X. (2021). PHF19 activates hedgehog signaling and promotes tumorigenesis in hepatocellular carcinoma. *Exp. Cell Res.* 406, 112690. doi:10.1016/j.yexcr.2021.112690.
- Xiao, A., Li, H., Shechter, D., Ahn, S. H., Fabrizio, L. A., Erdjument-Bromage, H., Ishibe-Murakami, S., Wang, B., Tempst, P., Hofmann, K., et al. (2009). WSTF regulates the H2A.X DNA damage response via a novel tyrosine kinase activity. *Nature* 457, 57–62. doi:10.1038/nature07668.
- Xiao, D., Yue, M., Su, H., Ren, P., Jiang, J., Li, F., Hu, Y., Du, H., Liu, H., and Qing, G. (2016). Polo-like Kinase-1 Regulates Myc Stabilization and Activates a Feedforward Circuit Promoting Tumor Cell Survival. *Mol. Cell* 64, 493–506. doi:10.1016/j.molcel.2016.09.016.
- Xu, C., Bian, C., Yang, W., Galka, M., Ouyang, H., Chen, C., Qiu, W., Liu, H., Jones, A. E., MacKenzie, F., et al. (2010a). Binding of different histone marks differentially regulates the activity and specificity of polycomb repressive complex 2 (PRC2). *Proc Natl Acad Sci USA* 107, 19266–19271. doi:10.1073/pnas.1008937107.
- Xu, G., Chapman, J. R., Brandsma, I., Yuan, J., Mistrik, M., Bouwman, P., Bartkova, J., Gogola, E., Warmerdam, D., Barazas, M., et al. (2015a). REV7 counteracts DNA double-strand break resection and affects PARP inhibition. *Nature* 521, 541–544. doi:10.1038/nature14328.
- Xu, H., Hu, Y.-W., Zhao, J.-Y., Hu, X.-M., Li, S.-F., Wang, Y.-C., Gao, J.-J., Sha, Y.-H., Kang, C.-M., Lin, L., et al. (2015b). MicroRNA-195-5p acts as an anti-oncogene by targeting PHF19 in hepatocellular carcinoma. *Oncol. Rep.* 34, 175–182. doi:10.3892/or.2015.3957.

- Xu, Y., Sun, Y., Jiang, X., Ayrapetov, M. K., Moskwa, P., Yang, S., Weinstock, D. M., and Price, B. D. (2010b). The p400 ATPase regulates nucleosome stability and chromatin ubiquitination during DNA repair. *J. Cell Biol.* 191, 31–43. doi:10.1083/jcb.201001160.
- Yang, Y., Ding, Y., Zhou, C., Wen, Y., and Zhang, N. (2019). Structural and functional studies of USP20 ZnF-UBP domain by NMR. *Protein Sci.* 28, 1606–1619. doi:10.1002/pro.3675.
- Yan, J., Kim, Y.-S., Yang, X.-P., Li, L.-P., Liao, G., Xia, F., and Jetten, A. M. (2007). The ubiquitin-interacting motif containing protein RAP80 interacts with BRCA1 and functions in DNA damage repair response. *Cancer Res.* 67, 6647–6656. doi:10.1158/0008-5472.CAN-07-0924.
- Yan, Q., Dutt, S., Xu, R., Graves, K., Juszczynski, P., Manis, J. P., and Shipp, M. A. (2009). BBAP monoubiquitylates histone H4 at lysine 91 and selectively modulates the DNA damage response. *Mol. Cell* 36, 110–120. doi:10.1016/j.molcel.2009.08.019.
- Yan, Q., Xu, R., Zhu, L., Cheng, X., Wang, Z., Manis, J., and Shipp, M. A. (2013). BAL1 and its partner E3 ligase, BBAP, link Poly(ADP-ribose) activation, ubiquitylation, and double-strand DNA repair independent of ATM, MDC1, and RNF8. *Mol. Cell Biol.* 33, 845–857. doi:10.1128/MCB.00990-12.
- Yang, C.-S., Jividen, K., Spencer, A., Dworak, N., Ni, L., Oostdyk, L. T., Chatterjee, M., Kuśmider, B., Reon, B., Parlak, M., et al. (2017). Ubiquitin Modification by the E3 Ligase/ADP-Ribosyltransferase Dtx3L/Parp9. *Mol. Cell* 66, 503-516.e5. doi:10.1016/j.molcel.2017.04.028.
- Yang, K., Moldovan, G.-L., and D'Andrea, A. D. (2010). RAD18-dependent recruitment of SNM1A to DNA repair complexes by a ubiquitin-binding zinc finger. *J. Biol. Chem.* 285, 19085–19091. doi:10.1074/jbc.M109.100032.
- Yilmaz, D., Furst, A., Meaburn, K., Lezaja, A., Wen, Y., Altmeyer, M., Reina-San-Martin, B., and Soutoglou, E. (2021). Activation of homologous recombination in G1 preserves centromeric integrity. *Nature* 600, 748–753. doi:10.1038/s41586-021-04200-z.
- Yin, Y., Seifert, A., Chua, J. S., Maure, J.-F., Golebiowski, F., and Hay, R. T. (2012). SUMO-targeted ubiquitin E3 ligase RNF4 is required for the response of human cells to DNA damage. *Genes Dev.* 26, 1196–1208. doi:10.1101/gad.189274.112.
- Yi, J., Lu, G., Li, L., Wang, X., Cao, L., Lin, M., Zhang, S., and Shao, G. (2015). DNA damage-induced activation of CUL4B targets HUWE1 for proteasomal degradation. *Nucleic Acids Res.* 43, 4579–4590. doi:10.1093/nar/gkv325.
- Yoshikawa, Y., Mori, T., Magome, N., Hibino, K., and Yoshikawa, K. (2008). DNA compaction plays a key role in radioprotection against double-strand breaks as revealed by single-molecule observation. *Chem. Phys. Lett.* 456, 80–83. doi:10.1016/j.cplett.2008.03.009.
- Young, L. C., McDonald, D. W., and Hendzel, M. J. (2013). Kdm4b histone demethylase is a DNA damage response protein and confers a survival advantage following γ -irradiation. *J. Biol. Chem.* 288, 21376–21388. doi:10.1074/jbc.M113.491514.
- Yu, M., Liu, K., Mao, Z., Luo, J., Gu, W., and Zhao, W. (2016). USP11 Is a Negative Regulator to γ H2AX Ubiquitylation by RNF8/RNF168. *J. Biol. Chem.* 291, 959–967. doi:10.1074/jbc.M114.624478.
- Zar, J. H. (1999). *Biostatistical analysis*. Prentice Hall.

- Zhang, H., Liu, H., Chen, Y., Yang, X., Wang, P., Liu, T., Deng, M., Qin, B., Correia, C., Lee, S., et al. (2016a). A cell cycle-dependent BRCA1-UHRF1 cascade regulates DNA double-strand break repair pathway choice. *Nat. Commun.* 7, 10201. doi:10.1038/ncomms10201.
- Zhang, Q., Karnak, D., Tan, M., Lawrence, T. S., Morgan, M. A., and Sun, Y. (2016b). FBXW7 Facilitates Nonhomologous End-Joining via K63-Linked Polyubiquitylation of XRCC4. *Mol. Cell* 61, 419–433. doi:10.1016/j.molcel.2015.12.010.
- Zhang, Q., Mady, A. S. A., Ma, Y., Ryan, C., Lawrence, T. S., Nikolovska-Coleska, Z., Sun, Y., and Morgan, M. A. (2019). The WD40 domain of FBXW7 is a poly(ADP-ribose)-binding domain that mediates the early DNA damage response. *Nucleic Acids Res.* 47, 4039–4053. doi:10.1093/nar/gkz058.
- Zhang, X., Chen, J., Wu, M., Wu, H., Arokiaraj, A. W., Wang, C., Zhang, W., Tao, Y., Huen, M. S. Y., and Zang, J. (2013). Structural basis for role of ring finger protein RNF168 RING domain. *Cell Cycle* 12, 312–321. doi:10.4161/cc.23104.
- Zhao, W., Steinfeld, J. B., Liang, F., Chen, X., Maranon, D. G., Jian Ma, C., Kwon, Y., Rao, T., Wang, W., Sheng, C., et al. (2017). BRCA1-BARD1 promotes RAD51-mediated homologous DNA pairing. *Nature* 550, 360–365. doi:10.1038/nature24060.
- Zhao, Y., Morgan, M. A., and Sun, Y. (2014). Targeting Neddylation pathways to inactivate cullin-RING ligases for anticancer therapy. *Antioxid. Redox Signal.* 21, 2383–2400. doi:10.1089/ars.2013.5795.
- Zheng, Q., Huang, T., Zhang, L., Zhou, Y., Luo, H., Xu, H., and Wang, X. (2016). Dysregulation of Ubiquitin-Proteasome System in Neurodegenerative Diseases. *Front. Aging Neurosci.* 8, 303. doi:10.3389/fnagi.2016.00303.
- Zheng, S., Li, D., Lu, Z., Liu, G., Wang, M., Xing, P., Wang, M., Dong, Y., Wang, X., Li, J., et al. (2018). Bre1-dependent H2B ubiquitination promotes homologous recombination by stimulating histone eviction at DNA breaks. *Nucleic Acids Res.* 46, 11326–11339. doi:10.1093/nar/gky918.
- Zhou, Y., Zhou, B., Pache, L., Chang, M., Khodabakhshi, A. H., Tanaseichuk, O., Benner, C., and Chanda, S. K. (2019). Metascape provides a biologist-oriented resource for the analysis of systems-level datasets. *Nat. Commun.* 10, 1523. doi:10.1038/s41467-019-09234-6.
- Zhu, Q., Huang, J., Huang, H., Li, H., Yi, P., Kloeber, J. A., Yuan, J., Chen, Y., Deng, M., Luo, K., et al. (2021). RNF19A-mediated ubiquitination of BARD1 prevents BRCA1/BARD1-dependent homologous recombination. *Nat. Commun.* 12, 6653. doi:10.1038/s41467-021-27048-3.

7. Annex

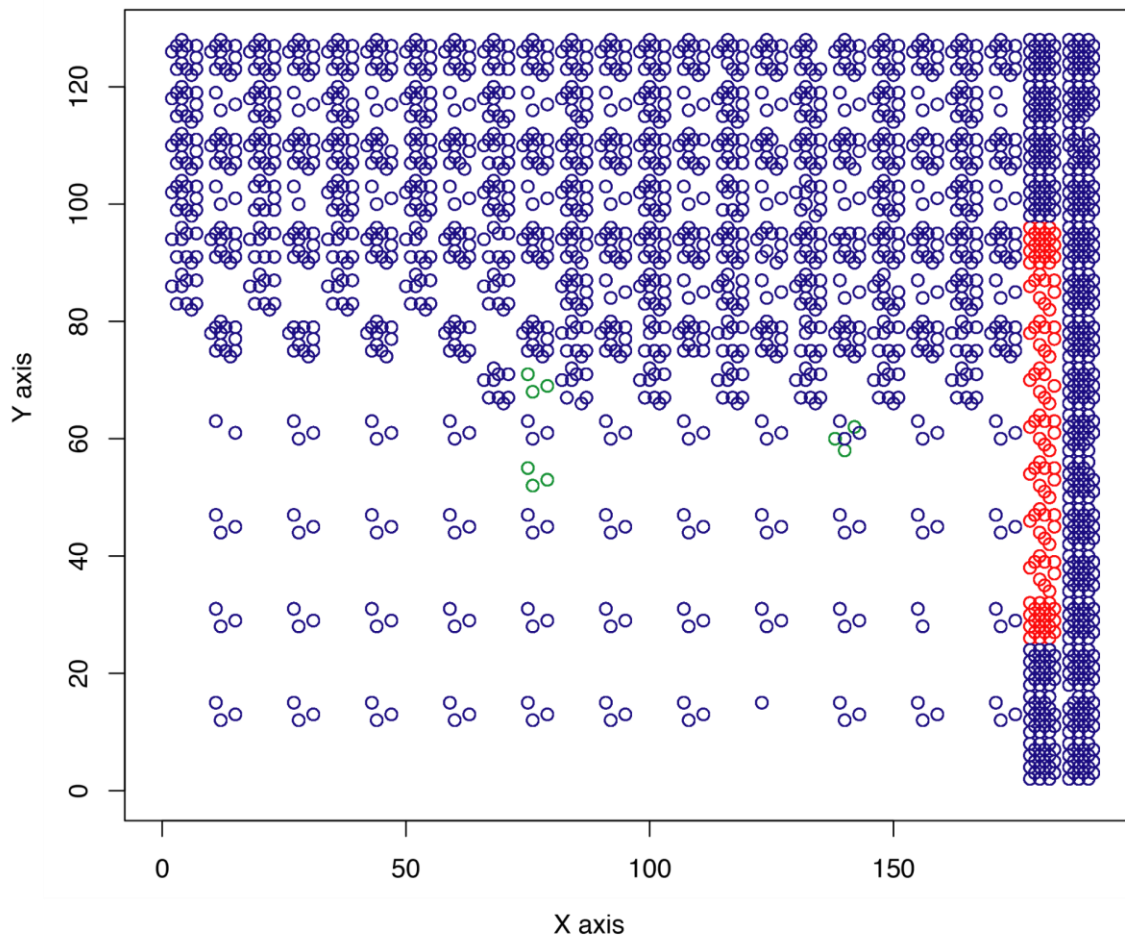
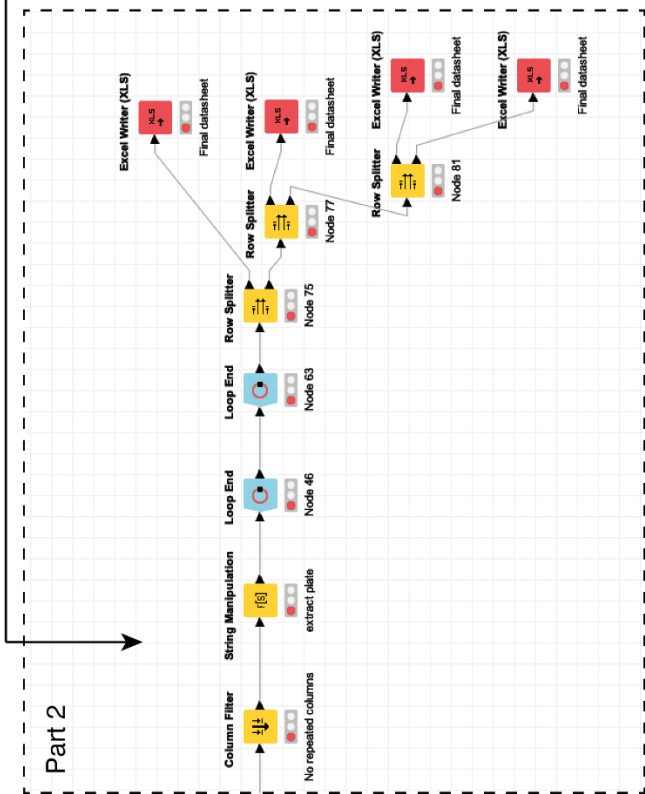
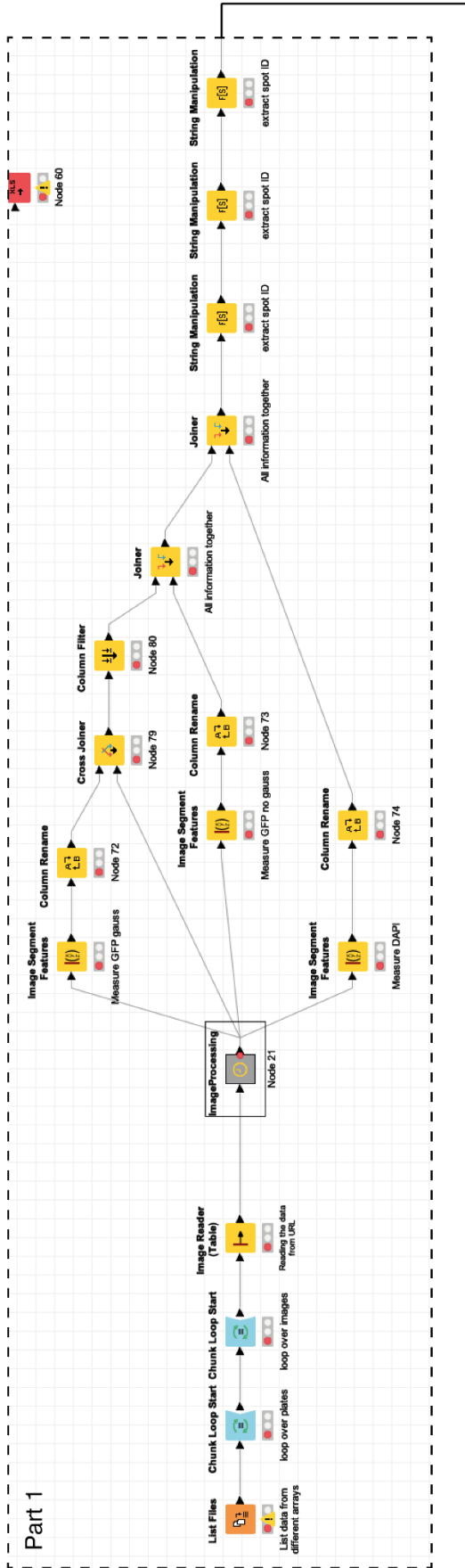


Figure 7.1. The layout of the negative controls on an array. Each circle represents a spot, where only negative controls are shown. Blue circles - non-siRNA treated spots, red - spots containing non-coding siRNA control (NCscr1), green - the spots containing only transfection reagent. X axis and Y axis represent index number of the spots on an array.

A



B

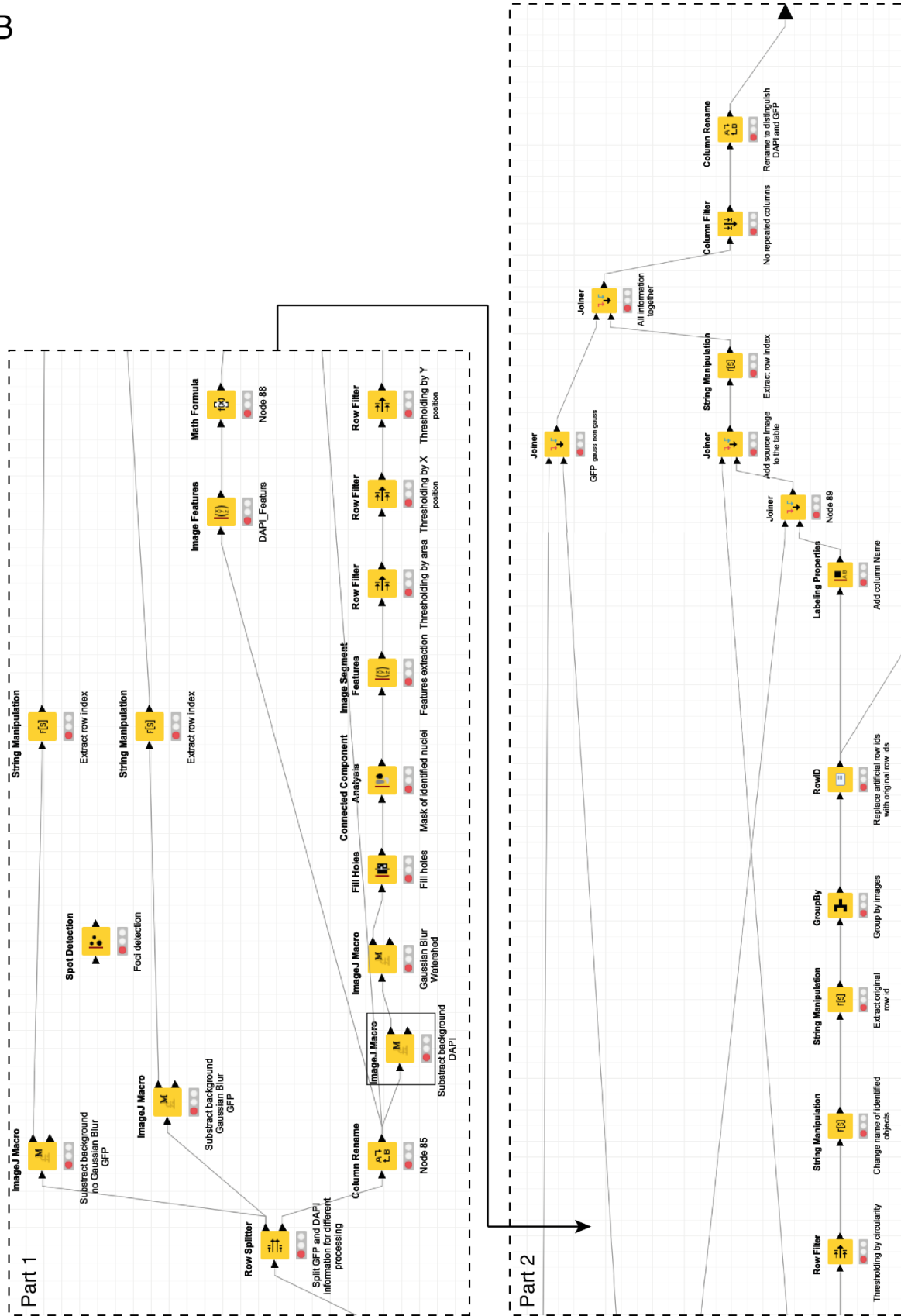
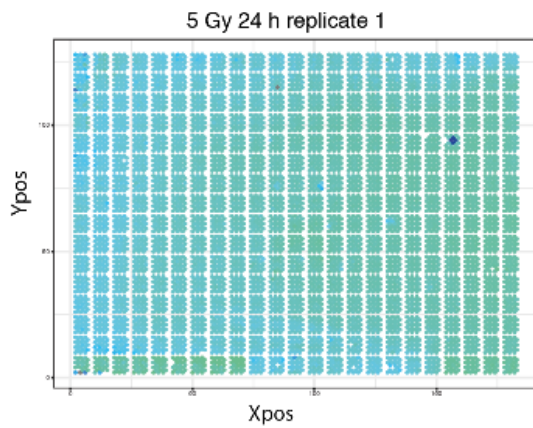
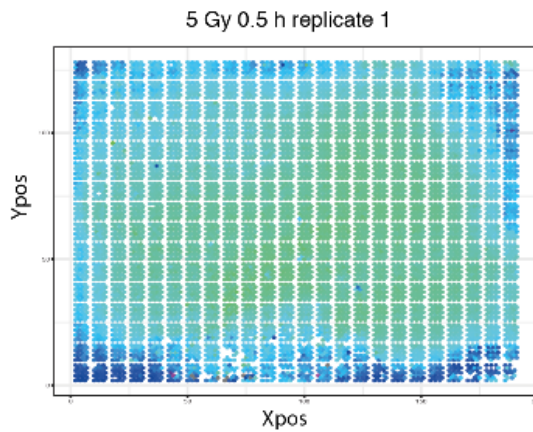
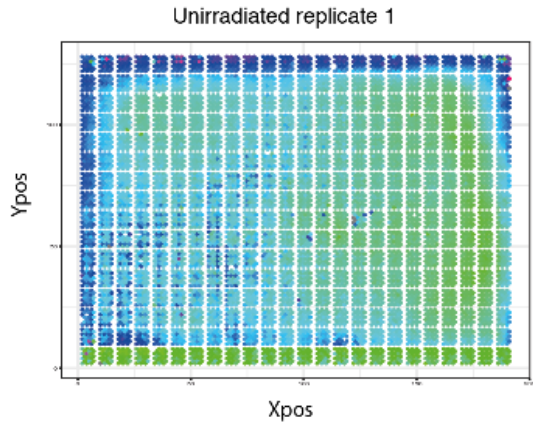
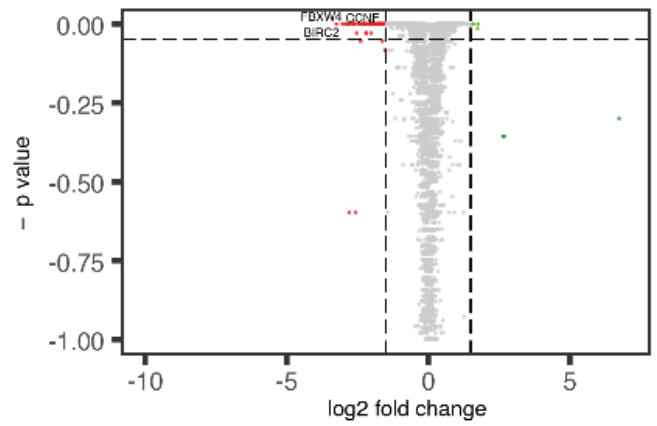
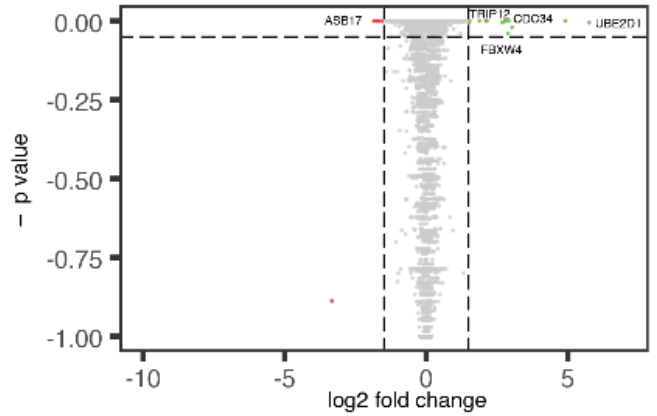
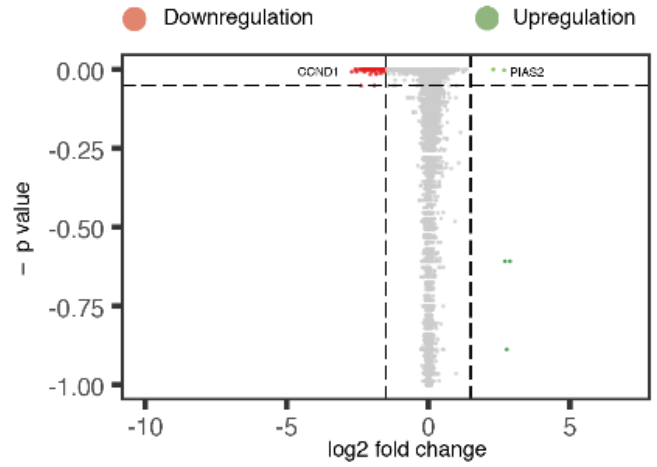
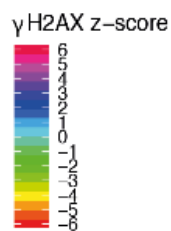


Figure 7.2. The KNIME Analytics image analysis pipeline. (A) Full image analysis workflow applied to the ubiquitinome-wide screening data. (B) Image Processing meta node content from the (A).



Legend



● not significant

Downregulation

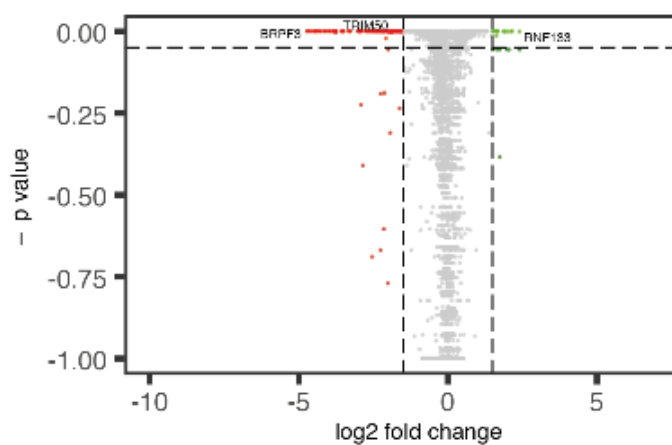
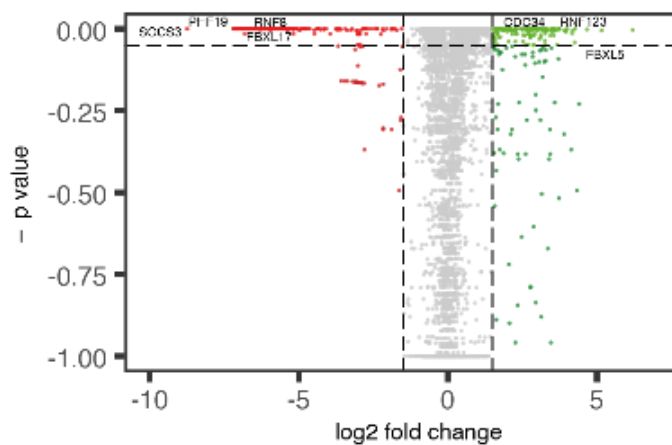
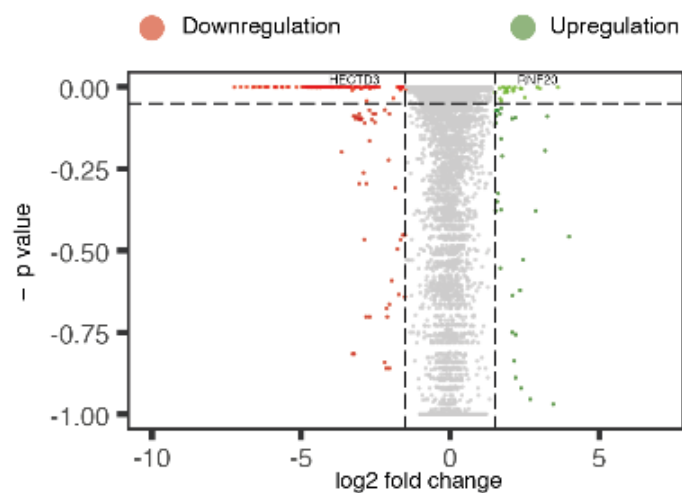
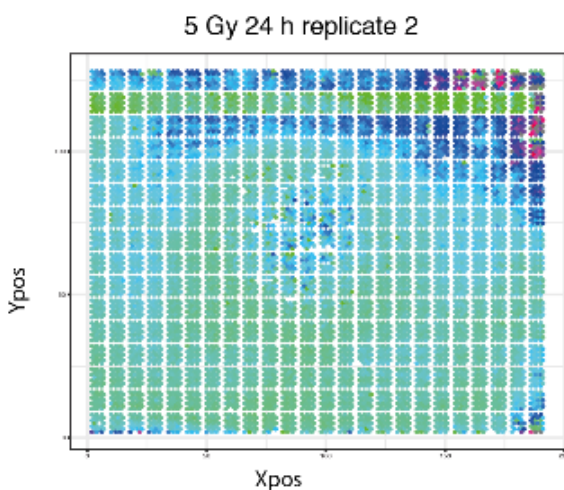
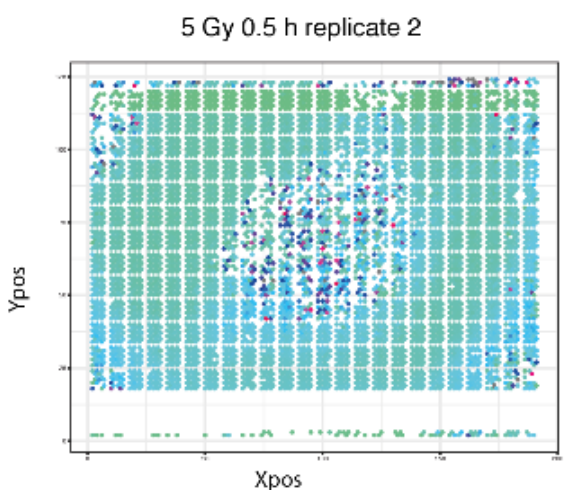
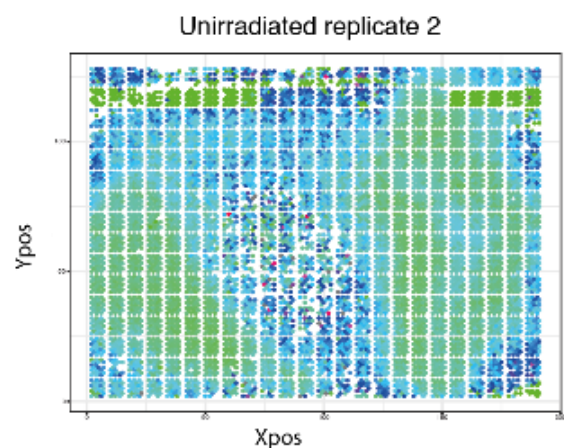
● log2 fold change significant

● both log2 fold change and p value significant

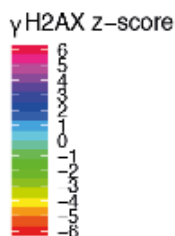
Upregulation

● log2 fold change significant

● both log2 fold change and p value significant



Legend



- not significant
- Downregulation**
 - log2 fold change significant
 - both log2 fold change and p value significant
- Upregulation**
 - log2 fold change significant
 - both log2 fold change and p value significant

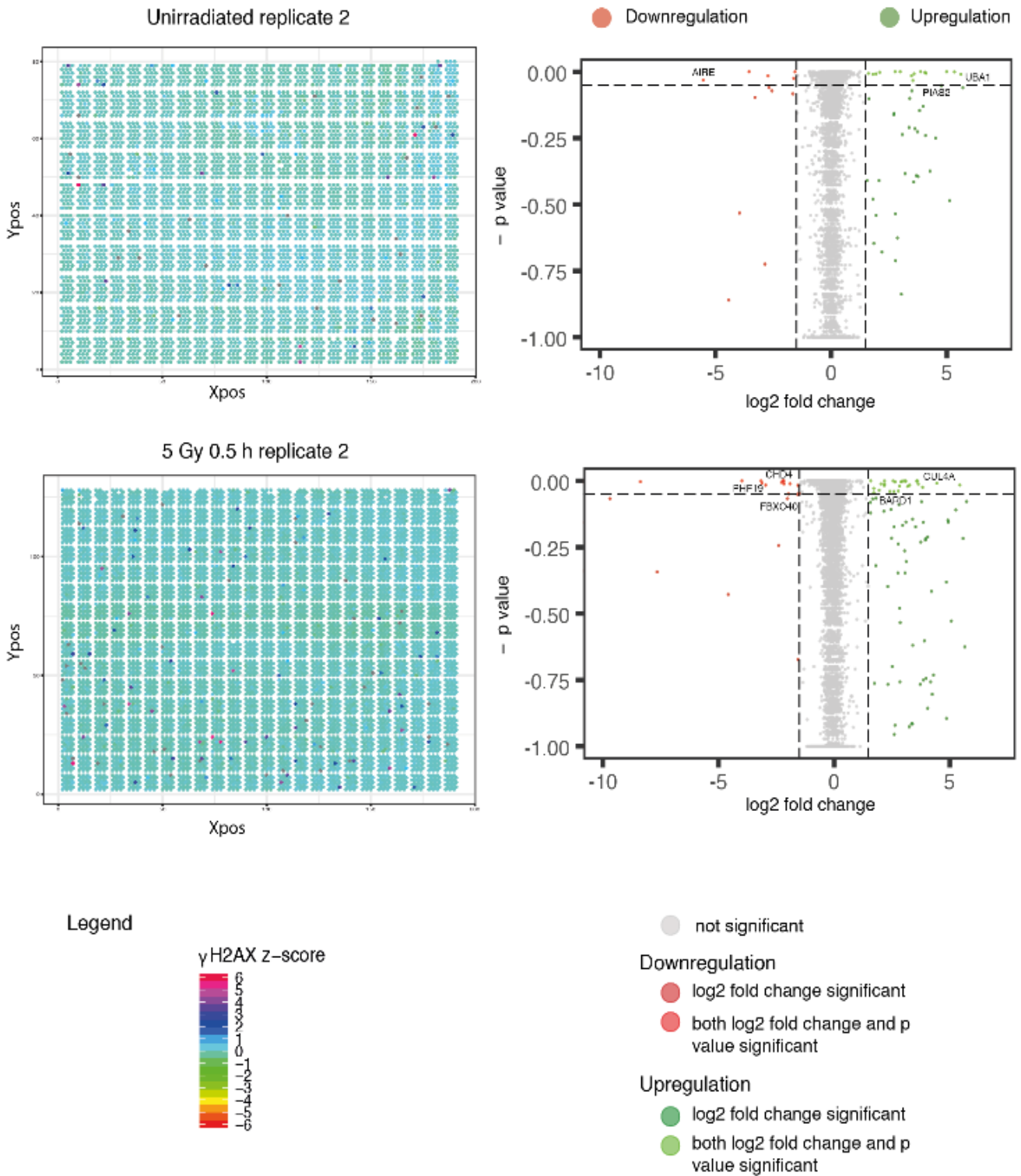
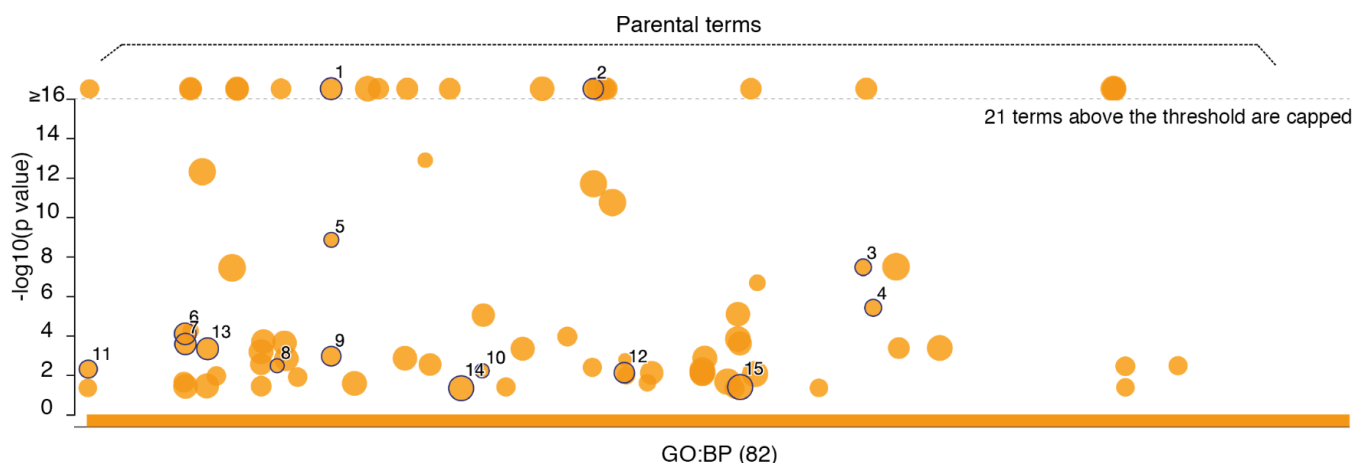


Figure 7.3. Data distribution and Volcano plots per array.

Figure 7.4. The functional profiling of the hits in undamaged cells. Results summary of the functional



ID	Database	Term ID	Term name	adjusted p value	colors for the log scale
1	GO:BP	GO:0016567	protein ubiquitination	1.244×10^{-58}	≥50
2	GO:BP	GO:0043161	proteasome-mediated ubiquitin-dependent protein catabolic process	4.740×10^{-26}	45
3	GO:BP	GO:0070534	protein K63-linked ubiquitination	3.525×10^{-8}	40
4	GO:BP	GO:0070936	protein K48-linked ubiquitination	4.000×10^{-6}	35
5	GO:BP	GO:0016574	histone ubiquitination	1.429×10^{-9}	30
6	GO:BP	GO:0006325	chromatin organization	8.285×10^{-5}	25
7	GO:BP	GO:0006338	chromatin remodeling	2.724×10^{-4}	20
8	GO:BP	GO:0010390	histone monoubiquitination	3.446×10^{-3}	15
9	GO:BP	GO:0016570	histone modification	1.142×10^{-3}	10
10	GO:BP	GO:0033522	histone H2A ubiquitination	6.237×10^{-3}	5
11	GO:BP	GO:0000086	G2/M transition of mitotic cell cycle	5.114×10^{-3}	0
12	GO:BP	GO:0044772	mitotic cell cycle phase transition	7.820×10^{-3}	
13	GO:BP	GO:0006974	DNA damage response	4.741×10^{-4}	
14	GO:BP	GO:0032774	RNA biosynthetic process	4.760×10^{-2}	
15	GO:BP	GO:0051252	regulation of RNA metabolic process	4.136×10^{-2}	

profiling for the hits from the undamaged cells (unir), irrespectively of up- or downregulation effect, GO:BP - biological process category. The hits list was cross-referenced with the biological process database comprising such evidence types as experiment, expression patterns, sequence or structural similarity, genomic context, and computational analysis. The resulting p values were corrected for the multiple testing with the in-house algorithm, significance threshold was set at 0.05. Only significant categories are plotted. 21 overrepresented terms (parental terms) with the highest p values were capped on the top of the plot to allow the visualization of the less represented but significant categories. 19 terms were manually selected, numbered and clustered in the categories (1, 2, 3, 4). The terms are listed in the table below. Each term has a corresponding ID number and the name presented. Category 1 - chromatin organization terms, 2 - cell cycle terms, 3 - DNA damage signaling/repair terms, 4 - RNA metabolism terms (special for the undamaged cells versus irradiated cells).

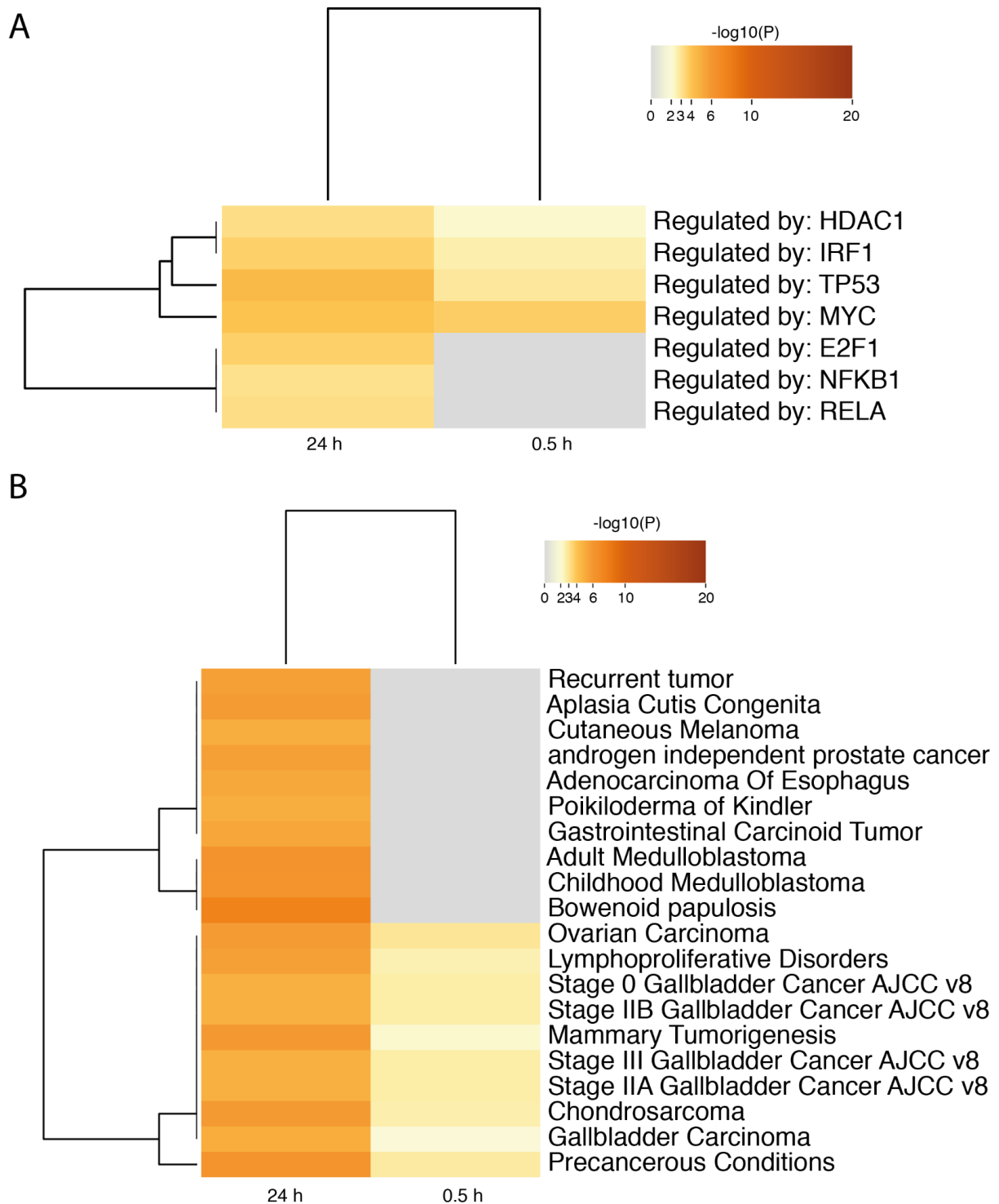


Figure 7.5. Comparative heatmaps of enriched transcriptional regulatory network and disease association terms across 0.5 h and 24 h hits lists, colored by p values. Terms with a p-value < 0.01, a minimum count of 3, and an enrichment factor > 1.5 are collected and grouped into clusters based on their membership similarities. Significant terms were then hierarchically clustered into a tree based on Kappa-statistical similarities among their gene memberships. Then 0.3 kappa score was applied as the threshold to cast the tree into term clusters. The term with the best p value within each cluster was chosen as its representative term and displayed in a dendrogram. The heatmap cells are colored by their p values, grey cells indicate the lack of enrichment for that term in the corresponding hit list. (A) Transcriptional regulatory networks heatmap, TRRUST database. (B) Gene-disease associations heatmap, DisGeNET database.

RNF8 KD

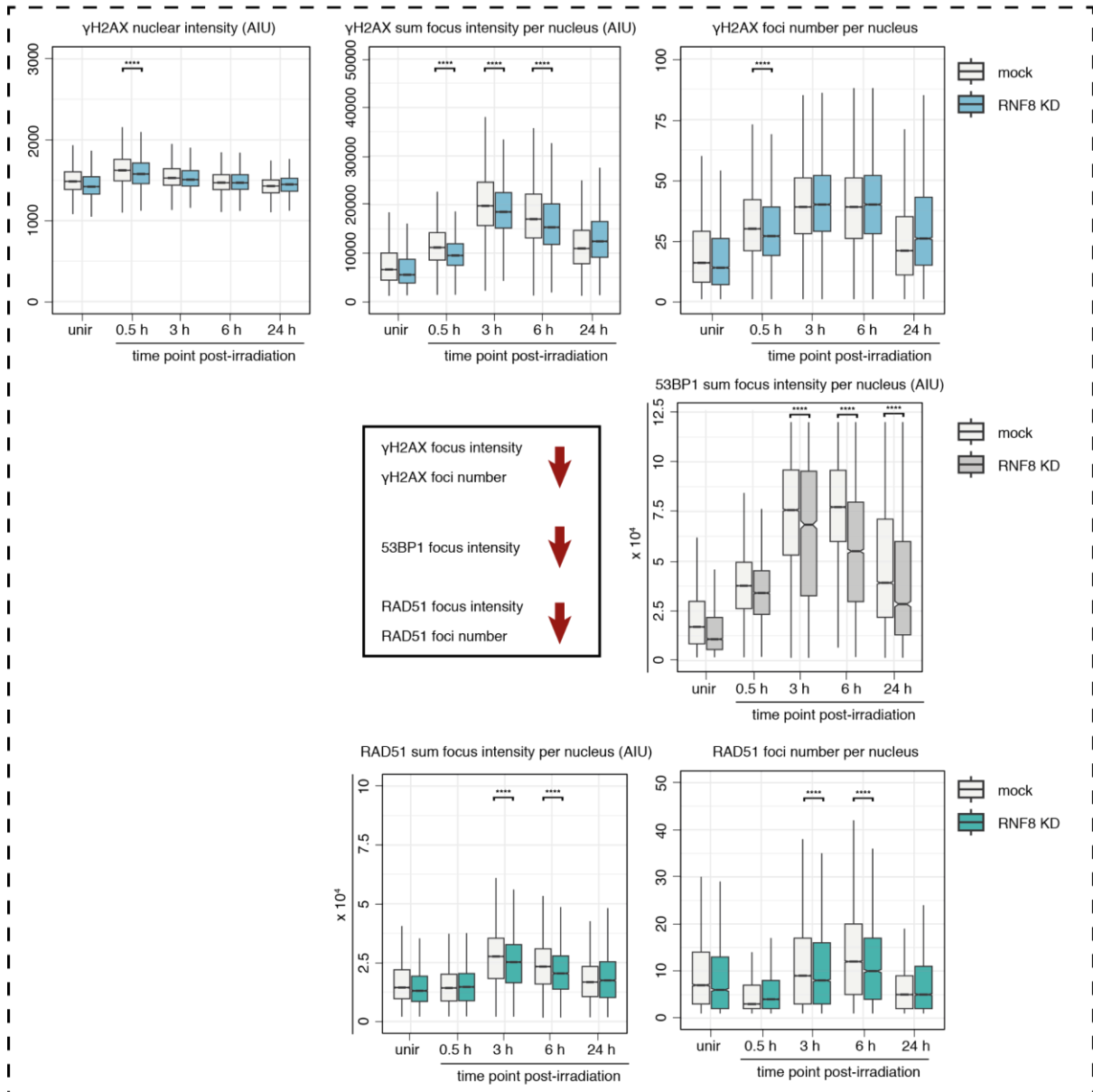


Figure 7.6. Depletion of RNF8 impairs γ H2AX, 53BP1, and RAD51 signaling in damaged cells. The quantification of the DDR kinetics in cells with knockdown of RNF8. For all plots, mock is a pooled population of mock-transfected and non-siRNA transfected cells from either one plate corresponding to the indicated time point (53BP1 and RAD51 response quantification, total 51 wells per plate, approx 200 cells per well) or two replicate plates corresponding to the indicated time point (γ H2AX response quantification, total 102 wells, approx 200 cells per well). The knockdown population was represented by the wells with three siRNA variants per gene of interest and their replicates (total minimum 9 wells per plate per gene, approx 200 cells per well) corresponding to the indicated time point. Whole nuclear intensity of γ H2AX per nucleus, mean focus intensity of γ H2AX, 53BP1, RAD51 foci per nucleus, and number of γ H2AX, RAD51 foci per nucleus were determined in HeLa Kyoto cells at the indicated times after DNA damage induction (5 Gy). The box plot description as above. The outliers were omitted and not presented at the plot. *** $p < 0.001$ by Wilcoxon rank-sum test, for knockdown sample versus mock/non-siRNA transfected sample.

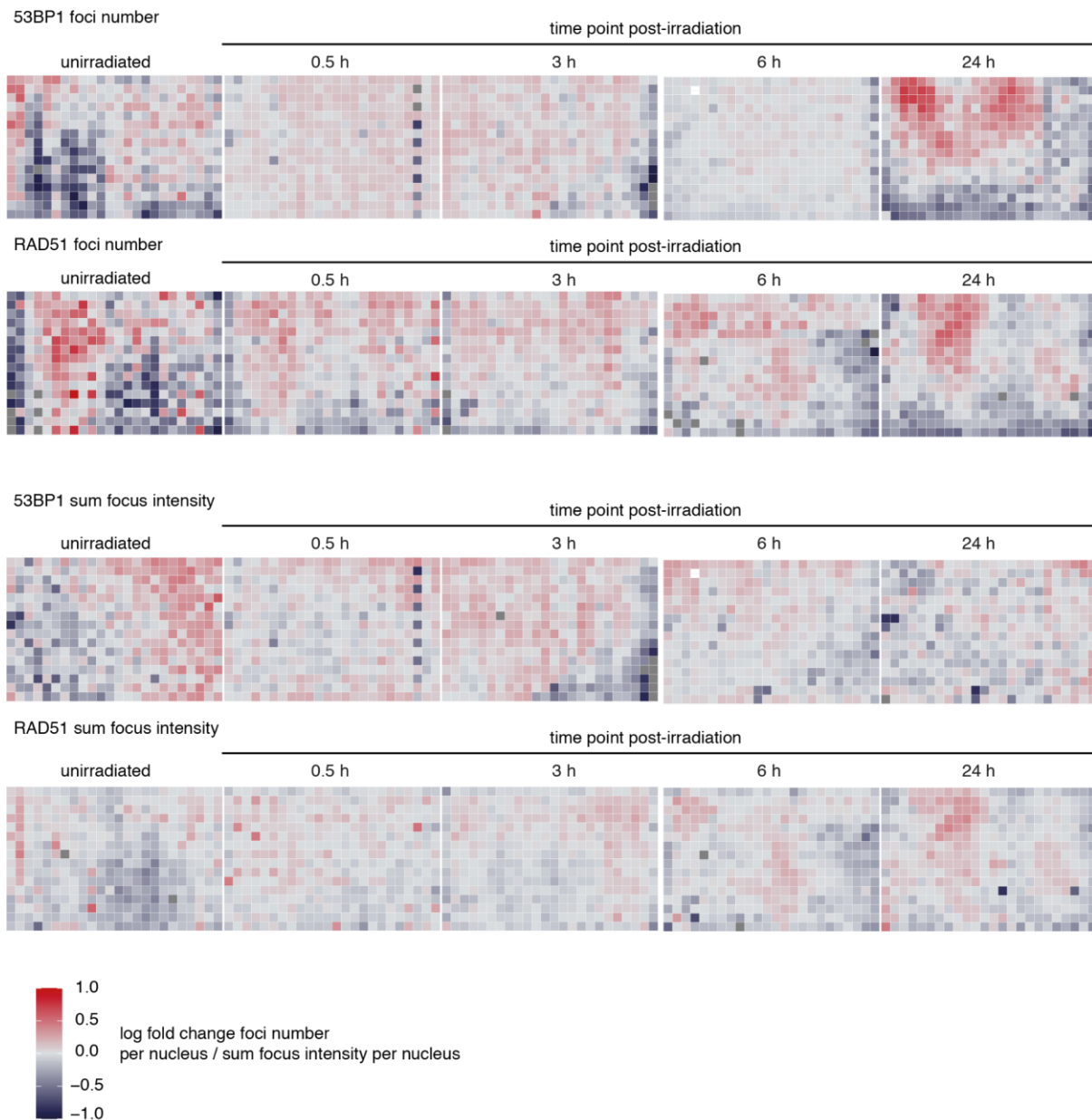


Figure 7.7. Heat maps of the 53BP1 and RAD51 foci number per nucleus and sum focus intensity per nucleus. The repair proteins 53BP1 and RAD51 foci number and sum focus intensity changes are represented by logarithmically transformed fold change values and depicted as heat maps with the plate layout. According to the scale, the red color represents the upregulation of the signal compared to the non-siRNA-treated/mock-transfected controls, the blue color represents the downregulation of the signal compared to the non-siRNA-treated/mock-transfected controls, the white color represents the value equal to the mean value of the non-siRNA-treated/mock-transfected controls. The grey wells represent a value outside of the range presented. The knockdown population was represented by the wells with three siRNA variants per gene of interest and their replicates (total minimum 9 wells per plate per gene, approximately 200 cells per well) corresponding to the indicated time point. The non-siRNA-treated/mock-transfected population was represented by the wells without siRNA printed, mock-transfected, and non-coding siRNA-transfected cells (total of 51 wells, approximately 200 cells per well).

Time-independent effects: γ H2AX compared to the common cluster

Phenotype	Foci	unir	0.5 h	3 h	6 h	24 h
CXXC1	count	↓	—	—	↓	—
	intensity	↓	↑	—	↓	—
RNF168	count	↑	—	↑	—	—
	intensity	↑	↓	↑	↓	—
RNF8	count	—	—	—	↑	—
	intensity	↓	—	↑	↓	↑
XIAP	count	—	↑	↓	—	↓
	intensity	—	—	↓	↓	↓

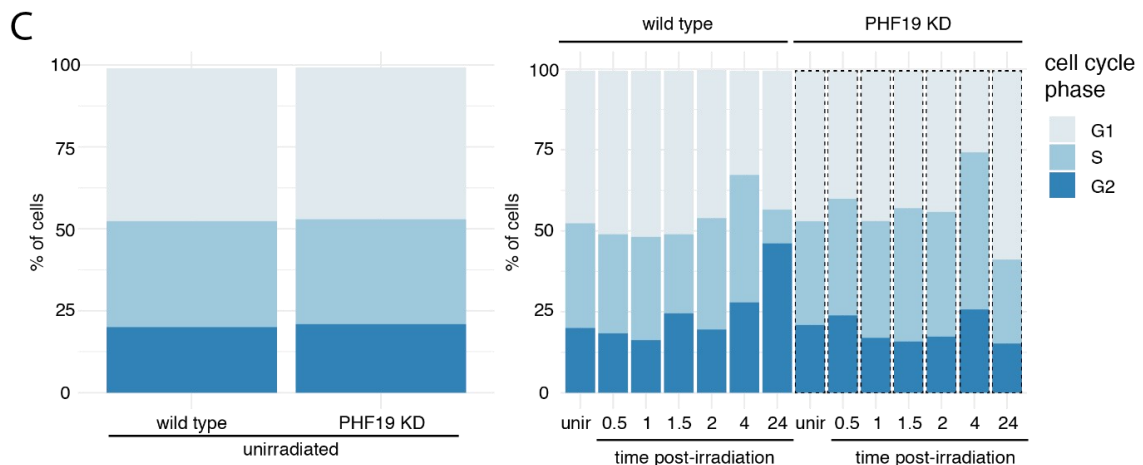
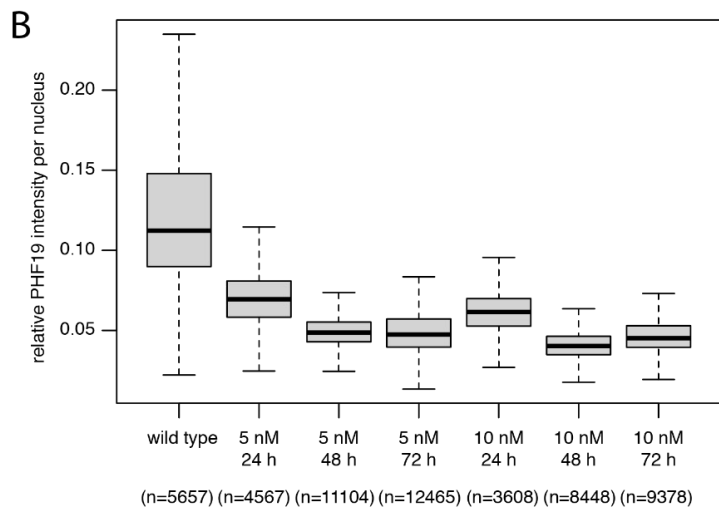
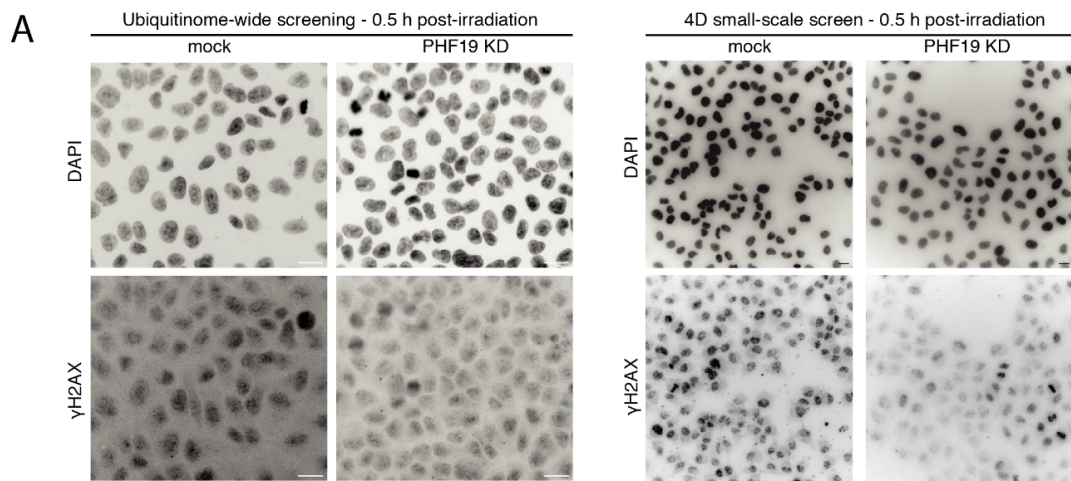
Time-independent effects: 53BP1 compared to the common cluster

Phenotype	Foci	unir	0.5 h	3 h	6 h	24 h
CXXC1	count	↓	—	—	↓	—
	intensity	↑	↑	—	↑	↑
RNF168	count	↑	—	↑	—	—
	intensity	↓	↓	—	↓	↓
RNF8	count	↓	↓	—	↓	↓
	intensity	↓	↓	↓	↓	↓
XIAP	count	—	—	↓	↓	↓
	intensity	↑	—	↓	↓	↑

Time-independent effects: **RAD51** compared to the common cluster

Phenotype	Foci	unir	0.5 h	3 h	6 h	24 h
CXXC1	count	↓	↑	↑	↑	↓
	intensity	—	↑	↑	↑	↓
RNF168	count	↓	↓	↓	↓	—
	intensity	—	↓	↓	↓	↓
RNF8	count	—	↓	↓	↓	—
	intensity	↑	↓	↓	↓	↓
XIAP	count	↓	—	↑	↓	↓
	intensity	↓	—	—	↓	↓

Figure 7.8 Characterization of the time-independent clusters. The γ H2AX, 53BP1, and RAD51 foci parameters of four single-gene knockdown phenotypes separated as time-independent clusters. The red arrow represents a strong (at least two-fold) downregulating effect compared to the common cluster of knockdowns, the green arrow indicates a strong (at least two-fold) upregulating effect compared to the common cluster of knockdowns, and the black line indicates no strong difference.



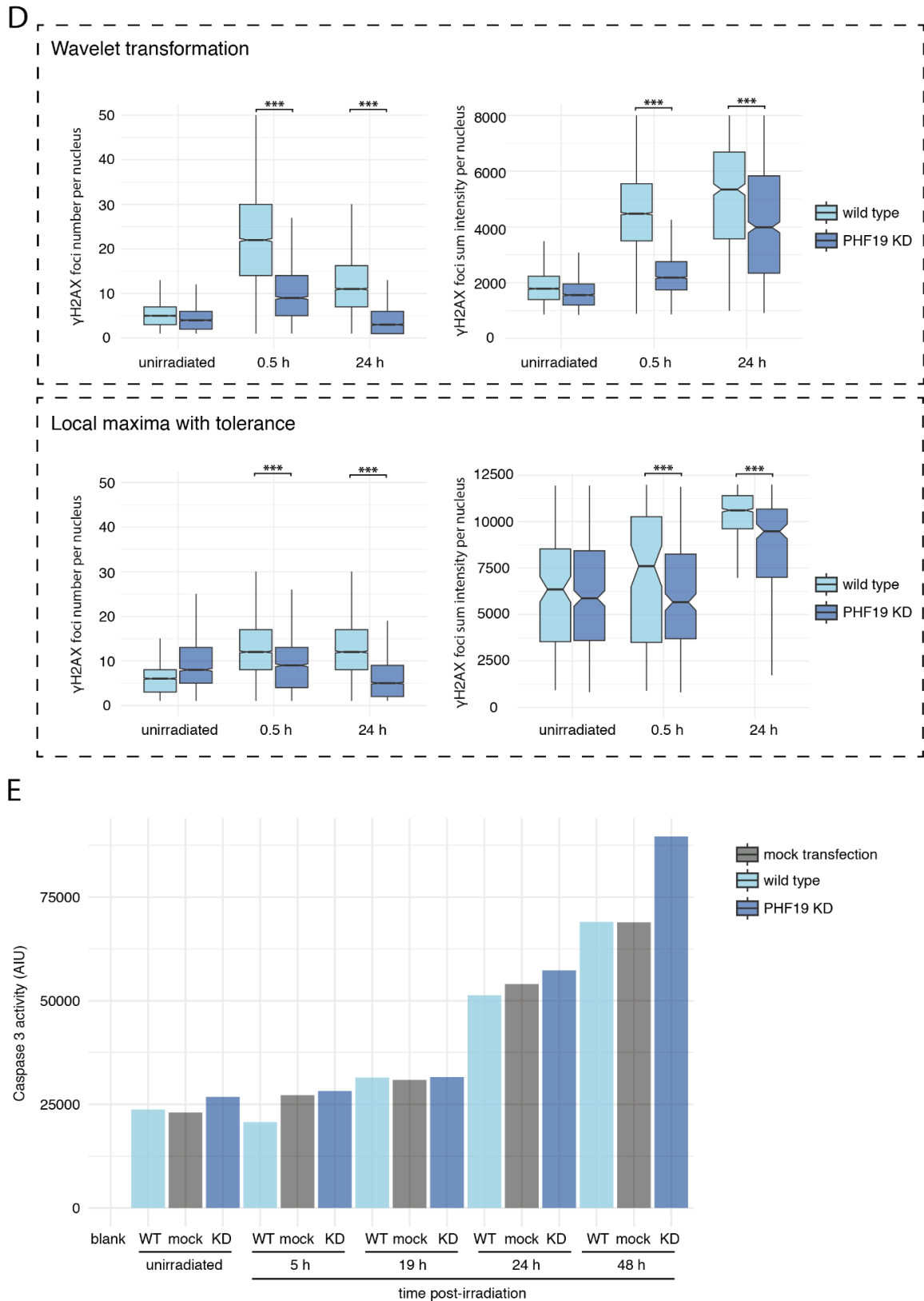


Figure 7.9. PHF19 depletion led to γ H2AX signaling downregulation and impaired DNA repair. (A) Representative images of the mock-transfected cells and PHF19-depleted cells showing the γ H2AX signal

0.5 h post-irradiation. Scale bar 20 μm . (B) The quantification of the PHF19 knockdown in the HeLa Kyoto cells at two different concentrations and three time points post-transfection. The number of cells analyzed per condition is specified under each box. Three replicates per condition were analyzed and pooled together. The box plot description as above. (C) Cell cycle analysis by flow cytometry. The unirradiated wild type and PHF19-depleted cells showed no difference in cell cycle distribution (left bar plot). After exposure to X-ray radiation, cells underwent cell cycle arrest and accumulated in G1- and S-phases up to four hours post IR (the biggest S-phase share among all the time points post-irradiation). After repair of DNA damage, cells progressed from the S-phase arrest into G2-phase (24 h). The knockdown cells showed delayed release into the G2 at 24 h post-irradiation. The bars representing the knockdown cells are highlighted by the dashed outline. Two independent experiments were performed and ~25000 cells per time point were analyzed. (D) The characterization of the γH2AX foci number and sum intensity per nucleus in the HeLa Kyoto wild type cells and HeLa Kyoto PHF19 knockdown. Two foci segmentation algorithms were compared for their ability to segment the γH2AX foci with various intensity: local maxima with tolerance is intensity-based segmentation, wavelet transform is both intensity- and texture-based segmentation approach. At least 2000 cells were analyzed per condition. The box plot description as above. The outliers are presented as single dots in the plot outside of the box area. *** $p < 0.001$ by t-test, for knockdown sample versus wild type sample. (E) The apoptosis analysis of the HeLa Kyoto wild type, mock-transfected and PHF19-depleted. Blank - only the lysis buffer readout, was subtracted from all other samples.

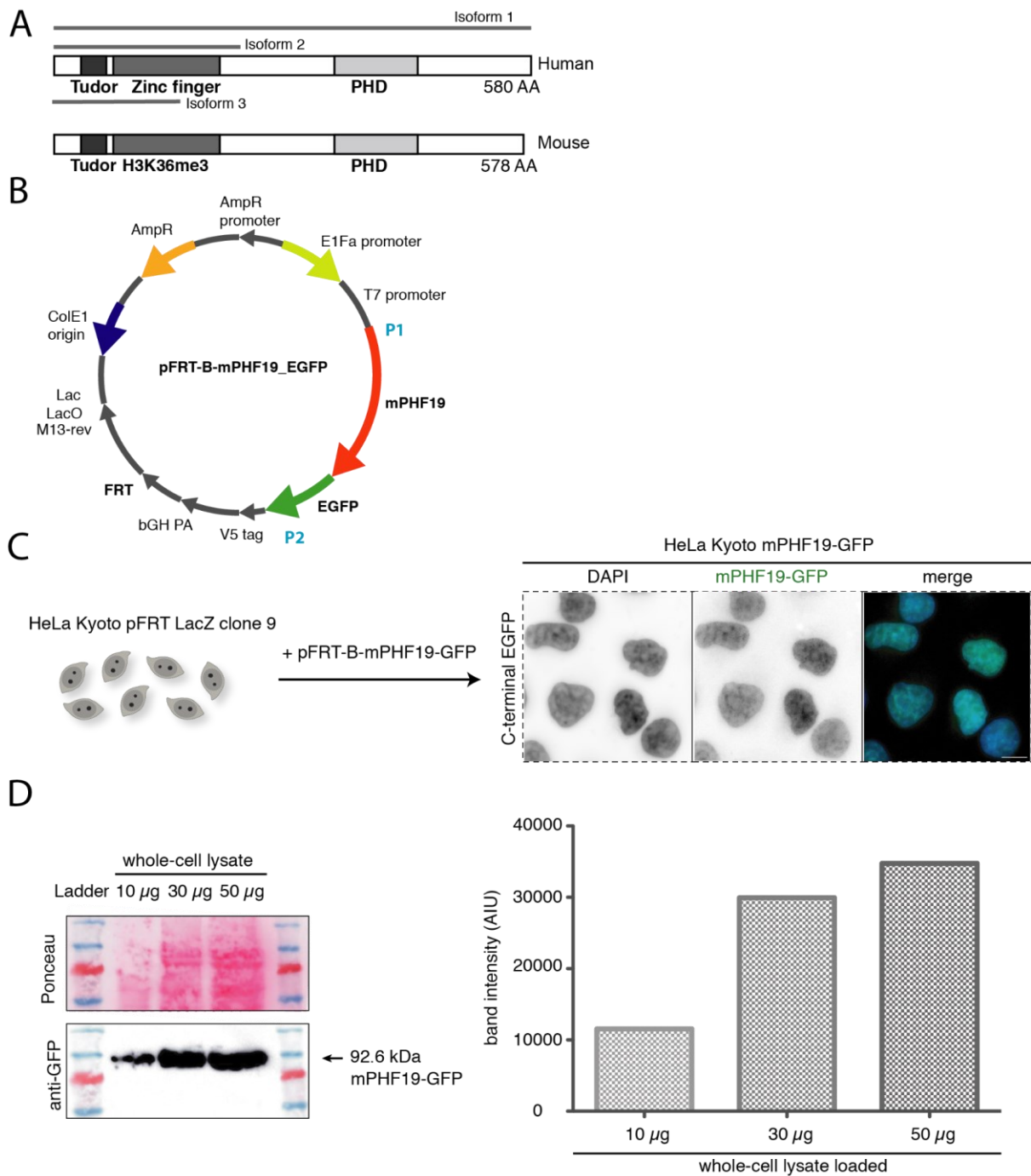


Figure 7.10. Creation of the HeLa Kyoto stable cell line with overexpression of mouse PHF19 tagged with GFP. (A) Comparison of the domain composition of human and mouse PHF19 proteins. The human PHF19 is produced as three isoforms where the longest isoform 1 is considered canonical and is studied in this thesis. (B) pFRT-B-mPHF19-GFP plasmid map. P1 and P2 demarcates the regions corresponding to primers. (C) Scheme of creation of the HeLa Kyoto mPHF19-GFP cell line with overexpression of the mPHF19 protein tagged with GFP. The cell line was created using site-directed Flp-FRT recombination technology. Scale bar 5 µm. (D) Western blot analysis of the mPHF19-GFP production in the stable cell line. The anti-GFP antibody recognized a product of the correct size (92.5 kDa). The bar plot represents the band intensity corresponding to the amount of the whole-cell lysate loaded, AIU - arbitrary intensity units.

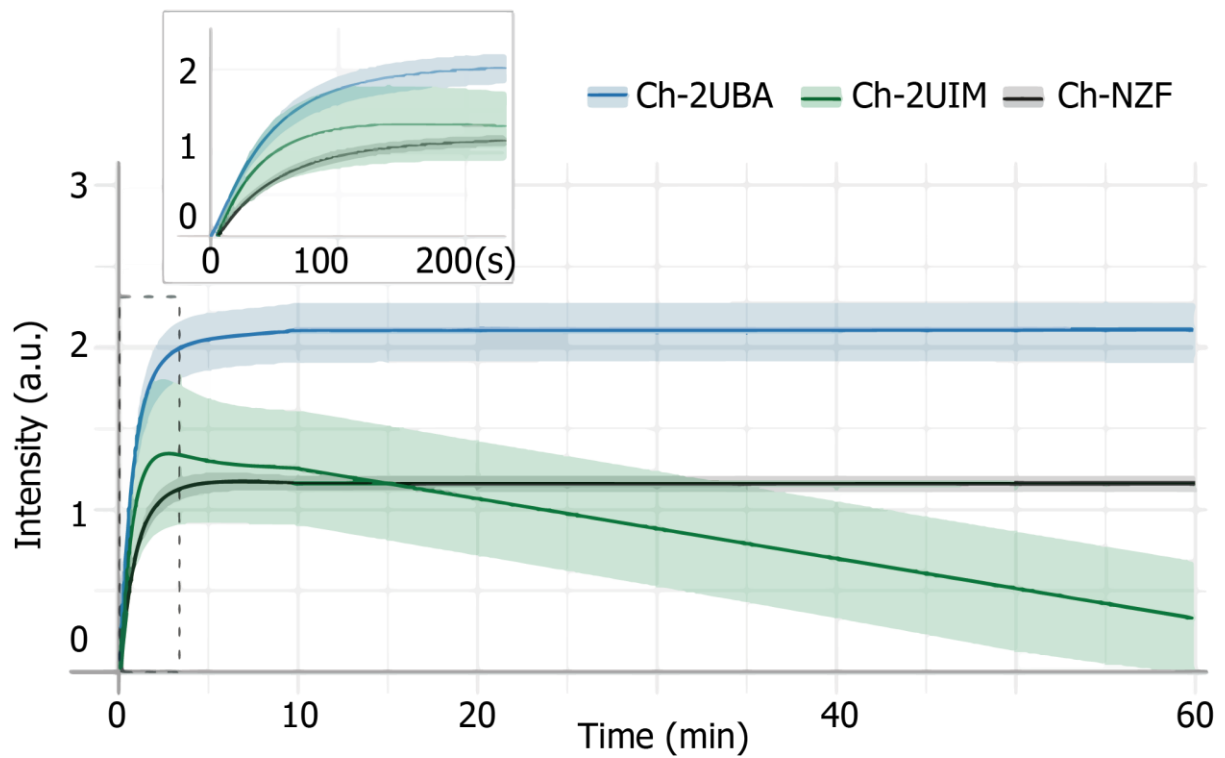


Figure 7.11. Ubiquitin probes recruitment curves - expanded time line. Recruitment curves displayed as mean \pm SEM for two or three independent experiments after DNA damage. For each experimental condition at least 25 cells were used. The dotted region is shown as a magnified insert to better illustrate the recruitments of ubiquitin probes within 200 seconds after DNA damage.

Table 7.1. List of the target genes and siRNA sequences used in the ubiquitinome-wide screening. Attached separately as a Word file because of the size.

Table 7.2. Selected hits for each time point. Red and green shadings correspond to hits leading to lower or higher γ H2AX intensity compared to control cells, respectively.

0.5 h	24 h	unirradiated
ASB17	CCNF	CCND1
PHRF1	APC*	AMFR
DCUN1D1	NEURL	PRICKLE3
LOC642219	UBE2K	CCNF
IRF2BP1	AIRE	APC*
ATG3	CDK1	CCNB1
SCEL	TRIP12*	NEURL
PHF19	UBE2A	UBE2K
FBXL17	BIRC2	AIRE
TRIM24	CDC34	CDK1
RNF11	FBXW4	TRIP12*
UBE2Z	UBE4A	TRIM27
SOCS2	UBE2B	CDC34
VPS41	CDK2*	FBXW4
FBXL15	SOCS5	BIRC3
HERC3	CBL	HLTF*
BRPF3	UBE2G2	CDK2*
ASB13	DZIP3	LPXN
HUWE1*	TRIM75	RNF7
HERC2*	DDX58_1	BARD1*
RNF115	IRF2BP1	JARID1C
FBXO31	ATG3	ESR1
HERC1	SCEL	TRAF4
ZNF330	PHF19	UBE2E1
FBXL18	DCUN1D3	SOCS5
UBE2D3	SOCS2	DZIP3
BTRC	VPS41	TNFRSF25
ESR1	FBXL15	ITCH
TRAF4	HERC3	IRF2BP1

PRPF19	BIRC3	ATG3
SPSB1	TRIM71	SCEL
SOCS3	BRPF3	PHF19
HMGCR	XIAP*	FBXL17
MYLIP	UFM1	FBXO8
FBXO11	HERC1	RNF24
RNF8*	TRIM50	MLLT6
UHRF1*	ZNF330	TRIM24
FBXO38	FBXL18	CUL4A*
BAZ1B*	FBXW8	SHPRH*
PDZRN4	BTRC	PCGF6
FBXO30	ESR1	RNF11
RNF6	ASB16	UBE2Z
CHD4*	PRPF19	TRIM13
UBE3C	TRAF4	FBXO21
UBE2C	SPSB1	DTX1
TRIM77	MARCH9	FBXO27
FBXO6	SOCS3	SOCS2
NEURL2	BMI1*	FBXL11
HRC	MYLIP	PSMB8
FBXO28	FBXO11	PHF20L1
FBXO40	ZNF592	RNF144A
BAHD1	RNF8*	VPS41
UBE2T	UHRF1*	UBE2N
PDZRN3	FBXO38	FBXL15
BMI1*	BAZ1B	UBR1
	PDZRN4	HERC3
	FBXO30	HECTD3
		BRPF3
		ASB13
		BTRC
		SPSB1
		RNF168*
		UHRF1*
		FBXO38
		FBXL12
		CBL
		BAZ1B
		PDZRN4

		FBXO30 AIRE FBXO2 FBXW8 ZNR2
TRIP12*	TNFRSF25	PIAS2
TRIM27	CCND1	FBXW2
FBXW4	PHF23	RNF20*
CDC34	UBE2D2	STUB1
UBE2B	PRICKLE2	FBXO28
BIRC3	PHF17	CNOT4
CDK2*	TRIM60	UFM1
LPXN	RNF133	NHLRC1
UBE2D1		FBXO3
RNF7		ASB10
ZNF592		PIAS4*
RNF123		UBA3
PHF23		TRIM5
FBXO17		ZMYND11
CBLC		TRIM8
UBE2H		FBXL7
PJA1		ASB17
RBBP6		TSG101
FBXL13		UBE2M*
MAGEC2		MARCH6
RFPL3		MARCH8
FBXL5		UBA1*
TRIM52		MARCH2
TRIM74		PHF2
DPF2		ASB7
TRIM39		FBXW10
CACUL1		similar_to_ring_finger_and_WD_repeat_domain_2
RNF43		MAVS2
ASB15		
UFM1		
FBXO48		
ZNR2		
FBXL4		

RNF185		
UBOX5		
FBXO3		
MARCH3		
RFPL2		
WHSC1L1		
RFPL1		
TRIM26		
LONRF3		
RNF145		
TRIM36		
ZC3HAV1		
ASB14		
TRAF3		
FBXW8		
ZMYND11		
RAD18*		
RNF113A		
HERC6		
TRAF5		
UNK		
MARCH9		
RNF183		
RNF168*		
RNF187		
FBXW5		
TRIM49		
ZNF185		
FBXO43		
TRAF6		
RNF222		
TRIM60		
TRIM46		
TRIM42		
FBXW10		
MID1		
KDM5B*		
RNF24		
CUL4A*		

RNF114 UBE2L3 FBXO18 TP53* UBE2V2 TRIM33* MARCH8 RNF181 TRIM6 FBXO22 LGR6 LNX2 TRIM68 ASB7 SMURF1* UBE2G2 similar_to_ring_finger_and_WD_repeat_domain_2 MAVS3 STUB1		
---	--	--

* Hits known to play a role in DNA damage and repair.

Table 7.3. The functional profiling of the hits list genes from the irradiated cells (0.5 h and 24 h post-irradiation).

Database	Term name	Term ID	adjusted p value	Term size	Hits list size	Intersection	Hits in the term
GO:BP	protein ubiquitination	GO:0016567	1.75E-123	792	153	112	ASB17,PHRF1,DCUN1D1,IRF2BP1,ATG3,FBXL17,TRIM24,RNF11,UBE2Z,SOCS2,FBXL15,HERC3,ASB13,HUWE1,HERC2,RNF115,FBXO31,HERC1,UBE2D3,BTRC,TRAF4,PRPF19,SPSB1,SOCS3,MYLIP,FBXO11,RNF8,UHRF1,FBXO38,FBXO30,RNF6,UBE3C,UBE2C,TRIM77,FBXO6,NEURL2,STUB1,FBXO28,UBE2T,PDZRN3,BMI1,TRIP12,TRIM27,CDC34,UBE2B,BIRC3,UBE2D1,RNF7,RNF123,PHF23,CBLC,UBE2H,RBBP6,MAGEC2,RFPL3,FBXL5,TRIM52,TRIM74,TRIM39,RNF43,ASB15,ZNRF1,RNF185,UBOX5,FBXO3,RFPL2,RFPL1,TRIM26,ASB14,TRAF3,FBXW8,RAD18,RNF113A,HERC6,TRAF5,RNF183,RNF168,RNF187,FBXW5,TRIM49,FBXO43,TRAF6,TRIM60,CUL4A,RNF114,UBE2L3,UBE2V2,TRIM33,MARCH8,RNF181,TRIM6,FBXO22,TRIM68,ASB7,SMURF1,UBE2G2,CCNF,UBE2K,UBE2A,BIRC2,UBE4A,SOCS5,CBL,DZIP3,TRIM75,DCUN1D3,TRIM71,XIAP,TRIM50,ASB16,UBE2D2,RNF133

GO:BP	protein modification by small protein conjugation	GO:0032446	2.16E-120	872	153	113	ASB17,PHRF1,DCUN1D1,IRF2BP1,ATG3,FBXL17,TRIM24,RNF11,UBE2Z,SOCS2,FBXL15,HERC3,ASB13,HUWE1,HERC2,RNF115,FBXO31,HERC1,UBE2D3,BTRC,TRAF4,PRPF19,SPSB1,SOCS3,MYLIP,FBXO11,RNF8,UHRF1,FBXO38,FBXO30,RNF6,UBE3C,UBE2C,TRIM77,FBXO6,NEURL2,STUB1,FBXO28,UBE2T,PDZRN3,BMI1,TRIP12,TRIM27,CDC34,UBE2B,BIRC3,UBE2D1,RNF7,RNF123,PHF23,CBLC,UBE2H,RBBP6,MAGEC2,RFPL3,FBXL5,TRIM52,TRIM74,TRIM39,RNF43,ASB15,UFM1,ZNRF1,RNF185,UBOX5,FBXO3,RFPL2,RFPL1,TRIM26,ASB14,TRAF3,FBXW8,RAD18,RNF113A,HERC6,TRAF5,RNF183,RNF168,RNF187,FBXW5,TRIM49,FBXO43,TRAF6,TRIM60,CUL4A,RNF114,UBE2L3,UBE2V2,TRIM33,MARCH8,RNF181,TRIM6,FBXO22,TRIM68,ASB7,SMURF1,UBE2G2,CCNF,UBE2K,UBE2A,BIRC2,UBE4A,SOCSS5,CBL,DZIP3,TRIM75,DCUN1D3,TRIM71,XIAP,TRIM50,ASB16,UBE2D2,RNF133
GO:BP	protein modification by small protein conjugation or removal	GO:0070647	3.55E-114	1019	153	114	ASB17,PHRF1,DCUN1D1,IRF2BP1,ATG3,FBXL17,TRIM24,RNF11,UBE2Z,SOCS2,FBXL15,HERC3,ASB13,HUWE1,HERC2,RNF115,FBXO31,HERC1,UBE2D3,BTRC,TRAF4,PRPF19,SPSB1,SOCS3,MYLIP,FBXO11,RNF8,UHRF1,FBXO38,FBXO30,RNF6,UBE3C,UBE2C,TRIM77,FBXO6,NEURL2,STUB1,FBXO28,UBE2T,PDZRN3,BMI1,TRIP12,TRIM27,CDC34,UBE2B,BIRC3,UBE2D1,RNF7,RNF123,PHF23,CBLC,UBE2H,RBBP6,MAGEC2,RFPL3,FBXL5,TRIM52,TRIM74,TRIM39,RNF43,ASB15,UFM1,ZNRF1,RNF185,UBOX5,FBXO3,RFPL2,RFPL1,TRIM26,ASB14,TRAF3,FBXW8,RAD18,RNF113A,HERC6,TRAF5,RNF183,RNF168,RNF187,FBXW5,TRIM49,FBXO43,TRAF6,TRIM60,CUL4A,RNF114,UBE2L3,UBE2V2,TRIM33,MARCH8,RNF181,TRIM6,FBXO22,TRIM68,ASB7,SMURF1,UBE2G2,CCNF,UBE2K,CDK1,UBE2A,BIRC2,UBE4A,SOCS5,CBL,DZIP3,TRIM75,DCUN1D3,TRIM71,XIAP,TRIM50,ASB16,UBE2D2,RNF133
GO:BP	post-translational protein modification	GO:0043687	8.27E-108	1276	153	117	ASB17,PHRF1,DCUN1D1,IRF2BP1,ATG3,FBXL17,TRIM24,RNF11,UBE2Z,SOCS2,FBXL15,HERC3,ASB13,HUWE1,HERC2,RNF115,FBXO31,HERC1,UBE2D3,BTRC,TRAF4,PRPF19,SPSB1,SOCS3,MYLIP,FBXO11,RNF8,UHRF1,FBXO38,BAZ1B,FBXO30,RNF6,CHD4,UBE3C,UBE2C,TRIM77,FBXO6,NEURL2,STUB1,FBXO28,UBE2T,PDZRN3,BMI1,TRIP12,TRIM27,CDC34,UBE2B,BIRC3,CDK2,UBE2D1,RNF7,RNF123,PHF23,CBLC,UBE2H,RBBP6,MAGEC2,RFPL3,FBXL5,TRIM52,TRIM74,TRIM39,RNF43,ASB15,UFM1,ZNRF1,RNF185,UBOX5,FBXO3,RFPL2,RFPL1,TRIM26,ASB14,TRAF3,FBXW8,RAD18,RNF113A,HERC6,TRAF5,RNF183,RNF168,RNF187,FBXW5,TRIM49,FBXO43,TRAF6,TRIM60,CUL4A,RNF114,UBE2L3,UBE2V2,TRIM33,MARCH8,RNF181,TRIM6,FBXO22,TRIM68,ASB7,SMURF1,UBE2G2,CCNF,UBE2K,CDK1,UBE2A,BIRC2,UBE4A,SOCS5,CBL,DZIP3,TRIM75,DCUN1D3,TRIM71,XIAP,TRIM50,ASB16,UBE2D2,RNF133
GO:BP	protein modification process	GO:0036211	3.40E-67	3409	153	124	ASB17,PHRF1,DCUN1D1,IRF2BP1,ATG3,FBXL17,TRIM24,RNF11,UBE2Z,SOCS2,FBXL15,HERC3,ASB13,HUWE1,HERC2,RNF115,FBXO31,HERC1,UBE2D3,BTRC,TRAF4,PRPF19,SPSB1,SOCS3,HMGCR,MYLIP,FBXO11,RNF8,UHRF1,FBXO38,BAZ1B,FBXO30,RNF6,CHD4,UBE3C,UBE2C,TRIM77,FBXO6,NEURL2,STUB1,FBXO28,UBE2T,PDZRN3,BMI1,TRIP12,TRIM27,CDC34,UBE2B,BIRC3,CDK2,UBE2D1,RNF7,ZNF592,RNF123,PHF23,CBLC,UBE2H,RBBP6,MAGEC2,RFPL3,FBXL5,TRIM52,TRIM74,TRIM39,CACUL1,RNF43,ASB15,UFM1,Z

							NRF1,RNF185,UBOX5,FBXO3,RFPL2,RFPL1,TRIM26,ASB14,TRAF3,FBXW8,RAD18,RNF113A,HERC6,TRAF5,RNF183,RNF168,RNF187,FBXW5,TRIM49,FBXO43,TRAF6,TRIM60,CUL4A,RNF114,UBE2L3,TP53,UBE2V2,TRIM33,MARCH8,RNF181,TRIM6,FBXO22,TRIM68,ASB7,SMURF1,UBE2G2,CCNF,APC,UBE2K,CDK1,UBE2A,BIRC2,UBE4A,SOCS5,CBL,DZIP3,TRIM75,DCUN1D3,TRIM71,XIAP,TRIM50,ASB16,CCND1,UBE2D2,RNF133
GO:BP	macromolecule modification	GO:0043412	6.14E-64	3628	153	124	ASB17,PHRF1,DCUN1D1,IRF2BP1,ATG3,FBXL17,TRIM24,RNF11,UBE2Z,SOCS2,FBXL15,HERC3,ASB13,HUWE1,HERC2,RNF115,FBXO31,HERC1,UBE2D3,BTRC,TRAF4,PRPF19,SPSB1,SOCS3,HMGCR,MYLIP,FBXO11,RNF8,UHRF1,FBXO38,BAZ1B,FBXO30,RNF6,CHD4,UBE3C,UBE2C,TRIM77,FBXO6,NEURL2,HRC,STUB1,FBXO28,UBE2T,PDZRN3,BMI1,TRIP12,TRIM27,CDC34,UBE2B,BIRC3,CDK2,UBE2D1,RNF7,ZNF592,RNF123,PHF23,CBLC,UBE2H,RBBP6,MAGEC2,RFPL3,FBXL5,TRIM52,TRIM74,TRIM39,CACUL1,RNF43,ASB15,UFM1,ZNRF1,RNF185,UBOX5,FBXO3,RFPL2,RFPL1,TRIM26,ASB14,TRAF3,FBXW8,RAD18,RNF113A,HERC6,TRAF5,RNF183,RNF168,RNF187,FBXW5,TRIM49,FBXO43,TRAF6,TRIM60,CUL4A,RNF114,UBE2L3,TP53,UBE2V2,TRIM33,MARCH8,RNF181,TRIM6,FBXO22,TRIM68,ASB7,SMURF1,UBE2G2,CCNF,APC,UBE2K,CDK1,UBE2A,BIRC2,UBE4A,SOCS5,CBL,DZIP3,TRIM75,DCUN1D3,TRIM71,XIAP,TRIM50,ASB16,CCND1,UBE2D2,RNF133
GO:BP	protein polyubiquitination	GO:0000209	6.31E-58	261	153	52	IRF2BP1,FBXL17,HUWE1,RNF115,UBE2D3,BTRC,TRAF4,PRPF19,RNF8,FBXO38,RNF6,UBE3C,UBE2C,STUB1,FBXO28,UBE2T,TRIP12,TRIM27,CDC34,UBE2B,UBE2D1,UBE2H,RFPL3,ZNRF1,RNF185,UBOX5,RFPL2,RFPL1,TRAF3,TRAF5,RNF183,RNF168,RNF187,TRAF6,RNF114,UBE2L3,UBE2V2,MARCH8,TRIM6,FBXO22,TRIM68,SMURF1,UBE2G2,UBE2K,UBE2A,BIRC2,UBE4A,CBL,DZIP3,TRIM71,XIAP,UBE2D2
GO:BP	ubiquitin-dependent protein catabolic process	GO:0006511	9.04E-55	696	153	67	FBXL17,RNF11,UBE2Z,FBXL15,HERC3,HERC2,RNF115,FBXO31,FBXL18,UBE2D3,BTRC,TRAF4,SPSB1,MYLIP,FBXO11,RNF8,UHRF1,FBXO38,RNF6,UBE3C,UBE2C,FBXO6,STUB1,TRIP12,FBXW4,CDC34,UBE2B,CDK2,UBE2D1,RNF7,RNF123,FBXO17,CBLC,UBE2H,RBBP6,FBXL13,FBXL5,TRIM39,CACUL1,RNF43,FBXO48,ZNRF1,FBXL4,RNF185,FBXO3,RFPL1,HERC6,RNF168,RNF187,FBXW5,CUL4A,RNF114,UBE2L3,FBXO22,SMURF1,UBE2G2,CCNF,APC,UBE2K,UBE2A,BIRC2,UBE4A,SOCS5,CBL,TRIM71,UBE2D2,RNF133
GO:BP	protein metabolic process	GO:0019538	1.62E-54	5373	153	133	ASB17,PHRF1,DCUN1D1,IRF2BP1,ATG3,FBXL17,TRIM24,RNF11,UBE2Z,SOCS2,FBXL15,HERC3,ASB13,HUWE1,HERC2,RNF115,FBXO31,HERC1,FBXL18,UBE2D3,BTRC,TRAF4,PRPF19,SPSB1,SOCS3,HMGCR,MYLIP,FBXO11,RNF8,UHRF1,FBXO38,BAZ1B,FBXO30,RNF6,CHD4,UBE3C,UBE2C,TRIM77,FBXO6,NEURL2,HRC,STUB1,FBXO28,UBE2T,PDZRN3,BMI1,TRIP12,TRIM27,FBXW4,CDC34,UBE2B,BIRC3,CDK2,UBE2D1,RNF7,ZNF592,RNF123,PHF23,FBXO17,CBLC,UBE2H,PJA1,RBBP6,FBXL13,MAGEC2,RFPL3,FBXL5,TRIM52,TRIM74,TRIM39,CACUL1,RNF43,ASB15,UFM1,FBXO48,ZNRF1,FBXL4,RNF185,UBOX5,FBXO3,RFPL2,RFPL1,TRIM26,ASB14,TRAF3,FBXW8,RAD18,RNF113A,HERC6,TRAF5,UNK,RNF183,RNF168,RNF187,FBXW5,TRIM49,FBXO43,TRAF6,TRIM60,CUL4A,RNF114,UBE2L3,TP53,UBE2V

							2,TRIM33,MARCH8,RNF181,TRIM6,FBXO22,TRIM68,ASB7,SMURF1,UBE2G2,CCNF,APC,UBE2K,AIRE,CDK1,UBE2A,BIRC2,UBE4A,SOCS5,CBL,DZIP3,TRIM75,DCUN1D3,TRIM71,XIAP,TRIM50,ASB16,CCND1,UBE2D2,RNF133
GO:BP	modification-dependent protein catabolic process	GO:0019941	2.37E-54	706	153	67	FBXL17,RNF11,UBE2Z,FBXL15,HERC3,HERC2,RNF115,FBXO31,FBXL18,UBE2D3,BTRC,TRAFA4,SPSB1,MYLIP,FBXO11,RNF8,UHRF1,FBXO38,RNF6,UBE3C,UBE2C,FBXO6,STUB1,TRIP12,FBXW4,CDC34,UBE2B,CDK2,UBE2D1,RNF7,RNF123,FBXO17,CBLC,UBE2H,RBBP6,FBXL13,FBXL5,TRIM39,CACUL1,RNF43,FBXO48,ZNRF1,FBXL4,RNF185,FBXO3,RFPL1,HERC6,RNF168,RNF187,FBXW5,CUL4A,RNF114,UBE2L3,FBXO22,SMURF1,UBE2G2,CCNF,APC,UBE2K,UBE2A,BIRC2,UBE4A,SOCS5,CBL,TRIM71,UBE2D2,RNF133
GO:BP	modification-dependent macromolecule catabolic process	GO:0043632	6.10E-54	716	153	67	FBXL17,RNF11,UBE2Z,FBXL15,HERC3,HERC2,RNF115,FBXO31,FBXL18,UBE2D3,BTRC,TRAFA4,SPSB1,MYLIP,FBXO11,RNF8,UHRF1,FBXO38,RNF6,UBE3C,UBE2C,FBXO6,STUB1,TRIP12,FBXW4,CDC34,UBE2B,CDK2,UBE2D1,RNF7,RNF123,FBXO17,CBLC,UBE2H,RBBP6,FBXL13,FBXL5,TRIM39,CACUL1,RNF43,FBXO48,ZNRF1,FBXL4,RNF185,FBXO3,RFPL1,HERC6,RNF168,RNF187,FBXW5,CUL4A,RNF114,UBE2L3,FBXO22,SMURF1,UBE2G2,CCNF,APC,UBE2K,UBE2A,BIRC2,UBE4A,SOCS5,CBL,TRIM71,UBE2D2,RNF133
GO:BP	proteolysis involved in protein catabolic process	GO:0051603	8.49E-52	807	153	68	FBXL17,RNF11,UBE2Z,FBXL15,HERC3,HERC2,RNF115,FBXO31,FBXL18,UBE2D3,BTRC,TRAFA4,PRPF19,SPSB1,MYLIP,FBXO11,RNF8,UHRF1,FBXO38,RNF6,UBE3C,UBE2C,FBXO6,STUB1,TRIP12,FBXW4,CDC34,UBE2B,CDK2,UBE2D1,RNF7,RNF123,FBXO17,CBLC,UBE2H,RBBP6,FBXL13,FBXL5,TRIM39,CACUL1,RNF43,FBXO48,ZNRF1,FBXL4,RNF185,FBXO3,RFPL1,HERC6,RNF168,RNF187,FBXW5,CUL4A,RNF114,UBE2L3,FBXO22,SMURF1,UBE2G2,CCNF,APC,UBE2K,UBE2A,BIRC2,UBE4A,SOCS5,CBL,TRIM71,UBE2D2,RNF133
GO:BP	protein catabolic process	GO:0030163	2.63E-49	1043	153	72	FBXL17,TRIM24,RNF11,UBE2Z,FBXL15,HERC3,HERC2,RNF115,FBXO31,FBXL18,UBE2D3,BTRC,TRAFA4,PRPF19,SPSB1,HMGCR,MYLIP,FBXO11,RNF8,UHRF1,FBXO38,RNF6,UBE3C,UBE2C,FBXO6,STUB1,TRIP12,FBXW4,CDC34,UBE2B,CDK2,UBE2D1,RNF7,RNF123,FBXO17,CBLC,UBE2H,PJA1,RBBP6,FBXL13,MAGEC2,FBXL5,TRIM39,CACUL1,RNF43,FBXO48,ZNRF1,FBXL4,RNF185,FBXO3,RFPL1,HERC6,RNF168,RNF187,FBXW5,CUL4A,RNF114,UBE2L3,FBXO22,SMURF1,UBE2G2,CCNF,APC,UBE2K,UBE2A,BIRC2,UBE4A,SOCS5,CBL,TRIM71,UBE2D2,RNF133
GO:BP	organonitrogen compound metabolic process	GO:1901564	3.30E-45	6362	153	133	ASB17,PHRF1,DCUN1D1,IRF2BP1,ATG3,FBXL17,TRIM24,RNF11,UBE2Z,SOCS2,FBXL15,HERC3,ASB13,HUWE1,HERC2,RNF115,FBXO31,HERC1,FBXL18,UBE2D3,BTRC,TRAFA4,PRPF19,SPSB1,SOCS3,HMGCR,MYLIP,FBXO11,RNF8,UHRF1,FBXO38,BAZ1B,FBXO30,RNF6,CHD4,UBE3C,UBE2C,TRIM77,FBXO6,NEURL2,HRC,STUB1,FBXO28,UBE2T,PDZRN3,BMI1,TRIP12,TRIM27,FBXW4,CDC34,UBE2B,BIRC3,CDK2,UBE2D1,RNF7,ZNF592,RNF123,PHF23,FBXO17,CBLC,UBE2H,PJA1,RBBP6,FBXL13,MAGEC2,RFPL3,FBXL5,TRIM52,TRIM74,TRIM39,CACUL1,RNF43,ASB15,UFM1,FBXO48,ZNRF1,FBXL4,RNF185,UBOX5,FBXO3,RFPL2,RFPL1,TRIM26,ASB14,TRAFA3,FBXW8,RAD18,RNF113A,HERC6,TRAFA5,UNK,RNF183,RNF1

							68,RNF187,FBXW5,TRIM49,FBXO43,TRAF6,TRIM60,CUL4A,RNF114,UBE2L3,TP53,UBE2V2,TRIM33,MARCH8,RNF181,TRIM6,FBXO22,TRIM68,ASB7,SMURF1,UBE2G2,CCNF,APC,UBE2K,AIRE,CDK1,UBE2A,BIRC2,UBE4A,SOCS5,CBL,DZIP3,TRIM75,DCUN1D3,TRIM71,XIAP,TRIM50,ASB16,CCND1,UBE2D2,RNF133
GO:BP	macromolecule catabolic process	GO:0009057	1.92E-42	1412	153	74	FBXL17,TRIM24,RNF11,UBE2Z,FBXL15,HERC3,HERC2,RNF115,FBXO31,FBXL18,UBE2D3,BTRC,TRAF4,PRPF19,SPSB1,HMGCR,MYLIP,FBXO11,RNF8,UHRF1,FBXO38,RNF6,UBE3C,UBE2C,FBXO6,STUB1,TRIP12,FBXW4,CDC34,UBE2B,CDK2,UBE2D1,RNF7,RNF123,FBXO17,CBLC,UBE2H,PJA1,RBBP6,FBXL13,MAGEC2,FBXL5,TRIM39,CACUL1,RNF43,FBXO48,ZNRF1,FBXL4,RNF185,FBXO3,RFPL1,ZC3HAV1,HERC6,TRAF5,RNF168,RNF187,FBXW5,CUL4A,RNF114,UBE2L3,FBXO22,SMURF1,UBE2G2,CCNF,APC,UBE2K,UBE2A,BIRC2,UBE4A,SOCS5,CBL,TRIM71,UBE2D2,RNF133
GO:BP	organonitrogen compound catabolic process	GO:1901565	9.62E-41	1386	153	72	FBXL17,TRIM24,RNF11,UBE2Z,FBXL15,HERC3,HERC2,RNF115,FBXO31,FBXL18,UBE2D3,BTRC,TRAF4,PRPF19,SPSB1,HMGCR,MYLIP,FBXO11,RNF8,UHRF1,FBXO38,RNF6,UBE3C,UBE2C,FBXO6,STUB1,TRIP12,FBXW4,CDC34,UBE2B,CDK2,UBE2D1,RNF7,RNF123,FBXO17,CBLC,UBE2H,PJA1,RBBP6,FBXL13,MAGEC2,FBXL5,TRIM39,CACUL1,RNF43,FBXO48,ZNRF1,FBXL4,RNF185,FBXO3,RFPL1,HERC6,RNF168,RNF187,FBXW5,CUL4A,RNF114,UBE2L3,FBXO22,SMURF1,UBE2G2,CCNF,APC,UBE2K,UBE2A,BIRC2,UBE4A,SOCS5,CBL,TRIM71,UBE2D2,RNF133
GO:BP	catabolic process	GO:0009056	3.55E-35	2616	153	86	ATG3,FBXL17,TRIM24,RNF11,UBE2Z,VPS41,FBXL15,HERC3,HUWE1,HERC2,RNF115,FBXO31,HERC1,FBXL18,UBE2D3,BTRC,TRAF4,PRPF19,SPSB1,HMGCR,MYLIP,FBXO11,RNF8,UHRF1,FBXO38,RNF6,UBE3C,UBE2C,FBXO6,STUB1,TRIP12,TRIM27,FBXW4,CDC34,UBE2B,CDK2,UBE2D1,RNF7,RNF123,PHF23,FBXO17,CBLC,UBE2H,PJA1,RBBP6,FBXL13,MAGEC2,RFPL3,FBXL5,TRIM39,CACUL1,RNF43,UFM1,FBXO48,ZNRF1,FBXL4,RNF185,FBXO3,RFPL2,RFPL1,ZC3HAV1,HERC6,TRAF5,RNF168,RNF187,FBXW5,CUL4A,RNF114,UBE2L3,TP53,TRIM6,FBXO22,TRIM68,SMURF1,UBE2G2,CCNF,APC,UBE2K,UBE2A,BIRC2,UBE4A,SOCS5,CBL,TRIM71,UBE2D2,RNF133
GO:BP	proteolysis	GO:0006508	1.12E-34	1766	153	73	FBXL17,RNF11,UBE2Z,FBXL15,HERC3,HERC2,RNF115,FBXO31,FBXL18,UBE2D3,BTRC,TRAF4,PRPF19,SPSB1,MYLIP,FBXO11,RNF8,UHRF1,FBXO38,RNF6,UBE3C,UBE2C,FBXO6,STUB1,TRIP12,FBXW4,CDC34,UBE2B,BIRC3,CDK2,UBE2D1,RNF7,RNF123,FBXO17,CBLC,UBE2H,RBBP6,FBXL13,FBXL5,TRIM39,CACUL1,RNF43,FBXO48,ZNRF1,FBXL4,RNF185,FBXO3,RFPL1,TRAF3,HERC6,RNF168,RNF187,FBXW5,CUL4A,RNF114,UBE2L3,TP53,FBXO22,SMURF1,UBE2G2,CCNF,APC,UBE2K,CDK1,UBE2A,BIRC2,UBE4A,SOCS5,CBL,TRIM71,XIAP,UBE2D2,RNF133
GO:BP	proteasome-mediated ubiquitin-	GO:0043161	3.34E-34	446	153	44	FBXL17,FBXL15,HERC2,FBXO31,FBXL18,UBE2D3,BTRC,TRAF4,SPSB1,FBXO38,UBE2C,FBXO6,STUB1,TRIP12,FBXW4,CDC34,UBE2B,CDK2,RNF7,FBXO17,UBE2H,FBXL13,FBXL5,TRIM39,FBXO48,ZNRF1,FBXL4,RNF185,FBXO3,RFPL1,RNF187,FBXW5,CUL4A,FBXO22,SMURF1,UBE2G2,CCNF,APC,UBE2K,CDK1,UBE2A,BIRC2,UBE4A,SOCS5,CBL,TRIM71,XIAP,UBE2D2,RNF133

	dependent protein catabolic process						URF1,UBE2G2,CCNF,APC,UBE2K,UBE2A,BIRC2,UBE4A,SOCS5,TRIM71
GO:BP	proteasomal protein catabolic process	GO:0010498	9.88E-33	515	153	45	FBXL17,FBXL15,HERC2,FBXO31,FBXL18,UBE2D3,BTRC,TRAF4,PRPF19,SPSB1,FBXO38,UBE2C,FBXO6,STUB1,TRIP12,FBXW4,CDC34,UBE2B,CDK2,RNF7,FBXO17,UBE2H,FBXL13,FBXL5,TRIM39,FBXO48,ZNRF1,FBXL4,RNF185,FBXO3,RFPL1,RNF187,FBXW5,CUL4A,FBXO22,SMURF1,UBE2G2,CCNF,APC,UBE2K,UBE2A,BIRC2,UBE4A,SOCS5,TRIM71
GO:BP	organic substance catabolic process	GO:1901575	1.47E-30	2173	153	75	FBXL17,TRIM24,RNF11,UBE2Z,FBXL15,HERC3,HERC2,RNF115,FBXO31,FBXL18,UBE2D3,BTRC,TRAF4,PRPF19,SPSB1,HMGCR,MYLIP,FBXO11,RNF8,UHRF1,FBXO38,RNF6,UBE3C,UBE2C,FBXO6,STUB1,TRIP12,FBXW4,CDC34,UBE2B,CDK2,UBE2D1,RNF7,RNF123,FBXO17,CBLC,UBE2H,PJA1,RBBP6,FBXL13,MAGEC2,FBXL5,TRIM39,CACUL1,RNF43,FBXO48,ZNRF1,FBXL4,RNF185,FBXO3,RFPL1,ZC3HAV1,HERC6,TRAF5,RNF168,RNF187,FBXW5,CUL4A,RNF114,UBE2L3,TP53,FBXO22,SMURF1,UBE2G2,CCNF,APC,UBE2K,UBE2A,BIRC2,UBE4A,SOCS5,CBL,TRIM71,UBE2D2,RNF133
GO:BP	protein K48-linked ubiquitination	GO:0070936	2.88E-24	79	153	21	RNF115,UBE2D3,BTRC,RNF8,FBXO38,RNF6,UBE3C,UBE2C,UBE2T,CDC34,UBE2B,UBE2D1,UBE2H,ZNRF1,RNF187,TRIM6,UBE2G2,UBE2K,UBE2A,BIRC2,UBE2D2
GO:BP	protein autoubiquitination	GO:0051865	1.23E-23	84	153	21	RNF11,RNF115,UBE2D3,RNF8,UHRF1,STUB1,UBE2T,UBE2B,TRIM52,RNF185,RAD18,RNF183,RNF187,TRAF6,RNF181,TRIM68,UBE2A,CBL,TRIM71,UBE2D2,RNF133
GO:BP	SCF-dependent proteasomal ubiquitin-dependent protein catabolic process	GO:0031146	4.11E-20	46	153	16	FBXL17,FBXL15,FBXO31,FBXL18,BTRC,FBXO38,FBXO6,FBXW4,FBXO17,FBXL13,FBXL5,FBXO48,FBXL4,FBXO3,FBXW5,CCNF
GO:BP	nitrogen compound metabolic process	GO:0006807	2.42E-19	12114	153	142	ASB17,PHRF1,DCUN1D1,IRF2BP1,ATG3,PHF19,FBXL17,TRIM24,RNF11,UBE2Z,SOCS2,FBXL15,HERC3,BRPF3,ASB13,HUWE1,HERC2,RNF115,FBXO31,HERC1,FBXL18,UBE2D3,BTRC,ESR1,TRAF4,PRPF19,SPSB1,SOCS3,HMGCR,MYLIP,FBXO11,RNF8,UHRF1,FBXO38,BAZ1B,FBXO30,RNF6,CHD4,UBE3C,UBE2C,TRIM77,FBXO6,NEURL2,HRC,STUB1,FBXO28,BAHD1,UBE2T,PDZRN3,BMI1,TRIP12,TRIM27,FBXW4,CDC34,UBE2B,BIRC3,CDK2,LPXN,UBE2D1,RNF7,ZNF592,RNF123,PHF23,FBXO17,CBLC,UBE2H,PJA1,RBBP6,FBXL13,MAGEC2,RFPL3,FBXL5,TRIM52,TRIM74,DPF2,TRIM39,CACUL1,RNF43,ASB15,UFM1,FBXO48,ZN

							RF1,FBXL4,RNF185,UBOX5,FBXO3,RFPL2,RFPL1,TRIM26,ZC3HAV1,ASB14,TRAF3,FBXW8,ZMYND11,RAD18,RNF113A,HERC6,TRAF5,UNK,RNF183,RNF168,RNF187,FBXW5,TRIM49,FBXO43,TRAF6,TRIM60,KDM5B,CUL4A,RNF114,UBE2L3,TP53,UBE2V2,TRIM33,MARCH8,RNF181,TRIM6,FBXO22,TRIM68,ASB7,SMURF1,UBE2G2,CCNF,APC,UBE2K,AIRE,CDK1,UBE2A,BIRC2,UBE4A,SOCS5,CBL,DZIP3,TRIM75,DCUN1D3,TRIM71,XIAP,TRIM50,ASB16,CCND1,UBE2D2,RNF133
GO:BP	macromolecular metabolic process	GO:0043170	2.22E-18	12326	153	142	ASB17,PHRF1,DCUN1D1,IRF2BP1,ATG3,PHF19,FBXL17,TRIM24,RNF11,UBE2Z,SOCS2,FBXL15,HERC3,BRPF3,ASB13,HUWE1,HERC2,RNF115,FBXO31,HERC1,FBXL18,UBE2D3,BTRC,ESR1,TRAF4,PRPF19,SPSB1,SOCS3,HMGCR,MYLIP,FBXO11,RNF8,UHRF1,FBXO38,BAZ1B,FBXO30,RNF6,CHD4,UBE3C,UBE2C,TRIM77,FBXO6,NEURL2,HRC,STUB1,FBXO28,BAHD1,UBE2T,PDZRN3,BMI1,TRIP12,TRIM27,FBXW4,CDC34,UBE2B,BIRC3,CDK2,LPXN,UBE2D1,RNF7,ZNF592,RNF123,PHF23,FBXO17,CBLC,UBE2H,PJA1,RBBP6,FBXL13,MAGEC2,RFPL3,FBXL5,TRIM52,TRIM74,DPF2,TRIM39,CACUL1,RNF43,ASB15,UFM1,FBXO48,ZNRF1,FBXL4,RNF185,UBOX5,FBXO3,RFPL2,RFPL1,TRIM26,ZC3HAV1,ASB14,TRAF3,FBXW8,ZMYND11,RAD18,RNF113A,HERC6,TRAF5,UNK,RNF183,RNF168,RNF187,FBXW5,TRIM49,FBXO43,TRAF6,TRIM60,KDM5B,CUL4A,RNF114,UBE2L3,TP53,UBE2V2,TRIM33,MARCH8,RNF181,TRIM6,FBXO22,TRIM68,ASB7,SMURF1,UBE2G2,CCNF,APC,UBE2K,AIRE,CDK1,UBE2A,BIRC2,UBE4A,SOCS5,CBL,DZIP3,TRIM75,DCUN1D3,TRIM71,XIAP,TRIM50,ASB16,CCND1,UBE2D2,RNF133
GO:BP	protein K63-linked ubiquitination	GO:0070534	6.88E-17	69	153	16	RNF115,TRAF4,PRPF19,RNF8,STUB1,UBE2T,TRIP12,TRIM27,UBE2B,TRAF3,TRAF5,RNF168,TRAF6,UBE2V2,BIRC2,XIAP
GO:BP	primary metabolic process	GO:0044238	7.04E-17	12666	153	142	ASB17,PHRF1,DCUN1D1,IRF2BP1,ATG3,PHF19,FBXL17,TRIM24,RNF11,UBE2Z,SOCS2,FBXL15,HERC3,BRPF3,ASB13,HUWE1,HERC2,RNF115,FBXO31,HERC1,FBXL18,UBE2D3,BTRC,ESR1,TRAF4,PRPF19,SPSB1,SOCS3,HMGCR,MYLIP,FBXO11,RNF8,UHRF1,FBXO38,BAZ1B,FBXO30,RNF6,CHD4,UBE3C,UBE2C,TRIM77,FBXO6,NEURL2,HRC,STUB1,FBXO28,BAHD1,UBE2T,PDZRN3,BMI1,TRIP12,TRIM27,FBXW4,CDC34,UBE2B,BIRC3,CDK2,LPXN,UBE2D1,RNF7,ZNF592,RNF123,PHF23,FBXO17,CBLC,UBE2H,PJA1,RBBP6,FBXL13,MAGEC2,RFPL3,FBXL5,TRIM52,TRIM74,DPF2,TRIM39,CACUL1,RNF43,ASB15,UFM1,FBXO48,ZNRF1,FBXL4,RNF185,UBOX5,FBXO3,RFPL2,RFPL1,TRIM26,ZC3HAV1,ASB14,TRAF3,FBXW8,ZMYND11,RAD18,RNF113A,HERC6,TRAF5,UNK,RNF183,RNF168,RNF187,FBXW5,TRIM49,FBXO43,TRAF6,TRIM60,KDM5B,CUL4A,RNF114,UBE2L3,TP53,UBE2V2,TRIM33,MARCH8,RNF181,TRIM6,FBXO22,TRIM68,ASB7,SMURF1,UBE2G2,CCNF,APC,UBE2K,AIRE,CDK1,UBE2A,BIRC2,UBE4A,SOCS5,CBL,DZIP3,TRIM75,DCUN1D3,TRIM71,XIAP,TRIM50,ASB16,CCND1,UBE2D2,RNF133
GO:BP	positive	GO:0031398	1.22E-12	123	153	16	DCUN1D1,HUWE1,BTRC,UBE2C,STUB1,BMI1,BIRC3,UBE2D1,PHF23,MAGEC2,TRAF6,UB

	regulation of protein ubiquitination						E2L3,UBE2V2,BIRC2,DCUN1D3,XIAP
GO:BP	organic substance metabolic process	GO:0071704	8.45E-12	13917	153	142	ASB17,PHRF1,DCUN1D1,IRF2BP1,ATG3,PHF19,FBXL17,TRIM24,RNF11,UBE2Z,SOCS2,FBXL15,HERC3,BRPF3,ASB13,HUWE1,HERC2,RNF115,FBXO31,HERC1,FBXL18,UBE2D3,BTRC,ESR1,TRAF4,PRPF19,SPSB1,SOCS3,HMGCR,MYLIP,FBXO11,RNF8,UHRF1,FBXO38,BAZ1B,FBXO30,RNF6,CHD4,UBE3C,UBE2C,TRIM77,FBXO6,NEURL2,HRC,STUB1,FBXO28,BAHD1,UBE2T,PDZRN3,BMI1,TRIP12,TRIM27,FBXW4,CDC34,UBE2B,BIRC3,CDK2,LPXN,UBE2D1,RNF7,ZNF592,RNF123,PHF23,FBXO17,CBLC,UBE2H,PJA1,RBBP6,FBXL13,MAGEC2,RFPL3,FBXL5,TRIM52,TRIM74,DPF2,TRIM39,CACUL1,RNF43,ASB15,UFM1,FBXO48,ZNR1,FBXL4,RNF185,UBOX5,FBXO3,RFPL2,RFPL1,TRIM26,ZC3HAV1,ASB14,TRAF3,FBXW8,ZMYND11,RAD18,RNF113A,HERC6,TRAF5,UNK,RNF183,RNF168,RNF187,FBXW5,TRIM49,FBXO43,TRAF6,TRIM60,KDM5B,CUL4A,RNF114,UBE2L3,TP53,UBE2V2,TRIM33,MARCH8,RNF181,TRIM6,FBXO22,TRIM68,ASB7,SMURF1,UBE2G2,CCNF,APC,UBE2K,AIRE,CDK1,UBE2A,BIRC2,UBE4A,SOCS5,CBL,DZIP3,TRIM75,DCUN1D3,TRIM71,XIAP,TRIM50,ASB16,CCND1,UBE2D2,RNF133
GO:BP	positive regulation of protein modification by small protein conjugation or removal	GO:1903322	1.11E-11	141	153	16	DCUN1D1,HUWE1,BTRC,UBE2C,STUB1,BMI1,BIRC3,UBE2D1,PHF23,MAGEC2,TRAF6,UBE2L3,UBE2V2,BIRC2,DCUN1D3,XIAP
GO:BP	metabolic process	GO:0008152	6.09E-11	14362	153	143	ASB17,PHRF1,DCUN1D1,IRF2BP1,ATG3,PHF19,FBXL17,TRIM24,RNF11,UBE2Z,SOCS2,VPS41,FBXL15,HERC3,BRPF3,ASB13,HUWE1,HERC2,RNF115,FBXO31,HERC1,FBXL18,UBE2D3,BTRC,ESR1,TRAF4,PRPF19,SPSB1,SOCS3,HMGCR,MYLIP,FBXO11,RNF8,UHRF1,FBXO38,BAZ1B,FBXO30,RNF6,CHD4,UBE3C,UBE2C,TRIM77,FBXO6,NEURL2,HRC,STUB1,FBXO28,BAHD1,UBE2T,PDZRN3,BMI1,TRIP12,TRIM27,FBXW4,CDC34,UBE2B,BIRC3,CDK2,LPXN,UBE2D1,RNF7,ZNF592,RNF123,PHF23,FBXO17,CBLC,UBE2H,PJA1,RBBP6,FBXL13,MAGEC2,RFPL3,FBXL5,TRIM52,TRIM74,DPF2,TRIM39,CACUL1,RNF43,ASB15,UFM1,FBXO48,ZNR1,FBXL4,RNF185,UBOX5,FBXO3,RFPL2,RFPL1,TRIM26,ZC3HAV1,ASB14,TRAF3,FBXW8,ZMYND11,RAD18,RNF113A,HERC6,TRAF5,UNK,RNF183,RNF168,RNF187,FBXW5,TRIM49,FBXO43,TRAF6,TRIM60,KDM5B,CUL4A,RNF114,UBE2L3,TP53,UBE2V2,TRIM33,MARCH8,RNF181,TRIM6,FBXO22,TRIM68,ASB7,SMURF1,UBE2G2,CCNF,APC,UBE2K,AIRE,CDK1,UBE2A,BIRC2,UBE4A,SOCS5,CBL,DZIP3,TRIM75,DCUN1D3,TRIM71,XIAP,TRIM50,ASB16,CCND1,UBE2D2,RNF133

GO:BP	positive regulation of post-translational protein modification	GO:1901875	9.03E-11	191	153	17	DCUN1D1,HUWE1,BTRC,BAZ1B,UBE2C,STUB1,BMI1,BIRC3,UBE2D1,PHF23,MAGEC2,TRAF6,UBE2L3,UBE2V2,BIRC2,DCUN1D3,XIAP
GO:BP	DNA damage response	GO:0006974	5.20E-10	890	153	31	HUWE1,HERC2,FBXO31,UBE2D3,PRPF19,RNF8,UHRF1,BAZ1B,CHD4,FBXO6,STUB1,UBE2T,TRIP12,UBE2B,CDK2,RBBP6,DPF2,TRIM39,RAD18,RNF113A,RNF168,TRAF6,CUL4A,TP53,UBE2V2,APC,CDK1,UBE2A,CBL,XIAP,CCND1
GO:BP	regulation of protein ubiquitination	GO:0031396	6.33E-10	215	153	17	DCUN1D1,HUWE1,BTRC,UBE2C,STUB1,BMI1,TRIP12,BIRC3,UBE2D1,PHF23,MAGEC2,TRAF6,UBE2L3,UBE2V2,BIRC2,DCUN1D3,XIAP
GO:BP	regulation of canonical NF-kappaB signal transduction	GO:0043122	1.21E-09	260	153	18	BTRC,ESR1,TRAF4,BIRC3,RFPL3,TRIM52,TRIM39,RFPL2,RFPL1,ZC3HAV1,TRAF3,ZMYND11,TRAF5,TRAF6,TRIM6,TRIM68,BIRC2,XIAP
GO:BP	cellular response to stress	GO:0033554	1.37E-09	1925	153	45	VPS41,HUWE1,HERC2,FBXO31,UBE2D3,TRAF4,PRPF19,RNF8,UHRF1,BAZ1B,CHD4,FBXO6,STUB1,UBE2T,TRIP12,UBE2B,CDK2,FBXO17,RBBP6,DPF2,TRIM39,UFM1,RNF185,TRAF3,ZMYND11,RAD18,RNF113A,TRAF5,RNF183,RNF168,TRAF6,MID1,CUL4A,TP53,UBE2V2,FBXO22,UBE2G2,APC,CDK1,UBE2A,UBE4A,SOCS5,CBL,XIAP,CCND1
GO:BP	regulation of post-translational protein modification	GO:1901873	7.36E-09	331	153	19	DCUN1D1,HUWE1,BTRC,BAZ1B,UBE2C,STUB1,BMI1,TRIP12,UBE2B,BIRC3,UBE2D1,PHF23,MAGEC2,TRAF6,UBE2L3,UBE2V2,BIRC2,DCUN1D3,XIAP
GO:BP	regulation of protein modification by small protein conjugation or removal	GO:1903320	9.38E-09	254	153	17	DCUN1D1,HUWE1,BTRC,UBE2C,STUB1,BMI1,TRIP12,BIRC3,UBE2D1,PHF23,MAGEC2,TRAF6,UBE2L3,UBE2V2,BIRC2,DCUN1D3,XIAP
GO:BP	canonical NF-kappaB signal transduction	GO:0007249	9.59E-09	294	153	18	BTRC,ESR1,TRAF4,BIRC3,RFPL3,TRIM52,TRIM39,RFPL2,RFPL1,ZC3HAV1,TRAF3,ZMYND11,TRAF5,TRAF6,TRIM6,TRIM68,BIRC2,XIAP

GO:BP	regulation of protein metabolic process	GO:0051246	1.18E-08	2389	153	49	DCUN1D1,HUWE1,BTRC,TRAF4,SOCS3,HMGCR,MYLIP,UHRF1,BAZ1B,UBE2C,HRC,STUB1,BMI1,TRIP12,TRIM27,UBE2B,BIRC3,CDK2,UBE2D1,ZNF592,PHF23,CBLC,MAGEC2,FBXL5,TRIM39,CACUL1,RNF185,RFPL1,TRAF3,UNK,TRAF6,CUL4A,UBE2L3,TP53,UBE2V2,TRIM6,FBXO22,SMURF1,CCNF,APC,UBE2K,AIRE,BIRC2,SOCS5,CBL,DCUN1D3,TRIM71,XIAP,CCND1
GO:BP	regulation of protein modification process	GO:0031399	1.12E-07	1385	153	35	DCUN1D1,HUWE1,BTRC,TRAF4,SOCS3,HMGCR,BAZ1B,UBE2C,HRC,STUB1,BMI1,TRIP12,TRIM27,UBE2B,BIRC3,UBE2D1,ZNF592,PHF23,CBLC,MAGEC2,CACUL1,TRAF6,UBE2L3,TP53,UBE2V2,TRIM6,CCNF,APC,UBE2K,BIRC2,SOCS5,CBL,DCUN1D3,XIAP,CCND1
GO:BP	positive regulation of ubiquitin-protein transferase activity	GO:0051443	2.34E-07	35	153	8	DCUN1D1,BTRC,UBE2C,STUB1,BMI1,MAGEC2,UBE2L3,DCUN1D3
GO:BP	regulation of signal transduction	GO:0009966	8.02E-07	2973	153	52	SCEL,FBXL17,TRIM24,SOCS2,FBXL15,RNF115,UBE2D3,BTRC,ESR1,TRAF4,SOCS3,HMGCR,RNF6,STUB1,BMI1,CDC34,UBE2B,BIRC3,LPXN,UBE2D1,ZNF592,CBLC,RFPL3,TRIM52,TRIM39,RNF43,UFM1,RNF185,RFPL2,RFPL1,ZC3HAV1,TRAF3,ZMYND11,RNF113A,TRAF5,RNF183,TRAF6,TRIM60,MID1,CUL4A,TP53,TRIM33,TRIM6,LGR6,TRIM68,SMURF1,APC,UBE2K,BIRC2,SOCS5,CBL,XIAP
GO:BP	DNA repair	GO:0006281	8.84E-07	602	153	22	HUWE1,HERC2,UBE2D3,PRPF19,RNF8,UHRF1,CHD4,FBXO6,STUB1,UBE2T,TRIP12,UBE2B,CDK2,DPF2,RAD18,RNF113A,RNF168,CUL4A,TP53,UBE2V2,CDK1,UBE2A
GO:BP	intracellular signal transduction	GO:0035556	9.33E-07	2609	153	48	ASB17,TRIM24,SOCS2,ASB13,FBXO31,BTRC,ESR1,TRAF4,PRPF19,SOCS3,HMGCR,RNF8,FBXO6,NEURL2,HRC,CDC34,UBE2B,BIRC3,CDK2,CBLC,RFPL3,TRIM52,TRIM39,ASB15,RFPL2,RFPL1,ZC3HAV1,ASB14,TRAF3,ZMYND11,TRAF5,RNF183,TRAF6,TRIM60,MID1,CUL4A,TP53,TRIM6,TRIM68,ASB7,APC,CDK1,BIRC2,SOCS5,CBL,XIAP,ASB16,CCND1
GO:BP	cell cycle phase transition	GO:0044770	1.07054E-06	551	153	21	FBXL15,FBXO31,PRPF19,UBE2C,FBXO6,CDC34,CDK2,DPF2,TRIM39,CACUL1,RFPL1,CUL4A,UBE2L3,TP53,CCNF,APC,CDK1,UBE2A,DCUN1D3,TRIM71,CCND1
GO:BP	response to stress	GO:0006950	1.20677E-06	3909	153	61	VPS41,HUWE1,HERC2,FBXO31,UBE2D3,ESR1,TRAF4,PRPF19,SOCS3,RNF8,UHRF1,BAZ1B,CHD4,TRIM77,FBXO6,STUB1,UBE2T,TRIP12,TRIM27,UBE2B,BIRC3,CDK2,FBXO17,RBBP6,RFPL3,TRIM52,DPF2,TRIM39,UFM1,RNF185,RFPL2,RFPL1,TRIM26,ZC3HAV1,TRAF3,ZMYND11,RAD18,RNF113A,TRAF5,RNF183,RNF168,TRIM49,TRAF6,MID1,CUL4A,TP53,UBE2V2,TRIM6,FBXO22,TRIM68,UBE2G2,APC,UBE2K,CDK1,UBE2A,BIRC2,UBE4A,SOCS5,CBL,XIAP,CCND1

GO:BP	cellular response to stimulus	GO:0051716	1.32386E-06	7399	153	91	ASB17,SCEL,FBXL17,TRIM24,SOCS2,VPS41,FBXL15,ASB13,HUWE1,HERC2,RNF115,FBXO31,UBE2D3,BTRC,ESR1,TRAF4,PRPF19,SOCS3,HMGCR,RNF8,UHRF1,BAZ1B,RNF6,CHD4,FBXO6,NEURL2,HRC,STUB1,UBE2T,BMI1,TRIP12,FBXW4,CDC34,UBE2B,BIRC3,CDK2,LPXN,UBE2D1,ZNF592,FBXO17,CBLC,RBBP6,RFPL3,TRIM52,DPF2,TRIM39,RNF43,ASB15,UFM1,RNF185,RFPL2,RFPL1,ZC3HAV1,ASB14,TRAF3,ZMYND11,RAD18,RNF113A,TRAF5,RNF183,RNF168,TRAF6,TRIM60,MID1,KDM5B,CUL4A,UBE2L3,TP53,UBE2V2,TRIM33,TRIM6,FBXO22,LGR6,TRIM68,ASB7,SMURF1,UBE2G2,APC,UBE2K,CDK1,UBE2A,BIRC2,UBE4A,SOCS5,CBL,TRIM71,XIAP,ASB16,TNFRSF25,CCND1,PRICKLE2
GO:BP	positive regulation of protein metabolic process	GO:0051247	1.63076E-06	1374	153	33	DCUN1D1,HUWE1,BTRC,TRAF4,MYLIP,UHRF1,BAZ1B,UBE2C,STUB1,BMI1,BIRC3,UBE2D1,PHF23,MAGEC2,FBXL5,CACUL1,RNF185,RFPL1,TRAF6,CUL4A,UBE2L3,TP53,UBE2V2,TRIM6,FBXO22,SMURF1,APC,UBE2K,BIRC2,SOCS5,DCUN1D3,XIAP,CCND1
GO:BP	response to stimulus	GO:0050896	2.73683E-06	8955	153	102	ASB17,SCEL,FBXL17,TRIM24,SOCS2,VPS41,FBXL15,ASB13,HUWE1,HERC2,RNF115,FBXO31,UBE2D3,BTRC,ESR1,TRAF4,PRPF19,SOCS3,HMGCR,RNF8,UHRF1,FBXO38,BAZ1B,RNF6,CHD4,TRIM77,FBXO6,NEURL2,HRC,STUB1,UBE2T,BMI1,TRIP12,TRIM27,FBXW4,CDC34,UBE2B,BIRC3,CDK2,LPXN,UBE2D1,RNF7,ZNF592,FBXO17,CBLC,RBBP6,RFPL3,TRIM52,DPF2,TRIM39,RNF43,ASB15,UFM1,RNF185,FBXO3,RFPL2,RFPL1,TRIM26,ZC3HAV1,ASB14,TRAF3,ZMYND11,RAD18,RNF113A,HERC6,TRAF5,RNF183,RNF168,TRIM49,TRAF6,TRIM60,MID1,KDM5B,CUL4A,UBE2L3,TP53,UBE2V2,TRIM33,MARCH8,TRIM6,FBXO22,LGR6,TRIM68,ASB7,SMURF1,UBE2G2,APC,UBE2K,AIRE,CDK1,UBE2A,BIRC2,UBE4A,SOCS5,CBL,DCUN1D3,TRIM71,XIAP,ASB16,TNFRSF25,CCND1,PRICKLE2
GO:BP	protein K11-linked ubiquitination	GO:0070979	2.98857E-06	30	153	7	UBE2D3,UBE2C,UBE2T,UBE2B,UBE2H,UBE2L3,UBE2A
GO:BP	histone ubiquitination	GO:0016574	3.83678E-06	31	153	7	RNF8,UHRF1,BMI1,TRIP12,UBE2B,RNF168,UBE2A
GO:BP	regulation of nitrogen compound metabolic process	GO:0051171	4.22341E-06	5587	153	75	DCUN1D1,IRF2BP1,PHF19,TRIM24,BRPF3,HUWE1,UBE2D3,BTRC,ESR1,TRAF4,PRPF19,SOCS3,HMGCR,MYLIP,RNF8,UHRF1,BAZ1B,RNF6,CHD4,UBE2C,HRC,STUB1,BAHD1,BMI1,TRIP12,TRIM27,UBE2B,BIRC3,CDK2,UBE2D1,ZNF592,PHF23,CBLC,RBBP6,MAGEC2,RFPL3,FBXL5,TRIM52,DPF2,TRIM39,CACUL1,RNF185,RFPL2,RFPL1,TRIM26,ZC3HAV1,TRAF3,ZMYND11,TRAF5,UNK,RNF168,RNF187,TRAF6,KDM5B,CUL4A,UBE2L3,TP53,UBE2V2,TRIM33,TRIM6,FBXO22,TRIM68,SMURF1,CCNF,APC,UBE2K,AIRE,CDK1,BIRC2,SOCS5,CBL,DCUN1D3,TRIM71,XIAP,CCND1

GO:BP	protein monoubiquitination	GO:0006513	4.67249E-06	72	153	9	HUWE1,UBE2D3,UHRF1,STUB1,UBE2T,BMI1,RAD18,BIRC2,CBL
GO:BP	positive regulation of nitrogen compound metabolic process	GO:0051173	7.85626E-06	3071	153	51	DCUN1D1,TRIM24,BRPF3,HUWE1,BTRC,ESR1,TRAF4,PRPF19,MYLIP,RNF8,UHRF1,BAZ1B,RNF6,CHD4,UBE2C,STUB1,BMI1,TRIM27,UBE2B,BIRC3,CDK2,UBE2D1,PHF23,MAGEC2,FBXL5,TRIM52,DPF2,CACUL1,RNF185,RFPL1,ZC3HAV1,RNF168,RNF187,TRAF6,CUL4A,UBE2L3,TP53,UBE2V2,TRIM6,FBXO22,SMURF1,APC,UBE2K,AIRE,CDK1,BIRC2,SOCS5,DCUN1D3,TRIM71,XIAP,CCND1
GO:BP	mitotic cell cycle phase transition	GO:0044772	8.45961E-06	447	153	18	FBXL15,FBXO31,UBE2C,CDC34,CDK2,DPF2,TRIM39,CACUL1,RFPL1,CUL4A,TP53,CCNF,APC,CDK1,UBE2A,DCUN1D3,TRIM71,CCND1
GO:BP	negative regulation of cell cycle process	GO:0010948	9.53119E-06	299	153	15	FBXO31,PRPF19,BAZ1B,FBXO6,CDK2,TRIM39,RFPL1,FBXO43,CUL4A,TP53,CCNF,APC,CDK1,DCUN1D3,CCND1
GO:BP	regulation of response to stimulus	GO:0048583	1.01406E-05	3909	153	59	SCEL,FBXL17,TRIM24,SOCS2,FBXL15,RNF115,UBE2D3,BTRC,ESR1,TRAF4,SOCS3,HMGR,RNF8,FBXO38,RNF6,STUB1,BMI1,TRIP12,TRIM27,CDC34,UBE2B,BIRC3,LPXN,UBE2D1,ZNF592,CBLC,RFPL3,TRIM52,DPF2,TRIM39,RNF43,UFM1,RNF185,RFPL2,RFPL1,ZC3HAV1,TRAF3,ZMYND11,RNF113A,TRAF5,RNF183,RNF168,TRAF6,TRIM60,MID1,CUL4A,TP53,UBE2V2,TRIM33,TRIM6,LGR6,TRIM68,SMURF1,APC,UBE2K,BIRC2,SOCS5,CBL,XIAP
GO:BP	regulation of cell communication	GO:0010646	1.14776E-05	3405	153	54	SCEL,FBXL17,TRIM24,SOCS2,FBXL15,RNF115,UBE2D3,BTRC,ESR1,TRAF4,SOCS3,HMGR,RNF6,HRC,STUB1,BMI1,CDC34,UBE2B,BIRC3,LPXN,UBE2D1,ZNF592,CBLC,RFPL3,TRIM52,TRIM39,RNF43,UFM1,RNF185,RFPL2,RFPL1,ZC3HAV1,TRAF3,ZMYND11,RNF113A,TRAF5,RNF183,TRAF6,TRIM60,MID1,KDM5B,CUL4A,TP53,TRIM33,TRIM6,LGR6,TRIM68,SMURF1,APC,UBE2K,BIRC2,SOCS5,CBL,XIAP
GO:BP	tumor necrosis factor-mediated signaling pathway	GO:0033209	1.17149E-05	108	153	10	TRAF4,BIRC3,TRAF3,TRAF5,TRAF6,TP53,UBE2K,BIRC2,XIAP,TNFRSF25
GO:BP	regulation of ubiquitin-protein transferase	GO:0051438	1.65472E-05	58	153	8	DCUN1D1,BTRC,UBE2C,STUB1,BMI1,MAGEC2,UBE2L3,DCUN1D3

	activity						
GO:BP	regulation of primary metabolic process	GO:0080090	1.87985E-05	5766	153	75	DCUN1D1,IRF2BP1,PHF19,TRIM24,BRPF3,HUWE1,UBE2D3,BTRC,ESR1,TRAF4,PRPF19,SOCS3,HMGCR,MYLIP,RNF8,UHRF1,BAZ1B,RNF6,CHD4,UBE2C,HRC,STUB1,BAHD1,BMI1,TRIP12,TRIM27,UBE2B,BIRC3,CDK2,UBE2D1,ZNF592,PHF23,CBLC,RBBP6,MAGEC2,RFPL3,FBXL5,TRIM52,DPF2,TRIM39,CACUL1,RNF185,RFPL2,RFPL1,TRIM26,ZC3HAV1,TRAF3,ZMYND11,TRAF5,UNK,RNF168,RNF187,TRAF6,KDM5B,CUL4A,UBE2L3,TP53,UBE2V2,TRIM33,TRIM6,FBXO22,TRIM68,SMURF1,CCNF,APC,UBE2K,AIRE,CDK1,BIRC2,SOCS5,CBL,DCUN1D3,TRIM71,XIAP,CCND1
GO:BP	positive regulation of macromolecule metabolic process	GO:0010604	2.5694E-05	3483	153	54	DCUN1D1,TRIM24,BRPF3,HUWE1,BTRC,ESR1,TRAF4,PRPF19,MYLIP,RNF8,UHRF1,BAZ1B,RNF6,CHD4,UBE2C,STUB1,BMI1,TRIM27,UBE2B,BIRC3,CDK2,UBE2D1,PHF23,MAGEC2,FBXL5,TRIM52,DPF2,CACUL1,RNF185,RFPL1,ZC3HAV1,TRAF3,TRAF5,RNF168,RNF187,TRAF6,KDM5B,CUL4A,UBE2L3,TP53,UBE2V2,TRIM6,FBXO22,SMURF1,APC,UBE2K,AIRE,CDK1,BIRC2,SOCS5,DCUN1D3,TRIM71,XIAP,CCND1
GO:BP	positive regulation of metabolic process	GO:0009893	2.64739E-05	3797	153	57	DCUN1D1,TRIM24,BRPF3,HUWE1,BTRC,ESR1,TRAF4,PRPF19,MYLIP,RNF8,UHRF1,BAZ1B,RNF6,CHD4,UBE2C,STUB1,BMI1,TRIM27,UBE2B,BIRC3,CDK2,UBE2D1,PHF23,MAGEC2,RFPL3,FBXL5,TRIM52,DPF2,CACUL1,RNF185,RFPL2,RFPL1,ZC3HAV1,TRAF3,TRAF5,RNF168,RNF187,TRAF6,KDM5B,CUL4A,UBE2L3,TP53,UBE2V2,TRIM6,FBXO22,TRIM68,SMURF1,APC,UBE2K,AIRE,CDK1,BIRC2,SOCS5,DCUN1D3,TRIM71,XIAP,CCND1
GO:BP	regulation of signaling	GO:0023051	2.99689E-05	3396	153	53	SCEL,FBXL17,TRIM24,SOCS2,FBXL15,RNF115,UBE2D3,BTRC,ESR1,TRAF4,SOCS3,HMGCR,RNF6,STUB1,BMI1,CDC34,UBE2B,BIRC3,LPXN,UBE2D1,ZNF592,CBLC,RFPL3,TRIM52,TRIM39,RNF43,UFM1,RNF185,RFPL2,RFPL1,ZC3HAV1,TRAF3,ZMYND11,RNF113A,TRAF5,RNF183,TRAF6,TRIM60,MID1,KDM5B,CUL4A,TP53,TRIM33,TRIM6,LGR6,TRIM68,SMURF1,APC,UBE2K,BIRC2,SOCS5,CBL,XIAP
GO:BP	regulation of catabolic process	GO:0009894	3.52375E-05	1013	153	26	HERC1,BTRC,HMGCR,MYLIP,STUB1,TRIM27,CDK2,PHF23,RFPL3,FBXL5,TRIM39,RNF185,RFPL2,RFPL1,ZC3HAV1,TRAF5,CUL4A,TP53,TRIM6,FBXO22,TRIM68,SMURF1,APC,UBE2K,SOCS5,TRIM71
GO:BP	positive regulation of canonical NF-kappaB signal transduction	GO:0043123	3.66328E-05	195	153	12	BIRC3,RFPL3,TRIM52,RFPL2,RFPL1,ZC3HAV1,TRAF5,TRAF6,TRIM6,TRIM68,BIRC2,XIAP
GO:BP	negative regulation of cellular	GO:0048523	4.12131E-05	5511	153	72	IRF2BP1,ATG3,PHF19,TRIM24,UBE2Z,SOCS2,HUWE1,RNF115,FBXO31,HERC1,UBE2D3,BTRC,ESR1,PRPF19,SOCS3,HMGCR,MYLIP,RNF8,UHRF1,BAZ1B,RNF6,CHD4,FBXO6,HRC,STUB1,BAHD1,BMI1,TRIP12,TRIM27,CDC34,UBE2B,BIRC3,CDK2,LPXN,UBE2D1,ZNF592,

	process						PHF23,CBLC,MAGEC2,DPF2,TRIM39,RNF43,UFM1,RFPL1,ZC3HAV1,ZMYND11,RNF113A,TRAF5,UNK,RNF168,FBXO43,TRAF6,TRIM60,TRIM46,MID1,KDM5B,CUL4A,TP53,TRIM33,TRIM6,SMURF1,UBE2G2,CCNF,APC,CDK1,BIRC2,SOCS5,CBL,DCUN1D3,TRIM71,XIAP,CCND1
GO:BP	mitotic cell cycle process	GO:1903047	5.73508E-05	757	153	22	FBXL15,FBXO31,BAZ1B,UBE2C,CDC34,CDK2,DPF2,TRIM39,CACUL1,RFPL1,TRIM36,FBXW5,FBXO43,CUL4A,TP53,CCNF,APC,CDK1,UBE2A,DCUN1D3,TRIM71,CCND1
GO:BP	DNA metabolic process	GO:0006259	5.8652E-05	1039	153	26	BRPF3,HUWE1,HERC2,UBE2D3,PRPF19,RNF8,UHRF1,CHD4,FBXO6,STUB1,UBE2T,BMI1,TRIP12,CDC34,UBE2B,CDK2,RBBP6,DPF2,RAD18,RNF113A,RNF168,CUL4A,TP53,UBE2V2,CDK1,UBE2A
GO:BP	cell cycle	GO:0007049	0.000122539	1811	153	35	FBXL15,FBXO31,BTRC,PRPF19,RNF8,UHRF1,BAZ1B,UBE2C,FBXO6,CDC34,UBE2B,BIRC3,CDK2,DPF2,TRIM39,CACUL1,RFPL1,TRIM36,ZMYND11,RAD18,FBXW5,FBXO43,CUL4A,UBE2L3,TP53,CCNF,APC,CDK1,UBE2A,BIRC2,TRIM75,DCUN1D3,TRIM71,XIAP,CCND1
GO:BP	positive regulation of biological process	GO:0048518	0.000127424	6253	153	77	DCUN1D1,SCEL,TRIM24,UBE2Z,SOCS2,FBXL15,BRPF3,HUWE1,UBE2D3,BTRC,ESR1,TRAF4,PRPF19,SOCS3,HMGCR,MYLIP,RNF8,UHRF1,FBXO38,BAZ1B,RNF6,CHD4,UBE2C,HR23,STUB1,BMI1,TRIM27,FBXW4,CDC34,UBE2B,BIRC3,CDK2,LPXN,UBE2D1,PHF23,MAGEC2,RFPL3,FBXL5,TRIM52,DPF2,TRIM39,CACUL1,RNF185,RFPL2,RFPL1,ZC3HAV1,TRAF3,FBXW8,RAD18,TRAF5,RNF183,RNF168,RNF187,TRAF6,TRIM46,MID1,KDM5B,CUL4A,UBE2L3,TP53,UBE2V2,TRIM6,FBXO22,LGR6,TRIM68,SMURF1,APC,UBE2K,AIRE,CDK1,BIRC2,SOCS5,CBL,DCUN1D3,TRIM71,XIAP,CCND1
GO:BP	positive regulation of protein modification process	GO:0031401	0.000227469	890	153	23	DCUN1D1,HUWE1,BTRC,TRAF4,BAZ1B,UBE2C,STUB1,BMI1,BIRC3,UBE2D1,PHF23,MAGEC2,CACUL1,TRAF6,UBE2L3,TP53,UBE2V2,TRIM6,UBE2K,BIRC2,DCUN1D3,XIAP,CCND1
GO:BP	cell cycle process	GO:0022402	0.000243232	1273	153	28	FBXL15,FBXO31,PRPF19,BAZ1B,UBE2C,FBXO6,CDC34,UBE2B,CDK2,DPF2,TRIM39,CACUL1,RFPL1,TRIM36,RAD18,FBXW5,FBXO43,CUL4A,UBE2L3,TP53,CCNF,APC,CDK1,UBE2A,TRIM75,DCUN1D3,TRIM71,CCND1
GO:BP	negative regulation of cell cycle	GO:0045786	0.000251041	383	153	15	FBXO31,PRPF19,BAZ1B,FBXO6,CDK2,TRIM39,RFPL1,FBXO43,CUL4A,TP53,CCNF,APC,CDK1,DCUN1D3,CCND1
GO:BP	negative regulation of biological process	GO:0048519	0.000361988	5913	153	73	IRF2BP1,ATG3,PHF19,TRIM24,UBE2Z,SOCS2,HUWE1,RNF115,FBXO31,HERC1,UBE2D3,BTRC,ESR1,PRPF19,SOCS3,HMGCR,MYLIP,RNF8,UHRF1,BAZ1B,RNF6,CHD4,FBXO6,HRC,STUB1,BAHD1,BMI1,TRIP12,TRIM27,CDC34,UBE2B,BIRC3,CDK2,LPXN,UBE2D1,ZNF592,PHF23,CBLC,MAGEC2,DPF2,TRIM39,RNF43,UFM1,RFPL1,TRIM26,ZC3HAV1,ZMYND11,R

							NF113A,TRAF5,UNK,RNF168,FBXO43,TRAF6,TRIM60,TRIM46,MID1,KDM5B,CUL4A,TP53,TRIM33,TRIM6,SMURF1,UBE2G2,CCNF,APC,CDK1,BIRC2,SOCS5,CBL,DCUN1D3,TRIM71,XIAP,CCND1
GO:BP	chromatin organization	GO:0006325	0.000514262	788	153	21	PHF19,BRPF3,HUWE1,ESR1,RNF8,UHRF1,BAZ1B,CHD4,BAHD1,BMI1,TRIP12,TRIM27,UBE2B,CDK2,DPF2,ZMYND11,RNF168,KDM5B,TP53,CDK1,UBE2A
GO:BP	regulation of cell cycle process	GO:0010564	0.000539903	721	153	20	FBXO31,PRPF19,BAZ1B,UBE2C,FBXO6,UBE2B,CDK2,DPF2,TRIM39,RFPL1,RAD18,FBXW5,FBXO43,CUL4A,TP53,CCNF,APC,CDK1,DCUN1D3,CCND1
GO:BP	chromatin remodeling	GO:0006338	0.000557212	655	153	19	PHF19,BRPF3,HUWE1,ESR1,RNF8,UHRF1,BAZ1B,CHD4,BAHD1,BMI1,TRIP12,TRIM27,CDK2,DPF2,RNF168,KDM5B,TP53,CDK1,UBE2A
GO:BP	DNA damage checkpoint signaling	GO:0000077	0.000740454	128	153	9	FBXO31,PRPF19,FBXO6,CDK2,TRIM39,CUL4A,TP53,CDK1,CCND1
GO:BP	negative regulation of cell cycle phase transition	GO:1901988	0.000744489	257	153	12	FBXO31,PRPF19,FBXO6,CDK2,TRIM39,RFPL1,CUL4A,TP53,APC,CDK1,DCUN1D3,CCND1
GO:BP	cell cycle G1/S phase transition	GO:0044843	0.000744489	257	153	12	FBXO31,CDC34,CDK2,DPF2,TRIM39,CACUL1,CUL4A,TP53,APC,DCUN1D3,TRIM71,CCND1
GO:BP	negative regulation of signal transduction	GO:0009968	0.000800611	1268	153	27	SOCS2,RNF115,UBE2D3,BTRC,ESR1,SOCS3,HMGCR,STUB1,BMI1,CDC34,UBE2B,LPXN,UBE2D1,ZNF592,CBLC,TRIM39,RNF43,ZMYND11,RNF113A,TRIM60,TP53,TRIM33,SMURF1,APC,SOCS5,CBL,XIAP
GO:BP	regulation of protein catabolic process	GO:0042176	0.000804344	363	153	14	BTRC,HMGCR,MYLIP,STUB1,CDK2,FBXL5,TRIM39,RNF185,RFPL1,CUL4A,FBXO22,APC,UBE2K,SOCS5
GO:BP	regulation of cell cycle	GO:0051726	0.000843553	1112	153	25	FBXO31,BTRC,PRPF19,BAZ1B,UBE2C,FBXO6,UBE2B,BIRC3,CDK2,DPF2,TRIM39,RFPL1,TRIM36,RAD18,FBXW5,FBXO43,CUL4A,TP53,CCNF,APC,CDK1,BIRC2,DCUN1D3,XIAP,CCND1

GO:BP	signal transduction	GO:0007165	0.000935957	5926	153	72	ASB17,SCEL,FBXL17,TRIM24,SOCS2,FBXL15,ASB13,RNF115,FBXO31,UBE2D3,BTRC,ESR1,TRAF4,PRPF19,SOCS3,HMGCR,RNF8,RNF6,FBXO6,NEURL2,HRC,STUB1,BMI1,FBXW4,CDC34,UBE2B,BIRC3,CDK2,LPXN,UBE2D1,ZNF592,CBLC,RFPL3,TRIM52,DPF2,TRIM39,RNF43,ASB15,UFM1,RNF185,RFPL2,RFPL1,ZC3HAV1,ASB14,TRAF3,ZMYND11,RNF113A,TRAF5,RNF183,TRAF6,TRIM60,MID1,CUL4A,TP53,TRIM33,TRIM6,LGR6,TRIM68,ASB7,SMURF1,APC,UBE2K,CDK1,BIRC2,SOCS5,CBL,TRIM71,XIAP,ASB16,TNFRSF25,CCND1,PRICKLE2
GO:BP	histone H2A ubiquitination	GO:0033522	0.001036729	23	153	5	RNF8,BMI1,TRIP12,RNF168,UBE2A
GO:BP	mitotic cell cycle	GO:0000278	0.001305901	908	153	22	FBXL15,FBXO31,BAZ1B,UBE2C,CDC34,CDK2,DPF2,TRIM39,CACUL1,RFPL1,TRIM36,FBXW5,FBXO43,CUL4A,TP53,CCNF,APC,CDK1,UBE2A,DCUN1D3,TRIM71,CCND1
GO:BP	DNA integrity checkpoint signaling	GO:0031570	0.001316298	137	153	9	FBXO31,PRPF19,FBXO6,CDK2,TRIM39,CUL4A,TP53,CDK1,CCND1
GO:BP	autophagy	GO:0006914	0.001711975	571	153	17	ATG3,VPS41,HUWE1,HERC1,STUB1,TRIM27,PHF23,RFPL3,UFM1,FBXL4,RNF185,RFPL2,RFPL1,TP53,TRIM6,TRIM68,SMURF1
GO:BP	process utilizing autophagic mechanism	GO:0061919	0.001711975	571	153	17	ATG3,VPS41,HUWE1,HERC1,STUB1,TRIM27,PHF23,RFPL3,UFM1,FBXL4,RNF185,RFPL2,RFPL1,TP53,TRIM6,TRIM68,SMURF1
GO:BP	G1/S transition of mitotic cell cycle	GO:0000082	0.001740357	229	153	11	FBXO31,CDC34,CDK2,DPF2,CACUL1,CUL4A,TP53,APC,DCUN1D3,TRIM71,CCND1
GO:BP	regulation of cellular process	GO:0050794	0.002582906	11758	153	114	ASB17,IRF2BP1,ATG3,SCEL,PHF19,FBXL17,TRIM24,UBE2Z,SOCS2,VPS41,FBXL15,BRPF3,ASB13,HUWE1,RNF115,FBXO31,HERC1,UBE2D3,BTRC,ESR1,TRAF4,PRPF19,SOCS3,HMGCR,MYLIP,FBXO11,RNF8,UHRF1,FBXO38,BAZ1B,RNF6,CHD4,UBE2C,TRIM77,FBXO6,NEURL2,HRC,STUB1,BAHD1,BMI1,TRIP12,TRIM27,FBXW4,CDC34,UBE2B,BIRC3,CDK2,LPXN,UBE2D1,ZNF592,PHF23,CBLC,RBBP6,MAGEC2,RFPL3,TRIM52,DPF2,TRIM39,CACUL1,RNF43,ASB15,UFM1,RNF185,RFPL2,RFPL1,TRIM26,TRIM36,ZC3HAV1,ASB14,TRAF3,FBXW8,ZMYND11,RAD18,RNF113A,TRAF5,UNK,RNF183,RNF168,RNF187,FBXW5,TRIM49,FBXO43,TRAF6,TRIM60,TRIM46,MID1,KDM5B,CUL4A,UBE2L3,TP53,UBE2V2,TRIM33,TRIM6,FBXO22,LGR6,TRIM68,ASB7,SMURF1,UBE2G2,CCNF,APC,UBE2K,AIRE,CDK1,BIRC2,SOCS5,CBL,DCUN1D3,TRIM71,XIAP,ASB16,TNFRSF25,CCND1,PRICKLE2

GO:BP	cell cycle checkpoint signaling	GO:0000075	0.002784739	193	153	10	FBXO31,PRPF19,FBXO6,CDK2,TRIM39,CUL4A,TP53,APC,CDK1,CCND1
GO:BP	negative regulation of nitrogen compound metabolic process	GO:0051172	0.002878667	2353	153	38	IRF2BP1,PHF19,TRIM24,UBE2D3,BTRC,ESR1,SOCS3,HMGCR,RNF8,UHRF1,CHD4,BAHD1,BMI1,TRIP12,TRIM27,UBE2B,CDK2,UBE2D1,CBLC,MAGEC2,DPF2,TRIM39,ZMYND11,TRAF5,UNK,RNF168,TRAF6,KDM5B,TP53,TRIM33,TRIM6,APC,SOCS5,CBL,DCUN1D3,TRIM71,XIAP,CCND1
GO:BP	positive regulation of catabolic process	GO:0009896	0.002900685	528	153	16	MYLIP,STUB1,RFPL3,FBXL5,RNF185,RFPL2,RFPL1,ZC3HAV1,CUL4A,TRIM6,FBXO22,TRIM68,SMURF1,APC,SOCS5,TRIM71
GO:BP	signal transduction in response to DNA damage	GO:0042770	0.002917953	194	153	10	FBXO31,PRPF19,RNF8,FBXO6,CDK2,TRIM39,CUL4A,TP53,CDK1,CCND1
GO:BP	regulation of viral entry into host cell	GO:0046596	0.002944403	50	153	6	RFPL3,RFPL2,RFPL1,TRIM26,TRIM6,TRIM68
GO:BP	protein-DNA complex organization	GO:0071824	0.003334055	885	153	21	PHF19,BRPF3,HUWE1,ESR1,RNF8,UHRF1,BAZ1B,CHD4,BAHD1,BMI1,TRIP12,TRIM27,UBE2B,CDK2,DPF2,ZMYND11,RNF168,KDM5B,TP53,CDK1,UBE2A
GO:BP	cell communication	GO:0007154	0.003645439	6495	153	75	ASB17,SCEL,FBXL17,TRIM24,SOCS2,VPS41,FBXL15,ASB13,RNF115,FBXO31,UBE2D3,BTRC,ESR1,TRAF4,PRPF19,SOCS3,HMGCR,RNF8,RNF6,FBXO6,NEURL2,HRC,STUB1,BMI1,FBXW4,CDC34,UBE2B,BIRC3,CDK2,LPXN,UBE2D1,ZNF592,CBLC,RFPL3,TRIM52,DPF2,TRIM39,RNF43,ASB15,UFM1,RNF185,RFPL2,RFPL1,ZC3HAV1,ASB14,TRAF3,ZMYND11,RNF113A,TRAF5,RNF183,TRAF6,TRIM60,MID1,KDM5B,CUL4A,TP53,TRIM33,TRIM6,FBXO22,LRG6,TRIM68,ASB7,SMURF1,APC,UBE2K,CDK1,BIRC2,SOCS5,CBL,TRIM71,XIAP,ASB16,TNFRSF25,CCND1,PRICKLE2
GO:BP	regulation of apoptotic process	GO:0042981	0.0039291	1463	153	28	TRIM24,UBE2Z,SOCS2,ESR1,TRAF4,SOCS3,FBXO11,BMI1,CDC34,UBE2B,BIRC3,TRIM39,UFM1,RFPL1,TRAF3,ZMYND11,TRAF5,RNF183,TRAF6,TP53,APC,CDK1,BIRC2,CBL,DCUN1D3,XIAP,TNFRSF25,CCND1

GO:BP	negative regulation of cell communication	GO:0010648	0.003961516	1378	153	27	SOCS2,RNF115,UBE2D3,BTRC,ESR1,SOCS3,HMGCR,STUB1,BMI1,CDC34,UBE2B,LPXN,UBE2D1,ZNF592,CBLC,TRIM39,RNF43,ZMYND11,RNF113A,TRIM60,TP53,TRIM33,SMURF1,APC,SOCS5,CBL,XIAP
GO:BP	negative regulation of signaling	GO:0023057	0.003961516	1378	153	27	SOCS2,RNF115,UBE2D3,BTRC,ESR1,SOCS3,HMGCR,STUB1,BMI1,CDC34,UBE2B,LPXN,UBE2D1,ZNF592,CBLC,TRIM39,RNF43,ZMYND11,RNF113A,TRIM60,TP53,TRIM33,SMURF1,APC,SOCS5,CBL,XIAP
GO:BP	cellular response to cytokine stimulus	GO:0071345	0.004346547	825	153	20	TRAF4,SOCS3,BMI1,CDC34,BIRC3,RNF185,TRAF3,RNF113A,TRAF5,TRAF6,KDM5B,TP53,TRIM6,UBE2G2,UBE2K,BIRC2,SOCS5,CBL,XIAP,TNFRSF25
GO:BP	regulation of macromolecule metabolic process	GO:0060255	0.004356937	6772	153	77	DCUN1D1,IRF2BP1,PHF19,TRIM24,BRPF3,HUWE1,UBE2D3,BTRC,ESR1,TRAF4,PRPF19,SOCS3,HMGCR,MYLIP,RNF8,UHRF1,BAZ1B,RNF6,CHD4,UBE2C,TRIM77,HRC,STUB1,BAHD1,BMI1,TRIP12,TRIM27,UBE2B,BIRC3,CDK2,UBE2D1,ZNF592,PHF23,CBLC,RBBP6,MAGEC2,RFPL3,FBXL5,TRIM52,DPF2,TRIM39,CACUL1,RNF185,RFPL2,RFPL1,TRIM26,ZC3HAV1,TRAF3,ZMYND11,TRAF5,UNK,RNF168,RNF187,TRIM49,TRAF6,KDM5B,CUL4A,UBE2L3,TP53,UBE2V2,TRIM33,TRIM6,FBXO22,TRIM68,SMURF1,CCNF,APC,UBE2K,AIRE,CDK1,BIRC2,SOCS5,CBL,DCUN1D3,TRIM71,XIAP,CCND1
GO:BP	regulation of protein polyubiquitination	GO:1902914	0.00499473	31	153	5	TRIP12,UBE2D1,UBE2V2,BIRC2,XIAP
GO:BP	cytokine-mediated signaling pathway	GO:0019221	0.004997588	486	153	15	TRAF4,BIRC3,RNF185,TRAF3,RNF113A,TRAF5,TRAF6,TP53,TRIM6,UBE2K,BIRC2,SOCS5,CBL,XIAP,TNFRSF25
GO:BP	regulation of transferase activity	GO:0051338	0.005120218	834	153	20	DCUN1D1,BTRC,TRAF4,HMGCR,UBE2C,STUB1,BMI1,TRIM27,CBLC,MAGEC2,CACUL1,TRAF6,UBE2L3,TP53,CCNF,APC,SOCS5,CBL,DCUN1D3,CCND1
GO:BP	positive regulation of cellular process	GO:0048522	0.005687191	5711	153	68	SCEL,TRIM24,UBE2Z,SOCS2,FBXL15,BRPF3,HUWE1,UBE2D3,BTRC,ESR1,TRAF4,PRPF19,SOCS3,HMGCR,RNF8,UHRF1,FBXO38,BAZ1B,RNF6,CHD4,UBE2C,STUB1,BMI1,TRIM27,FBXW4,CDC34,UBE2B,BIRC3,CDK2,RFPL3,TRIM52,DPF2,TRIM39,CACUL1,RNF185,RFPL2,RFPL1,ZC3HAV1,TRAF3,FBXW8,RAD18,TRAF5,RNF183,RNF168,RNF187,TRAF6,TRIM46,MID1,KDM5B,CUL4A,UBE2L3,TP53,UBE2V2,TRIM6,LGR6,TRIM68,SMURF1,APC,UBE2K,AIR

							E,CDK1,BIRC2,SOCS5,CBL,DCUN1D3,TRIM71,XIAP,CCND1
GO:BP	regulation of cell cycle phase transition	GO:1901987	0.006069142	431	153	14	FBXO31,PRPF19,UBE2C,FBXO6,CDK2,DPF2,TRIM39,RFPL1,CUL4A,TP53,APC,CDK1,DCUN1D3,CCND1
GO:BP	modulation by symbiont of entry into host	GO:0052372	0.006447692	57	153	6	RFPL3,RFPL2,RFPL1,TRIM26,TRIM6,TRIM68
GO:BP	regulation of programmed cell death	GO:0043067	0.006944086	1507	153	28	TRIM24,UBE2Z,SOCS2,ESR1,TRAF4,SOCS3,FBXO11,BMI1,CDC34,UBE2B,BIRC3,TRIM39,UFM1,RFPL1,TRAF3,ZMYND11,TRAF5,RNF183,TRAF6,TP53,APC,CDK1,BIRC2,CBL,DCUN1D3,XIAP,TNFRSF25,CCND1
GO:BP	positive regulation of DNA-binding transcription factor activity	GO:0051091	0.00857375	270	153	11	ESR1,TRIM27,RFPL3,TRIM52,RFPL2,RFPL1,TRIM26,TRAF5,TRAF6,TRIM6,TRIM68
GO:BP	signaling	GO:0023052	0.009258844	6396	153	73	ASB17,SCEL,FBXL17,TRIM24,SOCS2,FBXL15,ASB13,RNF115,FBXO31,UBE2D3,BTRC,ESR1,TRAF4,PRPF19,SOCS3,HMGCR,RNF8,RNF6,FBXO6,NEURL2,HRC,STUB1,BMI1,FBXW4,CDC34,UBE2B,BIRC3,CDK2,LPXN,UBE2D1,ZNF592,CBLC,RFPL3,TRIM52,DPF2,TRIM39,RNF43,ASB15,UFM1,RNF185,RFPL2,RFPL1,ZC3HAV1,ASB14,TRAF3,ZMYND11,RNF113A,TRAF5,RNF183,TRAF6,TRIM60,MID1,KDM5B,CUL4A,TP53,TRIM33,TRIM6,LGR6,TRIM68,ASB7,SMURF1,APC,UBE2K,CDK1,BIRC2,SOCS5,CBL,TRIM71,XIAP,ASB16,TNFRSF25,CCND1,PRICKLE2
GO:BP	regulation of mitotic cell cycle phase transition	GO:1901990	0.010382268	331	153	12	FBXO31,UBE2C,CDK2,DPF2,TRIM39,RFPL1,CUL4A,TP53,APC,CDK1,DCUN1D3,CCND1
GO:BP	positive regulation of protein polyubiquitination	GO:1902916	0.010673863	17	153	4	UBE2D1,UBE2V2,BIRC2,XIAP

GO:BP	cellular response to organic substance	GO:0071310	0.010754126	2001	153	33	TRIM24,SOCS2,BTRC,ESR1,TRAF4,SOCS3,RNF6,STUB1,BMI1,CDC34,BIRC3,ZNF592,UFM1,RNF185,TRAF3,RNF113A,TRAF5,TRAF6,KDM5B,UBE2L3,TP53,TRIM6,TRIM68,UBE2G2,UBE2K,CDK1,BIRC2,SOCS5,CBL,TRIM71,XIAP,TNFRSF25,CCND1
GO:BP	apoptotic process	GO:0006915	0.011111013	1910	153	32	ATG3,TRIM24,UBE2Z,SOCS2,UBE2D3,ESR1,TRAF4,SOCS3,FBXO11,BMI1,CDC34,UBE2B,BIRC3,DPF2,TRIM39,UFM1,RFPL1,TRAF3,ZMYND11,TRAF5,RNF183,TRAF6,CUL4A,TP53,APC,CDK1,BIRC2,CBL,DCUN1D3,XIAP,TNFRSF25,CCND1
GO:BP	regulation of biological process	GO:0050789	0.011298639	12331	153	116	ASB17,DCUN1D1,IRF2BP1,ATG3,SCEL,PHF19,FBXL17,TRIM24,UBE2Z,SOCS2,VPS41,FBXL15,BRPF3,ASB13,HUWE1,RNF115,FBXO31,HERC1,UBE2D3,BTRC,ESR1,TRAF4,PRPF19,SOCS3,HMGCR,MYLIP,FBXO11,RNF8,UHRF1,FBXO38,BAZ1B,RNF6,CHD4,UBE2C,TRIM77,FBXO6,NEURL2,HRC,STUB1,BAHD1,BMI1,TRIP12,TRIM27,FBXW4,CDC34,UBE2B,BIRC3,CDK2,LPXN,UBE2D1,ZNF592,PHF23,CBLC,RBBP6,MAGEC2,RFPL3,FBXL5,TRIM52,DPF2,TRIM39,CACUL1,RNF43,ASB15,UFM1,RNF185,RFPL2,RFPL1,TRIM26,TRIM36,ZC3HAV1,ASB14,TRAF3,FBXW8,ZMYND11,RAD18,RNF113A,TRAF5,UNK,RNF183,RNF168,RNF187,FBXW5,TRIM49,FBXO43,TRAF6,TRIM60,TRIM46,MID1,KDM5B,CUL4A,UBE2L3,TP53,UBE2V2,TRIM33,TRIM6,FBXO22,LGR6,TRIM68,ASB7,SMURF1,UBE2G2,CCNF,APC,UBE2K,AIRE,CDK1,BIRC2,SOCS5,CBL,DCUN1D3,TRIM71,XIAP,ASB16,TNFRSF25,CCND1,PRICKLE2
GO:BP	negative regulation of mitotic cell cycle phase transition	GO:1901991	0.012018492	179	153	9	FBXO31,CDK2,TRIM39,RFPL1,TP53,APC,CDK1,DCUN1D3,CCND1
GO:BP	epigenetic regulation of gene expression	GO:0040029	0.012315992	228	153	10	PHF19,RNF8,UHRF1,BAHD1,BMI1,TRIP12,TRIM27,CDK2,RNF168,TP53
GO:BP	regulation of biological process involved in symbiotic interaction	GO:0043903	0.012774591	64	153	6	RFPL3,RFPL2,RFPL1,TRIM26,TRIM6,TRIM68
GO:BP	cellular response to tumor necrosis	GO:0071356	0.012798897	229	153	10	TRAF4,BIRC3,TRAF3,TRAF5,TRAF6,TP53,UBE2K,BIRC2,XIAP,TNFRSF25

	factor						
GO:BP	regulation of proteolysis involved in protein catabolic process	GO:1903050	0.013298099	230	153	10	BTRC,STUB1,CDK2,TRIM39,RNF185,RFPL1,FBXO22,SMURF1,UBE2K,SOCS5
GO:BP	regulation of cell cycle G1/S phase transition	GO:1902806	0.017857569	188	153	9	FBXO31,CDK2,DPF2,TRIM39,CUL4A,TP53,APC,DCUN1D3,CCND1
GO:BP	response to cytokine	GO:0034097	0.020521571	916	153	20	TRAF4,SOCS3,BMI1,CDC34,BIRC3,RNF185,TRAF3,RNF113A,TRAF5,TRAF6,KDM5B,TP53,TRIM6,UBE2G2,UBE2K,BIRC2,SOCS5,CBL,XIAP,TNFRSF25
GO:BP	regulation of intracellular signal transduction	GO:1902531	0.021309076	1691	153	29	TRIM24,BTRC,ESR1,TRAF4,HMGCR,CDC34,UBE2B,BIRC3,CBL,RFPL3,TRIM52,TRIM39,RFPL2,RFPL1,ZC3HAV1,TRAF3,ZMYND11,TRAF5,RNF183,TRAF6,TRIM60,MID1,CUL4A,TP53,TRIM6,TRIM68,BIRC2,CBL,XIAP
GO:BP	regulation of proteasomal protein catabolic process	GO:0061136	0.022042466	193	153	9	BTRC,STUB1,CDK2,TRIM39,RNF185,RFPL1,FBXO22,UBE2K,SOCS5
GO:BP	programmed cell death	GO:0012501	0.023713427	1982	153	32	ATG3,TRIM24,UBE2Z,SOCS2,UBE2D3,ESR1,TRAF4,SOCS3,FBXO11,BMI1,CDC34,UBE2B,BIRC3,DPF2,TRIM39,UFM1,RFPL1,TRAF3,ZMYND11,TRAF5,RNF183,TRAF6,CUL4A,TP53,APC,CDK1,BIRC2,CBL,DCUN1D3,XIAP,TNFRSF25,CCND1
GO:BP	cell death	GO:0008219	0.025208604	1988	153	32	ATG3,TRIM24,UBE2Z,SOCS2,UBE2D3,ESR1,TRAF4,SOCS3,FBXO11,BMI1,CDC34,UBE2B,BIRC3,DPF2,TRIM39,UFM1,RFPL1,TRAF3,ZMYND11,TRAF5,RNF183,TRAF6,CUL4A,TP53,APC,CDK1,BIRC2,CBL,DCUN1D3,XIAP,TNFRSF25,CCND1
GO:BP	regulation of mitotic cell cycle	GO:0007346	0.027198512	492	153	14	FBXO31,UBE2C,CDK2,DPF2,TRIM39,RFPL1,FBXW5,FBXO43,CUL4A,TP53,APC,CDK1,DCUN1D3,CCND1
GO:BP	response to tumor necrosis	GO:0034612	0.027488056	250	153	10	TRAF4,BIRC3,TRAF3,TRAF5,TRAF6,TP53,UBE2K,BIRC2,XIAP,TNFRSF25

	factor						
GO:BP	negative regulation of G1/S transition of mitotic cell cycle	GO:2000134	0.029730993	74	153	6	FBXO31,CDK2,TP53,APC,DCUN1D3,CCND1
GO:BP	cell cycle G2/M phase transition	GO:0044839	0.031250023	154	153	8	FBXL15,CDK2,TRIM39,RFPL1,TP53,CDK1,UBE2A,CCND1
GO:BP	innate immune response	GO:0045087	0.033172118	947	153	20	ESR1,TRAF4,TRIM77,TRIM27,BIRC3,RFPL3,RNF185,RFPL2,RFPL1,TRIM26,ZC3HAV1,TRAF3,TRIM49,TRAF6,TP53,TRIM6,TRIM68,UBE2K,BIRC2,XIAP
GO:BP	negative regulation of response to stimulus	GO:0048585	0.033232159	1639	153	28	SOCS2,RNF115,UBE2D3,BTRC,ESR1,SOCS3,HMGCR,STUB1,BMI1,TRIM27,CDC34,UBE2B,LPXN,UBE2D1,ZNF592,CBLC,TRIM39,RNF43,ZMYND11,RNF113A,TRIM60,TP53,TRIM33,SMURF1,APC,SOCS5,CBL,XIAP
GO:BP	positive regulation of NF-kappaB transcription factor activity	GO:0051092	0.039367865	159	153	8	RFPL3,TRIM52,RFPL2,RFPL1,TRAF5,TRAF6,TRIM6,TRIM68
GO:BP	negative regulation of gene expression, epigenetic	GO:0045814	0.04058735	116	153	7	PHF19,UHRF1,BAHD1,BMI1,TRIP12,TRIM27,CDK2
GO:BP	regulation of DNA-binding transcription factor activity	GO:0051090	0.041241282	444	153	13	BTRC,ESR1,TRIM27,RFPL3,TRIM52,RFPL2,RFPL1,TRIM26,TRAF3,TRAF5,TRAF6,TRIM6,TRIM68
GO:BP	response to endoplasmic reticulum stress	GO:0034976	0.042495162	263	153	10	FBXO6,STUB1,FBXO17,UFM1,RNF185,RNF183,TP53,UBE2G2,UBE4A,CCND1

GO:BP	positive regulation of protein catabolic process	GO:0045732	0.043102087	210	153	9	MYLIP,STUB1,FBXL5,RNF185,RFPL1,CUL4A,FBXO22,APC,SOCS5
GO:BP	regulation of metabolic process	GO:0019222	0.044304816	7295	153	78	DCUN1D1,IRF2BP1,PHF19,TRIM24,BRPF3,HUWE1,HERC1,UBE2D3,BTRC,ESR1,TRAF4,PRPF19,SOCS3,HMGCR,MYLIP,RNF8,UHRF1,BAZ1B,RNF6,CHD4,UBE2C,TRIM77,HRC,STUB1,BAHD1,BMI1,TRIP12,TRIM27,UBE2B,BIRC3,CDK2,UBE2D1,ZNF592,PHF23,CBLC,RBBP6,MAGEC2,RFPL3,FBXL5,TRIM52,DPF2,TRIM39,CACUL1,RNF185,RFPL2,RFPL1,TRIM26,ZC3HAV1,TRAF3,ZMYND11,TRAF5,UNK,RNF168,RNF187,TRIM49,TRAF6,KDM5B,CUL4A,UBE2L3,TP53,UBE2V2,TRIM33,TRIM6,FBXO22,TRIM68,SMURF1,CCNF,APC,UBE2K,AIRE,CDK1,BIRC2,SOCS5,CBL,DCUN1D3,TRIM71,XIAP,CCND1
GO:BP	regulation of G1/S transition of mitotic cell cycle	GO:2000045	0.045037835	162	153	8	FBXO31,CDK2,DPF2,CUL4A,TP53,APC,DCUN1D3,CCND1
GO:BP	regulation of cellular response to stress	GO:0080135	0.045745777	658	153	16	TRAF4,RNF8,TRIP12,DPF2,RNF185,TRAF3,ZMYND11,TRAF5,RNF183,RNF168,TRAF6,MID1,CUL4A,TP53,UBE2V2,XIAP
GO:BP	negative regulation of cell cycle G1/S phase transition	GO:1902807	0.046528089	80	153	6	FBXO31,CDK2,TP53,APC,DCUN1D3,CCND1
GO:BP	negative regulation of DNA-templated transcription	GO:0045892	0.046813496	1309	153	24	IRF2BP1,PHF19,TRIM24,UBE2D3,BTRC,ESR1,RNF8,UHRF1,CHD4,BAHD1,BMI1,TRIM27,CDK2,UBE2D1,MAGEC2,DPF2,ZMYND11,RNF168,TRAF6,KDM5B,TP53,TRIM33,TRIM6,CCND1
GO:BP	entry into host	GO:0044409	0.047073575	163	153	8	RFPL3,RFPL2,RFPL1,TRIM26,TRIM6,TRIM68,CDK1,CBL

Table 7.4. The functional profiling of the hits list genes from the undamaged cells (unirradiated).

Database	Term name	Term ID	adjusted p value	Term size	Hits list size	Intersection	Hits in the term
GO:BP	protein modification by small protein conjugation	GO:0032446	9.38E-65	872	90	64	AMFR,CCNF,UBE2K,TRIP12,TRIM27,CDC34,BIRC3,HLTF,RNF7,BARD1,TRAF4,UBE2E1,SOCS5,DZIP3,ITCH,IRF2BP1,ATG3,FBXL17,TRIM24,CUL4A,SHPRH,PCGF6,RNF11,UBE2Z,TRIM13,DTX1,SOCS2,RNF144A,UBE2N,FBXL15,UBR1,HERC3,HECTD3,ASB13,BTRC,SPSB1,RNF168,UHRF1,FBXO38,FBXL12,CBL,FBXO30,FBXO2,FBXW8,ZNRF2,PIAS2,RNF20,STUB1,FBXO28,CNOT4,UFM1,NHLRC1,FBXO3,ASB10,PIAS4,UBA3,TRIM5,TRIM8,FBXL7,ASB17,UBE2M,MARCH8,UBA1,ASB7
GO:BP	protein modification by small protein conjugation or removal	GO:0070647	4.51E-62	1019	90	65	AMFR,CCNF,UBE2K,CDK1,TRIP12,TRIM27,CDC34,BIRC3,HLTF,RNF7,BARD1,TRAF4,UBE2E1,SOCS5,DZIP3,ITCH,IRF2BP1,ATG3,FBXL17,TRIM24,CUL4A,SHPRH,PCGF6,RNF11,UBE2Z,TRIM13,DTX1,SOCS2,RNF144A,UBE2N,FBXL15,UBR1,HERC3,HECTD3,ASB13,BTRC,SPSB1,RNF168,UHRF1,FBXO38,FBXL12,CBL,FBXO30,FBXO2,FBXW8,ZNRF2,PIAS2,RNF20,STUB1,FBXO28,CNOT4,UFM1,NHLRC1,FBXO3,ASB10,PIAS4,UBA3,TRIM5,TRIM8,FBXL7,ASB17,UBE2M,MARCH8,UBA1,ASB7
GO:BP	post-translational protein modification	GO:0043687	1.19E-60	1276	90	68	AMFR,CCNF,UBE2K,CDK1,TRIP12,TRIM27,CDC34,BIRC3,HLTF,CDK2,RNF7,BARD1,TRAF4,UBE2E1,SOCS5,DZIP3,ITCH,IRF2BP1,ATG3,FBXL17,TRIM24,CUL4A,SHPRH,PCGF6,RNF11,UBE2Z,TRIM13,DTX1,SOCS2,PHF20L1,RNF144A,UBE2N,FBXL15,UBR1,HERC3,HECTD3,ASB13,BTRC,SPSB1,RNF168,UHRF1,FBXO38,FBXL12,CBL,BAZ1B,FBXO30,FBXO2,FBXW8,ZNRF2,PIAS2,RNF20,STUB1,FBXO28,CNOT4,UFM1,NHLRC1,FBXO3,ASB10,PIAS4,UBA3,TRIM5,TRIM8,FBXL7,ASB17,UBE2M,MARCH8,UBA1,ASB7
GO:BP	protein ubiquitination	GO:0016567	1.24E-58	792	90	59	AMFR,CCNF,UBE2K,TRIP12,TRIM27,CDC34,BIRC3,HLTF,RNF7,BARD1,TRAF4,UBE2E1,SOCS5,DZIP3,ITCH,IRF2BP1,ATG3,FBXL17,TRIM24,CUL4A,SHPRH,PCGF6,RNF11,UBE2Z,TRIM13,DTX1,SOCS2,RNF144A,UBE2N,FBXL15,UBR1,HERC3,HECTD3,ASB13,BTRC,SPSB1,RNF168,UHRF1,FBXO38,FBXL12,CBL,FBXO30,FBXO2,FBXW8,ZNRF2,RNF20,STUB1,FBXO28,CNOT4,NHLRC1,FBXO3,ASB10,TRIM5,TRIM8,FBXL7,ASB17,MARCH8,UBA1,ASB7
GO:BP	protein modification process	GO:0036211	6.09E-40	3409	90	74	CCND1,AMFR,CCNF,APC,CCNB1,UBE2K,CDK1,TRIP12,TRIM27,CDC34,BIRC3,HLTF,CDK2,RNF7,BARD1,TRAF4,UBE2E1,SOCS5,DZIP3,ITCH,IRF2BP1,ATG3,FBXL17,TRIM24,CUL4A,SHPRH,PCGF6,RNF11,UBE2Z,TRIM13,DTX1,SOCS2,PHF20L1,RNF144A,UBE2N,FBXL15,UBR1,HERC3,HECTD3,ASB13,BTRC,SPSB1,RNF168,UHRF1,FBXO38,FBXL12,CBL,BAZ1B,FBXO30,FBXO2,FBXW8,ZNRF2,PIAS2,FBXW2,RNF20,STUB1,FBXO28,CNOT4,UFM1,NHLRC1,FBXO3,ASB10,PIAS4,UBA3,TRIM5,TRIM8,FBXL7,ASB17,TSG101,UBE2M,MARCH8,UBA1,PHF2,ASB7

GO:BP	ubiquitin-dependent protein catabolic process	GO:0006511	3.86E-39	696	90	45	AMFR,CCNF,APC,UBE2K,TRIP12,CDC34,FBXW4,CDK2,RNF7,TRAF4,UBE2E1,SOCS5,ITCH,FBXL17,FBXO8,CUL4A,RNF11,UBE2Z,TRIM13,FBXO21,FBXO27,PHF20L1,RNF144A,UBE2N,FBXL15,UBR1,HERC3,HECTD3,BTRC,SPSB1,RNF168,UHRF1,FBXO38,FBXL12,CBL,FBXO2,ZNRF2,RNF20,STUB1,CNOT4,NHLRC1,FBXO3,FBXL7,TSG101,UBA1
GO:BP	modification-dependent protein catabolic process	GO:0019941	7.34E-39	706	90	45	AMFR,CCNF,APC,UBE2K,TRIP12,CDC34,FBXW4,CDK2,RNF7,TRAF4,UBE2E1,SOCS5,ITCH,FBXL17,FBXO8,CUL4A,RNF11,UBE2Z,TRIM13,FBXO21,FBXO27,PHF20L1,RNF144A,UBE2N,FBXL15,UBR1,HERC3,HECTD3,BTRC,SPSB1,RNF168,UHRF1,FBXO38,FBXL12,CBL,FBXO2,ZNRF2,RNF20,STUB1,CNOT4,NHLRC1,FBXO3,FBXL7,TSG101,UBA1
GO:BP	modification-dependent macromolecule catabolic process	GO:0043632	1.38E-38	716	90	45	AMFR,CCNF,APC,UBE2K,TRIP12,CDC34,FBXW4,CDK2,RNF7,TRAF4,UBE2E1,SOCS5,ITCH,FBXL17,FBXO8,CUL4A,RNF11,UBE2Z,TRIM13,FBXO21,FBXO27,PHF20L1,RNF144A,UBE2N,FBXL15,UBR1,HERC3,HECTD3,BTRC,SPSB1,RNF168,UHRF1,FBXO38,FBXL12,CBL,FBXO2,ZNRF2,RNF20,STUB1,CNOT4,NHLRC1,FBXO3,FBXL7,TSG101,UBA1
GO:BP	macromolecule modification	GO:0043412	5.26E-38	3628	90	74	CCND1,AMFR,CCNF,APC,CCNB1,UBE2K,CDK1,TRIP12,TRIM27,CDC34,BIRC3,HLTF,CDK2,RNF7,BARD1,TRAF4,UBE2E1,SOCS5,DZIP3,ITCH,IRF2BP1,ATG3,FBXL17,TRIM24,CUL4A,SHPRH,PCGF6,RNF11,UBE2Z,TRIM13,DTX1,SOCS2,PHF20L1,RNF144A,UBE2N,FBXL15,UBR1,HERC3,HECTD3,ASB13,BTRC,SPSB1,RNF168,UHRF1,FBXO38,FBXL12,CBL,BAZ1B,FBXO30,FBXO2,FBXW8,ZNRF2,PIAS2,FBXW2,RNF20,STUB1,FBXO28,CNOT4,UFM1,NHLRC1,FBXO3,ASB10,PIAS4,UBA3,TRIM5,TRIM8,FBXL7,ASB17,TSG101,UBE2M,MARCH8,UBA1,PHF2,ASB7
GO:BP	proteolysis involved in protein catabolic process	GO:0051603	1.07E-37	807	90	46	AMFR,CCNF,APC,UBE2K,TRIP12,CDC34,FBXW4,CDK2,RNF7,TRAF4,UBE2E1,SOCS5,ITCH,FBXL17,FBXO8,CUL4A,RNF11,UBE2Z,TRIM13,FBXO21,FBXO27,PSMB8,PHF20L1,RNF144A,UBE2N,FBXL15,UBR1,HERC3,HECTD3,BTRC,SPSB1,RNF168,UHRF1,FBXO38,FBXL12,CBL,FBXO2,ZNRF2,RNF20,STUB1,CNOT4,NHLRC1,FBXO3,FBXL7,TSG101,UBA1
GO:BP	protein catabolic process	GO:0030163	2.43E-35	1043	90	48	AMFR,CCNF,APC,UBE2K,TRIP12,CDC34,FBXW4,CDK2,RNF7,BARD1,TRAF4,UBE2E1,SOCS5,ITCH,FBXL17,FBXO8,TRIM24,CUL4A,RNF11,UBE2Z,TRIM13,FBXO21,FBXO27,PSMB8,PHF20L1,RNF144A,UBE2N,FBXL15,UBR1,HERC3,HECTD3,BTRC,SPSB1,RNF168,UHRF1,FBXO38,FBXL12,CBL,FBXO2,ZNRF2,RNF20,STUB1,CNOT4,NHLRC1,FBXO3,FBXL7,TSG101,UBA1
GO:BP	protein metabolic process	GO:0019538	2.08E-33	5373	90	80	CCND1,AMFR,CCNF,APC,CCNB1,UBE2K,AIRE,CDK1,TRIP12,TRIM27,CDC34,FBXW4,BIRC3,HLTF,CDK2,RNF7,BARD1,TRAF4,UBE2E1,SOCS5,DZIP3,ITCH,IRF2BP1,ATG3,FBXL17,FBXO8,TRIM24,CUL4A,SHPRH,PCGF6,RNF11,UBE2Z,TRIM13,FBXO21,DTX1,FBXO27,SOCS2,PHF20L1,RNF144A,UBE2N,FBXL15,UBR1,HERC3,HECTD3,BTRC,SPSB1,RNF168,UHRF1,FBXO38,FBXL12,CBL,FBXO2,ZNRF2,RNF20,STUB1,CNOT4,NHLRC1,FBXO3,FBXL7,TSG101,UBA1

							S2,PSMB8,PHF20L1,RNF144A,UBE2N,FBXL15,UBR1,HERC3,HECTD3,ASB13,BTRC,SPSB1,RNF168,UHRF1,FBXO38,FBXL12,CBL,BAZ1B,FBXO30,FBXO2,FBXW8,ZNRF2,PIAS2,FBXW2,RNF20,STUB1,FBXO28,CNOT4,UFM1,NHLRC1,FBXO3,ASB10,PIAS4,UBA3,TRIM5,TRIM8,FBXL7,ASB17,TSG101,UBE2M,MARCH8,UBA1,PHF2,ASB7
GO:BP	organonitrogen compound catabolic process	GO:1901565	1.33E-29	1386	90	48	AMFR,CCNF,APC,UBE2K,TRIP12,CDC34,FBXW4,CDK2,RNF7,BARD1,TRAF4,UBE2E1,SOC S5,ITCH,FBXL17,FBXO8,TRIM24,CUL4A,RNF11,UBE2Z,TRIM13,FBXO21,FBXO27,PSMB8,PHF20L1,RNF144A,UBE2N,FBXL15,UBR1,HERC3,HECTD3,BTRC,SPSB1,RNF168,UHRF1,FBXO38,FBXL12,CBL,FBXO2,ZNRF2,RNF20,STUB1,CNOT4,NHLRC1,FBXO3,FBXL7,TSG101,UBA1
GO:BP	macromolecule catabolic process	GO:0009057	3.11E-29	1412	90	48	AMFR,CCNF,APC,UBE2K,TRIP12,CDC34,FBXW4,CDK2,RNF7,BARD1,TRAF4,UBE2E1,SOC S5,ITCH,FBXL17,FBXO8,TRIM24,CUL4A,RNF11,UBE2Z,TRIM13,FBXO21,FBXO27,PSMB8,PHF20L1,RNF144A,UBE2N,FBXL15,UBR1,HERC3,HECTD3,BTRC,SPSB1,RNF168,UHRF1,FBXO38,FBXL12,CBL,FBXO2,ZNRF2,RNF20,STUB1,CNOT4,NHLRC1,FBXO3,FBXL7,TSG101,UBA1
GO:BP	protein polyubiquitination	GO:0000209	1.86E-28	261	90	28	AMFR,UBE2K,TRIP12,TRIM27,CDC34,BARD1,TRAF4,UBE2E1,DZIP3,ITCH,IRF2BP1,FBXL17,SHPRH,RNF144A,UBE2N,BTRC,RNF168,FBXO38,CBL,ZNRF2,RNF20,STUB1,FBXO28,NHLRC1,TRIM5,TRIM8,FBXL7,MARCH8
GO:BP	proteolysis	GO:0006508	3.12E-28	1766	90	51	AMFR,CCNF,APC,UBE2K,CDK1,TRIP12,CDC34,FBXW4,BIRC3,CDK2,RNF7,BARD1,TRAF4,UBE2E1,SOC S5,ITCH,FBXL17,FBXO8,CUL4A,RNF11,UBE2Z,TRIM13,FBXO21,FBXO27,PSMB8,PHF20L1,RNF144A,UBE2N,FBXL15,UBR1,HERC3,HECTD3,BTRC,SPSB1,RNF168,UHRF1,FBXO38,FBXL12,CBL,FBXO2,ZNRF2,FBXW2,RNF20,STUB1,CNOT4,NHLRC1,FBXO3,UBA3,FBXL7,TSG101,UBA1
GO:BP	organonitrogen compound metabolic process	GO:1901564	8.90E-28	6362	90	80	CCND1,AMFR,CCNF,APC,CCNB1,UBE2K,AIRE,CDK1,TRIP12,TRIM27,CDC34,FBXW4,BIRC3,HLTF,CDK2,RNF7,BARD1,TRAF4,UBE2E1,SOC S5,DZIP3,ITCH,IRF2BP1,ATG3,FBXL17,FBXO8,TRIM24,CUL4A,SHPRH,PCGF6,RNF11,UBE2Z,TRIM13,FBXO21,DTX1,FBXO27,SOC S2,PSMB8,PHF20L1,RNF144A,UBE2N,FBXL15,UBR1,HERC3,HECTD3,ASB13,BTRC,SPSB1,RNF168,UHRF1,FBXO38,FBXL12,CBL,BAZ1B,FBXO30,FBXO2,FBXW8,ZNRF2,PIAS2,FBXW2,RNF20,STUB1,FBXO28,CNOT4,UFM1,NHLRC1,FBXO3,ASB10,PIAS4,UBA3,TRIM5,TRIM8,FBXL7,ASB17,TSG101,UBE2M,MARCH8,UBA1,PHF2,ASB7
GO:BP	proteasome-mediated ubiquitin-dependent protein catabolic	GO:0043161	4.74E-26	446	90	31	AMFR,CCNF,APC,UBE2K,TRIP12,CDC34,FBXW4,CDK2,RNF7,TRAF4,SOC S5,ITCH,FBXL17,CUL4A,TRIM13,FBXO27,PHF20L1,RNF144A,FBXL15,UBR1,HECTD3,BTRC,SPSB1,FBXO38,FBXL12,FBXO2,ZNRF2,STUB1,NHLRC1,FBXO3,FBXL7

	process						
GO:BP	proteasomal protein catabolic process	GO:0010498	3.91E-24	515	90	31	AMFR,CCNF,APC,UBE2K,TRIP12,CDC34,FBXW4,CDK2,RNF7,TRAF4,SOCS5,ITCH,FBXL17,CUL4A,TRIM13,FBXO27,PHF20L1,RNF144A,FBXL15,UBR1,HECTD3,BTRC,SPSB1,FBXO38,FBXL12,FBXO2,ZNRF2,STUB1,NHLRC1,FBXO3,FBXL7
GO:BP	catabolic process	GO:0009056	3.53E-23	2616	90	54	AMFR,CCNF,APC,UBE2K,TRIP12,TRIM27,CDC34,FBXW4,CDK2,RNF7,BARD1,TRAF4,UBE2E1,SOCS5,ITCH,ATG3,FBXL17,FBXO8,TRIM24,CUL4A,RNF11,UBE2Z,TRIM13,FBXO21,FBXO27,PSMB8,PHF20L1,RNF144A,VPS41,UBE2N,FBXL15,UBR1,HERC3,HECTD3,BTRC,SPSB1,RNF168,UHRF1,FBXO38,FBXL12,CBL,FBXO2,ZNRF2,RNF20,STUB1,CNOT4,UFM1,NHLRC1,FBXO3,TRIM5,TRIM8,FBXL7,TSG101,UBA1
GO:BP	organic substance catabolic process	GO:1901575	7.91E-21	2173	90	48	AMFR,CCNF,APC,UBE2K,TRIP12,CDC34,FBXW4,CDK2,RNF7,BARD1,TRAF4,UBE2E1,SOCS5,ITCH,FBXL17,FBXO8,TRIM24,CUL4A,RNF11,UBE2Z,TRIM13,FBXO21,FBXO27,PSMB8,PHF20L1,RNF144A,UBE2N,FBXL15,UBR1,HERC3,HECTD3,BTRC,SPSB1,RNF168,UHRF1,FBXO38,FBXL12,CBL,FBXO2,ZNRF2,RNF20,STUB1,CNOT4,NHLRC1,FBXO3,FBXL7,TSG101,UBA1
GO:BP	SCF-dependent proteasomal ubiquitin-dependent protein catabolic process	GO:0031146	1.33E-13	46	90	11	CCNF,FBXW4,FBXL17,FBXO27,FBXL15,BTRC,FBXO38,FBXL12,FBXO2,FBXO3,FBXL7
GO:BP	nitrogen compound metabolic process	GO:0006807	5.06E-13	12114	90	86	CCND1,AMFR,CCNF,APC,CCNB1,UBE2K,AIRE,CDK1,TRIP12,TRIM27,CDC34,FBXW4,BIRC3,HLTF,CDK2,LPXN,RNF7,BARD1,ESR1,TRAF4,UBE2E1,SOCS5,DZIP3,ITCH,IRF2BP1,ATG3,PHF19,FBXL17,FBXO8,MLLT6,TRIM24,CUL4A,SHPRH,PCGF6,RNF11,UBE2Z,TRIM13,FBXO21,DTX1,FBXO27,SOCS2,PSMB8,PHF20L1,RNF144A,UBE2N,FBXL15,UBR1,HERC3,HECTD3,BRPF3,ASB13,BTRC,SPSB1,RNF168,UHRF1,FBXO38,FBXL12,CBL,BAZ1B,FBXO30,FBXO2,FBXW8,ZNRF2,PIAS2,FBXW2,RNF20,STUB1,FBXO28,CNOT4,UFM1,NHLRC1,FBXO3,ASB10,PIAS4,UBA3,TRIM5,ZMYND11,TRIM8,FBXL7,ASB17,TSG101,UBE2M,MARCH8,UBA1,PHF2,ASB7
GO:BP	macromolecule metabolic process	GO:0043170	2.06E-12	12326	90	86	CCND1,AMFR,CCNF,APC,CCNB1,UBE2K,AIRE,CDK1,TRIP12,TRIM27,CDC34,FBXW4,BIRC3,HLTF,CDK2,LPXN,RNF7,BARD1,ESR1,TRAF4,UBE2E1,SOCS5,DZIP3,ITCH,IRF2BP1,ATG3,PHF19,FBXL17,FBXO8,MLLT6,TRIM24,CUL4A,SHPRH,PCGF6,RNF11,UBE2Z,TRIM13,FBXO21,DTX1,FBXO27,SOCS2,PSMB8,PHF20L1,RNF144A,UBE2N,FBXL15,UBR1,HERC3,H

							ECTD3,BRPF3,ASB13,BTRC,SPSB1,RNF168,UHRF1,FBXO38,FBXL12,CBL,BAZ1B,FBXO30,FBXO2,FBXW8,ZNRF2,PIAS2,FBXW2,RNF20,STUB1,FBXO28,CNOT4,UFM1,NHLRC1,FBXO3,ASB10,PIAS4,UBA3,TRIM5,ZMYND11,TRIM8,FBXL7,ASB17,TSG101,UBE2M,MARCH8,UBA1,PHF2,ASB7
GO:BP	primary metabolic process	GO:0044238	1.84E-11	12666	90	86	CCND1,AMFR,CCNF,APC,CCNB1,UBE2K,AIRE,CDK1,TRIP12,TRIM27,CDC34,FBXW4,BIRC3,HLTF,CDK2,LPXN,RNF7,BARD1,ESR1,TRAF4,UBE2E1,SOCS5,DZIP3,ITCH,IRF2BP1,ATG3,PHF19,FBXL17,FBXO8,MLLT6,TRIM24,CUL4A,SHPRH,PCGF6,RNF11,UBE2Z,TRIM13,FBXO21,DTX1,FBXO27,SOCS2,PSMB8,PHF20L1,RNF144A,UBE2N,FBXL15,UBR1,HERC3,HECTD3,BRPF3,ASB13,BTRC,SPSB1,RNF168,UHRF1,FBXO38,FBXL12,CBL,BAZ1B,FBXO30,FBXO2,FBXW8,ZNRF2,PIAS2,FBXW2,RNF20,STUB1,FBXO28,CNOT4,UFM1,NHLRC1,FBXO3,ASB10,PIAS4,UBA3,TRIM5,ZMYND11,TRIM8,FBXL7,ASB17,TSG101,UBE2M,MARCH8,UBA1,PHF2,ASB7
GO:BP	histone ubiquitination	GO:0016574	1.43E-09	31	90	8	TRIP12,BARD1,UBE2E1,PCGF6,UBE2N,RNF168,UHRF1,RNF20
GO:BP	organic substance metabolic process	GO:0071704	3.33E-08	13917	90	86	CCND1,AMFR,CCNF,APC,CCNB1,UBE2K,AIRE,CDK1,TRIP12,TRIM27,CDC34,FBXW4,BIRC3,HLTF,CDK2,LPXN,RNF7,BARD1,ESR1,TRAF4,UBE2E1,SOCS5,DZIP3,ITCH,IRF2BP1,ATG3,PHF19,FBXL17,FBXO8,MLLT6,TRIM24,CUL4A,SHPRH,PCGF6,RNF11,UBE2Z,TRIM13,FBXO21,DTX1,FBXO27,SOCS2,PSMB8,PHF20L1,RNF144A,UBE2N,FBXL15,UBR1,HERC3,HECTD3,BRPF3,ASB13,BTRC,SPSB1,RNF168,UHRF1,FBXO38,FBXL12,CBL,BAZ1B,FBXO30,FBXO2,FBXW8,ZNRF2,PIAS2,FBXW2,RNF20,STUB1,FBXO28,CNOT4,UFM1,NHLRC1,FBXO3,ASB10,PIAS4,UBA3,TRIM5,ZMYND11,TRIM8,FBXL7,ASB17,TSG101,UBE2M,MARCH8,UBA1,PHF2,ASB7
GO:BP	protein K63-linked ubiquitination	GO:0070534	3.52E-08	69	90	9	TRIP12,TRIM27,TRAF4,ITCH,UBE2N,RNF168,STUB1,TRIM5,TRIM8
GO:BP	metabolic process	GO:0008152	3.76E-08	14362	90	87	CCND1,AMFR,CCNF,APC,CCNB1,UBE2K,AIRE,CDK1,TRIP12,TRIM27,CDC34,FBXW4,BIRC3,HLTF,CDK2,LPXN,RNF7,BARD1,ESR1,TRAF4,UBE2E1,SOCS5,DZIP3,ITCH,IRF2BP1,ATG3,PHF19,FBXL17,FBXO8,MLLT6,TRIM24,CUL4A,SHPRH,PCGF6,RNF11,UBE2Z,TRIM13,FBXO21,DTX1,FBXO27,SOCS2,PSMB8,PHF20L1,RNF144A,VPS41,UBE2N,FBXL15,UBR1,HERC3,HECTD3,BRPF3,ASB13,BTRC,SPSB1,RNF168,UHRF1,FBXO38,FBXL12,CBL,BAZ1B,FBXO30,FBXO2,FBXW8,ZNRF2,PIAS2,FBXW2,RNF20,STUB1,FBXO28,CNOT4,UFM1,NHLRC1,FBXO3,ASB10,PIAS4,UBA3,TRIM5,ZMYND11,TRIM8,FBXL7,ASB17,TSG101,UBE2M,MARCH8,UBA1,PHF2,ASB7
GO:BP	protein autoubiquitination	GO:0051865	2.17E-07	84	90	9	AMFR,BARD1,ITCH,RNF11,TRIM13,UHRF1,CBL,STUB1,CNOT4

	ion						
GO:BP	protein K48-linked ubiquitination	GO:0070936	4.00026E-06	79	90	8	AMFR,UBE2K,CDC34,UBE2E1,ITCH,BTRC,FBXO38,ZNRF2
GO:BP	positive regulation of nitrogen compound metabolic process	GO:0051173	8.39538E-06	3071	90	36	CCND1,APC,UBE2K,AIRE,CDK1,TRIM27,BIRC3,HLTF,CDK2,BARD1,ESR1,TRAF4,UBE2E1,SOCS5,ITCH,MLLT6,TRIM24,CUL4A,TRIM13,DTX1,RNF144A,UBE2N,BRPF3,BTRC,RNF168,UHRF1,BAZ1B,RNF20,STUB1,CNOT4,NHLRC1,PIAS4,TRIM5,TRIM8,TSG101,PHF2
GO:BP	cellular response to stress	GO:0033554	9.37658E-06	1925	90	28	CCND1,AMFR,APC,CDK1,TRIP12,HLTF,CDK2,BARD1,TRAF4,SOCS5,ITCH,CUL4A,SHPRH,TRIM13,FBXO27,VPS41,UBE2N,RNF168,UHRF1,CBL,BAZ1B,FBXO2,STUB1,UFM1,NHLRC1,PIAS4,ZMYND11,UBA1
GO:BP	protein monoubiquitination	GO:0006513	5.84158E-05	72	90	7	BARD1,ITCH,PCGF6,UHRF1,CBL,RNF20,STUB1
GO:BP	chromatin organization	GO:0006325	8.28461E-05	788	90	17	CDK1,TRIP12,TRIM27,HLTF,CDK2,ESR1,PHF19,MLLT6,SHPRH,PCGF6,BRPF3,RNF168,UHRF1,BAZ1B,RNF20,ZMYND11,PHF2
GO:BP	regulation of protein catabolic process	GO:0042176	0.000114817	363	90	12	APC,UBE2K,CDK2,BARD1,SOCS5,ITCH,CUL4A,PHF20L1,RNF144A,BTRC,FBXO2,STUB1
GO:BP	regulation of nitrogen compound metabolic process	GO:0051171	0.000152728	5587	90	48	CCND1,CCNF,APC,CCNB1,UBE2K,AIRE,CDK1,TRIP12,TRIM27,BIRC3,HLTF,CDK2,BARD1,ESR1,TRAF4,UBE2E1,SOCS5,ITCH,IRF2BP1,PHF19,MLLT6,TRIM24,CUL4A,PCGF6,TRIM13,DTX1,PSMB8,PHF20L1,RNF144A,UBE2N,BRPF3,BTRC,RNF168,UHRF1,CBL,BAZ1B,FBXO2,PIAS2,RNF20,STUB1,CNOT4,NHLRC1,PIAS4,TRIM5,ZMYND11,TRIM8,TSG101,PHF2
GO:BP	regulation of signal transduction	GO:0009966	0.000201464	2973	90	33	AMFR,APC,CCNB1,UBE2K,CDC34,BIRC3,LPXN,BARD1,ESR1,TRAF4,SOCS5,ITCH,SCEL,FBXL17,FBXO8,TRIM24,CUL4A,TRIM13,DTX1,SOCS2,UBE2N,FBXL15,UBR1,BTRC,CBL,PIAS2,STUB1,UFM1,PIAS4,TRIM5,ZMYND11,TRIM8,TSG101
GO:BP	positive regulation of macromolecule	GO:0010604	0.000239942	3483	90	36	CCND1,APC,UBE2K,AIRE,CDK1,TRIM27,BIRC3,HLTF,CDK2,BARD1,ESR1,TRAF4,UBE2E1,SOCS5,ITCH,MLLT6,TRIM24,CUL4A,TRIM13,DTX1,RNF144A,UBE2N,BRPF3,BTRC,RNF168,UHRF1,BAZ1B,RNF20,STUB1,CNOT4,NHLRC1,PIAS4,TRIM5,TRIM8,TSG101,PHF2

	e metabolic process						
GO:BP	regulation of protein metabolic process	GO:0051246	0.000257234	2389	90	29	CCND1,CCNF,APC,CCNB1,UBE2K,AIRE,TRIP12,TRIM27,BIRC3,CDK2,BARD1,TRAF4,SOC S5,ITCH,CUL4A,PSMB8,PHF20L1,RNF144A,UBE2N,BTRC,UHRF1,CBL,BAZ1B,FBXO2,STU B1,CNOT4,NHLRC1,PIAS4,TSG101
GO:BP	chromatin remodeling	GO:0006338	0.000272445	655	90	15	CDK1,TRIP12,TRIM27,HLTF,CDK2,ESR1,PHF19,SHPRH,PCGF6,BRPF3,RNF168,UHRF1,BA Z1B,RNF20,PHF2
GO:BP	regulation of primary metabolic process	GO:0080090	0.000435609	5766	90	48	CCND1,CCNF,APC,CCNB1,UBE2K,AIRE,CDK1,TRIP12,TRIM27,BIRC3,HLTF,CDK2,BARD1 ,ESR1,TRAF4,UBE2E1,SOCS5,ITCH,IRF2BP1,PHF19,MLLT6,TRIM24,CUL4A,PCGF6,TRIM1 3,DTX1,PSMB8,PHF20L1,RNF144A,UBE2N,BRPF3,BTRC,RNF168,UHRF1,CBL,BAZ1B,FBX O2,PIAS2,RNF20,STUB1,CNOT4,NHLRC1,PIAS4,TRIM5,ZMYND11,TRIM8,TSG101,PHF2
GO:BP	protein-DNA complex organization	GO:0071824	0.000437788	885	90	17	CDK1,TRIP12,TRIM27,HLTF,CDK2,ESR1,PHF19,MLLT6,SHPRH,PCGF6,BRPF3,RNF168,UH RF1,BAZ1B,RNF20,ZMYND11,PHF2
GO:BP	intracellular signal transduction	GO:0035556	0.000472993	2609	90	30	CCND1,AMFR,APC,CCNB1,CDK1,CDC34,BIRC3,CDK2,BARD1,ESR1,TRAF4,SOCS5,ITCH, FBXO8,TRIM24,CUL4A,TRIM13,SOCS2,UBE2N,UBR1,ASB13,BTRC,CBL,ASB10,PIAS4,TRI M5,ZMYND11,TRIM8,ASB17,ASB7
GO:BP	DNA damage response	GO:0006974	0.000474116	890	90	17	CCND1,APC,CDK1,TRIP12,HLTF,CDK2,BARD1,CUL4A,SHPRH,UBE2N,RNF168,UHRF1,C BL,BAZ1B,STUB1,PIAS4,UBA1
GO:BP	positive regulation of metabolic process	GO:0009893	0.000671402	3797	90	37	CCND1,APC,CCNB1,UBE2K,AIRE,CDK1,TRIM27,BIRC3,HLTF,CDK2,BARD1,ESR1,TRAF4, UBE2E1,SOCS5,ITCH,MLLT6,TRIM24,CUL4A,TRIM13,DTX1,RNF144A,UBE2N,BRPF3,BTRC ,RNF168,UHRF1,BAZ1B,RNF20,STUB1,CNOT4,NHLRC1,PIAS4,TRIM5,TRIM8,TSG101,PHF 2
GO:BP	histone modification	GO:0016570	0.001142224	291	90	10	TRIP12,BARD1,UBE2E1,PCGF6,PHF20L1,UBE2N,RNF168,UHRF1,BAZ1B,RNF20
GO:BP	regulation of response to stimulus	GO:0048583	0.001420694	3909	90	37	AMFR,APC,CCNB1,UBE2K,TRIP12,TRIM27,CDC34,BIRC3,LPXN,BARD1,ESR1,TRAF4,SOC S5,ITCH,SCEL,FBXL17,FBXO8,TRIM24,CUL4A,TRIM13,DTX1,SOCS2,UBE2N,FBXL15,UBR1 ,BTRC,RNF168,FBXO38,CBL,PIAS2,STUB1,UFM1,PIAS4,TRIM5,ZMYND11,TRIM8,TSG101
GO:BP	regulation of signaling	GO:0023051	0.001437026	3396	90	34	AMFR,APC,CCNB1,UBE2K,CDC34,BIRC3,LPXN,BARD1,ESR1,TRAF4,SOCS5,ITCH,SCEL,F BXL17,FBXO8,TRIM24,CUL4A,TRIM13,DTX1,SOCS2,UBE2N,FBXL15,UBR1,BTRC,CBL,FBX O2,PIAS2,STUB1,UFM1,PIAS4,TRIM5,ZMYND11,TRIM8,TSG101

GO:BP	regulation of cell communication	GO:0010646	0.001530623	3405	90	34	AMFR,APC,CCNB1,UBE2K,CDC34,BIRC3,LPXN,BARD1,ESR1,TRAF4,SOCS5,ITCH,SCEL,FBXL17,FBXO8,TRIM24,CUL4A,TRIM13,DTX1,SOCS2,UBE2N,FBXL15,UBR1,BTRC,CBL,FBXO2,PIAS2,STUB1,UFM1,PIAS4,TRIM5,ZMYND11,TRIM8,TSG101
GO:BP	suppression of viral release by host	GO:0044790	0.001709507	17	90	4	TRIM27,TRIM13,TRIM5,TRIM8
GO:BP	regulation of catabolic process	GO:0009894	0.002874231	1013	90	17	APC,UBE2K,TRIM27,CDK2,BARD1,SOCS5,ITCH,CUL4A,TRIM13,PHF20L1,RNF144A,BTRC,FBXO2,STUB1,CNOT4,TRIM5,TRIM8
GO:BP	regulation of protein modification process	GO:0031399	0.002977195	1385	90	20	CCND1,CCNF,APC,CCNB1,UBE2K,TRIP12,TRIM27,BIRC3,TRAF4,SOCS5,ITCH,UBE2N,BTRC,CBL,BAZ1B,FBXO2,STUB1,NHLRC1,PIAS4,TSG101
GO:BP	regulation of protein modification by small protein conjugation or removal	GO:1903320	0.003432433	254	90	9	TRIP12,BIRC3,ITCH,UBE2N,BTRC,FBXO2,STUB1,NHLRC1,PIAS4
GO:BP	histone monoubiquitination	GO:0010390	0.003446032	20	90	4	BARD1,PCGF6,UHRF1,RNF20
GO:BP	regulation of post-translational protein modification	GO:1901873	0.003672022	331	90	10	TRIP12,BIRC3,ITCH,UBE2N,BTRC,BAZ1B,FBXO2,STUB1,NHLRC1,PIAS4
GO:BP	regulation of canonical NF-kappaB signal transduction	GO:0043122	0.004161395	260	90	9	BIRC3,ESR1,TRAF4,TRIM13,UBE2N,BTRC,TRIM5,ZMYND11,TRIM8
GO:BP	G2/M transition of mitotic cell	GO:0000086	0.005113603	138	90	7	CCND1,CCNB1,CDK1,CDK2,BARD1,FBXL15,FBXL7

	cycle						
GO:BP	positive regulation of biological process	GO:0048518	0.005850348	6253	90	48	CCND1,APC,CCNB1,UBE2K,AIRE,CDK1,TRIM27,CDC34,FBXW4,BIRC3,HLTF,CDK2,LPXN,BARD1,ESR1,TRAF4,UBE2E1,SOCS5,ITCH,SCEL,MLLT6,TRIM24,CUL4A,UBE2Z,TRIM13,DTX1,SOCS2,RNF144A,UBE2N,FBXL15,BRPF3,BTRC,RNF168,UHRF1,FBXO38,CBL,BAZ1B,FBXW8,RNF20,STUB1,CNOT4,NHLRC1,PIAS4,TRIM5,TRIM8,TSG101,UBE2M,PHF2
GO:BP	histone H2A ubiquitination	GO:0033522	0.006236587	23	90	4	TRIP12,BARD1,PCGF6,RNF168
GO:BP	mitotic cell cycle phase transition	GO:0044772	0.007820278	447	90	11	CCND1,CCNF,APC,CCNB1,CDK1,CDC34,CDK2,BARD1,CUL4A,FBXL15,FBXL7
GO:BP	positive regulation of nucleobase-containing compound metabolic process	GO:0045935	0.007882575	2039	90	24	AIRE,CDK1,TRIM27,HLTF,CDK2,ESR1,UBE2E1,MLLT6,TRIM24,TRIM13,DTX1,UBE2N,BRPF3,BTRC,RNF168,UHRF1,BAZ1B,RNF20,CNOT4,PIAS4,TRIM5,TRIM8,TSG101,PHF2
GO:BP	positive regulation of cellular process	GO:0048522	0.008061726	5711	90	45	CCND1,APC,CCNB1,UBE2K,AIRE,CDK1,TRIM27,CDC34,FBXW4,BIRC3,HLTF,CDK2,BARD1,ESR1,TRAF4,UBE2E1,SOCS5,ITCH,SCEL,MLLT6,TRIM24,CUL4A,UBE2Z,TRIM13,DTX1,SOCS2,UBE2N,FBXL15,BRPF3,BTRC,RNF168,UHRF1,FBXO38,CBL,BAZ1B,FBXW8,RNF20,STUB1,CNOT4,PIAS4,TRIM5,TRIM8,TSG101,UBE2M,PHF2
GO:BP	negative regulation of biological process	GO:0048519	0.008136934	5913	90	46	CCND1,AMFR,CCNF,APC,CCNB1,CDK1,TRIP12,TRIM27,CDC34,BIRC3,CDK2,LPXN,BARD1,ESR1,SOCS5,ITCH,IRF2BP1,ATG3,PHF19,TRIM24,CUL4A,PCGF6,UBE2Z,TRIM13,DTX1,SOCS2,PHF20L1,UBR1,BTRC,RNF168,UHRF1,CBL,BAZ1B,FBXO2,PIAS2,RNF20,STUB1,CNOT4,UFM1,NHLRC1,PIAS4,TRIM5,ZMYND11,TRIM8,TSG101,PHF2
GO:BP	cellular response to stimulus	GO:0051716	0.009044939	7399	90	53	CCND1,AMFR,APC,CCNB1,UBE2K,CDK1,TRIP12,CDC34,FBXW4,BIRC3,HLTF,CDK2,LPXN,BARD1,ESR1,TRAF4,SOCS5,TNFRSF25,ITCH,SCEL,FBXL17,FBXO8,TRIM24,CUL4A,SHPRH,TRIM13,DTX1,FBXO27,SOCS2,VPS41,UBE2N,FBXL15,UBR1,ASB13,BTRC,RNF168,UHRF1,CBL,BAZ1B,FBXO2,PIAS2,STUB1,UFM1,NHLRC1,ASB10,PIAS4,TRIM5,ZMYND11,TRIM8,ASB17,TSG101,UBA1,ASB7
GO:BP	cell cycle G2/M phase transition	GO:0044839	0.010599362	154	90	7	CCND1,CCNB1,CDK1,CDK2,BARD1,FBXL15,FBXL7

GO:BP	canonical NF-kappaB signal transduction	GO:0007249	0.011357774	294	90	9	BIRC3,ESR1,TRAF4,TRIM13,UBE2N,BTRC,TRIM5,ZMYND11,TRIM8
GO:BP	negative regulation of cell cycle process	GO:0010948	0.013018289	299	90	9	CCND1,CCNF,APC,CCNB1,CDK1,CDK2,BARD1,CUL4A,BAZ1B
GO:BP	response to stimulus	GO:0050896	0.022197163	8955	90	59	CCND1,AMFR,APC,CCNB1,UBE2K,AIRE,CDK1,TRIP12,TRIM27,CDC34,FBXW4,BIRC3,HLTF,CDK2,LPXN,RNF7,BARD1,ESR1,TRAF4,SOCS5,TNFRSF25,ITCH,SCEL,FBXL17,FBXO8,TRIM24,CUL4A,SHPRH,TRIM13,DTX1,FBXO27,SOCS2,VPS41,UBE2N,FBXL15,UBR1,ASB13,BTRC,RNF168,UHRF1,FBXO38,CBL,BAZ1B,FBXO2,PIAS2,STUB1,UFM1,NHLRC1,FBXO3,ASB10,PIAS4,TRIM5,ZMYND11,TRIM8,ASB17,TSG101,MARCH8,UBA1,ASB7
GO:BP	DNA repair	GO:0006281	0.023341646	602	90	12	CDK1,TRIP12,HLTF,CDK2,BARD1,CUL4A,SHPRH,UBE2N,RNF168,UHRF1,STUB1,PIAS4
GO:BP	negative regulation of gene expression, epigenetic	GO:0045814	0.025272649	116	90	6	TRIP12,TRIM27,CDK2,PHF19,UHRF1,PHF2
GO:BP	regulation of nucleobase-containing compound metabolic process	GO:0019219	0.027128514	4038	90	35	CCND1,AIRE,CDK1,TRIP12,TRIM27,HLTF,CDK2,BARD1,ESR1,UBE2E1,ITCH,IRF2BP1,PHF19,MLLT6,TRIM24,CUL4A,PCGF6,TRIM13,DTX1,PHF20L1,UBE2N,BRPF3,BTRC,RNF168,UHRF1,BAZ1B,PIAS2,RNF20,CNOT4,PIAS4,TRIM5,ZMYND11,TRIM8,TSG101,PHF2
GO:BP	response to stress	GO:0006950	0.036268779	3909	90	34	CCND1,AMFR,APC,UBE2K,CDK1,TRIP12,TRIM27,BIRC3,HLTF,CDK2,BARD1,ESR1,TRAF4,SOCS5,ITCH,CUL4A,SHPRH,TRIM13,FBXO27,VPS41,UBE2N,RNF168,UHRF1,CBL,BAZ1B,FBXO2,STUB1,UFM1,NHLRC1,PIAS4,TRIM5,ZMYND11,TRIM8,UBA1
GO:BP	positive regulation of catabolic process	GO:0009896	0.037555231	528	90	11	APC,BARD1,SOCS5,ITCH,CUL4A,TRIM13,RNF144A,STUB1,CNOT4,TRIM5,TRIM8
GO:BP	DNA-templated transcription	GO:0006351	0.038378036	3563	90	32	CCND1,AIRE,CDK1,TRIM27,HLTF,CDK2,LPXN,ESR1,UBE2E1,ITCH,IRF2BP1,PHF19,MLLT6,TRIM24,PCGF6,TRIM13,DTX1,PHF20L1,UBE2N,BRPF3,BTRC,RNF168,UHRF1,BAZ1B,PIAS

							2,RNF20,PIAS4,TRIM5,ZMYND11,TRIM8,TSG101,PHF2
GO:BP	response to endoplasmic reticulum stress	GO:0034976	0.04125002	263	90	8	CCND1,AMFR,TRIM13,FBXO27,FBXO2,STUB1,UFM1,NHLRC1
GO:BP	regulation of RNA metabolic process	GO:0051252	0.041361714	3753	90	33	CCND1,AIRE,CDK1,TRIM27,HLTF,CDK2,BARD1,ESR1,UBE2E1,ITCH,IRF2BP1,PHF19,MLLT6,TRIM24,PCGF6,TRIM13,DTX1,PHF20L1,UBE2N,BRPF3,BTRC,RNF168,UHRF1,BAZ1B,PIAS2,RNF20,CNOT4,PIAS4,TRIM5,ZMYND11,TRIM8,TSG101,PHF2
GO:BP	positive regulation of post-translational protein modification	GO:1901875	0.043264476	191	90	7	BIRC3,UBE2N,BTRC,BAZ1B,STUB1,NHLRC1,PIAS4
GO:BP	regulation of proteasomal protein catabolic process	GO:0061136	0.046270695	193	90	7	UBE2K,CDK2,SOCS5,PHF20L1,RNF144A,BTRC,STUB1
GO:BP	cell cycle checkpoint signaling	GO:0000075	0.046270695	193	90	7	CCND1,APC,CCNB1,CDK1,CDK2,BARD1,CUL4A
GO:BP	RNA biosynthetic process	GO:0032774	0.047595268	3600	90	32	CCND1,AIRE,CDK1,TRIM27,HLTF,CDK2,LPXN,ESR1,UBE2E1,ITCH,IRF2BP1,PHF19,MLLT6,TRIM24,PCGF6,TRIM13,DTX1,PHF20L1,UBE2N,BRPF3,BTRC,RNF168,UHRF1,BAZ1B,PIAS2,RNF20,PIAS4,TRIM5,ZMYND11,TRIM8,TSG101,PHF2
GO:BP	regulation of DNA-binding transcription factor activity	GO:0051090	0.048392214	444	90	10	TRIM27,ESR1,ITCH,TRIM13,UBE2N,BTRC,PIAS2,PIAS4,TRIM5,TRIM8

Table 7.5. Protein-protein interactions in tabular form, 0.5 h hits. Columns “Node 1” and “Node 2” at each row contain protein names interacting, columns “Node 1 accession number” and “Node 2 accession number” contain unique identifier of the String database. Column “Homology” contains homology value that the String database calculates from known interaction between the same proteins in other species. The experimentally determined interaction score combines the information from the BIND, DIP, GRID, HPRD, IntAct, MINT, and PID databases. The database annotated interaction score combines the information from the Biocarta, BioCyc, GO, KEGG, and Reactome. Combined score is calculated by combining the probabilities from the different evidence channels (experimental and annotated) and corrected for the probability of randomly observing an interaction.

node 1	node 2	node 1 accession number	node 2 accession number	homology	experimentally determined interaction	database annotated	combined score
ASB13	RNF7	9606.ENSP00000350331	9606.ENSP00000273480	0	0.468	0.4	0.667
ASB14	RNF7	9606.ENSP00000419199	9606.ENSP00000273480	0	0.09	0.4	0.43
ASB15	RNF7	9606.ENSP00000397655	9606.ENSP00000273480	0	0.09	0.4	0.43
ASB17	RNF7	9606.ENSP00000284142	9606.ENSP00000273480	0	0	0.4	0.4
ASB7	RNF7	9606.ENSP00000328327	9606.ENSP00000273480	0	0.61	0.4	0.756
BAZ1B	CHD4	9606.ENSP00000342434	9606.ENSP00000440542	0.547	0.581	0	0.581
BIRC3	TRAF5	9606.ENSP00000263464	9606.ENSP00000261464	0	0.066	0.9	0.902
BIRC3	UBE2L3	9606.ENSP00000263464	9606.ENSP00000400906	0	0.328	0.4	0.58
BIRC3	UBE2D3	9606.ENSP00000263464	9606.ENSP00000349722	0	0.612	0.5	0.798
BIRC3	UBE2D1	9606.ENSP00000263464	9606.ENSP00000363019	0	0.833	0.5	0.913
BIRC3	TRAF6	9606.ENSP00000263464	9606.ENSP00000433623	0	0.717	0.4	0.823
BIRC3	TRAF3	9606.ENSP00000263464	9606.ENSP00000376500	0	0.719	0.9	0.97
BMI1	TP53	9606.ENSP00000365851	9606.ENSP00000269305	0	0.625	0.5	0.804
BMI1	UBE2C	9606.ENSP00000365851	9606.ENSP00000348838	0	0.071	0.9	0.903
BMI1	UBE2D3	9606.ENSP00000365851	9606.ENSP00000349722	0	0.853	0	0.853
BMI1	CHD4	9606.ENSP000	9606.ENSP000	0	0.07	0.5	0.515

		00365851	00440542				
BRPF3	TP53	9606.ENSP000350267	9606.ENSP000269305	0	0.421	0.5	0.698
BRPF3	CHD4	9606.ENSP000350267	9606.ENSP000440542	0	0.07	0.4	0.418
BTRC	CDC34	9606.ENSP000359206	9606.ENSP000215574	0	0.839	0.5	0.916
BTRC	TP53	9606.ENSP000359206	9606.ENSP000269305	0	0.51	0	0.51
BTRC	RNF7	9606.ENSP000359206	9606.ENSP000273480	0	0.554	0	0.554
BTRC	UBE2D3	9606.ENSP000359206	9606.ENSP000349722	0	0.66	0	0.66
BTRC	SMURF1	9606.ENSP000359206	9606.ENSP000354621	0	0.523	0	0.523
BTRC	UHRF1	9606.ENSP000359206	9606.ENSP000479617	0	0.601	0	0.601
BTRC	FBXW8	9606.ENSP000359206	9606.ENSP000498999	0.558	0.51	0	0.51
BTRC	UBE2D1	9606.ENSP000359206	9606.ENSP000363019	0	0.358	0.8	0.866
BTRC	FBXO43	9606.ENSP000359206	9606.ENSP000403293	0	0	0.9	0.9
CACUL1	RNF7	9606.ENSP000358147	9606.ENSP000273480	0	0.573	0	0.573
CDC34	UBE2G2	9606.ENSP000215574	9606.ENSP000338348	0.915	0.09	0.4	0.43
CDC34	UBE2T	9606.ENSP000215574	9606.ENSP000494957	0.747	0	0.4	0.4
CDC34	UBE2B	9606.ENSP000215574	9606.ENSP000265339	0.868	0.073	0.4	0.42
CDC34	UBE2D1	9606.ENSP000215574	9606.ENSP000363019	0.855	0	0.4	0.4
CDC34	UBE2L3	9606.ENSP000215574	9606.ENSP000400906	0.731	0	0.4	0.4
CDC34	UBE2C	9606.ENSP000215574	9606.ENSP000348838	0.777	0	0.4	0.4
CDC34	UBE2H	9606.ENSP000215574	9606.ENSP000347836	0.72	0.061	0.4	0.412
CDC34	RNF7	9606.ENSP000215574	9606.ENSP000273480	0	0.691	0	0.691
CDC34	BTRC	9606.ENSP000215574	9606.ENSP000359206	0	0.839	0.5	0.916
CDK2	HERC2	9606.ENSP000266970	9606.ENSP000261609	0	0.05	0.5	0.504

CDK2	UBE2V2	9606.ENSPO00 00266970	9606.ENSPO00 00428209	0	0	0.5	0.499
CDK2	RNF168	9606.ENSPO00 00266970	9606.ENSPO00 00320898	0	0	0.5	0.499
CDK2	UBE2D1	9606.ENSPO00 00266970	9606.ENSPO00 00363019	0	0.091	0.5	0.526
CDK2	RNF8	9606.ENSPO00 00266970	9606.ENSPO00 00362578	0	0.091	0.5	0.526
CDK2	UBE2C	9606.ENSPO00 00266970	9606.ENSPO00 00348838	0	0.091	0.5	0.526
CDK2	TP53	9606.ENSPO00 00266970	9606.ENSPO00 00269305	0	0.778	0.5	0.884
CHD4	TP53	9606.ENSPO00 00440542	9606.ENSPO00 00269305	0	0.164	0.5	0.564
CHD4	BAZ1B	9606.ENSPO00 00440542	9606.ENSPO00 00342434	0.547	0.581	0	0.581
CHD4	BRPF3	9606.ENSPO00 00440542	9606.ENSPO00 00350267	0	0.07	0.4	0.418
CHD4	RNF8	9606.ENSPO00 00440542	9606.ENSPO00 00362578	0	0.519	0	0.519
CHD4	BMI1	9606.ENSPO00 00440542	9606.ENSPO00 00365851	0	0.07	0.5	0.515
CHD4	ZNF592	9606.ENSPO00 00440542	9606.ENSPO00 00452877	0	0.541	0	0.541
CUL4A	RAD18	9606.ENSPO00 00364589	9606.ENSPO00 00264926	0	0	0.5	0.499
CUL4A	UBE2B	9606.ENSPO00 00364589	9606.ENSPO00 00265339	0	0.059	0.5	0.509
CUL4A	TP53	9606.ENSPO00 00364589	9606.ENSPO00 00269305	0	0.51	0	0.51
CUL4A	RNF7	9606.ENSPO00 00364589	9606.ENSPO00 00273480	0	0.663	0	0.663
CUL4A	DCUN1D1	9606.ENSPO00 00364589	9606.ENSPO00 00292782	0	0.825	0.5	0.909
CUL4A	FBXW5	9606.ENSPO00 00364589	9606.ENSPO00 00313034	0	0.625	0.9	0.96
CUL4A	UBE2V2	9606.ENSPO00 00364589	9606.ENSPO00 00428209	0	0	0.5	0.499
DCUN1D1	TRIM39	9606.ENSPO00 00292782	9606.ENSPO00 00365844	0	0.407	0	0.407
DCUN1D1	UBE2D1	9606.ENSPO00 00292782	9606.ENSPO00 00363019	0	0	0.5	0.499
DCUN1D1	UBE2D3	9606.ENSPO00 00292782	9606.ENSPO00 00349722	0	0.292	0.5	0.63
DCUN1D1	CUL4A	9606.ENSPO00 00292782	9606.ENSPO00 00364589	0	0.825	0.5	0.909

ESR1	STUB1	9606.ENSPO00 00405330	9606.ENSPO00 00219548	0	0.788	0.5	0.889
ESR1	TP53	9606.ENSPO00 00405330	9606.ENSPO00 00269305	0	0.735	0	0.735
ESR1	TRIM24	9606.ENSPO00 00405330	9606.ENSPO00 00340507	0	0.836	0	0.836
ESR1	SMURF1	9606.ENSPO00 00405330	9606.ENSPO00 00354621	0	0.514	0	0.514
FBH1	RAD18	9606.ENSPO00 00369335	9606.ENSPO00 00264926	0	0.773	0	0.773
FBH1	UBE2B	9606.ENSPO00 00369335	9606.ENSPO00 00265339	0	0.411	0	0.41
FBXL5	HERC2	9606.ENSPO00 00344866	9606.ENSPO00 00261609	0	0.624	0	0.624
FBXL5	TP53	9606.ENSPO00 00344866	9606.ENSPO00 00269305	0	0	0.4	0.4
FBXL5	FBXW5	9606.ENSPO00 00344866	9606.ENSPO00 00313034	0	0	0.4	0.4
FBXL5	FBXW4	9606.ENSPO00 00344866	9606.ENSPO00 00499522	0	0	0.4	0.4
FBXL5	FBXW10	9606.ENSPO00 00344866	9606.ENSPO00 00379025	0	0	0.4	0.4
FBXL5	FBXO6	9606.ENSPO00 00344866	9606.ENSPO00 00365944	0	0	0.4	0.4
FBXO22	TP53	9606.ENSPO00 00307833	9606.ENSPO00 00269305	0	0.51	0	0.51
FBXO28	TRAF5	9606.ENSPO00 00355827	9606.ENSPO00 00261464	0	0.492	0	0.491
FBXO43	BTRC	9606.ENSPO00 00403293	9606.ENSPO00 00359206	0	0	0.9	0.9
FBXO6	TP53	9606.ENSPO00 00365944	9606.ENSPO00 00269305	0	0	0.4	0.4
FBXO6	FBXW5	9606.ENSPO00 00365944	9606.ENSPO00 00313034	0	0	0.4	0.4
FBXO6	FBXL5	9606.ENSPO00 00365944	9606.ENSPO00 00344866	0	0	0.4	0.4
FBXO6	FBXW10	9606.ENSPO00 00365944	9606.ENSPO00 00379025	0	0	0.4	0.4
FBXO6	FBXW4	9606.ENSPO00 00365944	9606.ENSPO00 00499522	0	0	0.4	0.4
FBXW10	TP53	9606.ENSPO00 00379025	9606.ENSPO00 00269305	0	0	0.4	0.4
FBXW10	FBXW5	9606.ENSPO00 00379025	9606.ENSPO00 00313034	0	0	0.4	0.4
FBXW10	FBXL5	9606.ENSPO00 00379025	9606.ENSPO00 00344866	0	0	0.4	0.4

FBXW10	FBXO6	9606.ENSPO00 00379025	9606.ENSPO00 00365944	0	0	0.4	0.4
FBXW10	FBXW4	9606.ENSPO00 00379025	9606.ENSPO00 00499522	0	0	0.4	0.4
FBXW4	TP53	9606.ENSPO00 00499522	9606.ENSPO00 00269305	0	0	0.4	0.4
FBXW4	FBXW5	9606.ENSPO00 00499522	9606.ENSPO00 00313034	0	0	0.4	0.4
FBXW4	FBXL5	9606.ENSPO00 00499522	9606.ENSPO00 00344866	0	0	0.4	0.4
FBXW4	FBXO6	9606.ENSPO00 00499522	9606.ENSPO00 00365944	0	0	0.4	0.4
FBXW4	FBXW10	9606.ENSPO00 00499522	9606.ENSPO00 00379025	0	0	0.4	0.4
FBXW5	TP53	9606.ENSPO00 00313034	9606.ENSPO00 00269305	0	0	0.4	0.4
FBXW5	ZNRF1	9606.ENSPO00 00313034	9606.ENSPO00 00335091	0	0.42	0	0.42
FBXW5	FBXO6	9606.ENSPO00 00313034	9606.ENSPO00 00365944	0	0	0.4	0.4
FBXW5	FBXW10	9606.ENSPO00 00313034	9606.ENSPO00 00379025	0	0	0.4	0.4
FBXW5	FBXL5	9606.ENSPO00 00313034	9606.ENSPO00 00344866	0	0	0.4	0.4
FBXW5	FBXW4	9606.ENSPO00 00313034	9606.ENSPO00 00499522	0	0	0.4	0.4
FBXW5	CUL4A	9606.ENSPO00 00313034	9606.ENSPO00 00364589	0	0.625	0.9	0.96
FBXW8	TP53	9606.ENSPO00 00498999	9606.ENSPO00 00269305	0	0.601	0	0.601
FBXW8	BTRC	9606.ENSPO00 00498999	9606.ENSPO00 00359206	0.558	0.51	0	0.51
HERC2	UBE2V2	9606.ENSPO00 00261609	9606.ENSPO00 00428209	0	0	0.5	0.499
HERC2	CDK2	9606.ENSPO00 00261609	9606.ENSPO00 00266970	0	0.05	0.5	0.504
HERC2	RNF168	9606.ENSPO00 00261609	9606.ENSPO00 00320898	0	0.292	0.5	0.63
HERC2	FBXL5	9606.ENSPO00 00261609	9606.ENSPO00 00344866	0	0.624	0	0.624
HERC2	TP53	9606.ENSPO00 00261609	9606.ENSPO00 00269305	0	0.787	0	0.787
HERC2	RNF8	9606.ENSPO00 00261609	9606.ENSPO00 00362578	0	0.786	0.7	0.933
HERC3	UBE2L3	9606.ENSPO00 00385684	9606.ENSPO00 00400906	0	0.461	0	0.461

HERC6	UBE2L3	9606.ENSPO00 00264346	9606.ENSPO00 00400906	0	0.461	0	0.461
HUWE1	TP53	9606.ENSPO00 00340648	9606.ENSPO00 00269305	0	0.636	0	0.636
HUWE1	UBE2D3	9606.ENSPO00 00340648	9606.ENSPO00 00349722	0	0.51	0	0.51
HUWE1	UBE2D1	9606.ENSPO00 00340648	9606.ENSPO00 00363019	0	0.833	0	0.833
HUWE1	UBE2L3	9606.ENSPO00 00340648	9606.ENSPO00 00400906	0	0.865	0	0.865
LGR6	RNF43	9606.ENSPO00 00356247	9606.ENSPO00 00463069	0	0	0.5	0.499
MARCHF8	UBE2H	9606.ENSPO00 00411848	9606.ENSPO00 00347836	0	0.51	0	0.51
MARCHF8	UBE2D3	9606.ENSPO00 00411848	9606.ENSPO00 00349722	0	0.525	0	0.525
MID1	UBE2D3	9606.ENSPO00 00414521	9606.ENSPO00 00349722	0	0.845	0	0.845
MID1	UBE2D1	9606.ENSPO00 00414521	9606.ENSPO00 00363019	0	0.83	0	0.83
MYLIP	UBE2D3	9606.ENSPO00 00349298	9606.ENSPO00 00349722	0	0.535	0	0.535
MYLIP	UBE2D1	9606.ENSPO00 00349298	9606.ENSPO00 00363019	0	0.972	0	0.972
NEURL2	RNF7	9606.ENSPO00 00361596	9606.ENSPO00 00273480	0	0	0.5	0.499
PJA1	UBE2D3	9606.ENSPO00 00355014	9606.ENSPO00 00349722	0	0.561	0	0.561
PRPF19	RNF113A	9606.ENSPO00 00227524	9606.ENSPO00 00360497	0	0.991	0	0.991
RAD18	CUL4A	9606.ENSPO00 00264926	9606.ENSPO00 00364589	0	0	0.5	0.499
RAD18	FBH1	9606.ENSPO00 00264926	9606.ENSPO00 00369335	0	0.773	0	0.773
RAD18	UBE2V2	9606.ENSPO00 00264926	9606.ENSPO00 00428209	0	0.088	0.5	0.524
RAD18	UBE2B	9606.ENSPO00 00264926	9606.ENSPO00 00265339	0	0.998	0.7	0.999
RFPL1	RFPL3	9606.ENSPO00 00346342	9606.ENSPO00 00249007	0.984	0.604	0	0.604
RFPL2	RFPL3	9606.ENSPO00 00383096	9606.ENSPO00 00249007	0.982	0.465	0	0.465
RFPL3	RFPL1	9606.ENSPO00 00249007	9606.ENSPO00 00346342	0.984	0.604	0	0.604
RFPL3	RFPL2	9606.ENSPO00 00249007	9606.ENSPO00 00383096	0.982	0.465	0	0.465

RNF11	UBE2D3	9606.ENSP000 00242719	9606.ENSP000 00349722	0	0.667	0	0.667
RNF11	UBE2D1	9606.ENSP000 00242719	9606.ENSP000 00363019	0	0.643	0	0.643
RNF113A	PRPF19	9606.ENSP000 00360497	9606.ENSP000 00227524	0	0.991	0	0.991
RNF114	UBE2D3	9606.ENSP000 00244061	9606.ENSP000 00349722	0	0.437	0	0.437
RNF114	UBE2D1	9606.ENSP000 00244061	9606.ENSP000 00363019	0	0.747	0	0.747
RNF115	UBE2D1	9606.ENSP000 00463650	9606.ENSP000 00363019	0	0.496	0	0.496
RNF123	UBE2D1	9606.ENSP000 00328287	9606.ENSP000 00363019	0	0.411	0	0.41
RNF168	HERC2	9606.ENSP000 00320898	9606.ENSP000 00261609	0	0.292	0.5	0.63
RNF168	CDK2	9606.ENSP000 00320898	9606.ENSP000 00266970	0	0	0.5	0.499
RNF168	UBE2D1	9606.ENSP000 00320898	9606.ENSP000 00363019	0	0.625	0	0.625
RNF168	UBE2V2	9606.ENSP000 00320898	9606.ENSP000 00428209	0	0	0.5	0.499
RNF168	UBE2D3	9606.ENSP000 00320898	9606.ENSP000 00349722	0	0.783	0	0.783
RNF168	RNF8	9606.ENSP000 00320898	9606.ENSP000 00362578	0	0	0.5	0.499
RNF181	UBE2D3	9606.ENSP000 00306906	9606.ENSP000 00349722	0	0.396	0.5	0.685
RNF181	UBE2D1	9606.ENSP000 00306906	9606.ENSP000 00363019	0	0.654	0.5	0.819
RNF185	UBE2D3	9606.ENSP000 00320508	9606.ENSP000 00349722	0	0.616	0	0.616
RNF43	LGR6	9606.ENSP000 00463069	9606.ENSP000 00356247	0	0	0.5	0.499
RNF7	CDC34	9606.ENSP000 00273480	9606.ENSP000 00215574	0	0.691	0	0.691
RNF7	ASB14	9606.ENSP000 00273480	9606.ENSP000 00419199	0	0.09	0.4	0.43
RNF7	NEURL2	9606.ENSP000 00273480	9606.ENSP000 00361596	0	0	0.5	0.499
RNF7	ASB17	9606.ENSP000 00273480	9606.ENSP000 00284142	0	0	0.4	0.4
RNF7	ASB15	9606.ENSP000 00273480	9606.ENSP000 00397655	0	0.09	0.4	0.43
RNF7	SPSB1	9606.ENSP000 00273480	9606.ENSP000 00330221	0	0.292	0.4	0.557

RNF7	CACUL1	9606.ENSP000 00273480	9606.ENSP000 00358147	0	0.573	0	0.573
RNF7	ASB13	9606.ENSP000 00273480	9606.ENSP000 00350331	0	0.468	0.4	0.667
RNF7	BTRC	9606.ENSP000 00273480	9606.ENSP000 00359206	0	0.554	0	0.554
RNF7	UBE2L3	9606.ENSP000 00273480	9606.ENSP000 00400906	0	0.417	0	0.417
RNF7	ASB7	9606.ENSP000 00273480	9606.ENSP000 00328327	0	0.61	0.4	0.756
RNF7	SOCS3	9606.ENSP000 00273480	9606.ENSP000 00330341	0	0.516	0.4	0.697
RNF7	UBE2C	9606.ENSP000 00273480	9606.ENSP000 00348838	0	0.691	0.36	0.794
RNF7	SOCS2	9606.ENSP000 00273480	9606.ENSP000 00481249	0	0.475	0.5	0.726
RNF7	UBE2D3	9606.ENSP000 00273480	9606.ENSP000 00349722	0	0.781	0.5	0.886
RNF7	UBE2D1	9606.ENSP000 00273480	9606.ENSP000 00363019	0	0.88	0.5	0.937
RNF7	CUL4A	9606.ENSP000 00273480	9606.ENSP000 00364589	0	0.663	0	0.663
RNF8	HERC2	9606.ENSP000 00362578	9606.ENSP000 00261609	0	0.786	0.7	0.933
RNF8	CDK2	9606.ENSP000 00362578	9606.ENSP000 00266970	0	0.091	0.5	0.526
RNF8	RNF168	9606.ENSP000 00362578	9606.ENSP000 00320898	0	0	0.5	0.499
RNF8	UBE2D3	9606.ENSP000 00362578	9606.ENSP000 00349722	0	0.76	0	0.76
RNF8	UBE2D1	9606.ENSP000 00362578	9606.ENSP000 00363019	0	0.577	0	0.577
RNF8	CHD4	9606.ENSP000 00362578	9606.ENSP000 00440542	0	0.519	0	0.519
RNF8	UBE2V2	9606.ENSP000 00362578	9606.ENSP000 00428209	0	0.647	0.5	0.816
SMURF1	TRAF4	9606.ENSP000 00354621	9606.ENSP000 00262395	0	0.525	0	0.525
SMURF1	UBE2D3	9606.ENSP000 00354621	9606.ENSP000 00349722	0	0.904	0	0.904
SMURF1	ESR1	9606.ENSP000 00354621	9606.ENSP000 00405330	0	0.514	0	0.514
SMURF1	UBE2D1	9606.ENSP000 00354621	9606.ENSP000 00363019	0	0.444	0	0.444
SMURF1	BTRC	9606.ENSP000 00354621	9606.ENSP000 00359206	0	0.523	0	0.523

SMURF1	UBE2L3	9606.ENSP000 00354621	9606.ENSP000 00400906	0	0.886	0	0.886
SOCS2	RNF7	9606.ENSP000 00481249	9606.ENSP000 00273480	0	0.475	0.5	0.726
SOCS2	SOCS3	9606.ENSP000 00481249	9606.ENSP000 00330341	0.764	0.303	0.9	0.927
SOCS3	RNF7	9606.ENSP000 00330341	9606.ENSP000 00273480	0	0.516	0.4	0.697
SOCS3	UBE2D1	9606.ENSP000 00330341	9606.ENSP000 00363019	0	0	0.5	0.499
SOCS3	UBE2D3	9606.ENSP000 00330341	9606.ENSP000 00349722	0	0	0.5	0.499
SOCS3	TRAF6	9606.ENSP000 00330341	9606.ENSP000 00433623	0	0.51	0	0.51
SOCS3	SOCS2	9606.ENSP000 00330341	9606.ENSP000 00481249	0.764	0.303	0.9	0.927
SPSB1	RNF7	9606.ENSP000 00330221	9606.ENSP000 00273480	0	0.292	0.4	0.557
STUB1	UBE2T	9606.ENSP000 00219548	9606.ENSP000 00494957	0	0.419	0	0.418
STUB1	UBE2L3	9606.ENSP000 00219548	9606.ENSP000 00400906	0	0.648	0	0.648
STUB1	TRAF6	9606.ENSP000 00219548	9606.ENSP000 00433623	0	0.634	0	0.634
STUB1	UBE2V2	9606.ENSP000 00219548	9606.ENSP000 00428209	0	0.47	0.72	0.845
STUB1	UBE2B	9606.ENSP000 00219548	9606.ENSP000 00265339	0	0.175	0.72	0.759
STUB1	ESR1	9606.ENSP000 00219548	9606.ENSP000 00405330	0	0.788	0.5	0.889
STUB1	TP53	9606.ENSP000 00219548	9606.ENSP000 00269305	0	0.916	0	0.916
STUB1	UBE2D3	9606.ENSP000 00219548	9606.ENSP000 00349722	0	0.968	0.5	0.983
STUB1	UBE2D1	9606.ENSP000 00219548	9606.ENSP000 00363019	0	0.996	0	0.996
TP53	STUB1	9606.ENSP000 00269305	9606.ENSP000 00219548	0	0.916	0	0.916
TP53	HERC2	9606.ENSP000 00269305	9606.ENSP000 00261609	0	0.787	0	0.787
TP53	CDK2	9606.ENSP000 00269305	9606.ENSP000 00266970	0	0.778	0.5	0.884
TP53	FBXW5	9606.ENSP000 00269305	9606.ENSP000 00313034	0	0	0.4	0.4
TP53	FBXW4	9606.ENSP000 00269305	9606.ENSP000 00499522	0	0	0.4	0.4

TP53	FBXW10	9606.ENSPO00 00269305	9606.ENSPO00 00379025	0	0	0.4	0.4
TP53	FBXO6	9606.ENSPO00 00269305	9606.ENSPO00 00365944	0	0	0.4	0.4
TP53	FBXL5	9606.ENSPO00 00269305	9606.ENSPO00 00344866	0	0	0.4	0.4
TP53	FBXO22	9606.ENSPO00 00269305	9606.ENSPO00 00307833	0	0.51	0	0.51
TP53	BRPF3	9606.ENSPO00 00269305	9606.ENSPO00 00350267	0	0.421	0.5	0.698
TP53	CHD4	9606.ENSPO00 00269305	9606.ENSPO00 00440542	0	0.164	0.5	0.564
TP53	BTRC	9606.ENSPO00 00269305	9606.ENSPO00 00359206	0	0.51	0	0.51
TP53	FBXW8	9606.ENSPO00 00269305	9606.ENSPO00 00498999	0	0.601	0	0.601
TP53	HUWE1	9606.ENSPO00 00269305	9606.ENSPO00 00340648	0	0.636	0	0.636
TP53	TRIM24	9606.ENSPO00 00269305	9606.ENSPO00 00340507	0	0.633	0	0.633
TP53	CUL4A	9606.ENSPO00 00269305	9606.ENSPO00 00364589	0	0.51	0	0.51
TP53	BMI1	9606.ENSPO00 00269305	9606.ENSPO00 00365851	0	0.625	0.5	0.804
TP53	ESR1	9606.ENSPO00 00269305	9606.ENSPO00 00405330	0	0.735	0	0.735
TRAF3	TRAF5	9606.ENSPO00 00376500	9606.ENSPO00 00261464	0.907	0.716	0.9	0.97
TRAF3	BIRC3	9606.ENSPO00 00376500	9606.ENSPO00 00263464	0	0.719	0.9	0.97
TRAF3	TRAF6	9606.ENSPO00 00376500	9606.ENSPO00 00433623	0.707	0.095	0.8	0.811
TRAF4	UBE2D1	9606.ENSPO00 00262395	9606.ENSPO00 00363019	0	0.58	0	0.58
TRAF4	SMURF1	9606.ENSPO00 00262395	9606.ENSPO00 00354621	0	0.525	0	0.525
TRAF4	TRAF6	9606.ENSPO00 00262395	9606.ENSPO00 00433623	0.74	0.606	0	0.606
TRAF5	FBXO28	9606.ENSPO00 00261464	9606.ENSPO00 00355827	0	0.492	0	0.491
TRAF5	UBE2V2	9606.ENSPO00 00261464	9606.ENSPO00 00428209	0	0	0.9	0.9
TRAF5	BIRC3	9606.ENSPO00 00261464	9606.ENSPO00 00263464	0	0.066	0.9	0.902
TRAF5	TRAF3	9606.ENSPO00 00261464	9606.ENSPO00 00376500	0.907	0.716	0.9	0.97

TRAF5	TRAF6	9606.ENSP000 00261464	9606.ENSP000 00433623	0.688	0.977	0.9	0.997
TRAF6	STUB1	9606.ENSP000 00433623	9606.ENSP000 00219548	0	0.634	0	0.634
TRAF6	TRAF5	9606.ENSP000 00433623	9606.ENSP000 00261464	0.688	0.977	0.9	0.997
TRAF6	TRAF4	9606.ENSP000 00433623	9606.ENSP000 00262395	0.74	0.606	0	0.606
TRAF6	BIRC3	9606.ENSP000 00433623	9606.ENSP000 00263464	0	0.717	0.4	0.823
TRAF6	SOCS3	9606.ENSP000 00433623	9606.ENSP000 00330341	0	0.51	0	0.51
TRAF6	UBE2D3	9606.ENSP000 00433623	9606.ENSP000 00349722	0	0.815	0.5	0.903
TRAF6	UBE2D1	9606.ENSP000 00433623	9606.ENSP000 00363019	0	0.393	0.5	0.683
TRAF6	ZMYND11	9606.ENSP000 00433623	9606.ENSP000 00371003	0	0.51	0	0.51
TRAF6	TRAF3	9606.ENSP000 00433623	9606.ENSP000 00376500	0.707	0.095	0.8	0.811
TRAF6	UBE2L3	9606.ENSP000 00433623	9606.ENSP000 00400906	0	0.674	0	0.674
TRAF6	UBE2V2	9606.ENSP000 00433623	9606.ENSP000 00428209	0	0.072	0.9	0.903
TRIM24	ZC3HAV1	9606.ENSP000 00340507	9606.ENSP000 00242351	0	0	0.5	0.499
TRIM24	TP53	9606.ENSP000 00340507	9606.ENSP000 00269305	0	0.633	0	0.633
TRIM24	TRIM33	9606.ENSP000 00340507	9606.ENSP000 00351250	0.928	0.863	0	0.863
TRIM24	ESR1	9606.ENSP000 00340507	9606.ENSP000 00405330	0	0.836	0	0.836
TRIM26	UBE2D3	9606.ENSP000 00410446	9606.ENSP000 00349722	0	0.414	0	0.414
TRIM27	UBE2D3	9606.ENSP000 00366404	9606.ENSP000 00349722	0	0.45	0	0.45
TRIM27	UBE2D1	9606.ENSP000 00366404	9606.ENSP000 00363019	0	0.714	0	0.714
TRIM33	TRIM24	9606.ENSP000 00351250	9606.ENSP000 00340507	0.928	0.863	0	0.863
TRIM33	UBE2D3	9606.ENSP000 00351250	9606.ENSP000 00349722	0	0.573	0	0.573
TRIM39	DCUN1D1	9606.ENSP000 00365844	9606.ENSP000 00292782	0	0.407	0	0.407
TRIM39	UBE2D3	9606.ENSP000 00365844	9606.ENSP000 00349722	0	0.501	0	0.501

TRIM39	UBE2D1	9606.ENSP000 00365844	9606.ENSP000 00363019	0	0.703	0	0.703
TRIP12	UBE2D1	9606.ENSP000 00373696	9606.ENSP000 00363019	0	0.835	0	0.835
TRIP12	UBE2L3	9606.ENSP000 00373696	9606.ENSP000 00400906	0	0.788	0	0.788
UBE2B	CDC34	9606.ENSP000 00265339	9606.ENSP000 00215574	0.868	0.073	0.4	0.42
UBE2B	STUB1	9606.ENSP000 00265339	9606.ENSP000 00219548	0	0.175	0.72	0.759
UBE2B	RAD18	9606.ENSP000 00265339	9606.ENSP000 00264926	0	0.998	0.7	0.999
UBE2B	UBE2T	9606.ENSP000 00265339	9606.ENSP000 00494957	0.863	0.136	0.4	0.459
UBE2B	FBH1	9606.ENSP000 00265339	9606.ENSP000 00369335	0	0.411	0	0.41
UBE2B	CUL4A	9606.ENSP000 00265339	9606.ENSP000 00364589	0	0.059	0.5	0.509
UBE2B	UNK	9606.ENSP000 00265339	9606.ENSP000 00464893	0	0.605	0	0.605
UBE2B	UBE2C	9606.ENSP000 00265339	9606.ENSP000 00348838	0.9	0.422	0.4	0.638
UBE2B	UBE2L3	9606.ENSP000 00265339	9606.ENSP000 00400906	0.811	0.479	0.4	0.674
UBE2B	UBE2V2	9606.ENSP000 00265339	9606.ENSP000 00428209	0	0.522	0.72	0.86
UBE2C	CDC34	9606.ENSP000 00348838	9606.ENSP000 00215574	0.777	0	0.4	0.4
UBE2C	UBE2B	9606.ENSP000 00348838	9606.ENSP000 00265339	0.9	0.422	0.4	0.638
UBE2C	CDK2	9606.ENSP000 00348838	9606.ENSP000 00266970	0	0.091	0.5	0.526
UBE2C	RNF7	9606.ENSP000 00348838	9606.ENSP000 00273480	0	0.691	0.36	0.794
UBE2C	UBE2G2	9606.ENSP000 00348838	9606.ENSP000 00338348	0.793	0.09	0.4	0.43
UBE2C	UBE2H	9606.ENSP000 00348838	9606.ENSP000 00347836	0.763	0.061	0.4	0.412
UBE2C	UNK	9606.ENSP000 00348838	9606.ENSP000 00464893	0	0.486	0	0.485
UBE2C	UBE2L3	9606.ENSP000 00348838	9606.ENSP000 00400906	0.706	0.053	0.4	0.407
UBE2C	UBE2T	9606.ENSP000 00348838	9606.ENSP000 00494957	0.809	0.071	0.4	0.418
UBE2C	UBE2D1	9606.ENSP000 00348838	9606.ENSP000 00363019	0.877	0.071	0.8	0.806

UBE2C	BMI1	9606.ENSP000 00348838	9606.ENSP000 00365851	0	0.071	0.9	0.903
UBE2D1	CDC34	9606.ENSP000 00363019	9606.ENSP000 00215574	0.855	0	0.4	0.4
UBE2D1	STUB1	9606.ENSP000 00363019	9606.ENSP000 00219548	0	0.996	0	0.996
UBE2D1	RNF11	9606.ENSP000 00363019	9606.ENSP000 00242719	0	0.643	0	0.643
UBE2D1	RNF114	9606.ENSP000 00363019	9606.ENSP000 00244061	0	0.747	0	0.747
UBE2D1	TRAF4	9606.ENSP000 00363019	9606.ENSP000 00262395	0	0.58	0	0.58
UBE2D1	BIRC3	9606.ENSP000 00363019	9606.ENSP000 00263464	0	0.833	0.5	0.913
UBE2D1	CDK2	9606.ENSP000 00363019	9606.ENSP000 00266970	0	0.091	0.5	0.526
UBE2D1	RNF7	9606.ENSP000 00363019	9606.ENSP000 00273480	0	0.88	0.5	0.937
UBE2D1	DCUN1D1	9606.ENSP000 00363019	9606.ENSP000 00292782	0	0	0.5	0.499
UBE2D1	RNF181	9606.ENSP000 00363019	9606.ENSP000 00306906	0	0.654	0.5	0.819
UBE2D1	UBE3C	9606.ENSP000 00363019	9606.ENSP000 00309198	0	0.845	0	0.845
UBE2D1	RNF168	9606.ENSP000 00363019	9606.ENSP000 00320898	0	0.625	0	0.625
UBE2D1	RNF123	9606.ENSP000 00363019	9606.ENSP000 00328287	0	0.411	0	0.41
UBE2D1	SOCS3	9606.ENSP000 00363019	9606.ENSP000 00330341	0	0	0.5	0.499
UBE2D1	ZNRF1	9606.ENSP000 00363019	9606.ENSP000 00335091	0	0.6	0	0.6
UBE2D1	UBE2G2	9606.ENSP000 00363019	9606.ENSP000 00338348	0.898	0.096	0.4	0.434
UBE2D1	HUWE1	9606.ENSP000 00363019	9606.ENSP000 00340648	0	0.833	0	0.833
UBE2D1	UBE2H	9606.ENSP000 00363019	9606.ENSP000 00347836	0.836	0.069	0.4	0.417
UBE2D1	UBE2C	9606.ENSP000 00363019	9606.ENSP000 00348838	0.877	0.071	0.8	0.806
UBE2D1	MYLIP	9606.ENSP000 00363019	9606.ENSP000 00349298	0	0.972	0	0.972
UBE2D1	UBE2D3	9606.ENSP000 00363019	9606.ENSP000 00349722	0.98	0.616	0.4	0.759
UBE2D1	UBE2Z	9606.ENSP000 00363019	9606.ENSP000 00354201	0.797	0	0.4	0.4

UBE2D1	SMURF1	9606.ENSP000 00363019	9606.ENSP000 00354621	0	0.444	0	0.444
UBE2D1	BTRC	9606.ENSP000 00363019	9606.ENSP000 00359206	0	0.358	0.8	0.866
UBE2D1	RNF8	9606.ENSP000 00363019	9606.ENSP000 00362578	0	0.577	0	0.577
UBE2D1	RNF115	9606.ENSP000 00363019	9606.ENSP000 00463650	0	0.496	0	0.496
UBE2D1	UFM1	9606.ENSP000 00363019	9606.ENSP000 00368970	0	0.603	0	0.603
UBE2D1	UBE2L3	9606.ENSP000 00363019	9606.ENSP000 00400906	0.887	0	0.4	0.4
UBE2D1	TRIM39	9606.ENSP000 00363019	9606.ENSP000 00365844	0	0.703	0	0.703
UBE2D1	TRIM27	9606.ENSP000 00363019	9606.ENSP000 00366404	0	0.714	0	0.714
UBE2D1	MID1	9606.ENSP000 00363019	9606.ENSP000 00414521	0	0.83	0	0.83
UBE2D1	TRAF6	9606.ENSP000 00363019	9606.ENSP000 00433623	0	0.393	0.5	0.683
UBE2D1	UHRF1	9606.ENSP000 00363019	9606.ENSP000 00479617	0	0.799	0	0.799
UBE2D1	TRIP12	9606.ENSP000 00363019	9606.ENSP000 00373696	0	0.835	0	0.835
UBE2D3	UBOX5	9606.ENSP000 00349722	9606.ENSP000 00217173	0	0.491	0	0.491
UBE2D3	STUB1	9606.ENSP000 00349722	9606.ENSP000 00219548	0	0.968	0.5	0.983
UBE2D3	RNF11	9606.ENSP000 00349722	9606.ENSP000 00242719	0	0.667	0	0.667
UBE2D3	RNF114	9606.ENSP000 00349722	9606.ENSP000 00244061	0	0.437	0	0.437
UBE2D3	BIRC3	9606.ENSP000 00349722	9606.ENSP000 00263464	0	0.612	0.5	0.798
UBE2D3	RNF7	9606.ENSP000 00349722	9606.ENSP000 00273480	0	0.781	0.5	0.886
UBE2D3	DCUN1D1	9606.ENSP000 00349722	9606.ENSP000 00292782	0	0.292	0.5	0.63
UBE2D3	RNF181	9606.ENSP000 00349722	9606.ENSP000 00306906	0	0.396	0.5	0.685
UBE2D3	UBE3C	9606.ENSP000 00349722	9606.ENSP000 00309198	0	0.535	0	0.535
UBE2D3	RNF185	9606.ENSP000 00349722	9606.ENSP000 00320508	0	0.616	0	0.616
UBE2D3	RNF168	9606.ENSP000 00349722	9606.ENSP000 00320898	0	0.783	0	0.783

UBE2D3	SOCS3	9606.ENSP000 00349722	9606.ENSP000 00330341	0	0	0.5	0.499
UBE2D3	HUWE1	9606.ENSP000 00349722	9606.ENSP000 00340648	0	0.51	0	0.51
UBE2D3	MYLIP	9606.ENSP000 00349722	9606.ENSP000 00349298	0	0.535	0	0.535
UBE2D3	TRIM26	9606.ENSP000 00349722	9606.ENSP000 00410446	0	0.414	0	0.414
UBE2D3	TRIM27	9606.ENSP000 00349722	9606.ENSP000 00366404	0	0.45	0	0.45
UBE2D3	TRIM39	9606.ENSP000 00349722	9606.ENSP000 00365844	0	0.501	0	0.501
UBE2D3	PJA1	9606.ENSP000 00349722	9606.ENSP000 00355014	0	0.561	0	0.561
UBE2D3	MARCHF8	9606.ENSP000 00349722	9606.ENSP000 00411848	0	0.525	0	0.525
UBE2D3	TRIM33	9606.ENSP000 00349722	9606.ENSP000 00351250	0	0.573	0	0.573
UBE2D3	UHRF1	9606.ENSP000 00349722	9606.ENSP000 00479617	0	0.729	0	0.729
UBE2D3	UBE2D1	9606.ENSP000 00349722	9606.ENSP000 00363019	0.98	0.616	0.4	0.759
UBE2D3	BTRC	9606.ENSP000 00349722	9606.ENSP000 00359206	0	0.66	0	0.66
UBE2D3	MID1	9606.ENSP000 00349722	9606.ENSP000 00414521	0	0.845	0	0.845
UBE2D3	RNF8	9606.ENSP000 00349722	9606.ENSP000 00362578	0	0.76	0	0.76
UBE2D3	SMURF1	9606.ENSP000 00349722	9606.ENSP000 00354621	0	0.904	0	0.904
UBE2D3	BMI1	9606.ENSP000 00349722	9606.ENSP000 00365851	0	0.853	0	0.853
UBE2D3	TRAF6	9606.ENSP000 00349722	9606.ENSP000 00433623	0	0.815	0.5	0.903
UBE2G2	CDC34	9606.ENSP000 00338348	9606.ENSP000 00215574	0.915	0.09	0.4	0.43
UBE2G2	UBE2D1	9606.ENSP000 00338348	9606.ENSP000 00363019	0.898	0.096	0.4	0.434
UBE2G2	UBE2C	9606.ENSP000 00338348	9606.ENSP000 00348838	0.793	0.09	0.4	0.43
UBE2G2	UBE2L3	9606.ENSP000 00338348	9606.ENSP000 00400906	0.784	0.094	0.4	0.433
UBE2G2	UBE2H	9606.ENSP000 00338348	9606.ENSP000 00347836	0.678	0	0.4	0.4
UBE2G2	UBE2Z	9606.ENSP000 00338348	9606.ENSP000 00354201	0.732	0.09	0.4	0.43

UBE2H	CDC34	9606.ENSPO00 00347836	9606.ENSPO00 00215574	0.72	0.061	0.4	0.412
UBE2H	UBE2G2	9606.ENSPO00 00347836	9606.ENSPO00 00338348	0.678	0	0.4	0.4
UBE2H	UBE2C	9606.ENSPO00 00347836	9606.ENSPO00 00348838	0.763	0.061	0.4	0.412
UBE2H	UBE2L3	9606.ENSPO00 00347836	9606.ENSPO00 00400906	0.733	0.069	0.4	0.417
UBE2H	UBE2D1	9606.ENSPO00 00347836	9606.ENSPO00 00363019	0.836	0.069	0.4	0.417
UBE2H	MARCHF8	9606.ENSPO00 00347836	9606.ENSPO00 00411848	0	0.51	0	0.51
UBE2L3	CDC34	9606.ENSPO00 00400906	9606.ENSPO00 00215574	0.731	0	0.4	0.4
UBE2L3	UBOX5	9606.ENSPO00 00400906	9606.ENSPO00 00217173	0	0.692	0	0.692
UBE2L3	STUB1	9606.ENSPO00 00400906	9606.ENSPO00 00219548	0	0.648	0	0.648
UBE2L3	BIRC3	9606.ENSPO00 00400906	9606.ENSPO00 00263464	0	0.328	0.4	0.58
UBE2L3	HERC6	9606.ENSPO00 00400906	9606.ENSPO00 00264346	0	0.461	0	0.461
UBE2L3	UBE2B	9606.ENSPO00 00400906	9606.ENSPO00 00265339	0.811	0.479	0.4	0.674
UBE2L3	RNF7	9606.ENSPO00 00400906	9606.ENSPO00 00273480	0	0.417	0	0.417
UBE2L3	UBE3C	9606.ENSPO00 00400906	9606.ENSPO00 00309198	0	0.822	0	0.822
UBE2L3	UBE2G2	9606.ENSPO00 00400906	9606.ENSPO00 00338348	0.784	0.094	0.4	0.433
UBE2L3	HUWE1	9606.ENSPO00 00400906	9606.ENSPO00 00340648	0	0.865	0	0.865
UBE2L3	UBE2H	9606.ENSPO00 00400906	9606.ENSPO00 00347836	0.733	0.069	0.4	0.417
UBE2L3	UBE2C	9606.ENSPO00 00400906	9606.ENSPO00 00348838	0.706	0.053	0.4	0.407
UBE2L3	UBE2Z	9606.ENSPO00 00400906	9606.ENSPO00 00354201	0	0	0.4	0.4
UBE2L3	SMURF1	9606.ENSPO00 00400906	9606.ENSPO00 00354621	0	0.886	0	0.886
UBE2L3	UBE2D1	9606.ENSPO00 00400906	9606.ENSPO00 00363019	0.887	0	0.4	0.4
UBE2L3	TRIP12	9606.ENSPO00 00400906	9606.ENSPO00 00373696	0	0.788	0	0.788
UBE2L3	HERC3	9606.ENSPO00 00400906	9606.ENSPO00 00385684	0	0.461	0	0.461

UBE2L3	UBE2T	9606.ENSP000 00400906	9606.ENSP000 00494957	0.797	0	0.4	0.4
UBE2L3	UBE2V2	9606.ENSP000 00400906	9606.ENSP000 00428209	0	0.432	0	0.432
UBE2L3	TRAF6	9606.ENSP000 00400906	9606.ENSP000 00433623	0	0.674	0	0.674
UBE2T	CDC34	9606.ENSP000 00494957	9606.ENSP000 00215574	0.747	0	0.4	0.4
UBE2T	STUB1	9606.ENSP000 00494957	9606.ENSP000 00219548	0	0.419	0	0.418
UBE2T	UBE2B	9606.ENSP000 00494957	9606.ENSP000 00265339	0.863	0.136	0.4	0.459
UBE2T	UBE2C	9606.ENSP000 00494957	9606.ENSP000 00348838	0.809	0.071	0.4	0.418
UBE2T	UBE2L3	9606.ENSP000 00494957	9606.ENSP000 00400906	0.797	0	0.4	0.4
UBE2V2	STUB1	9606.ENSP000 00428209	9606.ENSP000 00219548	0	0.47	0.72	0.845
UBE2V2	TRAF5	9606.ENSP000 00428209	9606.ENSP000 00261464	0	0	0.9	0.9
UBE2V2	HERC2	9606.ENSP000 00428209	9606.ENSP000 00261609	0	0	0.5	0.499
UBE2V2	RAD18	9606.ENSP000 00428209	9606.ENSP000 00264926	0	0.088	0.5	0.524
UBE2V2	UBE2B	9606.ENSP000 00428209	9606.ENSP000 00265339	0	0.522	0.72	0.86
UBE2V2	CDK2	9606.ENSP000 00428209	9606.ENSP000 00266970	0	0	0.5	0.499
UBE2V2	RNF168	9606.ENSP000 00428209	9606.ENSP000 00320898	0	0	0.5	0.499
UBE2V2	RNF8	9606.ENSP000 00428209	9606.ENSP000 00362578	0	0.647	0.5	0.816
UBE2V2	CUL4A	9606.ENSP000 00428209	9606.ENSP000 00364589	0	0	0.5	0.499
UBE2V2	UBE2L3	9606.ENSP000 00428209	9606.ENSP000 00400906	0	0.432	0	0.432
UBE2V2	TRAF6	9606.ENSP000 00428209	9606.ENSP000 00433623	0	0.072	0.9	0.903
UBE2Z	UBE2G2	9606.ENSP000 00354201	9606.ENSP000 00338348	0.732	0.09	0.4	0.43
UBE2Z	UBE2D1	9606.ENSP000 00354201	9606.ENSP000 00363019	0.797	0	0.4	0.4
UBE2Z	UBE2L3	9606.ENSP000 00354201	9606.ENSP000 00400906	0	0	0.4	0.4
UBE3C	UBE2D3	9606.ENSP000 00309198	9606.ENSP000 00349722	0	0.535	0	0.535

UBE3C	UBE2L3	9606.ENSP00000309198	9606.ENSP00000400906	0	0.822	0	0.822
UBE3C	UBE2D1	9606.ENSP00000309198	9606.ENSP00000363019	0	0.845	0	0.845
UBOX5	UBE2D3	9606.ENSP00000217173	9606.ENSP00000349722	0	0.491	0	0.491
UBOX5	UBE2L3	9606.ENSP00000217173	9606.ENSP00000400906	0	0.692	0	0.692
UFM1	UBE2D1	9606.ENSP00000368970	9606.ENSP00000363019	0	0.603	0	0.603
UHRF1	UBE2D3	9606.ENSP00000479617	9606.ENSP00000349722	0	0.729	0	0.729
UHRF1	BTRC	9606.ENSP00000479617	9606.ENSP00000359206	0	0.601	0	0.601
UHRF1	UBE2D1	9606.ENSP00000479617	9606.ENSP00000363019	0	0.799	0	0.799
UNK	UBE2B	9606.ENSP00000464893	9606.ENSP00000265339	0	0.605	0	0.605
UNK	UBE2C	9606.ENSP00000464893	9606.ENSP00000348838	0	0.486	0	0.485
ZC3HAV1	TRIM24	9606.ENSP00000242351	9606.ENSP00000340507	0	0	0.5	0.499
ZMYND11	TRAF6	9606.ENSP00000371003	9606.ENSP00000433623	0	0.51	0	0.51
ZNF592	CHD4	9606.ENSP00000452877	9606.ENSP00000440542	0	0.541	0	0.541
ZNRF1	FBXW5	9606.ENSP00000335091	9606.ENSP00000313034	0	0.42	0	0.42
ZNRF1	UBE2D1	9606.ENSP00000335091	9606.ENSP00000363019	0	0.6	0	0.6

Table 7.6. Protein-protein interactions in tabular form, 24 h hits. Columns “Node 1” and “Node 2” at each row contain protein names interacting, columns “Node 1 accession number” and “Node 2 accession number” contain unique identifier of the String database. Column “Homology” contains homology value that the String database calculates from known interaction between the same proteins in other species. The experimentally determined interaction score combines the information from the BIND, DIP, GRID, HPRD, IntAct, MINT, and PID databases. The database annotated interaction score combines the information from the Biocarta, BioCyc, GO, KEGG, and Reactome. Combined score is calculated by combining the probabilities from the different evidence channels (experimental and annotated) and corrected for the probability of randomly observing an interaction.

node 1	node 2	node 1 accession number	node 2 accession number	homology	experimentally determined interaction	database annotated	combined score
APC	BTRC	9606.ENSP00000257430	9606.ENSP00000359206	0	0.787	0.8	0.955

BIRC2	BIRC3	9606.ENSP000 00477613	9606.ENSP000 00263464	0.975	0.292	0.9	0.926
BIRC2	XIAP	9606.ENSP000 00477613	9606.ENSP000 00360242	0.863	0.818	0.9	0.981
BIRC2	UBE2D2	9606.ENSP000 00477613	9606.ENSP000 00381717	0	0.982	0.5	0.99
BIRC3	XIAP	9606.ENSP000 00263464	9606.ENSP000 00360242	0.862	0.527	0.9	0.95
BIRC3	BIRC2	9606.ENSP000 00263464	9606.ENSP000 00477613	0.975	0.292	0.9	0.926
BIRC3	UBE2D2	9606.ENSP000 00263464	9606.ENSP000 00381717	0	0.987	0.5	0.993
BTRC	CDC34	9606.ENSP000 00359206	9606.ENSP000 00215574	0	0.839	0.5	0.916
BTRC	APC	9606.ENSP000 00359206	9606.ENSP000 00257430	0	0.787	0.8	0.955
BTRC	DCUN1D3	9606.ENSP000 00359206	9606.ENSP000 00319482	0	0	0.5	0.499
BTRC	UHRF1	9606.ENSP000 00359206	9606.ENSP000 00479617	0	0.601	0	0.601
BTRC	FBXW8	9606.ENSP000 00359206	9606.ENSP000 00498999	0.558	0.51	0	0.51
BTRC	UBE2D2	9606.ENSP000 00359206	9606.ENSP000 00381717	0	0.932	0.8	0.986
CBL	SOCS2	9606.ENSP000 00264033	9606.ENSP000 00481249	0	0.066	0.5	0.513
CBL	UBE2D2	9606.ENSP000 00264033	9606.ENSP000 00381717	0	0.989	0	0.989
CCND1	FBXW8	9606.ENSP000 00227507	9606.ENSP000 00498999	0	0.51	0	0.51
CCND1	ESR1	9606.ENSP000 00227507	9606.ENSP000 00405330	0	0.625	0.75	0.902
CCND1	CDK1	9606.ENSP000 00227507	9606.ENSP000 00378699	0	0.866	0	0.866
CCND1	CDK2	9606.ENSP000 00227507	9606.ENSP000 00266970	0	0.901	0.8	0.979
CCNF	CDK2	9606.ENSP000 00380256	9606.ENSP000 00266970	0	0.402	0	0.402
CCNF	DCUN1D3	9606.ENSP000 00380256	9606.ENSP000 00319482	0	0	0.5	0.499
CCNF	CDK1	9606.ENSP000 00380256	9606.ENSP000 00378699	0	0.586	0	0.586
CDC34	UBE2G2	9606.ENSP000 00215574	9606.ENSP000 00338348	0.915	0.09	0.4	0.43
CDC34	UBE2B	9606.ENSP000 00215574	9606.ENSP000 00265339	0.868	0.073	0.4	0.42

CDC34	UBE2A	9606.ENSP000 00215574	9606.ENSP000 00360613	0.864	0.073	0.4	0.42
CDC34	UBE2K	9606.ENSP000 00215574	9606.ENSP000 00261427	0.726	0	0.4	0.4
CDC34	UBE2D2	9606.ENSP000 00215574	9606.ENSP000 00381717	0.822	0	0.4	0.4
CDC34	BTRC	9606.ENSP000 00215574	9606.ENSP000 00359206	0	0.839	0.5	0.916
CDK1	CCND1	9606.ENSP000 00378699	9606.ENSP000 00227507	0	0.866	0	0.866
CDK1	CDK2	9606.ENSP000 00378699	9606.ENSP000 00266970	0.968	0.47	0.4	0.668
CDK1	G3BP1	9606.ENSP000 00378699	9606.ENSP000 00377681	0	0.516	0	0.516
CDK1	CCNF	9606.ENSP000 00378699	9606.ENSP000 00380256	0	0.586	0	0.586
CDK2	CCND1	9606.ENSP000 00266970	9606.ENSP000 00227507	0	0.901	0.8	0.979
CDK2	RNF8	9606.ENSP000 00266970	9606.ENSP000 00362578	0	0.091	0.5	0.526
CDK2	CCNF	9606.ENSP000 00266970	9606.ENSP000 00380256	0	0.402	0	0.402
CDK2	CDK1	9606.ENSP000 00266970	9606.ENSP000 00378699	0.968	0.47	0.4	0.668
DCUN1D3	FBXL15	9606.ENSP000 00319482	9606.ENSP000 00224862	0	0	0.5	0.499
DCUN1D3	FBXO30	9606.ENSP000 00319482	9606.ENSP000 00237281	0	0	0.5	0.499
DCUN1D3	BTRC	9606.ENSP000 00319482	9606.ENSP000 00359206	0	0	0.5	0.499
DCUN1D3	FBXW4	9606.ENSP000 00319482	9606.ENSP000 00499522	0	0	0.5	0.499
DCUN1D3	CCNF	9606.ENSP000 00319482	9606.ENSP000 00380256	0	0	0.5	0.499
DCUN1D3	FBXW8	9606.ENSP000 00319482	9606.ENSP000 00498999	0	0.048	0.5	0.503
DCUN1D3	FBXL18	9606.ENSP000 00319482	9606.ENSP000 00371805	0	0	0.5	0.499
DCUN1D3	FBXO11	9606.ENSP000 00319482	9606.ENSP000 00384823	0	0	0.5	0.499
DZIP3	UBE2D2	9606.ENSP000 00355028	9606.ENSP000 00381717	0	0.429	0	0.429
ESR1	CCND1	9606.ENSP000 00405330	9606.ENSP000 00227507	0	0.625	0.75	0.902
FBXL15	DCUN1D3	9606.ENSP000 00224862	9606.ENSP000 00319482	0	0	0.5	0.499

FBXL18	DCUN1D3	9606.ENSP000 00371805	9606.ENSP000 00319482	0	0	0.5	0.499
FBXO11	DCUN1D3	9606.ENSP000 00384823	9606.ENSP000 00319482	0	0	0.5	0.499
FBXO30	DCUN1D3	9606.ENSP000 00237281	9606.ENSP000 00319482	0	0	0.5	0.499
FBXW4	DCUN1D3	9606.ENSP000 00499522	9606.ENSP000 00319482	0	0	0.5	0.499
FBXW8	CCND1	9606.ENSP000 00498999	9606.ENSP000 00227507	0	0.51	0	0.51
FBXW8	DCUN1D3	9606.ENSP000 00498999	9606.ENSP000 00319482	0	0.048	0.5	0.503
FBXW8	BTRC	9606.ENSP000 00498999	9606.ENSP000 00359206	0.558	0.51	0	0.51
G3BP1	CDK1	9606.ENSP000 00377681	9606.ENSP000 00378699	0	0.516	0	0.516
MYLIP	UBE2D2	9606.ENSP000 00349298	9606.ENSP000 00381717	0	0.535	0	0.535
RNF8	CDK2	9606.ENSP000 00362578	9606.ENSP000 00266970	0	0.091	0.5	0.526
SOCS2	CBL	9606.ENSP000 00481249	9606.ENSP000 00264033	0	0.066	0.5	0.513
SOCS2	SOCS5	9606.ENSP000 00481249	9606.ENSP000 00305133	0.724	0	0.54	0.54
SOCS2	SOCS3	9606.ENSP000 00481249	9606.ENSP000 00330341	0.764	0.303	0.9	0.927
SOCS3	SOCS5	9606.ENSP000 00330341	9606.ENSP000 00305133	0	0	0.54	0.54
SOCS3	UBE2D2	9606.ENSP000 00330341	9606.ENSP000 00381717	0	0	0.5	0.499
SOCS3	SOCS2	9606.ENSP000 00330341	9606.ENSP000 00481249	0.764	0.303	0.9	0.927
SOCS5	SOCS2	9606.ENSP000 00305133	9606.ENSP000 00481249	0.724	0	0.54	0.54
SOCS5	SOCS3	9606.ENSP000 00305133	9606.ENSP000 00330341	0	0	0.54	0.54
TRIP12	UBE2D2	9606.ENSP000 00373696	9606.ENSP000 00381717	0	0.426	0	0.426
UBE2A	CDC34	9606.ENSP000 00360613	9606.ENSP000 00215574	0.864	0.073	0.4	0.42
UBE2A	UBE2B	9606.ENSP000 00360613	9606.ENSP000 00265339	0.984	0.609	0.9	0.959
UBE2A	UBE2D2	9606.ENSP000 00360613	9606.ENSP000 00381717	0.91	0.136	0.4	0.459
UBE2B	CDC34	9606.ENSP000 00265339	9606.ENSP000 00215574	0.868	0.073	0.4	0.42

UBE2B	UBE2D2	9606.ENSPO00 00265339	9606.ENSPO00 00381717	0.908	0.136	0.4	0.459
UBE2B	UBE2A	9606.ENSPO00 00265339	9606.ENSPO00 00360613	0.984	0.609	0.9	0.959
UBE2D2	CDC34	9606.ENSPO00 00381717	9606.ENSPO00 00215574	0.822	0	0.4	0.4
UBE2D2	UBE2K	9606.ENSPO00 00381717	9606.ENSPO00 00261427	0.898	0.68	0.4	0.799
UBE2D2	BIRC3	9606.ENSPO00 00381717	9606.ENSPO00 00263464	0	0.987	0.5	0.993
UBE2D2	CBL	9606.ENSPO00 00381717	9606.ENSPO00 00264033	0	0.989	0	0.989
UBE2D2	UBE2B	9606.ENSPO00 00381717	9606.ENSPO00 00265339	0.908	0.136	0.4	0.459
UBE2D2	SOCS3	9606.ENSPO00 00381717	9606.ENSPO00 00330341	0	0	0.5	0.499
UBE2D2	UBE2G2	9606.ENSPO00 00381717	9606.ENSPO00 00338348	0.898	0.096	0.4	0.434
UBE2D2	MYLIP	9606.ENSPO00 00381717	9606.ENSPO00 00349298	0	0.535	0	0.535
UBE2D2	DZIP3	9606.ENSPO00 00381717	9606.ENSPO00 00355028	0	0.429	0	0.429
UBE2D2	BTRC	9606.ENSPO00 00381717	9606.ENSPO00 00359206	0	0.932	0.8	0.986
UBE2D2	XIAP	9606.ENSPO00 00381717	9606.ENSPO00 00360242	0	0.847	0	0.847
UBE2D2	UBE2A	9606.ENSPO00 00381717	9606.ENSPO00 00360613	0.91	0.136	0.4	0.459
UBE2D2	TRIP12	9606.ENSPO00 00381717	9606.ENSPO00 00373696	0	0.426	0	0.426
UBE2D2	UBE4A	9606.ENSPO00 00381717	9606.ENSPO00 00387362	0	0.423	0	0.423
UBE2D2	BIRC2	9606.ENSPO00 00381717	9606.ENSPO00 00477613	0	0.982	0.5	0.99
UBE2G2	CDC34	9606.ENSPO00 00338348	9606.ENSPO00 00215574	0.915	0.09	0.4	0.43
UBE2G2	UBE2K	9606.ENSPO00 00338348	9606.ENSPO00 00261427	0.749	0.09	0.4	0.43
UBE2G2	UBE2D2	9606.ENSPO00 00338348	9606.ENSPO00 00381717	0.898	0.096	0.4	0.434
UBE2K	CDC34	9606.ENSPO00 00261427	9606.ENSPO00 00215574	0.726	0	0.4	0.4
UBE2K	UBE2G2	9606.ENSPO00 00261427	9606.ENSPO00 00338348	0.749	0.09	0.4	0.43
UBE2K	UBE2D2	9606.ENSPO00 00261427	9606.ENSPO00 00381717	0.898	0.68	0.4	0.799

UBE4A	UBE2D2	9606.ENSP00000387362	9606.ENSP00000381717	0	0.423	0	0.423
UHRF1	BTRC	9606.ENSP00000479617	9606.ENSP00000359206	0	0.601	0	0.601
XIAP	BIRC3	9606.ENSP00000360242	9606.ENSP00000263464	0.862	0.527	0.9	0.95
XIAP	UBE2D2	9606.ENSP00000360242	9606.ENSP00000381717	0	0.847	0	0.847
XIAP	BIRC2	9606.ENSP00000360242	9606.ENSP00000477613	0.863	0.818	0.9	0.981

Table 7.7. Hits scored at both 0.5 h and 24 h post-irradiation time points. Ensembl ID and Gene ID are provided. The green coloring of the well corresponds to the upregulation of γ H2AX signal intensity, red corresponds to downregulation.

	Gene name	Ensembl ID	Gene ID	Damage 0.5 h	Repair 24 h
1	RNF8	ENSG00000112130	9025	↓	↓
2	TRIM27	ENSG00000204713	5987	↑	↓
3	PHF19	ENSG00000119403	26147	↓	↓
4	BMI1	ENSG00000168283	12151	↓	↓
5	IRF2BP1	ENSG00000170604	26145	↓	↓
6	BTRC	ENSG00000166167	8945	↓	↓
7	FBXO11	ENSG00000138081	80204	↓	↓
8	CDK2	ENSG00000123374	1017	↑	↓
9	ESR1	ENSG00000091831	2099	↓	↓
10	CDC34	ENSG00000099804	997	↑	↓
11	FBXL15	ENSG00000107872	79176	↓	↓
12	FBXO30	ENSG00000118496	84085	↓	↓
13	FBXW4	ENSG00000107829	6468	↑	↓
14	BIRC3	ENSG00000023445	330	↑	↓
15	FBXO38	ENSG00000145868	81545	↓	↓
16	FBXW8	ENSG00000174989	26259	↑	↓
17	HERC1	ENSG00000103657	8925	↓	↓
18	TRIP12	ENSG00000153827	9320	↑	↓
19	SOCS3	ENSG00000184557	9021	↓	↓
20	MARCH9	ENSG00000139266	92979	↑	↓
21	FBXL18	ENSG00000155034	80028	↓	↓
22	HERC3	ENSG00000138641	8916	↓	↓
23	ZNF592	ENSG00000166716	9640	↑	↓
24	BRPF3	ENSG00000096070	27154	↓	↓
25	MYLIP	ENSG00000007944	29116	↓	↓

26	BAZ1B	ENSG00000009954	9031	↓	↓
27	PDZRN4	ENSG00000165966	29951	↓	↓
28	CCND1	ENSG00000136155	8796	↓	↑
29	PRPF19	ENSG00000110107	27339	↓	↓
30	SOCS2	ENSG00000120833	8835	↓	↓
31	SPSB1	ENSG00000171621	80176	↓	↓
32	TRAF4	ENSG00000076604	9618	↓	↓
33	UBE2B	ENSG00000119048	7320	↑	↓
34	ATG3	ENSG00000144848	67841	↓	↓
35	UBE2G2	ENSG00000184787	7327	↑	↓
36	UFM1	ENSG00000120686	51569	↑	↓
37	UHRF1	ENSG00000276043	29128	↓	↓
38	VPS41	ENSG00000006715	27072	↓	↓
39	ZNF330	ENSG00000109445	27309	↓	↓

Table 7.8. Small-scale 4D screen layout.

Lot Number	Location (Row-Col)	RefSeq Accession Number	Gene Symbol	Gene ID	siRNA ID	Amount	Exon(s) Targeted	Sense siRNA Sequence	Antisense siRNA Sequence
AMO21R6P	A1	NM_006510	TRIM27	5987	s11959	0.25 nmole	2	GCUGAACUCUUG AGCCUAAtt	UUAGGCUCAAGA GUUCAGCtc
AMO21R6P	A2	NM_006510	TRIM27	5987	s11959	0.25 nmole	2	GCUGAACUCUUG AGCCUAAtt	UUAGGCUCAAGA GUUCAGCtc
AMO21R6P	A3	NM_025058	TRIM46	80128	s36934	0.25 nmole	3	GGGCUUUUCCGG AACCUGAtt	UCAGGUUCCGGA AAAGCCctg
AMO21R6P	A4	NM_025058	TRIM46	80128	s36934	0.25 nmole	3	GGGCUUUUCCGG AACCUGAtt	UCAGGUUCCGGA AAAGCCctg
AMO21R6P	A5	NM_152620	TRIM60	166655	s46623	0.25 nmole	3	GCCUUAUUUCUA UACUGGAtt	UCCAGUAUAGAAA UAAGGCca
AMO21R6P	A6	NM_152620	TRIM60	166655	s46623	0.25 nmole	3	GCCUUAUUUCUA UACUGGAtt	UCCAGUAUAGAAA UAAGGCca
AMO21R6P	A7	NM_001798	CDK2	1017	s204	0.25 nmole	Not Determined	CGGAGCUUGUUA UCGCAAAtt	UUUGCGAUACAA GCUCCGtc
AMO21R6P	A8	NM_001798	CDK2	1017	s204	0.25 nmole	Not Determined	CGGAGCUUGUUA UCGCAAAtt	UUUGCGAUACAA GCUCCGtc
AMO21R6P	A9	NM_183237	RNF7	9616	s18473	0.25 nmole	3	GCUUAUGGUUGA UCAGUUAtt	UAACUGAUCAACC AUAAGCat

AMO21R6P	A10	NM_183237	RNF7	9616	s18473	0.25 nmole	3	GCUUAUGGUUGA UCAGUUAtt	UAACUGAUCAACC AUAAGCat
AMO21R6P	A11	NM_004359	CDC34	997	s2762	0.25 nmole	5	AGUACUGCGUGA AGACCAAtt	UUGGUCUUCACG CAGUACUcg
AMO21R6P	A12	NM_004359	CDC34	997	s2762	0.25 nmole	5	AGUACUGCGUGA AGACCAAtt	UUGGUCUUCACG CAGUACUcg
AMO21R6P	A13	NM_001165	BIRC3	330	s1451	0.25 nmole	2,3	CACUCAUUACUU CCGGGUAtt	UACCCGGAAGUAA UGAGUGtg
AMO21R6P	A14	NM_001165	BIRC3	330	s1451	0.25 nmole	2,3	CACUCAUUACUU CCGGGUAtt	UACCCGGAAGUAA UGAGUGtg
AMO21R6P	A15	NM_012116	CBLC	23624	s24223	0.25 nmole	Not Determined	GGGAGGCCGUGA GUAUCUAtt	UAGAUACUCACGG CCUCCcag
AMO21R6P	A16	NM_012116	CBLC	23624	s24223	0.25 nmole	Not Determined	GGGAGGCCGUGA GUAUCUAtt	UAGAUACUCACGG CCUCCcag
AMO21R6P	A17	NM_004238	TRIP12	9320	s17808	0.25 nmole	32	GCACCUAGAUUG GAUAGAAtt	UUCUAUCCAAUC UAGGUGCaa
AMO21R6P	A18	NM_004238	TRIP12	9320	s17808	0.25 nmole	32	GCACCUAGAUUG GAUAGAAtt	UUCUAUCCAAUC UAGGUGCaa
AMO21R6P	A19	NM_001167	XIAP	331	s1454	0.25 nmole	2	GGAUUACUCAGU UAACAAtt	UUGUUAACUGAG UAUAUCCat
AMO21R6P	A20	NM_001167	XIAP	331	s1454	0.25 nmole	2	GGAUUACUCAGU UAACAAtt	UUGUUAACUGAG UAUAUCCat

AMO21R6P	A21	NM_004667	HERC2	8924	s17062	0.25 nmole	77	GCGAAAACAUGGA UGUUCUtt	AGAACAUCAUGU UUUCGctg
AMO21R6P	A22	NM_004667	HERC2	8924	s17062	0.25 nmole	77	GCGAAAACAUGGA UGUUCUtt	AGAACAUCAUGU UUUCGctg
AMO21R6P	A23	NM_014593	CXXC1	30827	s26935	0.25 nmole	Not Determined	ACUGCAUCCGGA UCACUGAtt	UCAGUGAUCCGG AUGCAGUcc
AMO21R6P	A24	NM_014593	CXXC1	30827	s26935	0.25 nmole	Not Determined	ACUGCAUCCGGA UCACUGAtt	UCAGUGAUCCGG AUGCAGUcc
AMO21R6P	B1	NM_006510	TRIM27	5987	s11959	0.25 nmole	2	GCUGAACUCUUG AGCCUAAtt	UUAGGCUCAAGA GUUCAGCtc
AMO21R6P	B2	NM_001798	CDK2	1017	s206	0.25 nmole	Not Determined	CAAGAUCUCAAGA AAUUCAtt	UGAAUUUCUUGA GAUCUUGgt
AMO21R6P	B3	NM_025058	TRIM46	80128	s36934	0.25 nmole	3	GGGCUUUUCCGG AACCUGAtt	UCAGGUUCCGGA AAAGCCctg
AMO21R6P	B4	NM_031407	HUWE1	10075	s19597	0.25 nmole	Not Determined	GGUCUAUCAUG CCGCAGAtt	UCUGCGGCAUGA UUAGACctt
AMO21R6P	B5	NM_152620	TRIM60	166655	s46623	0.25 nmole	3	GCCUUUUUUCUA UACUGGAtt	UCCAGUAUAGAAA UAAGGCca
AMO21R6P	B6	NM_001273	CHD4	1108	s2985	0.25 nmole	20	CACUCGAAAUUUU GAAGCAtt	UGCUUCAAAUUU CGAGUGag
AMO21R6P	B7	NM_001798	CDK2	1017	s204	0.25 nmole	Not Determined	CGGAGCUUGUUA UCGCAAAtt	UUUGCGAUAAACA GCUCCgtc
AMO21R6P	B8	NM_020901	PHRF1	57661	s33543	0.25 nmole	Not Determined	CCAGUUUCUUUU CAGCGAAtt	UUCGCUGAAAAGA AACUGGag
AMO21R6P	B9	NM_183237	RNF7	9616	s18473	0.25 nmole	3	GCUUAUGGUUGA UCAGUUAtt	UAACUGAUCAACC AUAAGCat

AMO21R6P	B10	NM_032408	BAZ1B	9031	s17210	0.25 nmole	Not Determined	CCUCAUUGCAUA CUACAAAtt	UUUGUAGUAUGC AAUGAGGtg
AMO21R6P	B11	NM_004359	CDC34	997	s2762	0.25 nmole	5	AGUACUGCGUGA AGACCAAtt	UUGGUCUUCACG CAGUACUcg
AMO21R6P	B12	NM_014948	UBOX5	22888	s22597	0.25 nmole	2,2	GCAACAAGAUauc AGCUGAtt	UCAGCUGAUauc UUGUUGCag
AMO21R6P	B13	NM_001165	BIRC3	330	s1451	0.25 nmole	2,3	CACUCAUUACUU CCGGGUAtt	UACCCGGAAGUAA UGAGUGtg
AMO21R6P	B14	NM_012116	CBLC	23624	s24225	0.25 nmole	Not Determined	CCGAAAGUGAGAC UCCUAAtt	UUAGGAGUCUCA CUUUCGGct
AMO21R6P	B15	NM_012116	CBLC	23624	s24223	0.25 nmole	Not Determined	GGGAGGCCGUGA GUAUCUAtt	UAGAUACUCACGG CCUCCcag
AMO21R6P	B16		SiSeL_NC1	0	s813	0.25 nmole	Not Determined		
AMO21R6P	B17	NM_004238	TRIP12	9320	s17808	0.25 nmole	32	GCACCUAGAUUG GAUAGAAtt	UUCUAUCCAAUC UAGGUGCaa
AMO21R6P	B18	NM_053056	CCND1	595	s228	0.25 nmole	5	GUAGGACUCUCA UUCGGGAtt	UCCCGAAUGAGA GUCCUACag
AMO21R6P	B19	NM_001167	XIAP	331	s1454	0.25 nmole	2	GGAUUACUCAGU UAACAAtt	UUGUUAACUGAG UAUAUCCat
AMO21R6P	B20	NM_004667	HERC2	8924	s17064	0.25 nmole	15	CCAUUGCUIUGA CGAAAGAtt	UCUUCGUCAAA GCAAUGGaa

AMO21R6P	B21	NM_004667	HERC2	8924	s17062	0.25 nmole	77	GCGAAAACAUGGA UGUUCUtt	AGAACAUCAUGU UUUCGctg
AMO21R6P	B22	NM_015695	BRPF3	27154	s25920	0.25 nmole	Not Determined	GCAUCGUAUCAG CAUCUAUtt	AUAGAUGCUGAUA CGAUGCag
AMO21R6P	B23	NM_014593	CXXC1	30827	s26935	0.25 nmole	Not Determined	ACUGCAUCCGGA UCACUGAtt	UCAGUGAUCCGG AUGCAGUcc
AMO21R6P	B24		SiSeL_NC1	0	s813	0.25 nmole	Not Determined		
AMO21R6P	C1	NM_007294	BRCA1	672	s457	0.25 nmole	Not Determined	GGGAUACCAUGC AACAUAtt	UUAUGUUGCAUG GUAUCCctc
AMO21R6P	C2	NM_007294	BRCA1	672	s457	0.25 nmole	Not Determined	GGGAUACCAUGC AACAUAtt	UUAUGUUGCAUG GUAUCCctc
AMO21R6P	C3	NM_024963	FBXL18	80028	s36850	0.25 nmole	Not Determined	CUGCAGCACAUG AAAUUCAtt	UGAAUUUCAUGU GCUGCAGga
AMO21R6P	C4	NM_024963	FBXL18	80028	s36850	0.25 nmole	Not Determined	CUGCAGCACAUG AAAUUCAtt	UGAAUUUCAUGU GCUGCAGga
AMO21R6P	C5	NM_003955	SOCS3	9021	s17189	0.25 nmole	2	UGAUUUGGUUUA AACCUGAtt	UCAGGUUUAAACC AAAUCAaa
AMO21R6P	C6	NM_003955	SOCS3	9021	s17189	0.25 nmole	2	UGAUUUGGUUUA AACCUGAtt	UCAGGUUUAAACC AAAUCAaa
AMO21R6P	C7	NM_053056	CCND1	595	s229	0.25 nmole	5	GGAGCAUUUUGA UACCAGAtt	UCUGGUUAUAAAA UGCUCcgg
AMO21R6P	C8	NM_053056	CCND1	595	s229	0.25 nmole	5	GGAGCAUUUUGA UACCAGAtt	UCUGGUUAUAAAA UGCUCcgg
AMO21R6P	C9	NM_030793	FBXO38	81545	s37602	0.25 nmole	11,11	GGACUCGAUUGG UUGAUUtt	AUAUCAACCAAUC GAGUCCat

AMO21R6P	C10	NM_030793	FBXO38	81545	s37602	0.25 nmole	11,11	GGACUCGAUUGG UUGAUUAtt	AUAUCAACCAUUC GAGUCCat
AMO21R6P	C11	NM_139048	HLTF	6596	s13136	0.25 nmole	4,4	GAAAAGCGGUUU CAGAUCAAtt	UGAUCUGAAACCG CUUUUCta
AMO21R6P	C12	NM_139048	HLTF	6596	s13136	0.25 nmole	4,4	GAAAAGCGGUUU CAGAUCAAtt	UGAUCUGAAACCG CUUUUCta
AMO21R6P	C13	NM_031966	CCNB1	891	s2515	0.25 nmole	6	GAAAUGUACCCUC CAGAAAtt	UUUCUGGAGGGU ACAUUUCtt
AMO21R6P	C14	NM_031966	CCNB1	891	s2515	0.25 nmole	6	GAAAUGUACCCUC CAGAAAtt	UUUCUGGAGGGU ACAUUUCtt
AMO21R6P	C15	NM_199320	PHF17	79960	s36724	0.25 nmole	6,6	CAGCGAUGCUCAC GACAAUAtt	UAUUGUCGUAGC AUCGCUGct
AMO21R6P	C16	NM_199320	PHF17	79960	s36724	0.25 nmole	6,6	CAGCGAUGCUCAC GACAAUAtt	UAUUGUCGUAGC AUCGCUGct
AMO21R6P	C17	NM_014630	ZNF592	9640	s18533	0.25 nmole	4	GCAUUUGCCUUA GAGAAGAtt	UCUUCUCUAAGG CAAUUCGct
AMO21R6P	C18	NM_014630	ZNF592	9640	s18533	0.25 nmole	4	GCAUUUGCCUUA GAGAAGAtt	UCUUCUCUAAGG CAAUUCGct
AMO21R6P	C19	NM_015649	IRF2BP1	26145	s25154	0.25 nmole	1	GGGCUUCAAGUA CCUCGAAtt	UUCGAGGUACUU GAAGCCGga
AMO21R6P	C20	NM_015649	IRF2BP1	26145	s25154	0.25 nmole	1	GGGCUUCAAGUA CCUCGAAtt	UUCGAGGUACUU GAAGCCGga

AMO21R6P	C21	NM_005861	STUB1	10273	s195025	0.25 nmole	1	GUCUGUUCGUGG GCCGAAAtt	UUUCGGCCCACG AACAGACga
AMO21R6P	C22	NM_005861	STUB1	10273	s195025	0.25 nmole	1	GUCUGUUCGUGG GCCGAAAtt	UUUCGGCCCACG AACAGACga
AMO21R6P	C23	NM_012167	FBXO11	80204	s37047	0.25 nmole	4,4,4	GAAACGAUUUAU AUGGAAtt	UUCCAUAUAUAU CGUUUCca
AMO21R6P	C24	NM_012167	FBXO11	80204	s37047	0.25 nmole	4,4,4	GAAACGAUUUAU AUGGAAtt	UUCCAUAUAUAU CGUUUCca
AMO21R6P	D1	NM_007294	BRCA1	672	s457	0.25 nmole	Not Determined	GGGAUACCAUGC AACAAAtt	UUAUGUUGCAUG GUAUCCctc
AMO21R6P	D2	NM_014952	BAHD1	22893	s22606	0.25 nmole	5	UUACAGACCUGAG CACUUAtt	UAAGUGCUCAGG UCUGUAAta
AMO21R6P	D3	NM_024963	FBXL18	80028	s36850	0.25 nmole	Not Determined	CUGCAGCACAUG AAAUUCAtt	UGAAUUUCAUGU GCUGCAGga
AMO21R6P	D4	NM_014593	CXXC1	30827	s26937	0.25 nmole	Not Determined	GUAUAAUCCUCAG AGCAAAtt	UUUGCUCUGAGG AUUAUACac
AMO21R6P	D5	NM_003955	SOCS3	9021	s17189	0.25 nmole	2	UGAUUUGGUUUA AACCUGAtt	UCAGGUUUAACC AAAUCAaa
AMO21R6P	D6	NM_152617	RNF168	165918	s46601	0.25 nmole	6	GAAGUAUAGCCGA CACUUUtt	AAAGUGUCGGCA UAUCUUCta
AMO21R6P	D7	NM_053056	CCND1	595	s229	0.25 nmole	5	GGAGCAUUUUGA UACCAGAtt	UCUGGUAUCAAAA UGCUCcg
AMO21R6P	D8		SiSeI_NC1	0	s813	0.25 nmole	Not Determined		

AMO21R6P	D9	NM_030793	FBXO38	81545	s37602	0.25 nmole	11,11	GGACUCGAUUGG UUGAUUtt	AUAUCAACCAUUC GAGUCCat
AMO21R6P	D10	NM_020640	DCUN1D1	54165	s28892	0.25 nmole	6	GCAGAUGACAUG UCUAAUtt	AAUUAGACAUGUC AUCUGCaa
AMO21R6P	D11	NM_139048	HLTE	6596	s13136	0.25 nmole	4,4	GAAAAGCGGUUU CAGAUCAtt	UGAUCUGAAACCG CUUUUCta
AMO21R6P	D12	NM_014502	PRPF19	27339	s26186	0.25 nmole	Not Determined	GCUCAUCGACAU CAAAGUtt	AACUUUGAUGUC GAUGAGCtg
AMO21R6P	D13	NM_031966	CCNB1	891	s2515	0.25 nmole	6	GAAAUGUACCCUC CAGAAAtt	UUUCUGGAGGGU ACAUUUCtt
AMO21R6P	D14	NM_001798	CDK2	1017	s206	0.25 nmole	Not Determined	CAAGAUCUCAAGA AAUUCAtt	UGAAUUUCUUGA GAUCUUGgt
AMO21R6P	D15	NM_199320	PHE17	79960	s36724	0.25 nmole	6,6	CAGCGAUGCUCAC GACAAUAtt	UAUUGUCGUAGC AUCGCUGct
AMO21R6P	D16	NM_031407	HUWE1	10075	s19597	0.25 nmole	Not Determined	GGUCUAAUCAUG CCGCAGAtt	UCUGCGGCAUGA UUAGACCtt
AMO21R6P	D17	NM_014630	ZNF592	9640	s18533	0.25 nmole	4	GCAUUUGCCUUA GAGAAGAtt	UCUUCUCUAAGG CAAUUGCgt
AMO21R6P	D18	NM_001273	CHD4	1108	s2985	0.25 nmole	20	CACUCGAAUUUU GAAGCAtt	UGCUUCAAAUUU CGAGUGag
AMO21R6P	D19	NM_015649	IRF2BP1	26145	s25154	0.25 nmole	1	GGGCUUCAAGUA CCUCGAAtt	UUCGAGGUACUU GAAGCCGa
AMO21R6P	D20	NM_020901	PHRF1	57661	s33543	0.25 nmole	Not Determined	CCAGUUUCUUUU CAGCGAAtt	UUCGCUGAAAAGA AACUGGag

AMO21R6P	D21	NM_005861	STUB1	10273	s195025	0.25 nmole	1	GUCUGUUCGUGG GCCGAAAtt	JUUCGGCCACG AACAGACga
AMO21R6P	D22	NM_032408	BAZ1B	9031	s17210	0.25 nmole	Not Determined	CCUCAUUGCAUA CUACAAAtt	JUUGUAGUAUGC AAUGAGGtg
AMO21R6P	D23	NM_012167	FBXO11	80204	s37047	0.25 nmole	4,4,4	GAAACGAUUAUUAU AUGGAAAtt	JUCCAUAUAUAU CGUUUCca
AMO21R6P	D24	NM_014948	UBOX5	22888	s22597	0.25 nmole	2,2	GCAACAAGAUUUC AGCUGAtt	UCAGCUGAUUUC UUGUUGCag
AMO21R6P	E1	NM_020165	RAD18	56852	s32295	0.25 nmole	Not Determined	CAUAUUAGAUGAA CUGGUAtt	UACCAGUUCAUC UAAUAUGcg
AMO21R6P	E2	NM_020165	RAD18	56852	s32295	0.25 nmole	Not Determined	CAUAUUAGAUGAA CUGGUAtt	UACCAGUUCAUC UAAUAUGcg
AMO21R6P	E3	NM_014593	CXXC1	30827	s26936	0.25 nmole	Not Determined	CAAGCUAGAGAUU CGCUAUtt	AUAGCGAAUCUCU AGCUUGgg
AMO21R6P	E4	NM_014593	CXXC1	30827	s26936	0.25 nmole	Not Determined	CAAGCUAGAGAUU CGCUAUtt	AUAGCGAAUCUCU AGCUUGgg
AMO21R6P	E5	NM_015651	PHF19	26147	s25160	0.25 nmole	2,2	GACUUGAUGUCC AAACUGAtt	UCAGUUUGGACA UCAAGUCtt
AMO21R6P	E6	NM_015651	PHF19	26147	s25160	0.25 nmole	2,2	GACUUGAUGUCC AAACUGAtt	UCAGUUUGGACA UCAAGUCtt
AMO21R6P	E7	NM_031407	HUWE1	10075	s19595	0.25 nmole	Not Determined	CAUUGGAAAGUG CGAGUUAtt	UAACUCGCACUU UCCAAUGtt
AMO21R6P	E8	NM_031407	HUWE1	10075	s19595	0.25 nmole	Not Determined	CAUUGGAAAGUG CGAGUUAtt	UAACUCGCACUU UCCAAUGtt
AMO21R6P	E9	NM_004238	TRIP12	9320	s17809	0.25 nmole	15	GAUUGAUCUUGU UCCACGAtt	UCGUGGAACAAGA UCAAUctg

AMO21R6P	E10	NM_004238	TRIP12	9320	s17809	0.25 nmole	15	GAUUGAUCUUGU UCCACGAtt	UCGUGGAACAAGA UCAAUctg
AMO21R6P	E11	NM_015695	BRPF3	27154	s25918	0.25 nmole	Not Determined	CCAACUGCAUGAA GUAUAAtt	UUUAUACUUAUG CAGUUGGta
AMO21R6P	E12	NM_015695	BRPF3	27154	s25918	0.25 nmole	Not Determined	CCAACUGCAUGAA GUAUAAtt	UUUAUACUUAUG CAGUUGGta
AMO21R6P	E13	NM_006510	TRIM27	5987	s11960	0.25 nmole	5	CAAAAUGUCUAU UCUUGAtt	UCAAGAAUAGACA UUUUUGgg
AMO21R6P	E14	NM_006510	TRIM27	5987	s11960	0.25 nmole	5	CAAAAUGUCUAU UCUUGAtt	UCAAGAAUAGACA UUUUUGgg
AMO21R6P	E15	NM_014948	UBOX5	22888	s22595	0.25 nmole	3,3	ACAGUAACUUUGG UGUAAAtt	UUUACACCAAAGU UACUGUct
AMO21R6P	E16	NM_014948	UBOX5	22888	s22595	0.25 nmole	3,3	ACAGUAACUUUGG UGUAAAtt	UUUACACCAAAGU UACUGUct
AMO21R6P	E17	NM_001273	CHD4	1108	s2983	0.25 nmole	12	CUAUCGCUAUGG GAUAAAAtt	UUUUAUCCCAUA GCGAUAGaa
AMO21R6P	E18	NM_001273	CHD4	1108	s2983	0.25 nmole	12	CUAUCGCUAUGG GAUAAAAtt	UUUUAUCCCAUA GCGAUAGaa
AMO21R6P	E19	NM_005861	STUB1	10273	s195026	0.25 nmole	2	CGCUGGUGGCCG UGUAUUAtt	UAAUACACGGCCA CCAGCGgg
AMO21R6P	E20	NM_005861	STUB1	10273	s195026	0.25 nmole	2	CGCUGGUGGCCG UGUAUUAtt	UAAUACACGGCCA CCAGCGgg

AMO21R6P	E21	NM_020640	DCUN1D1	54165	s28890	0.25 nmole	4	CCAGGACGAUUUA AGGAUUt	AAUCCUUAAAUCG UCCUGGt
AMO21R6P	E22	NM_020640	DCUN1D1	54165	s28890	0.25 nmole	4	CCAGGACGAUUUA AGGAUUt	AAUCCUUAAAUCG UCCUGGt
AMO21R6P	E23	NM_007294	BRCA1	672	s458	0.25 nmole	Not Determined	CAGCUACCCUUC CAUCAUAtt	UAUGAUGGAAGG GUAGCUGt
AMO21R6P	E24	NM_007294	BRCA1	672	s458	0.25 nmole	Not Determined	CAGCUACCCUUC CAUCAUAtt	UAUGAUGGAAGG GUAGCUGt
AMO21R6P	F1	NM_020165	RAD18	56852	s32295	0.25 nmole	Not Determined	CAUAUUAGAUGAA CUGGUAtt	UACCAGUUCAUC UAAUAUGcg
AMO21R6P	F2	NM_012116	CBLC	23624	s24225	0.25 nmole	Not Determined	CCGAAAGUGAGAC UCCUAAtt	UUAGGAGUCUCA CUUUCGGct
AMO21R6P	F3	NM_014593	CXXC1	30827	s26936	0.25 nmole	Not Determined	CAAGCUAGAGAUU CGCUAUtt	AUAGCGAAUCUCU AGCUUGgg
AMO21R6P	F4	NM_053056	CCND1	595	s228	0.25 nmole	5	GUAGGACUCUCA UUCGGGAtt	UCCCGAAUGAGA GUCCUACag
AMO21R6P	F5	NM_015651	PHE19	26147	s25160	0.25 nmole	2,2	GACUUGAUGUCC AAACUGAtt	UCAGUUUGGACA UCAAGUCt
AMO21R6P	F6	NM_004667	HERC2	8924	s17064	0.25 nmole	15	CCAUUGCUUUGA CGAAAGAtt	UCUUUCGUCAAA GCAAUGGaa
AMO21R6P	F7	NM_031407	HUWE1	10075	s19595	0.25 nmole	Not Determined	CAUUGGAAAGUG CGAGUUAtt	UAACUCGCACUU UCCAAUGt
AMO21R6P	F8	NM_015695	BRPF3	27154	s25920	0.25 nmole	Not Determined	GCAUCGUAUCAG CAUCUAUtt	AUAGAUGCUGAUA CGAUGCag
AMO21R6P	F9	NM_004238	TRIP12	9320	s17809	0.25 nmole	15	GAUUGAUCUUGU UCCACGAtt	UCGUGGAACAAGA UCAAUctg

AMO21R6P	F10		SiSeL_NC1	0	s813	0.25 nmole	Not Determined		
AMO21R6P	F11	NM_015695	BRPF3	27154	s25918	0.25 nmole	Not Determined	C AACUGCAUGAA GUAUAAtt	UUUAUCUUAUG CAGUUGGta
AMO21R6P	F12	NM_014952	BAHD1	22893	s22606	0.25 nmole	5	UUACAGACCUGAG CACUUAtt	UAAGUGCUCAGG UCUGUAAta
AMO21R6P	F13	NM_006510	TRIM27	5987	s11960	0.25 nmole	5	CAAAAUGUCUAU UCUUGAtt	UCAAGAAUAGACA UUUUUGgg
AMO21R6P	F14		SiSeL_NC1	0	s813	0.25 nmole	Not Determined		
AMO21R6P	F15	NM_014948	UBOX5	22888	s22595	0.25 nmole	3,3	ACAGUAACUUUGG UGUAAAtt	UUUACACCAAAGU UACUGUct
AMO21R6P	F16	NM_014593	CXXC1	30827	s26937	0.25 nmole	Not Determined	GUAUAAUCCUCAG AGCAAAtt	UUUGCUCUGAGG AUUAUACac
AMO21R6P	F17	NM_001273	CHD4	1108	s2983	0.25 nmole	12	CUAUCGCUAUGG GAUAAAAtt	UUUUAUCCCAUA GCGAUAGaa
AMO21R6P	F18	NM_152617	RNF168	165918	s46601	0.25 nmole	6	GAAGUAUGCCGA CACUUUtt	AAAGUGUCGGCA UAUCUUCta
AMO21R6P	F19	NM_005861	STUB1	10273	s195026	0.25 nmole	2	CGCUGGUGGCCG UGUAUUAtt	UAAUACACGGCCA CCAGCGgg
AMO21R6P	F20	NM_020640	DCUN1D1	54165	s28892	0.25 nmole	6	GCAGAUGACAUG UCUAAUtt	AAUAGACAUGUC AUCUGCaa
AMO21R6P	F21	NM_020640	DCUN1D1	54165	s28890	0.25 nmole	4	CCAGGACGAUUUA AGGAUtt	AAUCCUAAAUCG UCCUGGtt

AMO21R6P	F22		SiSeL_NC1	0	s813	0.25 nmole	Not Determined		
AMO21R6P	F23	NM_007294	BRCA1	672	s458	0.25 nmole	Not Determined	CAGCUACCCUUC CAUCAUAtt	UAUGAUGGAAGG GUAGCUGtt
AMO21R6P	F24	NM_014502	PRPF19	27339	s26186	0.25 nmole	Not Determined	GCUCAUCGACAU CAAAGUAtt	AACUUUGAUGUC GAUGAGCtg
AMO21R6P	G1	NM_152617	RNF168	165918	s46599	0.25 nmole	6	GAAGAGUCGUGC CUACUGAtt	UCAGUAGGCACG ACUCUUCat
AMO21R6P	G2	NM_152617	RNF168	165918	s46599	0.25 nmole	6	GAAGAGUCGUGC CUACUGAtt	UCAGUAGGCACG ACUCUUCat
AMO21R6P	G3	NM_020901	PHRF1	57661	s33541	0.25 nmole	Not Determined	CGAACUCUAUUUA AGUGCAtt	UGCACUUAAAUAG AGUUCGat
AMO21R6P	G4	NM_020901	PHRF1	57661	s33541	0.25 nmole	Not Determined	CGAACUCUAUUUA AGUGCAtt	UGCACUUAAAUAG AGUUCGat
AMO21R6P	G5	NM_152620	TRIM60	166655	s46624	0.25 nmole	3	CCAAGGAGAUUUU AUGUCUtt	AGACAUAAAUCU CCUUGGgt
AMO21R6P	G6	NM_152620	TRIM60	166655	s46624	0.25 nmole	3	CCAAGGAGAUUUU AUGUCUtt	AGACAUAAAUCU CCUUGGgt
AMO21R6P	G7	NM_003958	RNF8	9025	s17200	0.25 nmole	Not Determined	GAGGAUUUGGUG UCACAUAtt	UAUGUGACACCAA AUCCUCgt
AMO21R6P	G8	NM_003958	RNF8	9025	s17200	0.25 nmole	Not Determined	GAGGAUUUGGUG UCACAUAtt	UAUGUGACACCAA AUCCUCgt
AMO21R6P	G9	NM_012167	FBXO11	80204	s37048	0.25 nmole	5,5,5	GCAGUUGUAUAAA GGUGCAtt	UGCACCUUUUAUA CAACUGCtg
AMO21R6P	G10	NM_012167	FBXO11	80204	s37048	0.25 nmole	5,5,5	GCAGUUGUAUAAA GGUGCAtt	UGCACCUUUUAUA CAACUGCtg

AMO21R6P	G11	NM_183237	RNF7	9616	s18474	0.25 nmole	2	UCUUAGAUGUCAAGCUGAAtt	UUCAGCUUGACAUCUAAGAc
AMO21R6P	G12	NM_183237	RNF7	9616	s18474	0.25 nmole	2	UCUUAGAUGUCAAGCUGAAtt	UUCAGCUUGACAUCUAAGAc
AMO21R6P	G13	NM_001165	BIRC3	330	s1452	0.25 nmole	4,5	GGAGUUCAUCCGUAAGUUt	AACUUGACGGGAUUAACUCtg
AMO21R6P	G14	NM_001165	BIRC3	330	s1452	0.25 nmole	4,5	GGAGUUCAUCCGUAAGUUt	AACUUGACGGGAUUAACUCtg
AMO21R6P	G15	NM_015695	BRPF3	27154	s25919	0.25 nmole	Not Determined	GGAUUACACCGAAUGCAAUt	AUUGCAUUCGGUGAUUUCtg
AMO21R6P	G16	NM_015695	BRPF3	27154	s25919	0.25 nmole	Not Determined	GGAUUACACCGAAUGCAAUt	AUUGCAUUCGGUGAUUUCtg
AMO21R6P	G17	NM_012116	CBLC	23624	s24224	0.25 nmole	Not Determined	CCUAUGAUGAGGUCCAAGAtt	UCUUGGACCUCAUCAUAGGtg
AMO21R6P	G18	NM_012116	CBLC	23624	s24224	0.25 nmole	Not Determined	CCUAUGAUGAGGUCCAAGAtt	UCUUGGACCUCAUCAUAGGtg
AMO21R6P	G19	NM_004359	CDC34	997	s2763	0.25 nmole	2	GCCUUUCGGUUCUGACCAAtt	UGGUCAGGAACCGAAAGGctg
AMO21R6P	G20	NM_004359	CDC34	997	s2763	0.25 nmole	2	GCCUUUCGGUUCUGACCAAtt	UGGUCAGGAACCGAAAGGctg
AMO21R6P	G21	NM_030793	FBXO38	81545	s37603	0.25 nmole	18,18	CACCAAUUGUAAACCGAAUUt	AAUCGGUUUACAAUUGGUGca

AMO21R6P	G22	NM_030793	FBXO38	81545	s37603	0.25 nmole	18,18	CACCAAUUGUAAA CCGAUUt	AAUCGGUUUACAA UUGGUGca
AMO21R6P	G23	NM_014630	ZNF592	9640	s18534	0.25 nmole	4	CAAACACUCUGAC AGUUAUt	AUAACUGUCAGAG UGUUUGgg
AMO21R6P	G24	NM_014630	ZNF592	9640	s18534	0.25 nmole	4	CAAACACUCUGAC AGUUAUt	AUAACUGUCAGAG UGUUUGgg
AMO21R6P	H1	NM_152617	RNF168	165918	s46599	0.25 nmole	6	GAAGAGUCGUGC CUACUGAtt	UCAGUAGGCACG ACUCUUCat
AMO21R6P	H2		SiSeL_NC1	0	s813	0.25 nmole	Not Determined		
AMO21R6P	H3	NM_020901	PHRF1	57661	s33541	0.25 nmole	Not Determined	CGAACUCUAUUUA AGUGCAtt	UGCACUUAAAUAG AGUUCGat
AMO21R6P	H4	NM_001798	CDK2	1017	s206	0.25 nmole	Not Determined	CAAGAUCUCAAGA AAUUCAtt	UGAAUUUCUUGA GAUCUUGgt
AMO21R6P	H5	NM_152620	TRIM60	166655	s46624	0.25 nmole	3	CCAAGGAGAUUUU AUGUCUtt	AGACAUAAAUCU CCUUGGgt
AMO21R6P	H6	NM_031407	HUWE1	10075	s19597	0.25 nmole	Not Determined	GGUCUAAUCAUG CCGCAGAtt	UCUGCGGCAUGA UUAGACct
AMO21R6P	H7	NM_003958	RNF8	9025	s17200	0.25 nmole	Not Determined	GAGGAUUUGGUG UCACAUAtt	UAUGUGACACCAA AUCCUCgt
AMO21R6P	H8	NM_001273	CHD4	1108	s2985	0.25 nmole	20	CACUCGAAUUUU GAAGCAtt	UGCUUCAAAUUU CGAGUGag
AMO21R6P	H9	NM_012167	FBXO11	80204	s37048	0.25 nmole	5,5,5	GCAGUUGUAUAAA GGUGCAtt	UGCACCUUUUAU CAACUGCtg
AMO21R6P	H10	NM_020901	PHRF1	57661	s33543	0.25 nmole	Not Determined	CCAGUUUCUUUU CAGCGAAtt	UUCGCUGAAAAGA AACUGGag

AMO21R6P	H11	NM_183237	RNF7	9616	s18474	0.25 nmole	2	UCUUAGAUGUCAA GCUGAAtt	UUCAGCUUGACA UCUAAGAc
AMO21R6P	H12	NM_032408	BAZ1B	9031	s17210	0.25 nmole	Not Determined	CCUCAUUGCAUA CUACAAAtt	UUUGUAGUAUGC AAUGAGGtg
AMO21R6P	H13	NM_001165	BIRC3	330	s1452	0.25 nmole	4,5	GGAGUUCAUCCG UCAAGUAtt	AACUUGACGGAU GAACUCctg
AMO21R6P	H14	NM_014948	UBOX5	22888	s22597	0.25 nmole	2,2	GCAACAAGUAUUC AGCUGAtt	UCAGCUGUAUUC UUGUUGCag
AMO21R6P	H15	NM_015695	BRPF3	27154	s25919	0.25 nmole	Not Determined	GGAUUACACCGAA UGCAAAtt	AUUGCAUUCGGU GAUAUCctg
AMO21R6P	H16	NM_012116	CBLC	23624	s24225	0.25 nmole	Not Determined	CCGAAAGUGAGAC UCCUAAtt	UUAGGAGUCUCA CUUUCGct
AMO21R6P	H17	NM_012116	CBLC	23624	s24224	0.25 nmole	Not Determined	CCUAUGAUGAGG UCCAAGAtt	UCUUGGACCUCA UCAUAGGtg
AMO21R6P	H18		SiSeI_NC1	0	s813	0.25 nmole	Not Determined		
AMO21R6P	H19	NM_004359	CDC34	997	s2763	0.25 nmole	2	GCCUUUCGGUUC CUGACCAtt	UGGUCAGGAACC GAAAGGctg
AMO21R6P	H20	NM_053056	CCND1	595	s228	0.25 nmole	5	GUAGGACUCUCA UUCGGGAtt	UCCCGAAUGAGA GUCCUACag
AMO21R6P	H21	NM_030793	FBXO38	81545	s37603	0.25 nmole	18,18	CACCAAUUGUAAA CCGAUAtt	AAUCGGUUUACAA UUGGUGca

AMO21R6P	H22	NM_004667	HERC2	8924	s17064	0.25 nmole	15	CCAUUGCUUUGA CGAAAGAtt	UCUUUCGUCAAA GCAAUGGaa
AMO21R6P	H23	NM_014630	ZNF592	9640	s18534	0.25 nmole	4	CAAACACUCUGAC AGUUAUtt	AUAACUGUCAGAG UGUUUGgg
AMO21R6P	H24	NM_015695	BRPF3	27154	s25920	0.25 nmole	Not Determined	GCAUCGUAUCAG CAUCUAUtt	AUAGAUGCUGAUA CGAUGCag
AMO21R6P	I1	NM_139048	HLTE	6596	s13137	0.25 nmole	7,7	GCGAAAUGACUUA UACUAUtt	AUAGUAUAAGUCA UUUCGctg
AMO21R6P	I2	NM_139048	HLTE	6596	s13137	0.25 nmole	7,7	GCGAAAUGACUUA UACUAUtt	AUAGUAUAAGUCA UUUCGctg
AMO21R6P	I3	NM_025058	TRIM46	80128	s36935	0.25 nmole	1	GCACUGGUCCGC AUCAGUAtt	UACUGAUGCgGA CCAGUGCgt
AMO21R6P	I4	NM_025058	TRIM46	80128	s36935	0.25 nmole	1	GCACUGGUCCGC AUCAGUAtt	UACUGAUGCgGA CCAGUGCgt
AMO21R6P	I5	NM_015649	IRF2BP1	26145	s25155	0.25 nmole	1	CCGAUUUCGAGAA AGAGAAtt	UUCUCUUUCUCG AAAUCGGag
AMO21R6P	I6	NM_015649	IRF2BP1	26145	s25155	0.25 nmole	1	CCGAUUUCGAGAA AGAGAAtt	UUCUCUUUCUCG AAAUCGGag
AMO21R6P	I7	NM_032408	BAZ1B	9031	s17208	0.25 nmole	Not Determined	GAUCGAAACCAUA AUAGAUtt	AUCUAUUUAGGU UUCGAUCtg
AMO21R6P	I8	NM_032408	BAZ1B	9031	s17208	0.25 nmole	Not Determined	GAUCGAAACCAUA AUAGAUtt	AUCUAUUUAGGU UUCGAUCtg

AMO21R6P	I9	NM_014502	PRPF19	27339	s26184	0.25 nmole	Not Determined	GCGCAAGCUUAA GAACUUUtt	AAAGUUCUUAAGC UUGCGCag
AMO21R6P	I10	NM_014502	PRPF19	27339	s26184	0.25 nmole	Not Determined	GCGCAAGCUUAA GAACUUUtt	AAAGUUCUUAAGC UUGCGCag
AMO21R6P	I11	NM_014952	BAHD1	22893	s22604	0.25 nmole	2	CGCAGCUGCUUU CCUAAAAtt	UUUUAGGAAAGCA GCUGCGtt
AMO21R6P	I12	NM_014952	BAHD1	22893	s22604	0.25 nmole	2	CGCAGCUGCUUU CCUAAAAtt	UUUUAGGAAAGCA GCUGCGtt
AMO21R6P	I13	NM_199320	PHE17	79960	s36725	0.25 nmole	6,6	CGAAUAUGAUGAA GAUGUUtt	AACAUCUUCAUCA UAUUCGat
AMO21R6P	I14	NM_199320	PHE17	79960	s36725	0.25 nmole	6,6	CGAAUAUGAUGAA GAUGUUtt	AACAUCUUCAUCA UAUUCGat
AMO21R6P	I15	NM_024963	FBXL18	80028	s36851	0.25 nmole	Not Determined	ACACCGUGUUGC UGCAAAAtt	UUUUGCAGCAACA CGGUGUgg
AMO21R6P	I16	NM_024963	FBXL18	80028	s36851	0.25 nmole	Not Determined	ACACCGUGUUGC UGCAAAAtt	UUUUGCAGCAACA CGGUGUgg
AMO21R6P	I17	NM_020165	RAD18	56852	s32296	0.25 nmole	Not Determined	GGAUUUUCUAAU CAAGGAAtt	UUCCUUGAAUAGA UAAUCCat
AMO21R6P	I18	NM_020165	RAD18	56852	s32296	0.25 nmole	Not Determined	GGAUUUUCUAAU CAAGGAAtt	UUCCUUGAAUAGA UAAUCCat
AMO21R6P	I19	NM_014952	BAHD1	22893	s22605	0.25 nmole	2	AGAAUUACCCACU UCGUAAtt	UUACGAAGUGGG UAAUUCUtg
AMO21R6P	I20	NM_014952	BAHD1	22893	s22605	0.25 nmole	2	AGAAUUACCCACU UCGUAAtt	UUACGAAGUGGG UAAUUCUtg

AMO21R6P	I21	NM_031966	CCNB1	891	s2516	0.25 nmole	6	CACUUAUACUAAG CACCAAtt	UUGGUGCUUAGU AUAAGUGtt
AMO21R6P	I22	NM_031966	CCNB1	891	s2516	0.25 nmole	6	CACUUAUACUAAG CACCAAtt	UUGGUGCUUAGU AUAAGUGtt
AMO21R6P	I23	NM_020165	RAD18	56852	s32297	0.25 nmole	Not Determined	GUUCAGACAUCAU AAGAGAtt	UCUCUUUAUGAU UCUGAACtg
AMO21R6P	I24	NM_020165	RAD18	56852	s32297	0.25 nmole	Not Determined	GUUCAGACAUCAU AAGAGAtt	UCUCUUUAUGAU UCUGAACtg
AMO21R6P	J1	NM_139048	HLTE	6596	s13137	0.25 nmole	7,7	GCGAAAUGACUUA UACUAtt	AUAGUAUAAGUCA UUUCGctg
AMO21R6P	J2	NM_014952	BAHD1	22893	s22606	0.25 nmole	5	UUACAGACCUGAG CACUAtt	UAAGUGCUCAGG UCUGUAAta
AMO21R6P	J3	NM_025058	TRIM46	80128	s36935	0.25 nmole	1	GCACUGGUCCGC AUCAGUAtt	UACUGAUGC GGA CCAGUGCtg
AMO21R6P	J4	NM_014593	CXXC1	30827	s26937	0.25 nmole	Not Determined	GUAUAAUCCUCAG AGCAAAtt	UUUGCUCUGAGG AUUAUACac
AMO21R6P	J5	NM_015649	IRF2BP1	26145	s25155	0.25 nmole	1	CCGAUUUCGAGAA AGAGAAtt	UUCUCUUUCUGG AAAUCGgag
AMO21R6P	J6	NM_152617	RNF168	165918	s46601	0.25 nmole	6	GAAGUAUAGCCGA CACUUUtt	AAAGUGC GCGCA UAUCUUCta
AMO21R6P	J7	NM_032408	BAZ1B	9031	s17208	0.25 nmole	Not Determined	GAUCGAAACCAUA AUAGAAtt	AUCUAUU AUGGU UUCGAUCtg
AMO21R6P	J8	NM_020640	DCUN1D1	54165	s28892	0.25 nmole	6	GCAGAUGACAUG UCUAUUtt	AAUAGACAUGUC AUCUGCaa

AMO21R6P	J9	NM_014502	PRPF19	27339	s26184	0.25 nmole	Not Determined	GCGCAAGCUUAA GAACUUUtt	AAAGUUCUUAAGC UUGCGCag
AMO21R6P	J10	NM_014502	PRPF19	27339	s26186	0.25 nmole	Not Determined	GCUCAUCGACAU CAAAGUUtt	AACUUUGAUGUC GAUGAGCtg
AMO21R6P	J11	NM_014952	BAHD1	22893	s22604	0.25 nmole	2	CGCAGCUGCUUU CCUAAAAtt	UUUUAGGAAAGCA GCUGCGtt
AMO21R6P	J12		SiSeL_NC1	0	s813	0.25 nmole	Not Determined		
AMO21R6P	J13	NM_199320	PHF17	79960	s36725	0.25 nmole	6,6	CGAAUAUGAUGAA GAUGUUtt	AACAUCUUAUCA UAUUCGat
	J14		Mock						
AMO21R6P	J15	NM_024963	FBXL18	80028	s36851	0.25 nmole	Not Determined	ACACCGUGUUGC UGCAAAtt	UUUJGCAGCAACA CGGUGUgg
	J16		Mock						
AMO21R6P	J17	NM_020165	RAD18	56852	s32296	0.25 nmole	Not Determined	GGAUUUACUUAU CAAGGAAtt	UUCCUUGAAUAGA UAAUCCat
	J18		Mock						
AMO21R6P	J19	NM_014952	BAHD1	22893	s22605	0.25 nmole	2	AGAAUUACCCACU UCGUAAAtt	UUACGAAGUGGG UAAUUCUtg
	J20		Mock						
AMO21R6P	J21	NM_031966	CCNB1	891	s2516	0.25 nmole	6	CACUUUAUCUAAG CACCAAAtt	UUGGUGCUUAGU AUAAGUGtt

	J22		Mock						
AMO21R6P	J23	NM_020165	BAD18	56852	s32297	0.25 nmole	Not Determined	GUUCAGACAUCAU AAGAGAtt	UCUCUUAUGAUG UCUGAACtg
	J24		Mock						
AMO21R6P	K1	NM_053056	CCND1	595	s230	0.25 nmole	5	GCUAUUGGAGGA UCAGUUUtt	AAACUGAUCCUCC AAUAGCag
AMO21R6P	K2	NM_053056	CCND1	595	s230	0.25 nmole	5	GCUAUUGGAGGA UCAGUUUtt	AAACUGAUCCUCC AAUAGCag
AMO21R6P	K3	NM_032408	BAZ1B	9031	s17209	0.25 nmole	Not Determined	CCUUCGUAGUGA UCUCAUtt	AAUGAGAUCACUA CGAAGGaa
AMO21R6P	K4	NM_032408	BAZ1B	9031	s17209	0.25 nmole	Not Determined	CCUUCGUAGUGA UCUCAUtt	AAUGAGAUCACUA CGAAGGaa
AMO21R6P	K5	NM_020640	DCUN1D1	54165	s28891	0.25 nmole	6	CAUAAACGAUCAA UACCAAtt	UUGGUAUUGAUC GUUUUAGat
AMO21R6P	K6	NM_020640	DCUN1D1	54165	s28891	0.25 nmole	6	CAUAAACGAUCAA UACCAAtt	UUGGUAUUGAUC GUUUUAGat
AMO21R6P	K7	NM_004667	HERC2	8924	s17063	0.25 nmole	86	CUAUGGUACGCG AUCGUCAtt	UGACGAUCGCGU ACCAUAGtt
AMO21R6P	K8	NM_004667	HERC2	8924	s17063	0.25 nmole	86	CUAUGGUACGCG AUCGUCAtt	UGACGAUCGCGU ACCAUAGtt
AMO21R6P	K9	NM_001273	CHD4	1108	s2984	0.25 nmole	29	GCAAUUUUGCGAU AUGGUAtt	UACCAUAUCGCAU AAUUGCat

AMO21R6P	K10	NM_001273	CHD4	1108	s2984	0.25 nmole	29	GCAAUUAUGCGAU AUGGUAtt	UACCAUAUCGCAU AAUUGCAt
AMO21R6P	K11	NM_014502	PRPF19	27339	s26185	0.25 nmole	Not Determined	GCAGCUCAUCGA CAUCAAAtt	UUUGAUGUCGAU GAGCUGCtc
AMO21R6P	K12	NM_014502	PRPF19	27339	s26185	0.25 nmole	Not Determined	GCAGCUCAUCGA CAUCAAAtt	UUUGAUGUCGAU GAGCUGCtc
AMO21R6P	K13	NM_003955	SOCS3	9021	s17190	0.25 nmole	2	AGAAGAGCCUAAU ACAUCUtt	AGAUGUAAUAGGC UCUUCUgg
AMO21R6P	K14	NM_003955	SOCS3	9021	s17190	0.25 nmole	2	AGAAGAGCCUAAU ACAUCUtt	AGAUGUAAUAGGC UCUUCUgg
AMO21R6P	K15	NM_015651	PHF19	26147	s25161	0.25 nmole	3,3	GCCUCGUGACUU UCGAAGAtt	UCUUCGAAAGUCA CGAGGCag
AMO21R6P	K16	NM_015651	PHF19	26147	s25161	0.25 nmole	3,3	GCCUCGUGACUU UCGAAGAtt	UCUUCGAAAGUCA CGAGGCag
AMO21R6P	K17	NM_001167	XIAP	331	s1455	0.25 nmole	2	GAAUCUAAUAAU CGAAGUtt	ACUUCGAAUAAU AGAUUCcg
AMO21R6P	K18	NM_001167	XIAP	331	s1455	0.25 nmole	2	GAAUCUAAUAAU CGAAGUtt	ACUUCGAAUAAU AGAUUCcg
AMO21R6P	K19	NM_014948	UBOX5	22888	s22596	0.25 nmole	3,3	GUCUUACUGAAAA ACCAGAtt	UCUGGUUUUUA GUAAGACtt
AMO21R6P	K20	NM_014948	UBOX5	22888	s22596	0.25 nmole	3,3	GUCUUACUGAAAA ACCAGAtt	UCUGGUUUUUA GUAAGACtt

AMO21R6P	K21	NM_004238	TRIP12	9320	s17810	0.25 nmole	38	GCAAUUUGAUUC GUUCAGAtt	UCUGAACGAAUCA AAUUGCct
AMO21R6P	K22	NM_004238	TRIP12	9320	s17810	0.25 nmole	38	GCAAUUUGAUUC GUUCAGAtt	UCUGAACGAAUCA AAUUGCct
AMO21R6P	K23	NM_003955	SOCS3	9021	s17191	0.25 nmole	2	GCACCUUUCUGA UCCGCGAtt	UCGCGGAUCAGA AAGGUGCcg
AMO21R6P	K24	NM_003955	SOCS3	9021	s17191	0.25 nmole	2	GCACCUUUCUGA UCCGCGAtt	UCGCGGAUCAGA AAGGUGCcg
AMO21R6P	L1	NM_053056	CCND1	595	s230	0.25 nmole	5	GCUAUUGGAGGA UCAGUUUtt	AAACUGAUCCUCC AAUAGCag
	L2		MOCK						
AMO21R6P	L3	NM_032408	BAZ1B	9031	s17209	0.25 nmole	Not Determined	CCUUCGUAGUGA UCUCAUUt	AAUGAGAUACACUA CGAAGGaa
	L4		Mock						
AMO21R6P	L5	NM_020640	DCUN1D1	54165	s28891	0.25 nmole	6	CAUAAACGAUCAA UACCAAtt	UUGGUAUUGAUC GUUUUAGat
AMO21R6P	L6		SiSeI_NC1	0	s813	0.25 nmole	Not Determined		
AMO21R6P	L7	NM_004667	HERC2	8924	s17063	0.25 nmole	86	CUAUGGUACGCG AUCGUCAtt	UGACGAUCGCGU ACCAUAGtt
	L8		Mock						

AMO21R6P	L9	NM_001273	CHD4	1108	s2984	0.25 nmole	29	GCAAUUUGCGAU AUGGUAtt	UACCAUAUCGCAU AAUUGCAt
	L10		Mock						
AMO21R6P	L11	NM_014502	PRPF19	27339	s26185	0.25 nmole	Not Determined	GCAGCUCAUCGA CAUCAAAAtt	UUUGAUGUCGAU GAGCUGCtc
	L12		Mock						
AMO21R6P	L13	NM_003955	SOCS3	9021	s17190	0.25 nmole	2	AGAAGAGCCUAUU ACAUCUtt	AGAUGUAAUAGGC UCUUCUgg
	L14		Mock						
AMO21R6P	L15	NM_015651	PHE19	26147	s25161	0.25 nmole	3,3	GCCUCGUGACUU UCGAAGAtt	UCUUCGAAAGUCA CGAGGCag
	L16		Mock						
AMO21R6P	L17	NM_001167	XIAP	331	s1455	0.25 nmole	2	GAAUCUAAUUAUU CGAAGUtt	ACUUCGAAUUAUA AGAUUCcg
	L18		Mock						
AMO21R6P	L19	NM_014948	UBOX5	22888	s22596	0.25 nmole	3,3	GUCUUACUGAAAA ACCAGAtt	UCUGGUUUUUCA GUAAGACTt
AMO21R6P	L20		SiSel_NC1	0	s813	0.25 nmole	Not Determined		
AMO21R6P	L21	NM_004238	TRIP12	9320	s17810	0.25 nmole	38	GCAAUUUGAUUC GUUCAGAtt	UCUGAACGAAUCA AAUUGCct

	L22		Mock						
AMO21R6P	L23	NM_003955	SOCS3	9021	s17191	0.25 nmole	2	GCACCUUUCUGA UCCGCGAtt	UCGCGGAUCAGA AAGGUGCcg
	L24		Mock						
AMO21R6P	M1	NM_005861	STUB1	10273	s195027	0.25 nmole	2	CCAAUCUGCAGC GAGCUUAtt	UAAGCUCGCUGC AGAUUGGcg
AMO21R6P	M2	NM_005861	STUB1	10273	s195027	0.25 nmole	2	CCAAUCUGCAGC GAGCUUAtt	UAAGCUCGCUGC AGAUUGGcg
AMO21R6P	M3	NM_007294	BRCA1	672	s459	0.25 nmole	Not Determined	CAUGCAACUAAC CUGAUAtt	UAUCAGGUUAUG UUGCAUGgt
AMO21R6P	M4	NM_007294	BRCA1	672	s459	0.25 nmole	Not Determined	CAUGCAACUAAC CUGAUAtt	UAUCAGGUUAUG UUGCAUGgt
AMO21R6P	M5	NM_030793	FBXO38	81545	s37604	0.25 nmole	22,22	GGGUGUAUUUCA GCGAGUAtt	UACUCGCUGAAAU ACACCtt
AMO21R6P	M6	NM_030793	FBXO38	81545	s37604	0.25 nmole	22,22	GGGUGUAUUUCA GCGAGUAtt	UACUCGCUGAAAU ACACCtt
AMO21R6P	M7	NM_001798	CDK2	1017	s205	0.25 nmole	Not Determined	GAGUCCUGUUC GUACUUAtt	UAAGUACGAACAG GGACUCca
AMO21R6P	M8	NM_001798	CDK2	1017	s205	0.25 nmole	Not Determined	GAGUCCUGUUC GUACUUAtt	UAAGUACGAACAG GGACUCca
AMO21R6P	M9	NM_020901	PHRF1	57661	s33542	0.25 nmole	Not Determined	CCCAAUCUGUCU CAACGCAtt	UGCGUUGAGACA GAUUGGGca
AMO21R6P	M10	NM_020901	PHRF1	57661	s33542	0.25 nmole	Not Determined	CCCAAUCUGUCU CAACGCAtt	UGCGUUGAGACA GAUUGGGca

AMO21R6P	M11	NM_006510	TRIM27	5987	s11961	0.25 nmole	3	GCAGCUGUAUCA CUCCUUAtt	UAAGGAGUGAUAC AGCUGCtc
AMO21R6P	M12	NM_006510	TRIM27	5987	s11961	0.25 nmole	3	GCAGCUGUAUCA CUCCUUAtt	UAAGGAGUGAUAC AGCUGCtc
AMO21R6P	M13	NM_152617	RNF168	165918	s46600	0.25 nmole	1	GUGGAACUGUGG ACGAUAAtt	UUAUCGUCCACA GUUCCACgt
AMO21R6P	M14	NM_152617	RNF168	165918	s46600	0.25 nmole	1	GUGGAACUGUGG ACGAUAAtt	UUAUCGUCCACA GUUCCACgt
AMO21R6P	M15	NM_152620	TRIM60	166655	s46625	0.25 nmole	3	CUCUAUACUUUU AACGAUUtt	AAUCGUUAAAAGU AUAGAGaa
AMO21R6P	M16	NM_152620	TRIM60	166655	s46625	0.25 nmole	3	CUCUAUACUUUU AACGAUUtt	AAUCGUUAAAAGU AUAGAGaa
AMO21R6P	M17	NM_003958	RNF8	9025	s17201	0.25 nmole	Not Determined	GGAGAAUGCGGA GUAUGAAtt	UUCAUACUCCGC AUUCUCctt
AMO21R6P	M18	NM_003958	RNF8	9025	s17201	0.25 nmole	Not Determined	GGAGAAUGCGGA GUAUGAAtt	UUCAUACUCCGC AUUCUCctt
AMO21R6P	M19	NM_025058	TRIM46	80128	s36936	0.25 nmole	8	CCAGCGCACCUU UGCCUAUtt	AUAGGCAAAGGUG CGCUGGgt
AMO21R6P	M20	NM_025058	TRIM46	80128	s36936	0.25 nmole	8	CCAGCGCACCUU UGCCUAUtt	AUAGGCAAAGGUG CGCUGGgt
AMO21R6P	M21	NM_001165	BIRC3	330	s1453	0.25 nmole	2,3	GAUUCGUUCAGA GUCUAAAtt	UUUAGACUCUGAA CGAAUCtg

AMO21R6P	M22	NM_001165	BIRC3	330	s1453	0.25 nmole	2,3	GAUUCGUUCAGA GUCUAAAtt	UUUAGACUCUGAA CGAAUCtg
AMO21R6P	M23	NM_001167	XIAP	331	s1456	0.25 nmole	2	GCAGAUUUUAUCAA CGGCUUtt	AAGCCGUUGAUAA AUCUGCaa
AMO21R6P	M24	NM_001167	XIAP	331	s1456	0.25 nmole	2	GCAGAUUUUAUCAA CGGCUUtt	AAGCCGUUGAUAA AUCUGCaa
AMO21R6P	N1	NM_005861	STUB1	10273	s195027	0.25 nmole	2	CCAUCUGCAGC GAGCUUAtt	UAAGCUCGCUGC AGAUUGGcg
	N2		Mock						
AMO21R6P	N3	NM_007294	BRCA1	672	s459	0.25 nmole	Not Determined	CAUGCAACAUAA CUGAUAtt	UAUCAGGUUAUG UUGCAUGgt
	N4		Mock						
AMO21R6P	N5	NM_030793	FBXO38	81545	s37604	0.25 nmole	22,22	GGGUGUAUUUCA GCGAGUAtt	UACUCGCUGAAAU ACACCCtt
	N6		Mock						
AMO21R6P	N7	NM_001798	CDK2	1017	s205	0.25 nmole	Not Determined	GAGUCCCGUUC GUACUUAtt	UAAGUACGAACAG GGACUCca
AMO21R6P	N8		SiSeI_NC1	0	s813	0.25 nmole	Not Determined		
AMO21R6P	N9	NM_020901	PHRF1	57661	s33542	0.25 nmole	Not Determined	CCCAAUCUGUCU CAACGCAAtt	UGCGUUGAGACA GAUUGGGca
	N10		Mock						

AMO21R6P	N11	NM_006510	TRIM27	5987	s11961	0.25 nmole	3	GCAGCUGUAUCA CUCCUUAtt	UAAGGAGUGAUAC AGCUGCtc
	N12		MOCK						
AMO21R6P	N13	NM_152617	RNF168	165918	s46600	0.25 nmole	1	GUGGAACUGUGG ACGAUAAtt	UUAUCGUCCACA GUUCCACgt
	N14		Mock						
AMO21R6P	N15	NM_152620	TRIM60	166655	s46625	0.25 nmole	3	CUCUAUACUUUU AACGAUUtt	AAUCGUUAAAAGU AUAGAGaa
	N16		Mock						
AMO21R6P	N17	NM_003958	RNF8	9025	s17201	0.25 nmole	Not Determined	GGAGAAUGCGGA GUAUGAAtt	UUCAUACUCCGC AUUCUCctt
	N18		Mock						
AMO21R6P	N19	NM_025058	TRIM46	80128	s36936	0.25 nmole	8	CCAGCGCACCUU UGCCUAUtt	AUAGGCAAAGGUG CGCUGGgt
	N20		Mock						
AMO21R6P	N21	NM_001165	BIRC3	330	s1453	0.25 nmole	2,3	GAUUCGUUCAGA GUCUAAAtt	UUUAGACUCUGAA CGAAUCtg
AMO21R6P	N22		SiSeI_NC1	0	s813	0.25 nmole	Not Determined		
AMO21R6P	N23	NM_001167	XIAP	331	s1456	0.25 nmole	2	GCAGAUUUUAUCAA CGGCUUtt	AAGCCGUUGAUAA AUCUGCaa

	N24		Mock						
AMO21R6P	O1	NM_014630	ZNF592	9640	s18535	0.25 nmole	4	AGAUACGGAUUU GGGAUAtt	UAUCCCAAUCCG UUAUCUtt
AMO21R6P	O2	NM_014630	ZNF592	9640	s18535	0.25 nmole	4	AGAUACGGAUUU GGGAUAtt	UAUCCCAAUCCG UUAUCUtt
AMO21R6P	O3	NM_015649	IRF2BP1	26145	s25156	0.25 nmole	1	GGAUACGAGUUC GAGCUGAtt	UCAGCUCGAACU CGUAUCCtg
AMO21R6P	O4	NM_015649	IRF2BP1	26145	s25156	0.25 nmole	1	GGAUACGAGUUC GAGCUGAtt	UCAGCUCGAACU CGUAUCCtg
AMO21R6P	O5	NM_012167	FBXO11	80204	s37049	0.25 nmole	15,15,15	GUACUGAGAAGAA ACCGGAtt	UCCGGUUUCUUC UCAGUACtg
AMO21R6P	O6	NM_012167	FBXO11	80204	s37049	0.25 nmole	15,15,15	GUACUGAGAAGAA ACCGGAtt	UCCGGUUUCUUC UCAGUACtg
AMO21R6P	O7	NM_004359	CDC34	997	s2764	0.25 nmole	2	CGACUACCCAUA UCUCCAtt	UGGAGAGUAUGG GUAGUCGat
AMO21R6P	O8	NM_004359	CDC34	997	s2764	0.25 nmole	2	CGACUACCCAUA UCUCCAtt	UGGAGAGUAUGG GUAGUCGat
AMO21R6P	O9	NM_015651	PHF19	26147	s25162	0.25 nmole	2,2	GGUCAGCAGCUC UAAGCAAtt	UUGC UUAGAGCU GCUGACCct
AMO21R6P	O10	NM_015651	PHF19	26147	s25162	0.25 nmole	2,2	GGUCAGCAGCUC UAAGCAAtt	UUGC UUAGAGCU GCUGACCct

AMO21R6P	O11	NM_003958	RNF8	9025	s17202	0.25 nmole	Not Determined	GGACAAUUAUGGA CAACAAtt	UUGUUGUCCAUA AUUGUCCat
AMO21R6P	O12	NM_003958	RNF8	9025	s17202	0.25 nmole	Not Determined	GGACAAUUAUGGA CAACAAtt	UUGUUGUCCAUA AUUGUCCat
AMO21R6P	O13	NM_031407	HUWE1	10075	s19596	0.25 nmole	Not Determined	CUGUGAGAGUGA UCGGGAAtt	UUCCCGAUCACU CUCACAGtt
AMO21R6P	O14	NM_031407	HUWE1	10075	s19596	0.25 nmole	Not Determined	CUGUGAGAGUGA UCGGGAAtt	UUCCCGAUCACU CUCACAGtt
AMO21R6P	O15	NM_031966	CCNB1	891	s2517	0.25 nmole	8	CAACAUUACCUGU CAUAUAtt	UAUAUGACAGGUA AUGUUGta
AMO21R6P	O16	NM_031966	CCNB1	891	s2517	0.25 nmole	8	CAACAUUACCUGU CAUAUAtt	UAUAUGACAGGUA AUGUUGta
AMO21R6P	O17	NM_024963	FBXL18	80028	s36852	0.25 nmole	Not Determined	GCACAGAUCUGAU UCUGAAtt	UUCAGAAUCAGAU CUGUGCtg
AMO21R6P	O18	NM_024963	FBXL18	80028	s36852	0.25 nmole	Not Determined	GCACAGAUCUGAU UCUGAAtt	UUCAGAAUCAGAU CUGUGCtg
AMO21R6P	O19	NM_183237	RNF7	9616	s18475	0.25 nmole	3	ACCCAACUCUUAC UCUUAAtt	UUAAGAGUAAGAG UUGGGUtt
AMO21R6P	O20	NM_183237	RNF7	9616	s18475	0.25 nmole	3	ACCCAACUCUUAC UCUUAAtt	UUAAGAGUAAGAG UUGGGUtt
AMO21R6P	O21	NM_199320	PHF17	79960	s36726	0.25 nmole	4,4	GAAUCCGGAUGA GUACUAUtt	AUAGUACUCAUCC GGAUUCag
AMO21R6P	O22	NM_199320	PHF17	79960	s36726	0.25 nmole	4,4	GAAUCCGGAUGA GUACUAUtt	AUAGUACUCAUCC GGAUUCag
AMO21R6P	O23	NM_139048	HLTF	6596	s13138	0.25 nmole	8,8	GGAAUUAUAUGUU AACGAUtt	AUCGUUAACAUUA UAUUCctt

AMO21R6P	O24	NM_139048	HLTE	6596	s13138	0.25 nmole	8,8	GGAAUAUAUGUU AACGAUtt	AUCGUUACAUAU UAUUCctt
AMO21R6P	P1	NM_014630	ZNF592	9640	s18535	0.25 nmole	4	AGAUACGGAUUU GGGAUAtt	UAUCCCCAAUCCG UUAUCUtt
AMO21R6P	P2		SiSeL_NC1	0	s813	0.25 nmole	Not Determined		
AMO21R6P	P3	NM_015649	IRF2BP1	26145	s25156	0.25 nmole	1	GGAUACGAGUUC GAGCUGAtt	UCAGCUCGAACU CGUAUCctg
	P4		Mock						
AMO21R6P	P5	NM_012167	FBXO11	80204	s37049	0.25 nmole	15,15,15	GUACUGAGAAGAA ACCGGAtt	UCCGGUUUCUUC UCAGUACtg
	P6		Mock						
AMO21R6P	P7	NM_004359	CDC34	997	s2764	0.25 nmole	2	CGACUACCCAUA UCUCCAtt	UGGAGAGUAUGG GUAGUCGat
	P8		Mock						
AMO21R6P	P9	NM_015651	PHF19	26147	s25162	0.25 nmole	2,2	GGUCAGCAGCUC UAAGCAAtt	UUGCUUAGAGCU GCUGACCct
	P10		Mock						
AMO21R6P	P11	NM_003958	RNF8	9025	s17202	0.25 nmole	Not Determined	GGACAAUUAUGGA CAACAAtt	UUGUUGUCCAUA AUUGUCCat
	P12		Mock						
AMO21R6P	P13	NM_031407	HUWE1	10075	s19596	0.25 nmole	Not Determined	CUGUGAGAGUGA UCGGGAAtt	UCCCCGAUCACU CUCACAGtt

AMO21R6P	P14		SiSeL_NC1	0	s813	0.25 nmole	Not Determined		
AMO21R6P	P15	NM_031966	CCNB1	891	s2517	0.25 nmole	8	CAACAUUACCUGU CAUAUAtt	UUAUGACAGGUA AUGUUGta
	P16		Empty						
AMO21R6P	P17	NM_024963	FBXL18	80028	s36852	0.25 nmole	Not Determined	GCACAGAUCUGAU UCUGAAtt	UUCAGAAUCAGAU CUGUGCtg
	P18		Empty						
AMO21R6P	P19	NM_183237	RNF7	9616	s18475	0.25 nmole	3	ACCCAACUCUUAC UCUUAAtt	UUAAGAGUAAGAG UUGGGUtt
	P20		MOCK						
AMO21R6P	P21	NM_199320	PHF17	79960	s36726	0.25 nmole	4,4	GAAUCCGGAUGA GUACUAUtt	AUAGUACUCAUCC GGAUUCag
	P22		Mock						
AMO21R6P	P23	NM_139048	HLTF	6596	s13138	0.25 nmole	8,8	GGAAUUAUAUGUU AACGAUtt	AUCGUUAACAUUA UAUUCctt
	P24		Empty						



Acknowledgements

I would like to express my deep appreciation to Prof. Dr. Cristina Cardoso for her unique and strategic approach to supervision, which allowed me to fully explore the depths of independent research. The freedom I was given to navigate challenges has been instrumental in helping me acquire a diverse and extensive skillset. This journey has taught me the importance of resilience, self-reliance, and adaptability. The opportunity to work autonomously has not only broadened my knowledge but also honed my ability to tackle complex problems with confidence. Thanks to this experience, I have grown into a well-rounded and capable professional, equipped with the skills and expertise needed to thrive in my field. I am sincerely grateful for the trust placed in my abilities, which has undoubtedly played a significant role in shaping the researcher I am today.

I would like to say thanks to Dr. Alexander Rapp for everything he did and everything he didn't. Both affected my PhD life equally significantly. Thanks for teaching me.

I sincerely thank people who was with me in the lab since the start of my PhD journey. Anne, Diana, Manu were always supportive, understanding and willing to help whenever possible. I learned a lot from them; their kind words and advice raised my spirit too many times.

Among others, Florian, Patrick, Cathia, and Francesco welcomed me in the lab and shared their experience, methods tips and inspiration. I am deeply thankful for the opportunity to be part of this vibrant lab environment that pushed me beyond my comfort zone and helped me grow in ways I never imagined. Florian, your support and acceptance made a significant difference during my time here. Without your kindness and encouragement, it would have been hard for me to persevere to the thesis completion. Thank you for being a good friend and amazing party buddy.

I would like to thank my favorite postdocs and dear friends, Dr. Vadim Chagin and Dr. Beata Plitta-Michalak. Amid challenges and uncertainties, your encouragement and understanding were a constant source of strength for me.

Vadim, for all the conversations, shared experiences, and your belief in me, I am profoundly grateful. As a fellow countryman, you understood me in a way others could not. Your presence was a comforting reminder of home, and you brought with you the warmth, traditions, and spirit of our country. In a foreign place, having someone who shares the same roots and values was incredibly meaningful to me and your presence here during emotionally exhausting coronavirus pandemic made those difficult days easier to bear.

Beata, you have been both empowering and enlightening in and outside the lab. You took care of me and offered a shoulder to lean on so many times. You are an inspiring example of a successful woman in science for me. Seeing you navigate the challenges of balancing a demanding career and family life has been truly motivating. Your dedication has shown me that it is possible to excel in both areas, even when the path is not easy.

I send my heartfelt gratitude to my fellow PhD students and friends Stefania, Maruthi, Sunil, and Annika who stood by my side during this journey. You supported me through some of the darkest moments in my life, and even when we didn't always see eye to eye, we endured and grew stronger together. The challenges we faced tested us, but they also deepened our understanding of each other and transformed our relationship into a genuine friendship. Ste, I still remember the day we first met; thank you for going on all the adventures with me and your care for me. I hope that we will keep the friendship fire in our hearts until the end. Annika, your sensible advice was always at the right time in the right place, and I deeply appreciated it. Maruthi, you have been my first student to supervise in my PhD time and I am happy that it was you and we had a good match. Special thanks for your patience and support in my turbulent love life. Sunil, thanks for listening and always being on my side no matter what. I deeply appreciate your care and loyalty, coffee breaks and pond breaks we had every day.

I am grateful to Katrin who, among others, supported me during the PhD time. Katrin skillfully took on the role of a negotiator during a difficult conflict taking place in my life. Her calm and diplomatic approach helped to de-escalate the situation, and it is largely thanks to her efforts that no legal charges were pressed against me. Katrin, you brought so much positivity and good vibes to the lab.

I thank Stefania, Maruthi, Sunil, Annika and Katrin for all the memorable moments, late-night talks, and shared adventures.

I extend my heartfelt gratitude to all the former and current members of Cardoso lab.

I would like to thank all the members of the graduate college GrK 1657 and Flow for Life consortium.

I extend my gratitude to the faculty of the Technical University of Darmstadt for their guidance and dedication throughout my academic journey. I thank my thesis advisory committee members, Prof. Dr. Markus Löbrich, Prof. Dr. Patrick Heun and Dr. Burkhard Jakob, for taking their time in reading and evaluating my research work.

I would like to thank the Technical University of Darmstadt and the city of Darmstadt for hosting me during this chapter of my academic journey. My time here was not without its challenges; I faced many difficulties and moments of self-doubt. However, these experiences have been transformative for my personal and professional growth.

With warm feelings I think about my *alma mater* Kazan Federal (Volga region) University, the faculty, all professors and mentors, and my first lab of Prof. Dr. Albert Rizvanov, where my journey in science truly began. It was there that I was taught the essential methods and given the fundamental knowledge that became the foundation of my research career. They also nurtured my passion for science, encouraging curiosity, critical thinking, and integrity. I know that they are proud of the researcher I became now.

I send my love to my family and friends. The current work is devoted to my family who patiently endured years of separation between us and never doubted that I could do it and deserve it. Since the first day when my PhD route started, the world has changed beyond our imagination, and despite the distance between us my family and I went through life storms together. I know that no matter where my way will bring me and how many good and bad days will come, I always have a home to come back to.

I thank Steffen Heß for always being on my side, protecting me and feeding me. I am grateful for absolute support and love you gave me.

I thank Ryan Alexander Ward for enjoyable conversations, entertaining games and emotional support. I hope for our exciting collaborations in the future, and, in the end of the day, I am happy that we met.

I thank post-rock bands 65daysofstatic, God Is An Astronaut, Mogwai, I Am Waiting For You Last Summer, as well as Depeche Mode, Morcheeba and Radiohead for keeping me sane. I also thank the BioPhoniX band, their concerts have always been a highlight and brought me a lot of joy.

At last, “I want to thank me for believing in me, I want to thank me for doing all this hard work. I want to thank me for having no days off. I want to thank me for never quitting. I want to thank me for always being a giver and trying to give more than I receive. I want to thank me for trying to do more right than wrong. I want to thank me for being me at all times.” ©

CV

1- Personal information

Name: Ksenia G. Kolobynina

Gender: female

Nationality: Russia

Researcher ID (ORCID): 0000-0002-8035-8867

2- Scientific bio sketch

Since my early years I have always had a keen interest in science and in particular in biology, and this interest has led me into my career. I started out as a laboratory assistant in my early university years and have come to leading several interdisciplinary research projects. My research focus is how genome instability and flaws in the 3D genome organization contribute to the disease development and aging. With my star techniques of nuclear targets visualization, microscopy and image analysis I would like to decipher complex interactions between molecular processes and chromatin structure in physiology and disease and create new methodological solutions. My long-term career goal is to become a leader of my own research group that would contribute not only to new discoveries in the field of epigenetics and DNA repair but also to the society as to inspire, tutor and support new generation of researchers and science professionals.

3- Education

- **PhD student**

Technical University Darmstadt, Germany

July 2017 – July 2024

Graduate college 1675 “Radiation Biology”. Thesis title “Novel regulators of chromatin response to DNA damage”, supervisor Prof. Dr. M. Cristina Cardoso.

- **Research internship, Summer School of Molecular Medicine**

Jena University Hospital, Germany

Aug 2016 – Sep 2016

Projects “Signaling molecules in angiogenesis” and “Signal transduction via JAKs and STATs in cancer and chronic inflammation”. Hosting supervisor Prof. Dr. Regine Heller.

- **Master of Science in Biology (major - Genetics)**

Kazan (Volga region) Federal University, Russia **Sep 2015 – June 2017**

Master thesis “Impact of Tescalcin protein fluctuations on the differentiation of mesenchymal stem cells”, supervisor Prof. Dr. Albert Rizvanov. Grade 1.0 (excellent).

• **Trainee**

Pfizer Inc., Kazan, Russia **Nov 2015**

Participant of the program “Biomedicine of cardiovascular diseases. Translational pharmacology and innovations in therapy”.

• **Trainee**

Novartis Institutes for biomedical research, Kazan, Russia **Oct 2015**

Theoretical and practical training in courses “Clinical pharmacology”, “Target to therapy”.

• **Research internship, exchange academic program**

University of Regensburg, Germany **Sep 2014 – Feb 2015**

Research internship in the University Clinic of Regensburg, project “V3-loop mimetic peptides of HIV-1 gp120 as vaccine tool to induce neutralizing activity of antibodies”, supervisor Prof. Dr. Barbara Schmidt.

• **Bachelor of Science in Biology**

Kazan (Volga region) Federal University, Russia **Sep 2011 – June 2015**

Bachelor thesis “Phylogenetic, structural and functional analysis of Tescalcin protein”, supervisor Prof. Dr. Albert Rizvanov. Grade 1.0 (excellent).

4- Current and previous positions

• **Junior researcher**

Technical University Darmstadt, Germany **Apr 2019 – Present**

Responsible for the projects: “Novel regulators of chromatin response to DNA damage” and “3D organization of DNA double strand break in time and space”.

• **Junior researcher**

Kazan (Volga region) Federal University, Russia **Aug 2016 – July 2017**

Responsible for the project in collaboration with University of Miami, USA: “Tescalcin as a player of complex network of stem cells fate”.

• **Laboratory assistant**

Lab “Gene and cell technologies” at the Institute of fundamental medicine and biology

5- Fellowships and awards

- Travel grant award for the participation in the 5th Danube Conference on epigenetics, 2024, Hungary
- Fellowship of GrK 1675 “Radiation Biology”, Technical University Darmstadt, 2017, Germany
- Fellowship of the Summer School of Molecular Medicine, Jena University Hospital, 2016, Germany
- Grant for young researchers by Innovation Promotion Fund, 2016, Russia
- Winner of the “50 best innovation ideas for the Republic of Tatarstan”, category “Youth innovation project” by the Investment Venture Fund of the Republic of Tatarstan, 2016, Russia

6- Scientific communication

- The 6th German-French DNA Repair meeting, 13-15 September 2023, Mainz, Germany – poster
- Trends in Microscopy, 20-24 March 2023, Münsingen, Germany – speaker of three-days course on light-sheet microscopy in cooperation with Evident corporation (Olympus), communicated the results of the project Flow for Life
- IMB/SFB 1361 Conference – “Restore, Reorganize, Repurpose: The many faces of DNA repair”, 20-23 September 2022, Mainz, Germany – poster
- International conference GrK 1739 “DNA damage and beyond: from molecular mechanisms to innovative concepts in the treatment of cancer”, 25-26 October 2019, Essen, Germany – poster
- 21st Annual Meeting of the Society for Biological Radiation Research GBS, 17-19 September 2018, Frankfurt am Main, Germany – poster
- International conference “Translational medicine: current time and future”, 24-25 May 2016, Kazan, Russia – poster
- International conference “Biology – science of the XXI century”, 20-24 April 2015, Moscow, Russia

7- Major collaborations and international experience

- LOEWE research cluster FLOW FOR LIFE “An artificial network for organ-like 3D cell aggregates”, interdisciplinary project at the TU Darmstadt
- Collaboration with the AG Leonhardt at the Ludwig-Maximilians-University Munich on the two projects aiming to develop ubiquitin-binding fluorescent probes for the live-cell imaging and site-specific antibody fragment conjugates for reversible immunostaining
- “KAUVIR: combination instead of addition” network, funded by the Ministry of Education and Research of Germany (BMBF)
- Collaboration with the AG Kubben at the IMB Mainz for the novel common ubiquitin

modifiers in DNA damage repair and senescence

- Collaborative project with the University of Miami, Miller School of Medicine (Dr. Vladlen Z. Slepak)

8- Teaching and supervision

- Tutor of the practical master course MTB10 “Cell biology and epigenetics” at the TU Darmstadt
- Supervisor of the master project “Identification and test of the novel ubiquitin modifiers in the DNA damage signaling and repair”, TU Darmstadt
- Supervisor of two master students internships, TU Darmstadt
- Supervisor of undergraduate students group (8 members), Kazan (Volga region) Federal University

9- Institutional responsibilities and project management

- Graduate student representative at the Faculty of Biology, TU Darmstadt
- Organizer of the BioScience symposium for the graduate students and postdocs, TU Darmstadt
- Organizer of the grant writing and application workshop at the Faculty of Biology
- Organizer of the graduate college GrK 1675 one week long retreat to Kleinwalsertal, Austria
- Chairwoman of the student English club, Kazan (Volga region) Federal University
- Representative of the German Centre of education, science and culture at the Kazan (Volga region) Federal University

10- Other relevant activities

Completed trainings and attended seminars:

- Intense microscopy training at the Trends in Microscopy (20-24 March 2023), biennial conference of German Biolmaging – GMB e.V., hands-on workshops on different microscopy techniques
- Spring School “UV meets ionizing radiation: Exposure, Prevention and Therapy” (27-29 April 2022), Düsseldorf, organized by the KAUVIR consortium
- Course “Souverän und up to date: So kommunizieren Sie Forschungsergebnisse zeitgemäß – Theorie und Praxis” (“Scientific communication – Theory and Practice”, September 2022), professional development at the TU Darmstadt, tutor – Dr. Jan Martin Wiarda
- Course “Supervising Bachelor and Master Theses” (January 2021), professional development at TU Darmstadt
- Workshop “Teaching critical thinking” (September 2021), Module 2 of the Higher Education Teaching Certificate (“Zertifikat Hochschullehre”), HDA, TU Darmstadt
- Seminar “Self-management” (March 2019), TU Darmstadt and AKAWIDA
- Debate training for the awareness for gender related topics (October-November 2019), TU Darmstadt and Debate Consult
- Course “Grant Writing for Natural Scientists and Engineers” (October 2019), professional development at the TU Darmstadt
- Workshop “Strategic Career Building Based on Skills and Values” (March 2019), TU

Darmstadt and K.T.E. – Coaching, Mainz

- Workshop “Communication and Conflict Management” (May 2019), TU Darmstadt and K.T.E. – Coaching, Mainz
- Seminar “Molecular radiation biology: from the basics to clinical applications” (February 2018), University Hospital Frankfurt am Main, Germany
- 3rd Bioimage Analysis Course (27-29 November 2017), Heidelberg Center for Human Bioinformatics (HD-HuB), Heidelberg, Germany
- Winter School for Innovations in Research “Navigation for Innovator” (29 January – 4 February 2017), Open University Skolkovo, Russia

List of publications

Kolobynina KG. Ubiquitinome-wide screening reveals a novel role for Polycomb complex proteins in repair of DNA double-strand breaks / Kolobynina KG, Rapp A, Beneke J, Starkuviene V, Pabba MK, Erfle H, Cardoso MC. // in preparation

Rapp A. Exposure of cells to near infrared irradiation relaxes chromatin compaction and facilitates recognition of cyclo-butane pyrimidine dimers / Rapp A, Kolobynina KG, Plitta-Michalak B, Cardoso MC. // Scientific Reports 2024, under revision

Pabba MK. Replisome loading reduces chromatin motion independent of DNA synthesis / Pabba MK, Ritter C, Chagin VO, Meyer J, Celikay K, Stear JH, Loerke D, Kolobynina K, Prorok P, Schmid AK, Leonhardt H., Rohr K, Cardoso MC. // eLife 2023 : doi: 10.1101/2023.03.07.531331

Qin W. Probing protein ubiquitination in live cells / Qin W, Steinek C, Kolobynina K, Forné I, Imhof A, Cardoso MC, Leonhardt H. // Nucleic Acids Res 2022 : doi: 10.1093/nar/gkac805.

Kolobynina KG. Chromatin Ubiquitination Guides DNA Double Strand Break Signaling and Repair / Kolobynina KG, Rapp A, Cardoso MC. // Front Cell Dev Biol 2022 : doi: 10.3389/fcell.2022.928113

Schwach J. Site-Specific Antibody Fragment Conjugates for Reversible Staining in Fluorescence Microscopy / Schwach J, Kolobynina K, Brandstetter K, Gerlach M, Ochtrop P, Helma J, Hackenberger CPR, Harz H, Cardoso MC, Leonhardt H, Stengl A. // Chembiochem 2022 : doi: 10.1002/cbic.202000727

Kolobynina KG. Emerging roles of the single EF-hand Ca²⁺ sensor tescalcin in the regulation of gene expression, cell growth and differentiation / Kolobynina KG, Solovyeva VV, Levay K, Rizvanov AA, Slepak VZ // J Cell Sci 2016 : doi: 10.1242/jcs.191486

Kolobynina KG. Creation of Human Adipose-Derived Stem Cell Lines with Overexpression of TESC gene/ Kolobynina KG, Solovyeva VV, Gomzikova MO, Tazetdinova LG, Rizvanov AA // Bionanoscience. – 2016 DOI : 10.1007/s12668-016-0299-5

Solovyeva VV. Tescalcin overexpression by adipose derived stem cells results in increase in IL-6 secretion / Solovyeva VV, Kolobynina KG, Gomzikova MO, Tazetdinova LG, Martynova EV, Khaiboullina SF, Slepak VZ, Rizvanov AA // Book of abstracts Ensor Workshop Nanocarbon materials, biomaterials and composites. - 2015. - P. 11.